2003

Evaluation and analysis of acid sulphate soil remediation via tidal restoration

William Carlos Glamore
University of Wollongong

University of Wollongong

THESIS DECLARATION: Part A

This is to certify that I ..WILLIAM GLANCE..... being a candidate for the degree of .PhD Engineering..... am fully aware of the University of Wollongong's rules and procedures relating to the preparation, submission, retention and use of higher degree theses, and its policy on intellectual property. I acknowledge that the University requires the thesis to be retained in the Library for record purposes and that within copyright privileges of the author, it should be accessible for consultation and copying at the discretion of the Library officer in charge and in accordance with the Copyright Act (1968). I authorise the University of Wollongong to publish an abstract of this thesis.

Signature .....

Date 09-10-03.....

EVALUATION AND ANALYSIS OF ACID SULPHATE SOIL REMEDIATION VIA TIDAL RESTORATION

A thesis submitted in fulfilment of the requirements for the award of the degree

DOCTOR OF PHILOSOPHY

From

UNIVERSITY OF WOLLONGONG

By

WILLIAM CARLOS GLAMORE
B. Sci. (Hons)

FACULTY OF ENGINEERING
2003

DECLARATION

I, William C. Glamore, declare that this thesis, submitted in fulfilment of the requirements for the award of Doctor of Philosophy, in the Faculty of Engineering, University of Wollongong, is wholly my own work unless otherwise referenced or acknowledged. This document has not been submitted for qualifications at any other academic institution.

William C. Glamore

25 September 2003

PUBLICATIONS RELATED TO THIS RESEARCH

Refereed Journals:

Glamore, W., and Indraratna, B. (2003) Floodgate Management Techniques for Acid Sulphate Soils Remediation. *Australian Journal of Soil Science*, (accepted, in press).

Glamore, W., and Indraratna, B. (2003) The Biogeochemical Impact of Tidal Forcing on Acidic Subsoils Using Multi-port Piezometers and Finite Element Simulations Techniques. *Journal of Geotechnical and Geoenvironmental Engineering,* (in prep).

Indraratna, B., Glamore W., and Tularam, G. A. (2002) The effects of tidal buffering on low-lying ASS environments. *International Journal of Geotechnical and Geological Engineering* **20** (3) pp 181-199.

Tularam, G. A., Indraratna, B., and Glamore, W. (2002) Investigation of tidal buffering via salinity intrusion in flood mitigation drains in Berry, New South Wales (Australia). *Quarterly Journal of Engineering Geotechnics*, (accepted).

Refereed Conference Papers:

Glamore, W. C. and Indraratna, B. (2004) Acid Sulfate Soils, Lateral Soil Hydraulic Conductivity and Groundwater Salinity: Management Implications of a Case Study, Broughton Creek, NSW. In 8^{th} *National Conference on Hydraulics in Water Engineering,* Gold Coast, QLD, Institution of Engineers, July 14-16 (accepted).

Glamore, W. C. and Indraratna, B. (2004) Design of an automated floodgate control system to enhance tidal flushing: Case Study, Broughton Creek, NSW. In *8th National Conference on Hydraulics in Water Engineering,* Gold Coast, QLD, Institution of Engineers, July 14-16 (accepted).

Glamore, W. C., and Indraratna, B. (2002) Management of Acid Sulphate Soil Drainage via Floodgate Manipulation. In *Proceedings of 5th International Conference on Acid Sulphate Soils*, Tweed Heads, 25-30 August, pp 75-77.

Glamore, W. C., and Indraratna, B. (2001) The effects of floodgate modifications in acid sulfate soil terrains. In *Proceedings of 15th Australasian Coastal and Ocean Engineering Conf.*, Gold Coast, Qld. Published by The Institution of Engineers, Australia. pp 265-270.

Invited Theme Paper: Indraratna, B., Glamore, W. C., Blunden, B., and Tularam, G. A. (2001) Engineering Strategies for Controlling Acid Sulphate Soils Problems in Low-lying Coastal Areas. In *Proceedings of 2nd Australia-New Zealand Conference on Environmental Geotechnics*, Newcastle, (Smith, D.W., Fityus, S.G., and Allman, M.A. editors), Published by Australian Geomechanics Society Inc., pp. 133-146.

Tularam, G. A., Indraratna, B., and Glamore, W. C. (2001) Effect of tidal buffering via salinity intrusion in flood mitigation drains in Berry, NSW. In *Proceedings of International Symposium on Application of Natural Materials for Environmental Geotechnology*. Tokyo, Japan. (Minato, H, and Ogushi, N editors) Published by Japan Society for the Promotion of Science. pp 301-318.

Cibilic, A., Gibbs, J., Haskins, P., Currie, B., Glamore, W. C., Morris, T., Tunks, M., and Wilkinson, G. (2002) Large Scale Acid Sulfate Soil Remediation, NSW Australia-Comparison of Hot Spot Site Characteristics and Strategies. In *Proceedings of 5th International Conference on Acid Sulphate Soils*, Tweed Heads, 25-30 August, pp 110-112.

ACKNOWLEDGEMENTS

The success of this thesis is in large part due to the assistance, collaboration and generosity of many people involved over the past three years. I would like to thank Prof. Indraratna, my supervisor, for his constant encouragement, inspirational work ethic, invaluable advice and technical assistance. I would also like to thank Warwick Papworth, John Downey (Shoalhaven City Council), Roy Lawrie, Narwash Haddad (NSW Department of Agriculture), and Alan Lugg (NSW Fisheries) for their technical advice, encouragement and in-field assistance.

I must thank the technical and administrative staff and students at the University of Wollongong, Faculty of Engineering, for their assistance, friendship, and entertainment. Special thanks go to Alan Grant, Bob Rowlan, Ian Kirby, Jeff Kinley, Ian Bridge, Norm Gal, Joanne George, Pam Burnham, Leonie MacIntrye, Peter Harding, Marcus Morgan, and Jeff Price. These people not only provided me with excellent technical support but they kept me fit, entertained and up to speed on the finer points of cricket. I would also like to thank Associate Professor Michael Boyd and Senior Research Fellow Phil Flentje for freely sharing their wealth of knowledge without hesitation.

Without the generous support from local landholders, this project would not have been possible. Therefore, I would like to thank Roger Carolyn and Janice Hayes for providing me with a beautiful field site and showing me untold hospitality, patience, and technical advice throughout the long field trial. I would also like to thank the Timbs family for putting up with my constant field trips.

Importantly, I would like to thank my friend and colleague Dr. Bruce Blunden whose excellent research laid the foundations for this project and whose friendship and technical advice was invaluable throughout the study.

I am thankful to my large and extended family for there support and encouragement over the past few years. The entire Crinis family including Peter, Vicki, Aaron, Stan and Matthew became my family and provided laughter, support, inspiration and sustenance. Furthermore, my family overseas which is too large to name has supported my endeavours for years and years and I want to thank them for always being there for me. I consider myself very lucky to have such caring and supportive friends and family.

Finally, and most importantly, I want to thank my wife and best friend, Georgia Glamore. Your undying support, love, patience and belief throughout the past three years has been immeasurable. Your contagious smile helped me through difficult times and your sampling skills are one-of-a-kind. I look forward to finally getting back to all those things we have planned for so long. Thank you.

ABSTRACT

The effectiveness of a floodgate modification strategy that involved restoring tidal flushing via modified floodgates to improve surface water quality and combat acid sulphate soil leachate was investigated in a low-lying flood mitigation drain near Berry in southeastern NSW, Australia. Prior to floodgate modifications, extensive soil, groundwater and surface water analysis indicated ubiquitous acidic conditions that were exacerbated by low drain water levels maintained by the one-way floodgates. The floodgates also increased a range of environmental problems including metal flocculation, low dissolved oxygen levels, pyrite oxidation, and acid transport. Temporal data showed that total drain water acidity was highest after rainfall but decreased when buffering agents inherent in brackish creek water penetrated upstream of the floodgate.

Before floodgate modifications were undertaken, tidal restoration techniques and criteria were developed to address surface water quality, hydraulics, and design concerns. First, an ion-association mixing program was developed and calibrated to simulate water quality and reaction kinetics within the drain. Second, hydraulic calculations and GIS mapping techniques indicated that full tidal restoration could be permitted solely within the primary drain. Floodgate design criteria were then developed and two modified floodgates were constructed and installed. One of these designs, the automated 'Environmentally Controlled Smart Gate System', was developed to permit tidal flushing based on real-time environmental parameters while utilising state-of-the-art technologies.

After floodgate modifications, tidal buffering and dilution improved drain water quality during all flow regimes and was most effective during prolonged dry periods. Tidal flushing also decreased the acid reservoir effect, permitted fish passage, reduced soluble iron concentrations and elevated the groundwater table. The impact of tidal forcing on the groundwater table was investigated biogeochemically through multi-port piezometers, while saline intrusion was simulated using 3-Dimensional finite element techniques. These investigations showed that tidal forcing at the study site was limited due to moderate lateral soil hydraulic conductivity values. Furthermore, while calibrated for the study site conditions, the finite element model and tidal buffering techniques can be easily adopted to other low-lying estuarine sites throughout Australia.

The floodgate modification strategy was shown to improve drain water quality, decrease groundwater drawdown, and improve drain hydraulics. However, before future floodgate modifications are undertaken several concerns should be addressed. These concerns and the findings from the entire thesis were summarised within a comprehensive best management practice developed to assist in effectively, efficiently, and safely restoring tidal flushing to additional sites.

TABLE OF CONTENTS

TABLE OF FIGURES

TABLE OF TABLES

Chapter 1.0 Introduction

1.1 General Background

The negative environmental impacts of water control structures, such as dams and floodgates, are well reported throughout the world. Along the coastal fringe of Australia, the majority of water control structures are one-way tidal restricting floodgates. Pollard and Hannan (1999) reported more than 1200 floodgates installed on tidal estuaries within the state of New South Wales, Australia. Originally, the one-way floodgates were installed to provide flood mitigation to low-lying coastal areas effected by tidal inundation or prolonged surface ponding. However, by restricting tidal flushing one-way floodgates create a myriad of environmental problems. These problems are greatly increased when the floodgates are installed in regions containing acid sulphate soils.

Acid sulphate soils are commonly defined as soils containing sulphidic minerals, mainly in the form of pyrite (FeS_2), in either a reduced or oxidised state. When oxidised the pyrite dissociates to form high concentrations of dissolved Fe (II) and sulphuric acid. The acidic subsoil conditions can solubilize acidic cations such as aluminium and manganese. In certain conditions when the groundwater pH falls below 3.5, and sufficient organic material is present, the acid generating process becomes self-sustaining. This process, combined with poor management techniques, can result in widespread acidification of the soil matrix and adjacent surface waters. Though several attempts have been made to decrease acid production and the net discharge of acid products, currently there are no cost-effective remedial strategies.

In combination, acid sulphate soils and tidal restricting floodgates degrade the estuarine environment. Glamore and Indraratna (2001) suggested that one-way floodgates installed on acid sulphate soil terrains increase acid production and acid transport within the phreatic zone, enhance acid discharge, and exacerbate problems associated with iron flocculation in surface waters. Indraratna *et al.* (2002) suggested that tidal restoration via modified floodgates might decrease acid transport and increase buffering capacity. Several researchers, however, suggest that further studies are necessary before floodgate modifications are undertaken to (i) better understand the interrelationships between one-way tidal restricting floodgates and acid production, (ii) to quantify the influence of tidal flushing prior to floodgate modifications, and (iii) to ascertain the hydraulic, floodgate design and saline intrusion concerns of tidal intrusion.

This thesis examines the interrelationships between tidal restricting one-way floodgates and acid sulphate soils. Specifically, this thesis provides an in-depth description of the current management practices, the impact of floodgates on the soil, groundwater and surface water regimes, and the influence of restored tidal flushing via modified floodgates to an acid sulphate soil affected flood mitigation drain in southeastern New South Wales, Australia. This thesis covers all relevant aspects regarding tidal flows in estuarine environments, including water quality forecasting, concerns regarding overtopping of the levee bank, floodgate design criteria and innovative design concepts, and the influence of tidal restoration on the soil and groundwater matrix. This thesis concludes with the development of a best management practice for tidal restoration via modified floodgates at additional low-lying flood mitigation drains.

1.2 Research aims

The research described in this thesis aims to:

- Provide a critical literature review of acid sulphate soil research undertaken within southeastern Australia over the past 30 years, including in-depth analysis of applied management strategies;

- Describe the relationship between one-way tidal restricting floodgates, acid production, and acid transport within the soil and groundwater regime;

- Ascertain the influence of climatic and hydraulic factors on surface water acidity upstream of tidal restricting floodgates and acid discharge from the drainage system;

- Develop and calibrate numerical models and techniques to quantify the hydraulic and aqueous chemical concerns relating to tidal restoration within a low-lying flood mitigation drain prone to inundation;

- Investigate the extent and impact of increased drain water salinity and tidal forcing on the biogeochemical reactions within the soil matrix using extensive multi-port piezometer testing;

- Develop a field calibrated 3-D finite element groundwater model to simulate coupled flow and transport of saline contaminates over varying climatic and physical soil conditions using real-time field data inputs;

- Design and construct innovative floodgate structures based on design criteria developed specifically for acid sulphate soil low-lying flood mitigation drains;

- Determine the influence of modified two-way floodgates on surface water quality and drain hydrodynamics at a fully instrumented low-lying estuarine field site in southeastern New South Wales, Australia;

- Develop best management practices related to future floodgate modifications.

1.3 Thesis Structure

This research is divided into six major components. The description of each component and its corresponding Chapter is described below.

1.3.1 Part I: Critical Literature Review

Background information regarding acid sulphate soils formation, oxidation and chemical processes is detailed in the beginning of Chapter 2. This review begins with an in-depth description of acid production and its influence on chemical and physical parameters within the soil matrix. Tidal restricting floodgates are then described and their role in intensifying acid production and transport is illustrated. Finally, the theory of tidal buffering via modified floodgates is presented as a non-anthropogenic alternative management strategy to combat acid sulphate soil drainage and discharge.

In the second section of Chapter 2, an extensive critical analysis of acid sulphate soil background research is undertaken. This review provides a vital link between previous

acid sulphate soil management research conducted over the past 30 years, including chemical analysis, field techniques and numerical simulations, and their significance to current research. Furthermore, the critical review examines why former groundwater management strategies were not effective in controlling acid production or transport.

1.3.2 Part II: The influence of tidal restricting floodgates

A major component of this research involves investigating the influence of existing tidal restricting floodgates on the soil, groundwater, and surface water terrains at a fully instrumented field site in southeastern New South Wales, Australia. Chapter 3 describes the study site's location, geomorphology, and drainage history, including the monitoring regime initiated to understand the complex physical and chemical attributes of the groundwater, surface water, and climatic factors. The climatic conditions experienced over the entire study period (i.e. long-term rainfall and evapotranspiration rates) are also discussed at the end of this Chapter.

Chapter 4 describes the baseline soil and groundwater conditions at the study site prior to floodgate modifications, the role of tidal restricting floodgates in increasing acid production, and the physical properties of the soil. These baseline conditions depict the influence of tidal restricting floodgates on the soil matrix and illustrate how the gradient (i.e. slope) of the phreatic zone decreases with distance from the floodgate. This information is later employed during the initialisation of a finite element coupled flow and transport model (Chapter 9).

In Chapter 5, the chemical and hydraulic influence of tidal restricting one-way floodgates is examined with regard to surface water indicators and climatic factors.

Drain water quality is divided into three periods based on flow and floodgate leakage. During the majority of the study, one-way floodgates are shown to intensify acid conditions and create acid reservoirs, which acidify receiving waters during the ebb tide. Periods of floodgate leakage were associated with ingress of alkaline creek water and improved drain water quality. At the conclusion of Chapter 5, floodgate modifications, which allow tidal flushing and increase tidal buffering, are recommended to improve drain water quality and hydraulics.

1.3.3 Part III: Chemical and hydraulic concerns prior to floodgate modifications

Chapter 6 examines three major issues addressed prior to the restoration of tidal flushing, namely; (i) the change in drain water quality after floodgate modifications, (ii) the hydraulic impact of tidal flushing in regards to overtopping of the drain levee bank, and (iii) floodgate design criteria and prototype designs. First, the reaction kinetics of acid buffering within estuarine environments are examined through laboratory tests. An aqueous ion speciation program is then developed to simulate drain water quality following mixing with estuarine water of varying ionic strength. The findings from these experiments indicate that drain water quality will significantly improve after floodgate modifications. A spatial modelling technique, developed to determine the influence of tidal flushing on drain water hydraulics, is also presented to calculate the quantity of tidal water permitted within the flood mitigation drain without overtopping the levee bank.

A series of floodgate design criteria are presented to assist floodplain managers and civil engineers during constructing of modified two-way floodgates. Based on these criteria and hydraulic concerns, two innovative floodgate designs installed at the study

site are outlined. The first model is a manually controlled vertical lifting device designed to permit full tidal intrusion. The second model is a fully automated state-of-the-art 'intelligent' floodgate, designed to control the quantity of tidal flows based on real-time data retrieval and remote dial-up technologies.

1.3.4 Part IV: The impact of modified floodgates on surface water and groundwater indicators

The influence of floodgate modifications on the surface water and groundwater environments forms a major component of this research. Chapter 7 examines "Surface Water Quality and Hydrodynamics Following Floodgate Modifications". In this chapter, tidal flushing is shown to significantly improve drain water quality and drain hydraulics. While previously in excess of the Australian and New Zealand Environment and Conservation Council water quality guidelines (ANZECC, 1992), following floodgate modifications water quality generally improved due to tidal buffering and dilution. The extent of water quality improvements is shown to be reliant on climatic factors that limit acid transport and the concentration of buffering agents.

The response of the phreatic zone in regards to floodgate modifications is detailed in the second section of Chapter 7. Field indicators show that tidal forcing and increased drain water elevations recharged the phreatic zone. In doing so, the surface of the phreatic zone is maintained above the pyritic layer and groundwater drawdown is reduced. A series of field tests are presented to illustrate the influence of tidal forcing on groundwater levels with increasing distance from the drain.

1.3.5 Part V: The influence of modified floodgates on the biogeochemical reactions within the soil and groundwater zones

Limited research has been conducted on the biogeochemical impact of saline tidal forcing in acid sulphate soil environments. In Chapter 8, a series of field tests undertaken to calculate the zone of tidal intrusion using sophisticated monitoring techniques are presented. Multi-level groundwater analysis is conducted on a range of chemical parameters including pyrite oxidation products, saline indicators, and nutrient species. These findings provide detailed insight into the mechanisms for saline intrusion and their implications for the floodgate management strategy.

Chapter 9 examines the impact of saline intrusion on the soil matrix through the initialisation, calibration and simulation of a 3-D coupled flow and transport finite element computer model. The field-calibrated model is constructed to determine the extent and distribution of saline contaminates over a range of climatic variables, including prolonged droughts and groundwater recharge. Numerical simulations of saline intrusion over varied lateral hydraulic conductivity values were undertaken and the formulated guidelines based on the simulations are presented.

1.3.6 Part VI: Guidelines and recommendations

The findings presented throughout this thesis are summarised within Chapter 10. The recommendations are collated into a Best Management Practice (BMP) for use in future floodgate modifications. Some additional research directions and issues that require further study are also discussed.

Chapter 2.0 Critical Review of Acid Sulphate Soils and Tidal Restricting Floodgates with Reference to Southeastern New South Wales, Australia.

2.1 Introduction

Dent and Pons (1995) state that acid sulphate soils are the 'nastiest soils in the world'. Predominately located in low-lying floodplains, these soils contain sulphide minerals either in an oxidisable or partially oxidised state. The common form of sulphide mineral is pyrite (FeS_2), however, others, such as metastable monosulphides (greigite, marcasite and amorphous FeS), may also form (Fitzpatrick *et al.*, 1993). Pyrite concentrations typically range from innocuous levels below 0.01% Chromium Reducible Sulfide ($\%S_{cr}$), to extreme concentrations above 15.0% S_{cr} (Dent and Pons, 1995). Due to the depositional environment in which they form, subsurface concentrations in Australia are commonly above the management action criteria of 0.05% S_{cr} set by Stone *et al.* (1998).

Acid sulphate soils (ASS) remain chemically inert whilst in reducing conditions. When oxidation occurs as a result of climatic, hydrological or geological changes, the oxidised layer produces sulphuric acid and is termed an actual acid sulphate soil (AASS). This oxidation process can acidify the soil pore water, cause dissolution of heavy metals, and change the structure of the soil fabric. An actual acid sulphate soil layer will often overlie a reduced or potential acid sulphate soil layer (PASS). In general, the term acid sulphate soil is used to portray the hazards associated within the entire soil profile.

This Chapter is divided into three subject themes that describe the impact of acid sulphate soils on the surrounding environment and analyse previous research on acid

sulphate soil management. Within the first subject theme, the processes involved in pyrite formation, oxidation and sulphurisation are described. In particular, the physical and chemical properties of acid sulphate soils are detailed, as well as the various methods of pyrite oxidation and acid production. The impact of pyrite oxidation is also described with particular reference to soil development, and its influence on the soil matrix and agricultural productivity. Finally, the translocation of acidic oxidation products into adjacent receiving waters is addressed at the conclusion of this theme.

The second subject theme of this Chapter investigates the different aspects of hydrogeology and hydromechanics associated with acid sulphate soil seepage/drainage in floodplain environments. Specifically, subsurface groundwater flow across altered floodplain dynamics and climatic periods is examined. Artificial drainage and its ability to increase groundwater drawdown are also considered, and background information regarding flow analysis of groundwater under varied artificial drainage regimes is given. As a conclusion to this theme, the impact of tidal restricting one-way floodgates on acid sulphate soil drainage is reviewed and the theory of tidal buffering is suggested as an alternative management strategy.

The final subject theme of this Chapter critically reviews previous on-ground management and acid sulphate soil remediation strategies conducted in Australia. As such, background research conducted during the past 25 years is described with particular emphasis on the study site region (southeastern New South Wales). This research shows that regardless of previous efforts, an alternative management strategy is necessary to combat acidic discharges. To this point, the research hypothesis of this study is presented and the aims and expected outcomes are detailed.

2.2 Pyrite formation processes

Acid sulphate soils form in reducing environments where there is a supply of easily obtained decomposed organic matter, sulphate, iron and reducing bacteria. During the formation process, the bacterium *Desulfovibrio desulfuricans*, reduces sulphate to sulphide. Electrons generated in the microbial oxidation of organic matter reduce Fe (III) to Fe (II) (Fanning, 1993). This combined reaction, called sulphidisation, most commonly results in the production of pyrite (FeS_2). Warmer temperatures and slightly acidic conditions enhance the pyrite formation kinetics, which typically occurs slowly; say 100 years to form 1% pyrite by mass (Dent and Pons, 1995).

Equation 2.1 shows the generalised process for pyrite formation (Dent, 1986).

$$\underbrace{Fe_2O_{3(s)}}_{\text{iron}} + \underbrace{4SO_{4\,(aq)}^{2-}}_{\text{sulfate}} + \underbrace{8CH_2O}_{\text{organic matter}} + \tfrac{1}{2}O_2 \xrightarrow{\text{bacterial driven with reducing conditions}} \underbrace{FeS_{2(s)}}_{\text{pyrite}} + \underbrace{8HCO_3^-}_{\text{bicarbonate}} + 4H_2O \qquad (2.1)$$

The formation of acid sulphate soils can occur in a variety of geographical locations, however, the above conditions are most prevalent in coastal floodplains. In these regions, sulphate is obtained from brackish water (seawater concentration = ~2700 mg L^{-1}). Iron is commonly found within coastal clays, in iron oxides including oxyhydroxides such as goethite, FeOOH, and in hydroxides and oxides, such as hematite, Fe_2O_3 (Blunden, 2000). Abundant organic matter and reducing conditions are maintained through regular tidal inundation, a consistent supply of fresh water, and long retention periods characteristic of mangrove ecosystems. An illustration of favourable conditions and predominate sources for pyrite formation is shown in Figure 2.1.

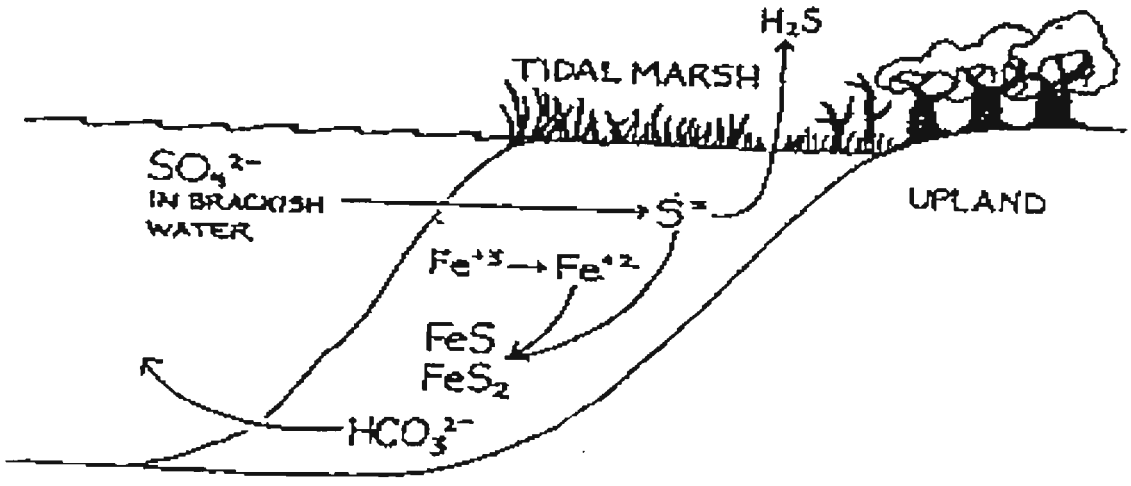

Figure 2.1 Typical conditions and inputs necessary for the formation of pyritic sediment (Fanning, 1993).

In these reduced, waterlogged environments, bicarbonate ions, a byproduct of Equation 2.1, remain soluble and are often lost from the soil by leaching and/or tidal flushing. Indeed, Fanning (1993) suggests that oyster communities commonly form on mangrove brace roots of *Rhizophora* by utilising bicarbonate from this process. Though this represents a significant reduction in the soil's potential neutralising capacity, the remnants of the oyster shells typically provide the main buffering reserve for most acid sulphate soils in the form of calcium carbonate (one part by mass of pyrite sulphur is buffered by three parts calcium carbonate). Other minor soil buffers can also exist, such as exchangeable bases, but in terms of neutralisation capacity they make up no more than 0.5% by mass of sulphur (Dent, 1992).

The above description is a simplified version of the actual chemical reactions carried out in the formation of sulphide minerals in coastal environments. In some cases, it has been suggested that hydrogen sulphide must be formed first (see Equation 2.2), and then reacted with iron oxides to produce pyrite (Bohn *et al.*, 1989). Although this process

(Equation 2.3) differs in that iron monosulphides are formed, the overall conditions and reaction mechanics are similar.

$$SO^{2-}_{4(aq)} + 2CH_2O_{(s)} \xrightarrow{\text{bacteria}} H_2S_{(g)} + 2HCO^{-}_{3(aq)} \quad (2.2)$$

$$3H_2S_{(g)} + 2FeOOH_{(s)} \longrightarrow FeS_{(s)} + FeS_{2(s)} + 4H_2O_{(l)} \quad (2.3)$$

2.3 Location of Acid Sulphate Soils

As part of the global sulphur cycle, acid sulphates soils are found worldwide. By restricting a survey to Holocene coastal plains and tidal swamp sediments, van Breeman (1980) estimated that there are 12-14 million ha worldwide where the topsoil either has the potential to become, or is already severely acidic. Table 2.1 shows initial estimates of the distribution of acid sulphate soils by region (Brinkman, 1982).

Table 2.1 Calculated distribution of acid sulphate soil by region.

Region	Area of ASS (x 10^6 ha)
Africa	3.7
Asia	6.7
Latin America	2.1
Australia	1.0

During regional mapping programs around New South Wales and Queensland, mounting evidence has shown that original calculations of 1 million ha. severely underestimates the quantity of acid sulphate soils. In Queensland alone, Powell *et al.* (1996) mapped 2,263,000 ha of acid sulphate soils and in NSW Naylor *et al.* (1995) calculated 400,000 – 600,000 ha (Figure 2.2). White *et al.* (1997) has shown that

similar conditions also exist in Western Australia and the Northern Territory. Large areas of acid sulphate soil have also been documented around Adelaide, South Australia and Westernport Bay near Melbourne, Victoria (Sammut *et al.*, 1996). With this in mind, recent conservative calculations of acid sulphate soils in Australia are now above 3 million ha (White *et al.*, 1997).

Acid sulphate soils occur mainly in low-lying coastal zones but have been noted in other environments. Primarily, acid sulphate soils are found in wave protected mangroves and marshes, outer barrier lakes, backswamp regions and salt water lakes or, importantly, remnants of such areas where suitable conditions previously existed for pyrite accumulation (Naylor *et al.*, 1995). Due to a lack of sulphate, pyrite formation has been documented in only a few fresh water locations and typically in low concentrations (Cohen *et al.*, 1984; Davison *et al.*, 1985; Marnette *et al.*, 1993; Kraus, 1998).

The presence of acid sulphate soils in many regions today is due to the relative sea levels during the Holocene and the associated depositional conditions. Most researchers agree that the last glacial maximum was at least 18000 years ago and current sea levels have been relatively stable for the last 3000 years (Thom and Chappell, 1975; Roy, 1984; Woodroffe *et al.*, 2000). The rise in sea levels during this period (approx. 10 m in the south coast of New South Wales) created conditions conducive to pyrite formation and resulted in large, laterally extensive deposits of sulphidic sediments (Woodroffe *et al.*, 2000). In most regions, the surface of the sulphidic horizon is at mean sea level from when it was formed, approximately 0-1 m above the current mean sea level, or 0-1 m Australian Height Datum (AHD). As sea levels receded, fluvial sedimentation

processes began to dominant, which fostered the deposition of an alluvial layer over the pyritic sediment. This layer is usually less than 5-10 m in height and mapping or reconnaissance of acid sulphate soils is generally restricted to < 10 m AHD (Atkinson *et al.*, 1996).

The content and location of pyritic sediments are directly related to its depositional environment and estuarine hydrodynamics. Though various arguments exist, Pons and van Breeman (1982) suggest that a slow sedimentation rate is likely to form high pyritic concentrations due to the kinetics of pyrite formation. In fact, rapid sedimentation may hinder the transformation of monosulphides to pyrite, as illustrated by Equation 2.2 (Goldhabar and Kaplan, 1982; Lin and Melville, 1994). When the basic components are abundant (eg. organic matter, sulphate, iron and reducing conditions), pyrite formation will be accelerated in shallow water due to low water pressure, by elevated temperatures that increase bacterial processes, and with tidal flushing. Tidal flushing, in particular, adds low concentrations of dissolved oxygen necessary to complete pyritisation of sulphate and remove bicarbonates, thereby maintaining favourable slightly acidic conditions (van der Kevie, 1973; Pons *et al.*, 1982). With this in mind, estuarine tidal flats with mangrove or reed communities, or remnants of such locations, provide the most favourable environment for high pyrite content.

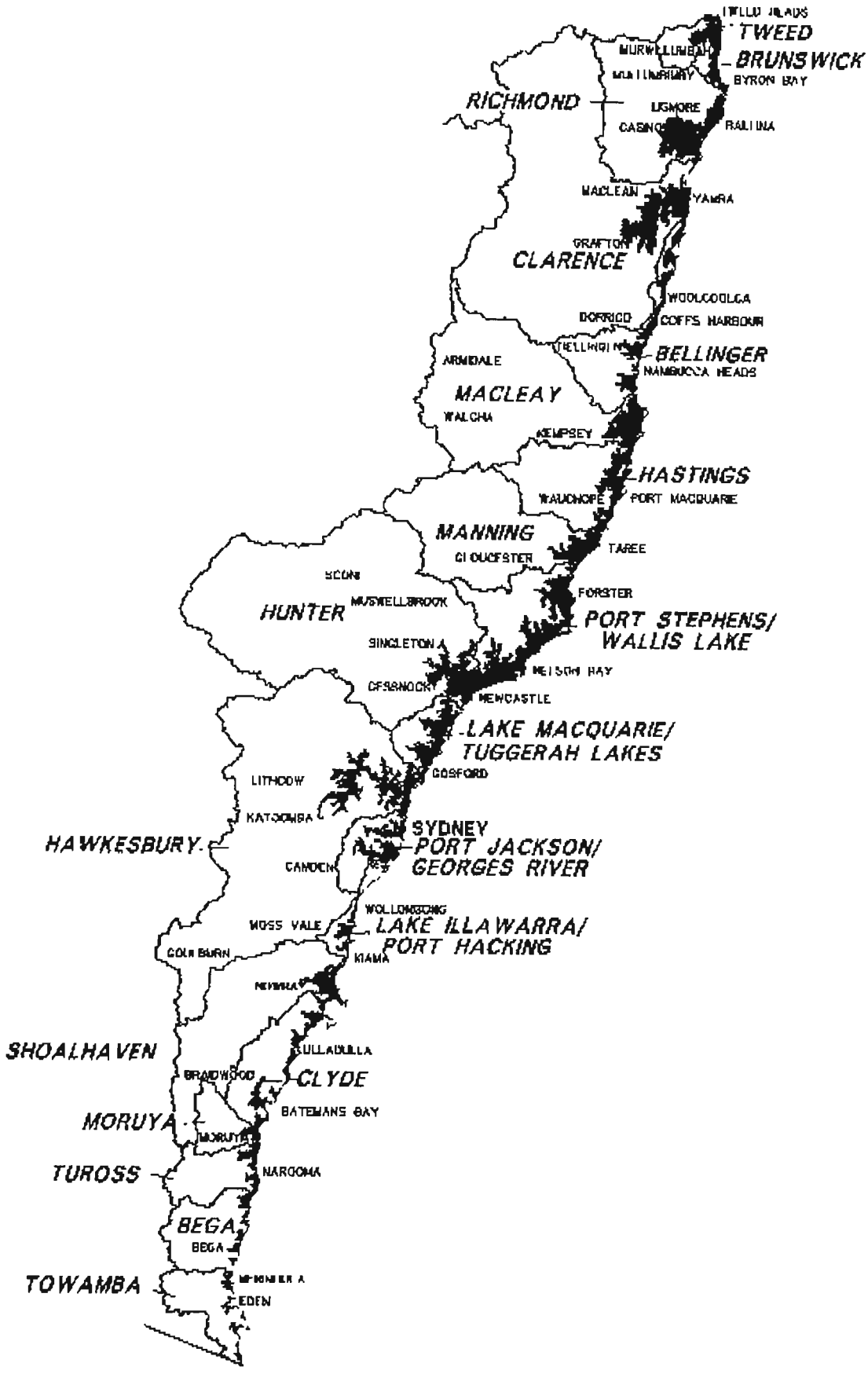

Figure 2.2 Risk map of acid sulphate soils within coastal NSW (Naylor *et al.*, 1995). Shaded regions represent high probability of occurrence of acid sulphate soils.

2.4 Properties of Acid Sulphate Soils

The processes and kinetics effecting pyrite oxidation and acid transport are complex and are still being understood. Indeed, one of the major stumbling blocks in managing acid sulphate soils has been controlling the various means of generating acid and its complex physical structure. This section provides an understanding of the mechanisms involved in pyrite oxidation, and the role soil structure plays in enhancing oxygen transport. It concludes with an examination of the impact of acid products on the soil, pore water, and surface water environment.

2.4.1 Pyrite oxidation processes

Pyrite oxidation occurs when sulphide minerals are exposed to atmospheric oxygen. The process is complex and there is no single rate law available to describe the general kinetics of the reaction in all cases. It involves chemical, biological, and electrochemical conditions and varies based on pH, pO_2, pyrite morphology, temperature, the presence of specific bacteria and hydrological conditions (Dent, 1984; Blunden, 2000). In short, the reaction involves the conversion of pyrite (FeS_2) to iron II and sulphate in the presence of oxygen and moisture. As shown in Equation 2.4, the byproduct of this reaction is H^+ ions that create acidic pore water (Stumm and Morgan, 1996; Indraratna *et al.*, 2001).

$$\underbrace{FeS_2}_{\text{pyrite}} + \underbrace{\tfrac{7}{2}O_2}_{\text{atmospheric oxygen}} + H_2O \longrightarrow \underbrace{Fe^{2+}}_{\text{dissolved iron}} + 2SO_4^{2-} + \underbrace{2H^+}_{\text{acid}} \qquad (2.4)$$

In acidic groundwater, Fe^{2+} produced in Equation 2.4 can further oxidise to Fe^{3+}, and in the process remove one of the H^+ ions. When Fe^{3+} flocculates as a hydroxide, three

moles of acid are generated for each dissolved ferric ion that precipitates. This reaction can be summarised as:

$$Fe^{3+} + 3H_2O \Leftrightarrow Fe(OH)_{3(s)} + 3H^+ \quad (2.5)$$

Initially, the oxidation of pyrite is a relatively slow process, but as pH decreases, Fe^{2+} remains soluble and the activity of Fe^{3+} increases. In a reduction reaction driven by the bacterium *Thiobacillius ferrooxidaans*, dissolved Fe^{3+} can directly oxidise pyrite in anaerobic conditions (Equation 2.6). Singer and Stumm (1970) showed that in mining waste, this process becomes the main mechanism of acid production. Importantly, the autotrophic organism *T. ferrooxidaans* accelerates the oxidation of Fe^{2+} into Fe^{3+} by a factor greater than 10^6, thus creating a continuous pyrite consumption and acid production cycle. This process will continue until all the Fe^{3+} is leached from the soil regardless of the oxidation state.

$$FeS_2 + 14Fe^{3+} + 8H_2O \longrightarrow 15Fe^{2+} + 2SO_4^{2-} + 16H^+ \quad (2.6)$$

Though greatly simplified, the overall process of complete pyrite oxidation is given as:

$$FeS_2 + {}^{15}\!/_4 O_2 + {}^{7}\!/_2 H_2O \longrightarrow Fe(OH)_3 + 2SO_4^{2-} + 4H^+ \quad (2.7)$$

In Equation 2.7, for every one mole of pyrite consumed, 4 moles of acid are generated.

2.4.2 Soil properties and development

The earliest surveys of acid sulphate soils were conducted during drainage of the big Harlemmermeer in Holland in 1852 (Dent and Pons, 1993). Since then, soil surveys have been undertaken throughout the world and a systematic method has been developed to classify acid sulphate soils based on their physical properties. This section details the physical attributes of acid sulphate soils and explains the processes of soil development from deposition to late stages of pyrite oxidation and consolidation.

In FAO soil taxonomy (FAO, 1974), potential acid sulphate soils are placed in the Order Entisols, as Sulfaquents if the sulphidic material is less than 0.5 m, or as Sulfic Hydraquents when it occurs between 0.5 and 1.0 m below the surface (Dent, 1992). These soils are generally saturated estuarine clays with moisture contents between 80-120%, and thus, have a gel-like appearance. Due to the depositional environment, the soil structure is texturally uniform with a fine, tortuous, heterogenous pore space (Blunden, 2000). Owing to the lack of pore volume, the hydraulic conductivity and oxygen diffusivity in these soils is extremely low and generally restricts pyrite oxidation. A list of physical properties from a typical potential acid sulphate soil taken from southeastern New South Wales (NSW), Australia is shown in Table 2.2.

Table 2.2 Physical properties of potential acid sulphate soil layer (Blunden and Indraratna, 2000).

Soil Layer	Bulk Density (kg/m^3)	Hydraulic Conductivity - vertical (m/day)	Hydraulic Conductivity - horizontal (m/day)	Porosity (%)	Residual moisture content – volumetric	Saturated moisture content-volumetric
Potential ASS	1030	2.02	0.20	61	0.06	0.49

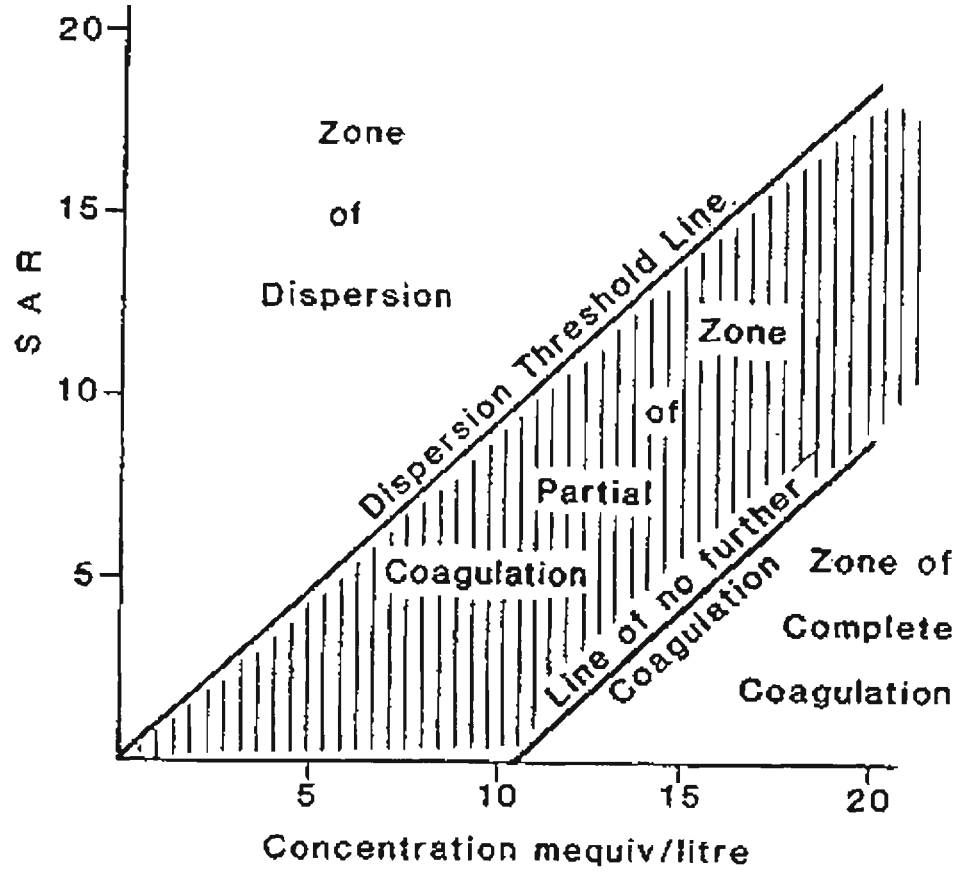

Figure 2.3 Sodium adsorption ratio versus concentration to determine coagulation limits (Mulvey, 1993).

The general development of an acid sulphate soil involves irreversible processes that change the structure and chemical constitution of the soil fabric. First, as fluvio-estuarine evolution reduces brackish flows, sodium is leached from the soil and replaced by higher valence cations such as calcium and magnesium. In a similar manner, aluminium and hydrogen ions are released from cation exchange complexes. This cation exchange process enlarges pore size due to clay flocculation and the formation of aggregates (Mulvey, 1993). As pore size increases, oxygen can diffuse into the soil matrix causing further clay flocculation. Clay flocculation increases pore size and allows plant roots and soil fauna to intrude. The combination of clay flocculation and plant and animal intrusion increases the soil macroporosity, permeability and

diffusivity. This progression of soil development triggers a cycle of clay flocculation, increased aeration, and further clay coagulation, which results in silt-sized structures called domains and macropores (Mulvey, 1993). Soil coagulation stops when the maximum sodium absorption ratio versus ionic concentration is established, as shown in Figure 2.3.

Soil development is enhanced by the establishment of surface vegetation which increases dewatering of the soil profile. The removal of moisture causes irreversible shrinkage of the soil colloid and general subsidence in soil elevation. This consolidation process can restrict plant growth through increased waterlogging and flooding. The rate of ripening is related to the rate at which the soil dries and in general terms, the watertable position. Therefore, in soils where a stable watertable is maintained, a marked boundary can exist between a ripened, acid producing actual acid sulphate soil layer and a massive, low permeability, potential acid sulphate soil layer. The conversion of potential acid sulphate soils to actual acid sulphate soils creates acidic pore water and causes an irreversible change in the colloidal structure of the clay.

2.4.3 The influence of pyrite oxidation on the soil matrix

The production of acid by pyrite oxidation significantly alters the soil's chemical composition. As pH levels fall, acidified pore water is transported above the pyritic layer due to capillary rise from evapotranspiration, or from an increase in the watertable due to rainfall. In this way, the soil matrix above the pyritic layer can become acidified over time. The acidification process changes the solubility of many iron oxidation products and the dissolution of clay minerals such as aluminium.

As shown in Equation 2.7, the oxidation of pyrite produces large concentrations of iron, sulphate and hydrogen ions. The solubility of each ion depends on its position in the watertable, the oxidation status (Eh) and the pH level (Ferguson and Eyre, 1996). For example, iron can range from insoluble Fe (III) oxides and hydroxides, such as goethite ($Fe_2O_3 \cdot H_2O$), to haematite in severely oxidised soils (Nordstrom, 1982).

Sulphates generated in an acidic environment remain soluble and are transported with ferrous iron minerals by diffusion or via mass flow. In evaporative conditions, hydrated ferrous sulphate minerals concentrate and precipitate primarily within macropores formed by old root channels, which provides space for accumulation and an evaporative surface. As described by Wilson (1995), the first of these to precipitate is melanterite ($FeSO_4 \cdot 7H_2O$), followed by rozenite ($FeSO_4 \cdot 4H_2O$), and possibly szomolnokite ($FeSO_4 \cdot H_2O$).

Marius (1985) suggested that ferrous sulphates (eg. rozenite) could accumulate on the soil surface through wicking or evapotranspiration. These white salts were originally thought to be aluminium sulphates, however, subsequent findings indicate that iron sulphate minerals are more common (Fanning, 1993). Though further oxidation of these salts is possible in the presence of highly soluble sulphate, such as in the creation of jarosite, ferrous sulphates can directly oxidize and solubilize to form iron oxides and sulphuric acid as described by:

$$\underbrace{FeSO_4}_{(aq)} + \underbrace{\tfrac{1}{4}4O_2}_{(aq)} + \underbrace{2\tfrac{1}{2}H_2O}_{(l)} \longrightarrow \underbrace{Fe(OH)_3}_{(s)} + \underbrace{H_2SO_4}_{(aq)} \qquad (2.8)$$

Fanning (1993) states that when working with acid sulphate soils, "one has in many cases to deal with acidity at the same time as salinity". Though the usual processes of Na^+ and Cl^- may cause salinisation in coastal environments, highly reactive processes involving iron and sulphate, such as those stated above, also occur. In fact, sodium sulphate salts may arise as a by-product of pyrite oxidation. In this reaction, Na^+ on the cation exchange complex replaces H^+ of H_2SO_4. The dissolved salt, Na_2SO_4, is then brought to the surface through capillary action, by an increase in watertable height due to rainfall, or by a change in hydrological conditions (Fanning, 1993). Drying by evaporation results in salt efflorescence at the surface, soil flocculation/cracking and hence, increased oxygen transport into the pyritic material.

As the pyrite layer develops and acid concentrations increase, silicate clay dissolution liberates metals into solution. In particular, at low pH levels aluminosilicate clays release aluminium that remain soluble and form aluminium hydroxy ions (e.g. $Al(OH)_2^+$). This process, as shown in Equation 2.9, blocks negatively charged sites in silicate clays, liberates other metals, and limits cation exchange (Nriagu, 1978).

$$(K_{0.5}Na_{0.36}Ca_{0.05})(Al_{1.5}Fe^{3+}_{0.25}Mg_{0.3})(Al_{0.45}Si_{3.46})(O_{10}OH)_2 + 7.41H^+ + 2.59H_2O \longrightarrow$$
$$0.5K^+ + 0.36Na^+ + 0.05Ca^{2+} + 0.3Mg^{2+} + 0.25Fe(OH)_3 + 1.95Al^{3+} + 3.46H_4SiO_4 \quad (2.9)$$

Within Australia, Blunden (2000) found that exchangeable aluminium saturation was above 90% for the majority of the soil profile (Figure 2.4). These extreme levels restrict the uptake of beneficial cations on cation exchange sites. Replacement by beneficial major cations via aluminium hydrolysis also contributes to soil acidity, as shown in Equations 2.10-2.12. Ritsema *et al.* (1992) found that the dissolution of aluminium

minerals into pore water increases soil buffering, as cations such as Mg^+ and Ca^+ can attach to the cation exchange complex. Clay dissolution from acidic pore water can strip high concentrations of Mn^+, Cd^+ and other heavy metals such as Pb^+ from the soil.

$$Al^{3+} + H_2O \rightarrow Al(OH)^{2+} + H^+ \quad (2.10)$$

$$Al(OH)^{2+} + H_2O \rightarrow Al(OH)_2^+ + H^+ \quad (2.11)$$

$$Al(OH)_2^+ + H_2O \rightarrow Al(OH)_3 + H^+ \quad (2.12)$$

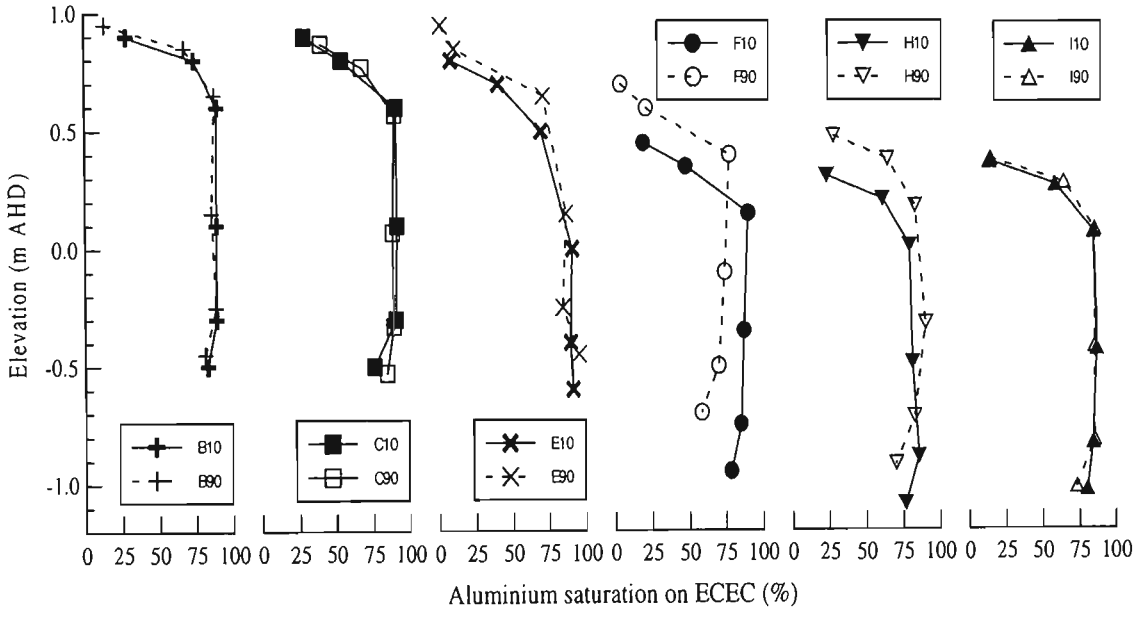

Figure 2.4 Typical aluminium saturation on the effective cation exchange capacity at 10 m and 90 m perpendicular to a flood mitigation drain for various piezometer transects (Blunden, 2000).

The characteristic formation of yellow jarositic mottles within the soil profile depends on oxidising conditions (Eh), the pH of the pore water, and a sufficient supply of K, Fe and SO_4 (Lin *et al.*, 1998). Generalised Eh/pH diagrams of Fe and S, shown in Figure 2.5, depict that jarosite precipitates in an acidic (pH < 4), strongly oxidising (Eh > 400) environment (Fanning and Fanning, 1989). These conditions normally occur in the transition zone between the actual acid producing layer and the non-pyritic layer, and

researchers often include a jarositic stratum as a third layer above the actual and potential acid sulphate soil layers. During the formation process, as shown in Equation 2.13, $FeSO_4$ transported upward by capillary rise, reacts with H_2O and K to form jarosite and sulphuric acid.

$$3FeSO_4 + O_2 + 4H_2O + K^+ \longrightarrow KFe_3(OH)_6(SO_4)_2 + H_2SO_4 \qquad (2.13)$$

Jarosite is part of the rhombohedral alunite group of minerals, and therefore, K may be substituted for Na, Pb, NH_4, H_3O, and Fe^{2+} for Fe^{3+} or Al^{3+}. As it is both insoluble in water and the predominant form of oxidized-S species in the soil (Lin *et al.*, 1998), jarosite represents a significant store of acid products and prevents extremely low soil pH levels (< 2.0). Similarly, the hydrolysis of jarosite as described below, occurs slowly, and thereby, serves as an acid reservoir.

$$KFe_3(SO_4)_2(OH)_6 + 3H_2O \rightarrow 3Fe(OH)_3 + SO_4^{2-} + K^+ + 3H^+ \qquad (2.14)$$

2.4.4 Impact of pyrite oxidation on soil productivity

Following pyrite oxidation, acid products are transported above their original production site through capillary rise due to evaporation, or from an increase in groundwater elevation in response to rainfall. As mentioned earlier, the accumulation of salt crusts and the dominance of Al and Fe on the cation exchange complex reduces plant health and may be toxic in high concentrations. Likewise, the diffusion of low pH pore water with elevated heavy metal concentrations can be toxic to surface flora important to agriculture.

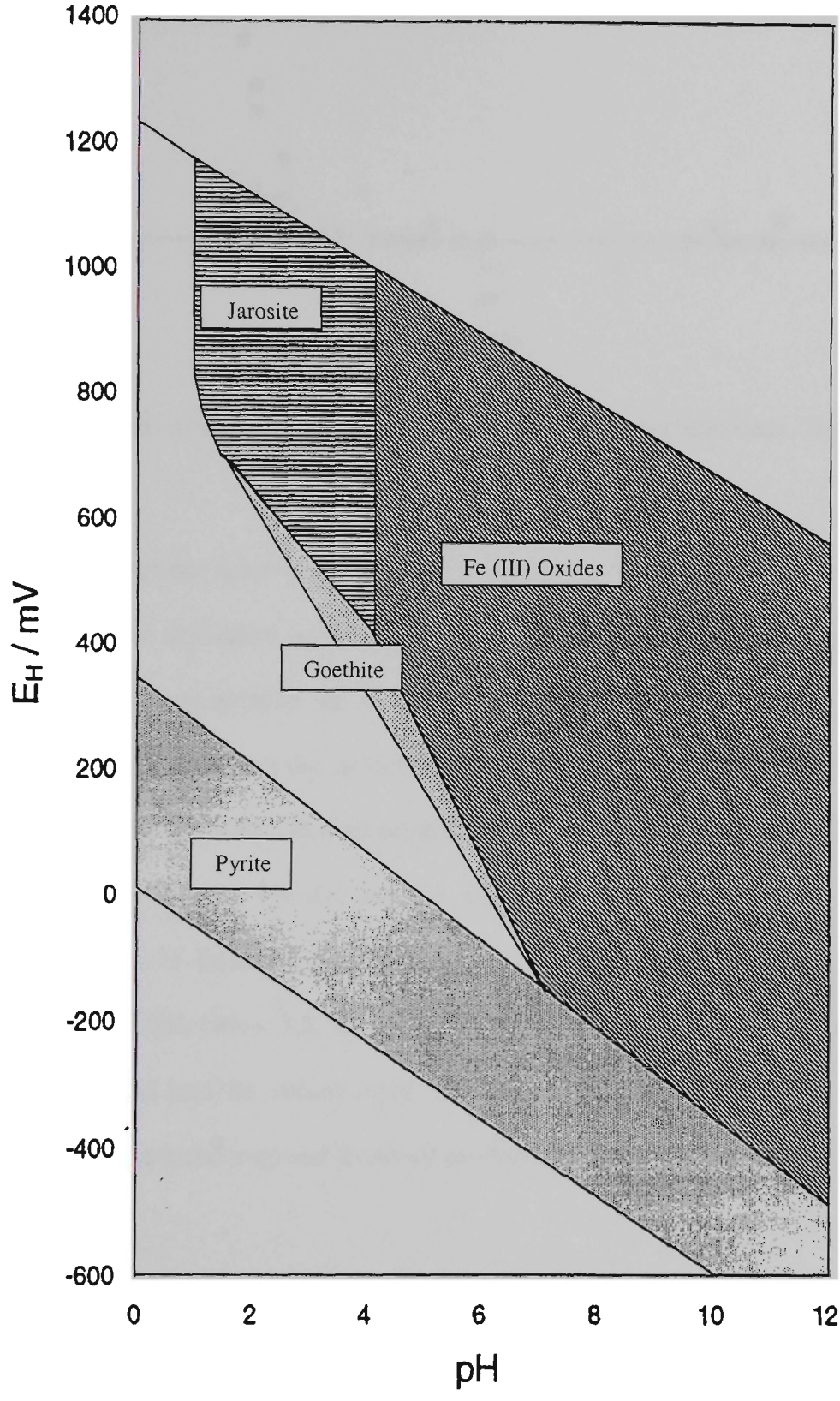

Figure 2.5 Diagram of major solid phases in acid sulphate soils (van Breeman, 1976).

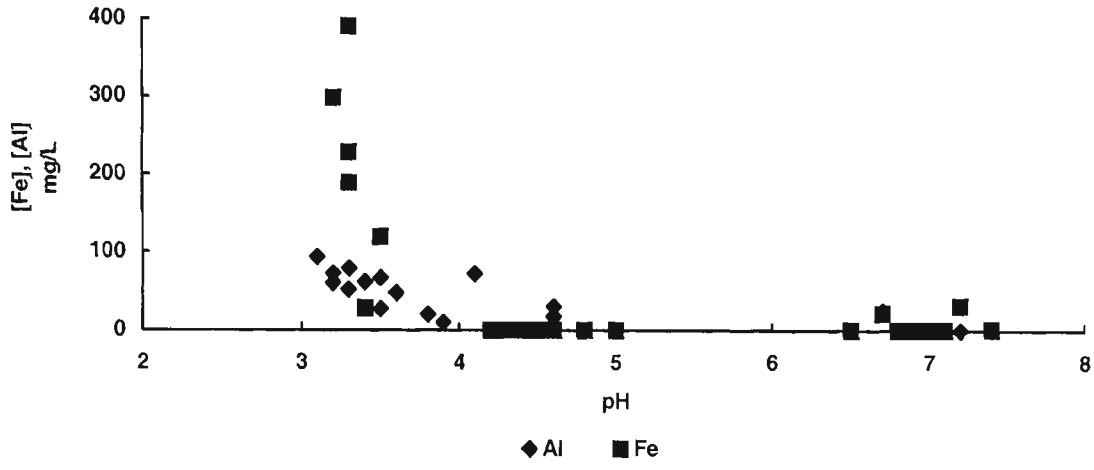

Figure 2.6 Relationship between pH and [Al3+], and [Fe3+] (Indraratna, Sullivan, and Nethery, 1995).

APHA (1985) defines heavy metals as ions with atomic weights over 65. The toxicity of these metals is dependent on the nature and concentration of the specific metal ions, the nature and concentration of suspended particular matter, pH, redox potential, temperature, competing cations, salinity, alkalinity, and other physio-chemical factors (Ferguson and Eyre, 1996). In acid sulphate soils, the most common heavy metals are Zn, Cd, Cu, Ni, Mn, Cr, Pb, Au, and Co, which may have substituted for Fe during pyrite formation in Equation 2.1 (Fanning *et al.*, 1988; van Breeman, 1993). As groundwater pH falls below 5.5, the solubility of most heavy metals increase and can be easily transported into the vadose layer. Elevated concentrations of heavy metals are associated with reduced crop and livestock productivity (Sammut, 1996).

While iron and aluminium's atomic weight are below that of traditional heavy metals, their abundance and impact on plant life are important to note. Many researchers (Indraratna *et al.*, 1999; Sammut *et al.*, 1996) have found that Al and Fe concentrations are logarithmically proportional to pH in acidic conditions (Figure 2.6). To ensure environmental protection, ANZECC (1992) guidelines permit 5 $\mu g\ L^{-1}$ of aluminium in

waters with pH levels below 5.5. In the southeastern coast of NSW, several researchers (Blunden, 2000; Ikin, 2001; Indraratna *et al.*, 2002) have found Al concentrations in excess of three orders of magnitude greater than recommended levels. High Al and Fe concentrations restrict plant growth and promote acid-tolerant species such as smartweed, thus reducing grazing areas for cattle (Sammut *et al.*, 1996).

In regions where the acid sulphate soil layer is exposed to the surface due to lack of alluvium coverage, or where overlying peat has been washed or burned away, large bare acid 'scalds' can exist. In these areas (reported up to 500 h^2), few plants survive and surface cracking enhances oxygen transport (Sammut *et al.*, 1996). Similarly, soil consolidation, through reduced surface elevation from subsidence, causes waterlogging and reduces plant growth and grazing area.

2.4.5 Influence of pyrite oxidation on the marine environment

Following pyrite oxidation and the development of acidic pore water, acid products are transported into surrounding surface waters with deleterious impacts. The input of acidic groundwater into pH neutral surface waters (eg. flood mitigation drains) dilutes acid concentrations but simultaneously increases the contamination zone. Although several researchers (Walker, 1972; Willet and Walker, 1982; Norwood, 1976) advised against disturbing acid sulphate soils, it was not until large-scale surface water acidification and fish kills occurred in the late 1980's that major combative research began in Australia (Indraratna *et al.*, 1999). While a great deal of work in this area has focused on marine life (Sammut *et al.*, 1996) and aquaculture (Simpson and Pedini, 1985), with the exception of White *et al.* (1997) limited research has been conducted on acid transport and flow in surface waters.

The leaching of acidic groundwater into surface drains impacts marine flora, fauna and engineering structures. As an environment becomes acidified (surface water pH < 4.0), acid tolerant flora species such as *Eleocharis* and *Nymphaea* dominate. In northern NSW, Sammut (1993) reported the exotic Cape waterlily (*Nymphaea caerulea*) growing profusely and saturating the water with dissolved oxygen causing 'gas bubble' disease in fish. The clarification of water by aluminium flocculation further acidifies the surface water and can lead to increased UVB infiltration, enhanced acid tolerant plant growth in deeper water, and increased temperature (Brierley, 1995).

The mixing of acidic drain water with pH neutral creek/river water increases acidity and causes additional environmental damage. High concentrations of soluble ferrous iron, inherent in acid sulphate soil oxidation, flocculate as iron oxyhydroxides and release H^+ ions. This process is commonly known as 'acid at a distance', because it occurs downstream of the oxidation source and creates a further two moles of acid. This reaction can be summarised as:

$$Fe^{2+} + \tfrac{1}{2}O_2 + \tfrac{3}{2}H_2O \longrightarrow \underbrace{FeOOH\downarrow}_{\text{red-brown floc}} + \underbrace{2H^+}_{\text{acid}} \qquad (2.15)$$

The flocculant, most commonly iron monosulphide, can further oxidise to produce H^+ ions if dredged or otherwise exposed to oxygen. During this reaction, oxygen is consumed and fish can asphyxiate from low dissolved oxygen levels. The flocculation process also smoothers the benthos layer leading to the destruction of fish eggs, loss of habitat, reduced recruitment, and decreased availability of nutrients (Sammut *et al*, 1996).

As clarified acid waters continue to discharge, mobile and sessile marine fauna are affected. Complex processes, such as increases in the pH of water passing over fish gills, affect aluminium and iron flocculation, and excessive flocculation can lead to clogged gills and suffocation. Similarly, Epizootic Ulcerative Syndrome, commonly known as red spot disease, is characteristic of acid drainage and occurs when the fungus *Aphenomyces* burrows beneath the skin to form subcutaneous ulcers in fish. Sammut (1993) suggests that aluminium rich, acid waters are responsible for lowering the immune system in fish and allowing them to be susceptible to the fungus.

In order to avoid acid water, mobile organisms often move to unaffected areas, which can become overcrowded and lead to physical stress. Sessile organisms, such as oysters and other bivalves, are robbed of shell building carbonate and may contain growth deformities. The impact of acid sulphate soils on marine fauna is of particular economic interest because 70% of all commercial fish species spend some portion of their life cycle in estuarine environments (Sammut *et al.*, 1996).

Engineering structures are also affected by acid sulphate soil leaching. Iron precipitates can clog pipes and drains, and weathering of acid sulphate soils can form a build-up of ettringite and gypsum, minerals that are associated with the breakdown of concrete structures (Holst and Westerveld, 1973). High concentrations of sulphuric acid corrode concrete and steel marine infrastructure, which is why costly sulphate resistant concrete is recommended in many coastal areas of Australia. Finally, due to their high volumetric moisture content, acid sulphate soils have a low bearing capacity and foundations often require extensive reinforcements to offset subsidence and localised failure (Dent, 1986).

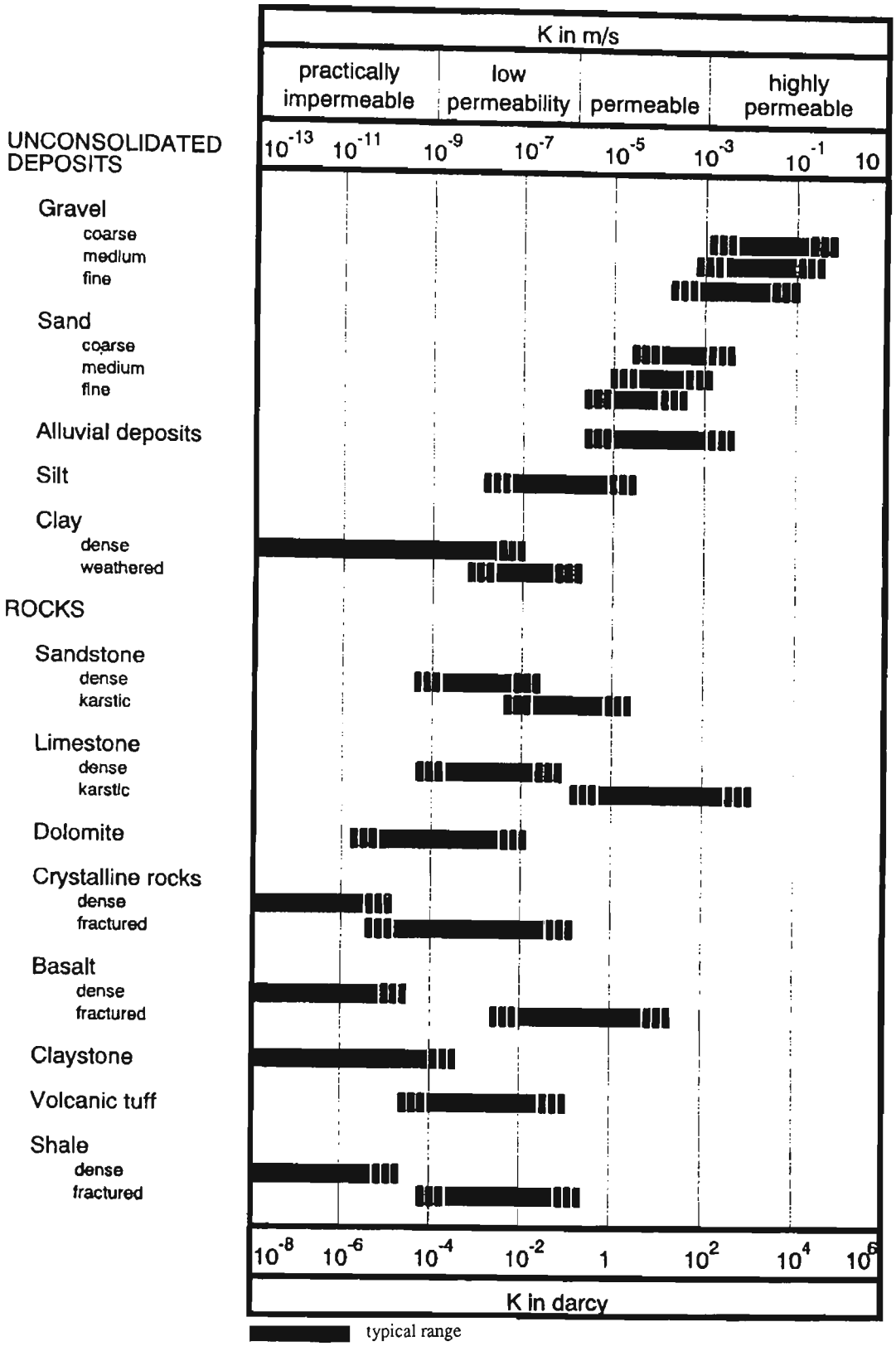

Figure 2.7 Range of hydraulic conductivity of geological formations (Spitz and Moreno, 1996). Note the difference between dense and weathered clays.

2.5 Aspects of hydrogeology and hydromechanics in acid sulphate soil affected floodplains

2.5.1 Subsurface water flow

The impact of acid sulphate soils in drainage waters is directly related to the quantity of groundwater discharged, and therefore, an understanding of groundwater hydrology and flow is vital in determining acid production and transport. In general, the movement of groundwater in the saturated phreatic zone is horizontal and primarily controlled by differences in hydraulic gradients, while flow in the unsaturated, vadose zone is predominately controlled by gravity and fluctuates in the vertical plain. The watertable surface, a mixture of water and air filled pores, separates the saturated and unsaturated zone and the main determinants of watertable elevation are rainfall, evapotranspiration, the presence of impermeable layers, boundary conditions (i.e. deep drains, tidal forcing, upland inflow, etc.), void geometry, soil porosity, and internal soil forces (Spitz and Moreno, 1999).

Darcy's Law is commonly used to depict the interrelationships between flux, pressure gradients, and hydraulic conductivity. Hydraulic conductivity, a function of soil porosity and an important component of Darcy's Law, is measured in velocity (m/s), and defined as the capacity of the porous media for transmitting water (Spitz *et al.*, 1996). A list of different hydraulic conductivities from a range of geological formations is presented in Figure 2.7. From this Figure, it is apparent that hydraulic conductivities of clay vary significantly depending on the degree of weathering. As hydraulic conductivity is proportional to the flow rate or velocity (flux) and the hydraulic gradient, a doubling of these variants will also double the flux and thereby, the extent of transport of acid products. Darcy's law is defined as:

$$q = -K\frac{\Delta h}{\Delta s} = -Ki \tag{2.16}$$

where, q = Darcy flux or specific discharge in [L/T], K = hydraulic conductivity in [L/T], Δh = head difference in [L], Δs = length of soil elements in [L], and i = hydraulic gradient in [l].

Darcy flux, q, is commonly referred to as Darcy velocity. Velocity, however, is defined as the rate of unit flow over unit cross sectional area perpendicular to the flow direction. Therefore, since in groundwater only pore water flows and not the entire soil matrix, Darcy velocity does not equal the velocity of water molecules. However, in acid sulphate soils research, the actual velocity of water in irregular pore spaces is of little interest, and the actual quantity of water discharged is the determinant factor. In situations where diffusion as well as advection is desired, such as in transport modelling of saline intrusion through tidal forcing (see Chapter 9), Fick's law (Equation 2.17) must be combined with Darcy's Law to form the advection-diffusion Equation 2.18 (Spitz and Moreno, 1996).

$$\underbrace{q_o}_{\text{diffusive flux}} = \underbrace{-D_o\frac{\partial c}{\partial x}}_{\text{concentration gradient}} \tag{2.17}$$

where, q_o = diffusive mass flux, D_o = diffusion coefficient in [L^2/T], c = concentration in [M/L^3], and x = direction of flow in [L].

$$\underbrace{\frac{\partial c}{\partial t}}_{\text{change in storage}} = \underbrace{-v\frac{\partial c}{\partial x}}_{\text{advective in/outflow}} + \underbrace{D_L\frac{\partial^2 c}{\partial x^2}}_{\text{diffusive and dispersive flux}} \qquad (2.18)$$

where, t = time in [T], and v = advective transport velocity in [L/T]

When determining the discharge of acid sulphate soils from groundwater flow through advection, Darcy's Law is only sufficient when the entire flow system is known. To determine groundwater flow in transient situations where only initial head distributions are known, the general flow equation described by Bear *et al.* (1999) is more appropriate. This equation is formulated by applying the law of conservation of mass over a control volume of groundwater in the flow field. The net inflow volume must equal the rate at which the groundwater volume accumulates and is described as (Bear *et al.*, 1999):

$$\frac{\partial}{\partial x_i}\left(K_{ij}\frac{\partial h}{\partial x_j}\right) = S_s\frac{\partial h}{\partial t} + Q \qquad (2.19)$$

In the above equation, S_s represents the specific storage coefficient or the amount of water volume released or gained in storage per unit change in head. A decrease in head corresponds to a discharge of water volume, but storage coefficients are typically small and range in the order of 10^{-4}. The term Q represents local sources and sinks per volume in [*1*/T] and can be a function of evaporation, rainfall, or water infiltrating to/from a river.

During the initialisation of numeric models, such as those depicted in Chapter 9, boundary conditions represent the inflow and environmental conditions and are an

important function to solve the general flow equation. Transient boundary conditions such as 'variable flux', which can be used to simulate tidal boundaries, will have significantly altered hydrological impacts in comparison to 'constant head' simulations used in the simulation of dammed, or weir boundary conditions (Indraratna and Blunden, 1999).

2.5.2 Floodplain watertable dynamics

The extent and magnitude of acid drainage is relative to the water balance of the floodplain and the characteristics of the drainage system. In this manner, floodplain hydrology determines the rate of oxidation via soil drainage, the permeability to air, and the soil temperature (Blunden, 2000). White *et al.* (1997) suggests that in coastal eastern Australia the key determinants of floodplain hydrology can be described as:

$$P + I + L_i = E_t + R + L_o + D + \Delta S \qquad (2.20)$$

Inputs Outputs Storage

where, on the input side, P is precipitation that falls on the floodplain, I is irrigation, and L_i is lateral inflow predominately from upland areas. In coastal Australia, irrigation is not generally applied, and can be considered a minor constituent. On the output/storage side, E_t is evapotranspiration, R is surface runoff, L_o is lateral outflow, D is vertical drainage to the shallow groundwater, and ΔS is the change in surface and soil water storage above the watertable (all units measured in volume per unit floodplain surface area, usually in mm of water).

When managing acid sulphate soils it is important to consider the depth of the sulphidic layer from the surface, the dynamics of the watertable relative to that layer, the influence of climate, drain and land management on the floodplain water balance, and its control of watertable dynamics and the export of oxidation products (White *et al.*, 1997). The impact of watertable dynamics on the management of acid sulphate soils can generally be described using Equation 2.20. Acid sulphate soils primarily occur where P and E_t are the dominant factors and $P > E_t$. In undrained areas, R and L_o result in a build-up of waters in backswamp and low-lying areas, and surface flooding can persist for prolonged periods. Under these conditions, consistent rainfall maintains an elevated watertable where minimal pyrite oxidation can occur. In dry summer periods when evapotranspiration rates increase (especially in tropic and sub-tropic regions with distinct seasonality), production and export of acidity depends on temporal variability and its impact on the change in soil water storage above the pyritic layer, ΔS.

The fluctuations in groundwater height determine the quantity and duration of acid generated. White *et al.* (1997) states that the change in watertable height, ΔH, at a given time, is a function of the vertical drainage, D, lateral groundwater inflows, L_{gi}, or outflows, L_{go}, direct evaporation from the water table, E_g, and the available porosity of the soil expressed as specific yield, Y_g (volume of groundwater per unit area per unit change in water table height). Therefore, the variations of a shallow groundwater table in the vertical direction can be described as:

$$Y_g \cdot \Delta H = D + L_{gi} - (E_g + L_{go}) \qquad (2.21)$$

Storage Inputs Outputs

The groundwater recharge rate, $E_g < E_t$ and $D - E_g$, is determined from comparing Equations 2.20 and 2.21.

2.5.3 Impact of prolonged wet and dry periods on floodplain hydrology

White *et al.* (1997) and Indraratna *et al.* (2002) suggest that markedly different drainage conditions, and thus chemical conditions, exist between wet and dry periods. In unconsolidated estuarine mud, the maximum change in soil water storage above a shallow water table is generally small (~ 50 cm), therefore during wet periods, the long-term flux of soil water storage is considerably less in comparison to rainfall, upland inflow and evapotranspiration. White *et al.* (1997) states that upland inflow depends on the area of the upland catchment A_u, upland rainfall P_u, and the fraction of rainfall r_u, which becomes inflow to the total floodplain area A_f so that:

$$L_i = \frac{r_u P_u A_u}{A_f} \tag{2.22}$$

During prolonged wet periods: $P_u \approx P$, $r_u \approx 1$, and the watertable is at or above the surface. Under these conditions, D is negligible and the main water storage is from ponded water on the surface, (ΔS_p). Therefore, the water balance for the floodplain under wet conditions can be described by:

$$P\frac{A_f + A_u}{A_f} \approx E_t + L_O + \Delta S_p \tag{2.23}$$

Although in eastern Australia most river catchments are relatively small (A_f/A_u of order 10), Equation 2.23 shows that upstream inflows can have a strong influence on the floodplain water balance during wet periods.

Historically, excess upstream inflows are retained within low-lying areas for prolonged periods, while overbank flow fills up depressions and backswamp areas during wet periods. Natural meandering channels, with low hydraulic gradients and a high roughness coefficient, further impede drainage, but once floodwaters have passed and the water level in the backswamp falls below the minimum elevation of the natural levees and drains, any remaining water is lost via evapotranspiration. White *et al.* (1997) suggests that since surface water levels are typically around 0.5 m, and average evapotranspiration is generally 5 mm day^{-1}, surface storage will persist for about 100 days.

The occurrence of low permeability, potential acid sulphate soils, underlying high permeability actual acid sulphate soils often increases groundwater drainage. In these circumstances, ponded surface water is quickly transmitted through the vadose layer through macropores and old root channels. The potential layer restricts further vertical drainage and acts as an impermeable base. The accumulated pore water then becomes acidified and transported laterally into adjacent drainage lines. In flooding conditions, the watertable rises above the soil surface and significant runoff can occur, while during dry periods when D, and L_{gi} are zero, the watertable falls quickly and oxygen is easily entrained into sulphidic sediments. White *et al.* (1997) terms this up and down water movement created by a permeable stratum on top of an impermeable layer the "leaky bucket" effect.

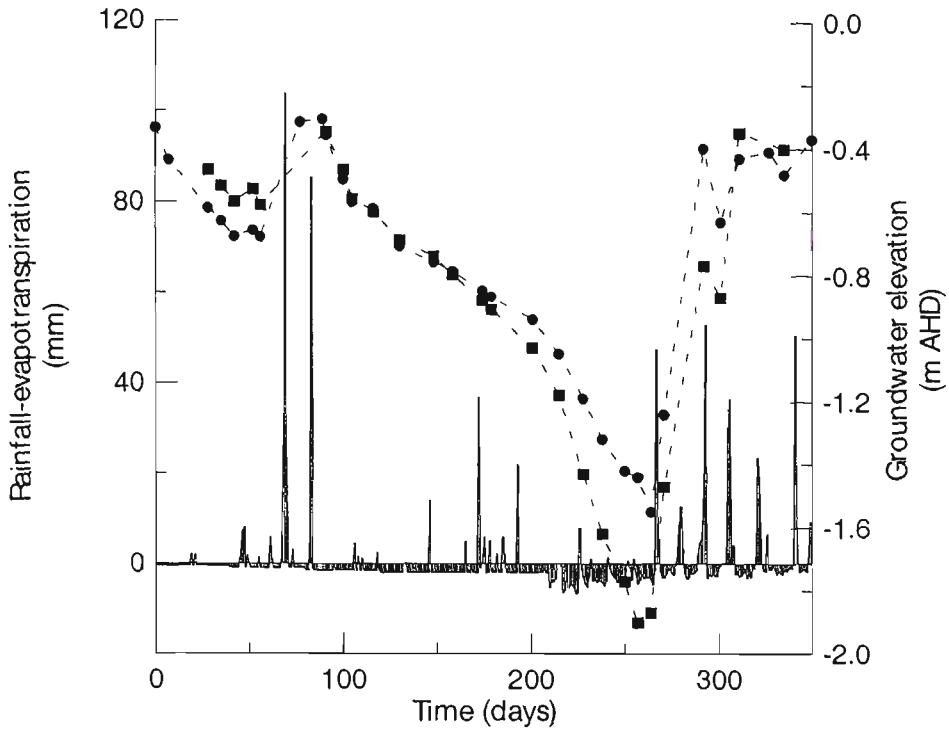

Figure 2.8 Groundwater elevations in response to rainfall and evapotranspiration at 10 m (•) and 90 m (■) perpendicular to a flood mitigation drain (Blunden, 2000).

During prolonged dry periods when inflow, drainage, and outflow are negligible, the watertable is solely determined by evaporation. This is best described as (White *et al.* 1997):

$$Y_g \cdot \Delta H = -E_g \qquad (2.24)$$

In an extensive groundwater study, Indraratna *et al.* (2001) showed the influence of evapotranspiration on reducing watertable height during a prolonged drought (Figure 2.8). Other researchers such as White and Melville (1993), and Wilson (1995) have illustrated similar results from vigorous deep rooting crops or where soil cracking is evident. Along the south coast of NSW, where less vigorous crops are used and the climate is temperate, Pease (1995) and Blunden (2000) showed that though strong evapotranspiration lowered the watertable, adjacent drainage lines recharged the

groundwater table. White *et al.* (1997) suggests that deeper drains in southeastern NSW (~3 m) increase the seepage gradient, which may explain the difference between findings in northern NSW where drains are typically shallow (~0.4 m deep). Furthermore, large variances in lateral soil hydraulic conductivity have been reported between acid sulphate soil sediments throughout Australia, possibly due to different management regimes and climatic factors.

2.5.4 Artificial drainage

Throughout the world, and particularly in coastal eastern Australia, artificial floodplain drainage has been undertaken to utilise a perceived agriculture benefit from fertile alluvium soils. In most cases, large drainage systems were constructed to protect coastal areas and encourage agriculture before any knowledge of acid sulphate soils existed. The deep drains with one-way tidal restricting floodgates lower the watertable (often below the sulphidic layer), and enhance pyrite oxidation. Swales (1982) stated, "It is well known drainage systems designed to alleviate flooding or improve agriculture drainage, generally have a detrimental impact on the environment".

Historically, flood mitigation works have been undertaken in coastal areas of Australia since the early 1900s. In response to large floods in the 1940s and 1950s, substantial funding was allocated for major drainage development (Middleton *et al.*, 1996). During this period, federal and state funding increased from a cumulative total of nearly $2 million up until 1960, to more than $80 million by 1980 (Pressey and Middleton, 1982). Additional funding, given by development authorities and local councils, totalled ~$20 million, which meant that within twenty years $100 million was spent on construction of levee banks, drainage channels, floodgates, bank stabilization, clearing works, and

the alignment of river channels (Pollard and Hannan, 1994). The main aim of these works was to guide overbank flow, prevent flood inundation, and to reduce the inundation by floodwaters (State Pollution Control Commission, 1978). Interestingly, the same SPCC (1978) inquiry found that the primary result of flood mitigation was to drain natural coastal wetlands outside of flood periods, which provided landowners with access to large tracts of land previously unsuitable for agriculture. Indeed, in 1976 the New South Wales State Fisheries stated, "In many cases these works appear more related to irrigation, drainage and water conservation needs than to flood mitigation."

Despite the fact that during dry periods most agriculture crops utilise shallow groundwater tables, flood mitigation drains were designed to significantly lower the watertable. Natural meandering channels were straightened, cleared and deepened. Adjoining secondary drains were constructed haphazardly and often without proper design. Tidal restricting floodgates were installed at the drainage point of each canal to maintain a low water level (about 0 m AHD) and restrict flooding from the creek/river. Figure 2.9 represents a typical flood mitigation system.

The presence of large flood mitigation works had a direct impact on groundwater levels and acid production. In particular, the mitigation works altered drainage characteristics, including recharge and discharge rates and the watertable elevation. Several methods for determining watertable elevation, and hence, the impact of drainage in altered landscapes are available. Bouwer (1974) gives the height of the watertable above the drains, H_m, at the midpoint between two parallel drains of spacing, S, for an average recharge rate of $D - E_d$ as:

$$\frac{D - E_d}{4K_s} \approx \frac{2H_m d + H_m^2}{S^2} \approx \frac{L_d}{4K_s} \qquad (2.24)$$

In the above equation, K_s is the saturated hydraulic conductivity of the top soil, L_d is the discharge rate (rate of volume outflow per unit area of drain discharge surface) and d is the effective depth from the water surface in the drains to an impermeable layer below the base of a drain. Efficient drain spacing can be obtained by dividing the floodplain area, A_f, by the total length of drains, $\sum_w$.

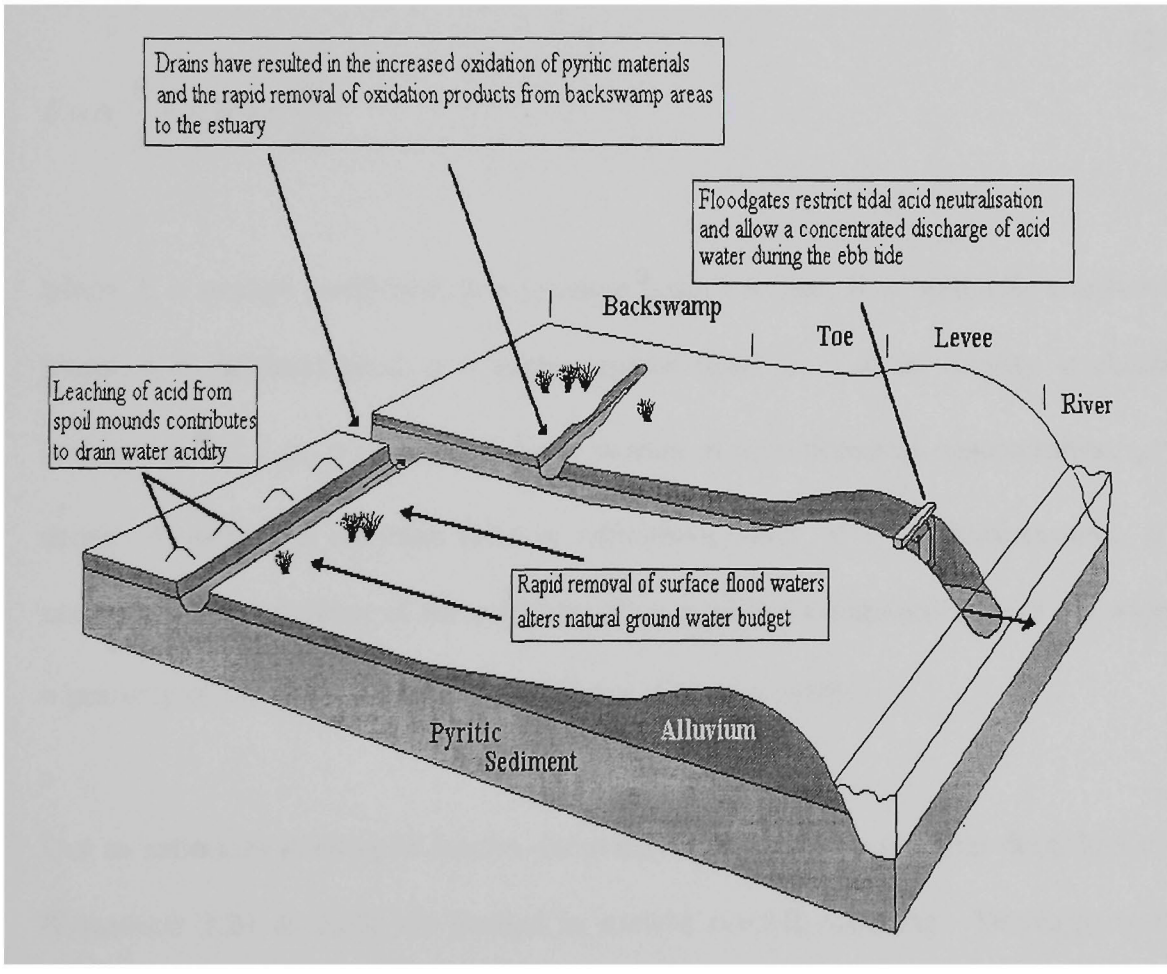

Figure 2.9 Typical flood mitigation scheme of an acid sulphate soil affected floodplain (Naylor *et al.*, 1993).

In a recent study, Blunden and Indraratna (2001) used a steady state three-dimensional finite element model, FEMWATER, to determine the height of the water table with varying drain water elevations in relation to an acid sulphate soil layer. By calibrating the model with field conditions and assuming the flux into and out of the model was zero ($d\theta/dt = 0$), the authors were able to determine the optimum drain water elevations required to minimise acid sulphate soil oxidation and transport. The governing flow equation used in FEMWATER is described as:

$$\frac{\rho}{\rho_o} F \frac{\partial h}{\partial t} = \nabla \cdot \left[K \cdot \left(\nabla h + \frac{\rho}{\rho_o} \nabla z \right) \right] + \frac{\rho^*}{\rho_o} q$$

$$F = \alpha' \frac{\theta}{n} + \beta' \theta + n \frac{dS}{dh} \qquad (2.25)$$

where, F = storage coefficient, h = pressure head, t = time, K = hydraulic conductivity tensor, z = potential head, q = source and/or sink, ρ = water density at chemical concentration C, ρ_o = referenced water density at zero chemical concentration, ρ^* = density of either the injection fluid or withdrawn water, θ = moisture content, α' = modified compressibility of the medium, β' = modified compressibility of the water, n = porosity of the medium, and S = saturation (Lin *et al.*, 1997).

Due to variations in climatic factors, the steady state analysis equations described above (Equations 2.24 & 2.25) are limited in eastern coastal Australia. Drainage systems based on these equations would not discharge enough water during the wet season (more pronounced in the tropic and subtropical zones), and would remove excessive amounts in the dry season. These drainage induced watertable variations lead to severe

oxidation of acid sulphate soils during dry periods and transport of oxidation products following rainfall. To this point, Sammut *et al.* (1996), Wilson (1995), and Pease (1995) have found that deep drainage of sulphidic sediment has led to acid production rates between 100 – 500 kg/ha/yr.

To manage the amount of acid water discharged from a poorly designed flood mitigation system, it is vital to understand the surface water drainage regime. As stated earlier (Equation 2.23), the major source of water during wet periods in coastal floodplains is from upland inflows. The quantity of water, Q (m/s), discharged from a drainage system can be determined from Manning's equation (Raadsma, 1974):

$$Q = \frac{A_w}{n} \cdot \frac{(A_w)^{2/3}}{(P_w)^{2/3}} G^{0.5} \qquad (2.26)$$

In the above equation, A_w is the wetted area of the channel (m), P_w is the wetted channel perimeter (m), and G is the hydraulic gradient [height of water (m)/length of channel (m)]. The Mannings roughness coefficient, n, varies from 0.02 in natural channels to 0.1 in smooth channels. Prior to flood mitigation works, natural meandering channels had low hydraulic gradients that were intensified by the accumulation of debris, plant growth, and tidal flows. Additional upland inflows could not discharge from the system and flooding of the backswamp areas was common.

The straightening, deepening, and clearing of channels, as well as the installation of tidal restricting floodgates, dramatically alters its roughness coefficient and hydraulic gradient. White *et al.* (1997) estimates that these drainage modifications can increase

discharge by at least two orders of magnitude and therefore, prior flooding that may have resided for up to 100 days is now drained within 5 days. This increase in discharge can have a significant impact on watertable dynamics and lead to a build up of acidic water behind tidal restricting floodgates.

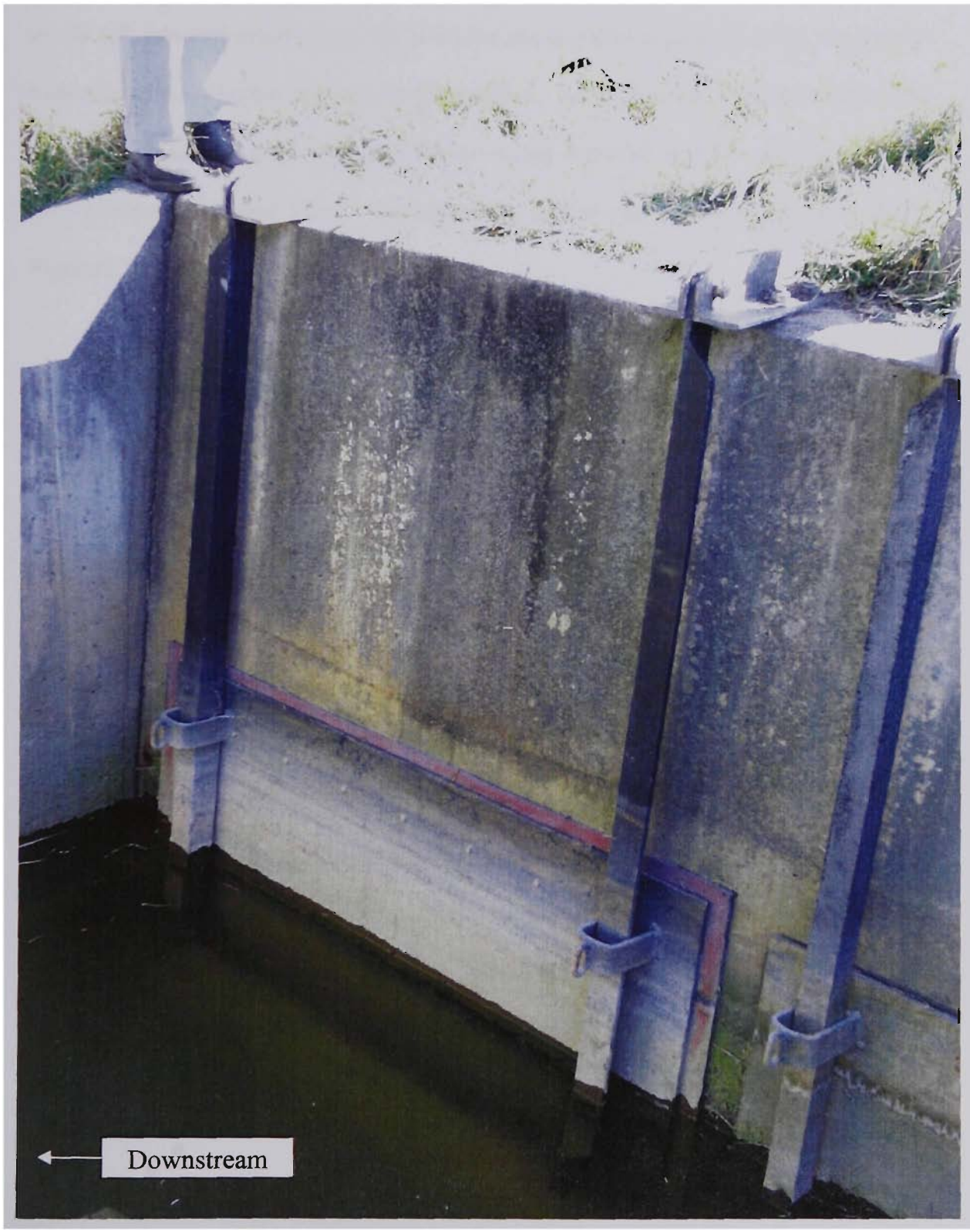

Figure 2.10 Typical top-hinged, one-way, tidal restricting floodgate installed on a flood mitigation drain in southeastern N.S.W.

2.5.5 One-way floodgates and acid drainage

Throughout New South Wales, Williams and Watford (1997) identified 1,035 tidal restricting floodgates. Initially designed to permit tidal flooding, one-way floodgates also maintain upstream water elevations at the low tide level. Top-hinged, one-way floodgates allow water to discharge under hydrostatic pressure, which normally occurs on the ebb tide and persists until the tide changes or following floods when the channel water elevation is higher than discharging waters. As well as draining backswamp and low-lying areas, one-way floodgates restrict saline intrusion and can provide livestock with a store of drinking water. A picture of a typical one-way floodgate is shown in Figure 2.10.

In areas affected by acid sulphate soils, one-way floodgates increase pyrite oxidation, create acid reservoirs that damage the marine environment, and restrict beneficial tidal buffering. As stated previously, floodgate sill levels are generally set to maintain upstream water levels at the low tide mark. Since the pyritic layer is normally at the mid to high tide level, by maintaining drain water elevations 1-2 m below the pyritic layer, one-way floodgates increase the hydraulic gradient between the drain water and groundwater. The difference in hydraulic gradients, shown in Figure 2.11, promotes the transport of oxygen into sulphidic subsoil material and the leaching of acid products into the drain. This is particularly evident following large rainfalls when floodgates quickly establish low drain water levels and the groundwater table is elevated (Glamore *et al.*, 2000). The flushing of acidic groundwater following large rainfalls (>50 mm/day) has been linked to fish kills and decreased pH levels (Sammut *et al.*, 1995).

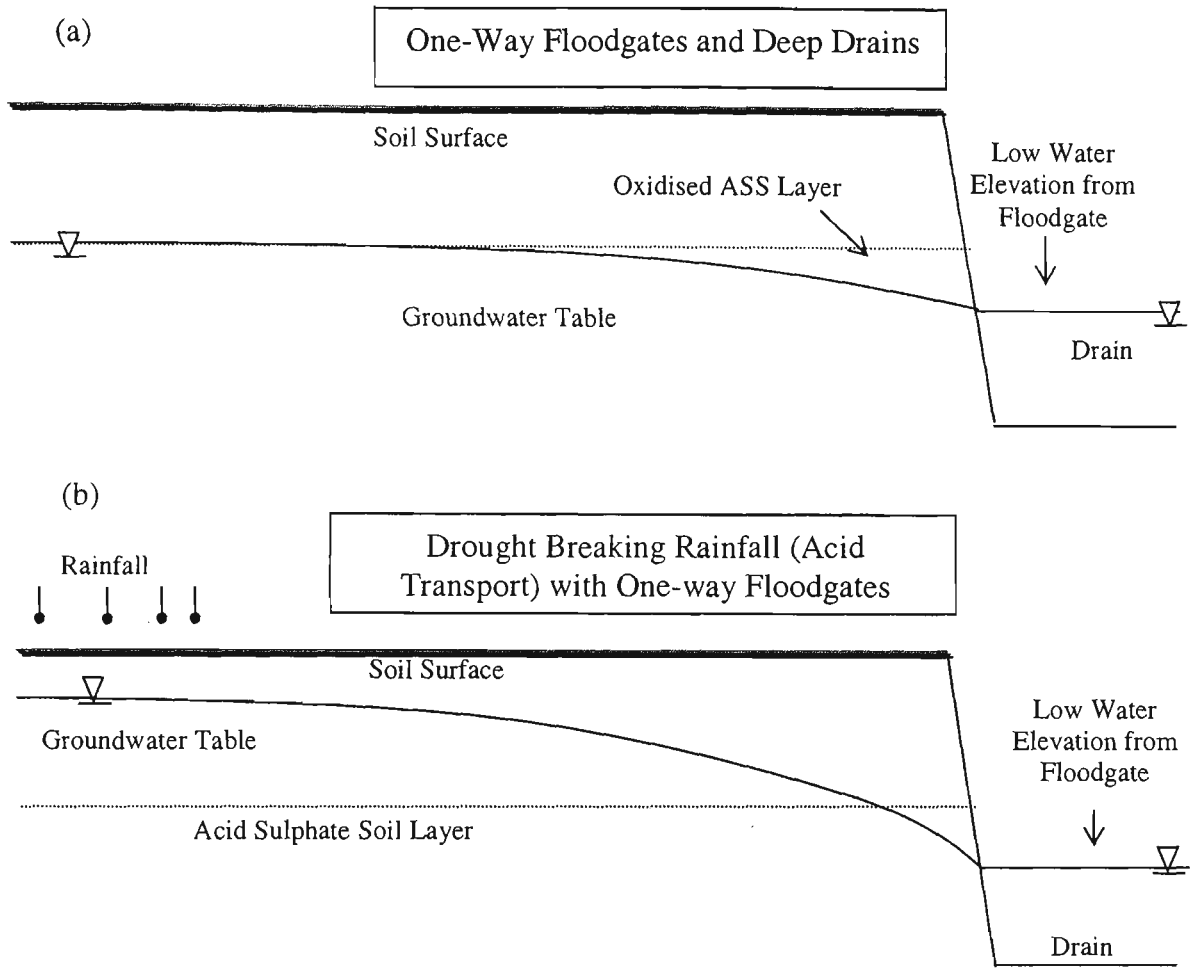

Figure 2.11 Influence of one-way floodgates on groundwater elevation under (a) normal and (b) flood conditions (adapted from Indraratna *et al.*, 2002).

Though not directly responsible for poor water quality, one-way floodgates aggravate environmental problems associated with acid sulphate soils. By restricting tidal flushing, one-way floodgates create an acid reservoir that is released either as a slug in subsequent flood events or as a consistent trickle with each ebb tide (White *et al*, 1997). This encourages aluminium flocculation and the acid generating 'acid at a distance' phenomenon. An acid reservoir also favours growth of acid tolerant flora and fauna species, which, if consumed, can be harmful to livestock. Similarly, one-way floodgates restrict turbulence so that the stagnant water is generally low in dissolved oxygen (< 5 ppm) and redox potential. For aquatic life, the constant closure of the flap

gate restricts passage into traditional, often vital breeding grounds. Furthermore, by eliminating saline intrusion one-way gates deny the beneficial process of carbonate/bicarbonate buffering (Glamore *et al.*, 2001).

2.5.6 Tidal buffering

Carbonate/bicarbonate buffering, herein referred to as tidal buffering, is based on the concept that incoming tides transport acid buffering agents throughout an estuary. The major buffering constituents of seawater are bicarbonate (HCO_3^-) and carbonate (CO_3^{2-}). As described by Indraratna, Glamore and Tularam (2002) the concentration of these buffering agents at any one point is dependent upon the stage of estuary development and the estuary hydrodynamics (eg. tidal height, wet vs. dry periods, salinity regime, etc.). In turn, the presence of bicarbonate or carbonate concentrations, or the alkalinity of the water (mg L^{-1} of HCO_3^-), varies with pH (Figure 2.12). Due to large freshwater inputs and a lack of strong alkaline minerals, estuarine pH is generally below 10.25 and, therefore, in most estuarine systems bicarbonates are the predominate buffering agent.

The key factor in tidal buffering is the consumption of H^+ ions and the production of weak carbonic acid. For every mole of available bicarbonate, one mole of H^+ ions is consumed. Equation 2.27 shows the buffering reaction of sulphuric acid ($pK_a = -3$) with bicarbonate to form carbonic acid ($pK_a = 3.8$) (Stumm and Morgan, 1996).

$$Ca^{2+} + \underbrace{HCO_3^-}_{\text{Saline water}} + \underbrace{H^+ + SO_4^{2-}}_{\text{ASS oxidation}} \rightarrow \underbrace{H_2CO_3}_{\text{Weak Carbonic Acid}} + Ca^{2+} + SO_4^{2-} \qquad (2.27)$$

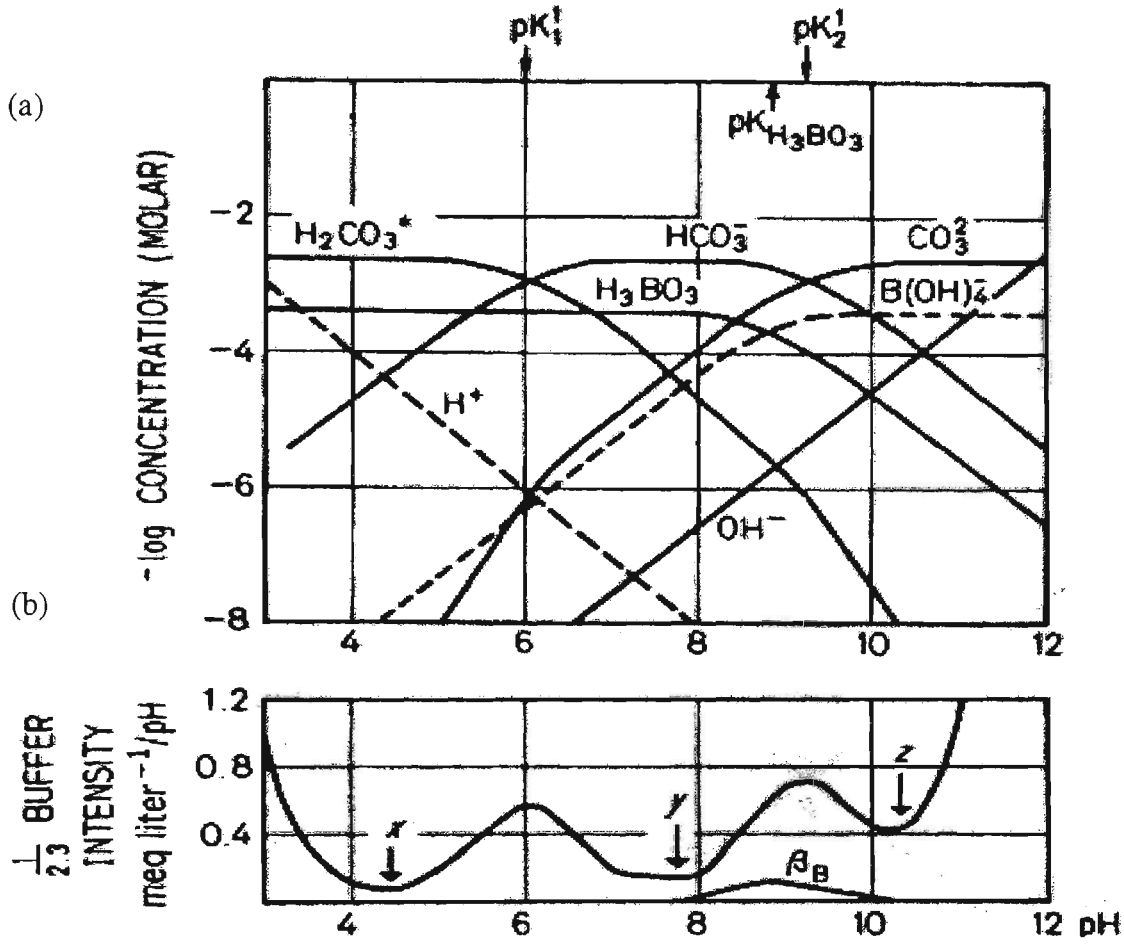

Figure 2.12 (a) Logarithmic equilibrium diagram for seawater and (b) the Buffer intensity of seawater.

In acidic water, sulphuric acid is highly ionised and sulphate and hydrogen ions exist freely in solution. Conversely, bicarbonate and carbonate anions have a larger affinity for the hydrogen ions due to the low ionisation capacity of carbonic acid. As shown in Equation 2.28 (a-c), the carbonic acid reaction proceeds towards the left, while the sulphate reaction largely proceeds towards the right. The removal of $[H^+]$ from solution by the formation of H_2CO_3 raises pH as depicted below (Indraratna *et al.*, 2002).

Strongly acidic, highly ionised:

$$H_2SO_4 \rightarrow 2H^+ + SO_4^{2-} \qquad (2.28a)$$

Weak acid, less ionised:

$$H_2CO_3 \leftarrow HCO_3^- + H^+ \quad (2.28b)$$

$$H_2CO_3 \leftarrow CO_3^- + 2H^+ \quad (2.28c)$$

By attaining the acid neutralising capacity of alkaline water, it is possible to determine the resultant pH when mixing occurs. For example, if brackish water with an alkalinity of 6.25×10^{-4} moles per litre (1/4 of seawater) is mixed in equal proportions with acidic water (say with a pH of 4.0), then the resulting pH will be 6.89 (Indraratna *et al.*, 2002). Although complete mixing may not be possible in the field, researchers in southeastern NSW (Glamore *et al.*, 2001; Blunden, 2000) have recorded alkalinity concentrations above 1.12×10^{-3} moles L^{-1}.

Many researchers (Blunden, 2000; Pease, 1995, Sammut *et al.*, 1995; Portnoy and Giblin, 1997; Dick and Osunkoya, 2000; Pollard and Hannan, 1994; Williams and Watford, 1997) have reported substantial improvements in water quality when leakage in one-way floodgates permits tidal buffering within acid affected flood mitigation drains. It has been suggested that allowing tidal flushing into flood mitigation drains via modified floodgates may: (i) decrease the 'acid reservoir effect', (ii) raise dissolved oxygen levels, (iii) decrease the hydraulic gradient between the drain and groundwater, (iv) diminish aluminium flocculation, (v) eliminate 'acid at a distance', (vi) combat exotic freshwater weeds, (vii) enhance runoff during wet periods and (viii) allow fish passage into important breeding grounds (Glamore *et al.*, 2001, Indraratna *et al.*, 2002). Based on this rationale, but without substantial scientific evidence, local councils and landholders are actively encouraging floodgate manipulations in many areas of coastal Australia. This thesis investigates the influence of tidal restoration, via modified floodgates, and the role of tidal buffering on controlling acid sulphate soil discharges.

2.6 Critical review of on-ground research and management strategies.

To date, the majority of field research to combat acid sulphate soils in Australia has focused on the manipulation of groundwater levels and the influence of acid drainage on marine ecosystems. The hypothesis for this research is that the intrusion of oxygen into the soil matrix is the key determinant of pyrite oxidation and subsequent acid production. Therefore, by limiting oxygen infiltration, via an elevated watertable, acid production can be controlled. As the impact of acid drainage on marine ecosystems is a function of the amount of acid generated, this review will concentrate on methods directly pertaining to controlling acid production and transport. While this critical review examines research throughout Australia, the primary focus is on research conducted along the south coast of New South Wales near the writer's study area. This is relevant as the majority of other research was conducted in tropical to subtropical regions with markedly different climatic factors, as well as different drainage regimes, agricultural uses (mainly sugar cane versus mainly dairy farms), and soil properties.

2.6.1 Background research

In 1972, Walker was the first in Australia to warn against the potential hazards of acid sulphate soils. Through radiocarbon dating, Walker found acid sulphate soils in the Macleay Valley dated back 3295 ± 95 years before present (YBP). Walker also categorised the presence of acid sulphate soils based on geomorphic formations (Figure 2.13) and suggested that as the alluvium layer decreased in elevation towards the backswamp region, both the acidity and salinity of the acid sulphate soil layer increased. Furthermore, Walker stated that soil pH and salinity were controlled by watertable fluctuations in the 'jarositic' layer, yet he only found a correlation between groundwater salinity and watertable fluctuations. Walker cautioned that unless elevated groundwater

levels were maintained and drainage works restricted, groundwater acidity would dramatically increase.

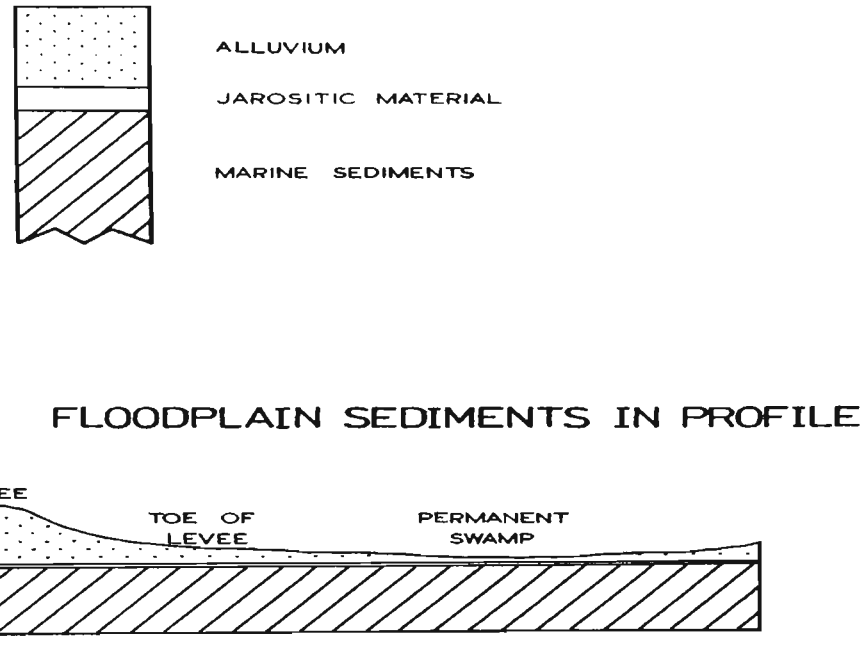

Figure 2.13 Geomorphic conditions and typical acid sulphate soil profiles (Walker, 1972).

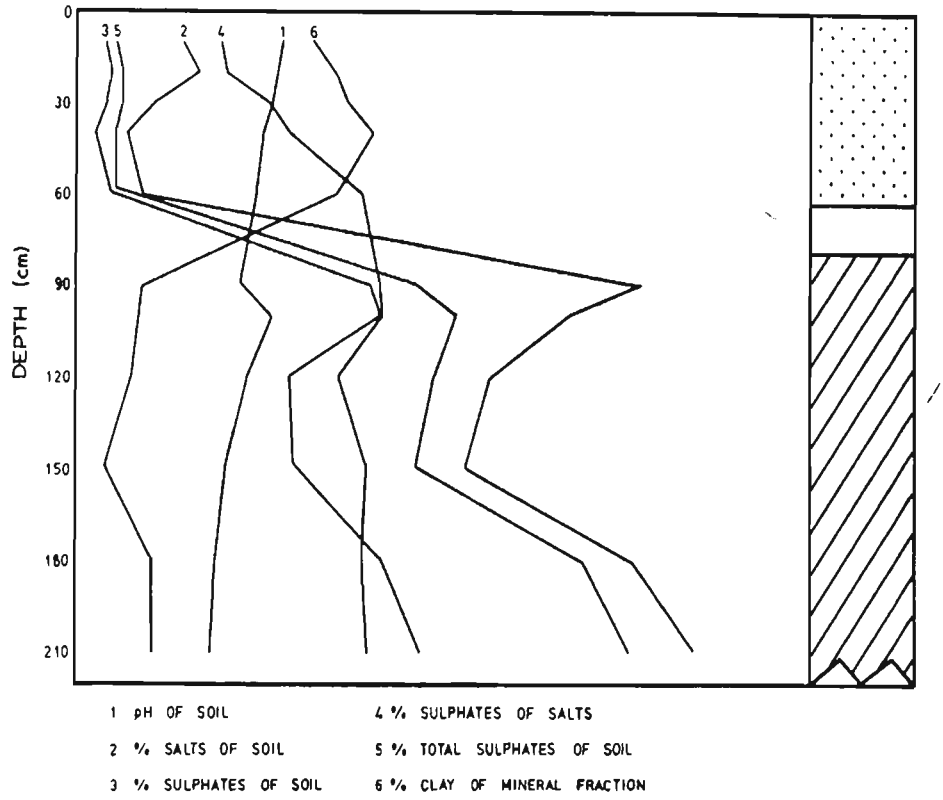

Figure 2.14 Mean soil property values of acid sulphate soils sampled by Norwood (1975).

Following this research and a preliminary study by the N.S.W. Department of Agriculture (1972), which stated that acid sulphate soils were prevalent in the Shoalhaven region, Norwood (1975) undertook preliminary steps in determining the distribution, location, and severity of acid sulphate soil in southern NSW. Using 40 sampling sites both north and south of the Shoalhaven River, Norwood found acidic conditions (pH<3.5) and the presence of jarositic mottles throughout the alluvial plains. Importantly, north of the Shoalhaven River, Norwood found consistent increases in soil acidity, salinity, and percentage of sulphates towards the backswamp region. By comparing the mean soil property values from 4 samples, Norwood showed that with increasing depth, soil pH and percent clay mineral fractions decreased, while precent salts and percent total sulphates increased (Figure 2.14). In contrast with Walker (1972), Norwood found a positive correlation between increased soil acidity and salinity with receding groundwater elevations.

2.6.2 Developmental research

Although the research conducted by Norwood (1975) and Walker (1972) stimulated concern for acid sulphate soils, no additional on-ground research was conducted in southeastern NSW till Pease (1994) examined the impact of flood mitigation drains on acid production and transport in the Shoalhaven region. Over this 20-year period, significant expansion and modifications of the flood mitigation system was conducted within the floodplain (Figures 2.15 and 2.16). These civil works lowered the groundwater table, decreased surface ponding and water retention, and increased the frequency of pyritic oxidation (Pease, 1997).

Figure 2.15 Aerial photo of Broughton Creek floodplain before large-scale flood mitigation works with natural flow paths highlighted (N.S.W. Dept of Lands, 1961).

Figure 2.16 Aerial photo of Broughton Creek floodplain after large-scale flood mitigation works (Courteous of Shoalhaven City Council, 1991). Note the extensive drainage network highlighted within the selected regions.

Pease's (1994) work focused on one flood mitigation drain along Broughton Creek, a north-bank tributary of the Shoalhaven River. The majority of this research was concerned with water quality changes associated with watertable fluctuations over an eight-month period. Pease compared boreholes in drained areas versus undrained areas in response to climatic factors, and found that drained regions had a faster response to rainfall/evapotranspiration and were more efficient at maintaining a hydraulic gradient towards the drain. Importantly, Pease (1994) postulated that drain water heights controlled groundwater elevations for at least 400 m, with evapotranspiration dominating as the distance increased.

Using a borehole typical of the region (Table 2.3), Pease (1994) showed that groundwater fluctuations in response to rainfall were followed by direct changes in pore water pH. The relationship between rainfall, groundwater elevation, and water chemistry for a borehole located 50 m perpendicular of a test drain can be seen in Figure 2.17 and 2.18, respectively. In Figure 2.17, the groundwater chloride/sulphate ratio shows a strongly oxidising environment with sulphate, aluminium and iron concentrations increasing as the watertable declined. In the drain (Figure 2.18), water elevations did not fluctuate widely due to tidal restricting floodgates installed at the drainage junction. Pease (1994) suggested that the low soluble iron concentrations in the drain were due to iron flocculating as iron hydroxides, and that high aluminium and sulphate concentrations were evidence of groundwater transport. Pease's work suggested that water-retaining structures, such as weirs, could be installed in the flood mitigation drains to maintain an elevated watertable and control acid production and transport.

(A)

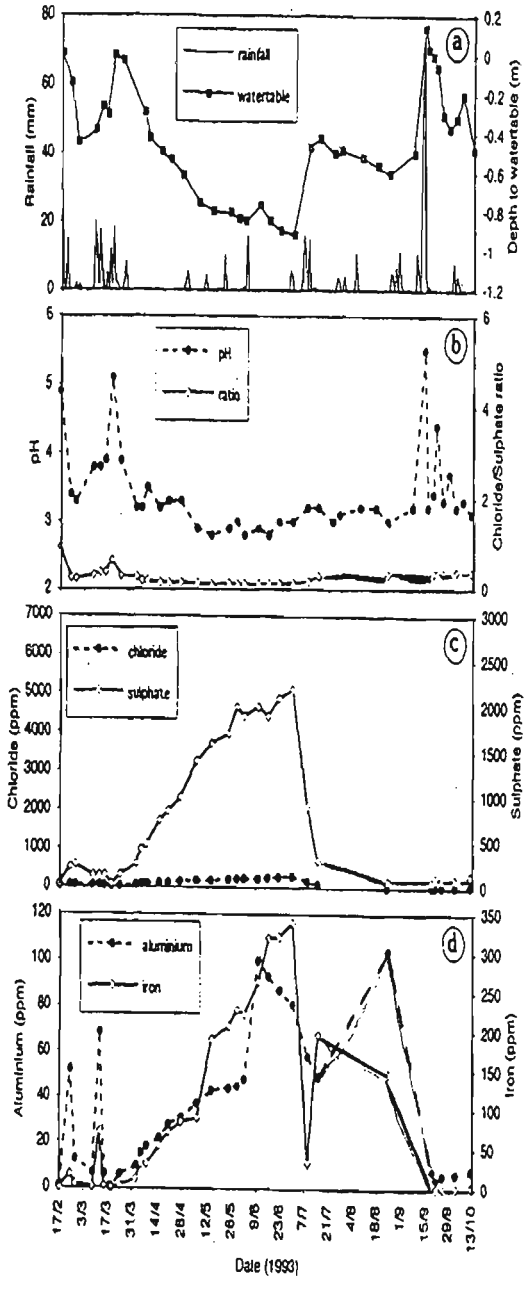

(B)

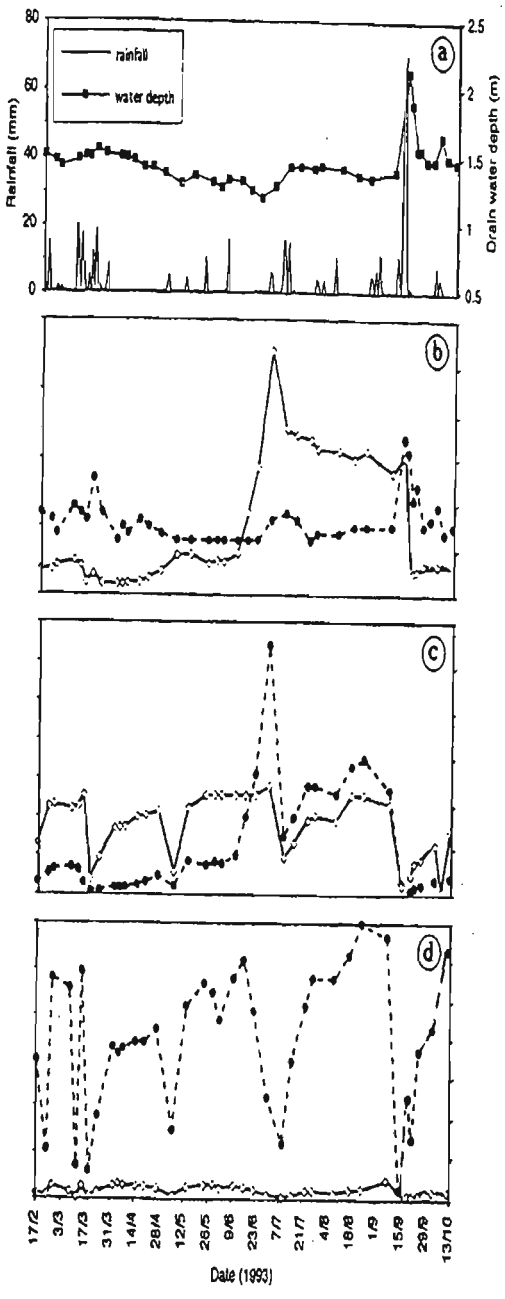

Figure 2.17 Water quality analysis from a typical borehole (A) located along the Broughton Creek floodplain over an 8 month period (Pease, 1997); a: Rainfall and Depth to watertable, b: pH and Chloride/Sulphate ratio, c: Chloride and Sulphate concentrations, d: Aluminium and Iron concentration.

Figure 2.18 Water quality analysis from a flood mitigation drain (B) located along the Broughton Creek floodplain over an 8 month period (Pease, 1997); a: Rainfall and Depth to watertable, b: pH and Chloride/Sulphate ratio, c: Chloride and Sulphate concentrations, d: Aluminium and Iron concentrations.

Table 2.3 Typical soil properties over depth taken from a borehole in the Shoalhaven Region of NSW, Australia (adapted from Pease *et al.*, 1997).

Soil property	0.15(m) depth	0.4 (m) depth	0.9(m) depth	1.89(M) depth
% Clay	39	38	30	41
% Silt	42	54	45	52
% Sand	19	8	25	7
pH (before drought)	4.1	3.3	2.9	6.5
pH (after drought)	3.2	2.7	2.5	1.8

Pease (1994) also noted an improvement in drain water quality when floodgates were either obstructed or poorly maintained. Indeed, the rise in chloride concentrations shown in Figure 2.17 & 2.18 was due to debris jammed in the floodgate, which allowed saline intrusion and a brief increase in pH levels. During a ten-week period, Pease found that pH values in the drain improved in proximity to the floodgates (Figure 2.19) and suggested that this improvement in drain water quality might be partly due to a deeper alluvium layer near the levee, as well as tidal buffering. Willet *et al.* (1993), White *et al.* (1993) and Willet and Bowman (1990) also reported similar trends of increasing water quality in relation to leaky floodgates on the north coast of NSW.

While Pease (1994) and Norwood (1975) investigated the relationship between chemical properties and the geomorphic characteristics of acid sulphate soils in the Shoalhaven Region, their research neglected the importance of soil physical properties or the implementation of on-ground remediation works. In fact, Pease (1997) pointed out that further research was necessary in regards to acid production, flow, and transport prior to any remediation techniques. To this end, a 120 ha field site was established in 1993 by the University of Wollongong, in collaboration with the NSW Environmental Protection Authority, to investigate the role water retaining structures play on acid production, transport and general trafficability in the northern section of Broughton

Creek, near the town of Berry. Initial topographical maps of the Berry field site are given by Chapman (1994) and Indraratna *et al.* (1995).

The main emphasis of Chapman's (1994) research was to determine the relationship between drain and groundwater interactions based on soil physical parameters. While Walker (1962) was the first to notice the prevalence of "buckshot nodules" within the soil profile, Chapman is credited as being the first to associate these "macro cracks", henceforth referred to as macropores, with oxygen diffusion into the pyritic layer.

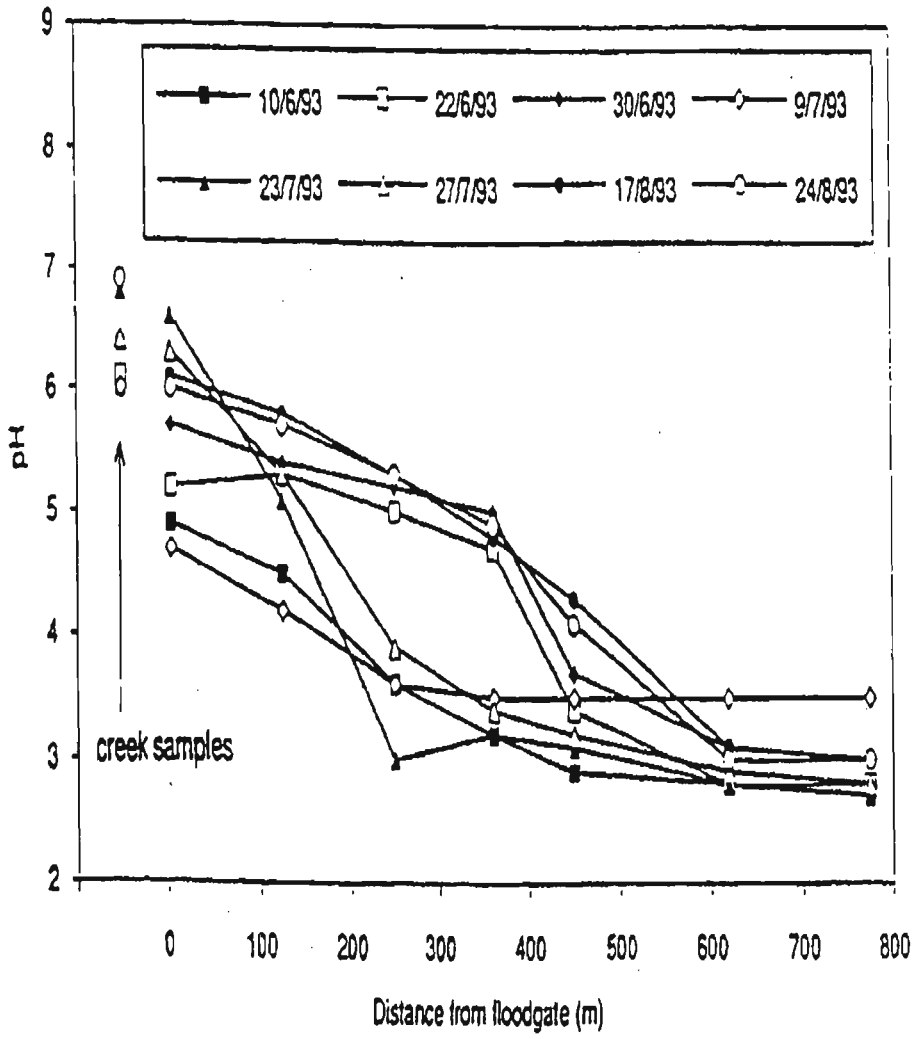

Figure 2.19 pH readings along the length of a flood mitigation drain analysed over a 10-week period in 1993. Creek samples were taken 50 m downstream of the tidal restricting floodgate (Pease, 1994).

Importantly, Chapman found an inverse relationship between drain water elevations and drain water pH at the Berry field site (Figure 2.20). Chapman also used a steady-state numerical seepage analysis program, PC-SEEP, to determine the critical drain water height necessary to inundate the pyritic layer while maintaining efficient agricultural production. Using this model, Chapman suggested that if the drain water level was maintained at 0.5 m below the ground surface, a large portion of the acid producing layer would be submerged. Optimistically, Chapman surmised that if drain water levels could be sustained, "the submerged acid sulphate soils would cease being raw and become potential acid sulphate soils and thus pose little environmental or agricultural concerns."

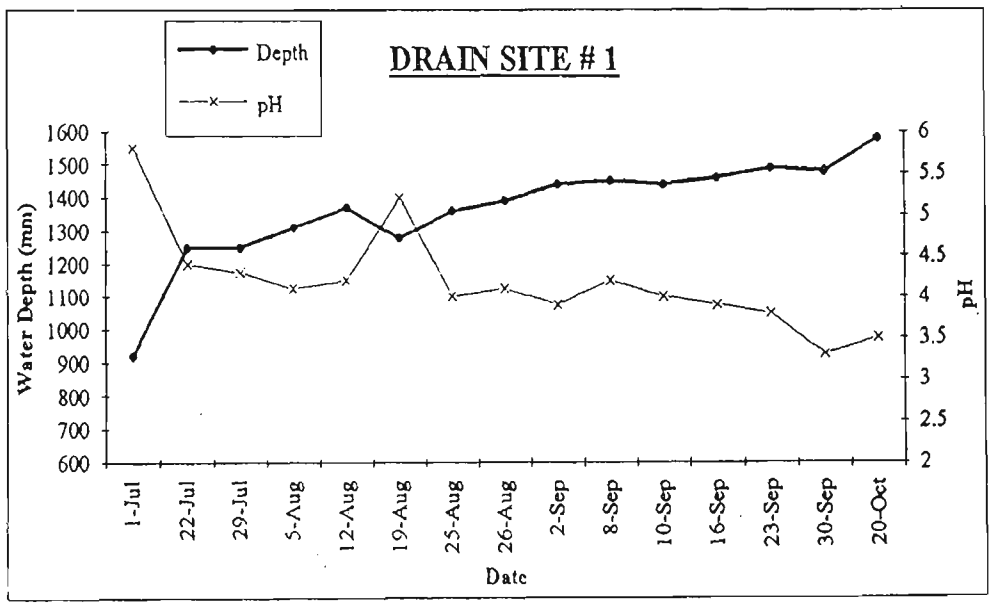

Figure 2.20 Relationship of drain water depth and pH over a four-month period (Chapman, 1994).

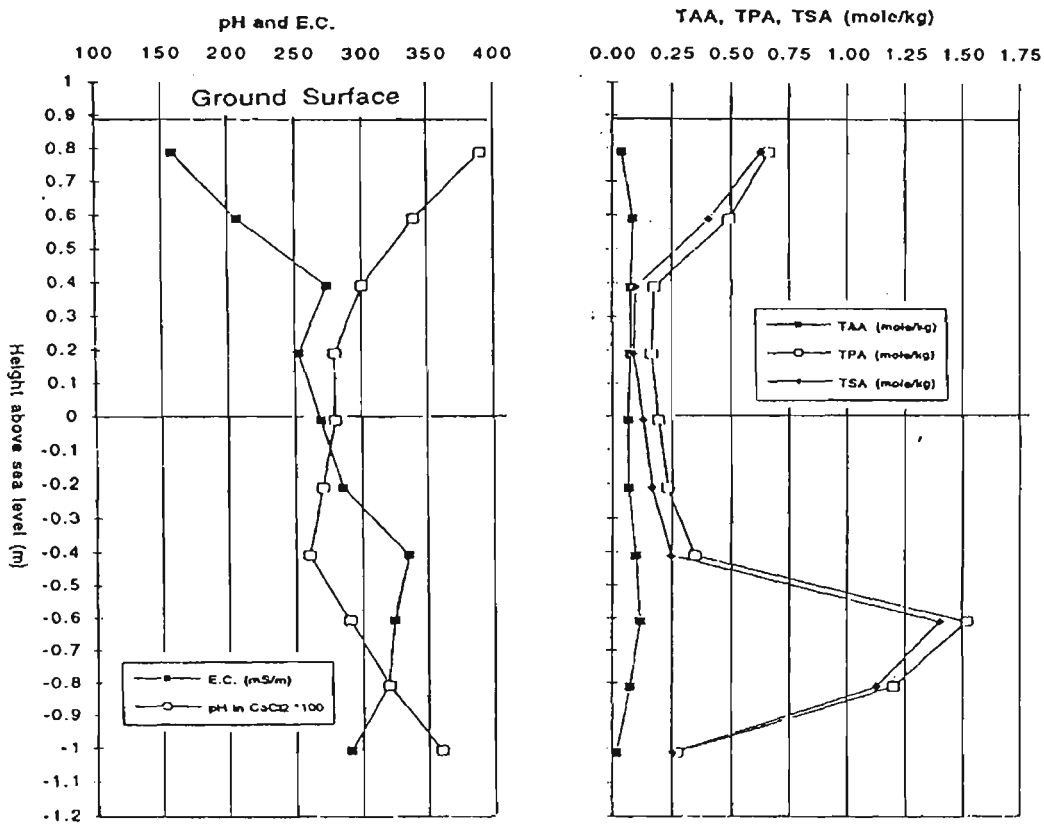

Figure 2.21 Typical plots of soil pH, electrical conductivity, total actual acidity, total potential acidity and total sulphur acidity over depth in the Shoalhaven floodplain (Sbeghan, 1995).

During the proceeding four years, several projects were conducted on the above field site to extend the work of Chapman (1994) and prepare the site for on-ground remediation works. Sullivan (1995) further developed the relationship between drain water and groundwater flow for the Berry field site but lacked seepage analysis, or soil physical properties. Sharman (1995) gathered additional water quality data and detailed the effects of acid and aluminium on pasture crops. Speghan (1995) was the first to analyse soil samples for total potential acidity (TPA), total sulphur acidity (TSA) and total actual acidity (TAA), and, as expected, found a significant increase in both TAA and TPA approximately 1.4 m below the surface (Figure 2.21). Speghan (1995) was also the first researcher in the Shoalhaven region to suggest complete removal of the

floodgates to increase the drain water elevation. Finally, Paynter (1995) compared ASS in the Illawarra region with those in the Shoalhaven using TAA/TPA results. Paynter's research showed that TPA/TAA analysis alone was not sufficient to distinguish between ASS and non-ASS sediments.

In 1997, Toniato's research analysed the impact of weirs on drain and groundwater hydrology at the Berry field site. Toniato calculated the hydraulic impact of weirs using 1 year and 10 year average recurrence interval storms and expanded Chapman's (1994) seepage model to include additional soil physical parameters over a field calibrated transient time period. As shown in Figure 2.22, Toniato suggested that the installation of weirs would not cause drain water to overtop the levee bank in either predicted storms. Once the hydraulic capacity of the weirs was deemed acceptable, Toniato (1997) determined the effectiveness of three weir heights on groundwater levels using a 2D finite element seepage package, SEEP/W. In this study, a finite element mesh was constructed, Figure 2.23, and run over a 100-day period. Using on-site environmental measurements, the model determined flux into and out of the groundwater mesh. Toniato suggested that drain water manipulation was most effective 0-50 m from the drain face and that evapotranspiration was the key element influencing water loss beyond this zone. Calculations showed that groundwater flux is dependent on rainfall, but pre-existing conditions play an important role in determining the amount of acid transported into the drain. Finally, Toniato concluded that while raising the groundwater table through increased drain water levels is a practical solution for reducing acidic discharges, additional three dimensional (3D) oxygen diffusion, pyrite oxidation, acid transport modelling was needed to better characterise the overall processes.

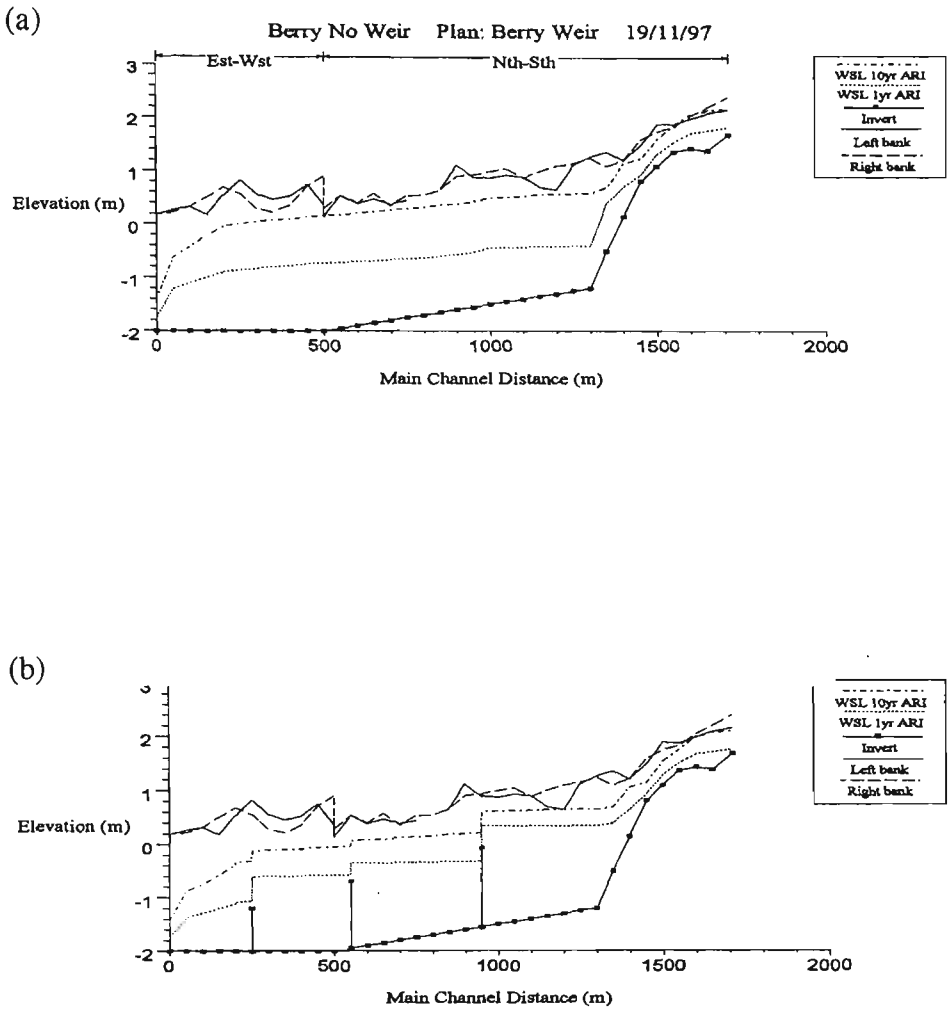

Figure 2.22 Drain water levels in existing (a) and under weir conditions (b) with simulated 1 yr and 10 yr storm events (Toniato, 1997).

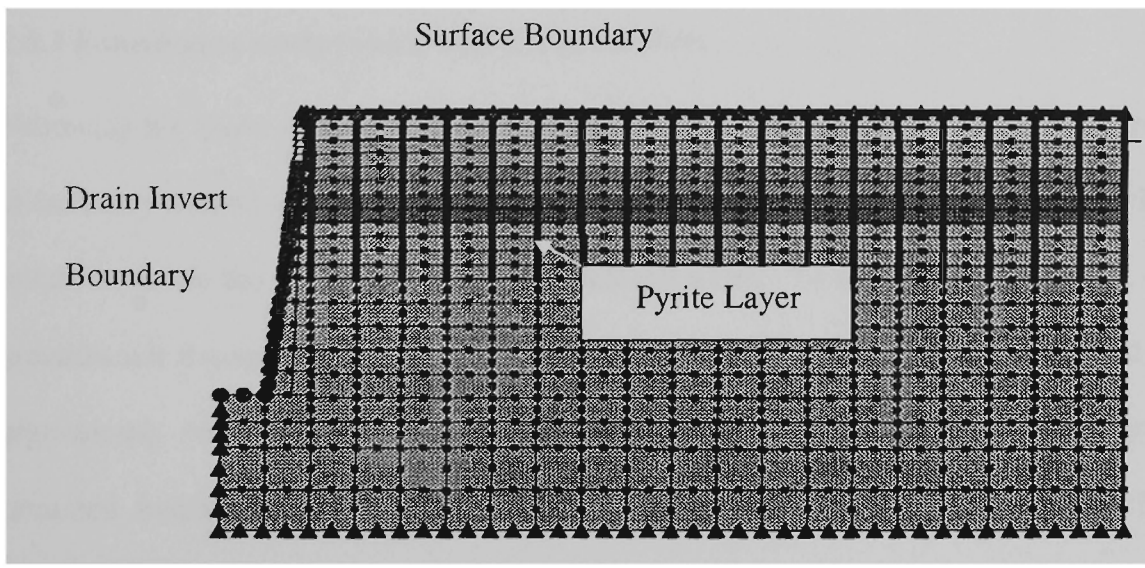

Figure 2.23 Diagram of finite element mesh constructed to evaluate optimum drain water heights to control pyrite oxidation (Toniato, 1997).

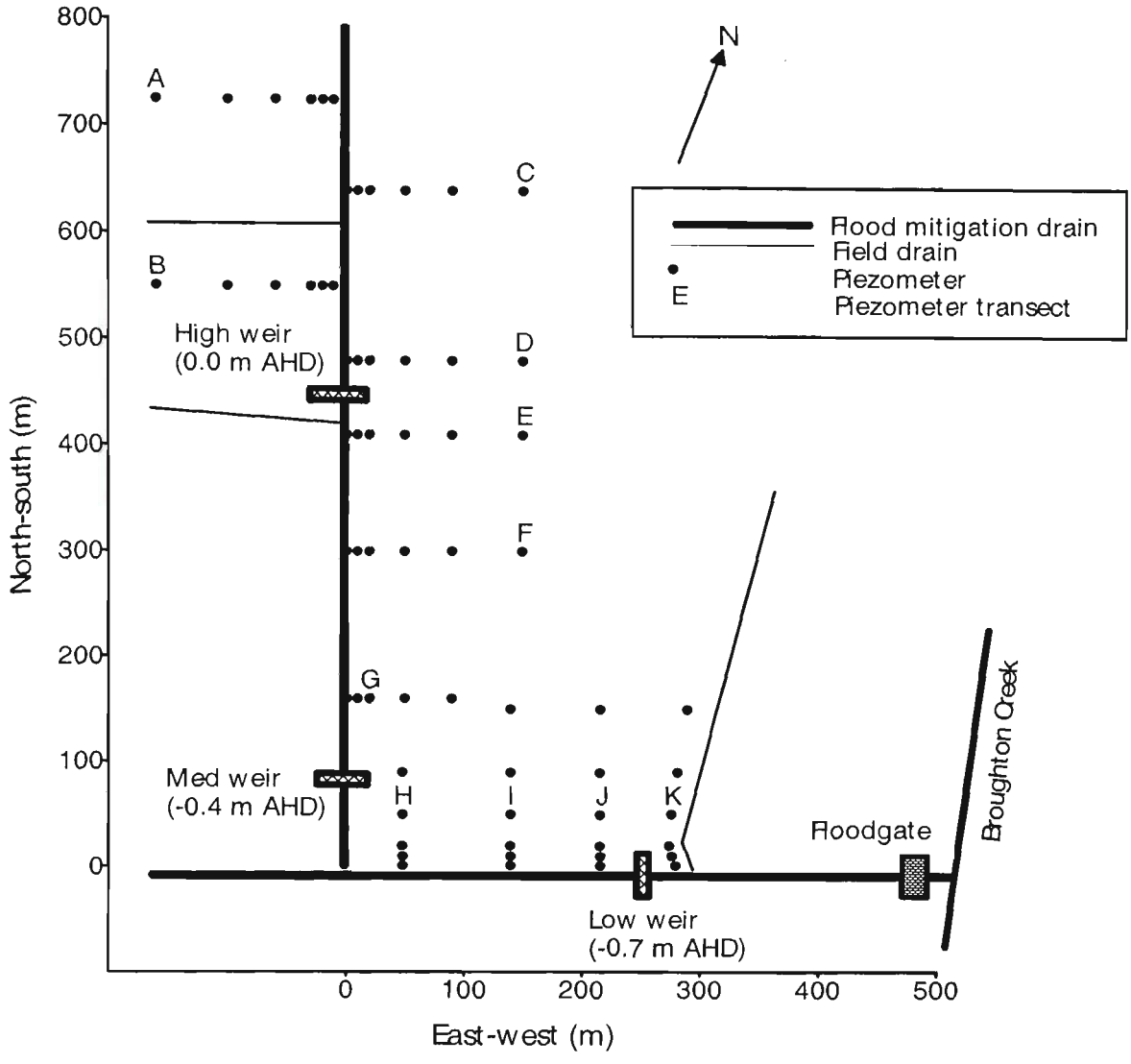

Figure 2.24 Location of sampling sites at the Berry field site (Blunden, 2000).

2.6.3 Remediation works (weirs) and acid production

Following the above research, Blunden (2000) commenced a three-year doctoral project at the Berry site, which focused on maintaining an elevated groundwater table above the pyritic layer via the installation of three v-notched weirs. To evaluate the processes of groundwater transport and acid production by oxygen diffusion, Blunden conducted a high-density soil sampling program including soil physical (bulk density, porosity, saturated hydraulic conductivity, moisture characteristic curves, particle and pyrite crystal size distribution and van gneutchen parameters), and chemical (carbon, pH, salinity, sulphate, chloride, exchangeable cations, oxidisable sulphur, aluminium,

calcium and base saturation, peroxide oxidisable sulphur concentrations) parameters over depth and distance. Table 2.4 shows typical soil physical properties found at the site. It is important to note from this table that the relatively high, saturated conductivity values in the vertical plane were attributed to macropores formed during the decomposition of organic matter. These vertical macropores enhance the transport of oxygen into the pyritic layer, thereby increasing acid production and the impact of evapotranspiration with distance from the drain. Furthermore, the relatively low saturated conductivity values and increased bulk density of the potential acid sulphate soil layer demonstrates its inundated, reduced state, and its role in maintaining the 'leaky bucket effect' discussed earlier. A schematic of sampling sites at the Berry field site is shown in Figure 2.24.

Table 2.4 Soil physical properties (adapted from Blunden, 2000).

Soil Layer	**Depth below surface (m)**	**Average dry bulk density (ρ_d) (t/m^3)**	**Porosity**	**Saturated Hydraulic Conductivity (vertical) (m day^{-1})**	**Saturated Hydraulic Conductivity (horizontal) (m day^{-1})**
Organic topsoil	0.3	0.80	0.70	3.95	3.72
Peat-Loam	0.6	1.11	0.58	3.84	3.76
Jarositic Layer	0.9	1.05	0.60	1.68	0.78
Actual ASS	1.2	0.95	0.64	2.08	0.88
Potential ASS	1.5	1.03	0.61	2.02	0.20
Pleistocene Clay	3.0	1.70	Not taken	0.20	0.20

Figure 2.25 shows dissolved sulphate and chloride concentrations at 10 m and 90 m perpendicular to a flood mitigation drain at the Berry field site. Sulphate concentrations show a defined actual acid sulphate soil layer 1.2 m below the soil surface with concentrations more than 3 orders of magnitude greater than the above layers. Interestingly, though the pyritic layer was formed in chloride rich environments, subsequent alluvial processes and mass flow has leached the majority of chloride concentrations out of the soil matrix. However, Blunden suggested that increased chloride concentrations at the surface were due to atmospheric seaspray. Floodgate leakage may have also allowed saline water to enter the flood mitigation drain, thus explaining the increase in chloride levels depicted at the 10 m site.

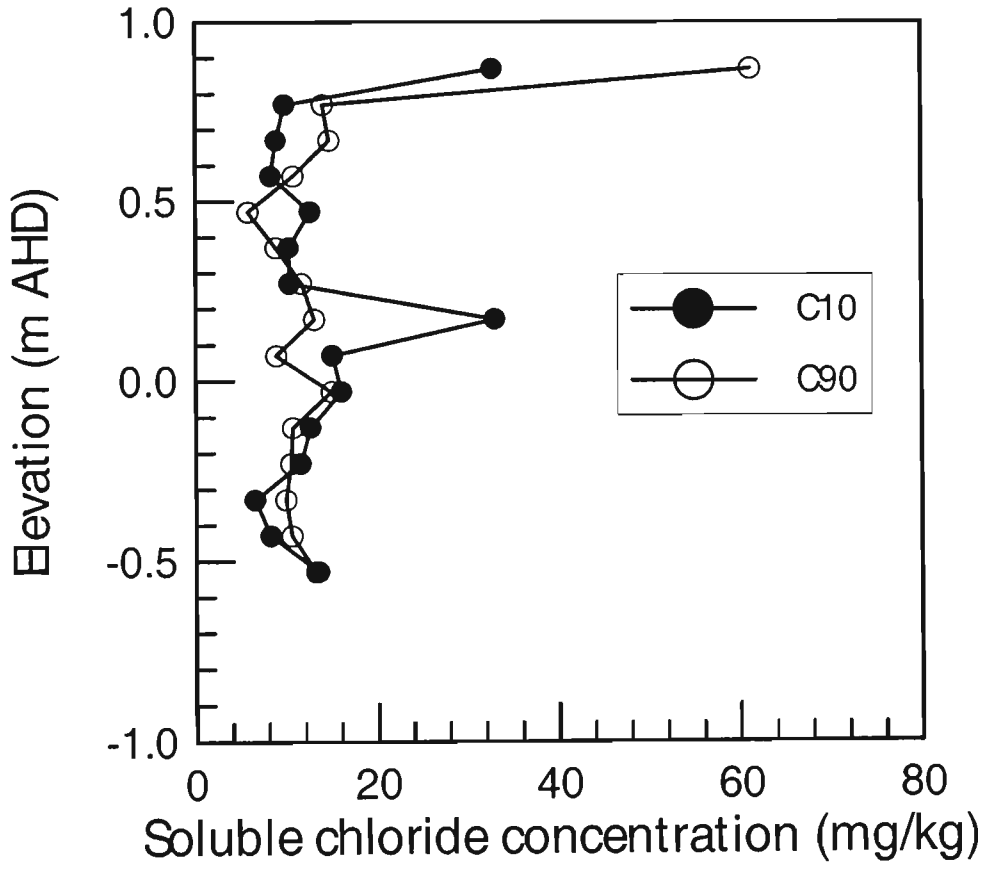

Figure 2.25 Dissolved soil chloride concentrations at 10 m and 90 m perpendicular to a flood mitigation drain (Blunden, 2000).

With ample soil data, Blunden and Indraratna (2001) went on to examine the affect of installing weirs on maintaining an elevated groundwater table. Pre-weir data (Figure 2.26) showed that the deep flood mitigation drain created a strong hydraulic gradient between the groundwater and drain water. This maintained the groundwater table below the pyritic layer, which was especially evident within 10 m perpendicular of the drain, and accelerated acid production. Furthermore, the strong velocity vectors combined with the relatively high saturated conductivity levels in the soils above the acidic layer, increased acid transport to the drain. This effect was most apparent following rainfall when tidal floodgates quickly restored low drain water elevations (Figure 2.27). During these periods, acidic groundwater was leached into the flood mitigation drain and quickly transported into the surrounding estuary. Indraratna *et al.* (1999) estimated that over the 1997-1998 summer more than 1.3 tonnes of H_2SO_4 ha^{-1} were generated at the Berry field site.

The installation of three v-notched weirs at the Berry field site was successful in maintaining the groundwater table at or above the pyritic layer. A comparison of pre- and post-weir groundwater elevations (Figure 2.28) shows that prior to weir installation the groundwater table fluctuated to a greater extent and was often below the pyritic layer, whereas, after weir installation the groundwater table was maintained above the pyritic layer and fluctuated within a smaller range. By maintaining a constant head within the drains, Blunden and Indraratna (2001) also demonstrated that the weirs reduced the hydraulic gradient between the drain and the phreatic zone. As shown in Figure 2.29, these modifications decreased the velocity vectors of acid transport.

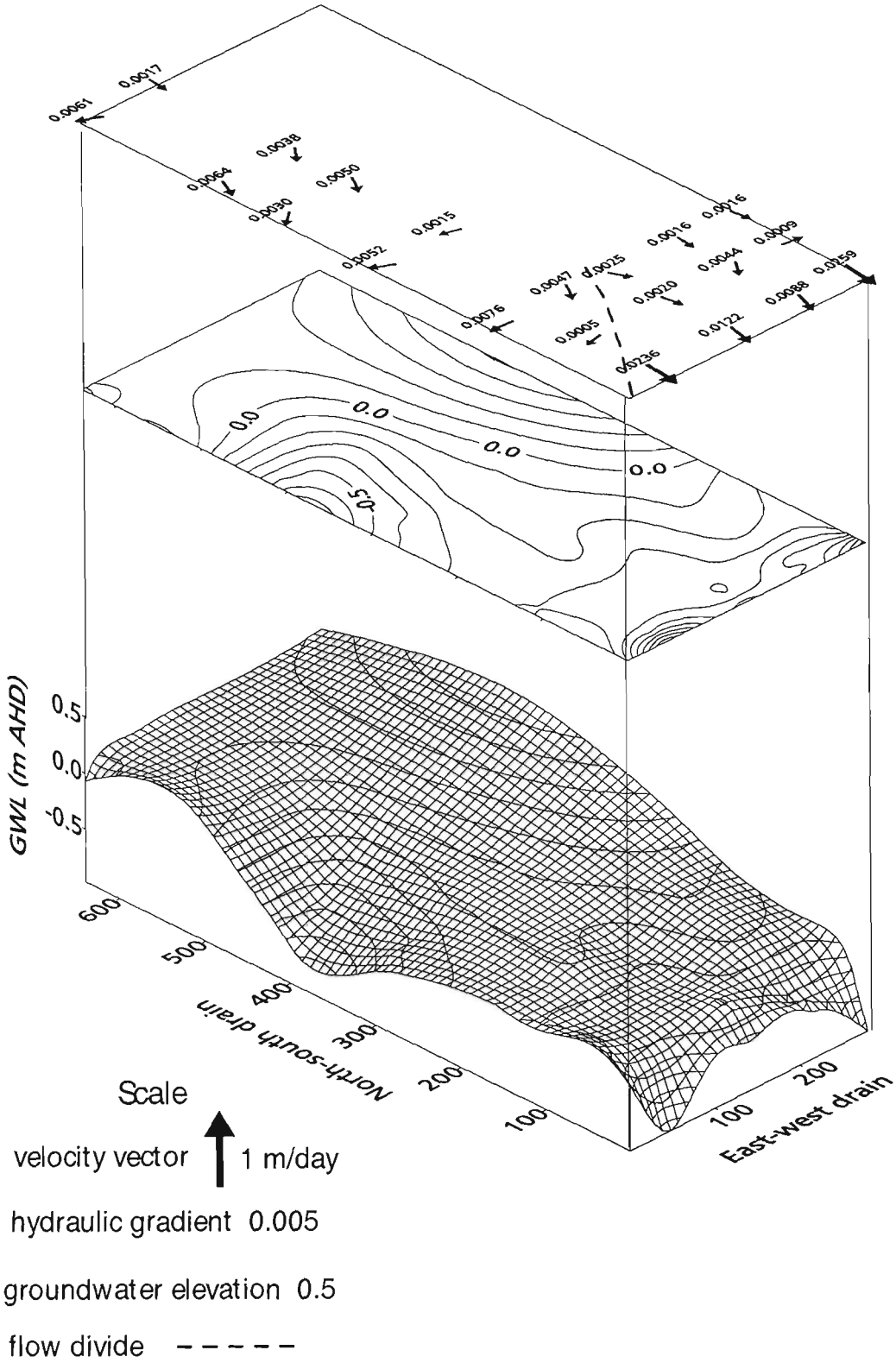

Figure 2.26 Typical groundwater elevation profile before weir installation (Indraratna *et al.*, 2001).

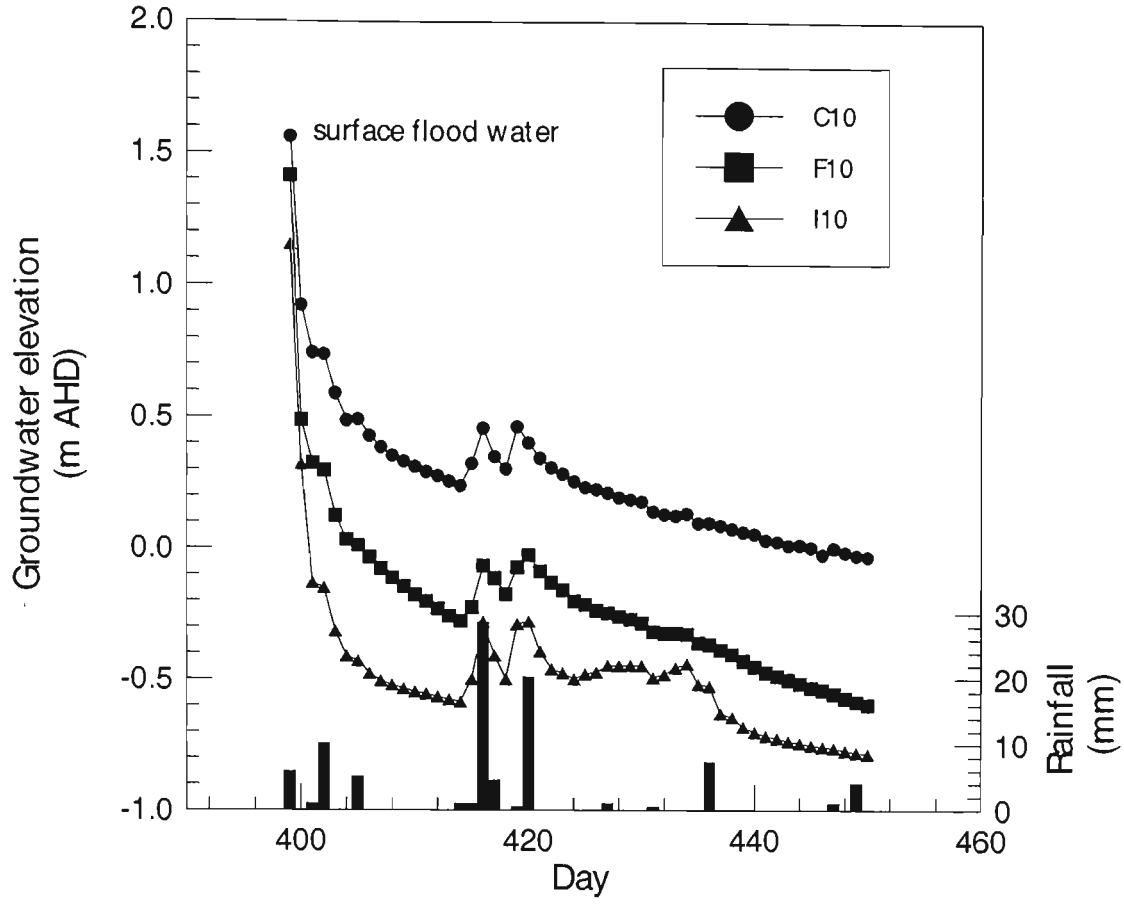

Figure 2.27 Decline of the groundwater level in three piezometer transects (labelled C, F, and I) after a flood event at 10 m perpendicular a flood mitigation drain (Blunden, 2000).

To quantify the impact of various water management strategies on acid production, Blunden (2000) applied two numerical models that predict the groundwater regime and acid production. Groundwater regimes were simulated using a 3D finite element flow and transport model for variable saturated media, FEMWATER (Lin *et al.*, 1997). Pyrite oxidation was simulated using the 1D Simulation Model for Acid Sulphate Soils (SMASS) developed by Bronswijk and Groenenberg (1992). Blunden (2000) compared the impact of irrigation strategies and weirs versus the existing conditions, and suggested that although a 7-day irrigation cycle produced the least amount of acid, installing weirs provided the most cost-effective solution. In fact, Blunden stated that installing a weir in the drain to maintain a drain water level above the pyritic layer resulted in a reduction of 25% to 43% compared to the existing situation at 10 m and 90

m from the drain, respectively. While this model provided a general estimate of acid production, its inherent 1D calculations restricted simulations over a realistic 3D plane.

To accurately simulate the impact of an elevated groundwater table on acid production in a 3D plane, Blunden and Indraratna (2001) developed the oxygen transport, pyrite oxidation model, ASS3D. In this model, the transport of oxygen through the soil matrix is assumed to predominate via macropores. The transport process, however, is 1D and ignores the component of lateral migration into the surrounding soil matrix (Figure 2.30). Additionally, the production of acid in ASS3D is solely based on pyrite oxidation via atmospheric oxygen and neglects other mechanisms such as ferric anaerobic oxidation.

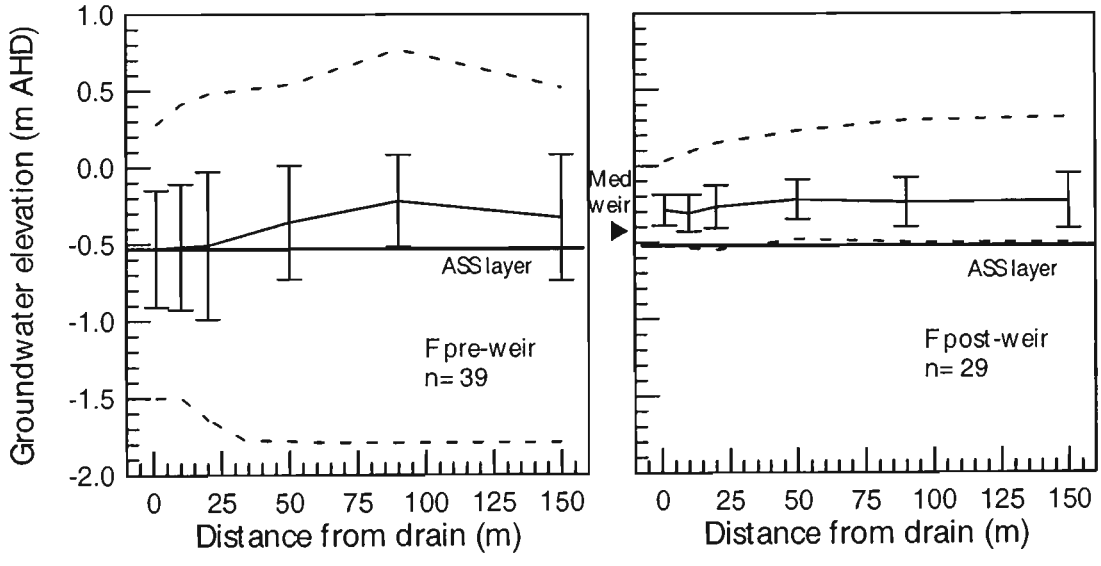

Figure 2.28 Comparison of the average groundwater elevation at a transect prior to and proceeding weir installation; also showing the maximum and minimum groundwater elevation and standard error bars (adapted from Indraratna *et al.*, 2001).

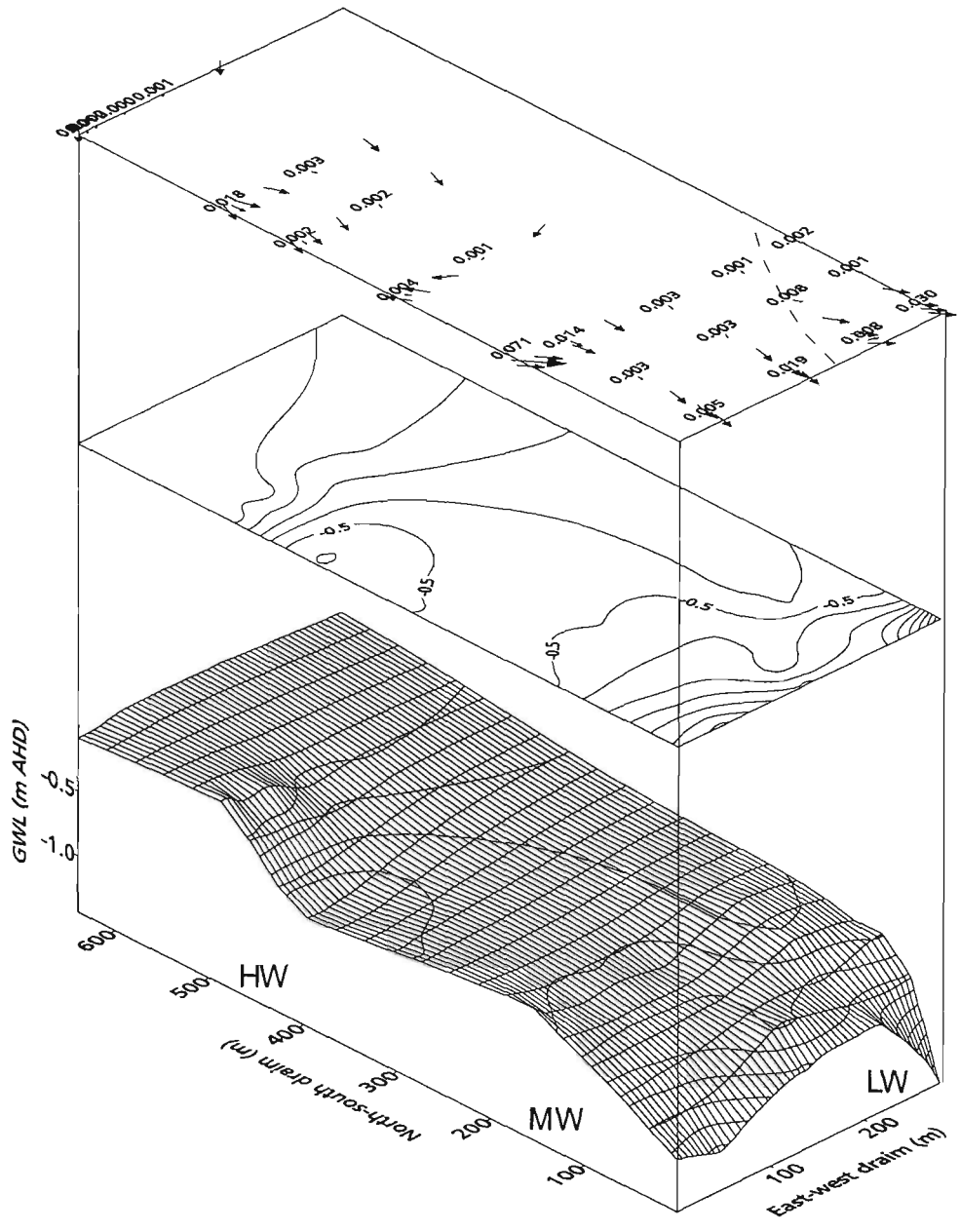

Figure 2.29 Typical groundwater elevation profile following weir installation (adapted from Indraratna *et al.*, 2001).

When linked to 3D soil moisture content distribution outputs produced from the simulation of saturated/unsaturated conditions using FEMWATER, ASS3D firstly determines the air-filled porosity of the soil profile. With this information, oxygen diffusion and consumption values are determined and the oxygen concentration in the soil matrix is then calculated. Secondly, the amount of pyrite oxidised is determined and the new pyrite content and diameter for the next time step is calculated. Finally, the

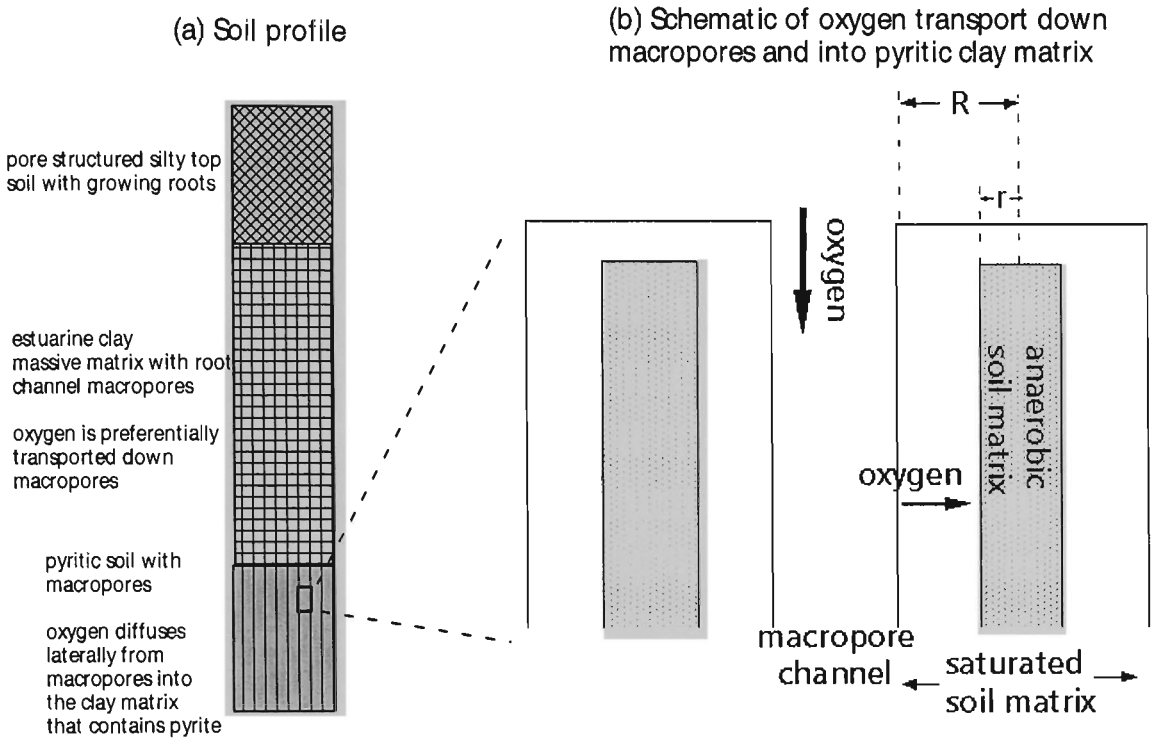

Figure 2.30 Schematic of the soil structure and oxygen transport in the pyrite oxidation model. R is the radius of the soil aggregates, and r is the radius of the anaerobic zone (Blunden and Indraratna, 2001).

amount of pyrite oxidation products (SO_4, Fe^{3+} and H^+) generated is calculated and written to an output file. A flow chart of the FEMWATER/ASS3D model is shown in Figure 2.31.

Following a rigorous comparison of analytical and numerical solutions, Blunden and Indraratna (2001) concluded that ASS3D was in strong agreement with the field data. To assess the effectiveness of weirs at reducing acid production they compared pyrite oxidation and sulphate production from the ASS3D model over a yearlong drought period in 1997-1998. This research revealed that a weir installed at 0.2 m above the pyritic zone maintained the groundwater table approximately 0.2 m above the non-weir simulation but varied spatially and temporally with distance from the drain. By reducing both the time and extent of pyrite oxidation, ASS3D predicted a 53% reduction in pyrite oxidation using weirs as opposed to the lower drain water levels that

occurred under normal drain operating conditions. Similarly, sulphate production was reduced from 91 x 10^3 mol to 42 x 10^3 mol with the installation of a weir over the 6000m^2 mesh. However, though the ASS3D model was useful in computing the magnitude and distribution of acid products, it provided no linkage between acid products and their concentration in groundwater or surface water.

2.6.4 The role of anaerobic oxidation

Subsequent research (Indraratna *et al.*, 2002; Rudens, 2001; Glamore *et al.*, 2001) undertaken at the Berry field site has found that acidic drain water conditions (pH < 4.0) persist regardless of drain water height. Blunden (2000) suggested that this might be partly due to the large store of acid products within the soil matrix from previous pyrite oxidation. This acid bank would continue to deposit oxidation products into the drain, especially proceeding rainfall when the groundwater table is elevated above the weirs. Furthermore, at the Berry field site a large portion of the drain (~250 m) is below the final weir, and within this region the watertable is consistently maintained below the pyritic layer by one-way floodgates.

Thong (1998) and Rudens (2001) in the south coast of New South Wales, and others worldwide (Evangelou, 1995; Dent, 1986; and Chapman and Murphy, 2000) predicted that acid production would persist even under reduced conditions. As stated earlier (Equation 2.6), under acidic conditions ferric iron can directly oxidise pyrite and this cycle is dependent upon a sufficient source of organic matter and the presence of the bacterium *T. ferrooxidans*. Initial investigations conducted by Thong (1998) suggest that these conditions may exist in the south coast of NSW and are possibly responsible for the continual acidic drain water conditions found at the Berry field site.

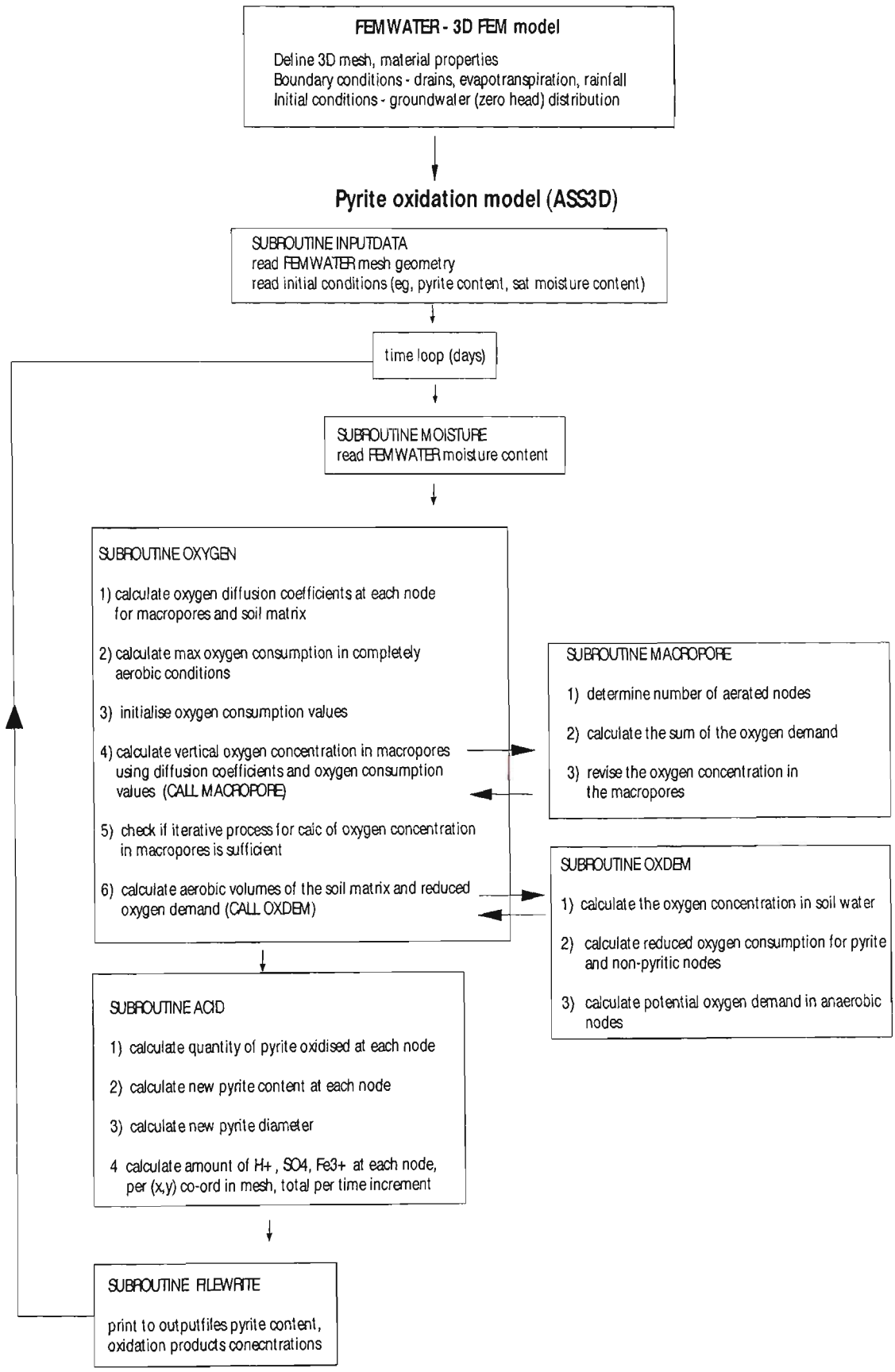

Figure 2.31 Flow chart of FEMWATER and ASS3D models (Blunden and Indraratna, 2001).

In an attempt to quantify the influence of groundwater manipulation on acid production, Thong's (1998) research compared field trials with numerical modelling. Using several soil columns at different water levels, Thong determined that in waterlogged, reduced conditions, the numerical model SMASS underestimated sulphate concentrations. Since sulphate production in SMASS is calculated solely by atmospheric oxidation, Thong postulated that anaerobic oxidation of pyrite must be occurring. Thong also developed a ratio of sulphate production in oxidised versus reduced columns, which illustrated that sulphate production under both conditions were initially similar, and attributed the sulphate production in the anaerobic columns to ferric oxidation. Taking into account the favourable acidic groundwater conditions prevalent across the floodplain, Thong (1998) hypothesized that, "the submergence of the pyritic layer will merely reduce the rate of acid production, but not prevent it". To this point, Rudens (2001) demonstrated that *T. ferrooxidans* were abundant in southeastern NSW subsoil and that their concentration was positively correlated with organic content. Rudens (2001) research suggested that acid production would persist even under submerged conditions as long as sufficient organic content was available (optimal level $\approx 5\%$ organic content) and the groundwater was acidic ($pH < 4.0$). As both of these criteria have been documented in several areas contaminated by acid sulphate soils, additional management strategies are necessary to combat acid drainage.

2.6.5 Alternative management strategies

Despite more than 25 years of research on acid sulphate soils in Australia, no successful management strategy has been developed to neutralise acidic discharges without the addition of anthropogenic chemicals. Therefore, to limit environmental degradation an alternative strategy is required. To this end, Pease (1995), Blunden (2000) Ikin (2001),

and Indraratna *et al.* (2002) in the south coast and several other researchers (Sammut *et al.*, 1995; Portnoy and Giblin, 1997; Dick and Osunkoya, 2000; Pollard and Hannan, 1994) in the north coast of New South Wales have noted improvements in surface water quality following tidal seepage upstream of one-way floodgates.

Several researchers have also suggested that tidal restoration via floodgate manipulation/modification will significantly improve drain water conditions. Blunden (2000) noted that saline flushing would act as an effective weed control mechanism in flood mitigation drains. Where saline flushing is restricted, as is the case upstream of weirs and tidal floodgates, freshwater weeds quickly establish and grow rapidly. High concentrations of dissolved sulphate in the drain from previous pyrite oxidation, as well as stagnant water from excessive weed growth, accelerate the precipitation of iron monosulphides (FeS) onto the drain invert. Sullivan and Bush (1999) showed that during floods or mechanical weed clearing, disturbance of the iron monosulphide sediment could lead to rapid acidification of the drain water. If regular saline flushing is permitted within the drains, weed growth is restricted and the formation of iron monosulphides is reduced. Additionally, Indraratna *et al.* (2002) suggested that limited weed growth would improve the hydraulic integrity of the drain, hence allowing it to perform efficiently during flood periods. Glamore and Indraratna (2001) postulated that tidal restoration may also reduce metal flocculation, increase dissolved oxygen and raise the groundwater table above the pyritic layer.

2.7 Current research strategy

Throughout coastal Australia, acid sulphate soils cause widespread environmental damage to land and drainage waters. Due to its complex nature, attempts to minimise

acid production and acid transport *in situ* have been largely unsuccessful. Similarly, efforts to neutralise acid drainage through the addition of anthropogenic chemicals such as lime or gypsum have been costly and ineffective in the long-term (Pearson and McDonell, 1975; Webb and Sasowsky, 1994). Preliminary data suggests that the restoration of tidal flushing via modified floodgates to allow for tidal buffering may provide a unique non-anthropogenic alternative to control acid sulphate soil drainage. To develop a management strategy for drained floodplains based on active floodgate manipulation, a thorough understanding of the complex interrelationship between estuarine hydrology, acid sulphate soils, groundwater transport, and buffer kinetics is required.

The hypothesis of this research is that the restoration of tidal flushing to acid sulphate soil affected flood mitigation drains will improve drain water quality without undue harm to agricultural productivity. The inappropriate design of one-way floodgates denies the beneficial effect of tidal buffering, perpetuates the acid producing-acid drainage cycle, and exacerbates environmental problems associated with acid sulphate soils. Therefore, the key objective of this thesis is to assess drain water and groundwater conditions, including hydraulic and chemical parameters, before and after the installation of modified floodgates, and to determine the effectiveness of tidal restoration as an effective drain water management strategy.

This study aims to provide:

(1) An understanding of the influence of one-way floodgates with regards to groundwater drawdown, soil conditions, and hydraulic gradients;

(2) A detailed description of floodplain hydrology prior to floodgate modifications, including estuarine dynamics and the impact of altered climatic periods on acidic discharges;

(3) A thorough understanding of the buffering kinetics involved including the calibration of an ion speciation mixing model to predict changes in drain water quality prior to civil works, and the simulation of altered drain hydraulic conditions through detailed geographic information system technique;

(4) A series of design criterion relating to floodgate modifications and two innovative floodgate designs directly applicable to the study site;

(5) Detailed quantitative and qualitative drain water quality results following floodgate modifications with specific reference to changes in total acidity, and the impact of altered hydraulic conditions;

(6) A comprehensive understanding of the impact of tidal forcing on the soil matrix and the role saline intrusion plays on pore water chemistry; and

(7) The development of a 3D finite element numerical model to simulate salinity flow and transport within the groundwater over varied climatic and soil property regimes.

To assess the effectiveness of the floodgate management strategy, the interrelationship between surface water chemistry and hydrology, groundwater and soil physics, estuarine dynamics and climatic influences were studied at a comprehensively instrumented and monitored flood mitigation drain along Broughton Creek, a left bank tributary to the Shoalhaven River in southeastern New South Wales, Australia. This study follows on from previous research undertaken at the Berry field site and provides a vital link between groundwater and surface water hydrology. This research

culminates in the formulation of a best management practice for acid sulphate soils and floodgate manipulation in southeastern NSW.

Chapter 3.0 Baseline Field Site Information: Location, Monitoring Details and Climatic Conditions

3.1 Introduction

In this chapter, the study site and monitoring regime devised to investigate the chemical and hydrological attributes of ground and surface water are described in detail. Climatic information obtained over the entire study period is also presented with particular reference to rainfall and evapotranspiration rates. In combination, this information provides vital background information regarding the environmental processes underlying the field trials.

A study site was selected to trial and assess the installation of modified floodgates within a low-lying flood mitigation drain. The study site is suitable for this purpose due to 3 major attributes, namely:

1. The site is underlain with acid sulphate soils;
2. An artificial drainage network with tidal restricting floodgates has been installed at the site;
3. Previous research in the region has demonstrated that acidic ground and surface water conditions exist regardless of the elevation of the phreatic zone.

The exact location of the study site, its geomorphology, and history of the drainage works are described in the first section of this chapter. To gain a better understanding of the hydrologic characteristics of the region, a comprehensive mapping program

involving the creation of digital elevation maps, catchment details and regions, drain surveying and creek bathymetry data is also provided.

In the second section of this chapter, the field equipment and monitoring program devised to test surface and groundwater quality is described. The location, operation, and monitoring schedule of piezometers, drain and creek sampling sites, as well as the chemical and hydraulic properties of the creek/drain are presented, including the methodology for collection and analysis of samples. An extensive array of continuous monitoring equipment, including submersible multi-parameter data loggers, bi-directional ultrasonic Doppler flow meters, and a weatherstation installed at the site is detailed.

The climatic conditions obtained over the entire study period are described in the final section of this chapter. The interrelationship between rainfall and evapotranspiration is highlighted because of their direct relationship with groundwater elevation, upland inflow rates, and the tidal regime. Moreover, the varied climatic conditions experienced over the trial period provide an optimal research environment to trial the management strategy.

3.2 Study site location

The study site is a flood mitigation drain, called Flying Fox Creek, situated on the south coast of New South Wales (NSW), approximately 3 km from the township of Berry (34^0S, 150^0E). The drain forms part of a small subcatchment (~468 ha) that discharges into Broughton Creek, a left bank tributary of the Shoalhaven River, and is located 10.2 kms from the junction of Broughton Creek and the Shoalhaven River. While Flying Fox Creek was originally a natural meandering waterway, in the 1960s the creek was straightened and deepened (~10 m wide x 3 m deep) for agricultural and flood mitigation purposes. At the same time, headworks consisting of two 2 m x 2 m top-hinged tidal restricting floodgates were installed to permit drainage under hydrostatic pressure, normally occurring at low tide. A location map and aerial photo of the study site are shown in Figures 3.1 and 3.2.

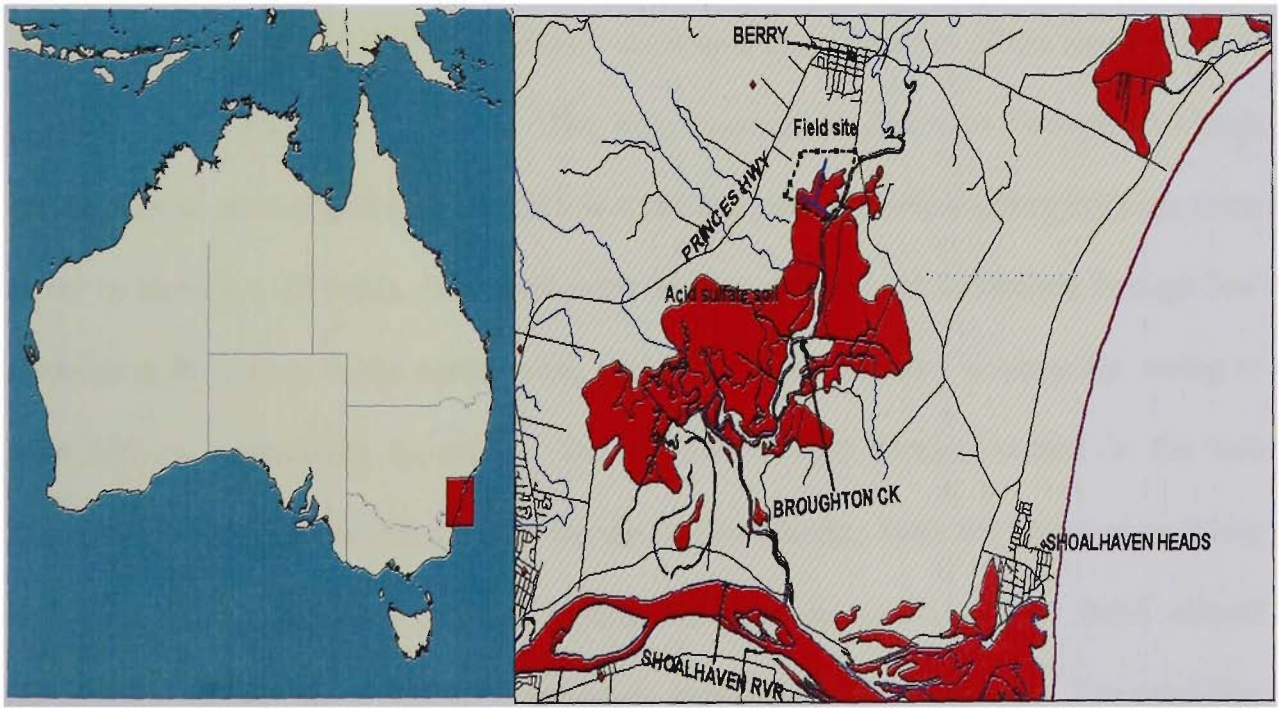

Figure 3.1 Location map of study site.

Figure 3.2 Aerial photo of study site and Broughton Creek.

3.2.1 Geomorphology

The Shoalhaven River is located 160 km south of Sydney on the tectonically stable south coast of New South Wales. The river drains a catchment of 9260 km^2 and in its lower reaches incises into Permo-Triassic sandstone and siltstones of the Sydney Basin (Figure 3.3, Umitsu *et al.*, 2001). The deltaic-estuarine plains of Broughton Creek encompass an area of 183 km^2 and follow a predominately north-south orientation from Berry to Bolong (~15 kms). The catchment of Broughton Creek is formed through low undulating hillslopes to the north, west, and south, with Mount Coolangattta, rising to over 300 m, controlling its route. To the east, a sand barrier formed in the late Quaternary separates the floodplain from the Pacific Ocean. Both the Shoalhaven River and Broughton Creek are highly channelised and are considered to have almost completely infilled the pre-existing estuarine embayment (Roy, 1984). The estuarine alluvial plains that characterise Broughton Creek presently support pastureland for mainly dairy farming.

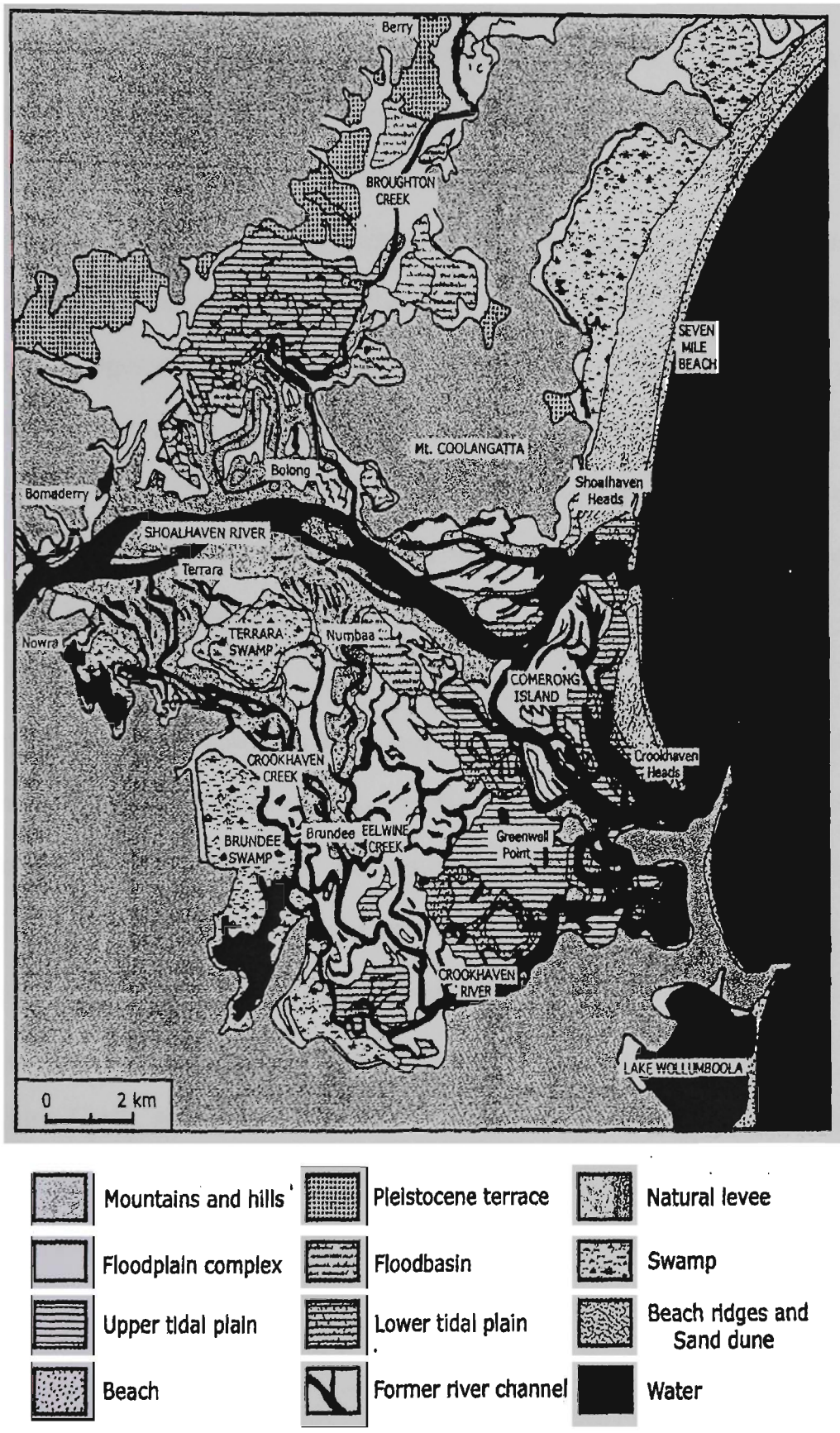

Figure 3.3 Landforms of the Shoalhaven River deltaic estuarine plains (Umitsu *et al.*, 2001).

Roy (1994) suggested that the formation of sulphidic sediments in the northern Shoalhaven was typical of processes associated with infilling of a barrier estuary. During a period of post-glacial marine transgression (approx. 8000 years ago), the underlying Pleistocene surface was flooded as sea levels rose and saline waters inundated previously terrestrial environments. Through radiocarbon dating of molluscan and diatom compositions, Willet and Walker (1982), and later Woodroffe *et al.* (2000), suggested that these conditions, conducive to the formation of pyritic sediments, persisted up to 4000 years ago. The formation of levees served to impound a series of low-lying flood basins with initial infilling occurring around the margins. As ocean heights receded and stabilised to current levels, pyrite formation ceased and freshwater alluvial processes dominated.

The evolution of the Shoalhaven River system from early stages of development to its current mature stage increased both the tidal range and amplitude (Figure 3.4). According to Roy (1984), estuary infilling creates sinuous channels with smooth level banks which promotes the attenuation of tides and enhances mixing within the water column. Broughton Creek has tidal fluctuations >1.0 m to Berry, more than 20 kms from the mouth of the Shoalhaven River (Pease, 1994). In the estuarine reaches of Broughton Creek, salinity is substantially reduced by floodwaters and by intermittent openings of Shoalhaven Heads. Since 1822, however, much of the flow of the Shoalhaven River has been diverted through Crookhaven Heads, via Berry's Canal.

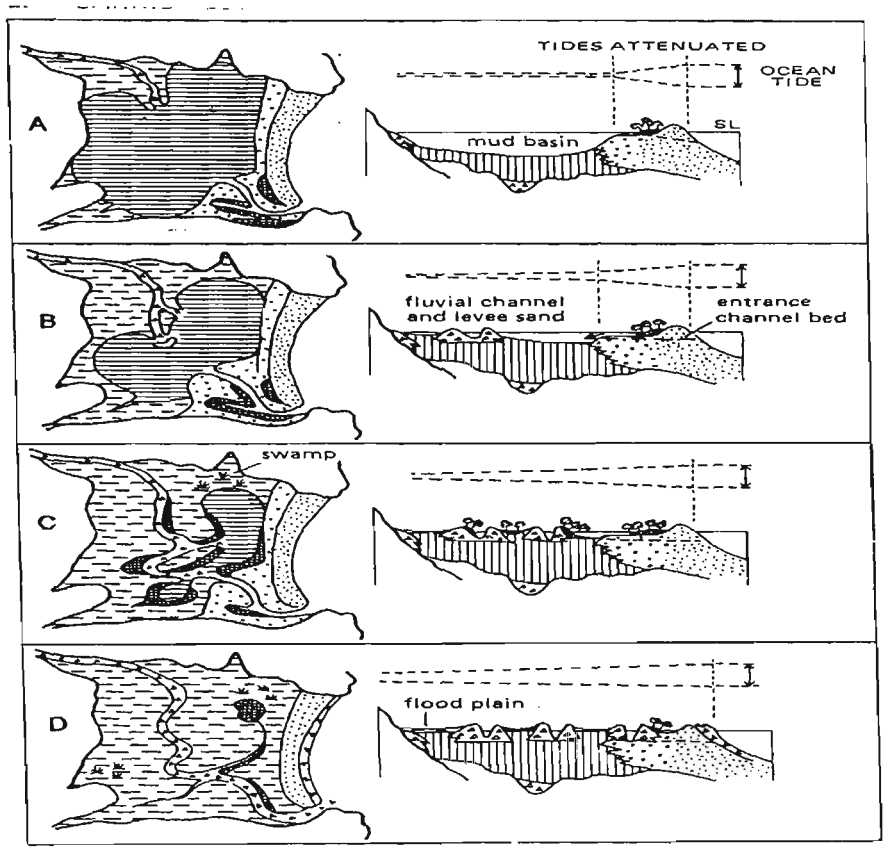

Figure 3.4 Evolution of the lower Shoalhaven River catchment with tidal characteristics (after Roy, 1984).

The presence of pyritic sediments in the Shoalhaven River, and Broughton Creek in particular, reflects their geomorphologic and palaeoecology evolution. According to the ASS risk maps described by Naylor *et al.* (1995), approximately 2500 ha of land with high risk of ASS occurrence are found in the Broughton Creek floodplain. In recognition of the large-scale deposition of ASS, the NSW Department of Land and Water Conservation has nominated Broughton Creek as one of seven ASS Hotspots in NSW. The distribution and location of ASS in the Broughton Creek Hotspot are shown in Figure 3.5.

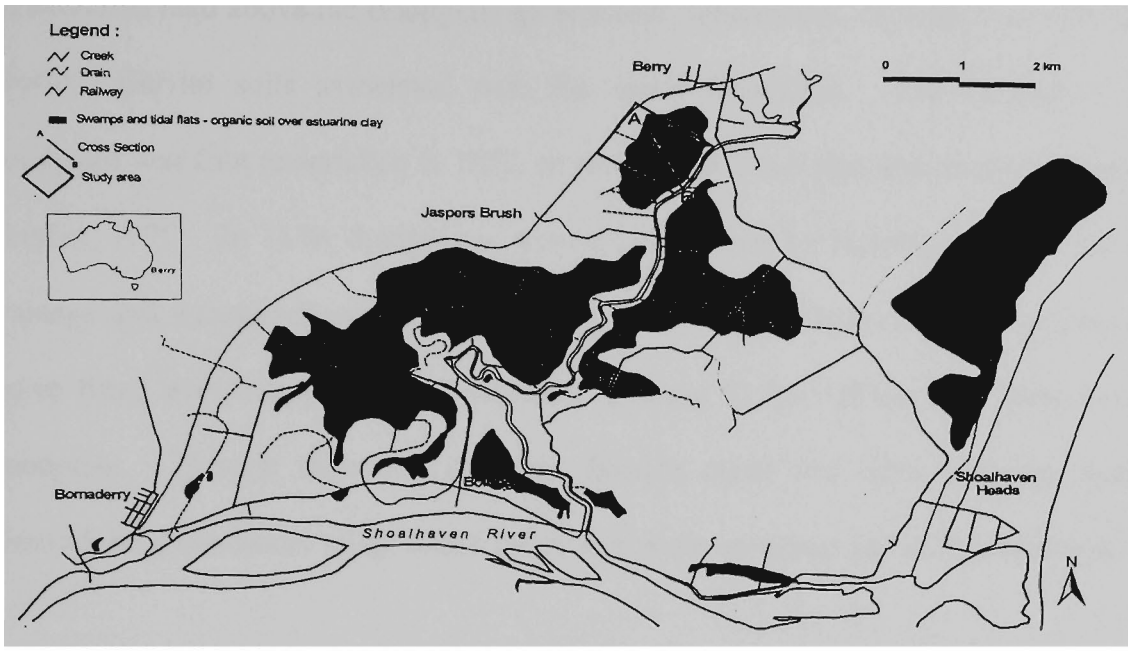

Figure 3.5 Location and distribution of acid sulphate soils along Broughton Creek.

3.2.2 History and evolution of flood mitigation in the Shoalhaven region

Prior to flood mitigation works, the area west of Broughton Creek was referred to as a 'large, continuous swamp' (Bayley, 1975). The first major works to alter creek hydrology in the Shoalhaven Region was the construction of Berry's Canal, commenced in 1840, which enabled the Shoalhaven River to discharge via the stable Crookhaven Heads. Anecdotal evidence suggests that the canal increased drainage and consequently, floodwaters in the 1860s and 1870s were said to recede faster. However, artificial drainage did not begin in earnest until the introduction of a 'tenant farming policy'. To promote development, this policy allocated twenty acre plots rent free on the condition they were cleared, fenced, and drained by the end of the two to five year lease (Bayley, 1975). By 1850, tenant farmers had established dairying as the primary industry of the Shoalhaven region.

As available land above the floodplain grew scarce, landholders attempted to utilise the "fertile" alluvial soils associated with the lower floodplain. The installation of floodgates was first undertaken in 1872, to restrict salt water that had threatened farms (Bayley, 1975). In 1879, dredging of Crookhaven Heads by bullock teams improved drainage and lessened flood damage. By 1901, landholders had installed 210 kms of drains fitted with floodgates and headwalls, draining 32 km^2 of the Broughton Creek floodplain. Through improved drainage, Berry's canal and other drainage works lowered the groundwater table, which promoted pyrite oxidation and acid production.

The network of flood mitigation drains in place today was mainly completed by 1949, although additional straightening, deepening and floodgating of the drains occurred from 1965-1972, in accordance with flood mitigation policy and funding. During this period, nineteen major drainage discharge points (18 with floodgates), as well as several minor drains, were upgraded and expanded on the Broughton Creek floodplain. Major drainage networks were installed using draglines (approximately 10 m wide) and drain inverts were set at –4 ft KAZI datum (20 centimetres below Australian Height Datum). While not standardised, drainage density across the floodplain is 0.0575 km/h, with 230 km of drains found on 4000 h of land prone to inundation (Pease, 1994). No additional major civil works or floodgate installations have been undertaken since 1972 (J. Downey, personnel communication), however, regular drain and floodgate maintenance (i.e. mechanical weed control) preserves the hydraulic efficiency of the drainage network. The flood mitigation drain located at the study site is shown in Figure 3.6.

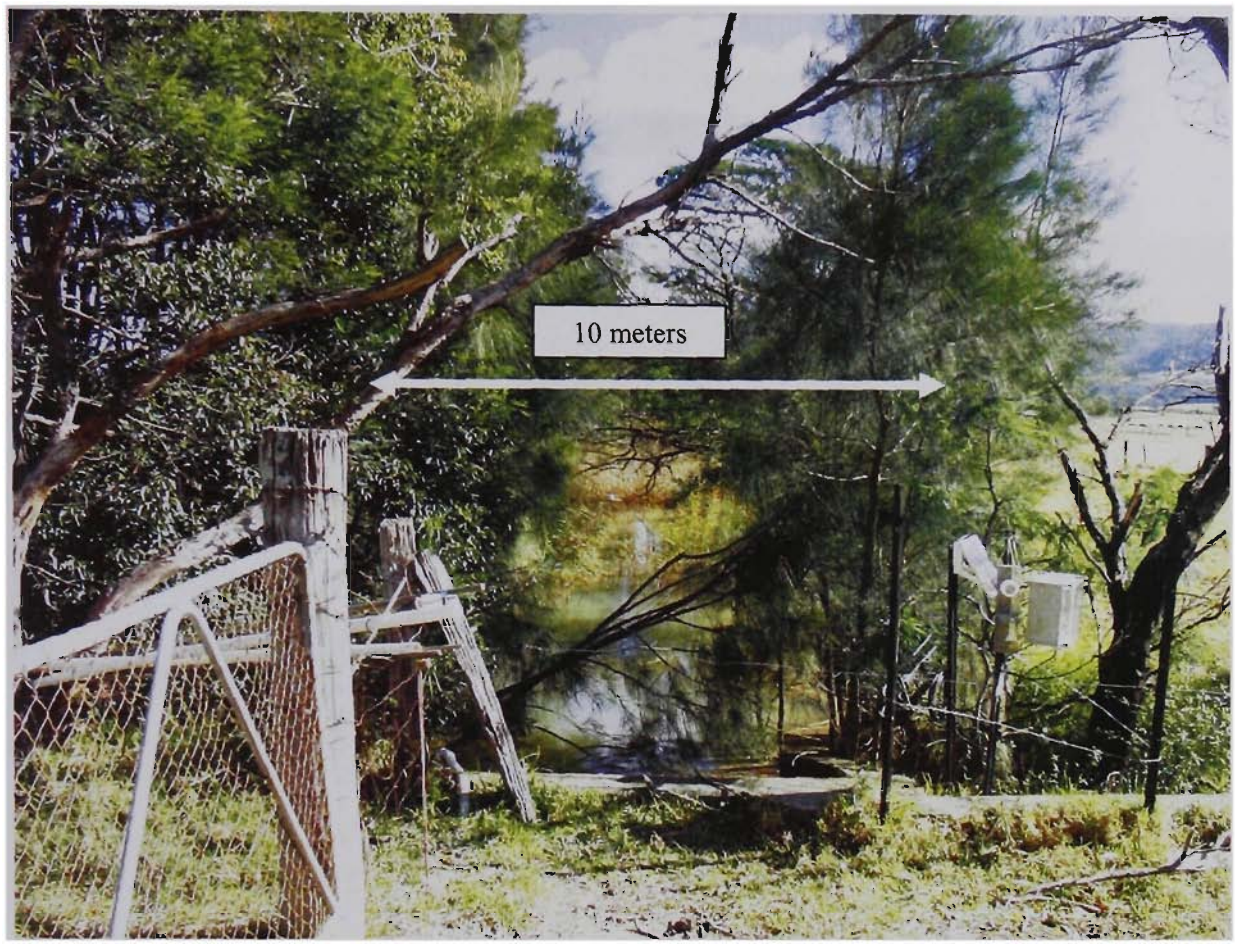

Figure 3.6 Picture of study site drain looking upstream from the floodgate. Drain width is approximately 10 m.

Tidal-restricting floodgates across the Broughton Creek floodplain range in size and capacity. Most consist of a battery of 1-4 concrete culverts (2 m x 2 m) with a top-hinged tidal restricting steel plate. A rubber seal, affixed to the back of the steel plate to create a compression seal between the headwall and the steel plate, minimises leakage. Nonetheless, as noted earlier Pease (1995) and Blunden (2000) noted minor leakage upstream of a floodgate when debris became jammed between the floodgate and the headwall, or when the rubber seal deteriorated. Several other floodgate styles are found in the Broughton Creek catchment, but are primarily smaller structures built on mole drains (i.e. circular gates attached to underground pipes) and function on the same hydraulic principles as larger gates. A selection of floodgates including those found at the study site is shown in Figure 3.7.

Figure 3.7 Typical tidal restricting floodgates installed on flood mitigation drains in the Broughton Creek estuary. Floodgates (a) and (c) are located at the study site. Floodgate (b) is the control floodgate located directly north of the study site.

Generally, the flood mitigation network installed on the Broughton Creek floodplain:

- Contain deep (~3 m) drains that efficiently remove surface and groundwater through straightened, cleared channels, increase the hydraulic gradient between the groundwater and the drain, and decrease the steady-state groundwater elevation.
- Contain one-way floodgates that eliminate tidal flushing within the flood mitigation drains, maintain the drain water level at the lowest downstream elevation (i.e., low tide), and quickly re-establish low drain water elevations following rainfall.

Assuming the pyritic (actual acid sulphate soil) layer is located at 0 m AHD, and the surface water level is maintained at low tide (approximately 1 m below the sulphidic layer), then the flood mitigation network increases acid production and transport. The low groundwater elevation enhances oxygen transport and, once generated, the strong hydraulic gradient created by the flood mitigation network assists in leaching the acid towards the drain. The hydraulic efficiency of the drain network quickly transports the acidic products into receiving waters, thereby causing environmental problems.

The geomorphology and soil characteristics of the Shoalhaven Floodplain and, particularly the Broughton Creek region, are typical of acid sulphate soil conditions throughout coastal NSW. The selected study site contains a pyritic layer approximately 1 m below the surface and a large flood mitigation drainage network (10 m wide x 3 m deep x 1500 m long) transects the site. Additional secondary drains (north-south direction) discharge into the primary drain (east-west direction), and contribute to its acid load. The primary drain contains a tidal restricting floodgate with two top-hinged

steel gates. Two additional control sites (one with a floodgate, one without a floodgate) were selected immediately north and south of the main drain. Figure 3.8 shows the location of the study site detailing the primary and secondary drains and the location of the control sites.

3.2.3 Study site elevation characteristics

A detailed survey was undertaken across Broughton Creek to evaluate floodplain topography in relation to ASS and to determine flow dynamics. High resolution airborne laser surveying (ALS), commisioned by the Shoalhaven City Council and composed by ESRI Australia, provided digital terrain maps that were interpolated to digital elevation maps (DEM) using ArcGIS. The topographical elevation data were related to the Australian Height Datum (AHD) and ground-truthing and benchmarking was accomplished via a handheld GPS device at all floodgates and weirs. A digital map of the Broughton Creek topography is shown in Figure 3.9.

Digital elevation maps (Figures 3.10) show that the surface topography of the study site is typical of ASS sites throughout NSW. Surface elevations in the catchment range from >4.0 m to <1.0 m AHD, and a levee bank, orientated in a north-south direction across the site, forms a ridge 1.5 m AHD that was created by the deposition of alluvial material from Broughton Creek. In the levee toe, surface elevations are between 1.0 m – 1.5 m AHD. The backswamp region starts approximately 100 m from the banks of Broughton Creek where elevations are less then 1.0 m AHD. From these maps, it is possible to recognise the relics of prior stream channels that were straightened and deepened during the construction of flood mitigation works.

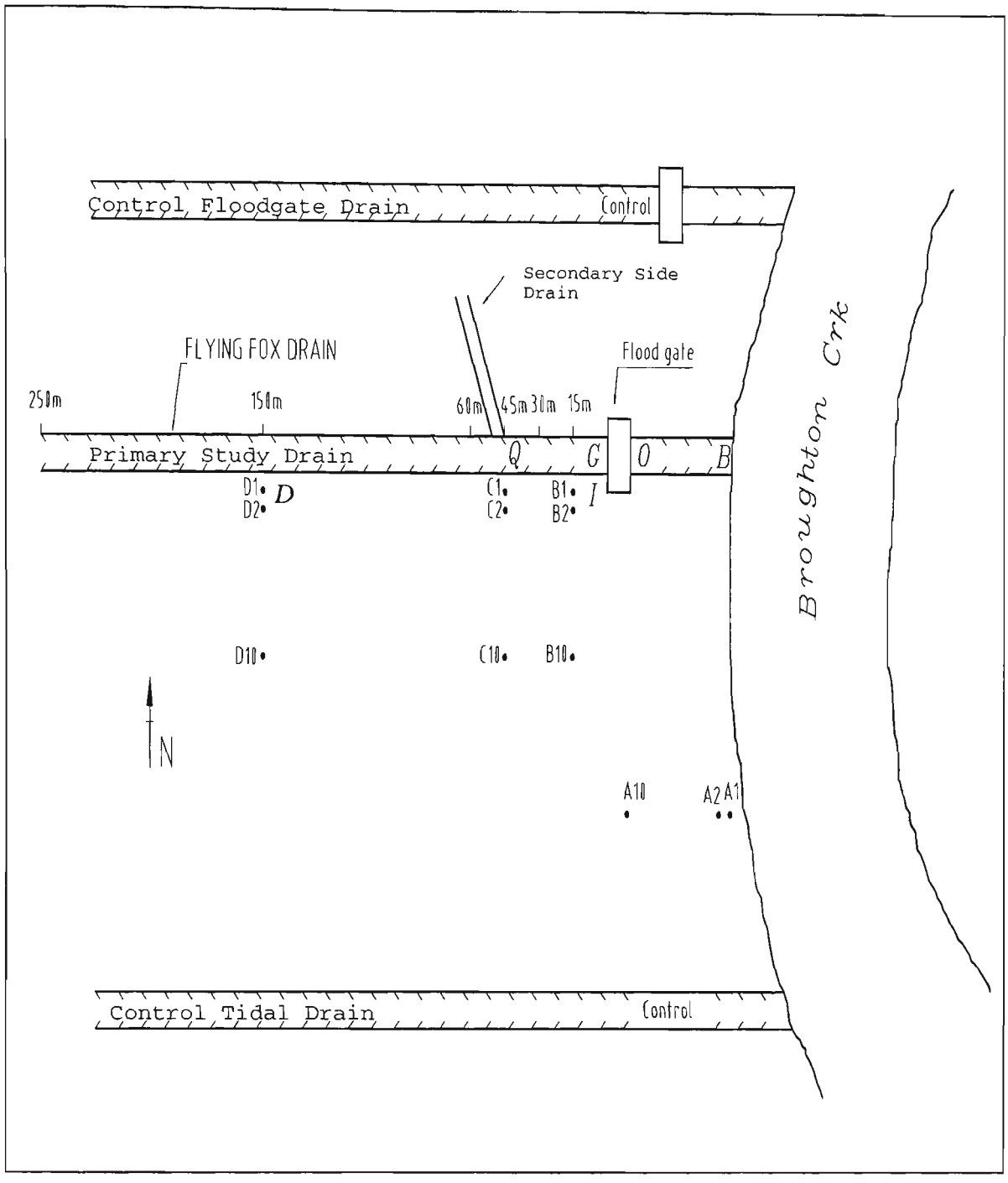

Figure 3.8 Location and description of the study site. Six dataloggers are labelled Q, G, O, B, D and I. Twelve observation bores are marked A1 – D10. Control drains are located north and south of the test drain.

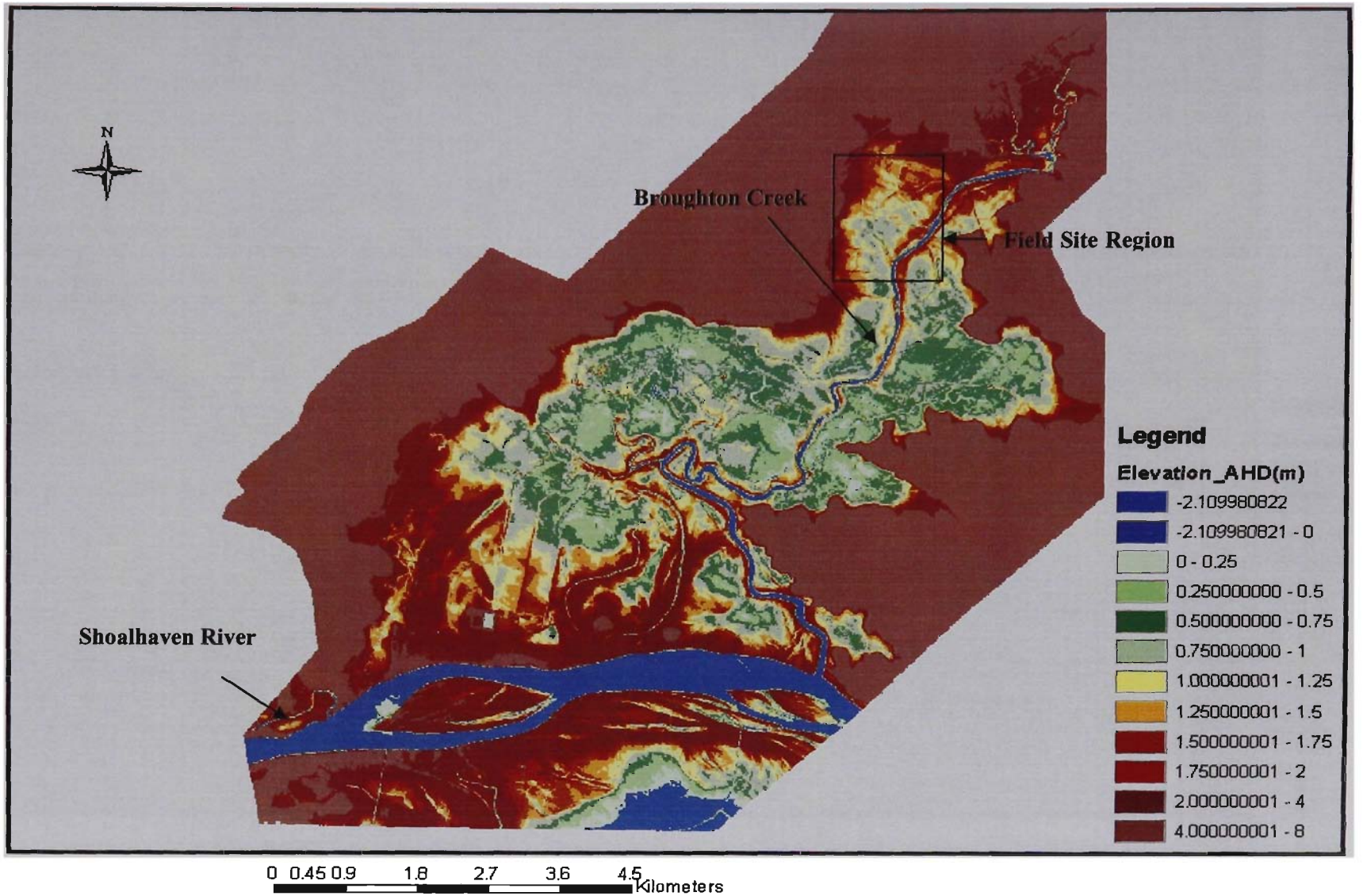

Figure 3.9 Digital Elevation Map (DEM) of the Broughton Creek floodplain.

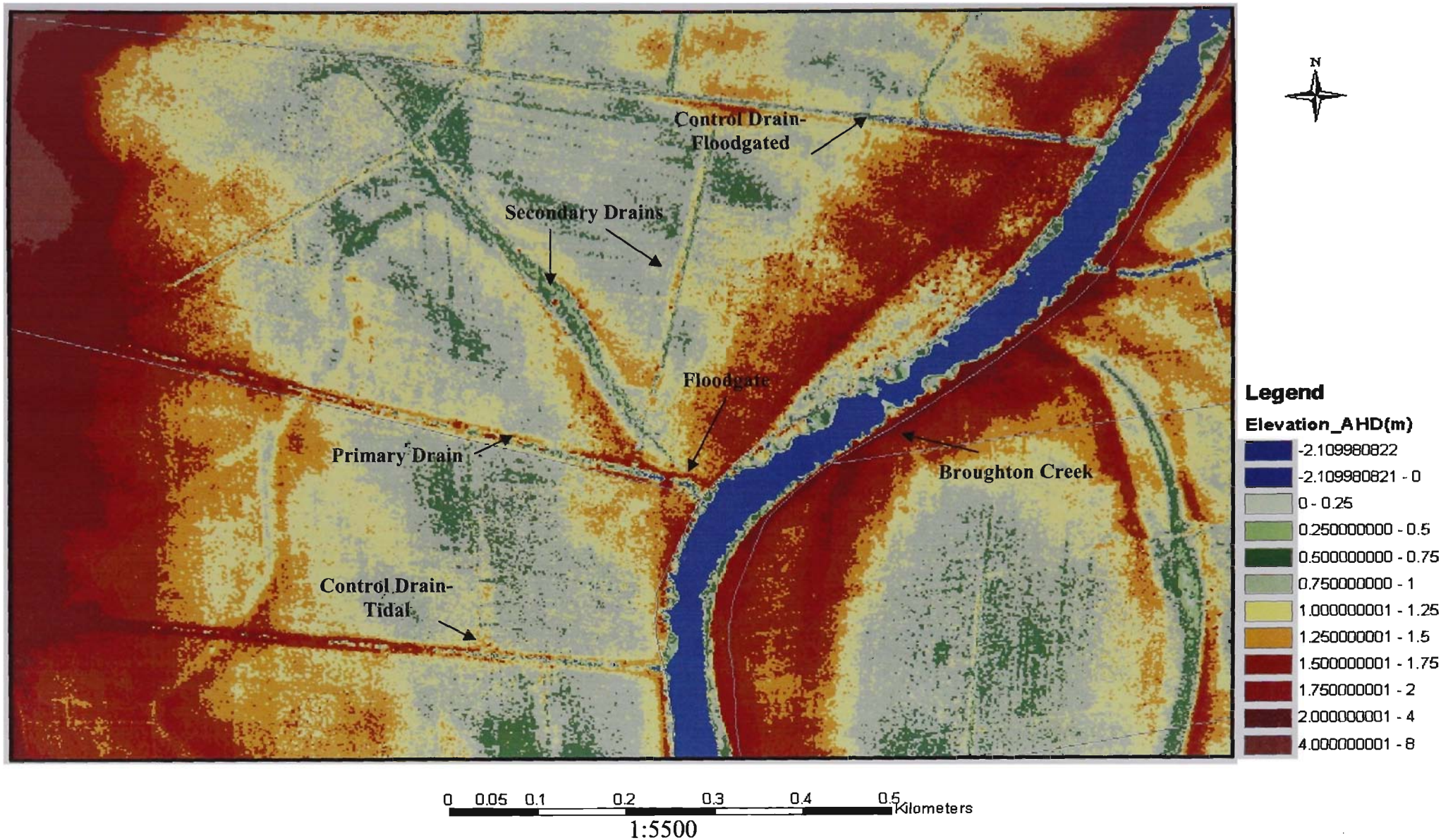

Figure 3.10 Digital elevation map of study site including control drains.

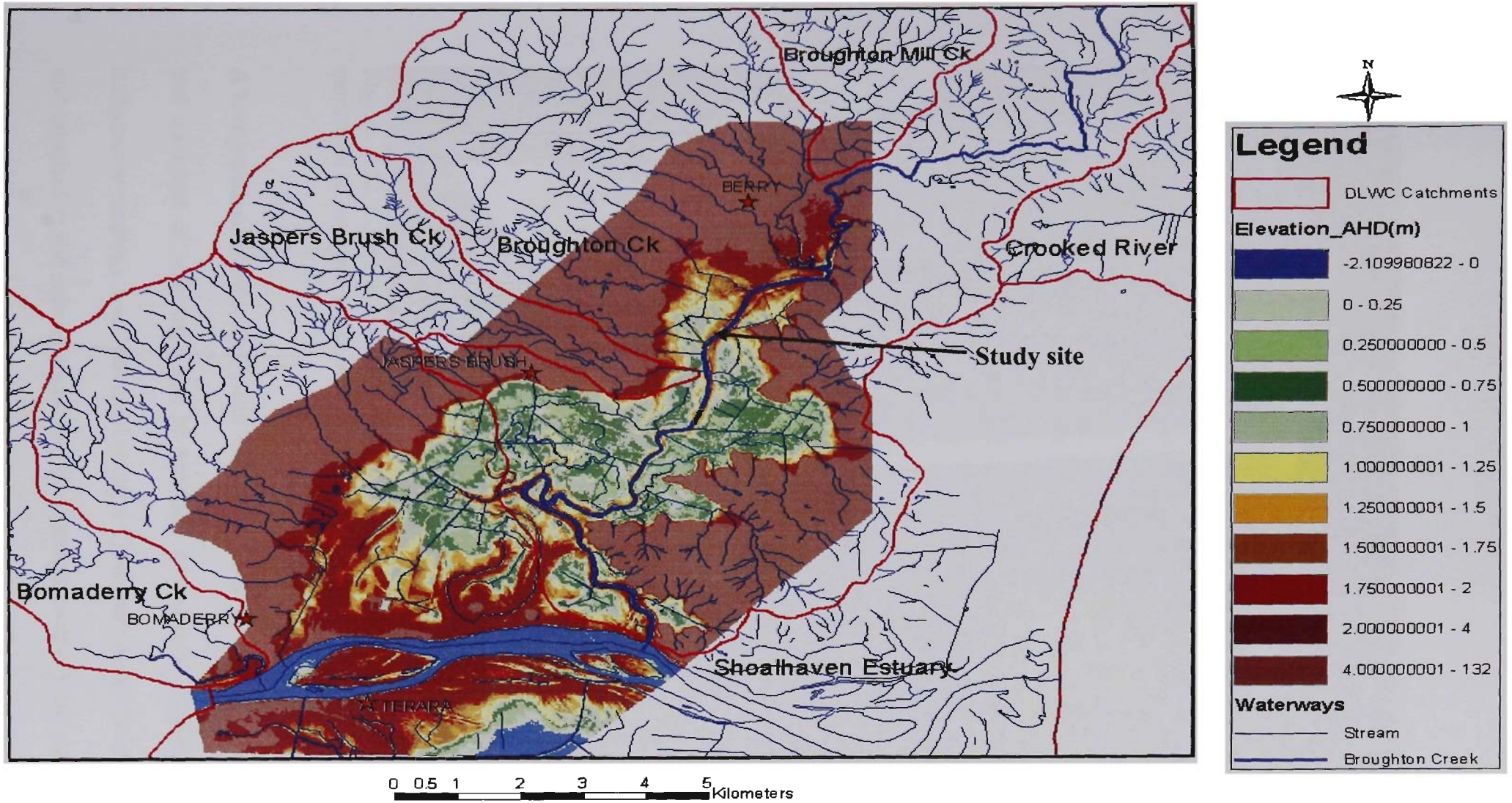

Figure 3.11 Catchment regions of the Broughton Creek floodplain (with elevation) as given by the Dept of Land and Water Conservation (1999).

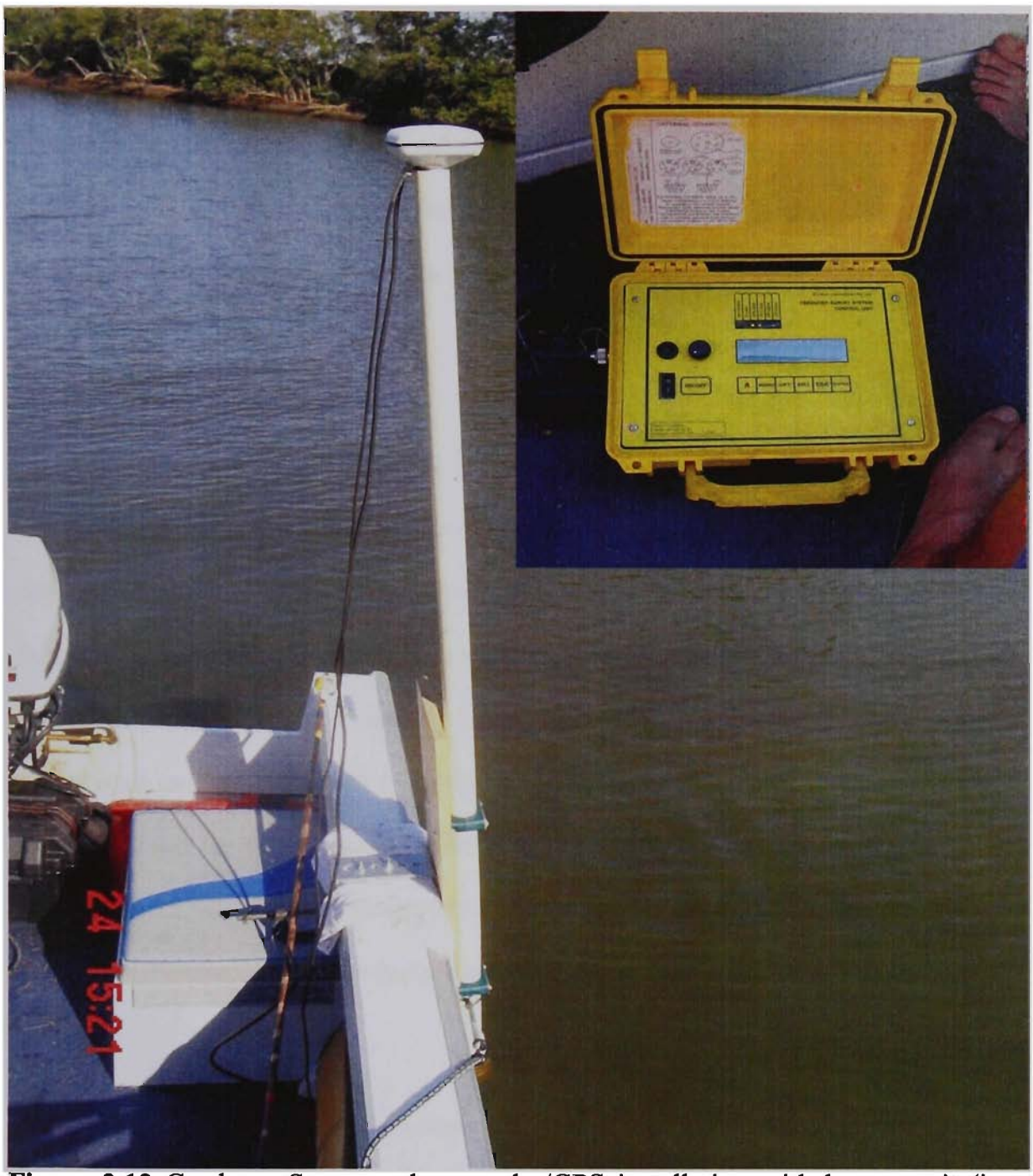

Figure 3.12 Ceeducer Survey echo-sounder/GPS installation with logger unit (insert) employed to measure creek bathymetry.

A comprehensive drain and creek bathymetry survey was conducted to simulate flow and transport of pollutants and to spatially model tidal flushing. Broughton Creek bathymetry readings were obtained using a Ceeducer survey control GPS/echo-sounder unit attached to the side of a boat and transported, over a 5 day period, in an 'S' shaped pattern along the length of the creek (Figure 3.12). The resultant data were filtered for errors, tidally corrected and adjusted for AHD, then processed through ArcGIS spatial

analyst and converted into raster format. A cross-section of the bathymetry results and their impact on hydrological conditions are described in Chapter 7. Due to the inaccessibility of the study site's flood mitigation drain, invert levels were taken with a handheld GPS unit every 25 m. The drain profile was then converted into a raster format and imported into the DEM for spatial analysis.

3.3 Field equipment and monitoring

A comprehensive monitoring program was conducted at the field site to investigate the relationship between drain and groundwater elevation and water quality before and after floodgates modifications. Monitoring of the drain and Broughton Creek hydrological conditions (i.e. flow rates and discharge) was also carried out. The monitoring program commenced on 2 January 2000 following the establishment of surface water sampling sites and lasted for 908 days. Baseline surface and groundwater data were collected until floodgate modifications occurred on 30 October 2000. Two control drain sites were also monitored for various surface water quality indicators throughout the project.

3.3.1 Surface and groundwater monitoring sites

Drain and groundwater sites were selected to provide a comprehensive understanding of the surface and sub-surface hydrochemistry of the site, whilst emphasising the region closest to the floodgate where significant saline and drain water mixing occurs. Surface water sites were selected at 1 m, 15 m, 30 m, 45 m, 60 m, and 250 m upstream of the floodgate, and at 1 m and 100 m downstream of the floodgate. Additional surface water samples were taken from a secondary drain, which discharged into the main drain, and from two control sites (see Figure 3.8). Within the floodgated control drain, samples

were taken 1 m and 250 m upstream of the floodgate and 1 m downstream of the floodgate. Within the non-floodgated control drain, surface water samples were taken 250 m upstream of the Broughton Creek/drain junction.

Surface water samples were collected from the middle of the drain in acid washed polyethylene plastic containers supplied by the NSW Environment Protection Authority. The bottles were rinsed 3 times with sample water and lowered through the water column using an elongated sampling pole. After collection, samples were immediately stored at 4°C until laboratory analysis. Surface water pH, salinity and alkalinity were measured in the field on a weekly basis and basic cations (Ca^{2+}, Mg^{2+}, Na^{+}, K^{+}), acidic cations (Al^{3+} and Fe^{2+}), and anions (Cl^{-} and SO_4^{2-}) were determined monthly.

Twelve observation bores arranged in 4 transects (Figure 3.8) were installed at the site to monitor the influence of floodgate manipulations on groundwater elevation and water quality. Three transects were located perpendicular to the adjacent flood mitigation drain, and one control transect was perpendicular to Broughton Creek. As the observation bores were designed to measure the fluctuations in the phreatic zone due to tidal flushing and the impact of altered drain water conditions on groundwater quality nearest the drain, the observation bores within each transect were spaced 1 m, 2 m, and 10 m from the drain/creek. Bore spacing was also dependent on the lateral hydraulic conductivity values measured during extensive soil testing in the area by Blunden and Indraratna (2000). Each transect was labelled with a letter (A-D) with individual bores within a transect identified by their distance from the drain (i.e., A1, B2, D10, etc.). The location of the observation bores at the study site is shown in Figure 3.8. An

additional transect of multi-port piezometers was installed at transect E and is further described in Chapter 8.

The observation bores were constructed using 2 m long, 50 mm external diameter, PVC pipes. Each unit was slotted, wrapped in geo-textile material and fitted with a PVC cap at the bottom. The distance from the drain was measured with a 100 m tape, and a 2.5 m deep well was drilled using the NSW Agriculture's Proline drill rig fitted with a 50 mm gouge auger. After drilling, a small amount of sand was placed at the bottom of the hole, the bore was forcefully placed into the well at ground level, and any space between the hole and the bore was then backfilled with previously removed soil. The snug fit of the observation bores and the swelling characteristics of the clay minimised seepage around the outside of the bore, which were capped in the field when not in use. Finally, the elevation of each bore was surveyed from known benchmarks using a total station survey level. Two 100 mm observation bores were constructed using the same method at B1 and D1 for installation of submersible data loggers.

Throughout the study period, the groundwater elevation of each bore was monitored weekly (every 6-10 days). Sampling was conducted by first inserting a rigid "plopper" made from a 2.5 m length of 10 mm rod. A PVC cone was affixed 100 mm from the end of the rod and, when lowered into the groundwater table, a 'plopping' sound could easily be heard. The distance from the groundwater table to the top of the bore was then read via a steel measuring tape attached to the rod; the distance was later converted to m AHD.

To obtain groundwater samples, a bailer was made from 1.5 m lengths of PVC pipe. The bailer was fitted with a 20 mm outlet to one end and a 25 mm stainless steel ball bearing was placed inside. When the bailer was lowered into the bore, water pressure pushed the ball bearing away from the hole and the bailer filled with water. After a few seconds, the ball bearing fell to the bottom of the bailer and formed a barrier. The bailer could then be removed and emptied into an acid washed sample bottle for testing. In this manner, pH and salinity were monitored weekly in the field and, following storage at 4°C, Cl^- and SO_4^{2-} concentrations were determined monthly in the laboratory.

Salinity and pH were measured in the field using a TPS WP-81 handheld probe that automatically compensated for temperature. The probes were calibrated before use with standard pH and salinity buffers, typically 4.0 and 6.88 and 2.65 mS/cm, respectively. Water quality analyses were performed at the University of Wollongong's Environmental Engineering Laboratory using standard methods described by Easton *et al.* (1995).

A brief description of the sample preparation and testing methodology is given below. Cations (Ca^{2+}, Mg^{2+}, Na^+, K^+, Al^{3+} and Fe^{2+}) were initially digested with concentrated nitric acid to dissolve any metal cations that formed complex ions or chemicals with organic matter and/or precipitated during storage. The samples were filtered through a 0.40-0.45 μm polycarbonate membrane to remove particulates and the metals were then measured using Atomic Absorption Spectrometry (AAS) under the appropriate wavelength and ion specific hallow cathode lamp.

Anion (Cl^- and SO_4^{2-}) samples were initially filtered through a 0.40-0.45 μm polycarbonate membrane to remove particulates and the sample were determined by ion chromatography with chemical suppression of eluent conductivity. The testing method IIC_A01 is fully described by Easton *et al.* (1995).

Alkalinity levels were determined through acid titration. A 200 ml aliquot of sample was titrated against 0.02M HCl^- until the known pH endpoint was reached (i.e., 4.5). To determine alkalinity in mg L^{-1}, the amount of acid titrated is multiplied by 50040, then multiplied by the molarity of the acid and divided by the quantity of the original sample. To obtain mg L^{-1} of bicarbonate, the product is multiplied by 1.219.

All results reported in mg L^{-1} were converted to mmol L^{-1} using appropriate stoichiometric conversions.

3.3.2 Water quality monitoring

Continuous monitoring of the surface and groundwater chemistry of the study site was conducted by four (three within the creek, one in the groundwater) Submersible Data Loggers (SDL) (Greenspan model CTDP300) that recorded pH, salinity, temperature and water height. Additionally, an SDL (Greenspan model CS304), located at the Broughton Creek-Flying Fox Creek junction, measured pH, salinity, dissolved oxygen (DO) and temperature. A sixth SDL (Greenspan model PS300) that solely measured water height was located in observation bore D1.

The SDLs were programmed to record at 1 hour intervals and were powered by a 12V gel cell battery recharged every 6 weeks. All sensors were downloaded monthly and

recalibrated, if necessary, every 8 weeks. Due to high levels of iron flocculation in the water column, the DO probe required additional maintenance every fortnight in order to maintain the porous membrane through which oxygen permeates. The SDLs were suspended in the middle of the channel, affixed to the floodgate's concrete headwall, or lowered down an observation bore (Figure 3.13). The elevation of each sensor was surveyed and the water height data was corrected to elevation in m AHD. At three sites, continuous water quality monitoring was interrupted when cows chewed through the logger's cable. On these occasions, the SDL was returned to the manufacturer for repairs and then reinstalled at the site. Nonetheless, the large amount of information obtained throughout the monitoring period provided data at a resolution never before obtained at an ASS landscape.

Two submersible ultrasonic Doppler bi-directional Flow Loggers (SFL) (Unidata's Starflow Instrument #6526-51) performed continuous monitoring of the drain and creeks flow regime. The SFLs were affixed to the bottom of Flying Fox Creek (directly upstream of the floodgate) and within Broughton Creek (approx. 1.5 k upstream of Flying Fox Creek) to record water height and velocity at 20-minute intervals. The readings were used to calculate discharge based on the cross-sectional area of the creek or drain. A 12V gel cell battery, recharged via a BP Solarex solar panel, powered the units and, if necessary, the SFLs were downloaded and calibrated monthly.

A Campbell Weatherwatch 2000 weather station was installed on elevated land approximately 700 m west of the site to continuously monitor climatic conditions. The weatherstation was mounted on a 3 m aluminium, lightning protected tower in excess of 100 m from the closest structure and measured temperature, humidity, wind speed, wind

direction, rainfall and solar radiation. The hourly measurements were stored on a CR10X data logger secured to the tower. The downloaded data provided various reports of the meteorological conditions, including the calculated Penman-Monteith evapotranspiration.

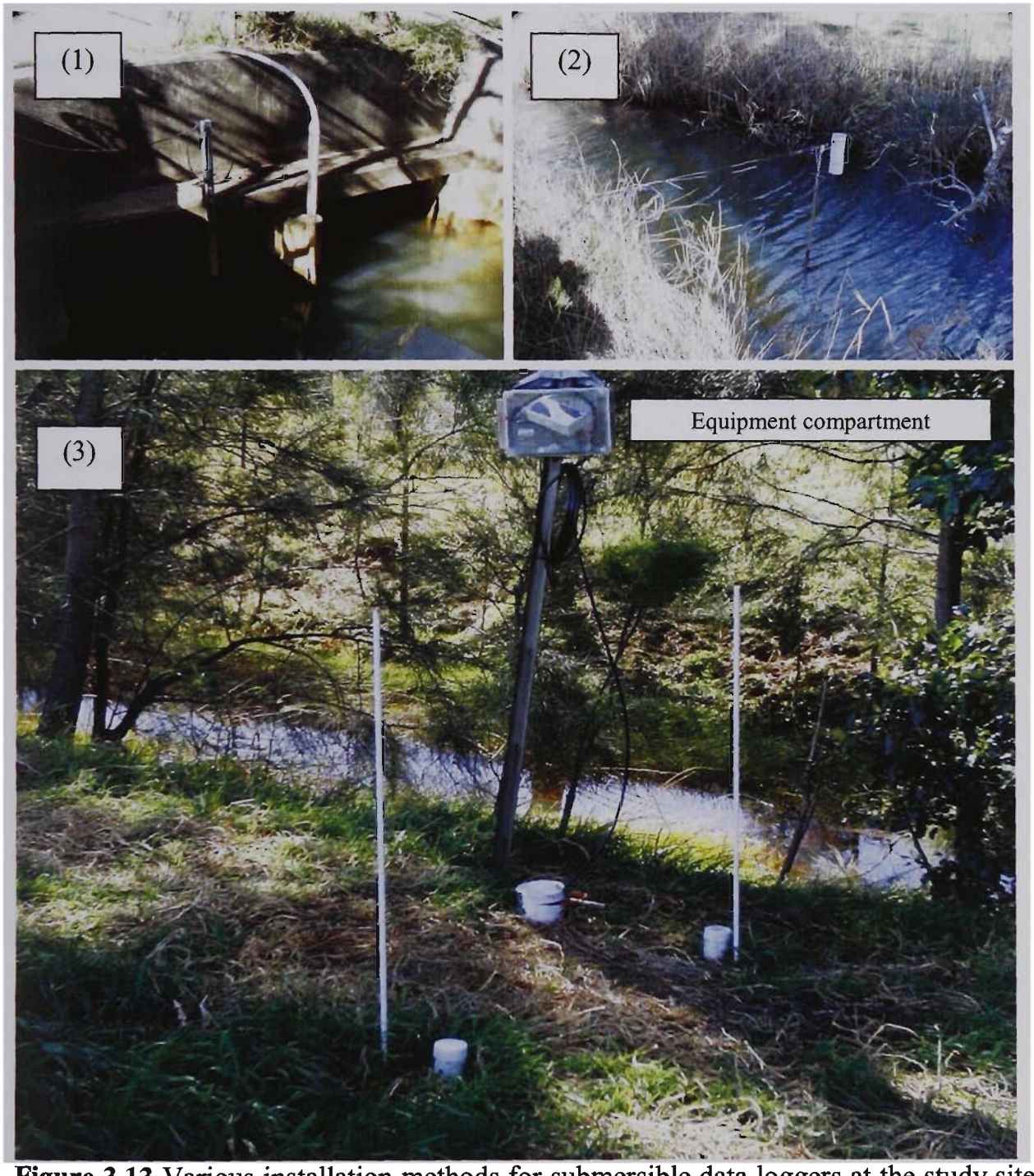

Figure 3.13 Various installation methods for submersible data loggers at the study site. In method (1), the data logger is affixed to the floodgate headwall to measure pressure. To calculate mid-water readings (2), the data logger was hung from a cable suspended across the drain. In groundwater situations (3), the data logger is lowered down a observation bore. The equipment compartment shown in (3) is typical of all data logger installations.

3.4 Climatic conditions: Implications for research

The successful management of acid sulphate soils via floodgate manipulation is reliant on a consistent supply of non-anthropogenic buffering agents. The concentration of buffering agents at any point within an estuary is complex but mainly reliant on tidal dynamics and forces of dispersion within the estuary. Furthermore, the tidal dynamics or tidal reach is largely dependent on the quantity of upland inflow discharging into the estuary, which is determined by varying amounts of rainfall/evapotranspiration in the sub-catchments. Therefore, the concentration of buffering agents within the tidal estuary is directly related to the rainfall/evapotranspiration relationship.

The rainfall/evapotranspiration relationship is also an important factor in determining the elevation of the groundwater table in coastal floodplains. During prolonged dry periods, with high rates of evapotranspiration, the watertable can fall below the pyritic layer, thus increasing acid production. In areas with sufficient hydraulic conductivity, adjoining surface waters (i.e., drains, creeks and rivers) recharge the groundwater table. However, when evapotranspiration exceeds precipitation the salinity of these waters increases, yet the extent of saline intrusion into the soil matrix (discussed further in Chapter 8 and 9) is related to the magnitude and duration of dry periods. Conversely, following rainfall, natural groundwater recharge promotes the transport of acid products into drains/creeks, and leaches soluble salts from the soil matrix. For these reasons, successful management of acid sulphate soils requires a thorough understanding of the rainfall and evapotranspiration rates at the study site.

In this section, the climatic conditions of the site are shown for the duration of the study period. Rainfall and evapotranspiration data taken from the weatherstation are broken

down into two periods; (i) prior to floodgate modifications (Days 1-306) and (ii) proceeding floodgate modifications (Days 307-908). With this information, a comparison of rainfall abundance and distribution between the two periods is presented and discussed. Long-term rainfall and evapotranspiration records are compared with the obtained site data to determine climatic variations. Additional climatic information including solar radiation and wind speed is given in Appendix A.

3.5 Weather conditions at the site

Climatic conditions at the site varied with time but were consistent with long-term averages. Overall, the weather conditions were characteristic of temperate regions with short to moderate dry periods followed by moderate rainfalls. The conditions experienced during the field trials were consistent with previous research in the region (Pease, 1994; Blunden, 2000).

Best efforts were made to source climatic data as close as possible to the study site. Rainfall and evapotranspiration data was obtained from the weatherstation located at the site and described previously. Long-term average rainfall data was acquired from the University of Wollongong (Berry Campus) located approximately 1 km from the study site. Long-term evapotranspiration data was obtained from a Bureau of Meteorology weatherstation approximately 3 kms inland.

3.5.1 Rainfall

Daily rainfall at the study site before and after floodgate modifications is shown in Figures 3.14 and 3.15, respectively. Prior to floodgate modifications, rainfall at the site

was predominately grouped into three events; Days 59-82, 182-186 and 271-295. Before Day 59, a prolonged dry period existed with only 78.4 mm recorded. During Days 59-82, consistent strong precipitation led to 218.4 mm of rain falling within 23 days. This event caused widespread flooding and surface ponding persisted for more than 5 days. From Days 83-181, a prolonged dry period returned and less then 88 mm fell over the 98-day period. Rainfall of 57.4 mm during Days 182-186 caused minor surface ponding and increased creek levels, but was followed by a prolonged dry period with only 29.3 mm received from Day 187 to 270 (83 days). Towards the end of the pre-modification period (days 271-295), strong rainfall (84.9 mm) triggered moderate creek and surface flooding.

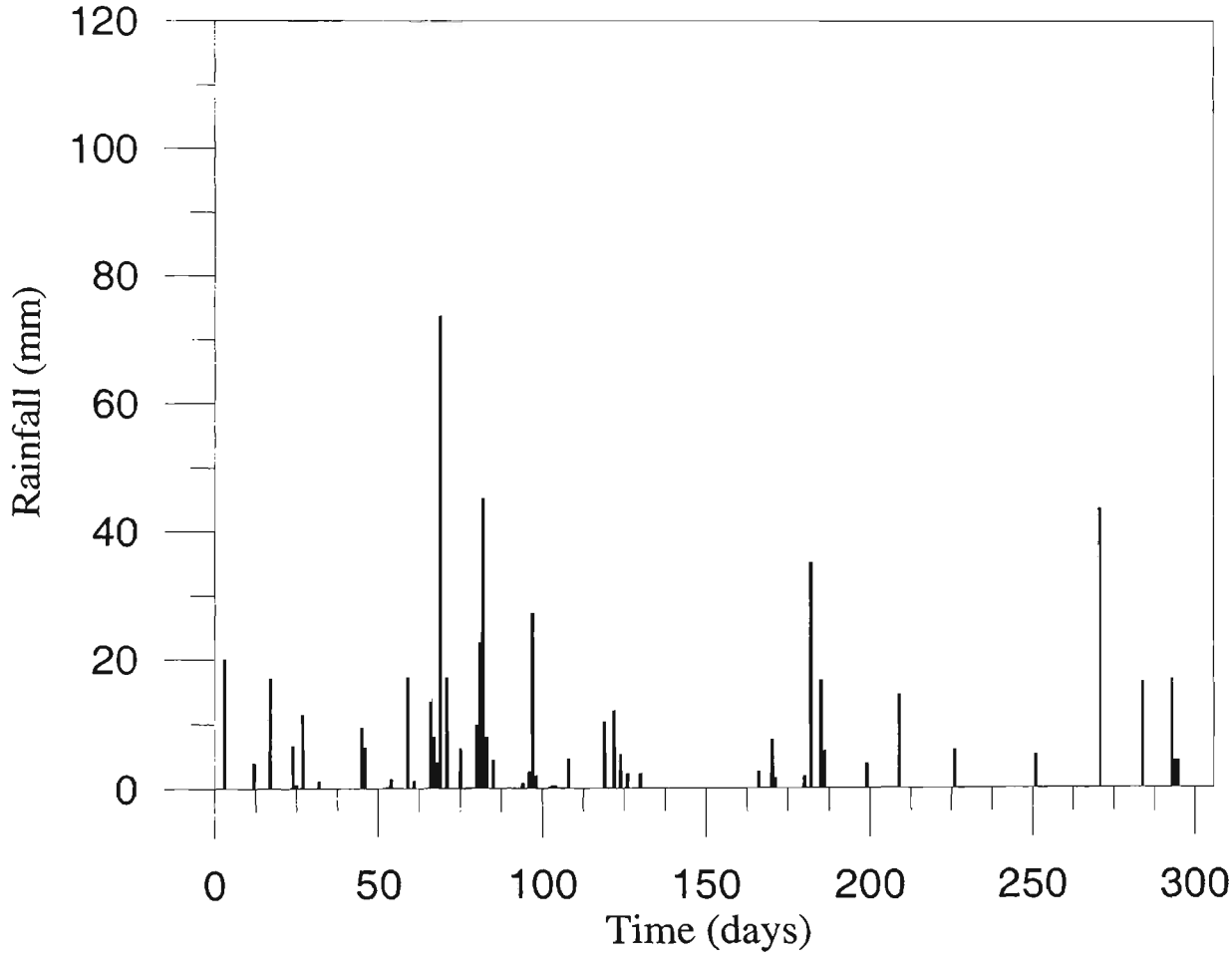

Figure 3.14 Rainfall at the study site prior to floodgate modifications.

From Figure 3.15, it is apparent that 5 major rainfall events occurred after floodgate modifications namely; Days 309-326 (203.8 mm), 397-407 (276.4 mm), 556-563 (120 mm), 747-773 (464.2 mm), and 811-821 (150.6 mm). During each of these events, creek and drain levels dramatically increased and surface flooding persisting for several days. Throughout the first three rainfall events, sufficient time existed between each event (69, 145, 182 days, respectively) to allow for the floodwaters to subside and drying conditions return. However, as there was only 36 days between the final two events, and minor rainfalls continued throughout, wet conditions persisted during the 72-day period.

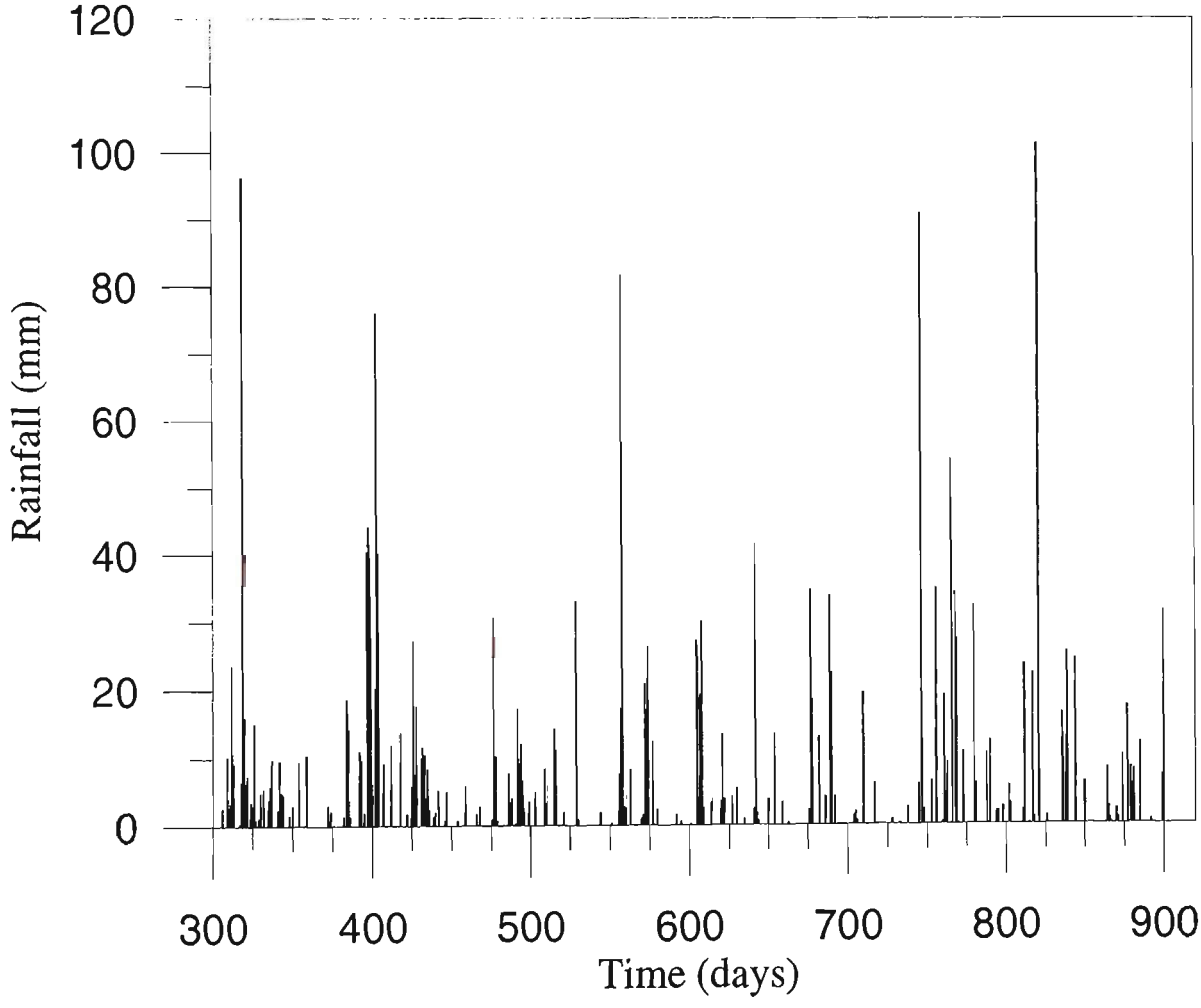

Figure 3.15 Rainfall at the study site following floodgate modifications.

The long-term average versus recorded monthly rainfall at the field site is shown in Figure 3.16. It is evident from this figure that average rainfall is generally consistent throughout the year, with minor summer dominance. In the first 300 days, rainfall was below average except for a long period of rainfall during the third month (March, 2000). The extended dry conditions coincide with the pre-modification period and depict drier than normal conditions before floodgate modifications.

Following floodgate modifications, rainfall at the site was close to average, however, both wet and dry conditions occurred. During this period, several rainfall events caused above average rainfall conditions on seven out of the 20 months. On two occasions (Day 403, February 2001 and Day 767, February 2002), these events caused large-scale flooding with surface ponding persisting for more than 5 days. Below average rainfall was also evident during the winter months of the study period, except for June 2001 where 106 mm fell over three days (556-558). The below average rainfall in the last three months of the study signified the beginning of an extended drought that lasted for more than 6 months. Indeed, this prolonged drought was the beginning of the driest period measured since records began.

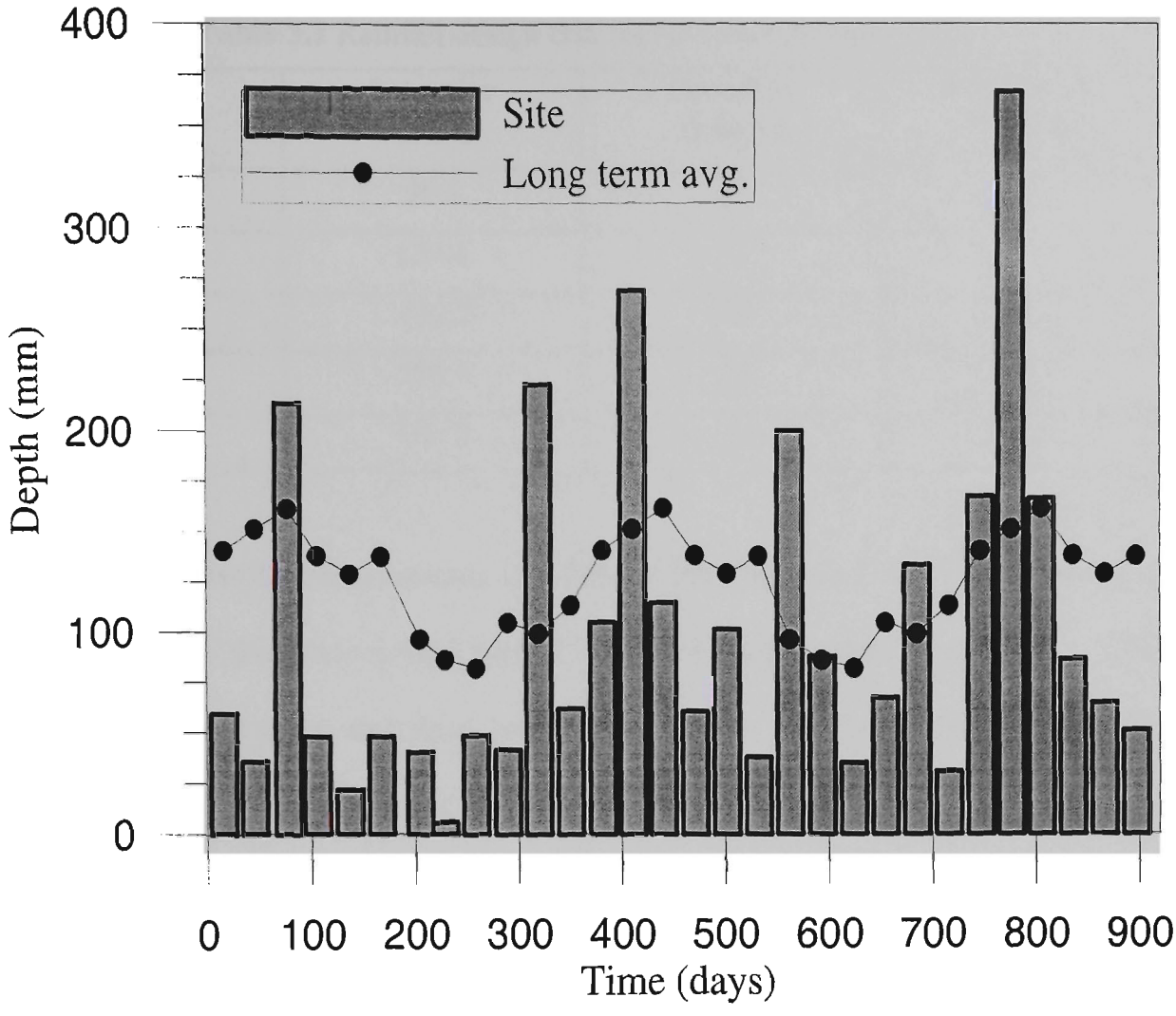

Figure 3.16 Rainfall at the study site versus the long-term average.

The calculated rainfall design criteria for major rainfall events during the study period are shown in Table 3.1. The majority of rainfall events received during the study were below the 1 year frequency interval and no 1 year events or greater were encountered before floodgate modifications. However, large sub-daily rainfall events that did occur may not have been detected because of the 24-hour rainfall intervals recorded by the weatherstation. Nonetheless, after modifications, several large storms were experienced which caused major flooding. Indeed, between days 766-768, a series of storms precipitated 258.4 mm over a 72-hour period, which coincides with a 5-year frequency interval. Within this rainfall event a 24 hour measurement of 170 mm equates to a 1 in 3 year storm event.

Table 3.1 Rainfall design criteria for major rainfall events.

Day	Intensity (mm)	Duration (hours)	Frequency (years)
319	96.2	24	1
402-404	136.6	72	1
767	170.2	24	3
766-768	258.4	72	5
821	101.2	24	1

The intensity-distribution-frequency calculations presented in Table 3.1 shows that for the majority of the study period typical environmental conditions prevailed. These conditions provided an excellent setting to test the tidal buffering theory and to determine the influence of saline intrusion on the soil matrix. Nevertheless, the above average rainfall events experienced towards the end of the study period offered important information on the efficiency and effectiveness of the modified floodgate design under extreme conditions.

In total, there were 255 rainfall events during the entire study period (908 days, minimum rainfall events calculated at 0.2 mm/day), with 54 events before and 201 events after floodgate modifications. This discrepancy between periods is partly because the pre-modification period was shorter then the post-modification period (306 days versus 601 days), but also because of the drier then normal pre-modification conditions. Overall, the number of rainfall events correlates well with similar length studies in the region (i.e. 233 rainfall events in 813 days for Blunden, 2000). Figures 3.17 and 3.18 show the distribution of rainfall by daily intensity for the pre- and post-modification period. In both figures, it is apparent that the majority of rainfall was less

than 5 mm/day (44% pre-modification and 47% post-modification) which is characteristic of temperate regions.

The major difference between rainfall intensity distributions before and after floodgate modifications is the high number of large rainfalls (>50 mm) that occurred during the post-modification period. For instance, in the pre-modification period there was only 1 rainfall greater then 50 mm, whereas after modifications there were 5 rainfall events between 50-100 mm and 2 over 100 mm. It is important to note that due to the relatively small and steep sub-catchments surrounding the study site, large daily rainfalls, such as those experienced during the post-modification period, can quickly discharge high quantities of water throughout the catchment which can lead to surface flooding and decreased drainage.

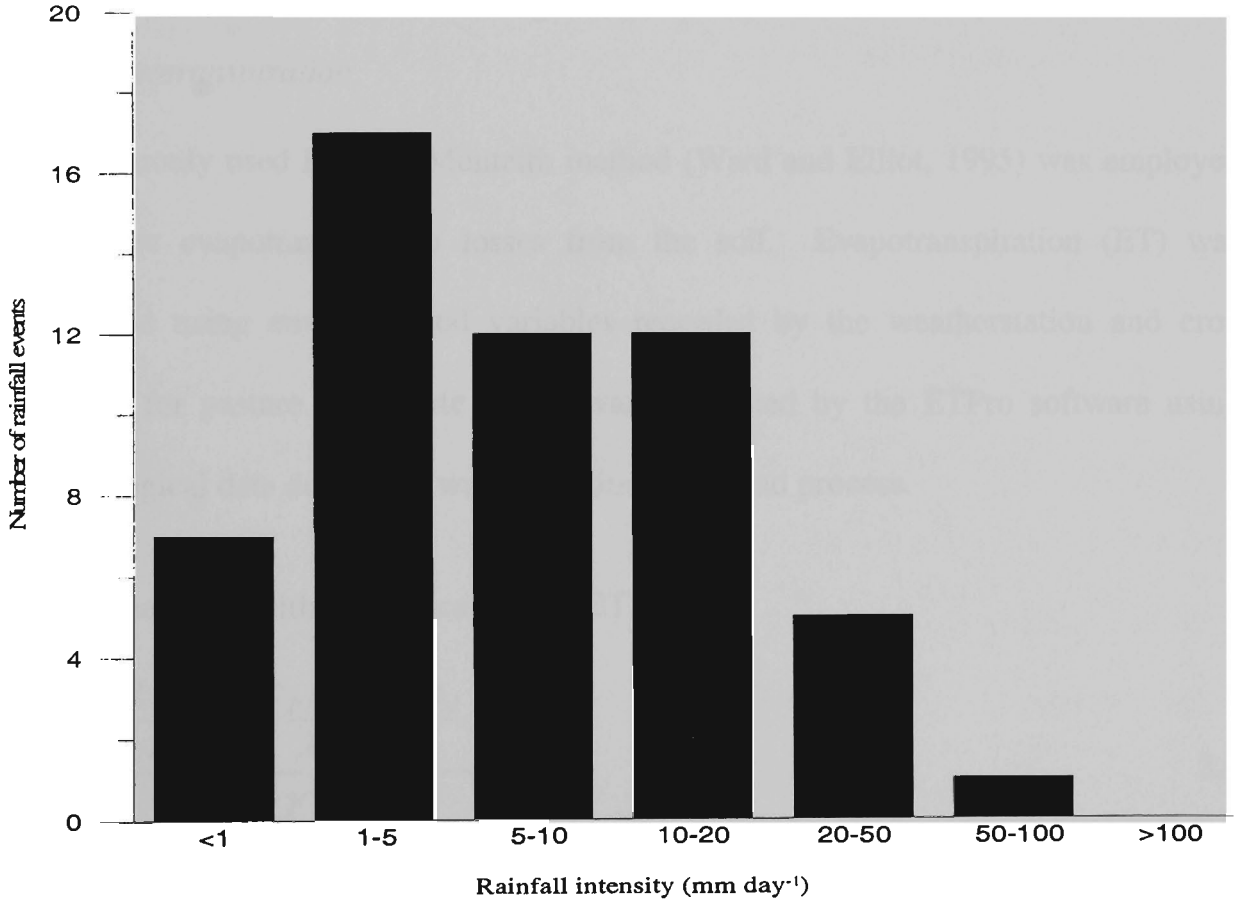

Figure 3.17 Rainfall intensity before floodgate modifications.

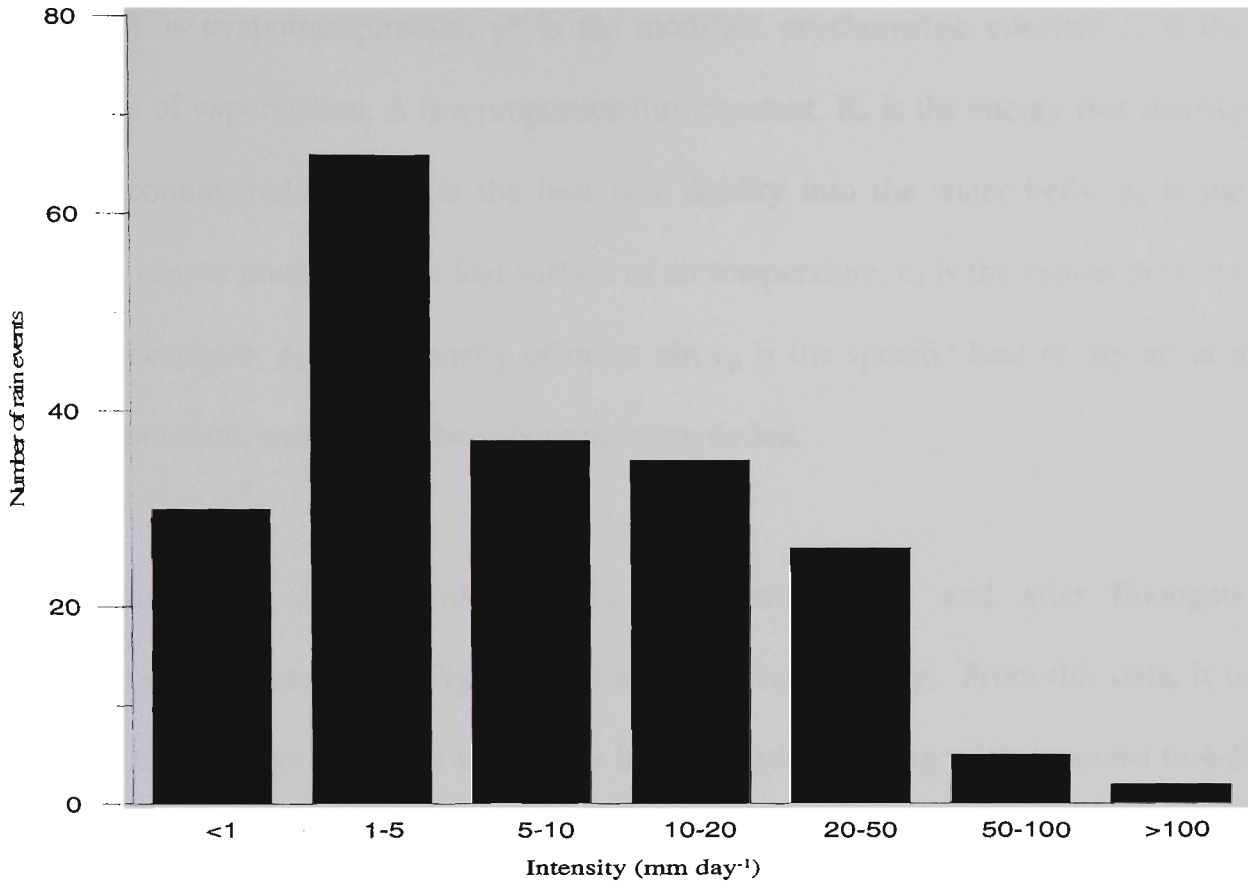

Figure 3.18 Rainfall intensity after floodgate modifications.

3.5.2 Evapotranspiration

The commonly used Penman-Monteith method (Ward and Elliot, 1995) was employed to measure evapotranspiration losses from the soil. Evapotranspiration (ET) was determined using environmental variables recorded by the weatherstation and crop constants for pasture. The rate of ET was calculated by the ETPro software using meteorological data during the weatherstation download process.

The Penman-Monteith method calculates ET as:

$$ET = \frac{\frac{\Delta(R_n - G)}{\lambda} + \frac{c_p \rho_a}{\lambda} \cdot \frac{e_a - e_d}{r_a}}{\Delta + \gamma^*} \qquad 3.1$$

where, ET is evapotranspiration, γ^* is the modified psychometric constant, λ is the latent heat of vaporisation, Δ is a proportionality constant, R_n is the energy flux density of net incoming radiation, G is the heat flux density into the water body, e_a is the saturated vapour pressure at the leaf surface of air temperature, e_d is the vapour pressure in the atmosphere, ρ_a is the density of moist air, c_p is the specific heat of dry air at a constant pressure, and e_a-e_d is the vapour pressure deficit.

Evapotranspiration data recorded at the study site before and after floodgate modifications is presented in Figures 3.19 and 3.20, respectively. From this data, it is apparent that average ET at the site ranges from 2 mm/day during winter months to 4-5 mm/day in summer months. Under extreme conditions, ET reached 8 mm/day during summer months due to elevated temperatures, increased solar radiation, low humidity and strong dry winds. Variances in daily rates were subject to changes in cloud cover (i.e., solar radiation), rainfall, humidity, and wind speed. While limited ET data exists for comparison, these findings are similar with those of Blunden (2000) taken from 1997-1999.

Long-term monthly average ET rates were similar to those found during the study period (Figure 3.21). It is apparent from this data, that two 'above average' ET periods existed both before (Days 83-181), and after (Days 584-647) modifications. However, it is important to consider that the long-term monthly average levels shown in Figure 3.21 were sourced from the Bureau of Meteorology Berry Mountain station, approximately 3 km west of the site and 250 m higher in elevation. The difference in elevation between the two sites may factor into the slightly higher than average rates

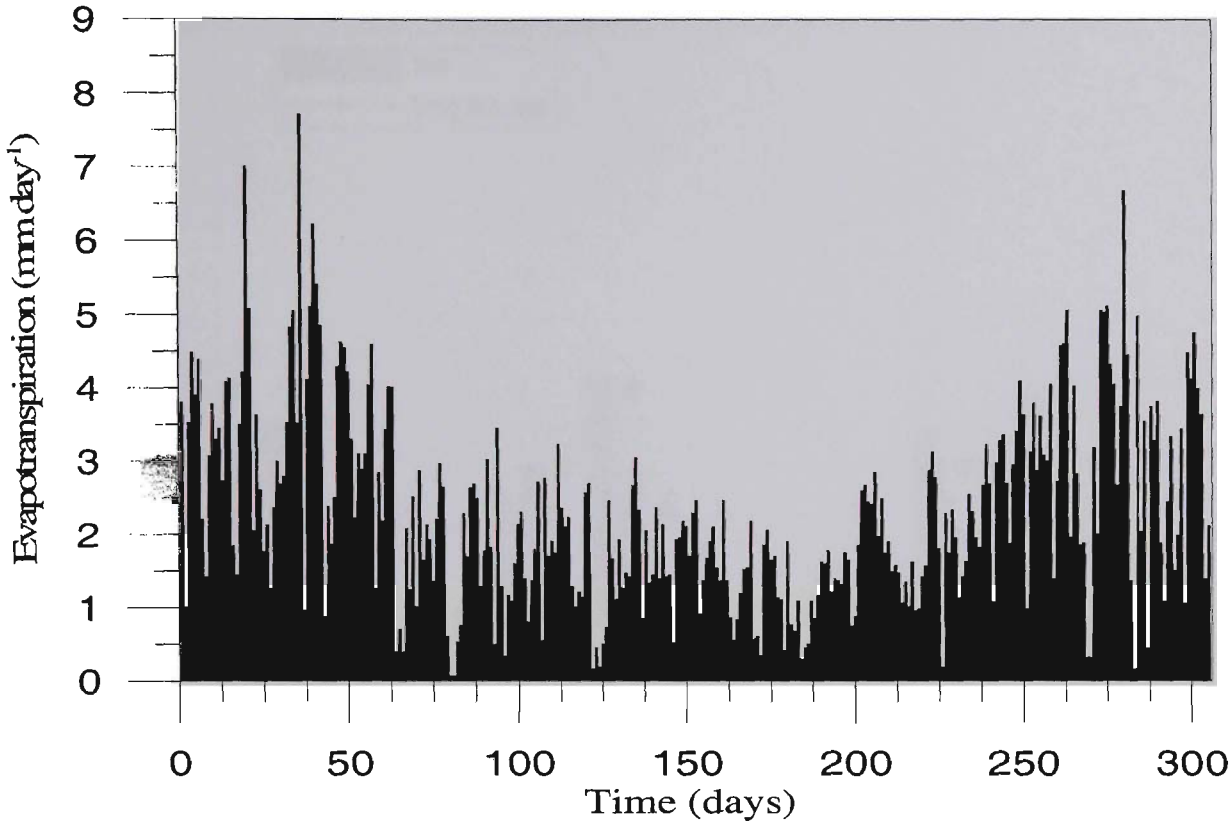

Figure 3.19 Evapotranspiration at the study site before floodgate modifications.

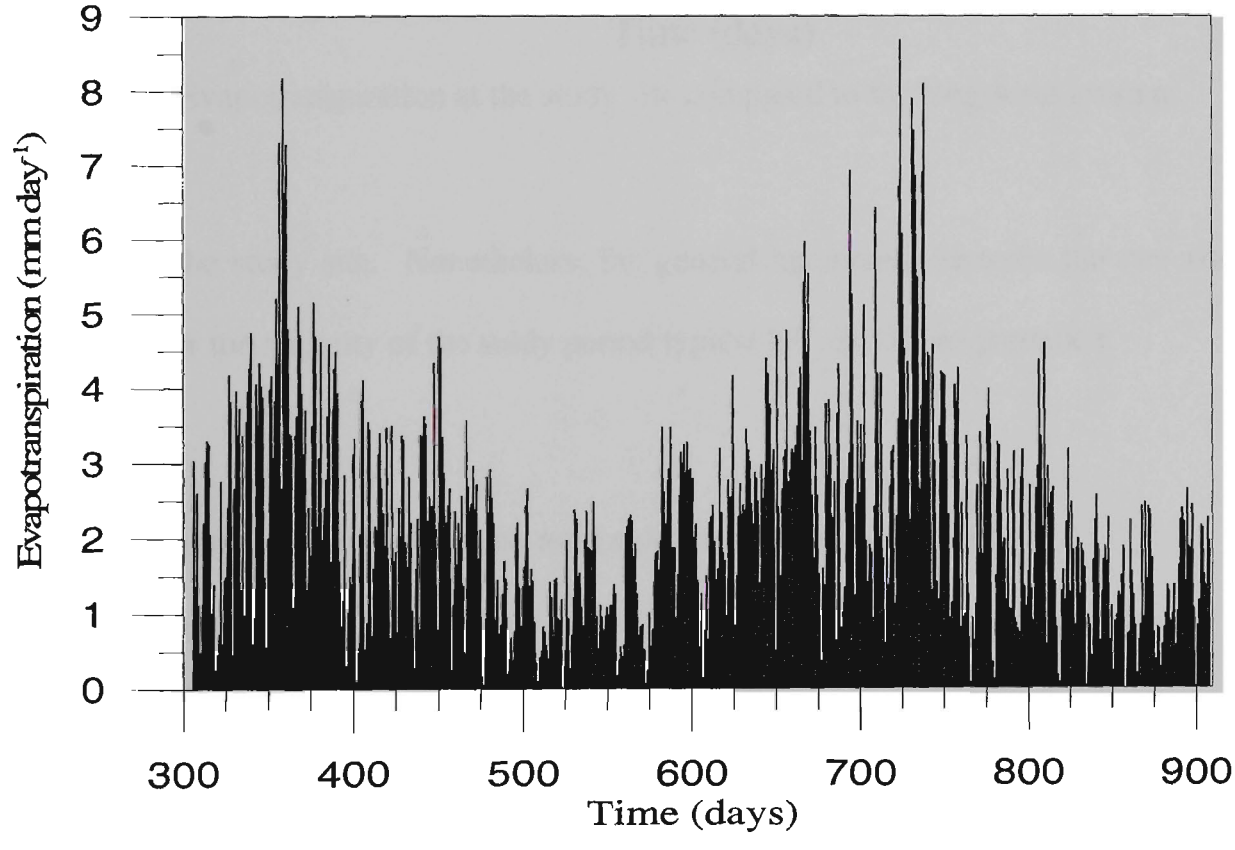

Figure 3.20 Evapotranspiration after floodgate modifications.

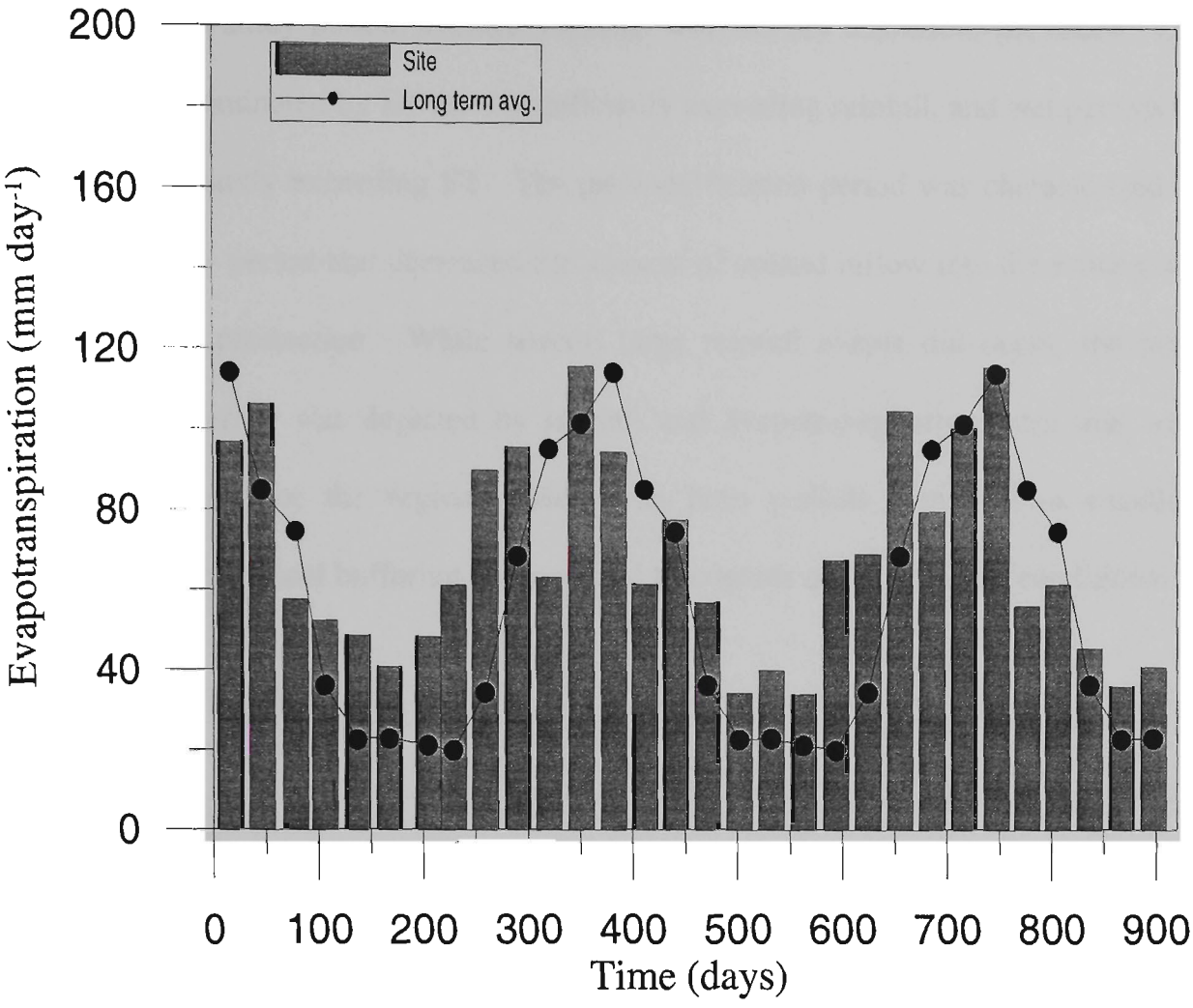

Figure 3.21 Evapotranspiration at the study site compared to the long-term average.

recorded at the study site. Nonetheless, the general agreement between the two sites shows that for the majority of the study period typical ET conditions prevailed.

3.6 Implications of climatic data on acid sulphate soil management

The interrelationship between rainfall and evapotranspiration plays an important role in determining the intrusion of tidal buffering agents within the estuary and the dynamics of the groundwater table in coastal floodplains. Furthermore, understanding the influence of rainfall and ET provides a vital link in optimising the proposed tidal buffering strategy. To this point, Figure 3.22 shows the relationship between rainfall and evapotranspiration at the study site.

Throughout the study period, average, extreme wet and dry conditions prevailed. Dry periods were dominated by ET rates significantly exceeding rainfall, and wet periods by rainfall significantly exceeding ET. The pre-modification period was characterised by an extended dry period that decreased the amount of upland inflow into the estuary and increased acid production. While several large rainfall events did occur, the post-modification period was depicted by rainfall and evapotranspiration rates that were close to average for the region. Moreover, both periods provided an excellent opportunity to trial tidal buffering via modified floodgates under 'normal' conditions.

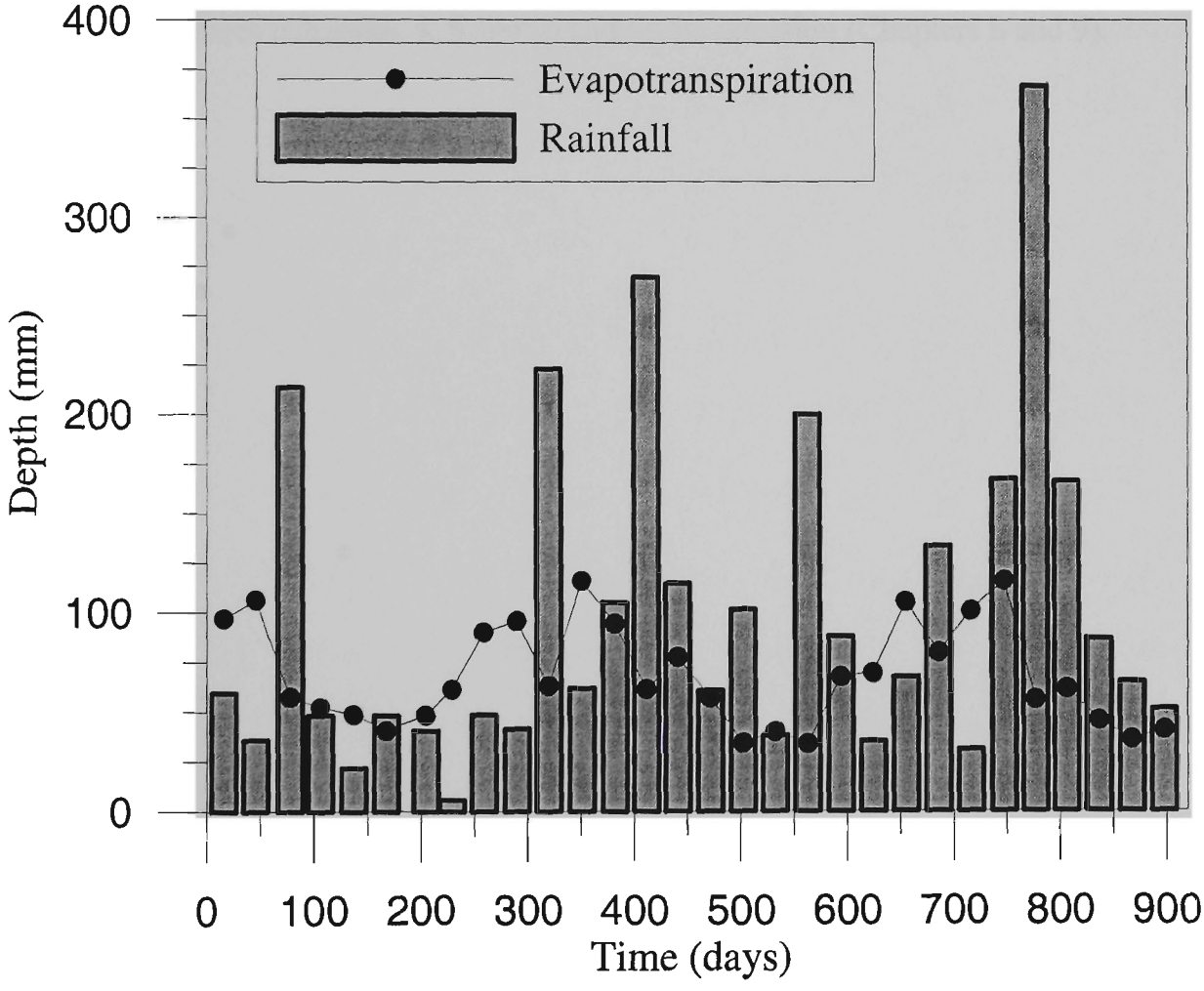

Figure 3.22 Rainfall versus evapotranspiration at the study site.

The climatic conditions recorded during the study trial influenced acid production, acid transport and estuarine hydrodynamics. Moreover, these conditions provided an ideal setting for investigating tidal buffering in respect to (i) alternative tidal regimes, (ii) response to floods and droughts, (iii) varying impacts on the groundwater table and acid dynamics, (iv) the hydrodynamic and spatial impacts of acid transport and buffering reactions, and (v) the hydraulic testing of various floodgate designs. To provide a detailed description of the above processes and their interrelationship with climatic conditions, a sophisticated network of continuous monitoring equipment, as well as the outlined sampling regime was devised. These interactions will be further discussed within the following Chapters with specific reference to soil chemistry (Chapter 4.0), estuarine dynamics (Chapters 5, 6 and 7) and saline intrusion (Chapters 8 and 9).

Chapter 4.0 The Impact of One-way Floodgates on Soil and Groundwater Conditions in Acid Sulphate Soil Terrains

4.1 Introduction

The climatic conditions presented in Chapter 3 illustrate that both wet and dry conditions prevailed throughout the study period. These varying climatic conditions have a direct impact on the elevation of the groundwater table and influence pyrite oxidation within the soil matrix. Furthermore, the wetting and drying of the vadose zone, perpetuated through climatic (i.e. rainfall and evapotranspiration) and hydraulic influences (i.e. one-way floodgates), increases soil development and alters its physical and chemical nature. To this point, this chapter investigates the groundwater dynamics across the study domain prior to floodgate modifications in order to ascertain the influence of varying boundary conditions on acid production and transport.

The first section of this chapter describes the baseline chemical, physical, and morphological properties of soil samples taken from the field site. This data was obtained to establish the extent of previous pyrite oxidation and is useful in (i) determining the influence of one-way floodgates on acid production, (ii) the potential for further acidification of drainage waters, and (iii) to ascertain baseline soil salinity conditions. Using this information, a base point was constructed so that future changes in the soils chemical attributes due to tidal flushing could be investigated. Extensive soil data was also acquired as inputs for the initialisation of numerical models (as shown in Chapter 8), which require a wide array of soil material properties for calibration and initialisation.

In the second section of this chapter, the temporal and spatial fluctuations in the phreatic zone over varied climatic conditions, including pore water acidification due to the mobilisation of pyrite oxidation products and the impact of one-way floodgates, are examined. Variations in the hydraulic gradient of the phreatic zone are also investigated to highlight how one-way floodgates maintain low drain water elevations, which, in turn, creates strong acid transport pathways. Finally, groundwater quality information is given to establish a base point for comparison after floodgate modifications.

4.2 Soil Investigations

A comprehensive sampling regime was undertaken to determine soil characteristics spatially and vertically across the study site. In every instance, well-established soil testing methods were employed that were current at the time of testing. Furthermore, detailed field descriptions were recorded to investigate the relationships between topographical and soil physical/chemical data at the study site.

4.2.1 Soil testing methods

Soil testing was conducted from a series of transects across the study site. The location of the testing sites in relation to the soil topography is shown in Figure 4.1. Testing sites were chosen based on their proximity to the floodgate and their relation to desired long-term variables (i.e. saline intrusion). In total, 18 soil cores were taken from 5 transects and the surface elevation of all sample sites varied less than 1.0 m.

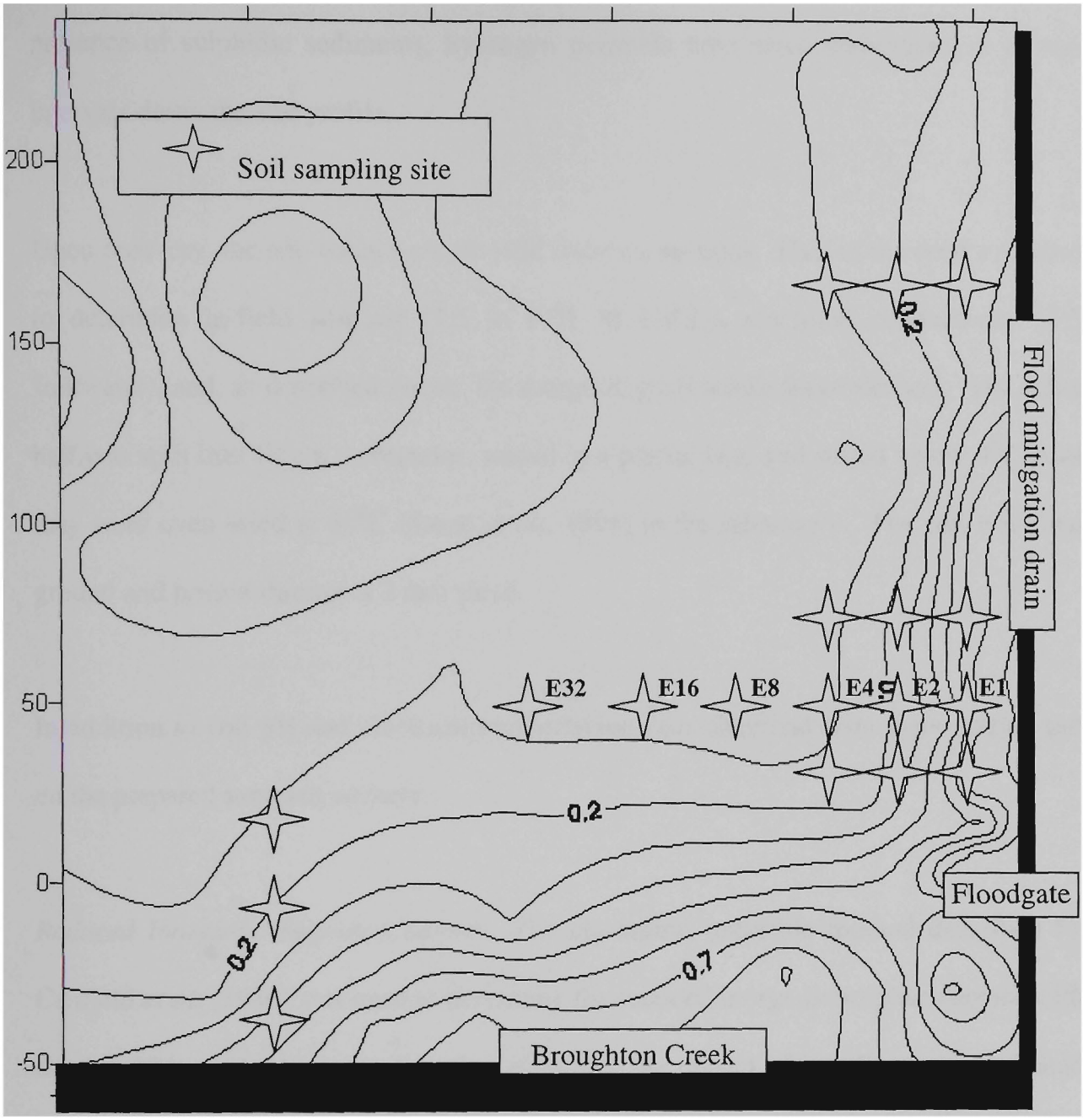

Figure 4.1 Location of soil sampling sites at the study site in relation to topography, the one-way floodgate and Broughton Creek.

Soil cores were obtained by mechanical push tube sampling to a depth of 2.0 m using a Pro-Line Drill Rig provided by the NSW Department of Agriculture. To determine the location and depth of the potential acid sulphate soil layer, samples at transect E (see Figure 4.1 for reference) were taken to a depth of 3.0 m. Recovered intact cores were described for soil texture, the presence of major horizons, and the location of features such as jarosite, iron mottles and the existence of macropores. To determine the

presence of sulphidic sediments, hydrogen peroxide tests were undertaken at 10 cm intervals down the soil profile.

Upon recovery, the soil cores were divided into two sections. Half of the core was used to determine in-field soil pH (1:5 in 0.01 M $CaCl_2$), electrical conductivity (1:5 soil/water), and, as described above, the morphological attributes of the soil. The other half was split into 10 cm increments, sealed in a plastic bag, and stored below 4^0C until they were oven dried at 85^0C (Stone *et al.*, 1998) in the laboratory. The soil was then ground and passed through a 2 mm sieve.

In addition to soil pH and electrical conductivity, four chemical tests were carried out on the prepared samples, namely:

Reduced Inorganic Sulphur Content: The chromium reducible method described by Canfield *et al.* (1986) was used to determine the reduced inorganic sulphur content with depth. This method was employed to eliminate the impact of interferences associated with organic matter, clays, and sulphate minerals (White and Melville, 1993) associated with previous methods, such as the POCAS method described by Ahern *et al.* (1998).

The Chromium reducible method involves reducing the inorganic sulphur content to H_2S by digestion with an acidified chromous chloride solution under a nitrogen atmosphere. The evolved H_2S is collected in a zinc acetate buffer as ZnS, and then acidified. Finally, the H_2S content is analysed by iodometric titration with the results being expressed as $\%S_{cr}$.

Total Actual Acidity: A 5 gram soil sample was suspended with 50 mL of KCl and shaken overnight. A filtered 25 ml aliquot was titrated with 0.25 M NaOH until a pH of 5.5 was attained. The recorded volume of alkali required to reach pH 5.5 determined the total actual acidity with the results expressed as mol H^+/tonne of dry soil.

Total Sulphate: Samples were extracted with a 1:5 potassium phosphate (0.01M KH_2PO_4) solution for phosphate extractable sulphate. Total sulphur in the extracts was analysed by ICP-AES and reported as extractable in mg/kg.

Chloride: Samples were extracted with a 1:5 water extract for water-soluble chloride (Method IIC_A01). Soluble chloride in the extracts was analysed by Ion Chromatography with the results being expressed as mg/kg.

In addition to chemical tests, physical soil testing was conducted to determine saturated hydraulic conductivity (lateral), and soil porosity. Four sampling locations were chosen; two immediately adjacent to the drain, and two 10 m inland from the drain. Test pits were dug to obtain duplicate samples at 0.2 m, 0.5 m, 1.0 m, 1.2 m and 1.5 m from the ground surface. Samples were taken by inserting a 100 mm diameter by 70 mm thick, thin walled brass core into the soil profile at the prescribed depths. Cores were carefully removed by hand to minimise disturbance, immediately wrapped in plastic wrap to avoid moisture loss, and stored at 4^0C until laboratory testing could be performed.

Lateral saturated hydraulic conductivity tests were determined using the falling head method described by ACLEP (1995). Following the tests, individual soil cores were

removed from the brass rings and dried at 105°C for 24 hours. The samples were then tested for dry bulk density and porosity.

4.2.2 Results and Discussion

4.2.2.1 Borehole stratigraphy

The soil stratigraphy found at the study site, and presented in Figure 4.2, is typical of soils found throughout the Shoalhaven floodplain (Willet and Walker, 1982; Pease, 1994; Blunden, 2000). In general, Holocene estuarine deposits overlie undisturbed Pleistocene clays, but within the Holocene sediments, an actual acid sulphate soil layer commonly overlies a potential acid sulphate soil layer. Above the estuarine clays, alluvial deposits, formed within the past 4000 years (Umitsu *et al.*, 2001), range in thickness depending on their geomorphic location (i.e. levee banks, levee toe, or backswamp).

While minor variations in the soil profiles were found, common soil properties can be assumed across the study site. In the backswamp region of the site (E32- Figure 4.2), the surface soil of a typical profile is a loamy alluvium generally 0.2 m thick. This dark brown silty loam contains a large mass of root material and is well aggregated. Below this layer is a dark brown to black (Munsel colour code 2.5Y2/0) peaty silty clay loam stratum approximately 0.2-0.35 m thick. This layer represents the extent of deposition due to freshwater infilling from former backswamp conditions. Further down the profile, a distinct, dark greyish brown (10YR4/2) silty clay layer, which hardens when dried, most likely represents the transition from alluvial to estuarine soils. Rusty mottles are found throughout this layer and increase with depth. Similarly, tubular iron concretions and jarosite mottles in this layer are commonly associated with vertical

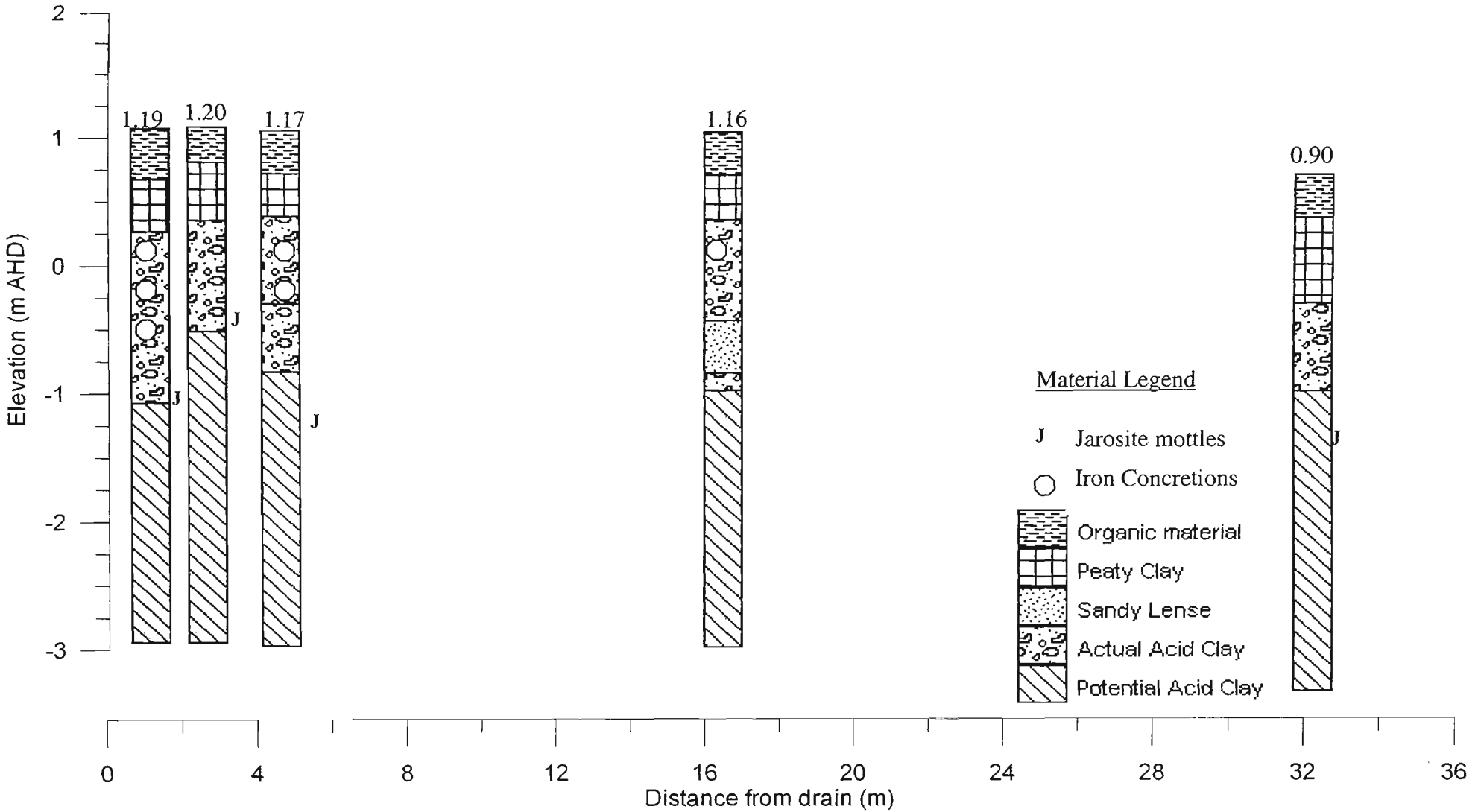

Figure 4.2 Description of soil profiles from transect E taken from the study site with surface elevations.

macropores that formed from decayed root matter. An increase in jarosite mottling typically occurs at the bottom of this layer (~1.2 m), and represents the transition zone from oxidised active minerals to the reduced sulphidic deposits. This layer is typically a dark grey (10YR4/1), massive silty clay with low hydraulic conductivities. The addition of hydrogen peroxide to soil taken from this stratum caused strong effervescence, which is indicative of sulphidic sediments. Underlying the potential acid sulphate soil layer is a dense, massive grey, clay layer. Both Roy (1985) and Umitsu *et al.* (2001) suggest that this clay layer is a Pleistocene deposit that formed the base for infilling Holocene sediments.

The thickness and distribution of the soil stratigraphy is controlled by the geomorphic characteristics of the study site and human disturbances. Moving from the backswamp to the levee toe, the layer of loamy alluvium overlying the actual acid sulphate soil layer increases in thickness. In the backswamp region, the layer of loamy alluvium is limited to 0.5 m, while in the levee toe it increases to 0.75 m. This is more apparent at the peak of the levee with increased alluvial deposition measuring more than 0.8 m above the pyritic layer.

As found in other sites in the Shoalhaven, the elevation of the pyritic layer gradually increases towards the backswamp. This increase was attributed to the gradual recession of estuarine waters during the Holocene, the subsidence of the soil due to draining, and varying levels of overburden. Across the field site, the top of the pyritic layer is consistently at 0.25 m AHD (about 1 m below the soil surface), however, slight undulations (20-25 mm) are found throughout. In soil profiles located adjacent to the

drain (E2), the increase in elevation of the actual acid sulphate soil layer is due to pyritic material being deposited along the banks during drain maintenance/construction.

The thickness of the pyritic layer varies across the site and is related to the physical properties of the soil. Generally, the pyritic layer is 0.5 m thick but this increases within the levee bank to 0.75 m and decreases with distance from the levee bank to 0.44 m in the backswamp. Large pyritic bands (0.69 m) are also found in proximity to the drain and these variations were attributed to the low surface elevations maintained by the deep drains and one-way floodgates.

4.2.2.2 Soil pH

The oxidation of pyrite produces H^+ ions as described in Equation 2.7. Under acidic groundwater conditions, additional H^+ ions are generated through the biologically enhanced ferrous-ferric oxidation/reduction reaction. In this manner, the concentration of H^+ ions is a strong indicator of acid production. pH is commonly used to measure the concentration of H^+ ions and is calculated as:

$$pH = -\log [H^+] \quad (4.1)$$

Stone *et al.* (1997) states that naturally occurring soils with a pH below 4.0 can be solely attributed to pyrite oxidation.

Soil pH readings, shown in Figure 4.3, depict acidic conditions throughout the soil profile. In the first 0.25 m, soil pH ranges from 4.09 to 5.41; this indicates acid production from organic matter decomposition, whereas underneath the peaty clay layer

(0.75-1.75 m below the surface) the soil pH falls below 4.0. This was attributed to the impact of pyrite oxidation within the actual sulphate soil layer, which produces H^+ ions and mineralises aluminium. At site E16, the slightly higher soil pH (3.92-4.64) is most likely due to a sandy band that transects this layer. While normally associated with low pH values, shell fragments found within this layer increase the buffering capacity of the soil. Similarly, the elevated hydraulic conductivity of the sandy band could have caused complete oxidation of the acidic minerals and previously generated acid would have been leached from the soil. The chemical and physical properties of this sandy layer are further discussed in Chapter 8.

Further down the soil profile (>1.75 m), increased pH and the absence of jarositic mottles indicates the presence of potential acid sulphate soils. In general, the soil pH rose above 6.0 deeper than 2.2 m below the surface, and continued to increase with depth. Nonetheless, throughout this circum-neutral pH layer, soil samples reacted vigorously with hydrogen peroxide, thereby depicting the presence of sulphidic minerals.

The pH values discussed above are typical of those found across the Shoalhaven floodplain and signify previously oxidised actual acid sulphate soils. Without increased soil buffering capacity, the acidity within the soil is likely to acidify groundwater and solubilise toxic metals through the dissolution of clay minerals. In areas with artificial drainage (i.e. flood mitigation drains and one-way floodgates), leaching of low pH groundwater will acidify adjacent surface waters and give rise to environmental degradation. Furthermore, by maintaining low drain water elevations, one-way

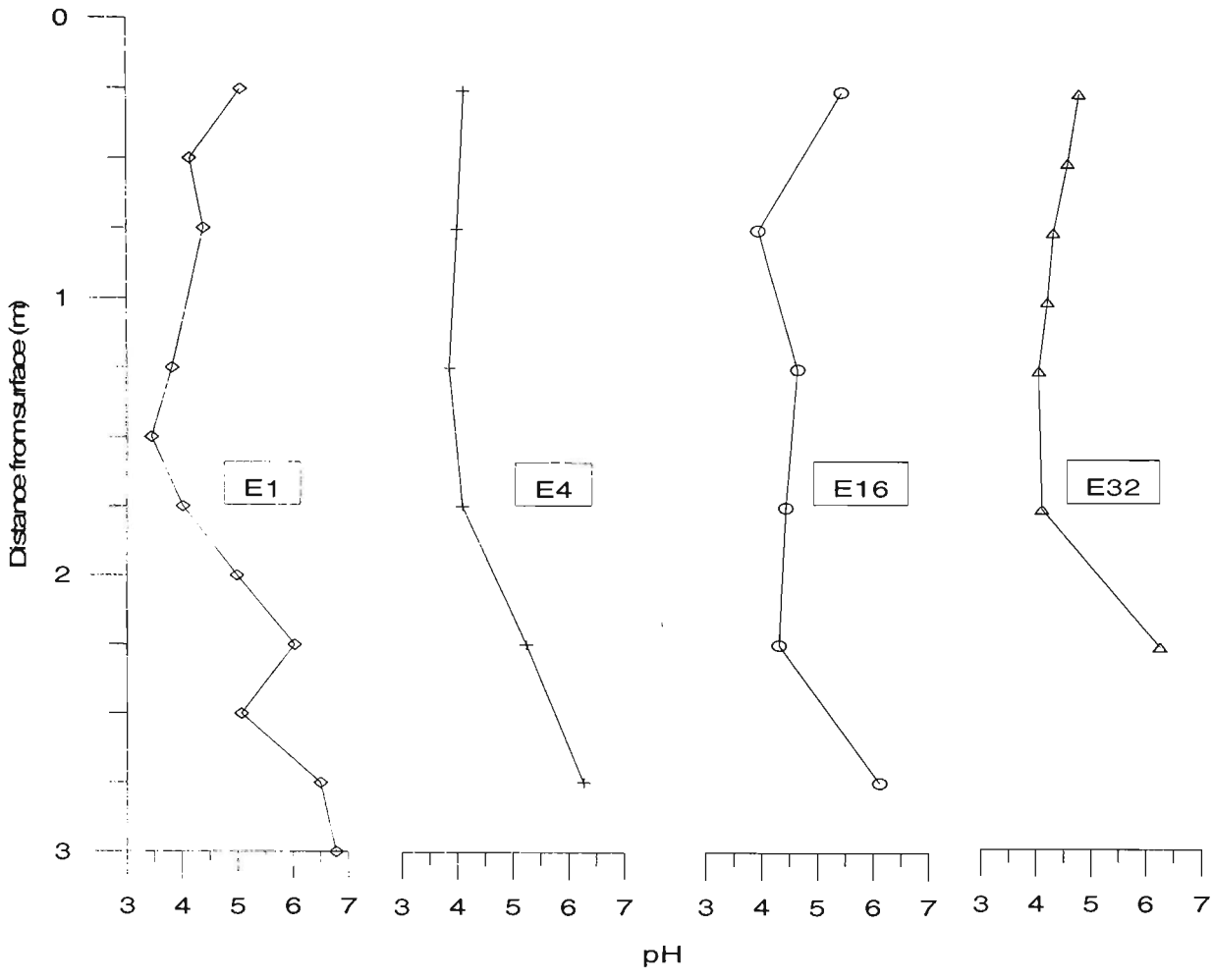

Figure 4.3 Typical soil pH profiles found at the study site with depth.

floodgates increase the sulphurisation process, which is depicted at the study site by both the low pH readings and the large oxidised zone nearest the drain (Figures 4.2 and 4.3). Conversely, the restoration of tidal flushing within the flood mitigation drain will increase drain water buffering capacity, and under favourable conditions, the transport of these buffering agents within the soil matrix may increase the buffering capacity within the soil. The influence of tidal ingress on soil acidity after floodgate modifications is described in Chapter 8.

4.2.2.3 Soil Electrical Conductivity

Electrical conductivity throughout the soil profile is low (<1.0 mS cm^{-1}), but increases with depth. Figure 4.4 shows that within 1.0 m from the surface, the electrical

conductivity is less than 0.15 mS cm^{-1}. At most sites, electrical conductivity peaks at 0.50 mS cm^{-1} in the pyrite oxidation zone, approximately 1.5 m below the surface. Beneath this layer, the electrical conductivity gradually declines below 0.40 mS cm^{-1}.

The electrical conductivity peak within the actual acid sulphate soil zone (1.5 m, Figure 4.4) is most likely due to the precipitation of ferrous sulphate salts. Though electrical conductivity is typically used to measure chloride concentrations, within actual acid sulphate soils sulphate is by far the dominant anion. In dry conditions, ferrous sulphate minerals such as copiapite ($Fe_2(SO_4)_3$) can form, which increase electrical conductivity (Fanning, 1993).

In samples located adjacent the drain and near the floodgate (E1), two electrical conductivity peaks are discernible. The first peak, approximately 1.5 m below the surface, is likely due to the generation of sulphate salts, however, the second peak at the bottom of the soil profile is associated with seepage of higher ionic strength creek water from the drain. On several occasions before floodgate modifications, debris became jammed between the floodgate and the headwall, which allowed for the intrusion of saline, high ionic strength water upstream of the floodgate. Ion exchange within the soil is more likely to occur within the pH neutral, potential acid sulphate soil layer, because sulphate ions block exchange sites within the oxidised soil layer. This was apparent at sampling site E1, located 15 m upstream of the floodgate and 1 m perpendicular of the drain. It is important to note, that even the highest levels recorded at E1 (0.949 mS cm^{-1}) are well below ANZECC criteria associated with saline soils. Furthermore, the elevated concentrations are located 3 m down the soil profile and pose little threat to agricultural productivity (mainly shallow rooted pasture crops such as paspalum).

Nonetheless, this indicates that saline ingress was occurring upstream of the floodgate before floodgate modifications without undue concern.

4.2.2.4 Total soluble chloride and sulphate

The concentration of sulphates bound within the soil profile is a strong indicator of previous pyrite oxidation. From Figure 4.5, it is apparent that the majority of sulphate production occurs approximately 1.75 m from the soil surface, which represents the bottom boundary of the actual acid sulphate soil layer. Gradually decreasing values above this point, represent the upward migration of sulphate ions due to capillary action and the presence of sulphate retaining minerals such as jarosite. The sharp decline in sulphate below the actual sulphate soil layer is indicative of the potential acid sulphate soil layer.

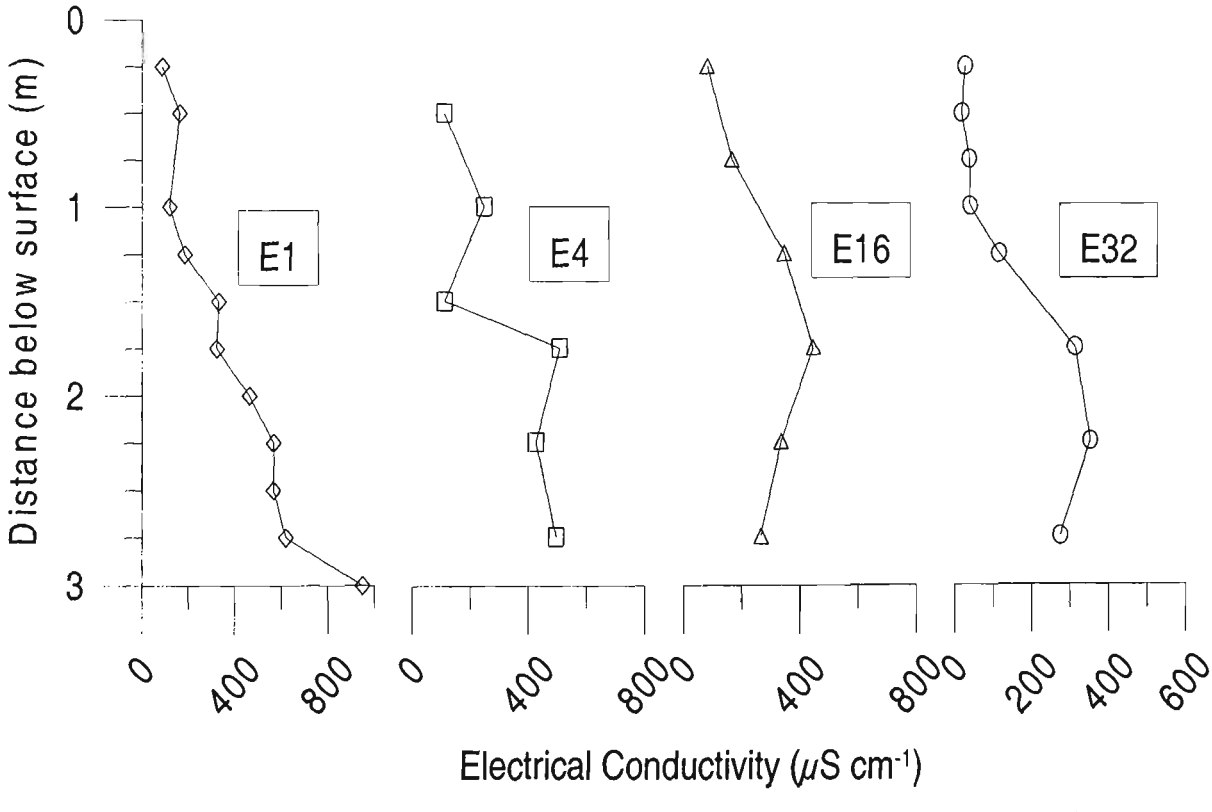

Figure 4.4 Soil electrical conductivity profiles found at the study site with depth.

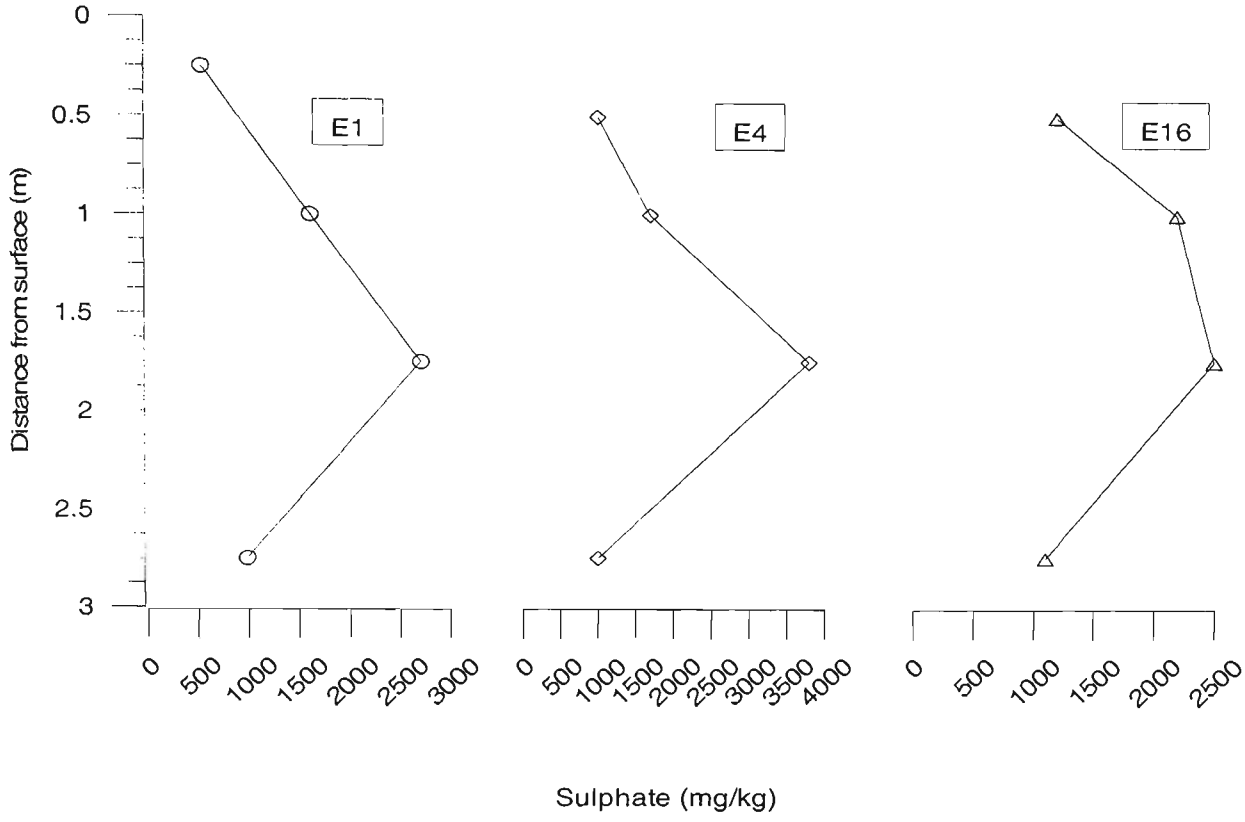

Figure 4.5 Total sulphate concentrations with depth.

The concentration of chloride down the soil profile at various locations is shown in Figure 4.6. In the top 1.0 m, low chloride concentrations (<500 kg/mg) are predominate due to the formation characteristics of the soil (i.e. mainly alluvial) and the consistent annual rainfall in the region, which promotes chloride leaching. In contrast with previous data in the region (Blunden, 2000), chloride concentrations below 1.0 m increased above 1000 mg/kg, and maintained this level until the bottom of the soil core (3 m below the surface). This is not surprising considering that acid sulphate soils were formed in estuarine (brackish) conditions with abundant chloride concentrations. Additionally, previous samples were from sites more than 1.2 kms from the floodgate/creek junction, whereas the samples presented here are 15 m from the floodgate/creek junction. As mentioned earlier, the proximity to the floodgate and its tendency to leak may have permitted saline water within the drain and promoted ion

exchange. These findings are important as they indicate that tidal restoration to the study drain will not drastically increase soil salinity.

According to Mulvey (1993), the chloride/sulphate ratio can be used to determine the level of pyrite oxidisation in acid sulphate soils. While the chloride/sulphate ratio of seawater on a mass basis is 7.2, values below 2.0 indicate sulphide oxidation. As shown in Figure 4.7, the highest chloride/sulphate ratio measured at the study site was 1.3 (E4-2.75 m) and within 2.0 m of the surface all samples were below 1.0. In conjunction with low soil pH (<4.0), these results demonstrate the strong oxidation environment within the actual acid sulphate soil zone and the weak buffering capacity of the soil. These findings are typical of chloride/sulphate ratios found throughout ASS affected floodplains in southeastern NSW (Sbeghan, 1995; Chapman, 1994; Sharman, 1995) and highlight the strong concentration of acid within the soil matrix and its potential to acidify the adjacent groundwater and surface water environments.

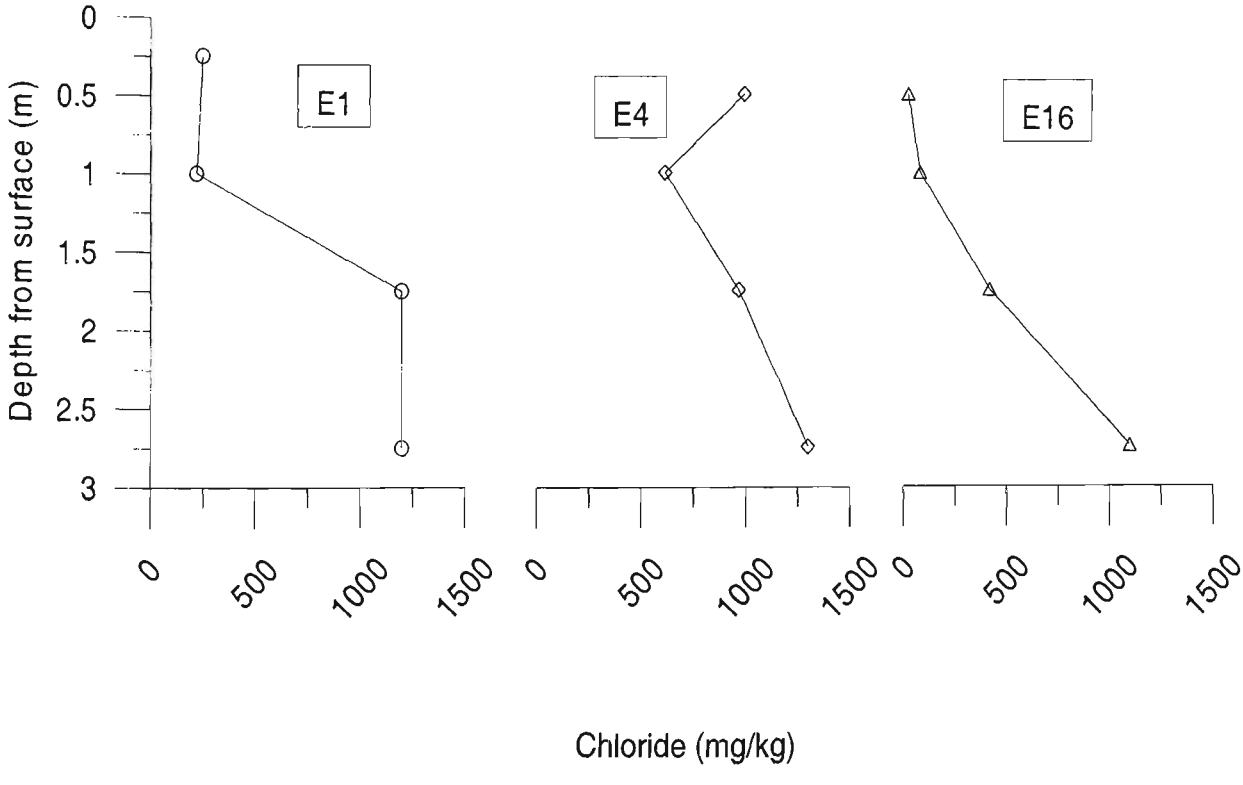

Figure 4.6 Soluble soil chloride concentrations with depth.

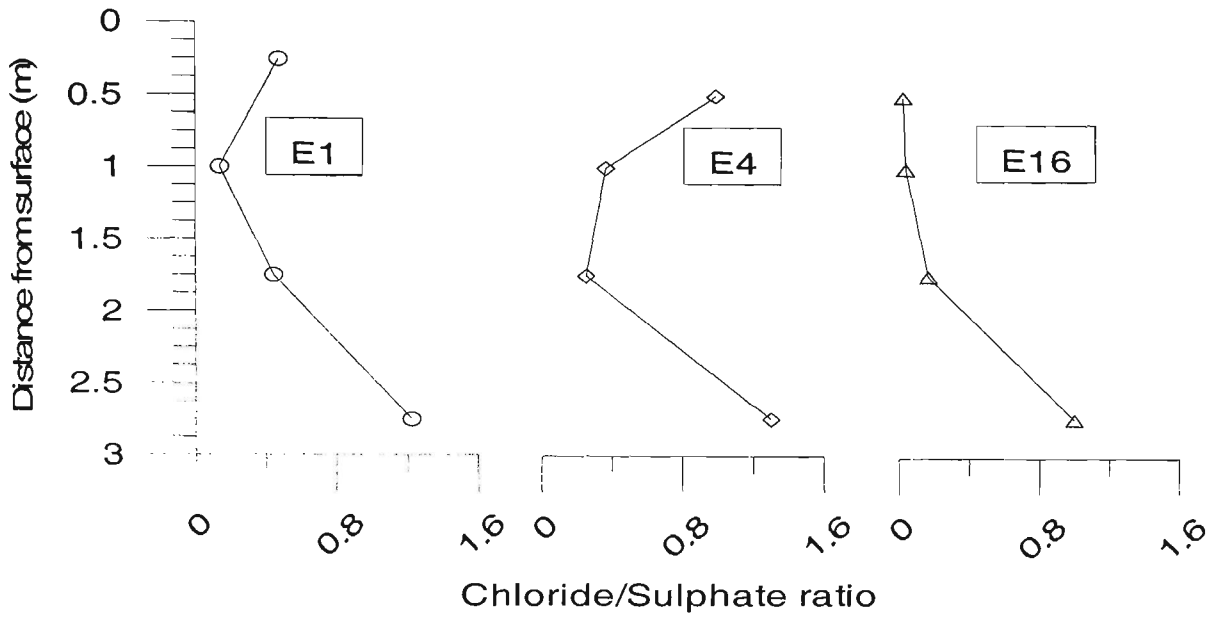

Figure 4.7 Typical chloride/sulphate ratios with depth found at the study site.

4.2.2.5 Total actual acidity

A typical soil profile for total actual acidity (TAA) or titratable acidity from the study site is shown in Figure 4.8. From this data, it is apparent that total actual acidity increases along the profile and peaks (64 mol H^+/tonne) 1.25 m from the surface. This peak in acidity corresponds well with the actual acid sulphate soil layer and represents acid generated from former pyrite oxidation. The decrease in total actual acidity below the oxidised layer (TAA of 0 at 1.75 m) represents the transition from actively oxidising pyritic material to the potential zone.

Lower acidity levels (<40 mol H^+/tonne) also exist within the top 1.0 m of the soil profile. The decomposition of organic matter is commonly associated with acid production and for every mole of decomposed material, one mole of acid is generated. Across the site, a rich organic layer was evident 0-0.5 m from the surface and is presumably the main form of acid production in this layer.

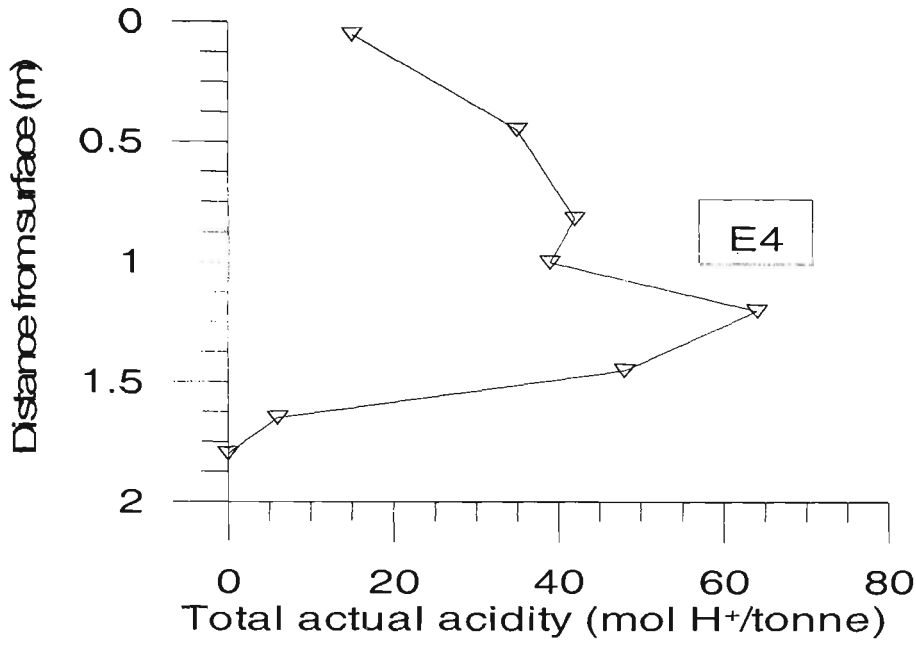

Figure 4.8 Total actual soil acidity with depth found at the study site.

Further down the soil profile, elevated TAA levels are a result of the upward movement of acid products due to capillary action and formation kinetics. Under acidic conditions, minerals such as ferrous sulphate and jarosite can form and/or be transported above the acid-producing layer. The hydrolysis of ferrous sulphate ions (Fanning, 1993), and the dissolution of jarosite, generates acid above the actual sulphate soil layer and adds to the total actual acidity concentration. The formation and hydrolysis of ferrous sulphate ions is shown in Equations 4.2 and 4.3.

$$FeSO_4 + \tfrac{1}{2} H_2SO_4 + \tfrac{1}{4} O_2 \rightarrow \tfrac{1}{2} Fe_2(SO_4)_3 + \tfrac{1}{2} H_2O \qquad (4.2)$$

$$FeSO_4 + \tfrac{1}{4} O_2 + \tfrac{5}{2} H_2O \rightarrow Fe(OH)_3 + H_2SO_4 \qquad (4.3)$$

Due to high total actual acidity concentrations, management of pyritic soils via traditional acid neutralisation techniques is not economically viable. For instance, using appropriate acid sulphate soil conversions (Stone *et al.*, 1998) approximately 30 tonnes H_2SO_4/ha is currently present within the upper 1.5 m of the soil profile. In terms of

buffering capacity, this equates to more than 47 tonnes/ha of lime, and therefore, a 100 ha property underlain with acid sulphate soils would need to invest more than $235,000 in agricultural lime to neutralise the current acidity. Considering the potential for additional acid production from underlying potential acid sulphate soils, the tendency of lime to be flushed from the soil profile with rainfall, and the extreme costs, other non-anthropogenic methods of controlling acid drainage such as tidal flushing are required.

4.2.2.6 Inorganic Reduced Sulphur

Inorganic reduced sulphur content is a measure of the potential acidity available along the soil profile in the forms of pyrite, marcasite and monosulphides. In contrast to TAA, the inorganic reduced sulphur content (S_{cr}%) measures the potential for further acid generation under oxidising conditions. The inorganic reduced sulphur content along a typical soil profile at the study site is shown in Figure 4.9.

The concentration of inorganic reduced sulphur is well above the management action criteria of 0.05% S_{cr} (Stone *et al.*, 1998). Below 1.25 m, the S_{cr}% increases from 0.024% S_{cr} to a maximum of 1.6% S_{cr} at 1.75 m from the surface. Inorganic reduced sulphur content in the upper 1.25 m is below the action criteria (minimum level 0.014% S_{cr}, at 0.82 m from the surface). However, as a result of the formation of monosulphides during prolonged periods of surface ponding, S_{cr}% within the topsoil is slightly above the action criteria.

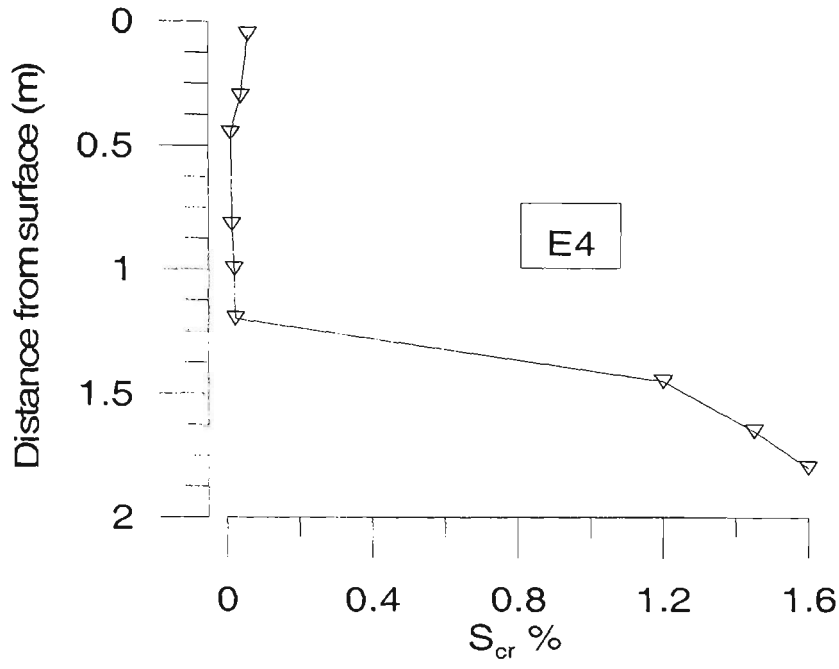

Figure 4.9 Inorganic reducible sulphur content with depth measured at the study site.

The concentration and distribution of inorganic reduced sulphur at the study site is typical of potential acid sulphate soils throughout the Shoalhaven Region. It is important to note that previous tests for potential acidity were conducted by oxidising sulphides with hydrogen peroxide (H_2O_2) and, as such, were susceptible to interferences with organic material and sulphate minerals. Since the chromium reducible method used in these tests are not predisposed to such interferences (Sullivan *et al.*, 1999), the slightly lower findings presented here (1.6% S_{cr} versus, say 2.4% S_{pos} presented by Blunden (2000)) may be attributed to those interferences. Nonetheless, these findings suggest a new management strategy is required to reduce further oxidation of the abundant pyritic material.

4.2.2.7 Hydraulic conductivity (lateral)

Saturated hydraulic conductivity tests in the lateral plane ($K_{sat(H)}$) were undertaken to determine the influence of drain water management strategies on groundwater levels and to initialise finite element models. In particular, $K_{sat(H)}$ measurements were required

to ascertain if tidal restoration within the study drain would impact contaminant transport of acidic products out of the soil matrix, and saline ingress into the soil matrix. The findings are compared with the extensive studies performed by Blunden and Indraratna (2001) at a nearby site.

The coefficient of permeability for a soil is the constant of proportionality relating to the ease at which a fluid can be transmitted through a soil. It can be calculated using the following formula:

$$k = \frac{aL}{At} \ln \frac{h_1}{h_2} \tag{4.4}$$

where, a = cross-sectional area of the burette, A = cross-sectional area of soil sample, h_1 = hydraulic head across sample at beginning of test (t = 0), and h_2 = hydraulic head across sample at end of test ($t = t_{test}$).

Overall, the soil results (Table 4.1) indicate that hydraulic conductivity is greatest in the organic layer, and decreases within the clayey, acid sulphate soil layer. Blunden and Indraratna (2000) showed a similar trend in K_{sat} measurements with slightly higher permeability rates (1.68 –3.95 m day^{-1}) due to the existence of vertical macropores from relic root channels. As the main objective of examining physical soil properties was to determine the lateral transport of groundwater contaminant either from the soil matrix into the drain or from the drain into the soil, the vertical permeability at the site was not determined. Nonetheless, the results presented in Table 4.1 show that saline ingress due to increased chloride concentrations in adjacent surface waters after floodgate modifications should not be a significant concern. However, further numerical

modelling (as given in Chapter 9) is required to determine saline intrusion under extreme situations, such as the drought experienced at the end of the study period.

Table 4.1 Soil physical properties

Depth (m)	**$K_{sat(H)}$ (mm s^{-1})**	**Porosity %**	**Saturated volumetric moisture content**
0.5	3.62	48	0.37
1.0	1.11	41	0.42
1.5	1.82	37	0.41
2.0	0.53	23	0.54

Recent soil findings within Australia demonstrate that the conductivity values presented at the study site are ideal for floodgate manipulation trials. Johnston *et al.* (2003) showed that in northern NSW highly oxidised acid sulphate soils could have permeability rates in excess of 25 m day^{-1}. In these areas, floodgate manipulation may not be feasible due to the impact of increased drain water height and salinity levels on soil and agronomic properties with distance from the study drain. Conversely, in southeastern Qld., MacDonald *et al.* (2002) reported lateral conductivity levels less than 0.05 m day^{-1} in acid sulphate soils overlain by sugarcane. In these circumstances, acid drainage would be primarily via surface runoff during flooding, and, while the concern of saline intrusion would be minimal, alternative in-situ acid treatment methods may be more effective. Nonetheless, the moderate hydraulic conductivity values found at the study site, and typical of many areas within Australia, are beneficial for floodgate manipulation because they confine saline intrusion within the area nearest the drain and reduce the hydraulic gradient of groundwater flow. The lateral transport of saline

contaminants and the impact of varying soil hydraulic conductivities on management strategies are further discussed in Chapter 8 and 9.

4.2.2.8 Soil porosity and moisture content

Porosity and moisture content measurements from the study site are given in Table 4.1. These results are similar with other findings within the Shoalhaven Region (Ford, 2002) and follow the same trend as Blunden (2000). Porosity is greatest (48%) in the top 0.5 m, but decreases with depth to 23% at 2.0 m. This is probably due to aggregation and flocculation of the organic and oxidised clay layers causing increased porosity, whereas the saturated potential clays remain unconsolidated. Similarly, moisture content increased with depth depicting high moisture content levels in the unconsolidated potential clays. Though not reported in southeastern NSW, White *et al.* (1993) stated that a potential ASS layer with a volumetric moisture content of 80% would consolidate up to 50% upon complete drying.

4.3 Groundwater conditions and watertable dynamics

As detailed above, actual and potential acidity within the soil matrix is abundant across the study site. The solubility and translocation of these contaminants and their impact on the groundwater regime is described in this section, with particular reference given to (i) the spatial distribution of acid products, (ii) the elevation of the groundwater table in relation to the pyritic layers, and (iii) the influence of one-way floodgates in maintaining a strong hydraulic gradient towards the drain. Finally, the influence of modifying one-way floodgates to re-establish tidal flushing and combat acid seepage is discussed.

4.3.1 Groundwater acidity

Groundwater conditions from the study site before floodgate modifications depict a strongly acidic environment typical of acid sulphate soil oxidation (Figure 4.10). Lacking additional acidic inputs, solubilisation and mobilisation of pyrite oxidation products are the probable causes of the acidic groundwater. Furthermore, low pH values (pH < 4.0) were found at every sample site and indicate the diffuse nature of acidic conditions.

Groundwater monitoring commenced on Day 101 and varied only slightly during the sampling period. Overall, groundwater pH ranged from 2.95 to 3.89, indicating limted soil buffering capacity within the soil matrix. From Day 101 to Day 150, groundwater pH generally decreased in response to a falling watertable. As this period follows a series of rainfalls, the decline in the watertable would have promoted the leaching of acidic products towards the drain. Consistent rainfall during Days 170-209 (86.5 mm) caused a general increase in groundwater pH values, however, as the groundwater became acidified, pH levels decreased to their lowest values (2.93, Day 248). In the final period before floodgate modifications (Days 271-305), 84.9 mm of rainfall slightly increased pH values.

Variations in groundwater pH were minor throughout the study period, and the median pH for all sites prior to floodgate modifications was 3.24. Individual median pH varied slightly between sites with the lowest reading at C10 (3.13) and the highest at D10 (3.73). Between transects, pH variance was low (0.245 pH units), hence depicting ubiquitous acidic conditions throughout the study site. These conditions are typical of

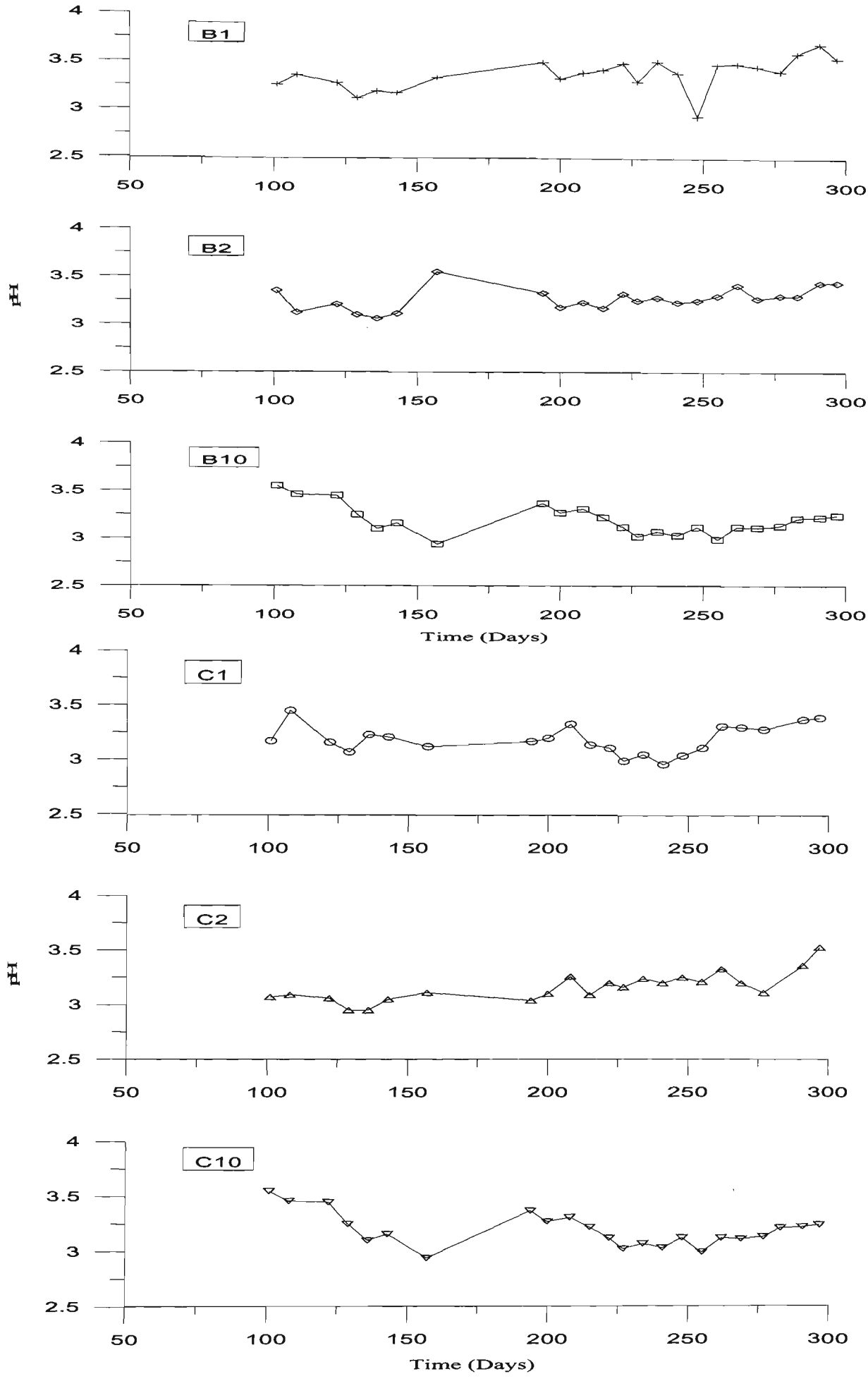

Figure 4.10 pH readings from piezometer B1-C10 before floodgate modifications.

those found across the Shoalhaven floodplain (Pease, 1997; Blunden and Indraratna, 1998) and indicate the strong pyrite oxidizing environment.

4.3.2 Chloride/Sulphate ratio

Naylor (1993), Mulvey (1993) and White and Melville (1993) recommend the determination of soluble chloride [Cl^-] and soluble sulphate [SO_4^{2-}] concentrations in acid sulphate soil groundwater. The Chloride/Sulphate ratios determined from groundwater taken from the study site supports the notion that a pyrite-oxidising, low buffering capacity soil environment prevailed before floodgate modifications. As shown in Figure 4.11, the Chloride/Sulphate ratio varied between 0.001-0.788, and was consistent temporally and spatially throughout the 306-day period. Ratios at piezometer B1, however, were somewhat elevated due to increased chloride concentrations and its proximity to the tidal creek. Excluding observation bore B1, the Chloride/Sulphate ratio at all sites ranged from 0.001-0.307 and averaged 0.1838. The elevated dissolved chloride concentrations nearest the floodgate again illustrates that saline water intruded upstream of the one-way floodgate, but the intrusion neither harmed nor benefited agricultural productivity.

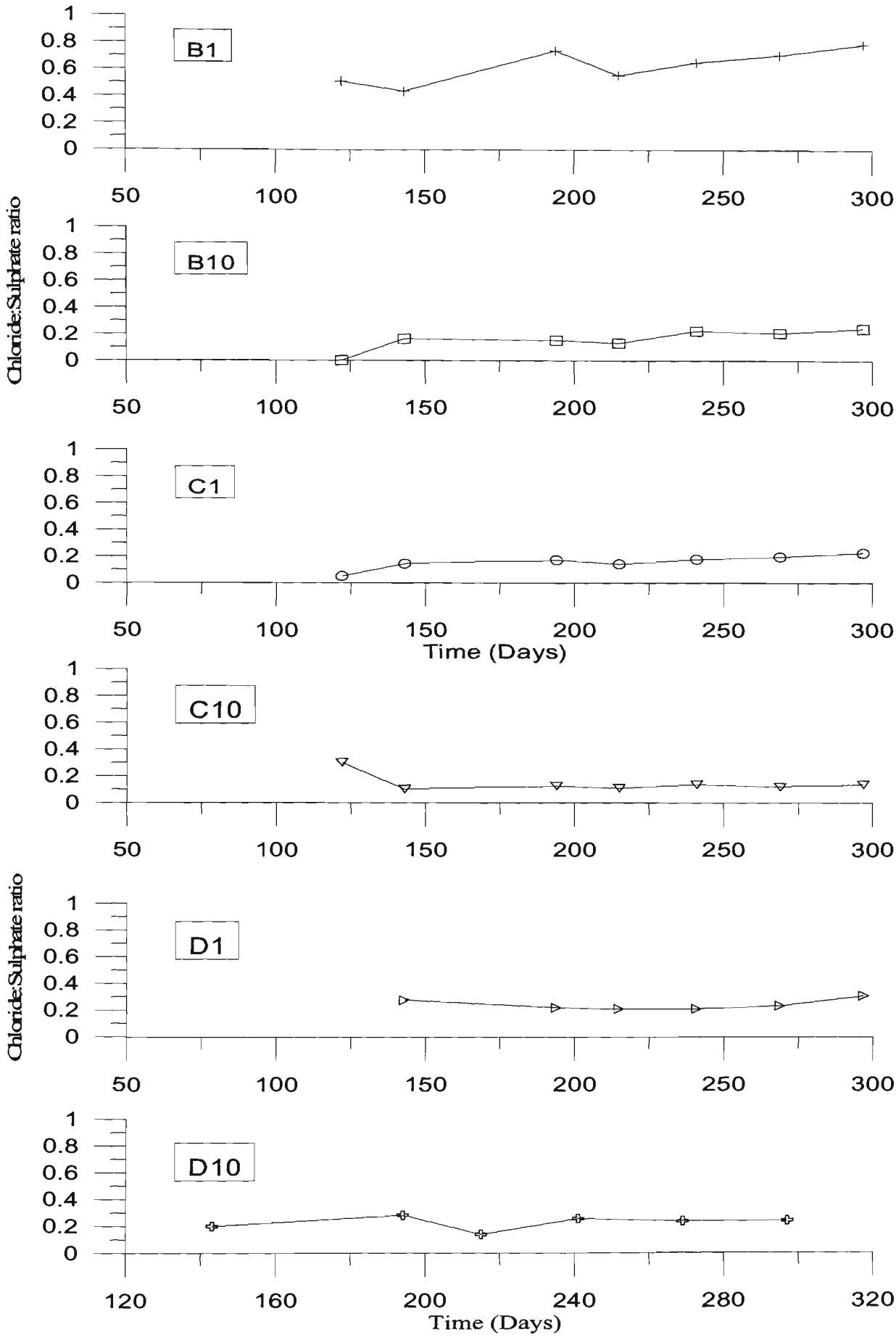

Figure 4.11 Chloride/Sulphate ratios before floodgate modifications at piezometer transects B, C, and D.

4.3.3 Hydraulic gradients and the impact of one-way floodgates

The translocation of acidic groundwater from the soil matrix into adjacent surface waters is related to the hydraulic gradient of the phreatic surface. The flow of water through soil, as described by Darcy's Law, states that under similar hydraulic conductivities, an increase in the hydraulic gradient (either vertically or laterally) will increase the mass flux. In low-lying floodplains, such as those found at the study site, the hydraulic gradient is mainly controlled by boundary (i.e. deep drains and floodgates) and environmental conditions (i.e. rainfall and evapotranspiration). In areas with deep flood mitigation drains, low surface water elevations, artificially created by one-way floodgates, maintain a strong hydraulic gradient towards the drain (Blunden and Indraratna, 2001). In this section, the elevation of the phreatic surface at the study site before floodgate modifications, as well as the capability for one-way floodgates to increase acid drainage, is described during both wet and dry periods.

The surface elevation of the phreatic zone prior to floodgate modifications (Table 4.2) indicates that the hydraulic gradient consistently sloped towards the drain. In fact, every measurement taken over the 23-week period depicted a sloping watertable, with the velocity vectors dependent on groundwater recharge from rainfall. Furthermore, the hydraulic gradient increased with proximity to the drain and the elevation of the watertable across the field site was primarily below the pyritic layer, thereby enhancing pyrite oxidation.

The long-term average groundwater elevation from each transect is shown in Table 4.2. From this data, three significant conclusions can be made. First, though the watertable was predominately static equi-distance from the drain (i.e. 1, 2, and 10 m), the

difference in elevation between transects B, C and D was attributed to the influence of the floodgate on increased seepage rates. Second, within transects the phreatic zone decreased in proximity to the drain, which shows that the phreatic surface predominately sloped towards the drain. Finally, as the top of the pyritic layer across the study site is located at 0.25 m AHD, and the average groundwater elevation at all sites is below this level, pyrite oxidation was abundant and ubiquitous prior to floodgate modification.

Table 4.2 Long-term average groundwater elevations with standard deviations taken before floodgate modifications.

Distance from drain (m)	**Piezometer Transect B** (m) AHD (n=23)	**Piezometer Transect C** (m) AHD (n=21)	**Piezometer Transect D** (m) AHD (n=21)	**Total Average** (m) AHD
1	-0.1485 ±0.097	-0.1113 ±0.103	-0.0829 ±0.128	-0.1143 ±0.112
2	-0.0695 ±0.103	-0.0813 ±0.122	-0.1089 ±0.138	-0.0591 ±0.122
10	-0.0020 ±0.108	-0.0006 ±0.086	0.0098 ±0.144	-0.0995 ±0.002

n equals the number of samples taken

Field investigations indicate that the extent and magnitude of sub-surface acid drainage is dependent on climatic factors such as rainfall, evapotranspiration, and the low drain water elevation maintained by one-way floodgates. A typical illustration of the groundwater surface at the field site during a prolonged dry period (Day 262) is shown in Figure 4.12. The increased velocity vectors 1-2 m across the drain boundary, and depicted in Figure 4.12, shows the impact of the low surface water elevation maintained by one-way floodgates. The influence of the one-way floodgate is also depicted by the

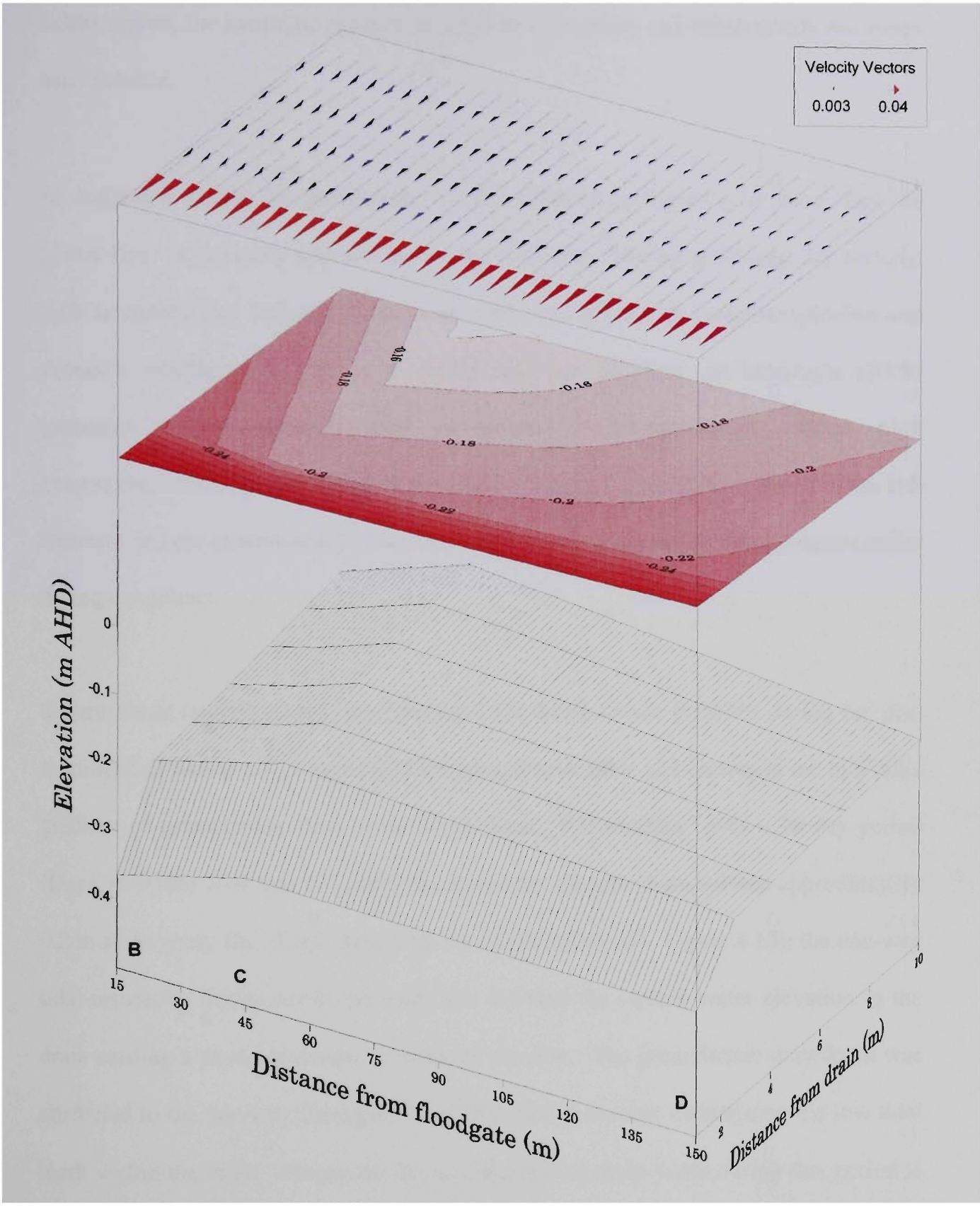

Figure 4.12 Groundwater elevation profile during a typical dry period before floodgate modifications (Day 262) with transects denoted by B, C, and D. Note that the surface of the pyrite layer is 0.25 m AHD, and that contours gradients and velocity vectors are in (m/day).

increased velocity vectors and decreased groundwater elevation nearest to the floodgate. In this region, the hydraulic gradient reaches its maximum, and subsequently decreases with distance.

As suggested earlier, the groundwater profile depicted in Figure 4.12 shows that the pyritic layer is generally exposed across the field site. During prolonged dry periods, such as around Day 262, the groundwater table can fall due to evapotranspiration and excessive drainage. In fact, in a nearby field site Blunden and Indraratna (2001) measured evapotranspiration rates in excess of 13 mm/day. These high evapotranspiration rates are likely due to the presence of vertical macropores in the soil structure and are exacerbated by clay flocculation and the formation of aggregates under drying conditions.

Several large rainfall events (see Chapter 3 for details) were recorded during the pre-modification period which recharged the groundwater table and increased the hydraulic gradient of groundwater flow towards the drain. For instance, over a 20-day period (Days 166-186) 70.4 mm of rainfall increased the phreatic zone surface approximately 0.2 m at the study site. Eight days after the rainfall (Day 194, Figure 4.13), the one-way tidal-restricting floodgates at the study site lowered the surface water elevation in the drain causing a strong hydraulic gradient to develop. The groundwater drawdown was attributed to the one-way floodgate restricting tidal flows and maintaining the low tidal mark within the drain. Moreover, the acidification of drain water during this period is supported by surface water records described in Chapter 5.

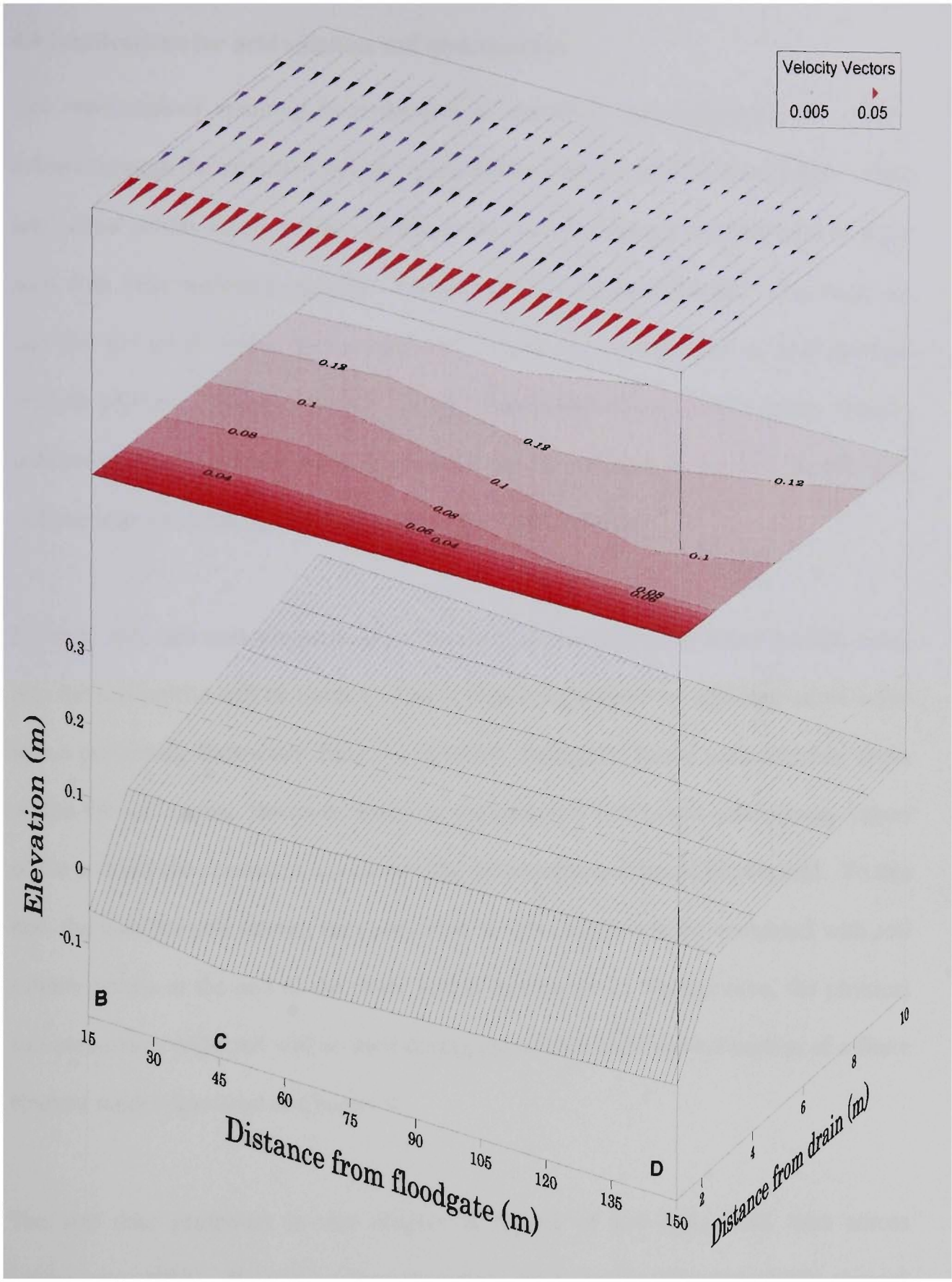

Figure 4.13 Groundwater elevation profile during a wet period before floodgate modifications (Day 194) with transects labelled B, C, and D. Note that the surface of the pyritic layer is depicted by the dotted line, and that the contour gradient and velocity vectors are in (m/day).

4.4 Implications for acid sulphate soil management

The repercussions resulting from decades of floodplain mismanagement are plainly evident through the extensive soil and groundwater data presented in this Chapter. High total actual acidity levels and low $Cl:SO_4$ ratios indicate strongly oxidised acid sulphate soils with little buffering capacity. Furthermore, the elevated sulphate concentrations and low pH levels within the groundwater suggest the translocation of acid products into the adjacent drainage network. In addition, chromium reducible sulphur contents indicate that a significant store of potential acidity remains in the soil profile and, without improved management, will add to the total acid load.

Physical soil data measurements show that lateral movements of saline surface water into the soil profile will be limited. This is important because by allowing saline water into a previously freshwater drain via modified floodgates, saline intrusion may occur within the soil matrix. However, based on the relatively low lateral conductivity values of the soil and the consistent annual rainfall, saline intrusion should be minimal. To this end, the baseline soil salinity data presented in this chapter will be compared with soil salinity values at the end of the study period in Chapter 7. Furthermore, the physical soil parameters collected will be used during the initialisation and calibration of a finite element model discussed in Chapter 9.

The soil data presented in this chapter is typical of low-lying ASS sites across southeastern NSW. Extensive physical testing conducted by Blunden (2000) showed hydraulic conductivity values were within 5% and soil porosity values were within 8% of this field site. Also, broad scale soil chemistry data taken from throughout the floodplain (Lawrie, 2002) showed similar trends with regards to TAA values and

chromium reducible sulphur contents. As the success of an acid sulphate soil management strategy such as tidal buffering, is directly related to the acidity and physical parameters of the soil, the conditions at this study site provide an optimal trial location.

Understanding the origin of acid drainage is the first step in effectively managing acid sulphate soils. The second step is to determine how the acid is transported through the phreatic zone and what its influence will be on receiving surface waters. The groundwater chemistry and elevation measurements presented in this Chapter indicate widespread acidification both spatially and temporally, while also demonstrating strong transport mechanisms generated by low drain water elevations maintained by the one-way floodgates. The impact of pyrite oxidation and transport on drain water quality before floodgate modification is discussed in Chapter 5.

Chapter 5.0 Drain Water Quality Before Floodgate Modifications

5.1 Introduction

As discussed in Chapter 4, various soil and groundwater parameters at the study site indicate extensive pyrite oxidisation and strong transport gradients of acid products towards the surface drain. In this Chapter, the extent, duration, and magnitude of drain water acidification associated with groundwater seepage prior to floodgate modifications are discussed. In particular, the role one-way floodgates play in exacerbating acidic conditions and the influence of altered climatic periods on buffering dynamics are examined.

To provide a concise discussion on the above themes, this chapter is divided into four major sections. In the first section, the spatial distribution of drain water quality is investigated to determine the extent of acidic groundwater seepage across the study domain. Total drain water acidity, the possible sources and abundance of each chemical species, and their variance with time are given to provide a detailed description of the drain water quality. This data is useful in determining the nature and mechanisms of acid inputs across the drain and in establishing baseline conditions.

The second section of this Chapter examines the temporal variations of drain and creek water acidity in response to climatic factors such as rainfall and evapotranspiration. Floodgate leakage is included as an additional factor controlling drain water quality This is because field records indicate that climatic factors can trigger changes in drain water quality depending on groundwater and estuarine dynamics, and that floodgate leakage fosters the intrusion of buffering agents.

The third section of this Chapter examines the environmental impacts of one-way floodgates, including the way in which an acid reservoir is created upstream of the one-way floodgate, and the subsequent discharge of acidic water on the ebb tide when the concentration of buffering agents and dilution are minimal. Examples of additional environmental problems associated with one-way floodgates such as limited fish passage, the growth of exotic weeds, low dissolved oxygen levels and the formation of mono-sulphide deposits are also described. This Chapter concludes with a comparison of water quality parameters from two control drains (with and without floodgates) located north and south on the study drain. These data highlights the beneficial impact of tidal buffering within flood mitigation drains and emphasises that tidal restoration via modified floodgates will not decrease agricultural productivity.

5.2 Spatial variance in drain water quality

In this section, drain water quality is described at various sampling sites to investigate the spatial distribution and extent of acid contamination before floodgate modifications. The baseline water quality data will also be used to determine the change in drain water quality after floodgate modifications (described in Chapter 7). To deliver a concise discussion on the subject, field results are limited to selected sites upstream of the floodgate. The remaining results are detailed in Appendix B.

5.2.1 Drain water pH

Figure 5.1 depicts the acidic drain water conditions prevalent within the flood mitigation drain at selected locations. Throughout the pre-modification period, drain water pH fluctuated between 2.57 (45 m, Day 80) to 7.30 (250 m, Day 157). Median

drain water pH at all locations was 4.47, however, by excluding the 250 m site, median pH decreased slightly to 4.32.

The complex drainage hydrology of the study site plays an important role in determining drain water acidity. The 45 m site was most acidic because a secondary side drain discharged extremely acidic water (pH < 3.0) into the primary drain at this point (see Figure 3.8 for reference). This smaller drain was designed to remove excess surface and groundwater runoff from a backswamp area north of the main drain, and was a significant contributor to the total acid load.

Conversely, due to upland inflow and diverted groundwater flows, the 250 m site had the highest pH measurements. This was attributed to circum-neutral pH waters being discharged into the drain from the upland sub-catchment, which diluted acidic groundwater. In addition, as detailed in Chapter 4, the one-way floodgates influence over the hydraulic gradient decreases with distance from the floodgate, and, as this site is 250 m from the floodgate, pyrite oxidation is limited. Furthermore, during the study the landholder deepened an existing surface drain which flows in a southerly direction away from the study drain. This drain discharged into the control non-floodgated drain and may have diverted some acidic groundwater flows away from the trial drain.

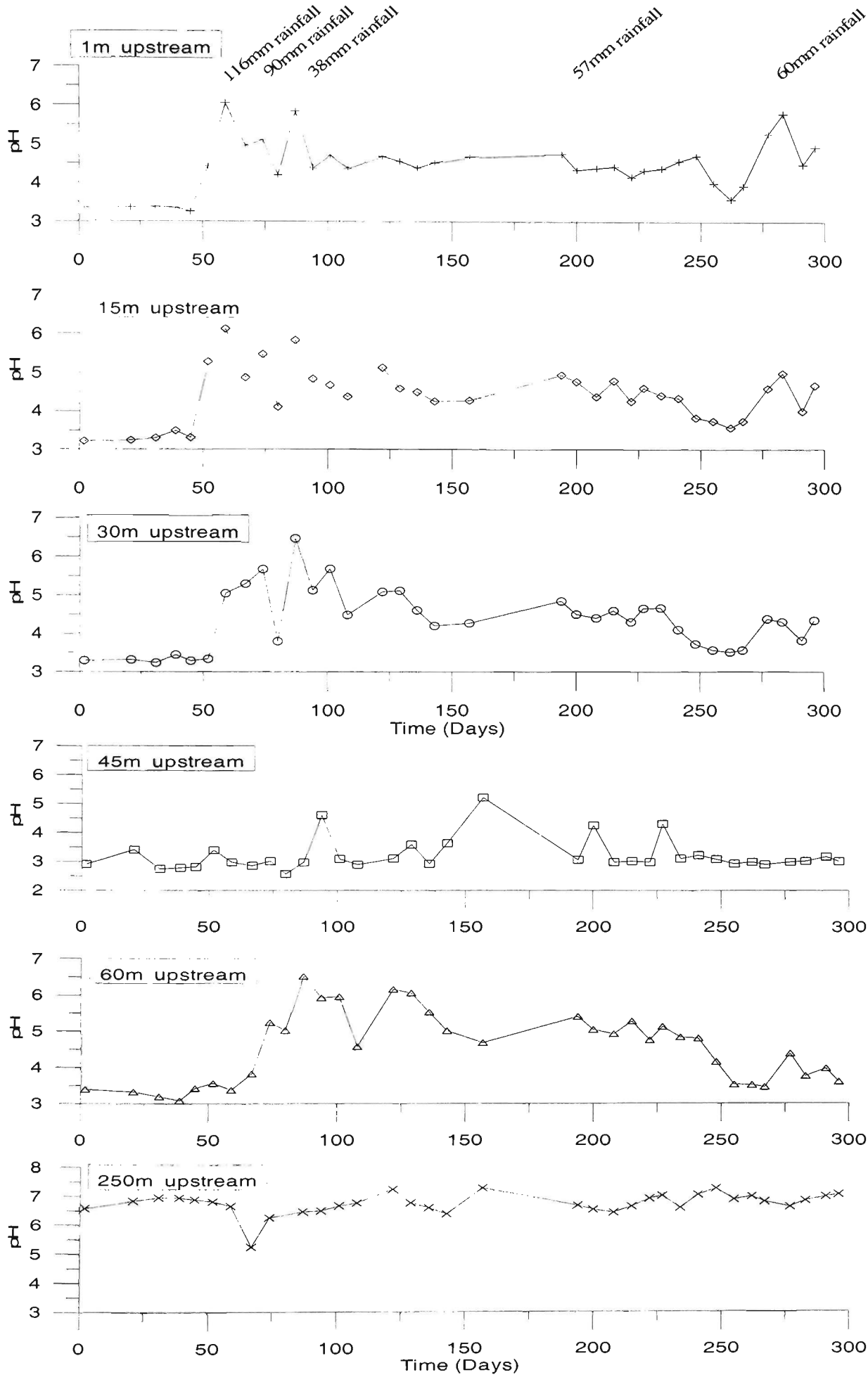

Figure 5.1 Drain water pH readings upstream of the floodgate with rainfall.

The low pH levels found within the study drain illustrate the influence of pyrite oxidation on surface water acidity and are typical of other acid sulphate soils in the region. ANZECC guidelines (1992) require marine waters to have a pH between 6.5-9.0, however, drain water pH immediately upstream of the floodgate ranged from 3.24 to 6.04, with a median pH of 4.41. This demonstrates that water discharging from the study drain was consistently below ANZECC criteria and that drainage of these waters through one-way floodgates will degrade the estuarine environment. Moreover, these pH readings are typical of other floodgated drains throughout the Broughton Creek floodplain (Pease *et al.*, 1997; Chapman, 1995; Indraratna *et al.*, 1995), and illustrate the urgent need for new management strategies such as tidal buffering via modified floodgates.

5.2.2 Acidic cations

The high concentration of dissolved monomeric aluminium and total dissolved iron within surface drainage waters is due to the solubility of dissolved aluminium and iron minerals, formed as a consequence of groundwater acidification from pyrite oxidation, and the release of cations bound on cation exchange sites. The concentration of these metals within the drain at several locations is shown in Figures 5.2 and 5.4, respectively.

5.2.2.1 Aluminium concentrations

ANZECC guidelines state that when the pH is less than 6.5, aluminium levels must not exceed 0.005 mmol L^{-1}. Throughout the pre-modification period, drain water aluminium concentrations generally exceeded this level by more than one order of magnitude. As with pH, aluminium levels were highest 45 m upstream of the floodgate

and lowest 250 m upstream. Concentrations ranged from 0.007 mmol L^{-1} (Day 31, 250 m upstream) to 4.35 mmol L^{-1} (Day 296, 45 m upstream), and averaged 0.62 mmol L^{-1}. Pease *et al.* (1997) and Blunden (2000) reported similar maximum Al^{3+} concentrations of 4.4 mmol L^{-1} and 5.2 mmol L^{-1}, respectively.

The solubility of aluminium in surface water is complex and reliant on several factors including ionic concentrations and pH. The elevated Al concentrations shown in Figure 5.2 are primarily due to the dissolution of silicate clays and aluminium minerals under acidic groundwater conditions. As detailed in Equation 2.9, the hydrolysis of illite, a common estuarine clay, releases 1.95 moles of aluminium for every mole of illite. This process is pH dependent and several researchers (Blunden and Indraratna, 1997; Sammut *et al.*, 1996) have found inverse correlations between pH and aluminium concentrations.

The relationship between surface water aluminium and pH levels at the study site is shown in Figure 5.3. As depicted in this Figure, a decrease in pH levels, which signifies an increase in H^+ ions, correlates to an exponential increase in inorganic monomeric aluminium concentrations. Based on this analysis, increasing drain water pH above 6.5 will lower aluminium below ANZECC (1992) guidelines (100 mmol when pH >6.5). Furthermore, the linear regression analysis ($r^2 = 0.88$) presented may provide a quick, first approximation method in determining *in-situ* aluminium concentrations as a function of pH.

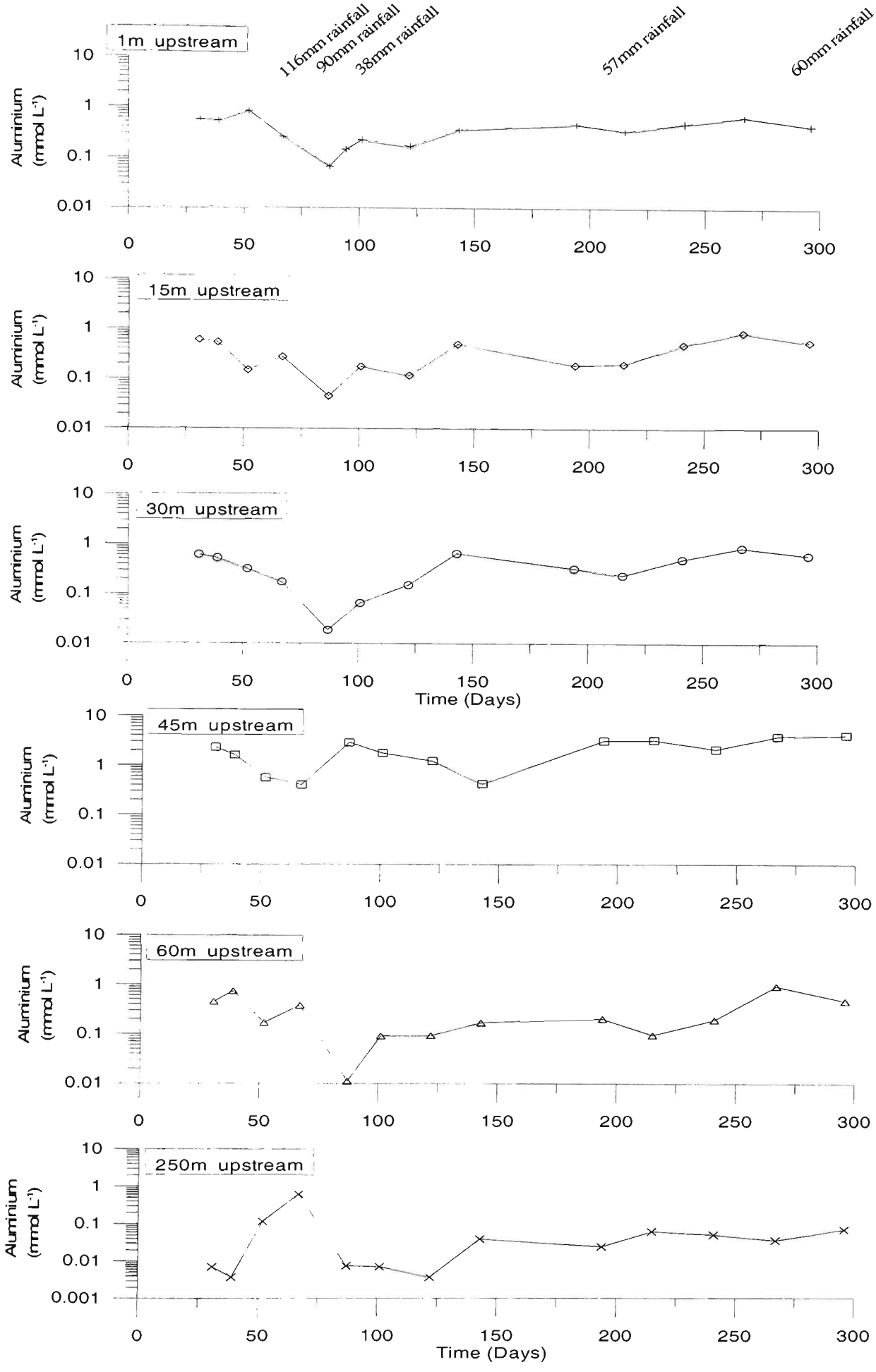

Figure 5.2 Dissolved inorganic monomeric Al^{3+} concentrations in drain water upstream of the floodgate with rainfall.

It is interesting to note, that although pH and Al^{3+} concentrations are highly correlated in drainage waters, the slope of the correlation line is flatter than in previous groundwater studies. Several researchers (Sposito, 1995; Neal, 1988) have reported a slope greater than –3.0 within groundwater samples, however, in Figure 5.3 the slope is –0.179. The difference between groundwater and surface water findings was attributed to increased cation exchange capacity and the formation of aluminium sulphate minerals within the groundwater. The flatter slope may also be due to the dilution of the original groundwater effluent with low ionic upland inflow from the catchment. Nonetheless, this correlation indicates that improved drain water pH conditions created by tidal buffering will result in a significant decrease in dissolved inorganic aluminium.

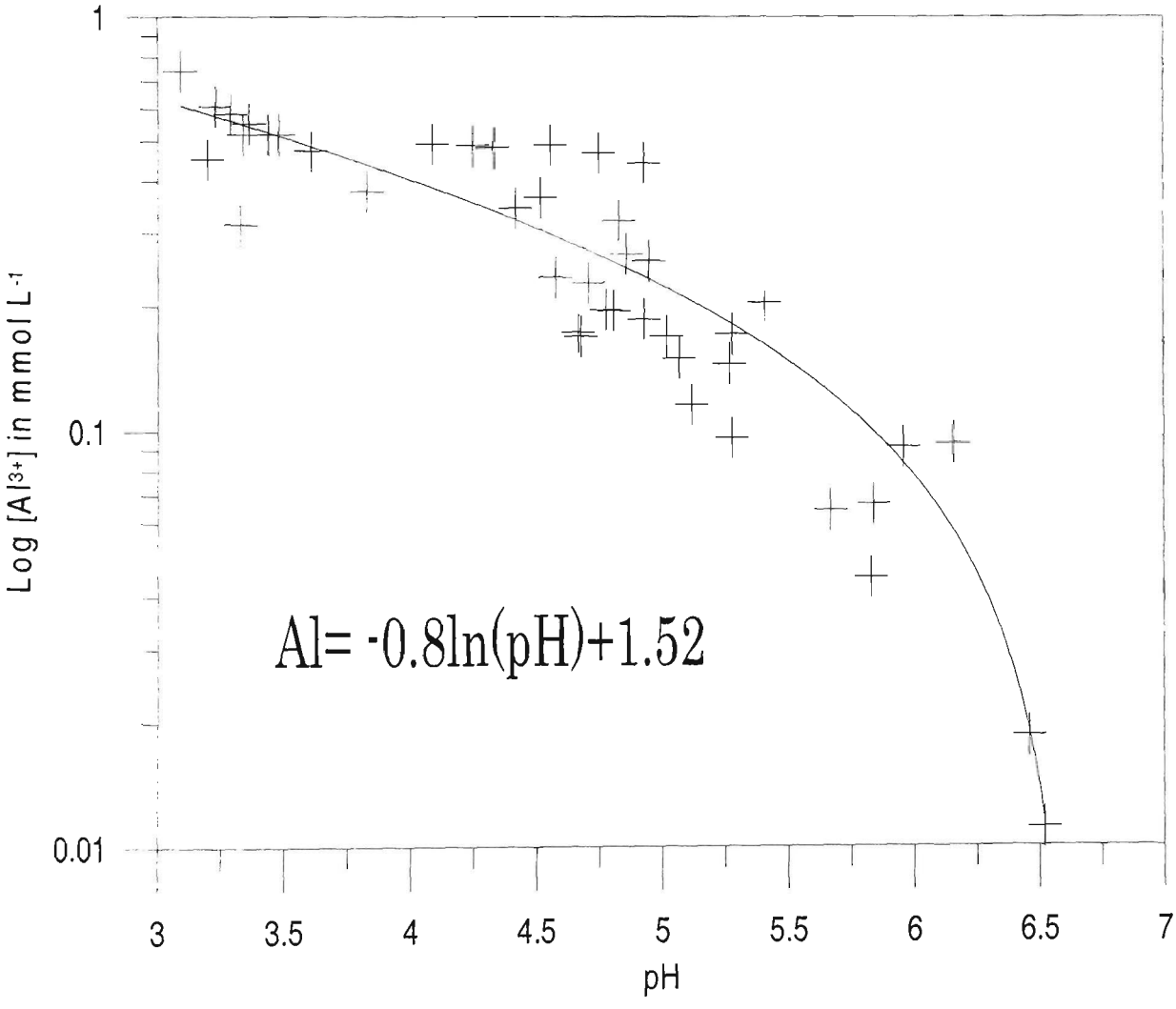

Figure 5.3 Correlation between drain water pH and dissolved aluminium concentrations.

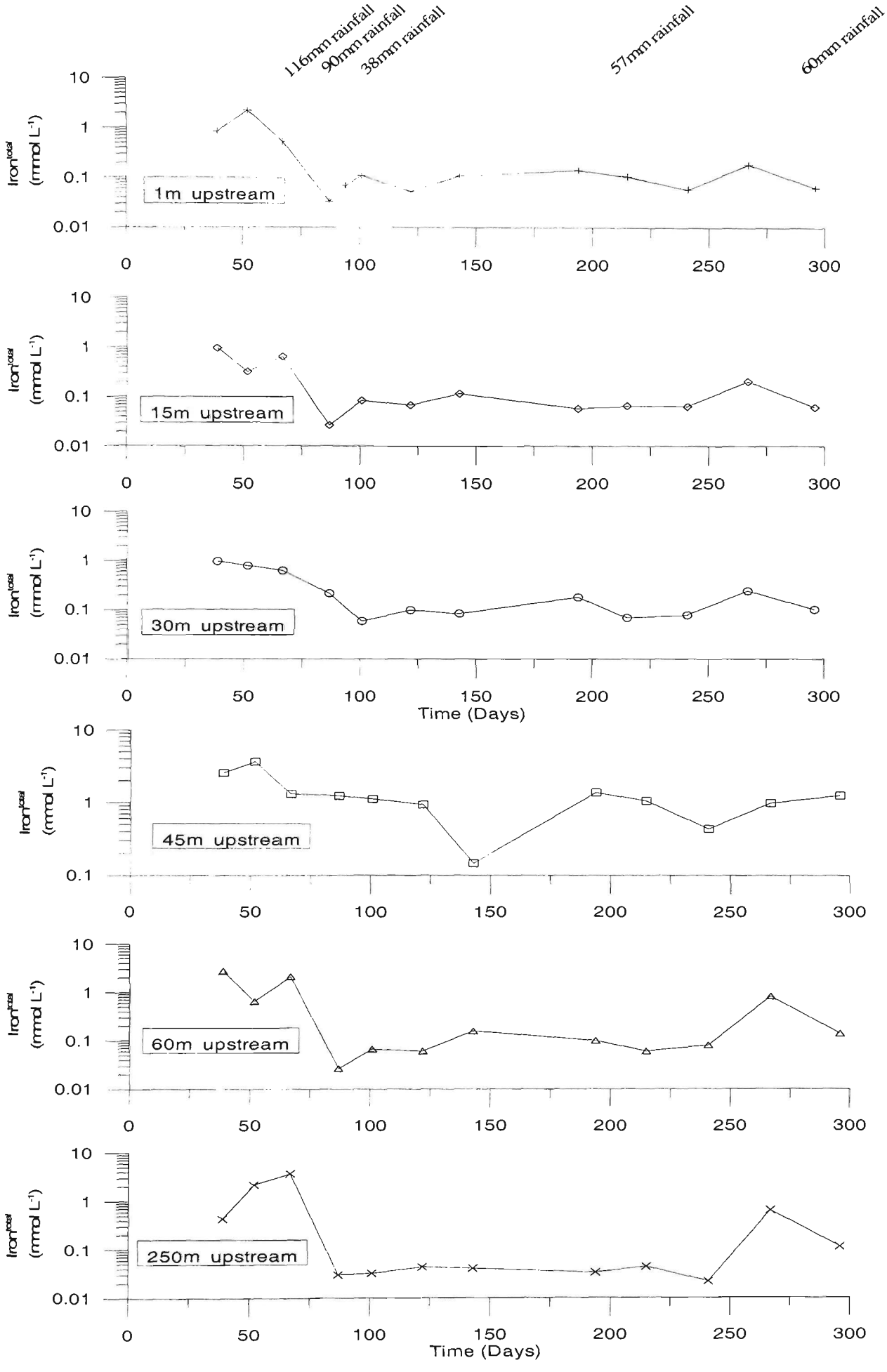

Figure 5.4 Total dissolved iron concentrations in drain water upstream of the floodgate before floodgate modifications with rainfall.

5.2.2.2 Iron concentrations

Elevated total iron concentrations upstream of the floodgate before floodgate modifications were indicative of strong acid sulphate soil oxidation and leaching. Total iron concentrations were measured in order to include both soluble ferrous and ferric contributions in the form of suspended particulate. Ferric particulates were measured because of the electrochemical impact of halmyrolysis and ion exchange in estuaries.

The concentration of Fe^{total} throughout the drain before floodgate modifications is shown in Figure 5.4. ANZECC (1992) guidelines require dissolved iron concentrations below 0.009 mmol L^{-1} for the protection of aquatic ecosystems. Concentrations above this level have been associated with fish disease and deoxygenation of surface waters. In all cases, total dissolved iron concentrations within the study drain were above previous findings and in excess of ANZECC (1992) criteria. Fe^{total} levels averaged 0.57 mmol L^{-1} and peaked on Day 52 at 3.69 mmol L^{-1} (45 m upstream). These conditions show the strong pyrite oxidation environment present throughout the sub-soil. Furthermore, the maximum concentration is nearly one order of magnitude greater than previous studies conducted in the Shoalhaven region by Blunden (2000) (0.45 mmol L^{-1}) and Pease *et al.* (1997) (0.4 mmol L^{-1}). This increase is partly due to the calculation of total dissolved iron versus ferrous iron conducted by previous researchers, but also due to the extreme acidic conditions discharging from the secondary drain 45 m upstream of the floodgate.

The generation of ferrous iron from the oxidation of pyrite and the secondary oxidation of ferrous to ferric iron, termed 'acid at a distance', is expressed as:

$$FeS_2 + 7/2\,O_2 + H_2O \rightarrow Fe^{2+} + 2SO_4^{2+} + 2H^+ \qquad (5.1)$$

$$Fe^{2+} + \tfrac{1}{4}O_2 + H^+ \rightarrow Fe^{3+} + \tfrac{1}{2}H_2O \quad (5.2)$$

The temporal fluctuations in Fe^{total} are due to its chemical interrelationships with pH and redox potential. As pH increased, the concentration of Fe^{total} decreased due to iron flocculation in the form of iron monosulphides (Equation 5.2). To this point, a significant store of iron monosulphides was noted covering the drain invert and when oxidised, either through dredging or during storm events, these minerals produce additional acidity and consume dissolved oxygen. Furthermore, the spatial distribution of Fe^{total} was more consistent throughout the drain than pH or aluminium, which illustrates widespread pyrite oxidation and acid seepage.

5.2.3 Total drain acidity

Hicks *et al.* (1999) proposed the determination of total acidity to evaluate the contribution of acidic cations relative to H^+ ions. In acid sulphate soil environments, the primary contributing acidic cations are iron and aluminium.

Total acidity, calculated as the sum of H^+, Fe^{total} and Al^{3+}, is shown in Figure 5.5 for selected drain sampling sites. At these sites, aluminium and iron were the main contributors to the total acid load within the first 87 days. Specifically, on Day 52 (1 m upstream) total acidity was more than 0.003 mol L^{-1} due primarily to the aforementioned high iron and aluminium concentrations (72% and 26%) and to a lesser extent from H^+ ions (2%). The concentration of total acidity is described below for the remaining pre-modification period.

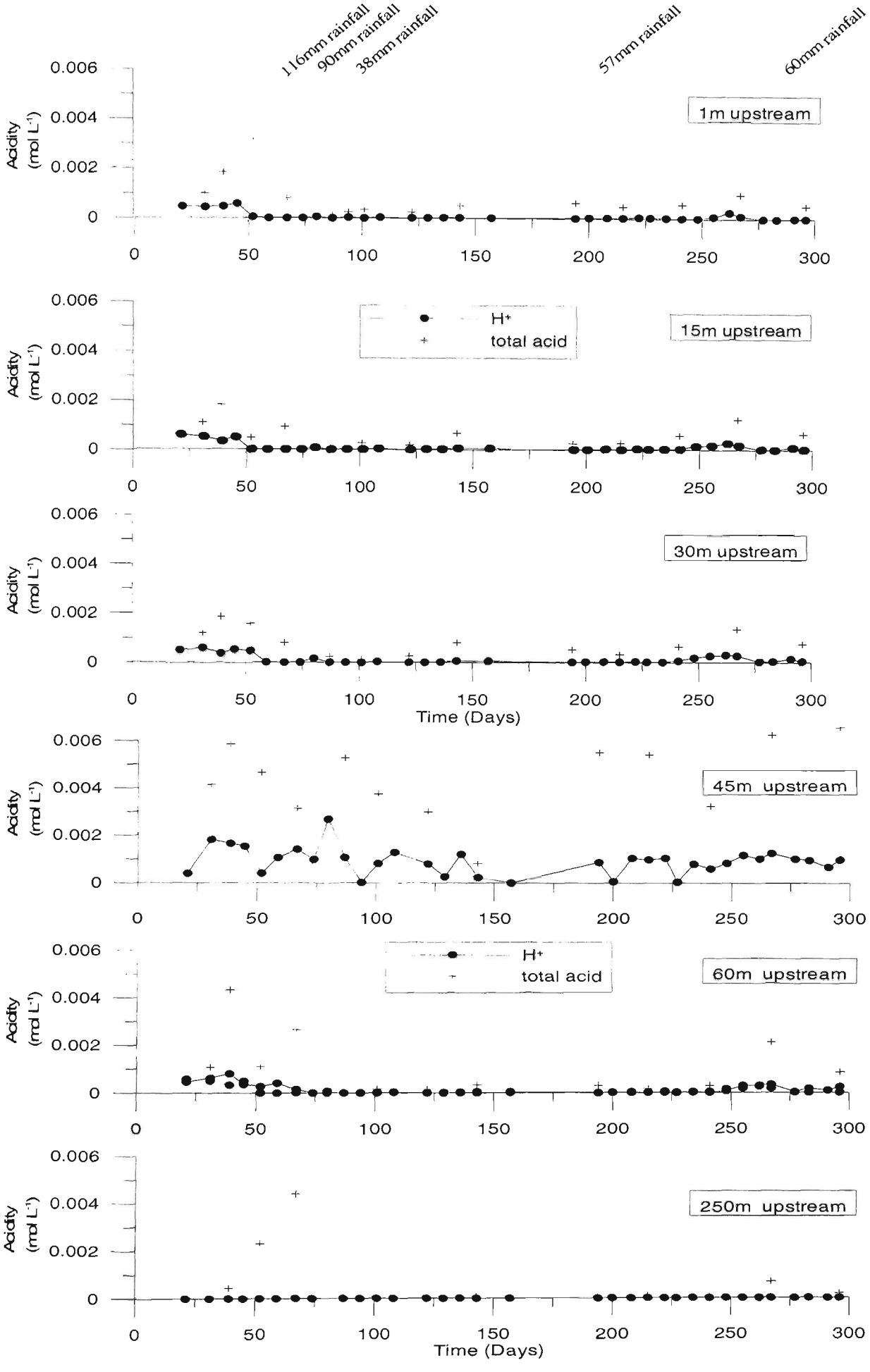

Figure 5.5 Drain water total acidity upstream of the floodgate before modifications with rainfall.

Overall, total drain water acidity decreased from Day 87 to Day 241, due to a combination of factors including (i) floodgate leakage, which increased aluminium and iron flocculation and removed soluble concentrations from the water column, and (ii) a long dry period, which lowered the groundwater table. As the groundwater table fell, the potential energy of the hydraulic gradient decreased and the mass transport of oxidation products was reduced. However, the lower total acidity measurements during this period are disproportionably represented by acidic cations, with aluminium and iron constituting 72% and 22% respectively, of the total acid load.

Towards the end of the pre-modification period (Days 241-296), the total acid load increased. Due to the extreme conditions which were discharging from the side drain (> 0.004 mol L^{-1}) total acidity was near or above 0.001 mol L^{-1} on Day 267, at 1, 15, 30, 45 and 60 m upstream of the floodgate. This period was similar to the initial conditions and suggests cyclical acid inputs triggered by rainfall. The temporal variance of each chemical species due to climatic factors and floodgate performance is discussed in more detail in Section 5.3.

Total acidity levels within the drain are typical of acid conditions throughout the Shoalhaven region. Blunden (2000) reported total acidity levels of a similar magnitude (maximum concentration = 0.007 mol/L) and noted that pH alone underestimates total drain water acidity. Once discharged from the flood mitigation drain, the high acidity poses a significant threat to aquatic life. For instance, conversion of total acidity to pH on Day 52 (conservatively assuming 1 mole per acidic cation = 1 mole H^+ ions) depicts a decrease in pH of nearly two orders of magnitude from 4.41 to 2.44. Therefore, total

drain water acidity, as well as pH, needs to be considered when implementing acid neutralisation management strategies such as tidal buffering via modified floodgates.

5.2.4 Anion, cations and electrical conductivity

The concentration of soluble anion and basic cations in the drain water upstream of the floodgate provides insight into the pyrite oxidation conditions occurring within the sub-soil, the spatial distribution of pyrite oxidation products across the study site, and the impact of one-way floodgates in restricting tidal buffering. Furthermore, electrical conductivity, as a function of total dissolved solids and/or chloride concentrations, is useful in determining the relative contributions of fresh, acidic, and saline water to drain water hydrochemistry. The concentration of basic cations, anions, and electrical conductivity across the drain prior to floodgate modification is shown in Figures 5.6-5.10, respectively.

5.2.4.1 Basic cations

The relative contribution of basic cations (Na^+, Ca^{2+}, Mg^{2+}, and K^+) within drain water is shown in Figure 5.6. Overall, Na^+ was dominate, Ca^{2+} and Mg^{2+} contributed in relatively equal proportions, and K^+ concentrations were generally the lowest. Within the drain profile, cations were typically highest 1 m upstream of the floodgate and decreased to their lowest levels 250 m upstream. However, the site 45 m upstream showed elevated concentrations of all species, except Na^+, due to the secondary drainage line discharging extremely acidic water into the primary drain. The concentration range of each cation was uniform throughout the pre-modification period, except for increases in Ca^{2+} and K^+ in the first 75 days, and increases in all cations after Day 241.

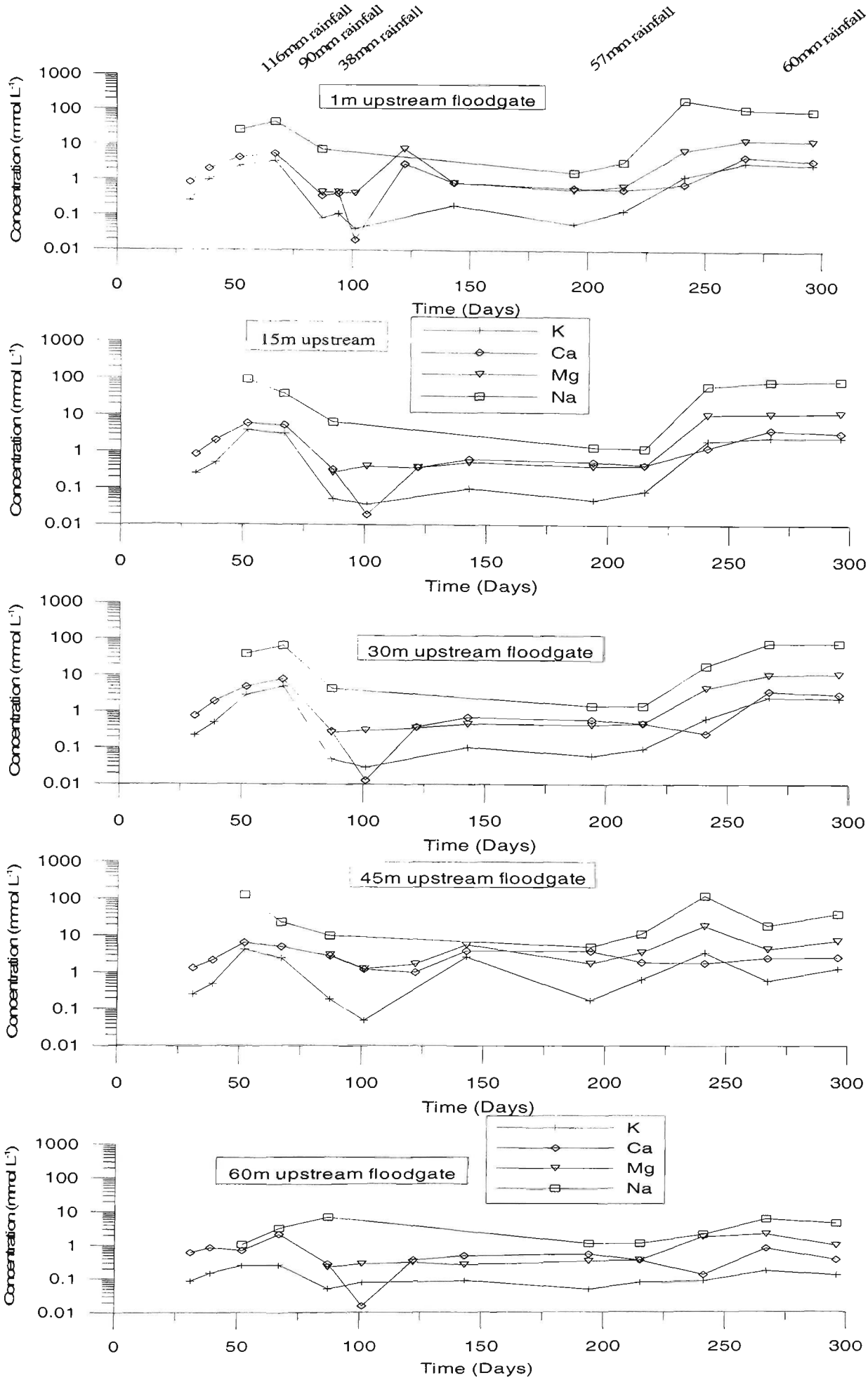

Figure 5.6 Soluble cation concentrations upstream of the floodgate with rainfall.

The concentration of Na^+ ions within the drain is indicative of clay dissolution under acidic conditions and the relative upland discharge versus saline ingress through floodgate leakage. In regards to clay dissolution, the hydrolysis of Na^+ clays liberate 0.36 moles of Na^+ for every mole of illite, which may account for Na^+ in regions where little to no tidal water was found. However, the concentration of Na^+ in seawater is high (10,500 mg L^{-1}), and the abundance of Na^+ in the drain is likely due to saline water penetrating upstream of the floodgate. Though the ingress of saline tidal water is the main objective of floodgate modifications, the quantity of tidal water intruding via seepage upstream of the leaky floodgates is substantially less and does not generally provide sufficient buffering capacity to improve water quality. This hypothesis is further substantiated by decreasing Na^+ concentrations with distance from the floodgate (i.e. 1 m versus 250 m upstream) and high drain water acidity.

The abundance and distribution of Ca^{2+} is similar to Na^+ and is related to floodgate performance and groundwater conditions. Blunden (2000) suggests that the high concentration of Al^{3+} released during hydrolysis of estuarine clays may exchange with Ca^{2+} from the cation exchange complex and release Ca^{2+} into solution. Ca^{2+} concentrations in the drain water may also be due to advective/diffusion transport upstream (i.e. seawater concentration = 400 mg L^{-1}) of the floodgates or the solubilisation and mobilisation of agricultural lime ($CaCO_3$).

A wide concentration range of Ca^{2+} was recorded during the pre-modification study period. From Figure 5.6, it is evident that the highest concentrations are evident 1 m and 45 m upstream of the floodgate, which lends credence to both brackish water ingress via leaky floodgates and dissolution of estuarine clays and subsequent

groundwater seepage. In the initial 70 days, Ca^{2+} concentrations increased from 0.8 to 5.0 mmol L^{-1} (1 m upstream), but the increase was less notable with distance from the drain. This increase is in line with a rise in pH and EC levels, which is indicative of saline water ingress. Rainfall prior to Day 100 enhanced drain water flushing and decreased Ca^{2+} concentrations, except at 45 m upstream where Ca^{2+} levels were maintained through acidic runoff discharging soluble Ca^{2+}. For the remainder of the pre-modification period, Ca^{2+} levels were relatively stable and decreased with distance from the floodgate. The slight increase shown at the end of this period was attributed to creek water leakage caused by floodgate manipulation trials.

Magnesium and potassium measurements are similar with those presented by Blunden (2000) in a nearby site. While Mg^{2+} levels were consistently higher then K^+, the temporal fluctuations of both cations were consistent across the drain. During this period, K^+ and Mg^{2+} concentrations followed those of Na^+ and Ca^{2+}. In the first 70 days, concentrations initially increased but then fell to a stable level until around Day 250 when they returned to earlier concentration levels. The supply of Mg^{2+} and K^+ may also be due to saline ingress (1300 mg L^{-1} and 380 mg L^{-1} in seawater, respectively), or the dissolution of estuarine clays. Low K^+ concentrations were attributed to the formation of jarosite or alunite within the soil profile, which requires soluble K^+, SO_4^{2-} and an acidic environment. As noted in Chapter 4, jarositic mottles were abundant in the active acid sulphate soil layer and are the main store of K^+ in the soil profile.

5.2.4.2 Anion Concentrations

Soluble chloride and sulphate concentrations are shown in Figure 5.7. Chloride is a conservative species and hence, a strong indicator of saline ingress upstream of the

floodgate. Therefore, the three periods of high soluble Cl^- concentrations (i.e. the initial 70 days, Days 140-175, and the final 50 days), and its decreasing concentrations with distance from the floodgate is evidence that saline ingress occurred prior to modifications. This is important to note because it depicts that chloride salts were not causing undue harm to agricultural productivity, which is a major concern to landholders involved with the study. This also suggests a source for the elevated soil chloride concentrations found with depth upstream of the floodgate and discussed in Chapter 4. Moreover, other researchers (Pease, 1997; Wilson *et al.*, 1999; Johnston *et al.*, 2003) have noted elevated chloride levels upstream of one-way floodgates, and, thus, the conventional belief that one-way floodgates restrict saline intrusion is unfounded, and, as long as overtopping is restricted, saline intrusion should not pose a significant concern to the soil matrix.

High sulphate levels within the drain are characteristic of acid sulphate soil leaching and at the study site dissolved sulphate concentrations were consistent both spatially and temporally. Average sulphate concentration at all sites was 4.71 mmol L^{-1}, but concentrations were significantly greater 45 m upstream of the floodgate (average 12.36 mmol L^{-1}). Excluding the 45 m sampling site, sulphate concentrations were greatest at the floodgate (enhanced by saline ingress and the increased hydraulic gradient of groundwater nearest the floodgate), and least 250 m upstream. Nonetheless, the consistently high sulphate concentrations throughout the drain depict the overall influence of acid sulphate soil contamination.

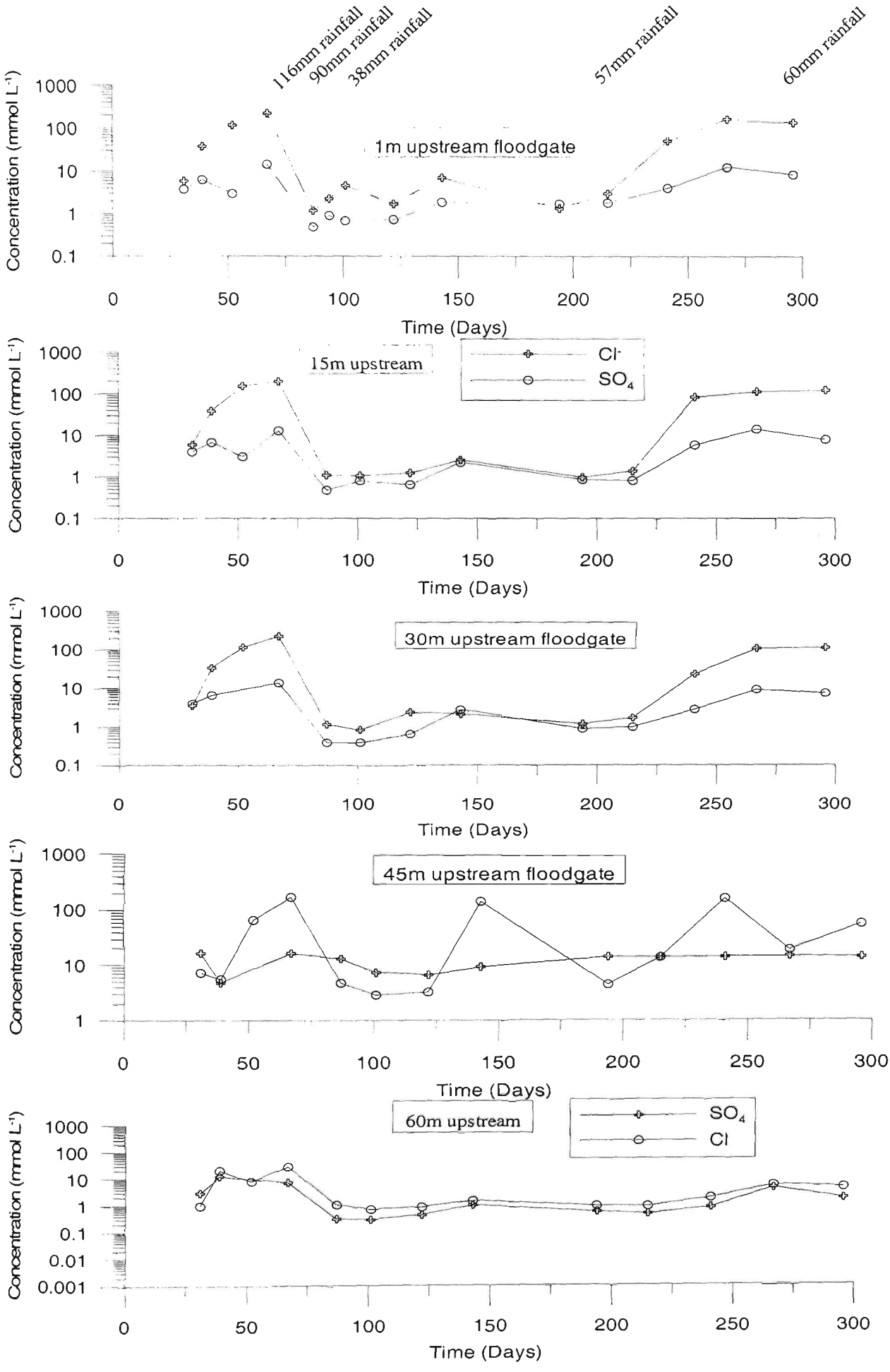

Figure 5.7 Dissolved Cl^- and SO_4 concentrations upstream of the floodgate with rainfall.

As described in Chapter 4, the chloride/sulphate ratio shown in Figure 5.8 is primarily used to determine the extent of pyrite oxidising conditions. At the field site, the influence of elevated chloride concentrations due to tidal leakage (chloride/sulphate ratio > 2) is apparent at the beginning, around Day 150, and at the end of the trial period 1 m upstream of the floodgate. However, at 60 m upstream of the floodgate, and during the majority of the study at 1 m upstream, the chloride/sulphate ratio was below 2.0 and primarily below 1.0. These results indicate (i) a strong acid sulphate soil oxidising environment within the soil matrix, (ii) the limited amount of buffering agents within the drain, and (iii) the capacity for one-way floodgates to maintain acidic conditions. Floodgate modifications to restore tidal flushing will increase the chloride/sulphate ratio by neutralising drain water acidity and increasing chloride concentrations.

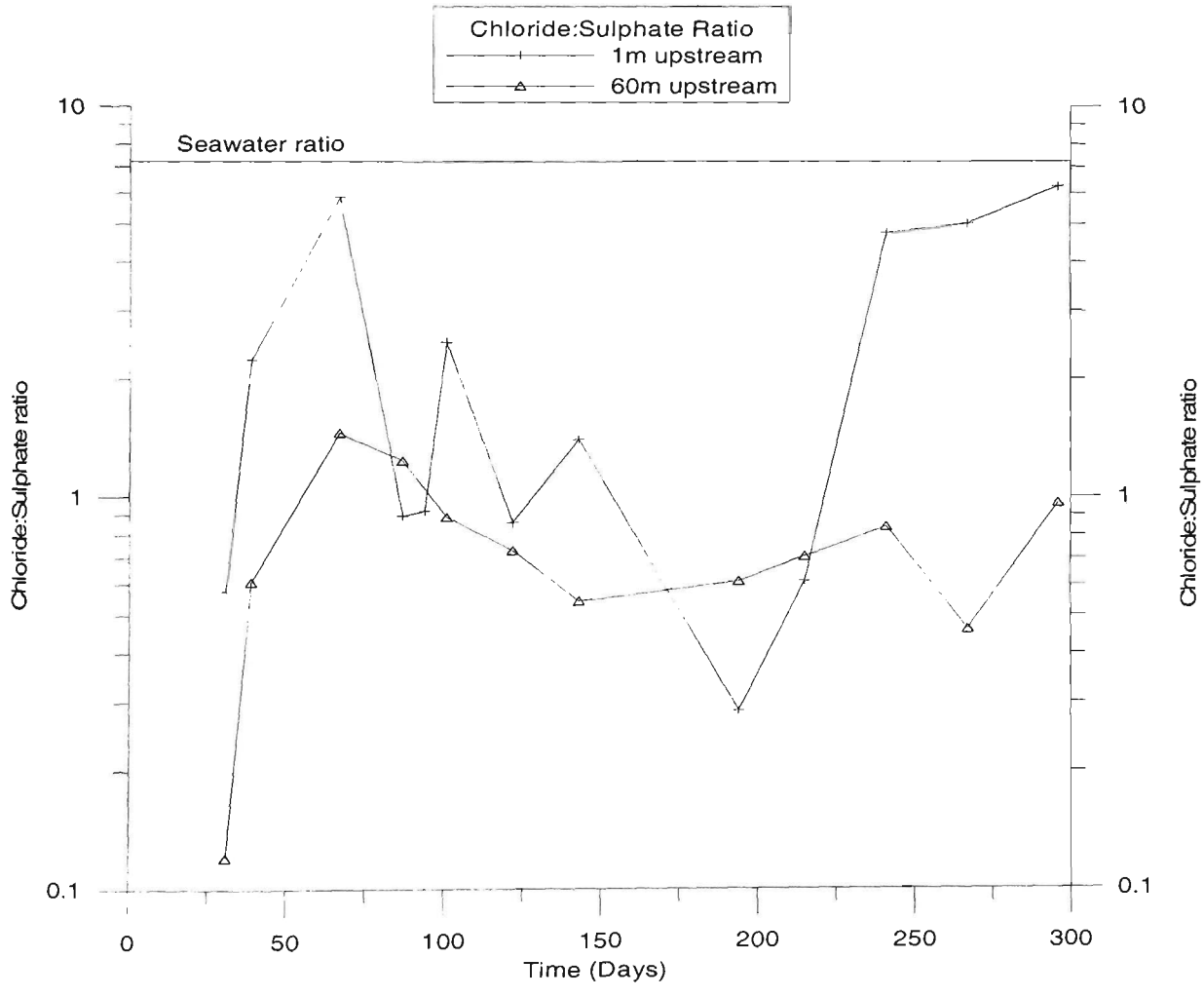

Figure 5.8 Chloride: sulphate ratio upstream of the floodgate prior to modifications.

5.2.4.3 Electrical conductivity

Electrical conductivity (EC) is a measure of the concentration of dissolved solids present within the drain water. As a result, EC readings in coastal areas primarily indicate the presence of salts such as sulphates, chlorides, bi/carbonates, calcium, magnesium or sodium. In acid sulphate soil affected drains, EC also signifies the generation of pyrite oxidation products such as aluminium and iron. Therefore, EC readings provide a useful measure as to the extent and magnitude of the tidal front within the estuary (seawater EC = 40 dS/m), and the presence of pyrite oxidation products within the drain.

Electrical conductivity measurements of water samples taken from Broughton Creek, and 1 m and 60 m upstream of the floodgate are presented in Figure 5.9. Generally, Broughton Creek samples were brackish to saline with sharp declines in EC after rainfall, thereby indicating low resident periods. Upstream of the floodgate, EC was significantly lower with drain water readings 1 m upstream more than 50% below Broughton Creek levels. Similarly, EC measurements 60 m upstream of the floodgate were one order of magnitude less than records taken 1 m upstream during dry periods. The difference in EC at the three sites was attributed to the one-way floodgates ability to restrict tidal flows, and, although minor leakage was evident, the low EC readings 60 m upstream indicate that saline intrusion decreased with distance. EC readings at all sites are given in Appendix B.

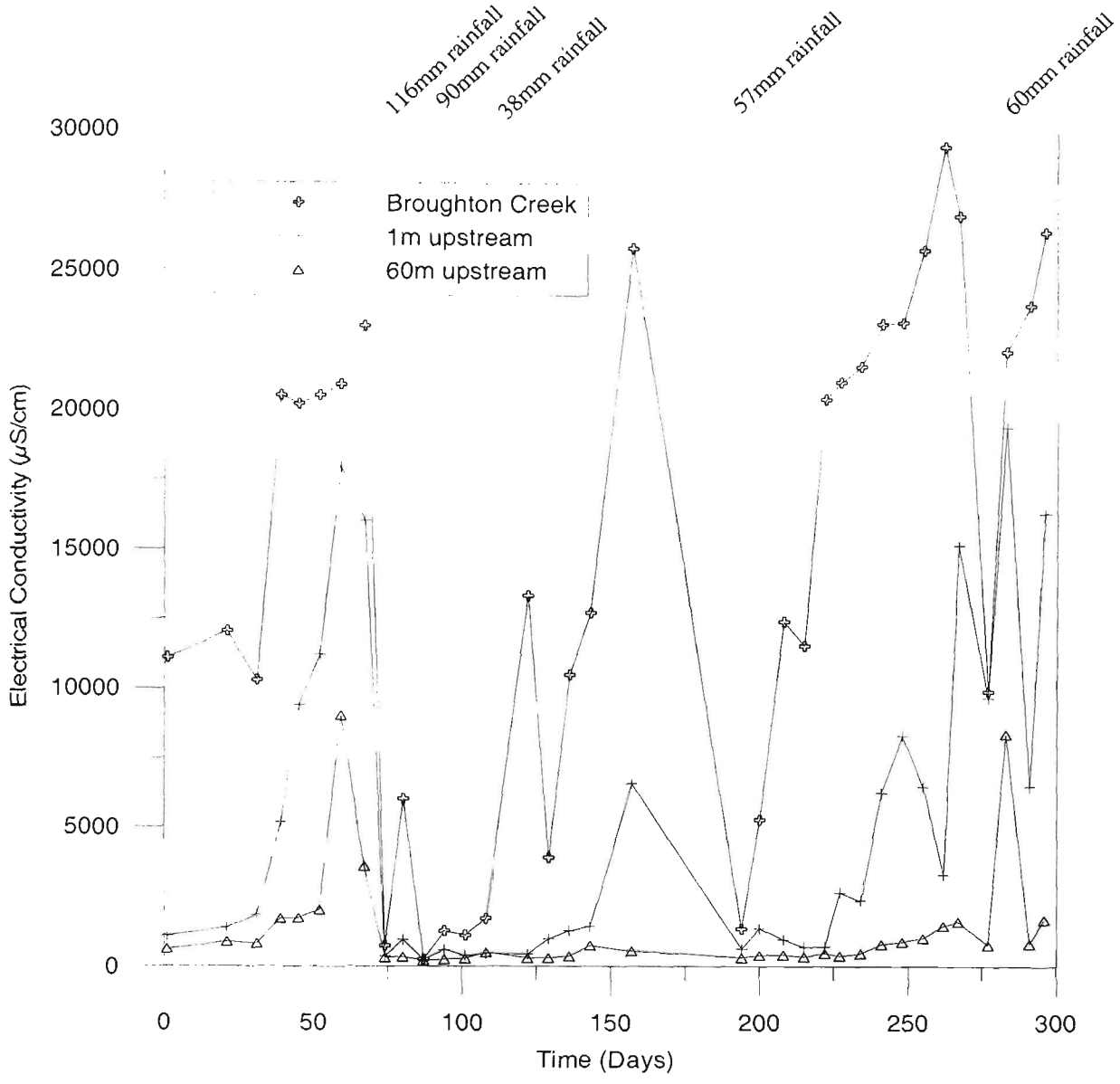

Figure 5.9 Electrical conductivity readings in Broughton Creek, 1 m upstream and 60 m upstream of the one-way floodgate.

Electrical conductivity fluctuated with rainfall both upstream and downstream of the floodgate. During the first 40 days, low EC (< 5000 µS/cm) conditions prevailed upstream of the floodgate indicating strong freshwater/acid water flows. Lacking additional rainfall, EC increased from Days 40-75 but then sharply fell to <1000 µS/cm from Days 75-143. This decline was attributed to 212.4 mm of rainfall recorded over a 20-day period, which flushed saline water from the creek/drain. With the return of the tidal front, brackish conditions (5000-1500 µS/cm) were recorded 1 m upstream of the floodgate during Days 143-194. Rainfall of 57.4 mm again flushed dissolved solids

from the drain and low EC conditions returned from Days 194-234. During the final 72 days of the pre-modification period, drain water EC increased to saline levels (>15000 μS/cm) 1 m and 60 m upstream due to drying conditions and floodgate manipulation trials. However, a brief decline in EC was noted around Day 262 due to 43.4 mm of rainfall.

While similar to upstream readings, EC measurements within Broughton Creek were significantly higher than within the drain. EC readings in the creek ranged from 250 μS/cm to 29,500 μS/cm and averaged 14,978 μS/cm. In comparison, EC averaged 5,215 μS/cm 1 m upstream, and 1,298 μS/cm 60 m upstream. Hourly electrical conductivity readings taken from a submersible datalogger downstream of the floodgate (Figure 5.10) depict consistently high EC readings (>20,000) in the creek throughout the pre-modification period interspersed with two freshwater periods caused by large rainfall. The influence of temporal fluctuations in EC relative to drain and creek water quality and floodgate leakage is further examined in Section 5.3.

5.3 Temporal fluctuations in drain water quality

Temporal fluctuations in drain water quality are dependant on climatic variables and inflows. In low-lying floodplains, the primary inflows are groundwater seepage (acidic), upland inflows from surface drainage (pH circum-neutral), and tidal flows (varying buffering capacity). White *et al.* (1997) suggested that water quality in tidal restricted flood mitigation drains could be categorised into wet or dry periods based on the prevailing hydrodynamics (i.e. groundwater seepage or upland inflow), however, a third condition termed 'tidal leakage' is presented here because of its unique chemical attributes.

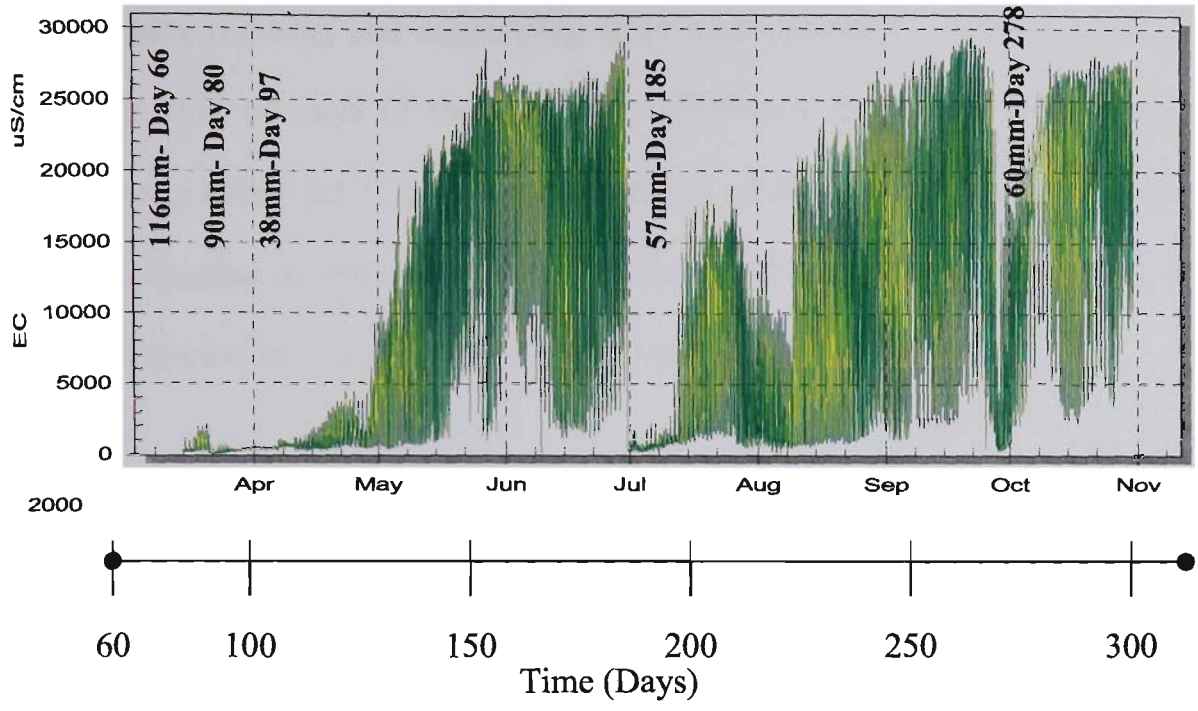

Figure 5.10 Electrical conductivity readings taken 1 m downstream of the floodgate (Datalogger O) before floodgate modifications.

In this section, water quality changes over the pre-modification period are described in regards to wet, dry and tidal leakage conditions due to fluctuations in inflow, groundwater response to climatic variables, creek hydrodynamics, and the salinity/carbonate regime. Continuous drain water pH readings taken from data loggers G and Q (Figure 3.8) located 1 m and 45 m upstream of the floodgate and rainfall data shown in Figure 3.14 are used to illustrate the different drainage periods. The prevalence of fresh or saline water within the drain is shown through electrical conductivity readings (Figures 5.9 and 5.10) and the commonly used sodium/chloride ratio shown in Figure 5.11.

5.3.1 Dry conditions (Days 1-60)

Dry periods were characterised by low pH levels and increasing total acidity. Under these conditions, one-way floodgates promoted groundwater leaching towards the drain

by continually restoring and maintaining drain water elevations at the low tidemark. During the first 60 days of the study, dry conditions maintained drain water pH predominately below 3.5 (Figure 5.1), and dissolved monomeric aluminium and total iron concentrations at most sites within the drain were greater than 1 mmol L^{-1}; more than 1000 times in excess of ANZECC (1992) guidelines.

As dry conditions continued, upland inflow from run-off decreased, which enhanced the intrusion of the highly ionic tidal front and increased electrical conductivity, as shown in Figure 5.9. To this point, Bear *et al.* (1993) states that a sodium/chloride ratio below 0.9 is indicative of saline intrusion. As shown in Figure 5.11, the Na/Cl ratio within drainage waters decreased during this period from strongly freshwater dominant (Na: Cl ratio > 2.0) to strongly saline dominant (Na/Cl ratio < 0.3). As with other dry periods, minor seepage through the floodgates was not sufficient to cause significant tidal buffering, and poor quality water was chronically discharged through the one-way floodgates.

5.3.2 Wet conditions (Days 60-100)

Neutral pH and low EC values, best depicted in data logger readings taken upstream of the floodgate (Figures 5.12), characterise the wet period beginning Day 60. Precipitation of 263.4 mm over the 40-day period triggered localised flooding and prolonged surface ponding, while the increased upland inflows briefly raised pH from 3.36 to 6.87, and maintained electrical conductivity below 500 $\mu S\ cm^{-1}$. These findings are predictable considering the 200% increase in drain water elevations measured at data loggers G and Q, and the dilution of acid waters. Similarly, increased flushing restricted tidal reach and the Na/Cl ratio increased to 2.45.

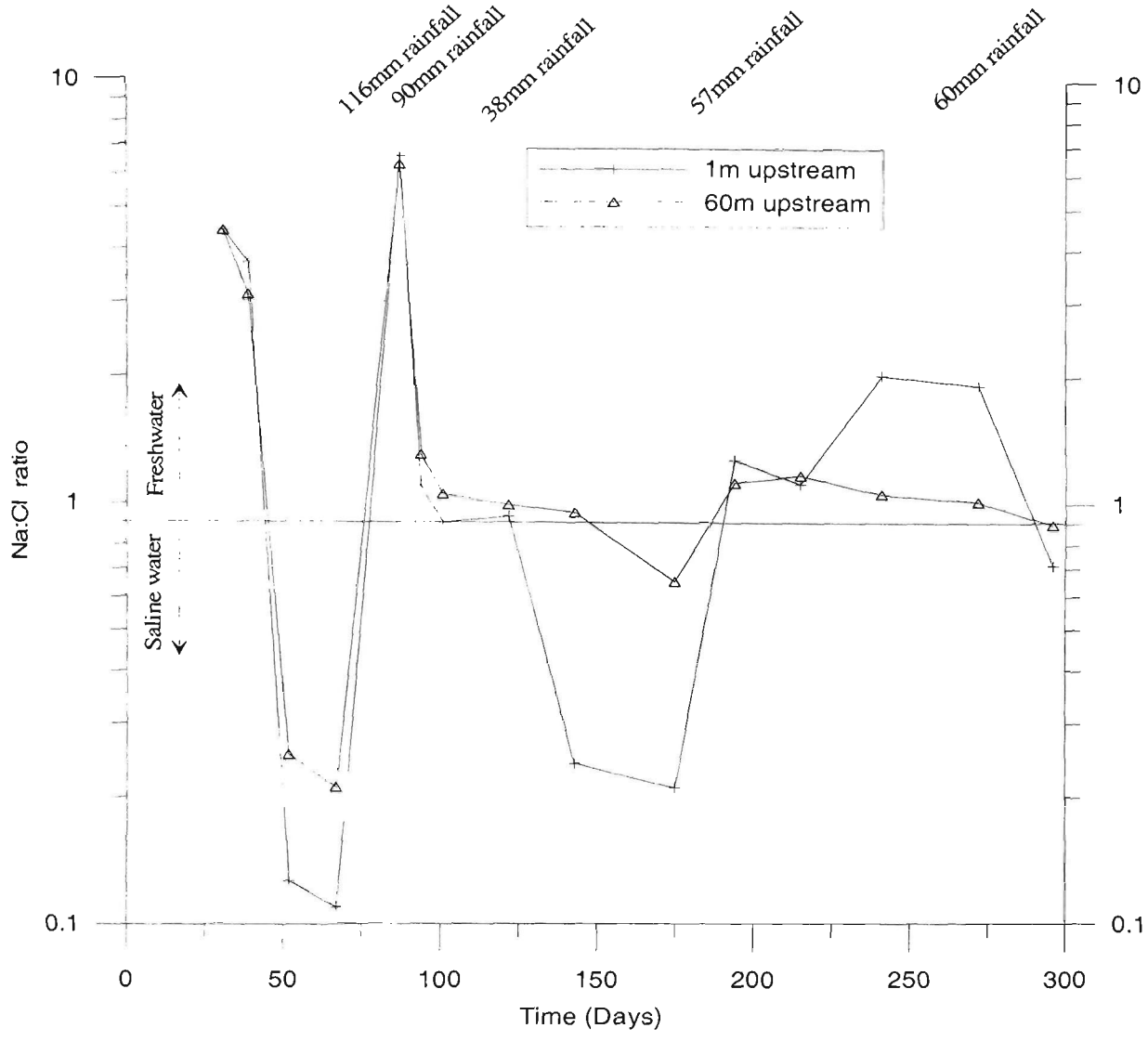

Figure 5.11 The Sodium:Chloride ratio upstream of the floodgate with rainfall.

While initially improving drain water quality through dilution, wet periods were mainly characterised by extended (3-11 week) acidic conditions caused by groundwater seepage following recharge of the phreatic zone. In particular, soils with a low specific yield (water depth applied/rise in watertable) and a low lateral hydraulic conductivity, such as those found at the study site, are prone to extended periods of groundwater seepage from small rainfalls. In addition, one-way floodgates quickly restore low drain water elevations, which enhance groundwater seepage (i.e. the hydraulic gradient). Furthermore, until the tidal reach is re-established minimal buffering capacity exists within the drain and water discharged through the floodgates can cause fish kills and other environmental problems.

5.3.3 Dry conditions (Days 100-140)

The translocation of acidic groundwater into the drain caused poor drain water quality over the 40-day period beginning Day 100. During this dry period, drain water pH varied between 3.27 and 5.66 (median pH = 4.47) and EC was < 2000 μS/cm. While initially decreasing during the wet period, inorganic monomeric aluminium and total dissolved iron concentrations increased to 0.1497 mmol L^{-1} and 0.0987 mmol L^{-1}, respectively. Moreover, with pH below 5.0, aluminium concentrations were more than 1000 times in excess of ANZECC (1992) guidelines.

As upland inflows diminished, electrical conductivity increased downstream of the floodgate and minor tidal seepage decreased the Na/Cl ratio from 6.6 to 0.93, indicating partial brackish water ingress. Although the seepage was not sufficient to improve drain water quality at all sampling sites, a slight increase in long-term average pH between data logger G (4.71- 1 m upstream) and Q (4.49- 45 m upstream) was attributed to the tidal seepage. Within southeastern NSW, Pease *et al.*, (1997) Chapman (1994), and Blunden (2000) found similar poor quality surface water conditions in other ASS affected drains during negative estuarine flow periods (i.e. increased tidal reach due to low discharge rates). Considering the increased buffering potential of highly ionic water, one of the main objectives of restoring tidal flushing via modified floodgates was to increase drain water quality during these 'dry' periods.

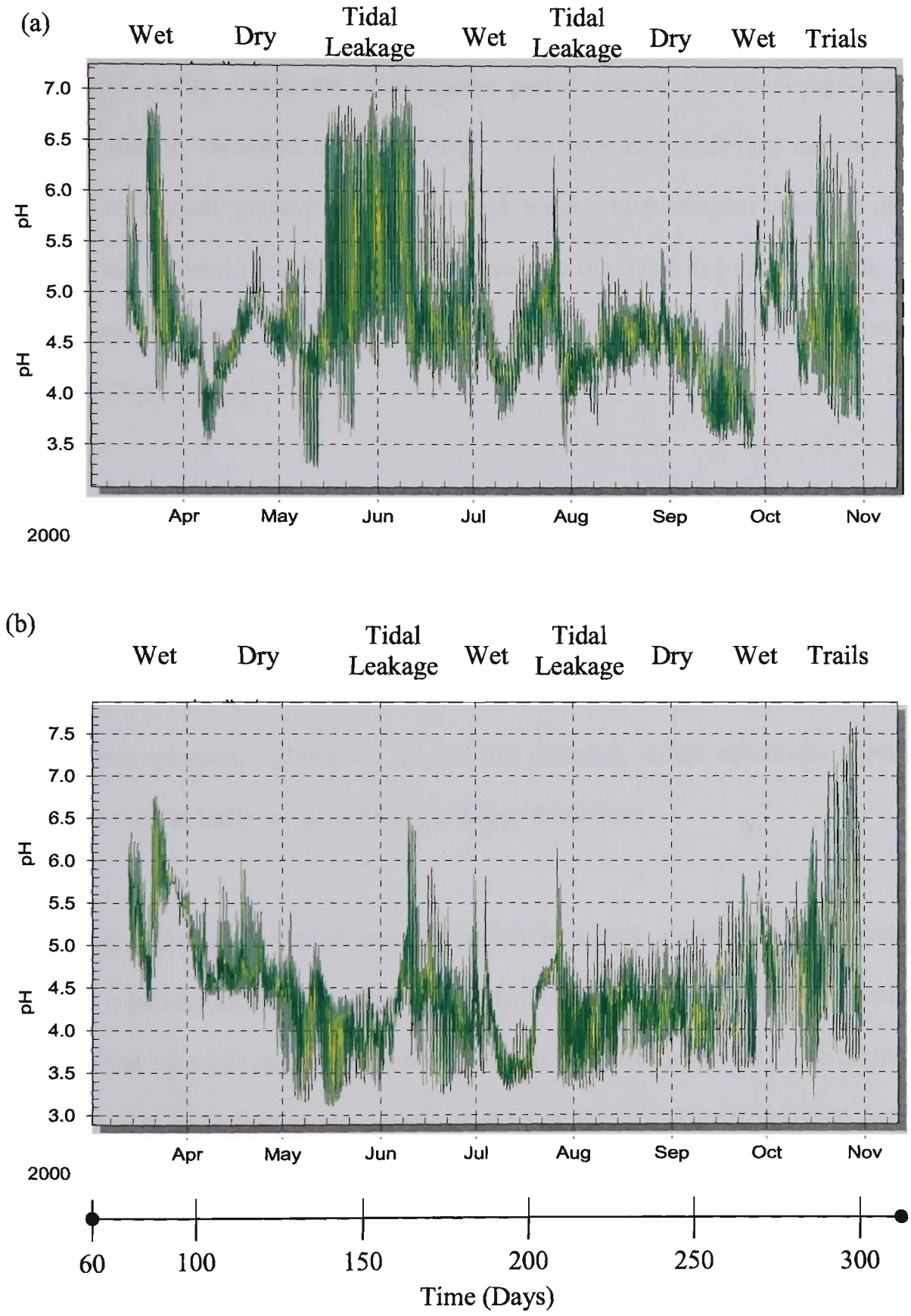

Figure 5.12 Pre-modification pH readings in response to rainfall, estuary hydrodynamics, and floodgate leakage from (a) 1 m and (b) 45 m upstream of the floodgate.

5.3.4 Tidal leakage conditions (Days 140-180)

Drain water quality during the tidal leakage period (Figure 5.12) was significantly improved due to increased tidal buffering. The increased buffering capacity was attributed to a small quantity of alkaline creek water which intruded upstream of the floodgate due to debris that was jammed between the floodgate flap and headwall. The alkaline water buffered the acidic drain water and drain water pH was consistently above 6.0 (Figure 5.12).

Figure 5.13 shows the improved drain water quality 1 m upstream of the floodgate during the tidal leakage period. The leaking and continual inter-mixing of acid drainage water with brackish (buffer-rich) estuarine water raised the drain water pH from 4.37 to 6.93. Considering the logarithmic nature of pH, this equates to a 100-fold decrease in H^+ ion concentration. However, as the tide receded, acidic conditions resumed, indicating that the buffering effect was limited to flood tides.

Interestingly, during the tidal leakage period iron and aluminium concentrations remained relatively unchanged. This was likely due to the sample collection period (i.e. low tide) and the small quantity of buffering agents permitted upstream of the floodgate. This was also attributed to the increased drain water elevations from tidal leakage initially recharging the phreatic zone and mobilising groundwater contaminants. Under these conditions, the decrease in surface water elevations during the ebb tide can re-establish a hydraulic gradient towards the drain and enhance groundwater drawdown. This effect is likely to occur in situations when floodgates are periodically opened and closed to permit short-term tidal flushing, and is why it is strongly recommended that permanent restoration of tidal flushing be maintained whenever feasible.

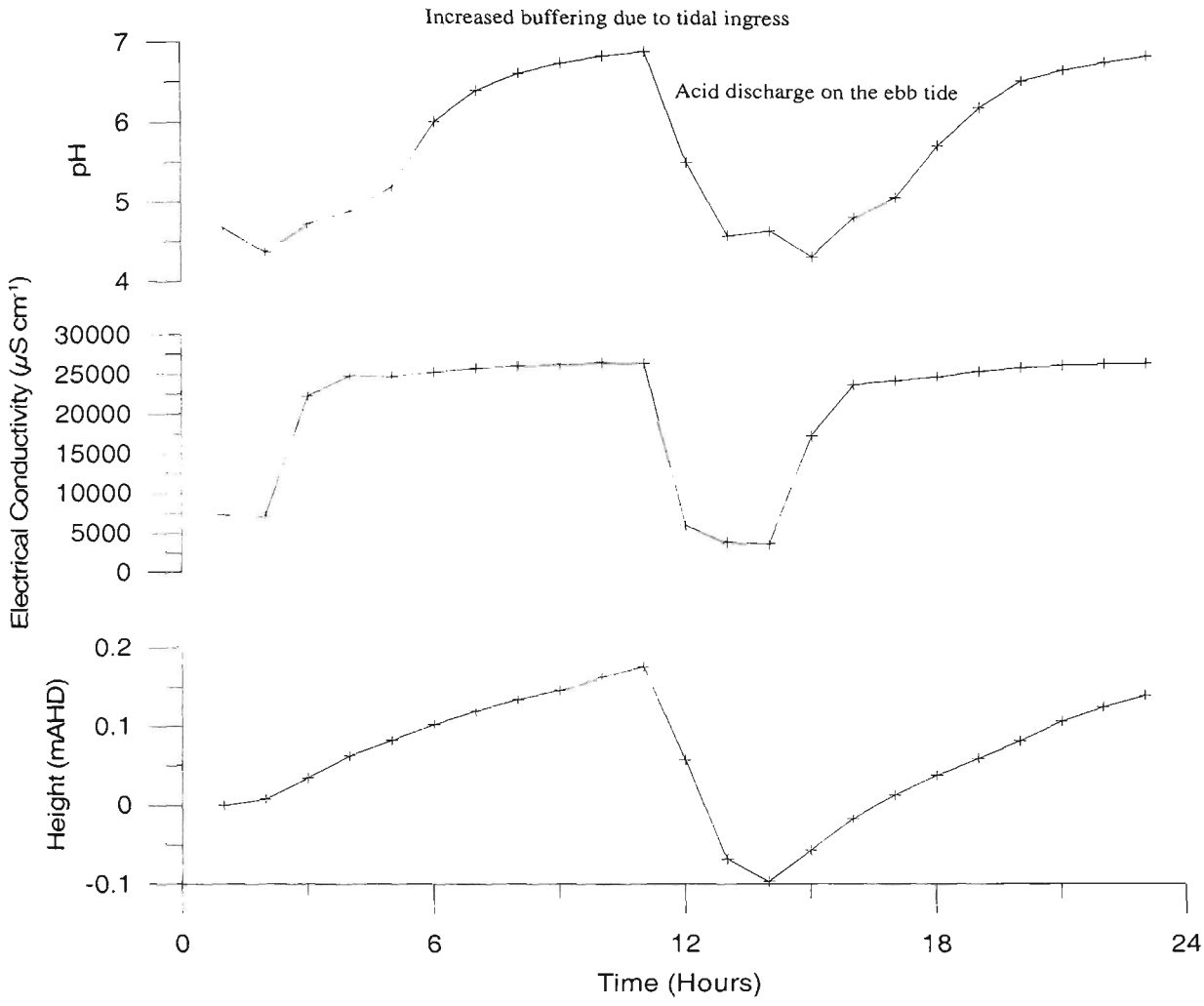

Figure 5.13 pH, electrical conductivity and elevation readings from Data logger G (1 m upstream) on Day 151.

The difference in drain water pH 1 m and 45 m upstream of the floodgate during the tidal leakage period, and shown in Figure 5.12, was attributed to the small quantity of tidal leakage and the consumption of buffering agents nearest the floodgate. Figure 5.9 indicates that while EC rises to over 6000 µS cm^{-1} 1 m upstream, only a slight change is discernable 60 m upstream. Similarly, the Na/Cl ratio (Figure 5.11) during the leakage period shows a strong saline front at the floodgate with brackish to freshwater dominance with distance. Therefore, due to the high concentration of H^+ ions within the drain (pH < 4.5) and the low concentration of buffering agents, the neutralising capacity of intruding water during tidal leakage periods will be limited with distance.

Several researchers (Pease, 1994; Russell and Helmke, 2002; Indraratna *et al.*, 2002) have attributed leaky floodgates to improved drain water quality. The results presented here verify previous findings and provide field evidence to support the floodgate modification strategy. Moreover, floodgate modifications that permit full tidal intrusion will increase the concentration and distribution of buffering agents and allow for the beneficial effects of tidal buffering throughout the entire drain. Floodgate modifications will also provide control over the quantity of brackish water within the drain and give floodplain managers the ability to optimise tidal buffering and improve drain water quality. Additional environmental benefits of floodgate manipulations and the related buffering kinetics are discussed in Section 5.4 and Chapter 6, respectively.

5.3.5 Wet conditions (Day 180-200)

Rainfall of 63 mm between Days 180-200 returned wet conditions to the study site, increased upland inflow and decreased electrical conductivity. As shown in Figure 5.14, pH levels initially increased to greater than 6.0 because of rain water dilution, but as runoff receded, groundwater contaminants were mobilised due to a strong hydraulic gradient imposed by the one-way floodgate. Subsequent groundwater seepage increased drain water acidity, which caused a 12-day period of extremely low pH levels (all readings < 4.5) where aluminium and iron flocculation plumes were noted discharging from the flood mitigation drain.

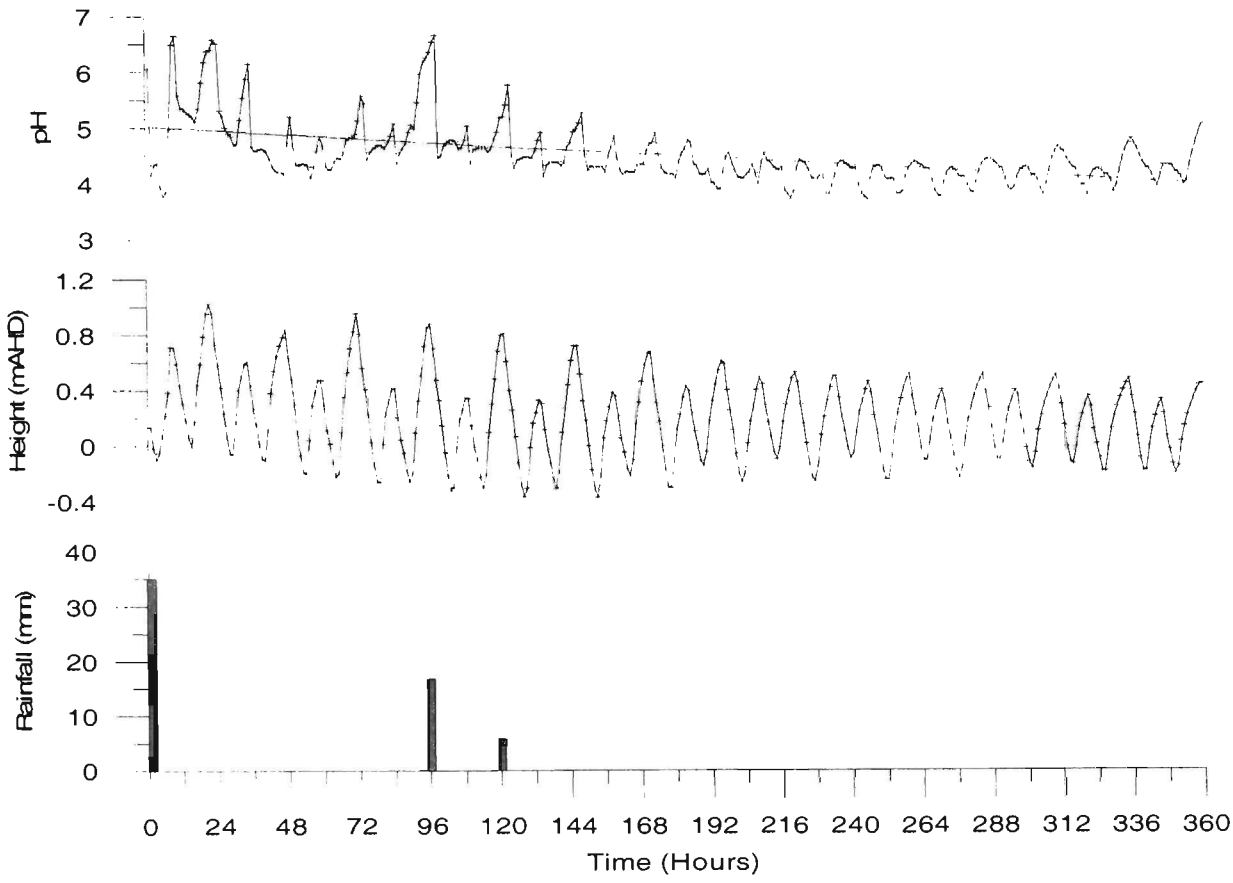

Figure 5.14 pH, drain water levels and rainfall measurements 1 m upstream of the floodgate on Days 182-196. Note the decreasing trend in pH as displayed by the solid line.

5.3.6 Dry conditions (Days 200-305)

Following a brief (10-day) tidal leakage period that was characterised by neutral pH levels, an extended dry period dominated from Days 200-270. This dry period was characterised by high drain water acidity and increased electrical conductivity values, with drain water pH ranging from 3.46 to 5.45 (median pH = 4.38). The dry conditions and one-way floodgates fostered groundwater seepage, which increased inorganic monomeric aluminium (0.978 mmol L^{-1}) and total dissolved iron (0.264 mmol L^{-1}) concentrations.

Hourly drain water elevations and pH during this dry period are presented in Figure 5.15. From this figure it is important to note the decline in surface water elevation on

the ebb tide due to the discharge of water through the floodgate under hydrostatic pressure. The continual re-establishment of low drain water elevations by the one-way floodgates promoted groundwater transport as shown in Chapter 4. Similar to previous dry periods, drain water pH fluctuated within a small acidic range (4.18-5.13, median pH = 4.7) and, following discharge on the ebb tide, caused downstream acidification.

Several small rainfalls (84.9 mm over 35 days) and a series of floodgate manipulation trials dominated the remainder of the pre-modification field trial. Rainfall flushed saline water from the creek, which briefly lowered electrical conductivity and increased the Na/Cl ratio (>0.9). The anticipated increase in drain water acidity was averted by several floodgate openings during the construction of the modified floodgates, which resulted in a decrease in iron concentrations and an increase in drain water pH.

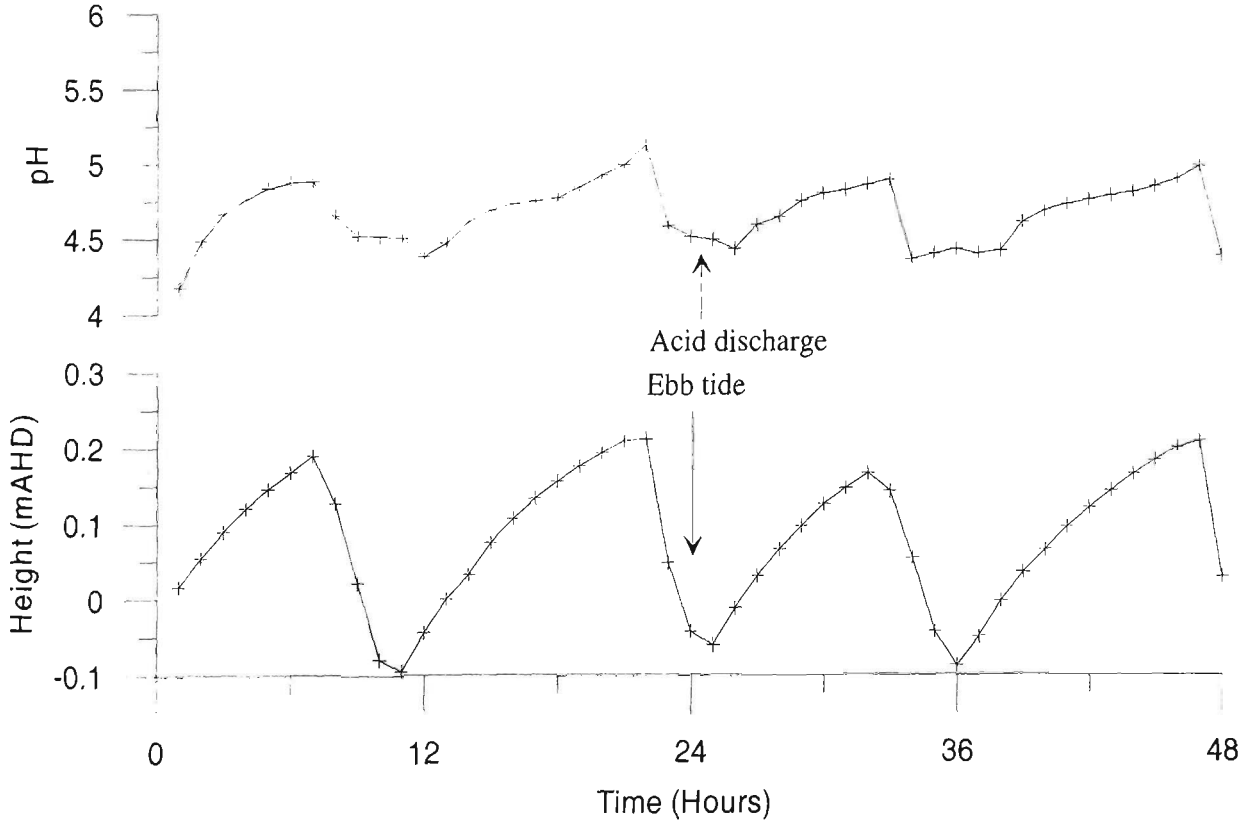

Figure 5.15 pH and drain water elevation measurements from data logger G (1 m upstream) between Days 237-238.

5.4 The influence of one-way floodgates on acid buffering and water quality

As shown above, acidic drain water conditions were prevalent both spatially and temporally across the study site prior to floodgate modifications. In this section, the role of one-way floodgates in exacerbating acid drainage and decreasing estuarine water quality is presented. Specific reference is given to:

- The capacity for one-way floodgates to create acid reservoirs and the impact of these reservoirs on metal flocculation.
- The inefficient design of one-way floodgates, including the tendency to discharge water solely on the ebb tide when dilution and buffering are minimal.
- The impact of drain water quality and, in particular dissolved oxygen levels, on receiving waters within Broughton Creek.

As well as the hydro-chemical and hydrodynamic impact of one-way floodgates on drain and creek water quality, additional environmental problems associated with one-way floodgates are discussed. These include lack of fish passage, the infestation of exotic weeds, and the accumulation of mono-sulphidic black oozes. Floodgate modifications that permit tidal flushing are presented as a means to control the above problems.

5.4.1 One-way floodgates and acid reservoirs

By restricting tidal flows into a drainage system, one-way floodgates form reservoirs of acidic water. Figure 5.16 shows typical pH readings upstream and downstream of the floodgate before modifications. While ANZECC (1992) guidelines state that surface

waters must have a pH between 6.5-9.0, and that waters discharging into a system must be within 0.2 pH units, Figure 5.16 shows extremely acidic drain water quality (pH < 4.5) upstream of the floodgate and circum-neutral pH waters downstream. The considerable difference in pH (6.68 versus 4.56 for Day 241, and 6.31 versus 3.92 on Day 269) upstream versus downstream of the floodgate is more than one order of magnitude in excess of ANZECC (1992) guidelines.

The acid reservoir upstream of the one-way floodgate also contained elevated concentrations of dissolved iron and aluminium. Figure 5.17 shows dissolved Al^{3+} and Fe^{total} measurements during discharge events on Days 241 and 269. In comparison with pH levels, Al^{3+} and Fe^{total} concentrations were 10 times greater upstream versus downstream. As the acid plume discharged from the drain, intermixing with pH neutral water decreased soluble Fe^{total} and Al^{3+} levels but increased monosulphide and aluminium hydroxide concentrations, as previously described in Equations 2.10 and

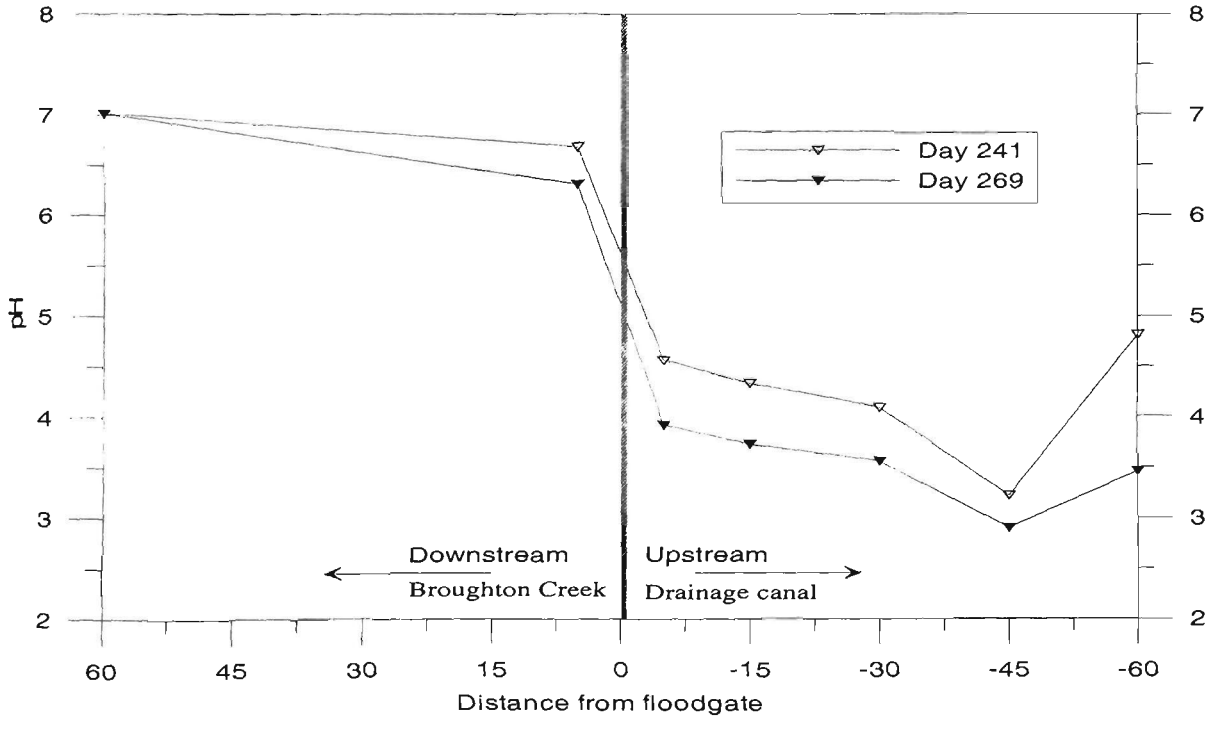

Figure 5.16 Drain and creek water pH levels upstream and downstream of the floodgate.

2.15. Large blue-grey plumes caused by aluminium flocculation were often seen emanating from the floodgate and have been linked with Epizootic Ulcerative Syndrome (red spot disease) in fish (Sammut *et al.*, 1997). Similarly, Fe^{2+} oxidation can cause deoxygenation of the water column and lead to asphyxiation and fish kills. However, floodgate modifications that permit tidal flushing would eliminate the acid reservoir effect and allow tidal buffering to occur on the soil-water interface.

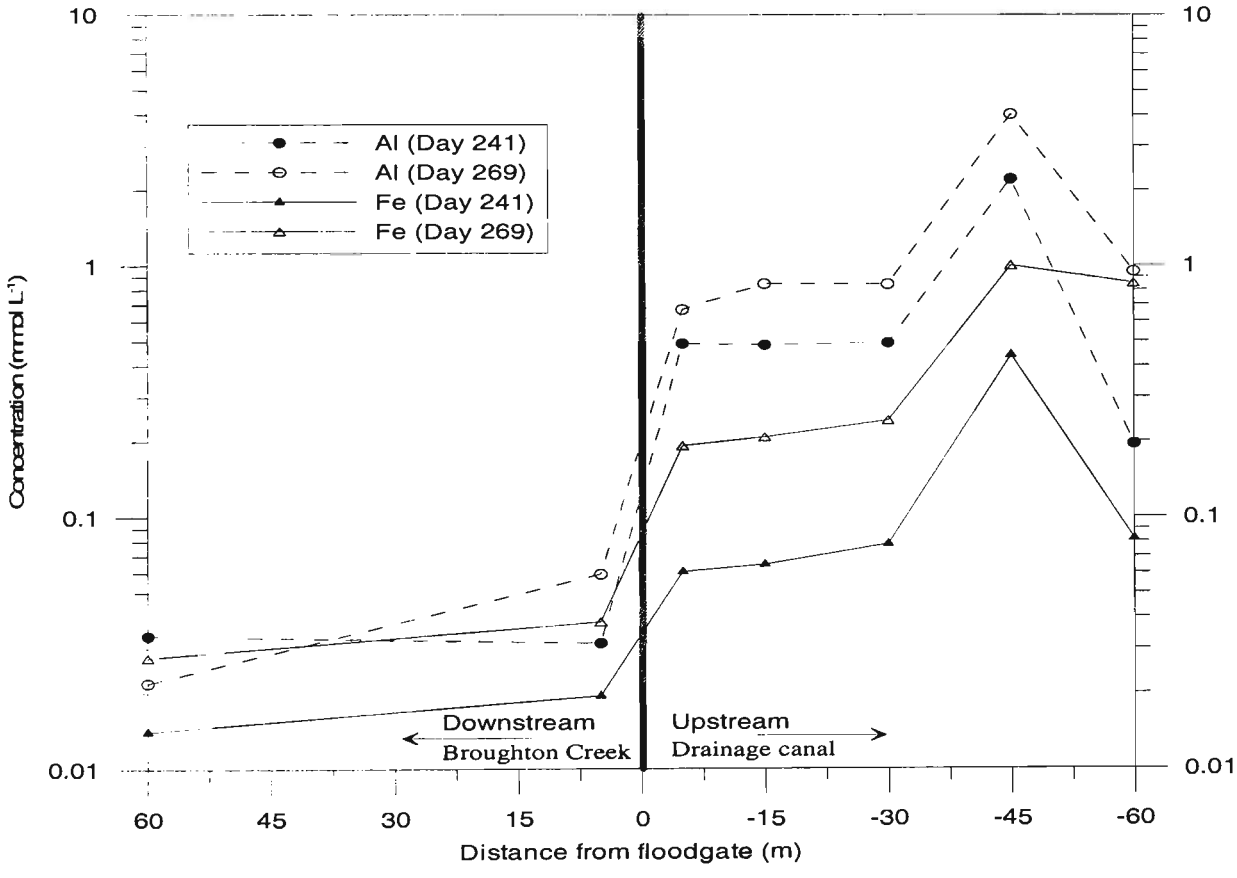

Figure 5.17 Inorganic monomeric aluminium and total dissolved iron concentrations upstream and downstream of the floodgate.

5.4.2 Dilution and buffering concerns associated with one-way floodgates

5.4.2.1 Dilution and one-way floodgates

One-way floodgates are designed to discharge water when the hydrostatic pressure is greater upstream than downstream. Except during flood periods, this normally occurs on the ebb tide when the downstream water elevation falls below the drain water level.

As long as the positive head gradient is maintained, drainage of acidic water will persist until downstream water levels rise above the drain water elevation. The discharge of acid slugs through one-way floodgates on the ebb tide increases the environmental impact of acid sulphate soil drainage because as the tide recedes the quantity of water within the creek decreases, thus reducing the amount of water available for dilution. To calculate this effect, the dilution capacity of Broughton Creek was determined over varying tidal cycles.

The volume of water within Broughton Creek was measured using the ArcGIS spatial analyst tool and comprehensive drain echo-sounding data. First, an aerial photograph of the Broughton Creek floodplain (with AMG projections) was imported into ArcGIS version 8.2. A detailed polygon was drawn along the perimeter of the creek excluding areas upstream of floodgates. A shape file was generated from the polygon, and using detailed (17,490 elevation points) tidal-corrected bathymetry data collected for this study, a digital elevation map of the creek was produced. Second, average tidal heights and ranges were determined from submersible pressure sensors adjusted to the Australian Height Datum (m AHD). Three sensors were installed (i) at the mouth of Broughton Creek, (ii) 5kms upstream from the mouth and (iii) at the junction of the study drain and Broughton Creek (10.2 kms upstream from the mouth). These data loggers were used to determine the moving average of high, mid, and low tidal heights. Finally, total Broughton Creek volumes were calculated by setting the creek water elevation to low, average, and high tide levels in the spatial analyst (raster calculator) tool. The total volumes are similar to those of Pease (1994) (2.33×10^9 versus 1.81×10^9), but differ due to a larger total area (709316 m^2 versus 603750 m^2) and a deeper

average creek depth (3.29 m versus 3.0 m for low tide). The flow capacity results are shown in Table 5.1.

Table 5.1 Calculations for total volume of Broughton Creek with tidal variations.

Tide	Average Tidal Height (m AHD)	Average Broughton Creek depth (m)	Total Volume (L) (Area= 709316m^2)
Low	-0.130	3.29	2.33 x 10^9
Average	0.265	3.69	2.62 x 10^9
High	0.710	4.14	2.94 x 10^9

Based on these results, by solely discharging during the ebb tide, one-way floodgates eliminate the beneficial effects of in-drain acid dilution. This is especially apparent during wet periods when buffering agents have been flushed from the estuary and dilution is the main acid neutralisation mechanism. During the ebb tide, 610 million litres of pH neutral creek water are flushed from the estuary and, following acid discharge, creek acidification is likely considering the 19 major floodgated drainage channels affected by ASS within the Broughton Creek floodplain.

Modified floodgates that permit tidal flushing and increase dilution will improve drain water quality. Detailed drain survey data (presented in Chapter 6) shows that tidal reach within the drain is approximately 250 m upstream of the floodgate and that the average drain width is 10 m. Using comprehensive (5777 readings) drain water elevation readings from submersible data loggers, average drain water depth was calculated at 1.27 m AHD, giving a total drain water volume of 3175 m^3. By allowing tidal flushing within the drain, average water elevation would increase by 0.66 m, and an additional 1650 m^3 would be available for dilution. To this point, before floodgate modifications

total average acidity within the whole drain was 1.39 mmol L^{-1}, however, by increasing drain water height by 52% total acid concentrations would be expected to decrease to 0.66 mmol L^{-1}. This represents nearly a one-unit change in pH across the entire drain, and is a significant result with regards to aluminium and iron flocculation.

The impact of acidic drain water discharged through one-way floodgates on the low tide is shown in Figure 5.18. Immediately prior to these readings, 57.4 mm of rainfall was recorded over a 3-day period, which increased upland inflow and flushed the majority of buffering agents from Broughton Creek (bicarbonate concentrations <10 mg L^{-1}). The rainfall also recharged the vadose zone, and due to low drain water levels maintained by the one-way floodgate, the total acid load within the creek increased. The negative slope of the pH readings over the 4-day period shows the increased acidity of the creek.

Lacking sufficient buffering agents for neutralisation, improvements in water quality due to dilution are most evident during flood tides. As shown in Figure 5.18, a positive correlation exists between creek water height and pH. For instance, the highest tide over the period and the highest pH were recorded on the 24th hour. Similarly, on smaller high tides, such as around the 12th, 37th, and 63rd hour (Figure 5.18), a smaller increase in pH was measured. These results are typical of drain/creek water quality during low alkaline conditions, and depict the need for floodgate modifications.

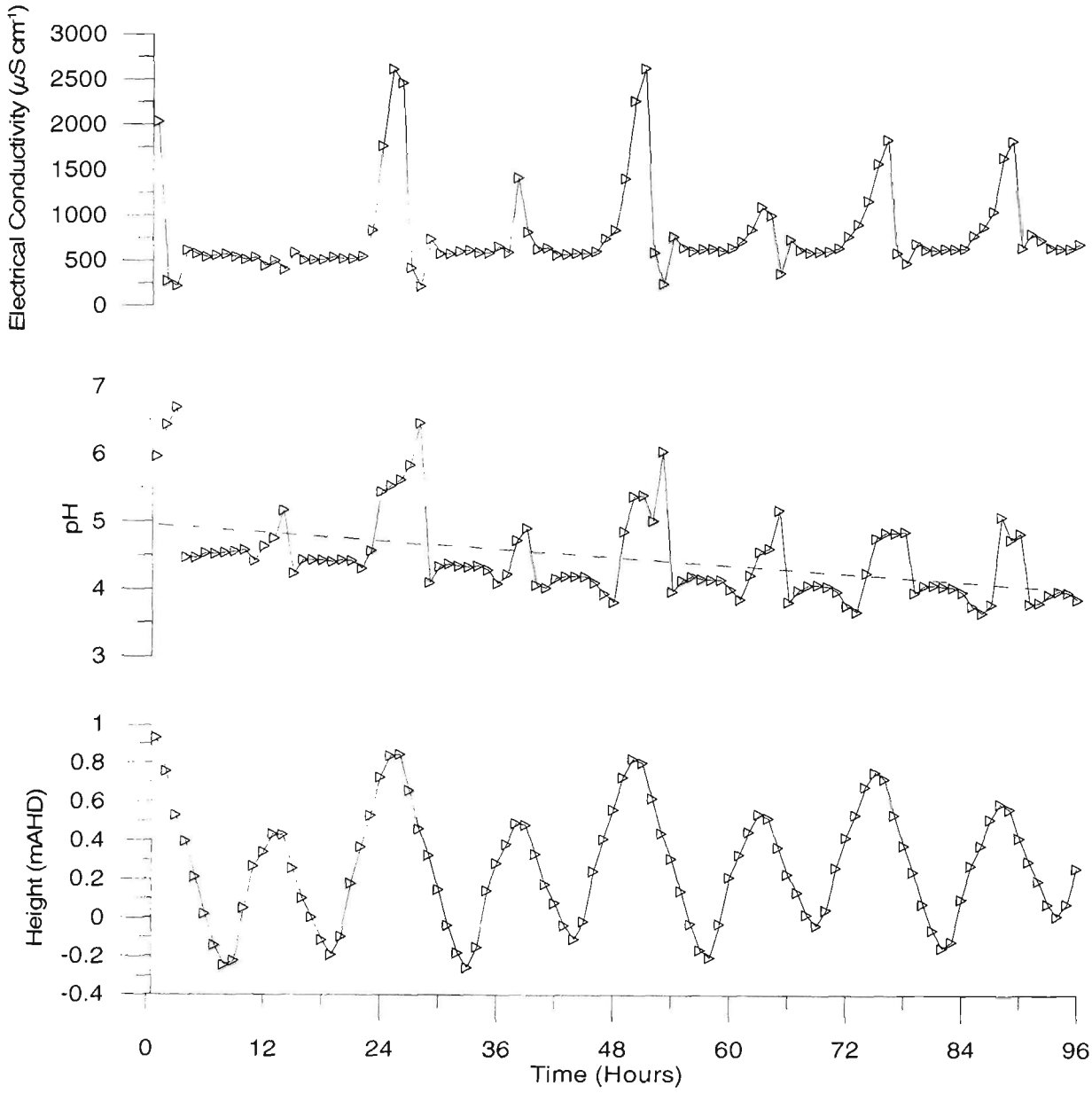

Figure 5.18 Surface water elevation, pH and electrical conductivity 1 m downstream of the floodgate on Days 187-190.

5.4.2.2 Tidal Buffering and one-way floodgates

Over daily timeframes (i.e. diurnal tidal cycles), with steady-state environmental conditions, the concentration of buffering agents is controlled by the tidal cycle (Ward and Elliot, 1995). As a result, the concentration of buffering agents increase during the flood/high tide and decrease during the ebb/low tide. Consequently, by discharging acid water during the ebb tide one-way floodgates have a negative impact on receiving waters.

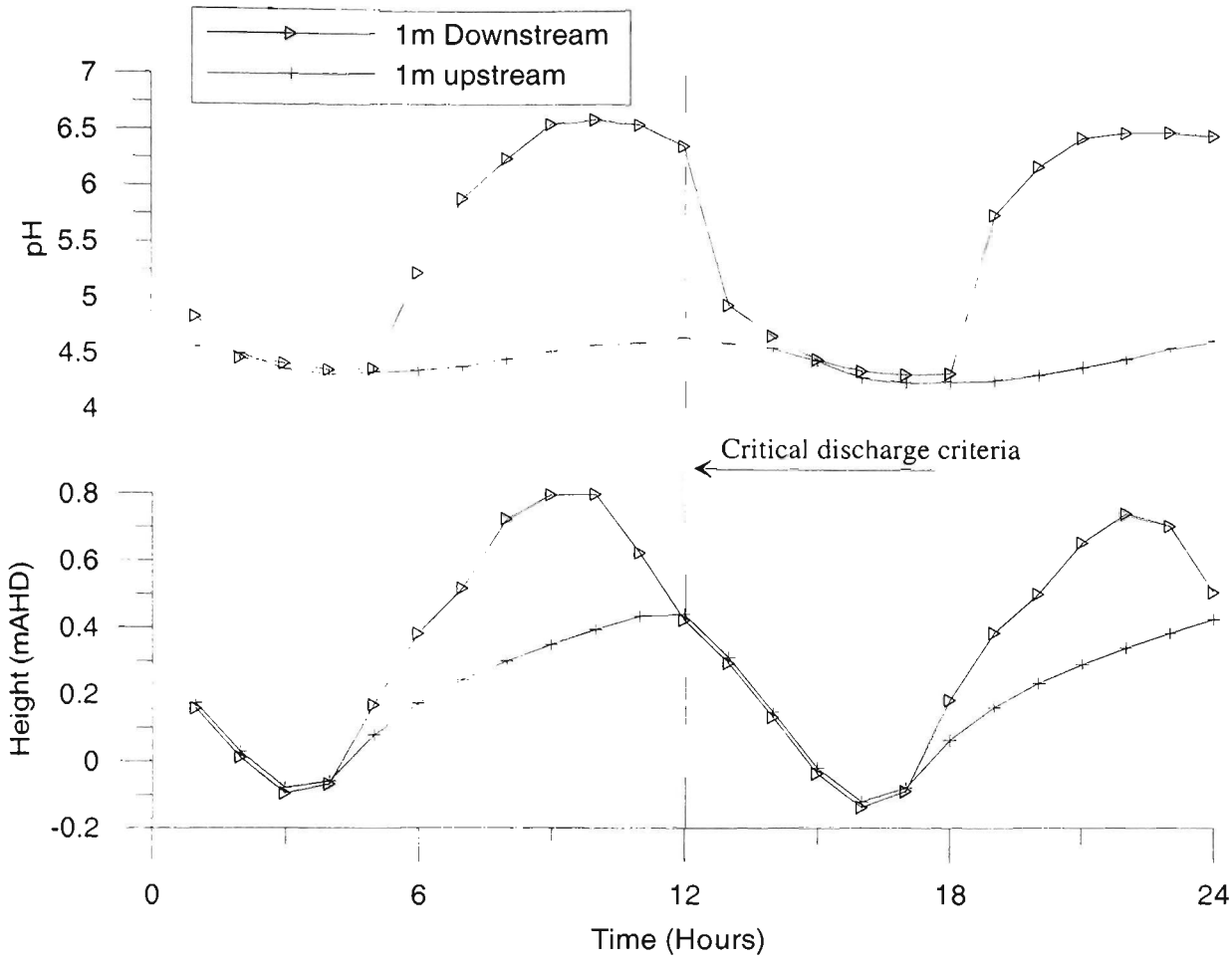

Figure 5.19 Drain and creek water elevation and pH on Day 107.

The hydrodynamics and chemical interactions of creek water over a 24-hour dry period are shown in Figure 5.19. In this figure, electrical conductivity depicts the fluctuations in bicarbonate levels with the tide, which is reasonable because of the strong correlation (r^2= 0.90) between EC and bicarbonate readings taken over the length of the study period (Figure 5.20). The relationship between electrical conductivity and bicarbonate concentrations in creek water is further discussed in Chapter 6.

During the ebb tide, once the critical downstream water elevation is reached (shown by a vertical dotted line in Figure 5.19) acidic water is discharged into pH neutral creek water with low buffering potential. On Day 107 (Figure 5.19), during the first 4 hours the tide initially fell, but then rose to a peak on the 10th hour. Creek water EC increased with the tide depicting increased buffering capacity as shown by pH levels above 6.5.

Over this period, the water level upstream of the floodgate slightly increased (0.52 m) due to upland inflow and groundwater seepage, but pH readings upstream of the floodgate remained below 5.0, and fluctuated within a small range (< 0.4 pH units). Furthermore, drain water EC remained below 2000 μS cm^{-1}, and therefore, lacked sufficient buffering capacity to neutralise acid products (Figure 5.20). When the downstream water elevation fell below upstream levels (12^{th} hour), hydrostatic pressure promoted drain water discharge. This caused creek water pH to decrease from 6.35 to 4.93 within one hour, and to remain below 4.7 until the flood tide returned on the 18^{th} hour. With this in mind, buffering as well as dilution is an important mechanism in improving drain water quality after tidal restoration.

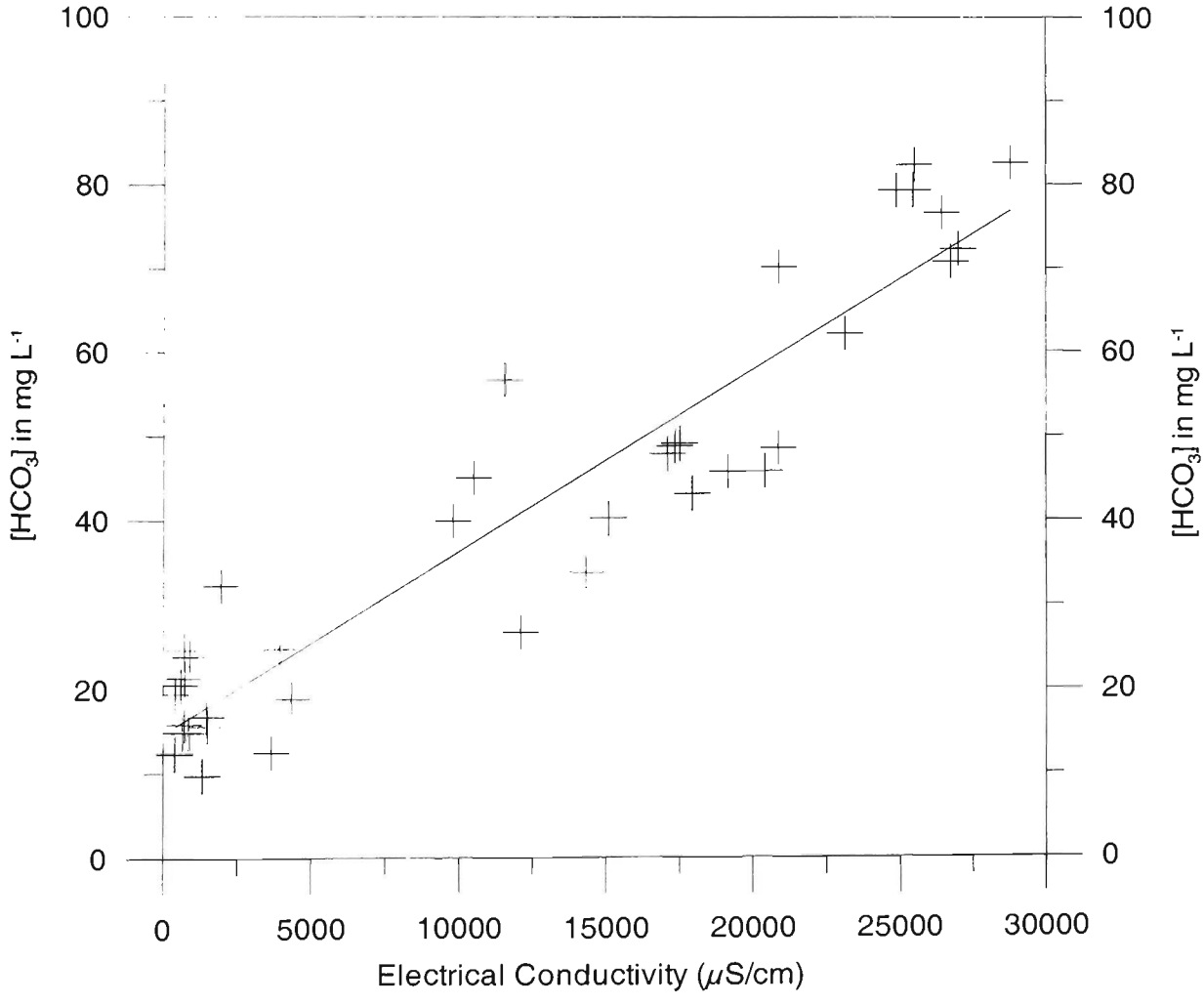

Figure 5.20 Linear correlation between electrical conductivity and bicarbonate readings taken from Broughton Creek samples.

5.4.3 Dissolved Oxygen Levels

Low dissolved oxygen (DO) levels are commonly associated with tidal restricting floodgates and acid sulphate soils (Dick and Osunkoya, 2000; Pollard and Hannah, 1994). In particular, one-way floodgates create environments with stagnant water and abundant organic matter. Acid sulphate soil products can also reduce DO by ferrous oxidation and through oxidation of mono-sulphidic deposits. It is widely recognised that dissolved oxygen levels below 6 ppm can have deleterious impacts on aquatic life including respiratory distress and skin/muscle damage (Sammut and Melville, 1994).

Figure 5.21 shows typical DO readings taken from the study drain over a two-week period. Unfortunately, technical problems with the data logger limited the amount of DO data in this period, however, available results clearly indicate that DO levels within the drain were below recommended levels. Overall DO measurements fluctuated in a wide range (0.5ppm to 11.65ppm) but averaged 3.58 ppm.

The DO results presented in Figure 5.21 are typical of readings from other floodgated drains affected by acid sulphate soils (Johnson *et al.*, 2003). To improve DO levels within flood mitigation drains, several researchers (Dick and Osunkoya, 2000; Pollard and Hannah, 1994; Sammut and Melville, 1994) have recommended the restoration of tidal flushing. While this may improve floodgate related DO problems, the increased flows may also mobilise mono-sulphide deposits causing secondary ferrous oxidation.

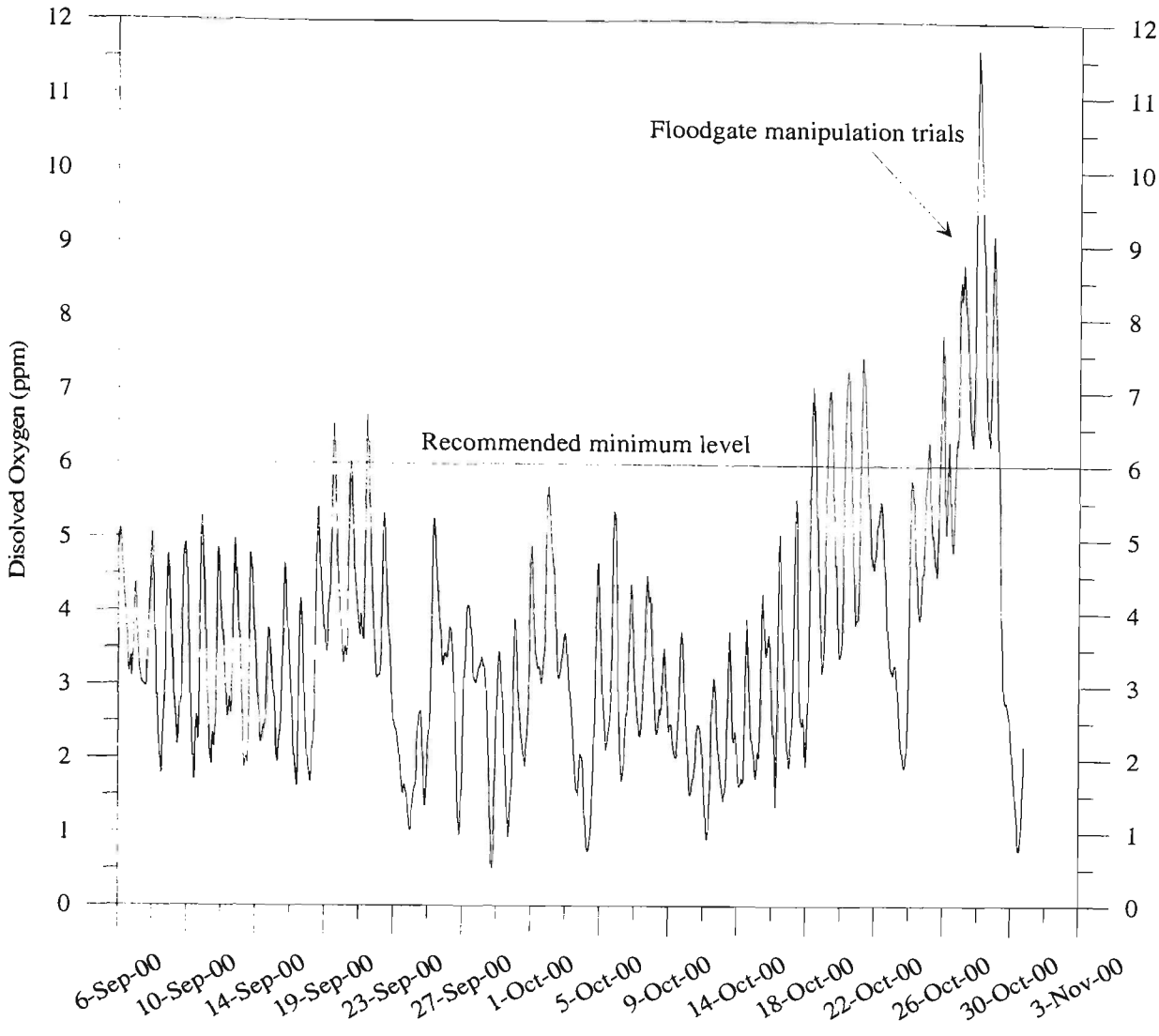

Figure 5.21 Drain water dissolved oxygen measurements taken before floodgate modifications.

5.4.4 Additional environmental problems associated with one-way floodgates

One-way floodgates create environmental problems similar to those commonly associated with weirs or dams. In general, floodgates restrict tidal flushing, and create an artificial freshwater environment, which encourages the growth of exotic species. To this end, the impact of the Cape waterlily on drain hydrodynamics in northern NSW is well documented (Sammut, 1996). In the southeastern NSW, environmental conditions do not suite the Cape waterlily but an acidophilic freshwater sedge, *Eleocharis equisetina*, can invade drains and reduce hydraulic efficiency. A photo of weed infestation in the control floodgated drain is shown in Figure 5.22.

In addition to reducing the hydraulic efficiency of the flood mitigation drains, weed infestations increase the organic matter content. The decomposition of organic matter reduces dissolved oxygen levels and simultaneously enhances the formation of mono-sulphide black oozes (MBOs). Sullivan and Bush (2000) suggest that weed accumulation and a high concentration of dissolved sulphate from previously oxidised pyrite provides an ideal environment for MBO deposition on the drain invert. Disturbing these sulphidic sediments via mechanical weed clearing or during floods, can induce secondary oxidation and increase drain and creek water acidity. Regular tidal flushing will reduce weed growth, decrease MBO formation and improve the hydraulic efficiency of the drain.

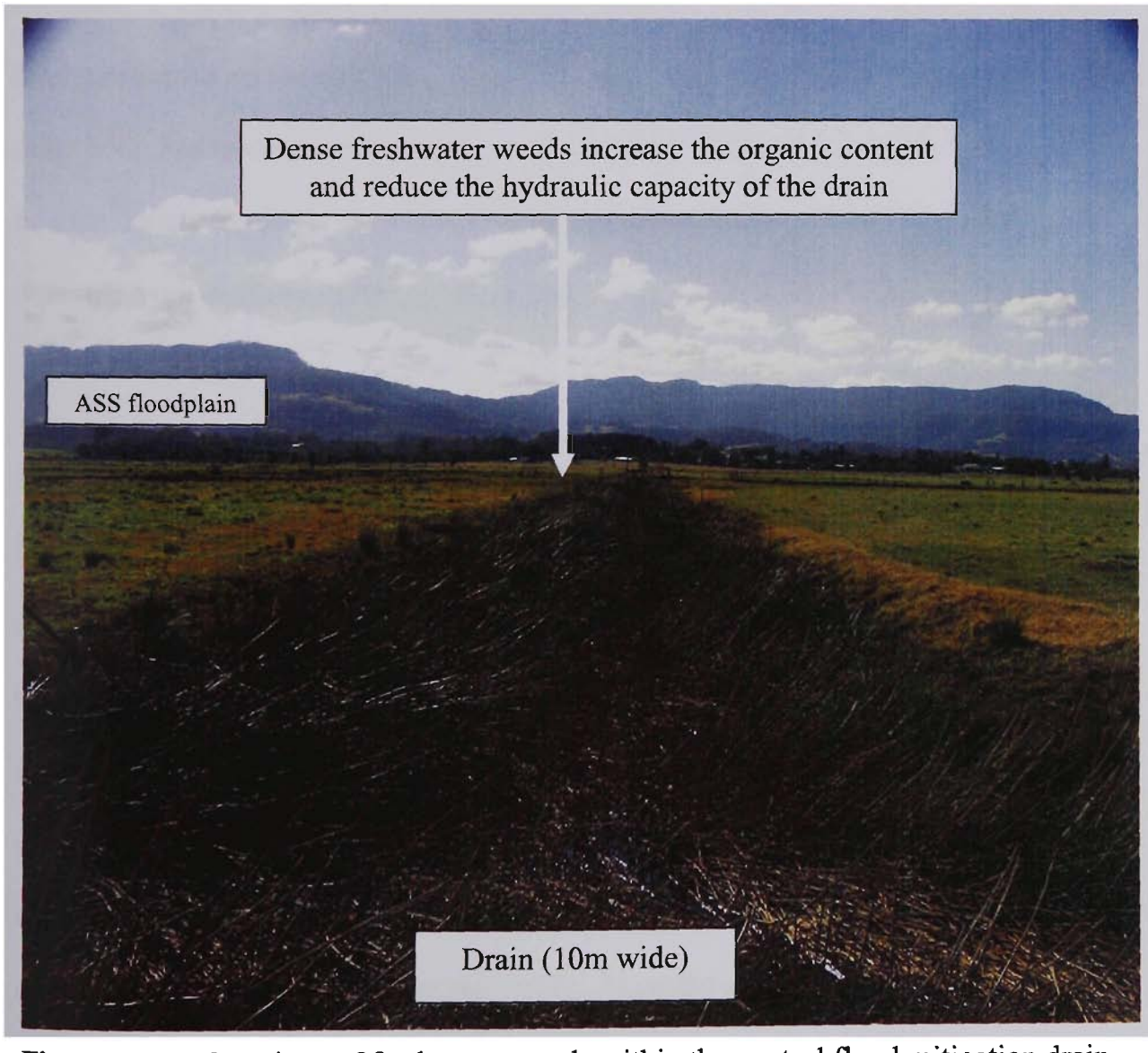

Figure 5.22 Infestations of freshwater weeds within the control flood mitigation drain.

One-way floodgates also restrict fish passage into traditional breeding areas. Pollard and Hannah (1994) suggest that one-way floodgates cause alienation of habitat areas, restrict fish passage and block larval transport, whereas Gibbs *et al.* (1997) found that the quantity of fish species significantly increased in drains with 'leaky' floodgates. It is envisioned that active floodgate management, which permits tidal flushing, will increase the number of species assemblages within ASS drainage systems.

5.5 Control sites versus trial site

To assess the effectiveness of tidal buffering, and to provide comparison for future reference, 2 control drains were selected. One of the control drains contained a floodgate similar to the trial site, while the other drain immediately to the south of the study drain has never been floodgated. The reader is advised to consult Figure 3.8 for location details regarding the control floodgated drain and the control tidal drain. Drain water pH from the three drains before floodgate modifications is shown in Figure 5.23.

5.5.1 Trial drain versus control floodgated drain

Before floodgate modifications, water quality at the control floodgated site and the trial drain site showed similar pH and metal concentrations. Mean pH between the drains was within 0.17 pH units (4.47 for the primary study drain versus 4.31 for the control floodgated drain), indicating that both drains were affected by acid sulphate soils. A slightly greater pH variance at the control floodgated site (0.90) versus the primary study site (0.45) was attributed to the control floodgated drain carrying excess surface runoff from the town of Berry during floods. Nonetheless, as shown in Figure 5.23, pH fluctuations over time were similar in both drains.

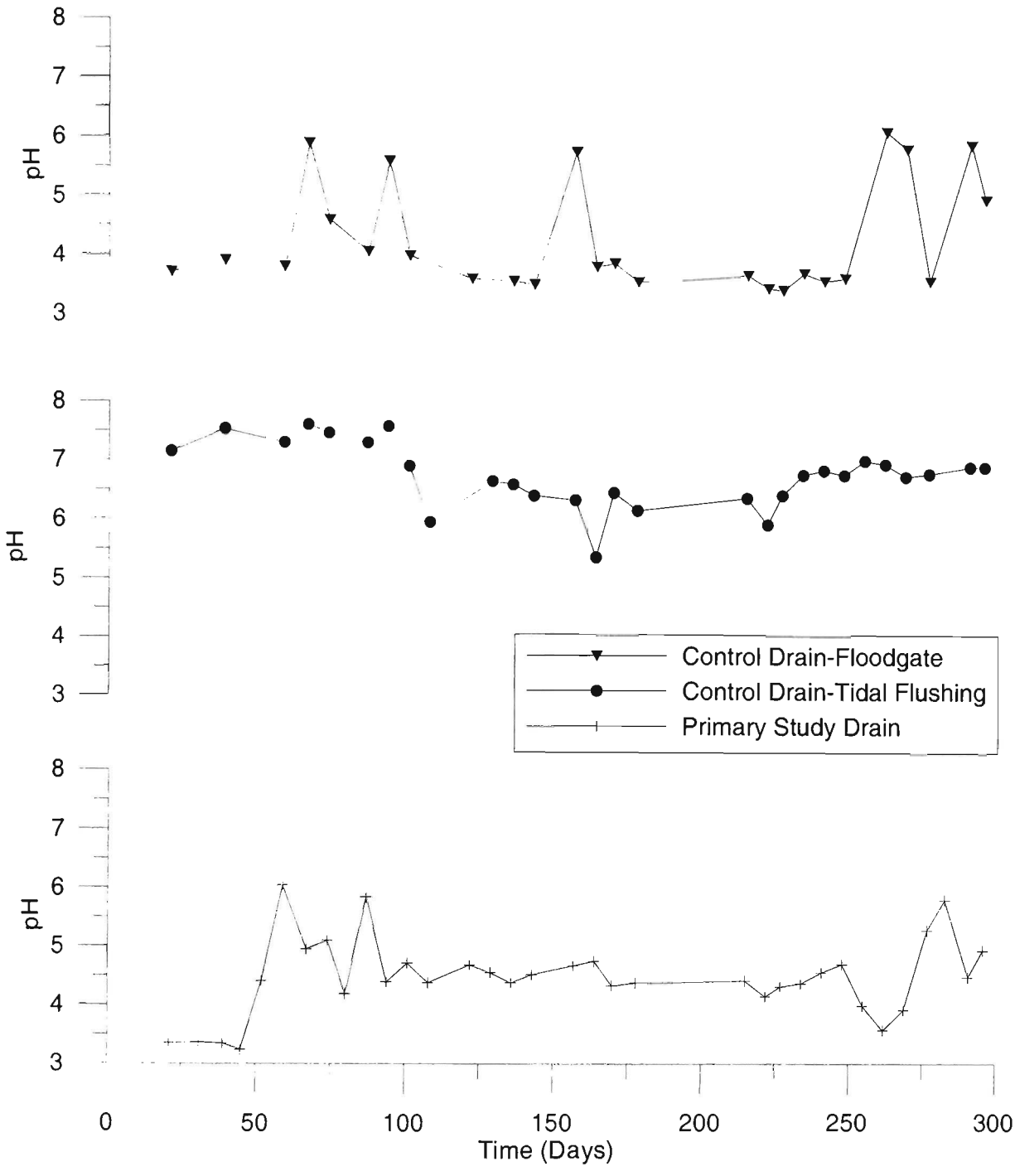

Figure 5.23 pH readings taken from the primary study drain and two control drains (with and without floodgates) before floodgate modifications.

Although aluminium concentrations were comparable in both drains, iron concentrations differed due to drain hydrochemistry. Aluminium concentrations at the trial site averaged 0.383 mmol L^{-1}, while $[Al^{3+}]$ in the control floodgated drain averaged 0.4354 mmol L^{-1}. Conversely, soluble iron concentrations averaged 0.293 mmol L^{-1} versus 0.122 mmol L^{-1} in the trial drain and control floodgated drain, respectively. The

difference in iron concentrations between the two drains was attributed to iron flocculating as MBOs in the control floodgated drain. This is to be expected considering the abundance of aquatic weeds within the drain, which provide optimal conditions for mono-sulphide formation. However, the long-term average for both metal species was in excess of ANZECC (1992) criteria and less than one standard deviation apart.

The similar water quality features of the two drains were expected considering their comparable catchment area, pyritic elevations, drain characteristics, locations and floodgates. Nonetheless, acid sulphate soil remediation works (i.e. weirs) installed at the control floodgated drain in 1998 may affect drain water quality by decreasing acid production and transport rates. With this in mind, all the drain water samples in the control floodgated drain were taken below the lowest weir, approximately 150 m upstream of the floodgate. However, the analogous nature of these drains provides a base point for determining the effectiveness of the floodgate modification strategy.

5.5.2 Trial drain versus the control tidal drain

Drain water conditions at the control tidal drain were significantly different from the study drain. Lacking a floodgate at the site, tidal flushing was permitted within the control drain and sufficient buffering agents were available for acid neutralisation. Mean drain water pH at the control tidal drain was 6.77, more than two orders of magnitude greater then the study drain, and in line with ANZECC (1992) guidelines. Similarly, average $[Al^{3+}]$ and $[Fe^{total}]$ in the control tidal drain were close to an order of magnitude lower then in the primary study drain; soluble aluminium averaged 0.044 mmol L^{-1} in the control drain versus 0.383 mmol L^{-1} in the primary study drain.

Similarly, total dissolved iron averaged 0.027 mmol L^{-1} in the control tidal drain versus 0.293 mmol L^{-1} within the trial drain. and acidic plumes were not noted discharging from the control tidal drain. Considering the similar nature of the two drains (i.e. drain depth, catchment area, pyritic content, pyrite depth, and location), improved water quality conditions at this site were attributed to tidal buffering.

5.6 Conclusions

The findings presented within this Chapter describe in a detailed scale the interrelationship between one-way floodgates installed on a flood mitigation drain affected by acid sulphate soil leachate and surface water hydrodynamics. Substantial temporal and spatial data was presented to show that one-way floodgates exacerbate acid conditions and to floodgate modifications that restore tidal flushing will improve both drain and estuarine waters. Furthermore, extensive data obtained from a series of continuous submersible data loggers provided detailed background information on drain water chemistry in relation to climatic conditions and floodgate leakage. The broad range of data collected provides ample baseline information for comparison with results after floodgate modifications.

Drain water chemistry measurements showed that before floodgate modifications the study drain was consistently acidic and in excess of several ANZECC (1992) criteria. Extremely acidic conditions were recorded 45 m upstream of the floodgate due to an adjoining secondary drain. Similarly, inorganic monomeric aluminium and total dissolved iron concentrations indicated that conditions at the study site were typical or greater than other affected drains in the region.

Surface water quality within the primary study drain fluctuated in response to climatic conditions and floodgate leakage. During wet periods, rainwater initially increased drain water pH, but following recharge of the groundwater table, seepage of acidic groundwater decreased pH below 4.5. These conditions were enhanced by the strong hydraulic gradient maintained by one-way floodgates, and their tendency to preclude buffering agents from the drain. During periods of tidal leakage, buffering agents were permitted upstream of the floodgate, which improved drain water quality.

Assessment of water quality indicators showed that one-way floodgates create acid reservoirs and exacerbate the impact of acid drainage. Acid reservoirs contain high concentrations of dissolved aluminium and iron, which when discharged during the low tide create additional acidity and smother the benthos layer. Furthermore, discharging drain water on the ebb tide intensifies problems associated with acid sulphate soils because of the reduced neutralising and dilution capacity of estuarine waters. Additionally, low dissolved oxygen readings indicate that drain water upstream of the floodgates was consistently below ANZECC (1992) criteria.

Water quality measurements given throughout this Chapter show that floodgate manipulation to permit tidal buffering would improve drain water quality. For instance, the tidal leakage period, drain water pH increased to its highest level and remained circum-neutral until the debris was removed. In addition, although other environmental and hydrological factors were similar to the study drain, pH levels within the control tidal drain were within ANZECC (1992) guidelines. Indeed, dissolved aluminium and iron concentrations within the control tidal drain were close to an order of magnitude lower.

Based on these findings, floodgate modifications were proposed to restore tidal flushing and improve drain water quality by:

- Permitting buffering agents upstream of the floodgate during all tidal phases;
- Increasing dilution rates during wet periods;
- Reducing the hydraulic gradient of groundwater towards the drain;
- Decreasing the total acidity by neutralising acid seepage on the soil/water interface and eliminating the acid reservoir effect; and
- Increasing DO levels through increased flushing and decreased ferrous oxidation.

Ancillary benefits of restoring tidal flushing include freshwater weed control, increased hydraulic efficiency, reduced MBO accumulation, and improved fish passage. The methodology, predicted outcomes, concerns and infrastructure designs regarding floodgate modifications are presented in Chapter 6.

Chapter 6.0 The Role of Buffering Kinetics and Tidal Flushing on the Design of Two-Way Floodgates

6.1 Introduction

As discussed in Chapter 5, acidic surface water conditions existed within the study drain due to groundwater seepage from oxidised acid sulphate soils. One-way floodgates exacerbated drain water conditions by eliminating tidal buffering/flushing, reducing acid dilution, maintaining drain water elevation at the low tide mark, creating acid reservoirs, and acidifying receiving waters. These acidic conditions were particularly prevalent during extended dry periods when sufficient buffering agents were available within creek water but transport was restricted by the one-way floodgates.

Significant improvements in drain water quality were recorded during periods of tidal leakage or in control drains without floodgates. These improvements, as well as anecdotal evidence, suggest that floodgate modifications to permit tidal buffering/flushing will combat acid leachate. However, modifying floodgates that are installed on productive agricultural pastures involves changing the hydrodynamics of the study drain, and several environmental and hydraulic concerns must be addressed prior to commencing civil works. The concerns include:

1. Assessing the potential change in drain water quality due to tidal flushing/buffering.
2. Calculating the quantity of tidal water permitted within the drain without overtopping the levee bank or reducing agricultural productivity.

3. Investigating the impact of increased salinity on the sub-soil matrix.
4. Determining the optimal design for floodgate modifications.

Based on the above concerns, this Chapter is divided into 3 subject themes. The first theme addresses buffering kinetics and water quality issues. This involves determining the buffering kinetics of the creek water and then incorporating this chemical information into an ion association program (PHREEQC) to predict drain water quality after floodgate modifications. These results assist in calculating the quantity of creek water required within the drain to reach a desired drain water quality level and in assessing the reaction path kinetics of undesirable metals such as aluminium.

The second subject theme addresses concerns regarding levee overtopping. To this end, a spatial technique or methodology is developed using extensive field data and Geographic Information Systems (GIS) to determine the quantity of water safely permitted within the drain. The results from the spatial technique and chemical analysis are then coupled to determine the expected drain water quality based on the predicted water levels. A flow chart, which outlines the coupled process, is given in Figure 6.1.

Based on these findings, and using specific design criteria, two modified floodgate designs were developed and installed. The first structure is a manually controlled vertical lifting floodgate operated on-site by a hand winch. The second 'intelligent' structure employs real-time data logging units installed upstream and downstream of the floodgate, which determine whether an aperture within the gate should be opened or closed. The design criteria, objectives, and operational procedures related to the modified floodgates are presented within the third subject theme of this chapter.

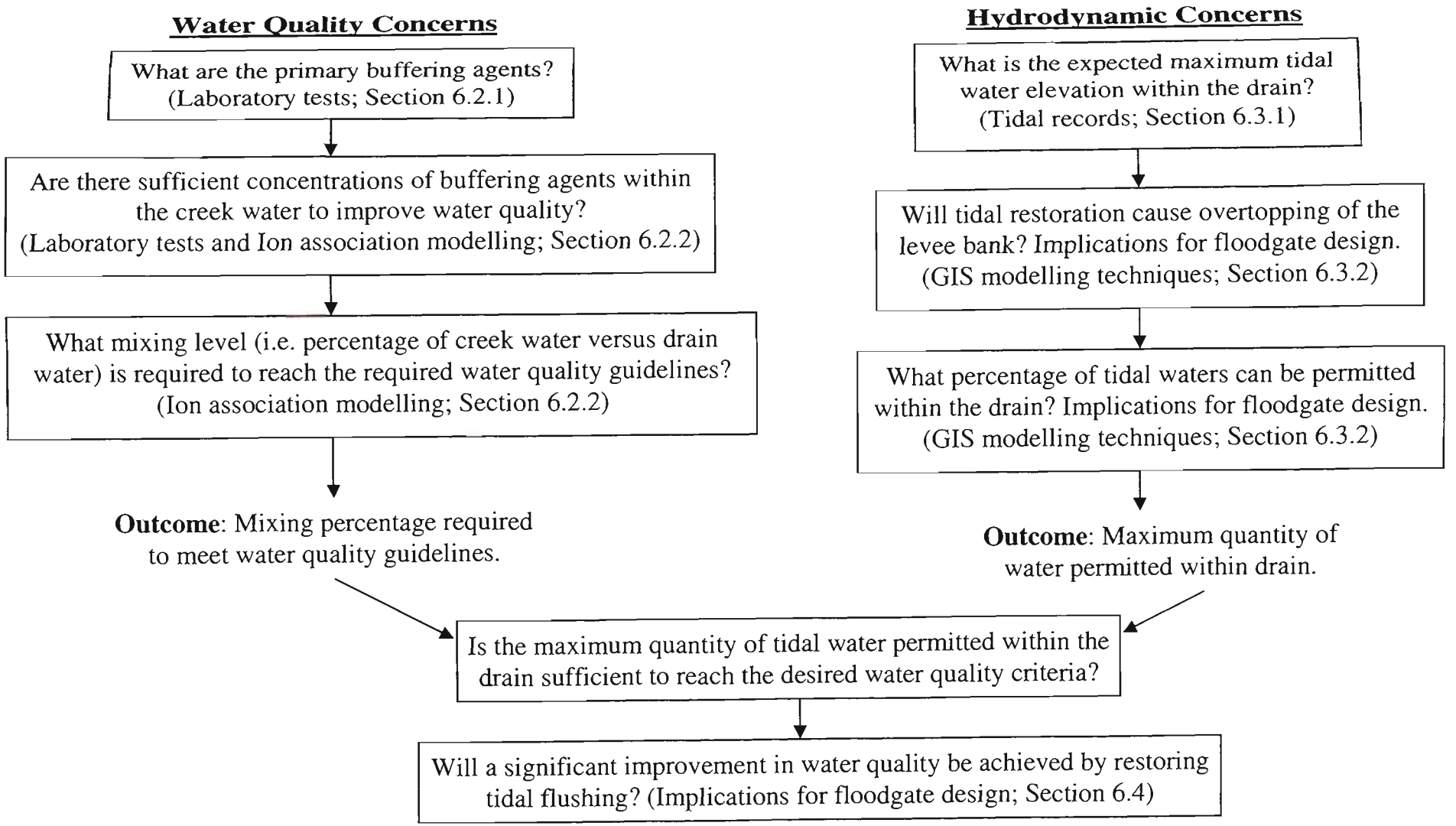

Figure 6.1 Flow chart outlining the structure of the water quality and hydrodynamic subject themes within this chapter.

The extent of saline intrusion into the sub-surface soil matrix is reliant on several complex factors such as spatial and temporal fluctuations in the phreatic zone; these concerns are detailed separately in Chapters 8 and 9.

6.2 Buffering kinetics and predictive ion speciation modelling

6.2.1 Buffering kinetics

The effective management of one-way floodgates requires an understanding of the source, reaction kinetics, and availability of buffering agents. In natural water systems void of clay sediments, three primary buffering species exist: bi/carbonates, phosphates and borates. However, in natural waters, phosphates ($H_2PO_4^-$) and borates (HBO_4^-) concentrations are negligible, and do not significantly contribute to the buffering cycle. In systems abundant with clay sediments, soluble silicate particles may also provide buffering capacity through ion exchange, yet this is only significant in buffering of acidic groundwater. Therefore, the primary concern in neutralising acidic drain water is the abundance and reaction kinetics of bicarbonates and/or carbonates.

The main source of bicarbonates and/or carbonates in natural waters is from either the dissolution of limestone or the diffusion/advection of soluble ions in tidal waters. Due to the availability and low cost of limestone, several attempts have been made to neutralise acidic drain water by installing limestone barriers within flood mitigation drains or by using limestone treatment tanks (Pearson and McDonnell, 1975; Webb and Sasowsky, 1994; Desmier *et al.*, 2002). The effectiveness of these acid neutralisation strategies is often limited by drain hydraulics (i.e. the low hydraulic gradient of the drains reduces the amount of water flowing over the limestone), the hydro-chemistry of

ferrous-ferric reactions (i.e. formation of iron hydroxides can coat the limestone unless manually agitated), and the reaction kinetics of calcium carbonate.

With regards to reaction kinetics, the solubility of limestone ($CaCO_3$) is complex and dependant on a range of external factors. Evangelou (1995) showed that calcium concentrations, and hence, limestone (1:1 molar ratio) is dependant on pH and pCO_2 by:

$$\text{Log } Ca^{2+} = 9.76 - 2pH + \log 1/pCO_2 \qquad (6.1)$$

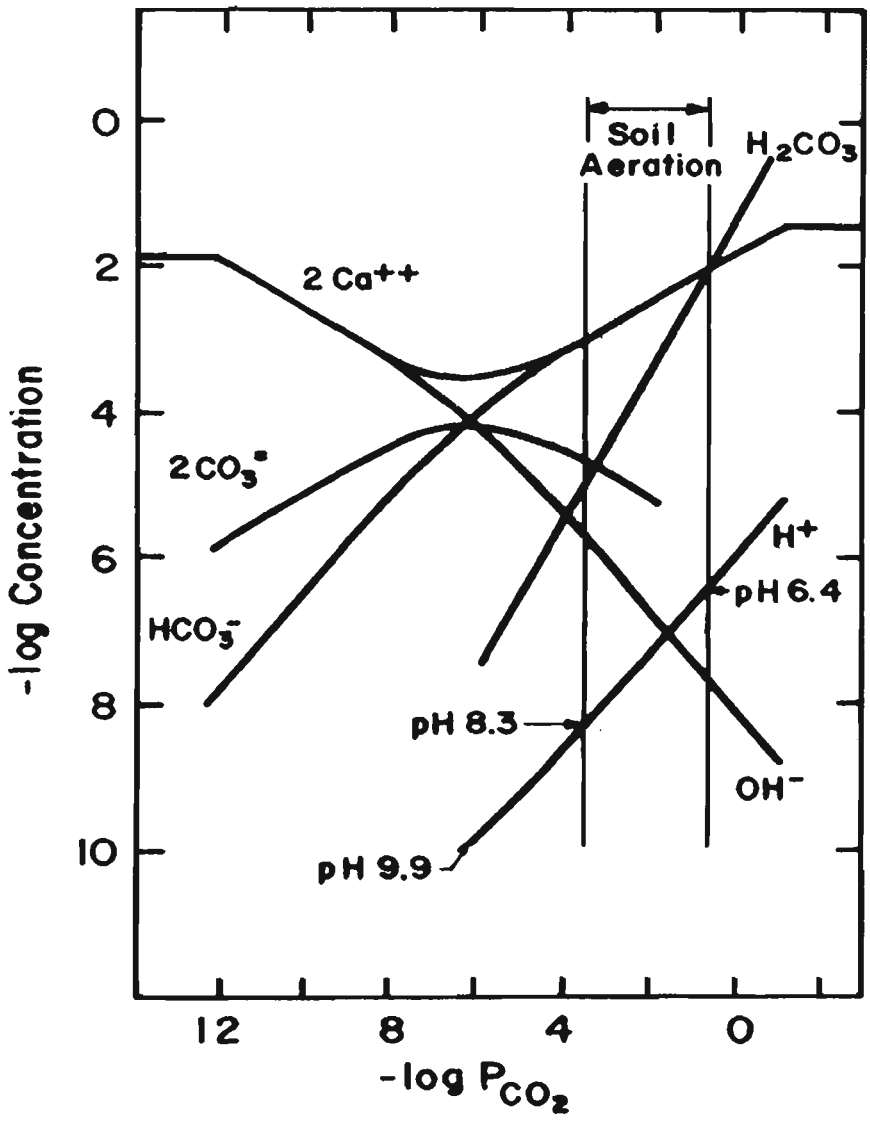

Figure 6.2 Stability diagram of limestone in natural water systems (adapted from Evangelou, 1995).

The solution of Equation 6.1 (i.e. Figure 6.2) illustrates that although alkalinity increases (in the form of bicarbonates) with increasing calcium concentrations, pH decreases. This represents a significant problem when treating acidic water with limestone because the majority of aqueous chemical reactions are driven by pH. This is important because of the high potential for H^+ ions to react with solution chemical species due to its small size and high electron accepting potential. Therefore, to remove common undesirable ions such as Mn^{2+}, the solution pH must be greater than 9.0. As shown in Figure 6.2, to obtain a drain water pH above 9.0, pCO_2 must be below atmospheric levels, yet in most natural systems pCO_2 is generally above that of the atmosphere. As a direct result, neutralisation of acidic drain water by limestone barrier treatments does not represent an effective long-term management strategy, and when feasible, buffering with a stronger base (i.e. NaOH or $Ca(OH)_2$), or with bicarbonates from tidal waters, is recommended.

The speciation of carbonate ions in relation to pH is shown in Figure 6.3. Since pH levels within Broughton Creek fluctuated from 4.86 to 8.02, and median pH was 6.74, the primary buffering agent is bicarbonate (HCO_3^-). Maximum buffering capacity within the carbonate system occurs when carbonic acid concentrations equal bicarbonate concentrations (pH 6.4), or when bicarbonate concentrations equal carbonate concentrations (pH 10.3). As stated in Chapter 5, concentrations of bicarbonates at any point within the estuary are dependent on penetration of the tidal front within the estuary, and, in mature well-mixed estuaries such as Broughton Creek, the tidal intrusion rate is mainly reliant on the quantity of upland inflow.

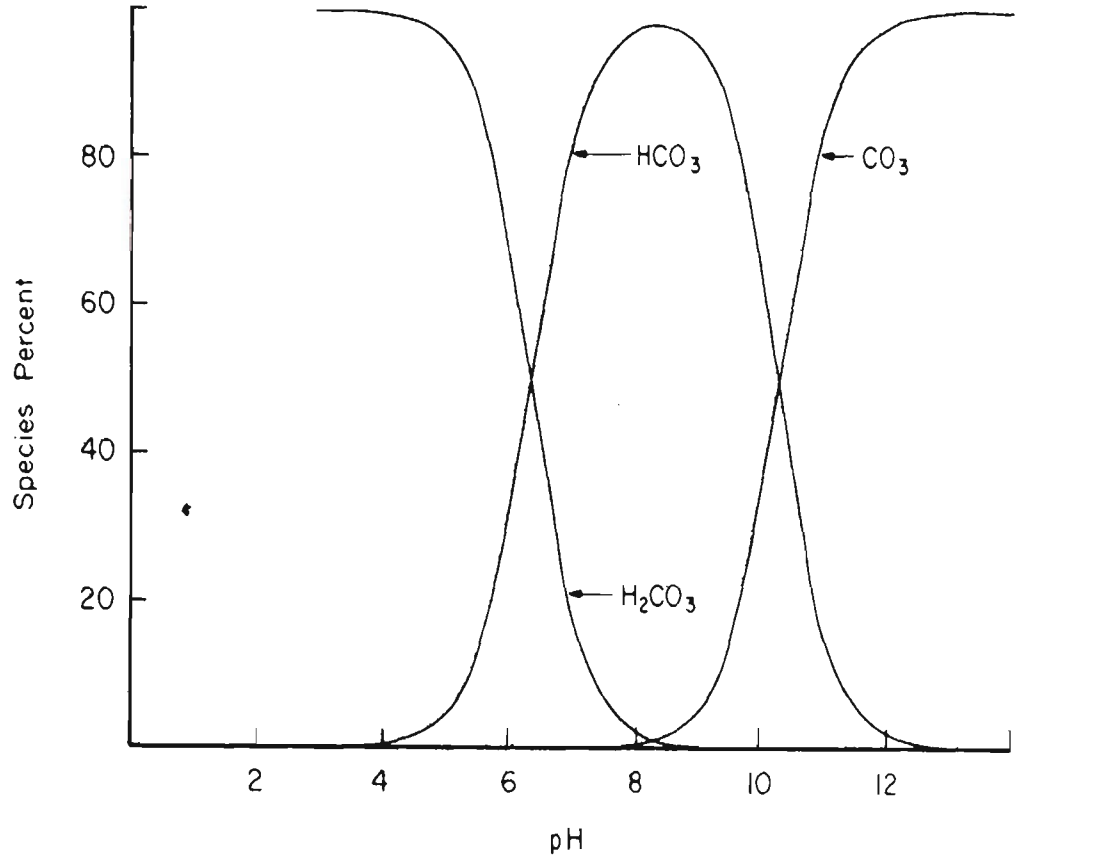

Figure 6.3 Speciation of carbonate system in natural waters (adapted from Evangelou, 1995).

6.2.1.1 Laboratory tests

To determine the contribution of bicarbonates and other buffering agents over varying ionic concentrations a series of laboratory test were performed. First, three sites were selected to obtain freshwater (0-5000 μS/cm), brackish water (5000-15000 μS/cm), and saline water (above 15000 μS/cm) samples. These sites were located at the mouth of Broughton Creek, 7.2 kms upstream, and 15.1 kms upstream, respectively. Grab samples, taken weekly over a 6 week period, were immediately measured for pH and electrical conductivity, and refrigerated until alkalinity analysis could be performed in the laboratory using the single endpoint titration method described by Neal (2001). To determine if bicarbonates were the sole contributor to alkalinity, a standard sample was prepared using 'milleq' deionised water and the equivalent quantity of standardised

bicarbonate solution. The standard sample was then titrated with acid of the same molarity and these results were compared against previous tests. The results were converted to mg L^{-1} of bicarbonate using the formulas (Raymont and Higginson, 1992):

$$\text{Total alkalinity} = \frac{T \times M \times 50040}{A} \quad (6.2)$$

$$HCO_3^- \text{ alkalinity} = \text{Total alkalinity} \times 1.219 \quad (6.3)$$

where, T equals the amount of titrate necessary to reach the selected endpoint, M equals the molarity of the titrate, and A equals the original volume of sample used. It was hypothesized that any difference between the two results was attributable to additional buffers within the creek. Averaged laboratory results from these experiments are shown in Table 6.1.

Within Broughton Creek, bicarbonates form the primary buffering agent with other neutralising agents contributing only slightly to the buffering system. Bicarbonates make up 99.14%, 99.16% and 98.37% of the buffering component at freshwater, brackish water and saline water sites, respectively. This was not surprising considering that seawater has a high concentration of bicarbonates (seawater concentration = 140 mg L^{-1}). Interestingly, it was hypothesised that due to the application of super-phosphates or ortho-phosphates for agricultural purposes, phosphates leached into the adjacent waterways may significantly contribute to the buffering component. However, the acidic soil and sub-soil conditions found across the floodplain tightly bind the phosphates with aluminium minerals on the soil colloid, hence reducing solubility.

Some silicate buffering was expected considering the abundance of clay sediments and the acidic groundwater environment, which can breakdown the clay lattice structure. To quantify silicate buffering, field samples were vacuum pumped through 0.45μm microfibre filters to remove soluble particulates, and then titrated in the same manner as described above. The proposed difference in filtered versus unfiltered samples was attributed to the impact of silicate buffering and is reported in Table 6.1.

The minor difference between filtered and unfiltered samples was attributed to the precipitation of oxides during the neutralisation process. The process of halmyrolysis encourages cation exchange and can remove dissolved components with a high affinity for solid phases, such as Fe (II). Furthermore, to test for silicate contributions to the total alkalinity, all of the samples taken had a pH above 6.25. However, leaching of silicates via groundwater seepage occurs under acidic conditions. As shown in Chapter 5, during mixing with pH neutral water both aluminium and iron oxidise to form precipitates. Flocculation and coagulation of precipitates is enhanced by the negatively charged silicate ion and, in this manner, particulates are removed from the water column.

Table 6.1 Averaged alkalinity concentrations to determine bicarbonate input.

Ionic strength	**Total Alkalinity $[HCO_3^-]$ in mg L^{-1}**	**Standard Solution $[HCO_3^-]$ in mg L^{-1}**	**Filtered Samples $[HCO_3^-]$ in mg L^{-1}**
Low (Fresh)	46.73±0.6	46.33±0.5	46.51±0.7
Medium (Brackish)	83.79±0.9	83.09±0.7	83.16±0.5
High (Saline)	117.55±1.1	115.64±1.8	115.77±1.1

6.2.2 Predictive ion speciation modelling

6.2.2.1 Model parameters, limitations and input criteria

The above tests demonstrate that bicarbonates are the primary buffer within Broughton Creek. However, the effectiveness of bicarbonate buffering is reliant on several electro and chemical gradients, which are often difficult to measure. The Davies Equation (Davies, 1962) approximates the electrical gradient of individual ions based on the activity coefficient, with the ionic strength of the solution acting as the controlling factor. This is significant because the solubility of most minerals is directly related to the ionic strength of the solution. The Davies Equation is given as:

$$\text{Log } \gamma_j = -AZ_j^2 \left[I^{1/2} / (1 + I^{1/2}) - 0.3I \right] \qquad (6.4)$$

where, γ is the activity coefficient of ionic species j, Zj is the charge of ionic species, A is a constant equal to 0.512, and I is the ionic strength given as:

$$I = 1/2 \sum_{j=1}^{n} Z_j^2 \, m_j \qquad (6.5)$$

where, m_j is the effective molar concentration of ionic species.

To calculate the complex reactions between differently charged ions over varying ionic strengths, several researchers such as Davies (1962), Sposito (1984), and Amacher (1984) have employed ion association models. One such model, PHREEQC, is an open interface program which has been developed to simulate chemical reactions in natural or polluted waters based on equilibrium chemistry of aqueous solutions reacting with minerals, gases, solid solutions, exchangers and sorption surfaces, including the

capability to model kinetic reactions. To account for high ionic strength (sodium chloride dominated) solutions, PHREEQC incorporates the ionic-strength term within the Debye-Hückel expression. PHREEQC is applicable to this study due to its capability to simulate chemical speciation and mixing over varying salinities. Additional information regarding PHREEQC, including governing and aqueous charge balance equations, are detailed by Parkhurst and Appelo (1999).

In this section, a mixing program is presented that was written and incorporated into the 1D ion association aqueous model, PHREEQC. The program was then modified, calibrated, and applied to evaluate the resultant product of mixing alkaline creek water of varying ionic strengths with acidic drain water rich in aluminium and iron.

The mixing program developed within this study, and run within the PHREEQC framework, was employed to simulate *in situ* water quality conditions over a range of buffering concentrations and ionic strengths, and was calibrated with experimental field data. The program measures elemental concentrations of selected species including aluminium, iron, sulphate, magnesium, and chloride, as well as pH, electrical conductivity and redox potential over a range of mixing proportions. Two assumptions and theoretical considerations for the mixing program are summarised below:

1. Creek water entering the drain completely mixes with acidic drain water. This assumption was justified at the study site following an in-depth study by Ikin (2001), who reported that due to the relatively shallow depth of the drain (~3 m), the high friction coefficient (Manning's n value > 0.25), and the induced mixing

caused by tidal ingress through modified floodgates, minimal stratification will occur within the drain.

2. Bicarbonate concentrations are equally distributed throughout the drain. Though the conversion of bicarbonate ions to carbonic acid will reduce buffering capacity with distance, the continual tidal influx replenishes bicarbonate concentrations. Nonetheless, further expansion of the model to incorporate 2-dimensional bicarbonate consumption is recommended if further application to significantly larger drainage systems is required.

The main inputs to the mixing program were elemental concentrations and electrical conductivity (i.e. ionic strength). These variables were determined from samples taken from the 3 alkaline sampling sites described above, and 1 extremely acidic sample (pH < 3.5) taken from the secondary side drain located at the study site. The samples were chemically tested in the laboratory using the methods previously described in Chapter 3. The initial chemical data of each sample was then used as an input via keywords and identifiers to the computer code and the program was developed to simulate mixing in 10% intervals (i.e. 10%, 20%, 30%, etc.), until there was twice as much alkaline water as acid water (i.e. 200%). In this regard, the modelling process represents a novel application of PHREEQC in simulating *in situ* acid neutralising conditions over varying ionic strengths. This procedure is also a significant improvement on current methods, which rely on trial and error methods to determine the resultant drain water quality. The developed program file is given in Appendix C.

6.2.2.2 Mixing model calibration and results

In conjunction, the developed program file and the ion association models within PHREEQC, henceforth referred to as the mixing model, were in strong agreement with laboratory results. To calibrate the mixing model, water samples were mixed in the same proportions as listed above, and chemically tested using standard laboratory procedures. The outputs from the mixing model simulations were then plotted against the laboratory results. The results for the highest and weakest ionic strength samples versus PHREEQC simulations are shown in Figures 6.4 and 6.5, respectively.

Both the mixing model simulations and the laboratory results indicate that drain water quality improved with mixing. In general, higher ionic strength samples (Figure 6.5) decreased acidity with less mixing than weaker ionic strength samples (Figure 6.4) due to the decreased solubility rates of highly ionic solutions and the increased concentration of buffering agents in the saline samples. The following section details the reaction path kinetics for anion and cations to highlight the decrease in ion solubility with increased mixing.

Generally, aluminium solubility (as shown in Figures 6.4 and 6.5) is pH dependent and aluminium is typically insoluble between pH 5-9. Monomeric inorganic aluminium solubility is complex due to the formation of partially dissociated $Al(OH)_3$ species and complexing between aluminium and organic matter. Aluminium commonly complexes with dissolved sulphate as $AlSO_4$ or as $Al(SO_4)_2$ in acidic conditions if sulphate is abundant, but as pH increases, Al^{3+} undergoes hydrolysis resulting in a series of OH^- complexes ($Al(OH)^{2+}$ and $Al(OH)^{+}_2$), and reduced solubility. The formation of aluminium hydroxide precipitates is shown in Equations 6.6 and 6.7.

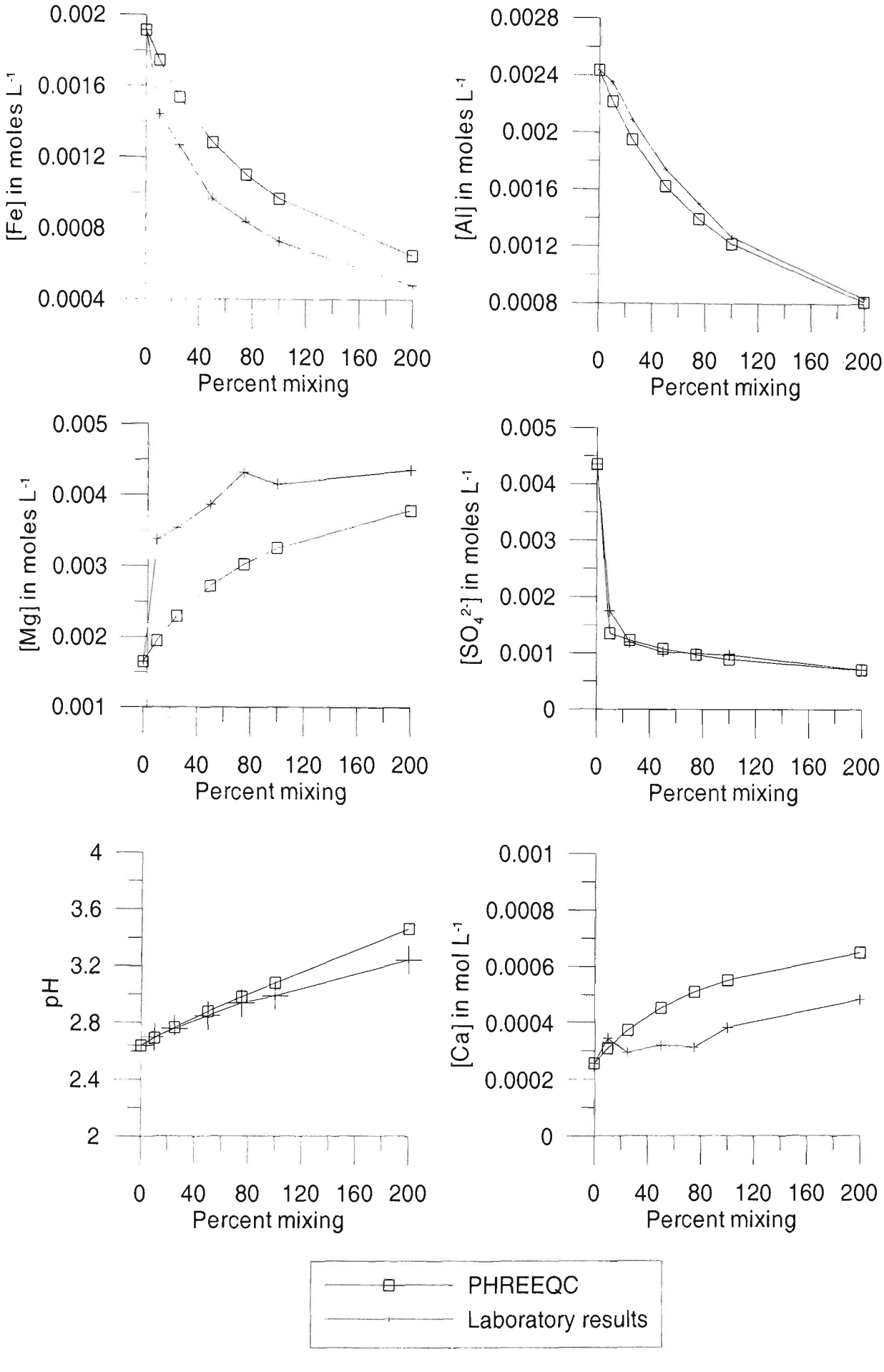

Figure 6.4 Laboratory results compared to PHREEQC simulations for low ionic strength samples taken from Broughton Creek.

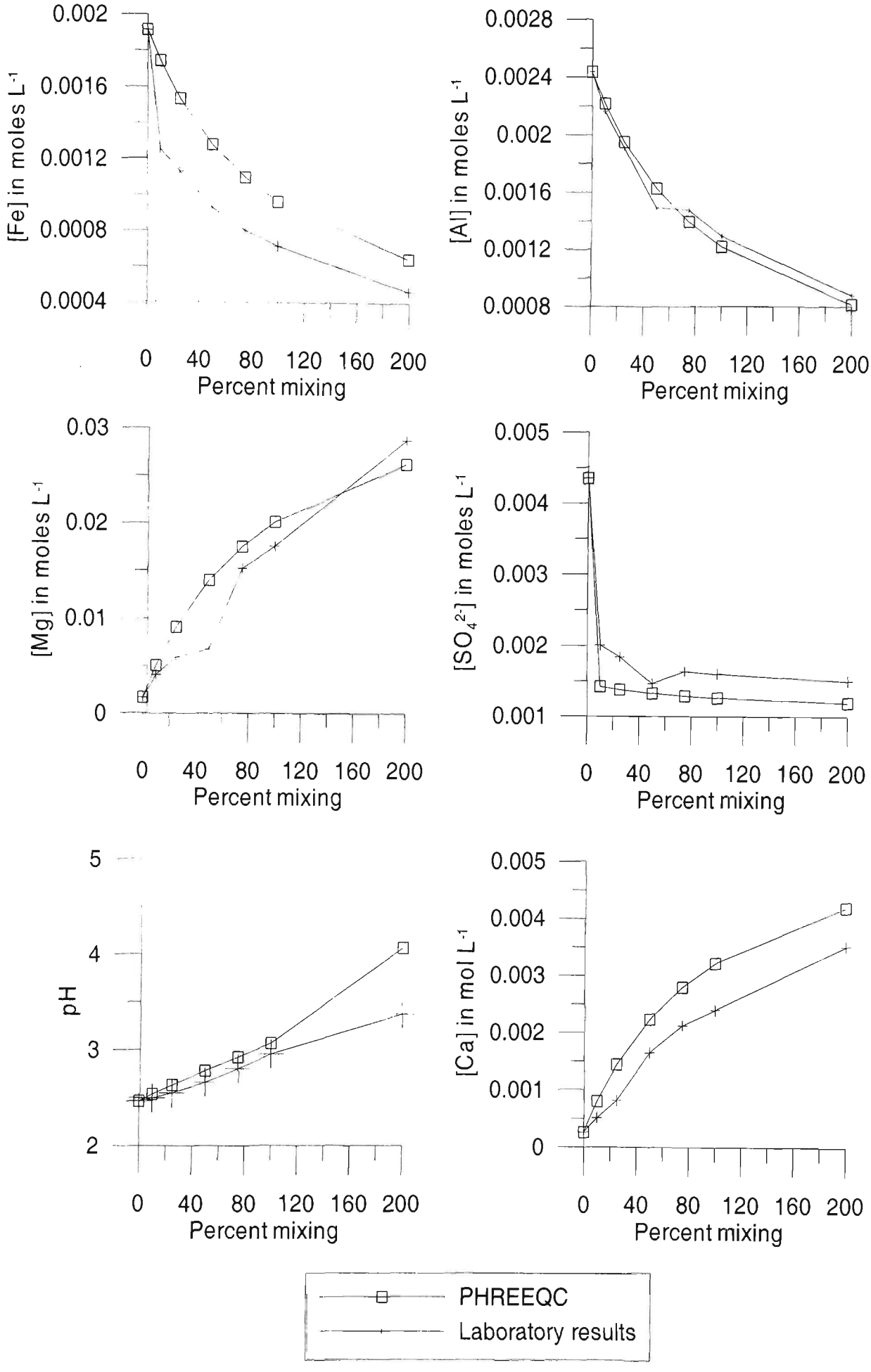

Figure 6.5 Laboratory results compared to PHREEQC simulations for high ionic strength samples taken from Broughton Creek.

$$Al^{3+}_{(aq)} + 3OH^{-}_{(aq)} \leftrightarrow Al(OH)_{3(s)} \quad (6.6)$$

$$Al(OH)_{3(s)} + OH^{-}_{(aq)} \leftrightarrow Al(OH)^{-}_{4} \quad (6.7)$$

The mixing model and the laboratory results indicate that increased drain water pH due to tidal buffering will decrease soluble aluminium concentrations. As the toxicity of soluble Al^{3+} is significantly reduced in drainage waters with a pH above 6.5, one of the major objectives of restoring tidal flushing is to maintain circum-neutral pH levels.

Total dissolved iron concentrations are dependent on pH and redox potential measurements; iron is generally only soluble under low redox or acidic conditions as Fe (II). Dick and Osunkoya (2000) showed that one-way floodgates promote reducing conditions because they restrict tidal flushing. At the study site, drain water quality (as shown in Chapter 5) was acidic with low dissolved oxygen levels, however, the mixing model results (Figures 6.4 and 6.5) suggest that modifying the floodgate to permit tidal flushing will increase Eh and remove soluble Fe (II) from the drainage waters. Conversely, the oxidation of Fe (II) and the formation of insoluble iron hydroxides generates H^{+} ions and explains the limited increase in pH during initial mixing as shown in Figure 6.4.

In contrast with aluminium and iron concentrations, sulphate solubility is not generally pH dependent. In Figures 6.4 and 6.5, the majority of sulphate ions were removed from solution within 20% mixing. This was attributed to the affinity of sulphates to bind with calcium to form gypsum ($CaSO_4 \cdot 2H_2O$). Gypsum is generally insoluble because when sulphate complexes with calcium the salts charge over the ionic radius decreases. Under reducing conditions with high iron content, sulphates can also precipitate as iron

monosulphides or MBOs (monosulphide black oozes), and form porous iron flocculate that releases acidity upon oxidation. Finally, dissolved sulphates can also be derived from tidal waters (seawater concentrations = 2700 mg L^{-1}) that mask acid contributions.

The above results indicate that alkaline buffering will improve water quality by increasing the pH and decreasing metal solubility. Based on these findings and using the calibrated model, a series of simulations were undertaken to determine resultant drain water quality under fluctuating tidal/climatic regimes (i.e. highly ionic versus lowly ionic conditions). In combination with the tidal leakage data presented in Chapter 5, these predictions were used to determine whether floodgate modifications would significantly improve drain water quality at the study site, and to calculate the volume of tidal water required within the drain. The results from these tests for both wet and dry climatic periods are shown in Figure 6.6.

The water quality simulations depicted in Figure 6.6 were developed using pre-modification drain and creek water data during wet and dry periods. The model inputs were divided into high ionic (low upland flow, strong buffering capacity) versus low ionic (strong upland flow, weak buffering capacity) periods based on electrical conductivity. All water quality samples under 5000 $\mu S\ cm^{-1}$ were deemed low ionic, while all samples over 15,000 $\mu S\ cm^{-1}$ were deemed highly ionic. Acid water inputs were obtained by averaging all relevant drain water quality records before floodgate modification, and the resultant concentrations were then used as inputs in the numerical code. The concentration of individual species is given in Appendix B.

The mixing model simulations of post-modification water quality at the study site (Figure 6.6) indicates that drain water quality will significantly improve during both high and low ionic creek conditions. In general, with increased mixing, acidic cation solubility decreased in a non-linear fashion, thus illustrating that buffering as well as dilution is important for removal of metal contaminants. The small disparity in water quality results between ionic conditions was attributed to the increased salt quantities in solution, which have a tendency to suppress metal-ion activity and/or increase solution pairing/complexation.

As shown in Figure 6.6, pH values rapidly increased with creek water mixing and varied between ionic conditions. Under highly ionic conditions, pH increased from 4.49 to 6.02 in less then 50% mixing, which was attributed to the elevated bicarbonate concentrations of highly ionic waters (87.86 mg L^{-1} in high ionic versus 17.98 mg L^{-1} in low ionic waters). In terms of management practices, it is important to note that the abrupt increase in pH levels indicates that only a relatively small quantity (~50%) of tidal water is required to significantly improve drain water conditions. Additionally, during the modelling process pH levels fluctuated greatest in response to variations in aluminium concentrations. This demonstrates that the removal of aluminium via mineral precipitates or through mineral surface sorption will correlate to an increase in drain water pH.

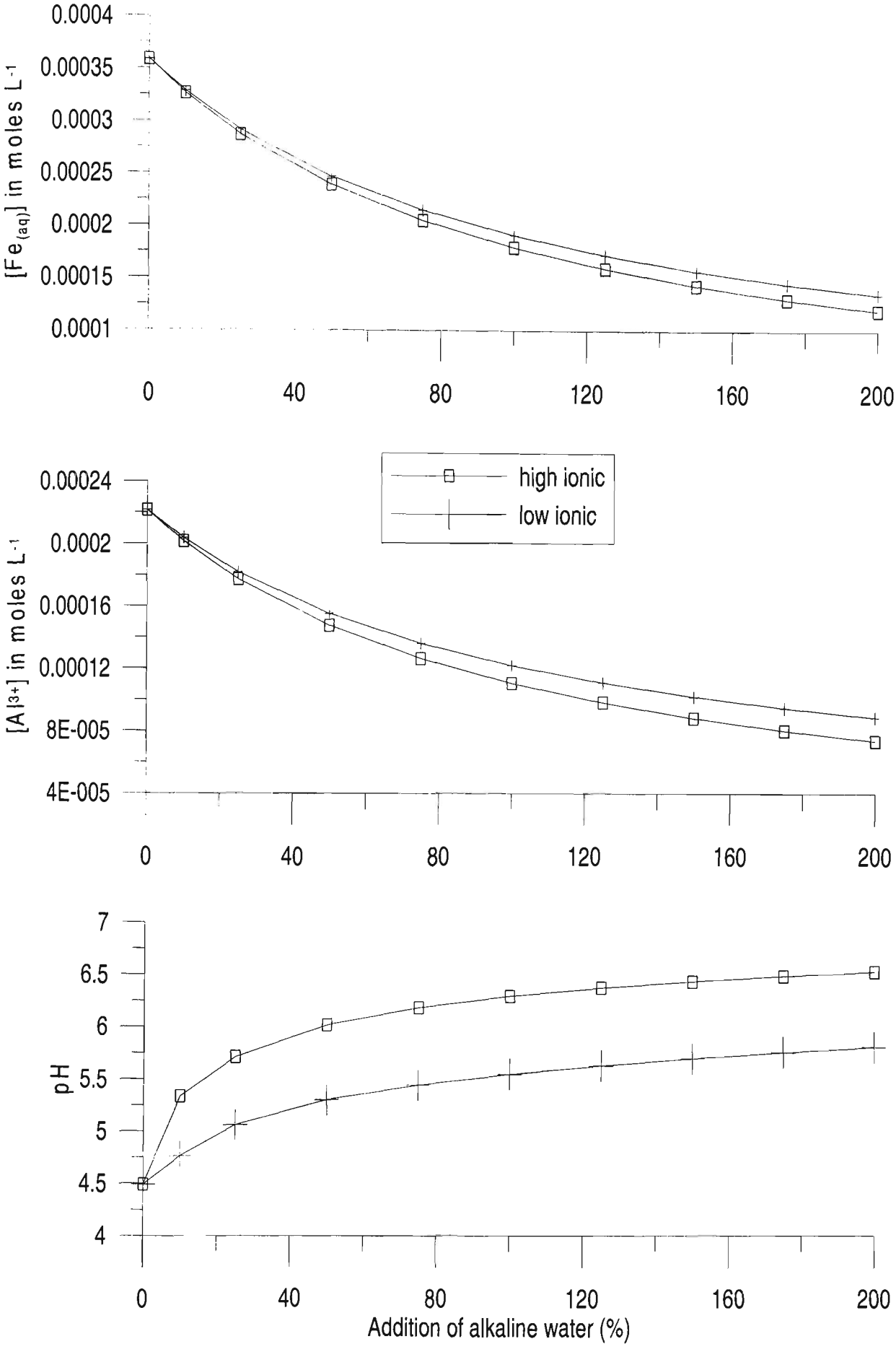

Figure 6.6 Simulations of drain water quality following mixing with alkaline creek water.

The above results show that mixing alkaline creek water with acidic drain water will improve water quality and that a significant improvement is attainable with only a small quantity of intruding water (50-100%). Understanding the potential change in water quality is vital in optimising floodgate design and in quantifying the benefits of modifications before costly civil works. The mixing model presented here and given in Appendix C is easy to use, cost-effective, and provides an accurate method of predicting the effect of tidal flushing on drain water quality. Furthermore, the above results indicate the reaction path kinetics for several undesirable ions during the buffering process. These simulations will be compared to post-modification results in Chapter 7.

6.3 Drain hydro-dynamics and overtopping concerns.

6.3.1 Tidal dampening and creek water levels

Based on the above simulations, increased tidal flushing rates equate to improved water quality. However, water levels within the creek are controlled by upland inflow and tidal characteristics. Along the southeastern coast of NSW Australia, tidal variations are predominately less than 1.6 m, with king tides (the strongest spring tides) around 1.9 m.

Within an estuary, tidal dampening due to friction, energy loss, and changes in surface elevation reduce tidal heights below coastal levels (Dyer, 1973). As the study site is 10.2 kms from the junction with the Shoalhaven River, and an additional 9.75 kms from where it discharges into the Tasman Sea, tidal variations are significantly attenuated. The influence of tidal dampening and tidal variations with distance from the mouth of the Shoalhaven River is shown in Figure 6.7.

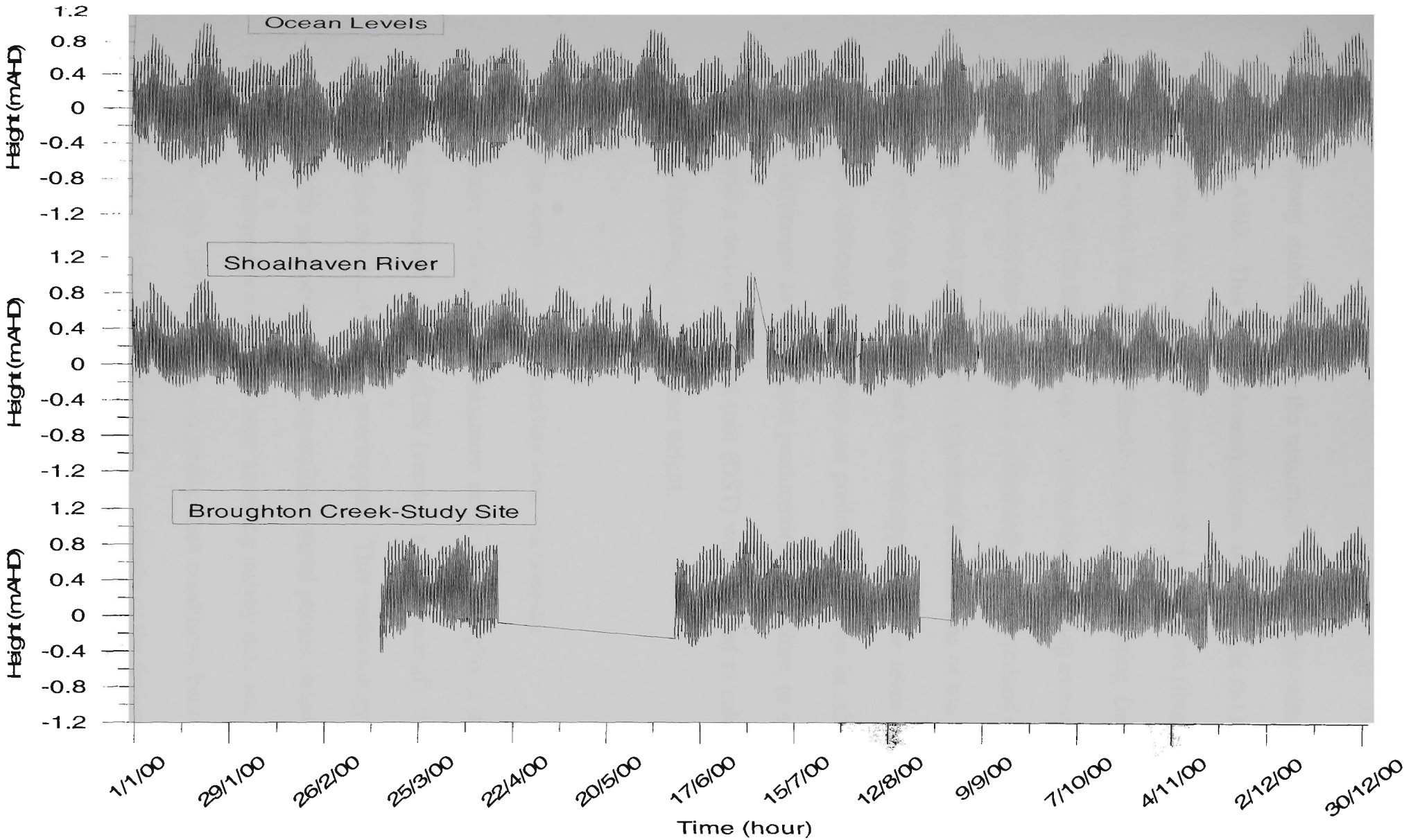

Figure 6.7 Tidal variations with distance from the ocean (missing data due to equipment malfunction).

Excluding strong rainfall events, the maximum water height within Broughton Creek was 0.91 m AHD. This is significantly below ocean levels (>1.0 m AHD), yet still represents strong tidal action. Measurements above this level (total readings = 11,465) were only recorded during peak flooding periods (i.e. during Days 180-186), which equated to 0.7% of the total readings. During these flooding events, overtopping of the levee banks occurred due to increased upland inflow and overland mass flow following saturation of the soil pores. This is important because one of the primary concerns in relation to modifying the floodgates is overtopping of the levee bank with saline or brackish water (although floodwaters are predominately low in salt concentrations and hence, not detrimental to agricultural productivity). Therefore, to avoid overtopping of the levee bank a decision support tool (DST) was required to calculate the impact of restoring tidal flushing on drain water height.

6.3.2 Decision support tool for assessing levee overtopping

Using the above tidal levels as maximum drain water heights, a decision support tool (DST) was developed using ArcGIS (version 8.2) to quantify the amount of water permitted within the drain without overtopping. This methodology was designed using various field site parameters including digitised aerial photos, detailed drain bathymetry information, comprehensive aerial laser scanning survey data and the aforementioned tidal records. The DST is limited to steady state conditions because of the low flow rates within the drain and the relatively flat topography of the region.

The presented method is a major improvement on current time consuming and imprecise methods, which rely on extensive drain levee sandbagging in 'assumed' critical spots. Furthermore, the DST provides visual reference to the critical areas

within the drain levee, and, when combined with site attribute information (i.e. soil and groundwater data), can be used to generate broad scale characterisations of the floodplain. This technique was also designed to be user-friendly and is applicable to other field sites within the Broughton Creek catchment and throughout Australia.

The DST was developed using extensive site-specific survey information to accurately simulate field site conditions. First, an aerial photograph of the area with AMG projections was imported into ArcGIS. Second, a comprehensive airborne laser scanning (ALS) survey was undertaken to determine topographical features. This survey data was ground-truthed using hand-held GPS surveying instruments on selected benchmarks including the floodgate headwall. As ALS does not effectively penetrate below the water surface, drain bathymetry data was obtained via hand-held GPS surveying of multiple transects in 50 m intervals. Additional transects were made in areas with unique topographic features such as low spots in the drain levee. Third, detailed echo-sounding data (see Chapter 5) was incorporated into the model to determine the creek bathymetry and then the various relative levels (RLs) were converted to meters Australian Height Datum (m AHD) and imported into ArcGIS as spot points. An aerial photo of the site with drain survey transects is shown in Figure 6.8.

Within ArcGIS, the survey data was integrated to form a digital elevation map (DEM) of the study area. The DEM was created by drawing a polygon around the spot points and using the 'create tin from features' tool from the 3D analyst extension within ArcGIS. The tin was clipped based on the polygon's features using the spatial analyst extension. The tin was then converted to raster format in 3D analyst and the raster data

was evaluated using the raster calculator in the spatial analyst extension. Finally, several DEMs were joined by 'mosaicing' each polygon within the grid calculator extension. The DEM of the study area was shown previously in Figure 3.9.

After the DEM was created, drain water elevations were set using the raster calculator tool within the spatial analyst extension to determine appropriate freeboard levels. Specifically, drain water elevations were set at 0.91 m AHD and 0.71 m AHD, representing the highest drain water elevation anticipated and the average high tide level (95% of all creek readings were less then 0.71 m AHD), respectively. The outputs for these simulations are shown in Figures 6.9 and 6.10.

Simulations using this technique showed that drain overtopping did not occur when water elevations were set to 0.71 m AHD. As depicted in Figure 6.9, tidal intrusion extends 234 m upstream of the floodgate within the primary study drain and throughout the length of the secondary side drain. The levee bank along both drains prevents overtopping, which suggests that for 95% of the study period full tidal flushing could be permitted within both drainage networks.

In contrast, when the drain water level was set at 0.91 m AHD significant overtopping was noted in the secondary side drain (Figure 6.10). However, close-up examination of the primary drain in Figure 6.11 shows that the drain levee bank is sufficient to restrict overtopping at this height. Nonetheless, a large area above and below the drain levee bank is subject to flooding by the lateral movement of surface water through the vadose layer, yet the short timeframe of king tides (1-3 hours) and the low hydraulic conductivity of the soil in the lateral plane will restrict flooding. Nonetheless, the

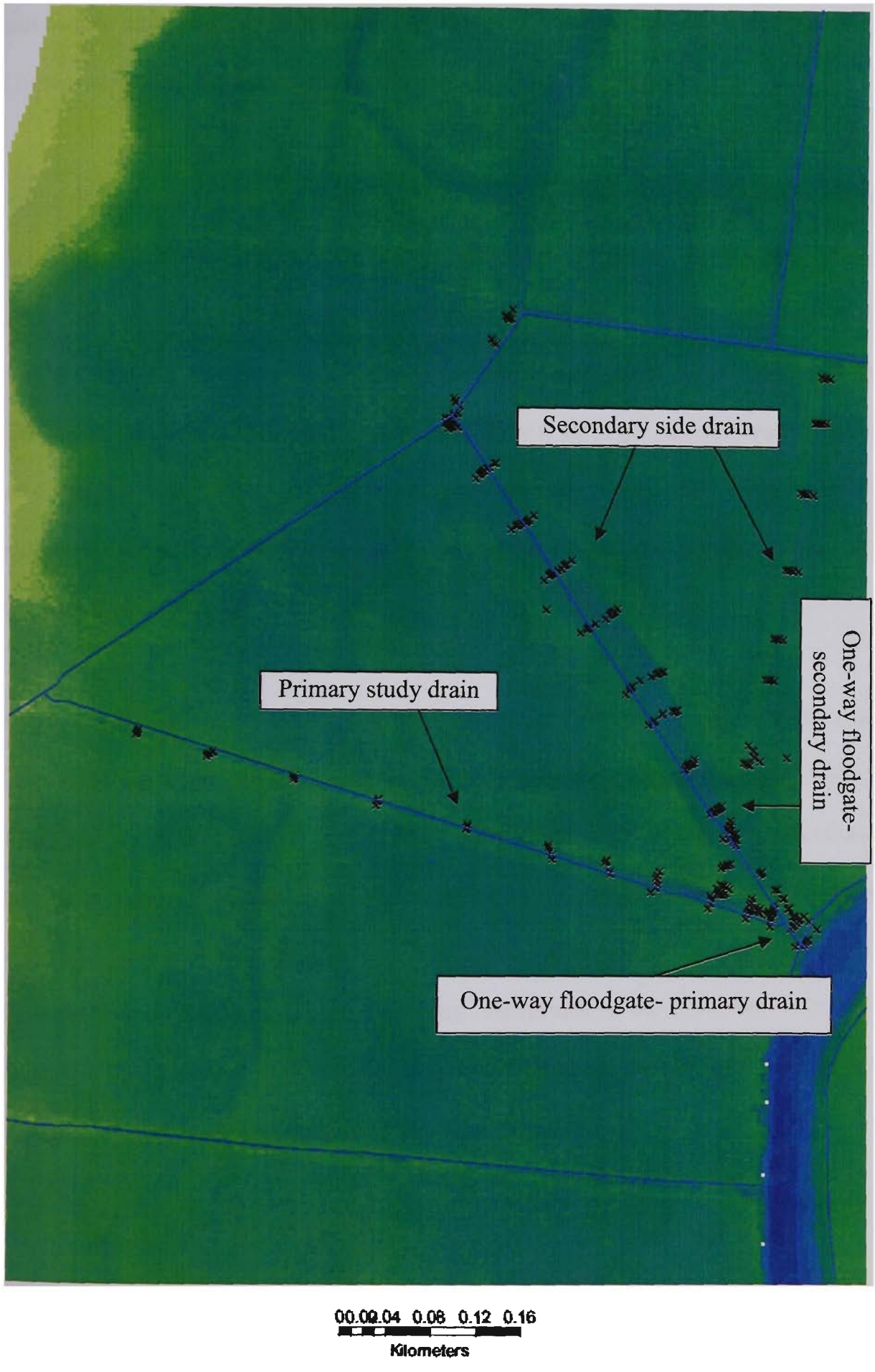

Figure 6.8 Drain cross-sectional survey transects with creek bathymetry data.

groundwater table was monitored after floodgate modifications to determine the affect of increased drain water elevations on the phreatic zone (see Chapter 7).

Results from the DST (Figure 6.10) show that surface flooding of the secondary side drain during peak flooding periods (0.91m AHD) would be via overtopping of the backswamp low-lying region, and, once this occurs, tidal waters would infill large areas north and south of the drain. Interestingly, the areas most likely to be submerged are relic stream channels, which previously flowed directly through the backswamp region, and are visible in aerial photographs. These areas have been previously linked to strong acid production and transport zones (Blunden, 2000; Lawrie and Eldridge, 2002) and may help explain the high acid concentrations within the secondary side drain.

Based on the above methodology, full tidal restoration should be restricted to the main study drain to avoid surface flooding. This is feasible because the side drain is floodgated and thus, changes in the main study drain will not cause a discernable increase in surface water levels. Conversely, if the tide is regulated and drain water levels are restricted to less then 0.71 m AHD, then the floodgates attached to the side drain can be modified to permit tidal flushing. Nevertheless, the outcomes of the DST emphasise the importance of floodgate design and highlight the necessity for different floodgate designs to achieve different water quality goals.

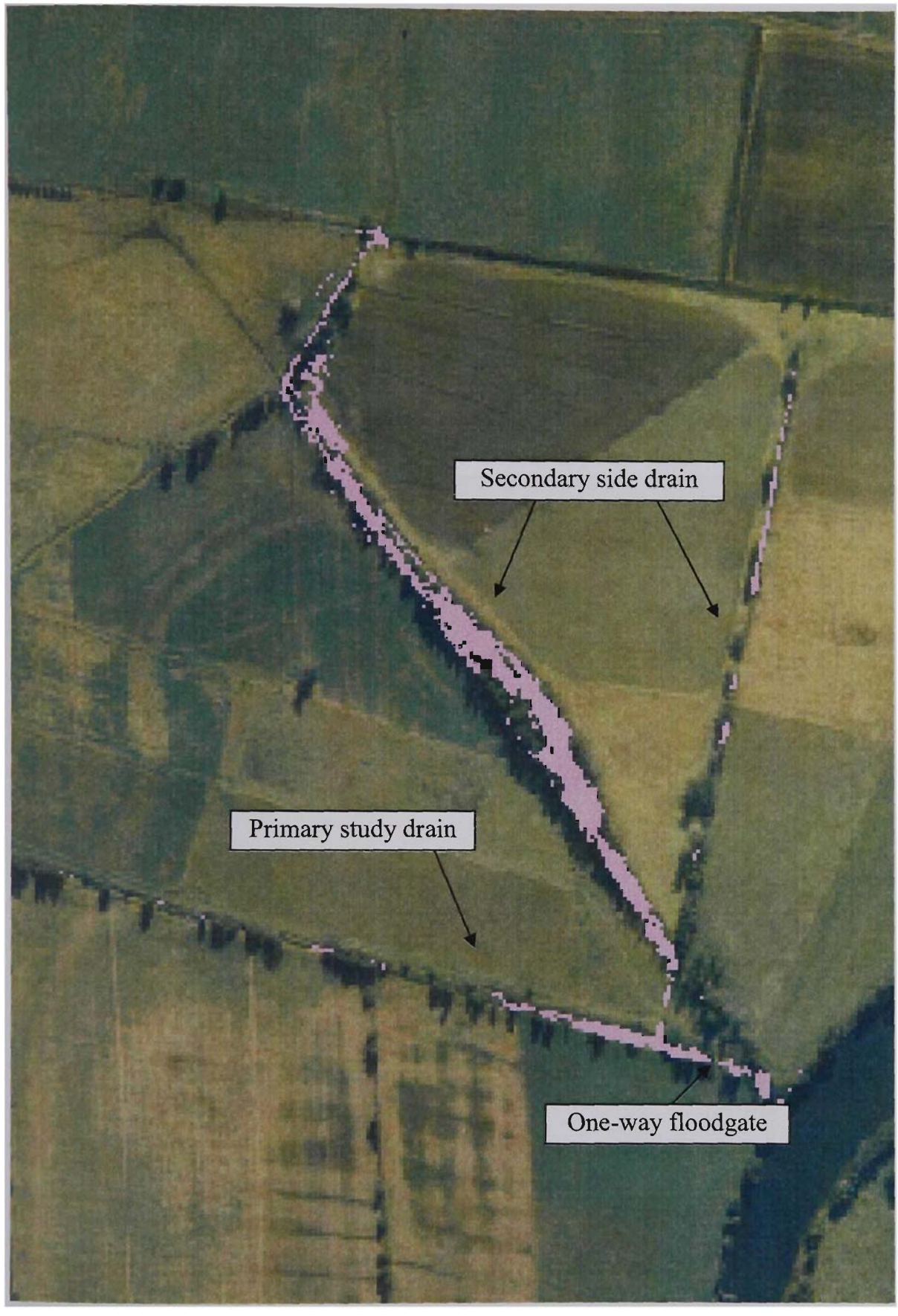

Figure 6.9 Drain water elevations at 0.71 m AHD within the study drain and secondary side drain.

Figure 6.10 Drain water elevation at 0.91 m AHD within the study drain and secondary side drain.

In conjunction, the spatial technique and the chemical mixing model emphasize the interrelationship between tidal intrusion rates and drain water quality. As shown above, the DST demonstrates that a 58% increase can be expected in drain water levels, and, when used in tandem with the PHREEQC mixing model, this equates to a rise in pH from 4.49 to 6.10 during highly ionic periods. The increase in drain water pH will also decrease soluble aluminium and iron concentrations, as well as lowering the manganese and sulphate levels. Based on the cost of floodgate modifications and the selected environmental objectives stated previously, these levels were deemed sufficient to commence trial floodgate modifications.

Figure 6.11 Levee bank region with drain water elevation set at 0.91 m AHD.

6.4 Modified floodgate designs: concerns, objectives and parameters.

The negative influence of tidal restricting structures with regards to ecological effects on aquatic life (Pollard and Hannan, 1994; Sammut *et al.*, 1994; Hyne and Wilson, 1997), wetland development and productivity (Dick and Osunkoya, 2000; Hutchings and Saenger, 1987), and acid sulphate soils (Indraratna *et al.*, 2002; Glamore and Indraratna, 2001) are now well recognised throughout Australia. Williams and Watford (1997) reported that within the state of New South Wales, 5300 tidal restricting structures exist. Of these, 1035 consist of top-hinged floodgates (or flap gates) similar to those found at the study site which are considered modifiable. Currently, no standard modification codes to redesign flap gates have been developed, and consequently, local government councils often undertake modifications haphazardly and without proper consideration of design objectives or hydraulic concerns. This section addresses the design and hydraulic issues regarding floodgate modifications, with particular reference to the multitude of concerns involved before floodgate modifications. In the latter part of this section, two floodgate designs are presented. Both designs were implemented at the study site and successfully achieved their design objectives.

6.4.1 Top-hinged flap gate design

At the study site, indeed in most flood mitigation systems throughout coastal Australia, the majority of floodgates in use are top-hinged flap gates (for reference see Figure 3.7). The working objective of flap gates is to permit drainage upstream of the floodgate and prevent flood and tidal flows from downstream waterways into the drained area. While other styles such as radial and sluice gates are used in a similar fashion, the following discussion will focus on top-hinged flap gates because of their relevance to this study.

As shown in Figure 6.12, top-hinged floodgates operate under 3 design criteria. First, when upstream water levels are higher than downstream levels hydrostatic pressure opens the gate and water is discharged from the drain. Assuming these conditions remain, water will continue to discharge until the drain invert or the sill level is reached. Second, when the downstream water elevation is higher then upstream levels hydrostatic pressure closes the gate and no reverse flow can occur. Finally, when the water level is equal on both sides the gate remains closed and acts like a non-return valve. Slanting the headwall enhances gate closure and attaching a natural rubber L-shaped seal between the flap face and the headwall structure improves sealing. Typical components of a top-hinged flap gate are presented in Figure 6.13.

The above drainage conditions imply that flap gates normally operate automatically except when manual debris removal from between the seal and headwall is necessary. Drainage will not occur unless there is a significant difference between water levels, therefore the rate of fall upstream of the gate cannot be greater than the rate of fall downstream. Nonetheless, drainage times are site specific and related to a number of factors including:

(1) The relationship between water height and volume stored in a particular area;

(2) The size of the floodgate structure;

(3) The design of the floodgate;

(4) The size of the drain; and

(5) The hydraulic efficiency of the drain.

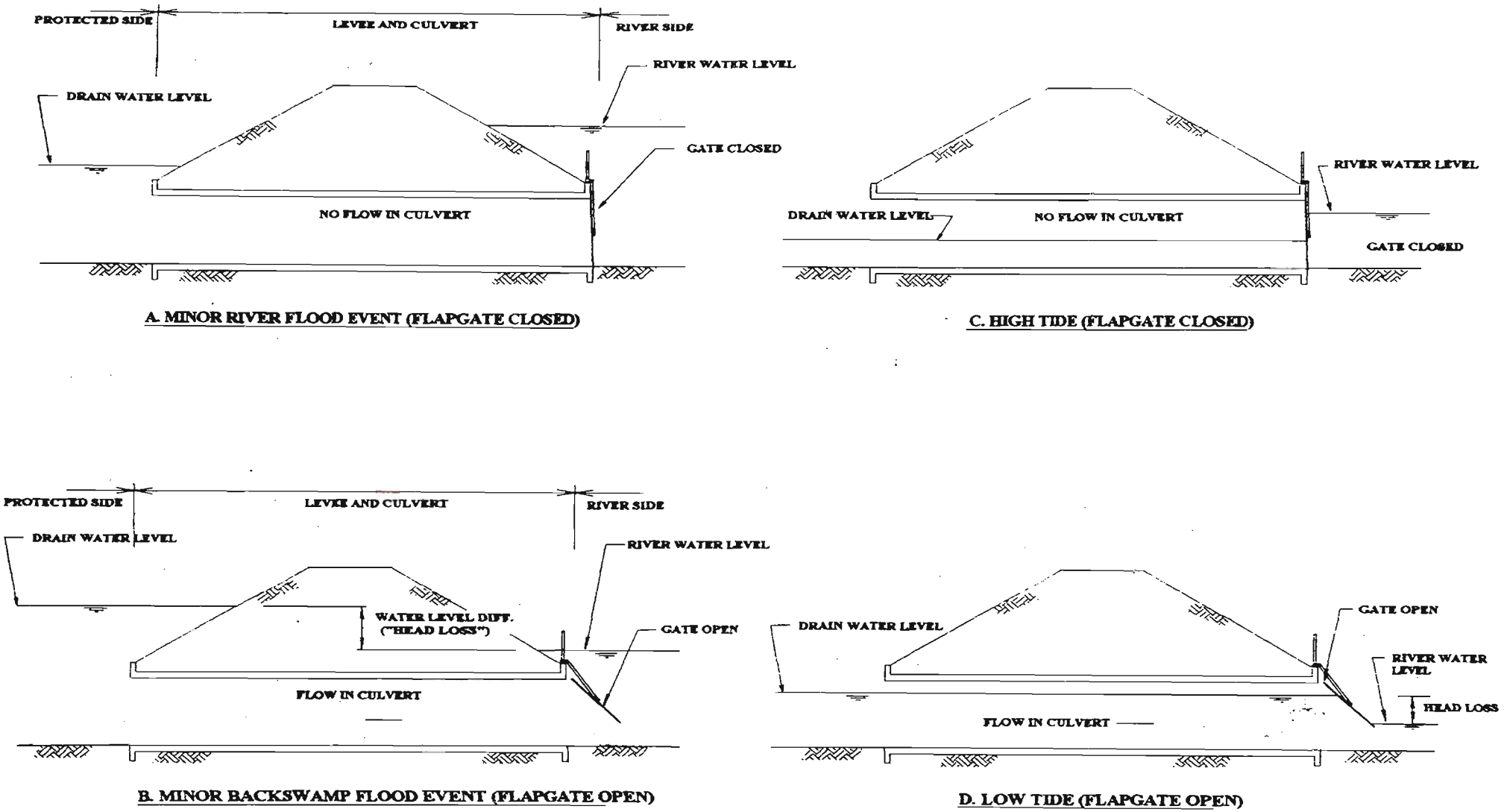

Figure 6.12 Operational conditions for top-hinged flap gates (adapted from Patterson and Smith, 2000). Note head loss has been exaggerated for illustration.

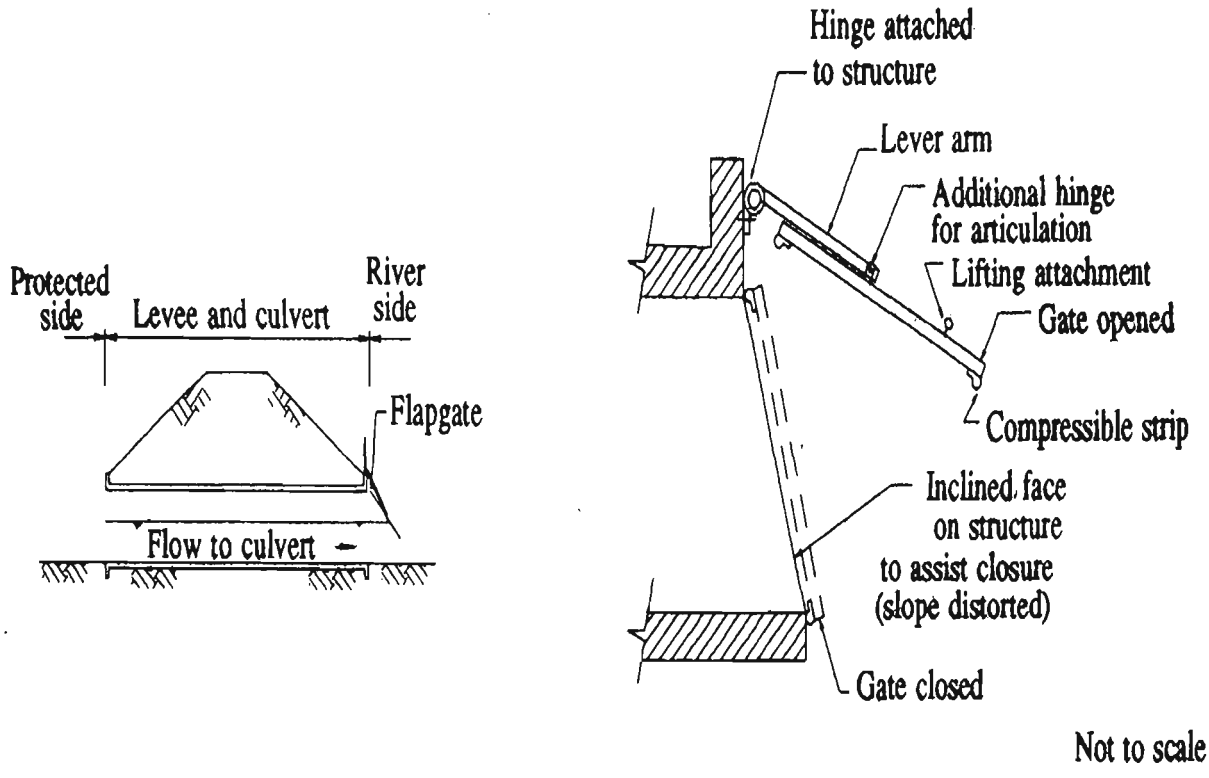

Figure 6.13 Typical components of a top-hinged flap gate (adapted from Patterson and Smith, 2000).

6.4.2 Hydraulic considerations

Limited information is available on the hydraulic considerations and stage discharge relationship of top-hinged flap gates. The majority of available information concerns the discharge of water through multiple gates and its impact on flow interference. Specifically, when a series of flap gates are close to each other, such as at this study site, discharge under and around the gate causes flow interferences and results in hydraulic loss (Figure 6.14). To maximise discharge and reduce bed-scour from flow interferences, training walls and aprons were installed at the study site. Therefore, any major structural modifications to the floodgate infrastructure must consider the interactions between adjoining floodgates and compensate for reduced discharge.

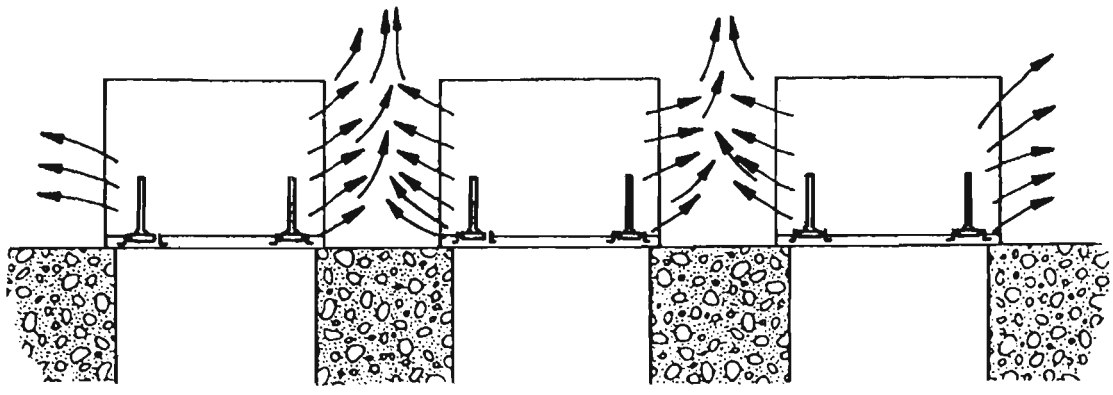

Figure 6.14 Sideways flow interference caused by top-hinged flap gates (Lewin, 1995).

Pethick and Harrison (1981) established the hypothetical treatment of the stage discharge relationship of a rectangular flap gate using 2 different theoretical concepts. The flap gate relationship was expressed as a 3 dimensionless parameter plot for free flow where, q = discharge per unit width of flap gate, ρ = density of fluid, h = upstream head, L = depth of flap, βL = distance from hinge to the centre of gravity of the flap, m = mass per unit width of flap gate and g = gravity constant

Using the constant mass parameter from Figure 6.15 ($2\beta m/\rho L^2$), and the variable h/L factor determined from field values, the stage-discharge relationship can be calculated. Based on the study drain dimensions, the calculated mass parameter of the floodgates at the study site is 0.12. Using surface water height data obtained from the submersible pressure sensors following a rainfall event, the dimensionless variable h/L fluctuated from 0.61 to 1.01. Therefore, the discharge per unit width of the flap gate varied between 2301 m^2/h to 5570 m^2/h.

Using the above calculations, the mass of the floodgate also plays an important role in determining the discharge coefficient through top-hinged flap gates. By reducing the mass by half and maintaining the same head levels, the discharge ranged from 2906

m^2/h to 7024 m^2/h, or an increase of 21%. This indicates that the weight of the floodgate flap has a significant impact on discharge, yet this relationship is valid only if the downstream head levels are maintained lower than upstream elevations. To calculate the impact of floodgate mass on preferential flow through modified floodgates, a series of hydraulic tests were conducted at the field site. The findings from those tests are given in Chapter 7.3.

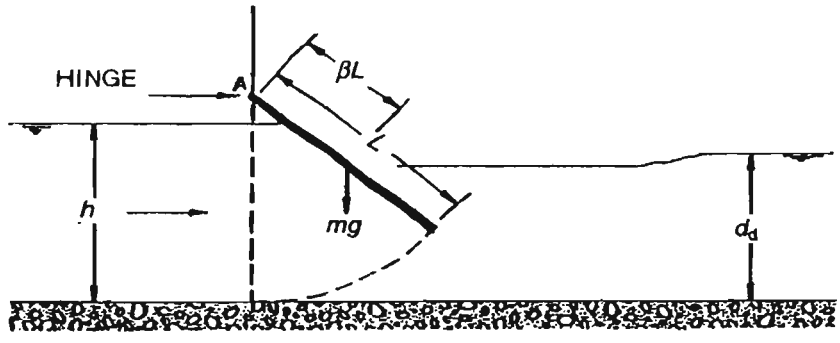

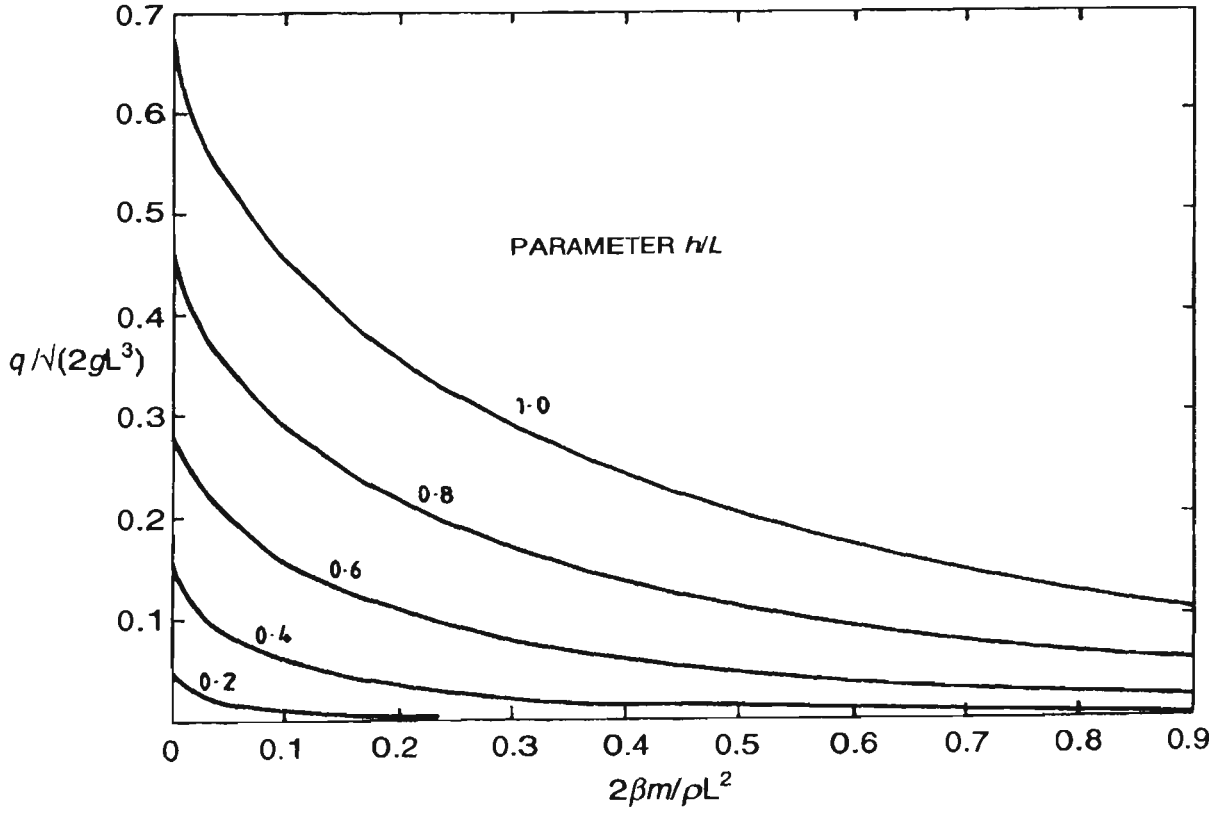

Figure 6.15 Stage discharge relationship of a top-hinged flap gate (adapted from Pethick and Harrison, 1981).

6.4.3 Floodgate design criteria

Based on the water quality and overtopping concerns detailed within the first two sections of this chapter, and working within the infrastructure and hydraulic constraints present at the study site, modifications of the floodgate structure were required to fall within strict operational guidelines. Whereas the main objective in regards to water quality was to restore tidal flushing to the drainage system, floodgate modifications were restricted by other hydrodynamic, environmental and agricultural criteria. These criteria are applicable to all floodgate modifications and include:

1. Maintaining flood mitigation characteristics (i.e. not reducing hydraulic efficiency of drain during storm events).
2. Prevention of saline water ponding on agricultural land.
3. Control of infrastructure to allow adjustments during critical events such as flooding and/or gate obstruction (i.e. debris removal).
4. Sufficient flexibility to trial several management strategies including optimising water levels and seasonal variations.
5. Low maintenance and safe to operate.
6. Long lasting, vandal resistant, and reasonably costed.
7. Will permit fish passage upstream of the floodgate.
8. Ability to be implemented within existing infrastructure.
9. Easily transported and installed with potential for widespread application.
10. Designed to function during extreme rainfall and discharge events.

These criteria are further detailed within individual floodgate design parameters set out in the following sections.

6.4.4 Winch driven vertical lifting gate

The modified vertical lifting gate (VLG) design initially installed at the study site is shown in Figure 6.16. It was developed to allow tidal flushing within the drain while maintaining on-site control of the infrastructure and upholding the hydraulic efficiency of the drainage system. The VLG complies with all of the design criteria and optimises tidal flushing at the study site by:

- Permitting dense alkaline creek water to intrude through an opening at the bottom of the gate.
- Allowing simple user-controlled mechanisms (i.e. hand winches) to raise and lower the floodgate to optimise the floodgate aperture and provide manual control during flood events.

The VLG is constructed from long-lasting materials (aluminium and stainless steel), does not require extensive maintenance, allows fish passage, has a widespread application, is easily adaptable to other locations, and is relatively inexpensive. However, the lifting mechanism of the VLG and the long tidal period (i.e., 6 hours) means that the VLG effectively acts as an on/off valve. Nonetheless, this was anticipated and tested with the spatial technique (i.e. the DST) before installation, and did not alter the design objectives.

Figure 6.16 Photo of two winch driven vertical lifting floodgates at the study site.

Two VLGs with mirrored designs were installed at the study site (one per flap). During construction, I-beams were welded to a base plate, and four 20 mm holes were drilled into the plate to align with the existing headwall bolts. Two 40 mm load-compensating arms were installed within the gate with one inserted through holes drilled within the I-Beams, and the other bolted onto the arms of the flap gate. A hoist drum was then welded onto one end of the top load-compensating arm and a winch plate was welded onto the I-beam 40 cm below the hoist drum. Stainless steel wire ropes (safety factor of 10) were then run between the winch and the hoist drum, and between the load-compensating arms. The wire ropes were designed so that if one rope failed the other would continue to operate. Finally, to raise and lower the gate easily the natural rubber seal and L-shaped hinge were removed from the back of the flap gate. This decreased seating efficiency of the floodgate but the leakage was not considered significant. The design components of the VLG are depicted in Figure 6.17.

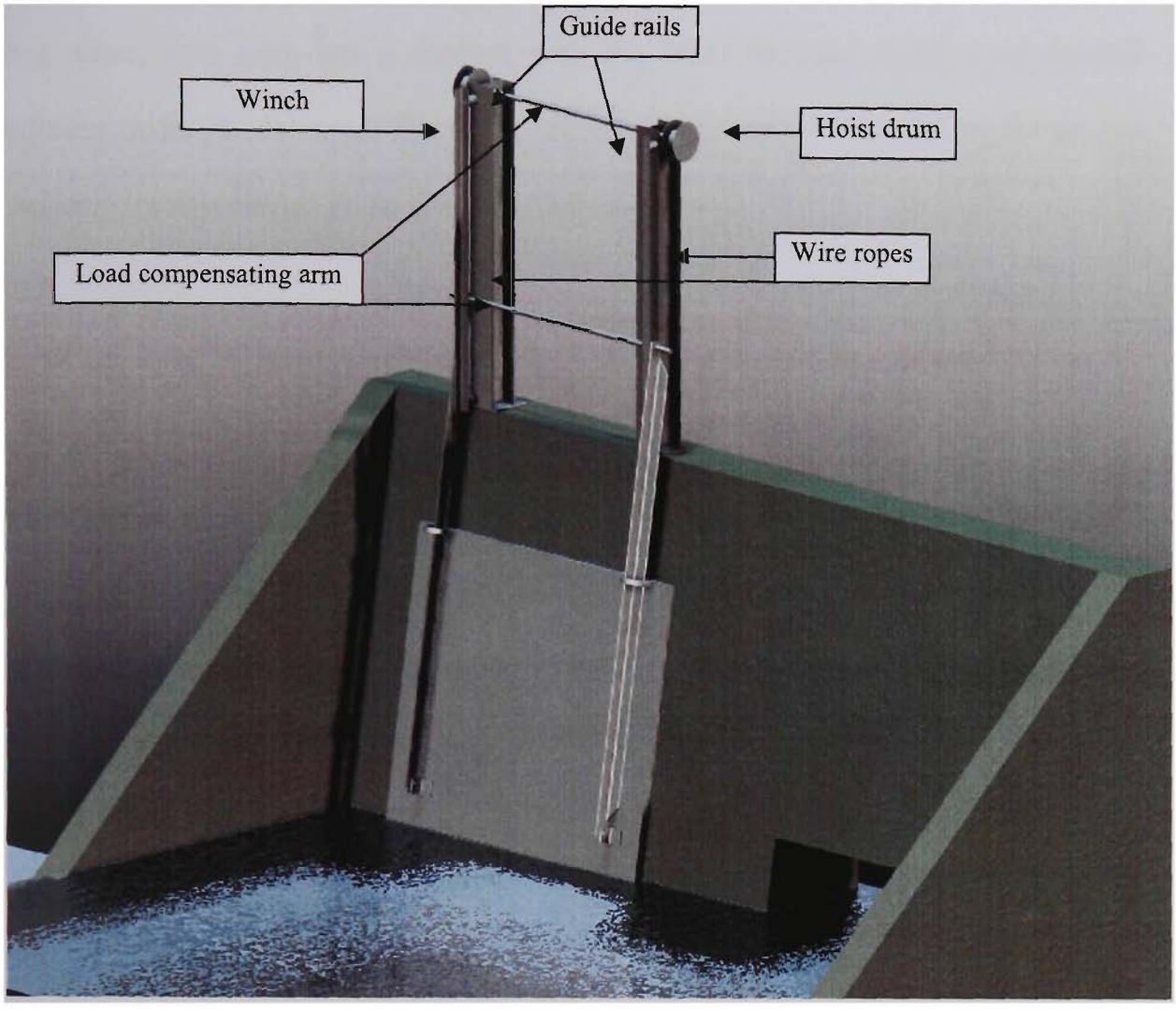

Figure 6.17 Schematic of vertical lifting gate (VLG).

With most vertical lifting gates opening is the critical emergency operation, yet to restrict tidal flows the VLG's critical emergency operation position is closed. Therefore, unlike other vertical gates, the mass of the flap was not overbalanced and the main drive effort was in opening. To enhance this 'fail-safe' design, a series of guides were installed along the exterior of the I-Beams that enclosed the lower load-compensating arm. These guides allow the gate to rise within a 50 mm slot, while maintaining the gate pivot point along the lower load-compensating arm. The bottom bolts on the guides also stop the gate from being lowered too far, which could damage the flap and the headwall and act as a catch in the unlikely case of dual wire rope failure. To combat vandalism, the winch arms were locked into place with a U-Bolt lock. Furthermore, while hydraulic downpull forces are important in high-headed

lifting gates, they were not a concern with the VLG because under open channel conditions hydraulic downpull forces are negligible and can be absorbed by the margin of hoisting force provided in the gate installation.

The VGLs were installed on October 30, 2000 and operated successfully during the entire post-modification period (>700 Days). They were subject to a range of environmental conditions including a one in five year storm event. Optimal gate aperture height was calculated at 0.3 m, based on the volume of water within the drain, operational stresses on the gate, and fish passage. This level also ensured that the gate opening was always submerged and therefore, floating debris (flotsam) could not intrude upstream of the floodgate.

6.4.5 Environmentally Controlled Smart Gate System

While the VLG was successful in restoring tidal flushing to the main study drain, it does not provide incremental control over the quantity of water within the drain. As shown above, the volume of tidal water within the drain determines drain water quality and/or the extent of floodgate manipulations (i.e. overtopping concerns). In these instances, the VLG is not suitable for drainage systems where only a small volume of tidal water is required to improve drain conditions or where full tidal flushing will cause drain overtopping. This situation is common in extremely low-lying drainage systems throughout the Broughton Creek catchment, in tertiary drains such as the side drain at the study site, and in various backswamp drains with small levee banks around coastal Australia.

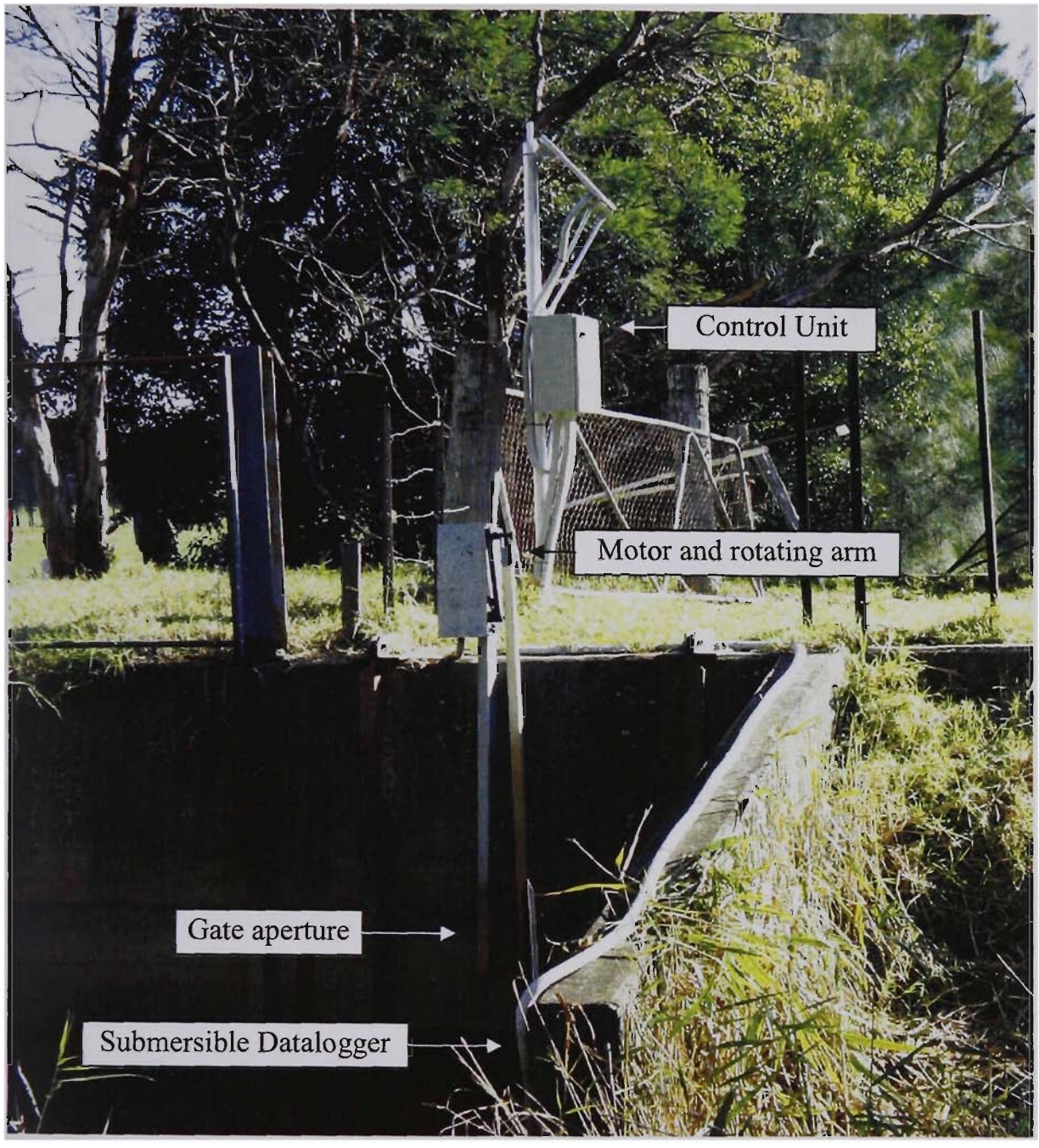

Figure 6.18 Photo of the 'Smart Gate' installed at the study site.

Access to manually controlled floodgates is also a concern during extreme events because tidal restricting flap gates are usually located along the levee bank junction where the drainage system flows into a creek or estuary. In these conditions, the floodgates can become isolated and access to the gates may become hazardous. Therefore, floodgates that incorporate a remote access feature are advantageous because they can be operated from a central control network.

Similarly, under prolonged dry conditions salinity levels within creeks/estuaries can rise to near seawater and only a small volume of tidal flushing is required to reduce drain water acidity (i.e. low groundwater seepage) and increase creek water alkalinity. In areas with high lateral soil hydraulic conductivity (> 5 m day^{-1}), tidal flushing may need to be restricted based on salinity concentrations. Based on these and the aforementioned operational requirements, the 'Environmentally Controlled Smart Gate System' was developed and installed at the field site.

A picture of the 'Environmentally Controlled Smart Gate System' (or 'Smart Gate') installed at the study site is shown in Figure 6.18. The 'Smart Gate' was designed to allow a specific volume of tidal water into the study drain based on real-time water quality variables. Within the system, submersible multi-parameter data loggers located upstream and downstream of the flap gate input pH, electrical conductivity, water temperature, and water elevation into a central data-logging unit at 15-minute intervals. The control unit then compares these readings to previously set trigger points and determines whether a slotted aperture within the floodgate should be opened or closed. If a trigger point is reached, the control unit closes the appropriate electrical circuit to drive a DC motor in the open (up) or closed (down) direction.

An example of a typical gate operation is explained below:

1. Gate is open to allow tidal flushing.
2. Data logger measurements uploaded to the control unit every 15 minutes.
3. With the incoming tide, data logger readings exceed manually set trigger levels and the control system activates the close gate protocols.
4. The motor closes the gate and the system awaits further readings.

5. When acceptable levels return, the gate reopens.

The primary objectives of the 'Smart Gate' are to control the volume of water upstream of the floodgate and optimise tidal buffering. To accomplish these objectives, a range of user defined triggers based on real-time data logger readings have been layered into the systems program. To specify these statements, a set of 'pseudo-codes' was written and is shown below:

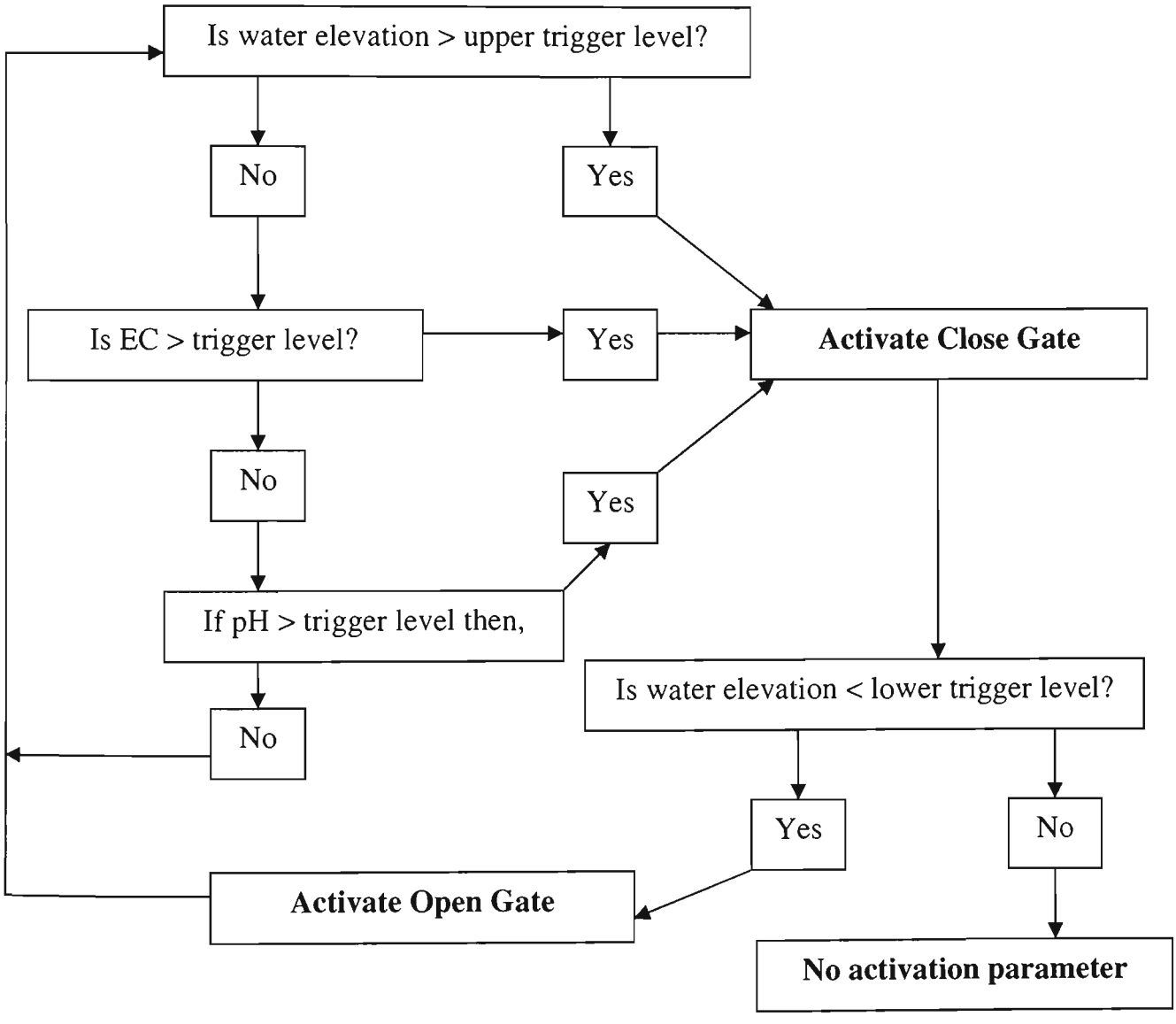

Based on these pseudo-codes, a sequence of program language files were written and incorporated into the main control data logger unit (Campbell CR10X). The complete program files are given in Appendix D.

To increase robustness and enable remote control of the system, various 'intelligent' designs were built-in to the program. First, using a standard 56K modem and appropriate data logger support software (Campbell Scientific PC208W) the user can remotely 'dial-in' to the system. Once connected, the user can view current conditions, download previous data, change trigger levels, and override automatic functions. This ability is particularly important during flooding periods when access to the site may be restricted. Second, the control unit is also equipped with 'dial-out' technologies which were used to increase on-site safety. These safety protocols are designed to alert the user to specific problems concerning 'Smart Gate' operations (i.e., low battery, jammed gate, energy surge, etc.) or preset water quality variables (i.e., low pH, high salinity, high flow) via a SMS text message to their mobile phone. The message will read 'Gate Error Number 1-15' and, based on the gate error number, the user can determine an appropriate plan of action. This function can also be used to alert a floodplain manager to activate an automatic sampler based on real-time drain water parameters.

Photos of the 'Smart Gate' during different phases of construction are shown in Figure 6.19. The 'Smart Gate' was constructed by initially modifying a standard flap gate. First, a 1000 mm x 150 mm slot was cut into the flap using an oxy/acetylene torch, 10 mm holes were then drilled along the gate aperture and a specially designed Kevlar plastic runner assembly was bolted onto the slot. Second, a stainless steel plate was fitted inside the slide assembly and an aluminium drive shaft welded to the plate (Figure 6.19a). To maintain the motor (Hargil Dynamics 0.37 Kw, 9.9 rpm, 24Volt, DC geared motor with single output shaft) above flood levels, a 2.5 m stainless steel brace was bolted to the flap gate and the motor, covered in an aluminium shroud, was secured to the top of the brace. The motor was then joined to the aluminium drive shaft via a

rotating arm (Figure 6.19b) attached to the solid output shaft. Finally, two magnetic reed switches were placed 180^0 perpendicular to each other outside the output shaft, and a magnet was bolted onto the shaft. As the drive shaft rotates, either opening or closing the aperture, the magnet encounters one of the reed switches which indicates the current position.

The electrical components were designed to provide optimal flexibility within a wide range of compatible components. A schematic of the internal components is shown in Figure 6.20. The central processing unit within the control panel is the Campbell Scientific CR10X measurement and control data logger. This unit is programmed to output to the appropriate relay according to external data loggers, which then input through individual converter boxes. The converter boxes allow multiple sensors (up to 10, with 10 parameters per sensor) to be connected via this port without absorbing existing analogue and digital ports on the control unit. Based on this information, the relevant relay circuit is closed and the motor rotates in the correct direction. When the motor reaches its full position, the reed switches send a return pulse to the control unit to stop the motor. Active readings within the control unit determine when/if the GSM modem should be activated and what message to send. The entire unit, including the external data loggers and the motor, is powered by two 12V gel cell batteries connected in series. A BP 20-watt solar panel trickle charges the batteries through a solar regulator. For safety and convenience, all external cables are concealed within flexible conduit buried underground, and the external data loggers are dyna-bolted to the headwalls and encased in slotted PVC sheath.

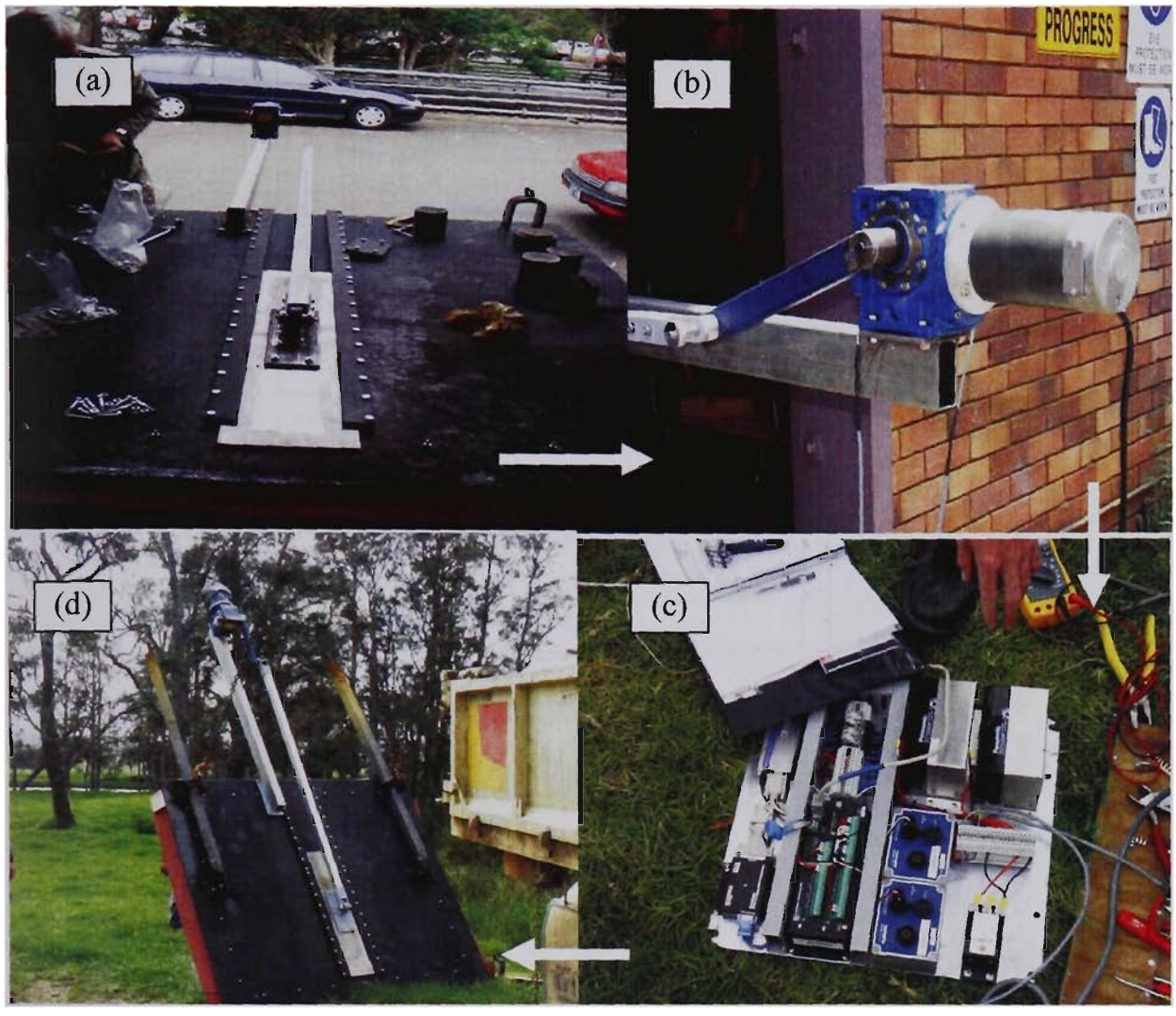

Figure 6.19 Construction phases of 'Smart Gate' including (a) the slide gate mechanism, (b) fitting of the motor, (c) assembly of internal electrical components and (d) installation of completed unit.

The 'Smart Gate' was installed at the study site on December 20th 2001 and has been operating successfully for the remainder of the trial period (>14 months). Installation involved removing one of the two VLGs and reinstalling the original hinging mechanisms. The 'Smart Gate' infrastructure was constructed and tested in the laboratory (including tests for sealant efficiency) and transported to the site as one unit. The electrical components were re-assembled at the site and total installation time was less than 4 hours.

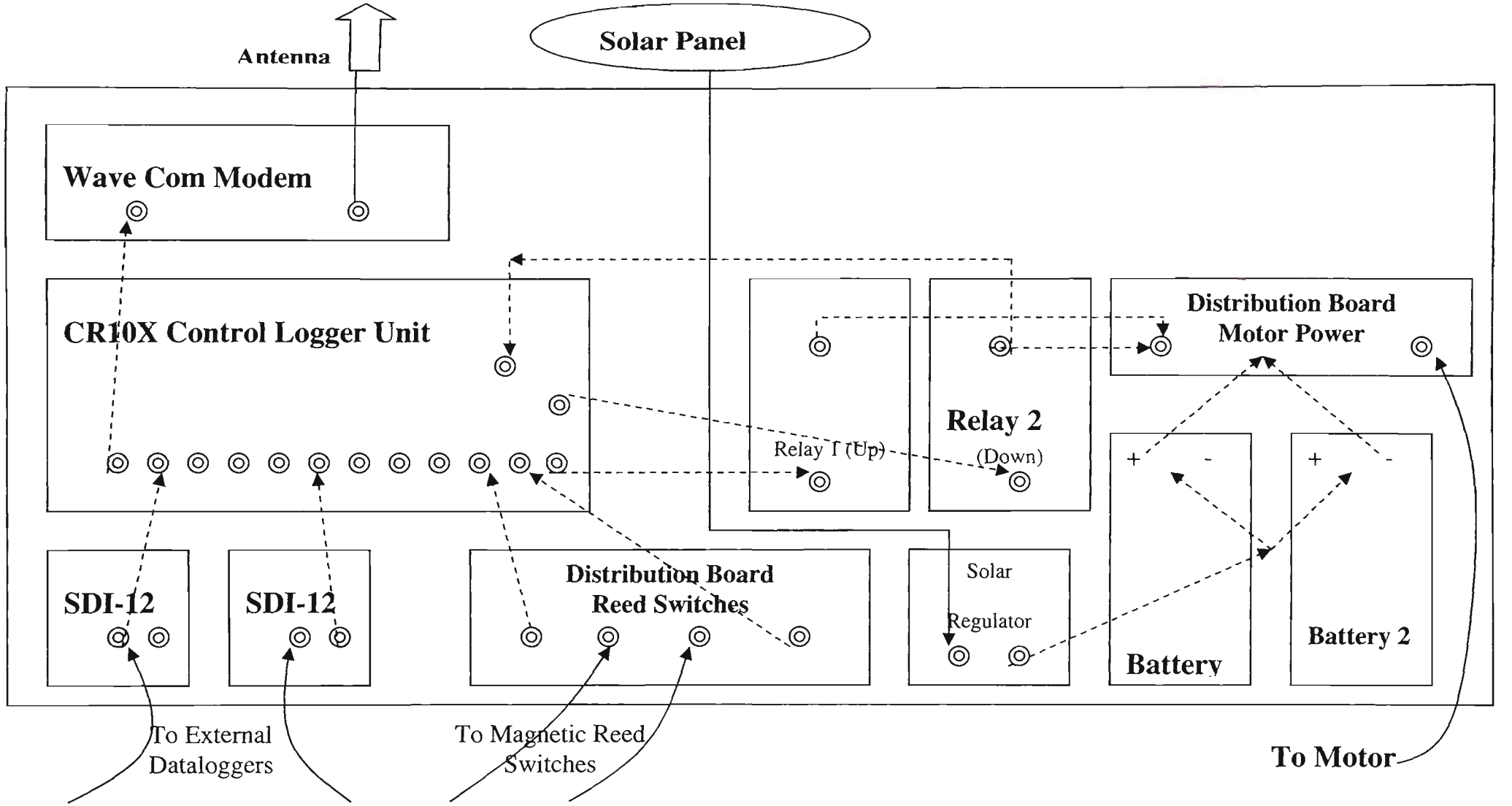

Figure 6.20 Schematic of 'Smart Gate' control panel. External leads are shown with solid lines and internal leads are shown with dashed lines.

With regard to the design objectives, the 'Smart Gate' complies with all the stated aims and is an improvement on manual designs because:

- It permits tidal flushing/buffering in areas where manual gates would cause overtopping;
- It can be controlled remotely allowing access to the gate during floods or from a central network. This is particularly important when multiple gates are installed across a large floodplain;
- It is extremely flexible to operate and can be adjusted to trial several management strategies. The unit may be incorporated into a larger flood mitigation scheme involving pumping stations, or will allow smaller individual units such as flow meters and automatic sampling units to be attached.

In comparison with other buoyancy driven 'automatic' gates driven solely by hydrostatic pressure, the 'Smart Gate's' critical advantage is that it can operate using multiple parameters including pH, electrical conductivity, water temperature, dissolved oxygen, and bi-directional flows to vary water elevation levels upstream or downstream of the floodgate. This is significant because improved water quality, and not water elevation, is the key factor in restoring tidal flushing in ASS terrains.

6.5 Conclusions

The development of an ion association mixing model program calibrated with laboratory tests demonstrated that restoring tidal flushing to the study drain would improve drain water quality. The degree of change is related to the ionic strength of the solution, the concentration of bicarbonates, and the amount of water permitted within the drain. Simultaneously, a sophisticated spatial modelling technique was developed to

show that full tidal flushing could be allowed within the primary study drain without overtopping the levee banks, but unrestricted tidal flushing within the acidic secondary drain will cause flooding of the low-lying areas. These results highlight the potential for improved drain management and accentuate the importance of floodgate design.

The spatial and chemical methodologies presented in this Chapter reduce uncertainty and hazards involved in manipulating floodgates. They also represent a significant improvement on current methods, which are mainly trial and error combined with labour intensive sandbagging techniques. Furthermore, the techniques are easily transferable to additional low-lying sites throughout Australia.

In response to the developed floodgate design criteria, two modified floodgate designs were presented. The winch driven vertical lifting gate was employed to allow unrestricted tidal flushing to the study drain while providing manual lifting control. This design was effective in trialling tidal flushing, yet did not provide incremental upstream water elevation control. Conversely, the environmental controlled 'Smart Gate' system incorporates intelligent technologies and real-time data processing to control tidal flushing based on *in-situ* environmental conditions. Enhanced functionality and remote gate control within the 'Smart Gate' optimises tidal buffering based on multiple water quality parameters.

Following the installation of the modified floodgates, significant changes in surface water quality were recorded. The spatial and temporal fluctuations of drain and ground water quality in comparison to pre-modification results are presented in Chapter 7.

Chapter 7.0 Surface Water Quality and Hydrodynamics after Floodgate Modifications

7.1 Introduction

Based on the techniques developed in Chapter 6, floodgate modifications to restore tidal flushing and investigate the influence of tidal buffering on drain water conditions were undertaken on October 31st 2000 (Day 305). Baseline research presented in Chapter 5, suggested that restoring tidal flushing would impact the adjacent groundwater table, the hydrodynamics of the drain, and the surface water quality. The aim of this chapter is to examine the extent of these changes and their relevance to the overall management strategy.

This chapter is broken into three sections. The first section investigates the impact of floodgate modifications and tidal buffering on drain water quality by comparing the biogeochemical indicators recorded after Day 305 with long-term measurements taken before floodgate modifications. From these findings, it is evident that drain water quality significantly improved following floodgate modifications.

In the second section of this chapter, the hydrodynamic conditions of the drain following floodgate modifications are examined. Particular reference is given to the acid reservoir effect, the fluctuations in the long-term drain water elevation, the optimal conditions for monosulphide formation and the mass export of acid products. The extensive data collected demonstrates that modifying floodgates to permit tidal flushing reduces the problems associated with aluminium and iron flocculation, and improves dissolved oxygen levels.

In the final section of this Chapter, the influence of altered drain hydrodynamics is considered with regards to changes in the groundwater regime. Specifically, the surface elevation of the phreatic zone is examined to determine whether increased drain water elevations decreased groundwater drawdown. In addition, groundwater acidity measurements are given to ascertain the tidal buffering intrusion zone.

7.2 Surface water quality after floodgate modifications

The primary aim of this study was to determine the impact of restoring tidal flushing/buffering on drain water quality via redesigned floodgates. As shown in Chapter 5, before floodgate modifications drain water was predominately acidic with pH levels consistently below 4.5, and soluble aluminium and iron concentrations more than 100 times in excess of ANZECC (1992) guidelines. These conditions were particularly evident during extended dry periods when low drain water elevations enhanced groundwater seepage and one-way floodgates restricted tidal buffering.

This section examines the extent of water quality improvements after modifications during both wet and dry periods. In contrast to Chapter 5, the temporal (552 Days) and spatial data are simultaneously addressed to obtain a comprehensive understanding of the changes across the drain in response to fluctuating concentrations of buffering agents. To facilitate a concise discussion, the data presented in this section is limited to sampling locations immediately upstream and downstream of the floodgate and from within the control drains. Remaining water quality information can be found in Appendix B.

7.2.1 Drain water quality: pre-modification versus post-modification

The restoration of tidal flushing within the study drain increased drain water pH. As shown in Table 7.1, drain water pH was above 6.0 and remained at this level for the majority of the post-modification period. Median pH at all upstream sites was 6.04 and fluctuated between 4.19-7.36. Excluding the site 45 m upstream, which received acidic discharges from the floodgated secondary drain, median pH at all upstream sites was 6.43. In comparison with pre-modification data (median pH 4.32), this represents a decrease in H^+ ions by more then two orders of magnitude.

Table 7.1 Average surface water quality indicators before (pre) and after (post) floodgate modifications.

	Total	**1m u/s**	**15m u/s**	**30m u/s**	**45m u/s**	**60m u/s**	**250 u/s**	**CT**	**CF**	**Side Drain**	**Exc. 45m**
pH (pre)	4.32	4.41	4.44	4.35	3.01	4.72	6.82	6.78	3.72	N/a	N/a
pH (post)	6.04	6.29	6.21	6.20	4.25	6.24	6.69	6.45	4.17	3.03	6.43
Al^{3+} (pre)	11.33	16.64	15.43	13.79	13.03	4.15	3.64	2.46	2.15	N/a	8.94
Al^{3+} (post)	4.38	2.80	1.96	1.69	17.94	1.21	0.70	4.02	6.79	42.46	1.39
% change	+62	+83	+87	+88	-27	+71	+81	-39	-69		+85
Fe^{2+} (pre)	23.07	31.89	29.41	27.17	26.08	14.47	9.38	1.117	0.876	N/a	22.46
Fe^{2+} (post)	10.33	5.75	3.85	3.74	42.95	3.46	2.23	6.08	7.14	86.23	3.17
% change	+56	+82	+87	+86	-40	+77	+76	-82	-88		+86

Note all relevant concentrations are in mg L^{-1}, CT = control tidal drain, CF = control floodgated drain, and Exc. 45m = average concentrations excluding the 45 m upstream site.

Long-term average dissolved monomeric aluminium concentrations (Figure 7.1) decreased in response to tidal buffering. Soluble Al^{3+} concentrations averaged 0.163 mmol L^{-1} throughout the study drain and 0.105 mmol L^{-1} when the 45 m upstream site was excluded. Concentrations ranged from 0.005 mmol L^{-1} (250 m upstream, Days 763 and 857) to 3.16 mmol L^{-1} (45 m upstream, Day 563), whereas before tidal buffering dissolved inorganic monomeric aluminium averaged 0.62 mmol L^{-1}. This represents a 26% decrease in soluble aluminium and, while still in excess of ANZECC guidelines, when viewed in conjunction with pH readings near 6.5 does not represent as significant a threat to aquatic life.

As forecasted by ion association modelling in Chapter 6, total dissolved iron concentrations decreased after floodgate modifications. Average concentrations fell 33% from 0.62 mmol L^{-1} to 0.163 mmol L^{-1}. Spatially, soluble iron decreased at every sampling location except 45 m upstream of the floodgate, indicating strong buffering potential throughout the drain. Soluble iron levels also fluctuated within a smaller range, with concentrations varying between 0.008 mmol L^{-1} on Day 703 at 1 m upstream, to 2.36 mmol L^{-1} on Day 824 at 45 m upstream (Figure 7.1). However, when the 45 m upstream site is excluded the maximum concentration is significantly less (0.522 mmol L^{-1}, Day 521 at 1 m upstream), which suggests that iron discharged from the secondary side drain was buffered out of the system either in the form of oxhydroxides or monosulphides.

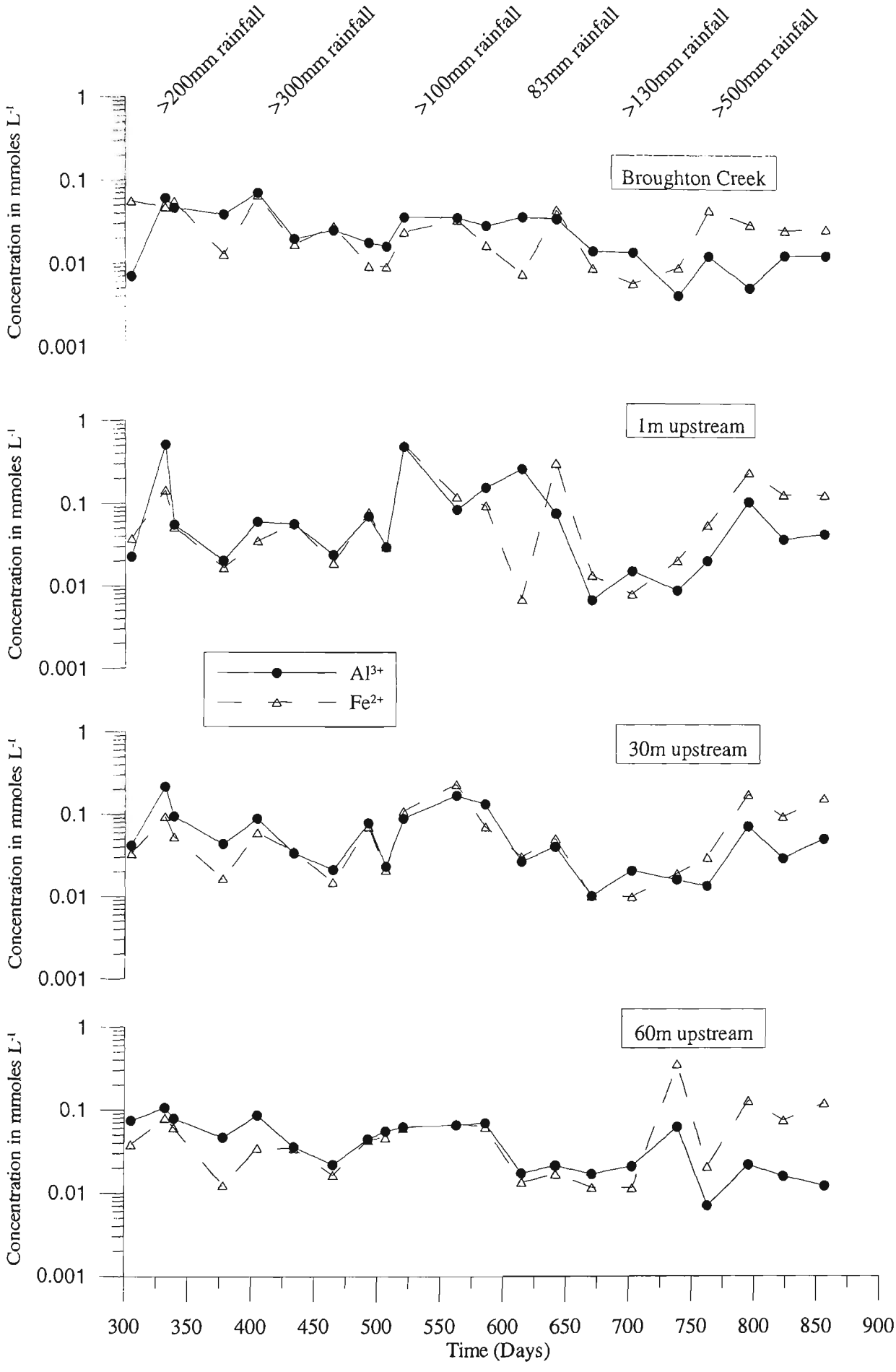

Figure 7.1 Soluble monomeric aluminium and total iron concentrations after floodgate modifications with rainfall.

It is important to note that acid concentrations 45 m upstream of the floodgate remained elevated following floodgate modifications, while upstream and downstream concentrations decreased. These conditions were attributed to the secondary side drain, which discharged into the primary drain at this location. As detailed in Chapter 6, this singular 600 mm circular floodgate was not modified following extensive predictive flood modelling. Throughout the study, however, water quality upstream of this floodgate was extremely poor (median pH = 3.03, average [Al] and [Fe]= 1.574 mmol L^{-1} and 1.544 mmol L^{-1}, respectively). Though this illustrates the limitations of tidal buffering, the improved readings upstream and downstream of the sampling site shows that within a relatively short distance (15 m), sufficient neutralising capacity existed to buffer the acid inputs.

Because of the decrease in inorganic monomeric aluminium, total dissolved iron, and hydrogen ions, total acidity decreased more than one order of magnitude following floodgate modifications. Similar to pre-modification results, and as shown in Figure 7.2, total acidity was still primarily composed of aluminium and iron, with hydrogen contributing 1.2% on average. Aluminium and iron contributed to total acidity in near equal proportion of 49% and 50%, respectively. The highest total acidity readings were taken just upstream of the floodgate and were a result of the mass transport of acid products from previously oxidised sites. Nonetheless, considering that all other factors remained unchanged, the decrease in total acidity was directly attributed to tidal buffering.

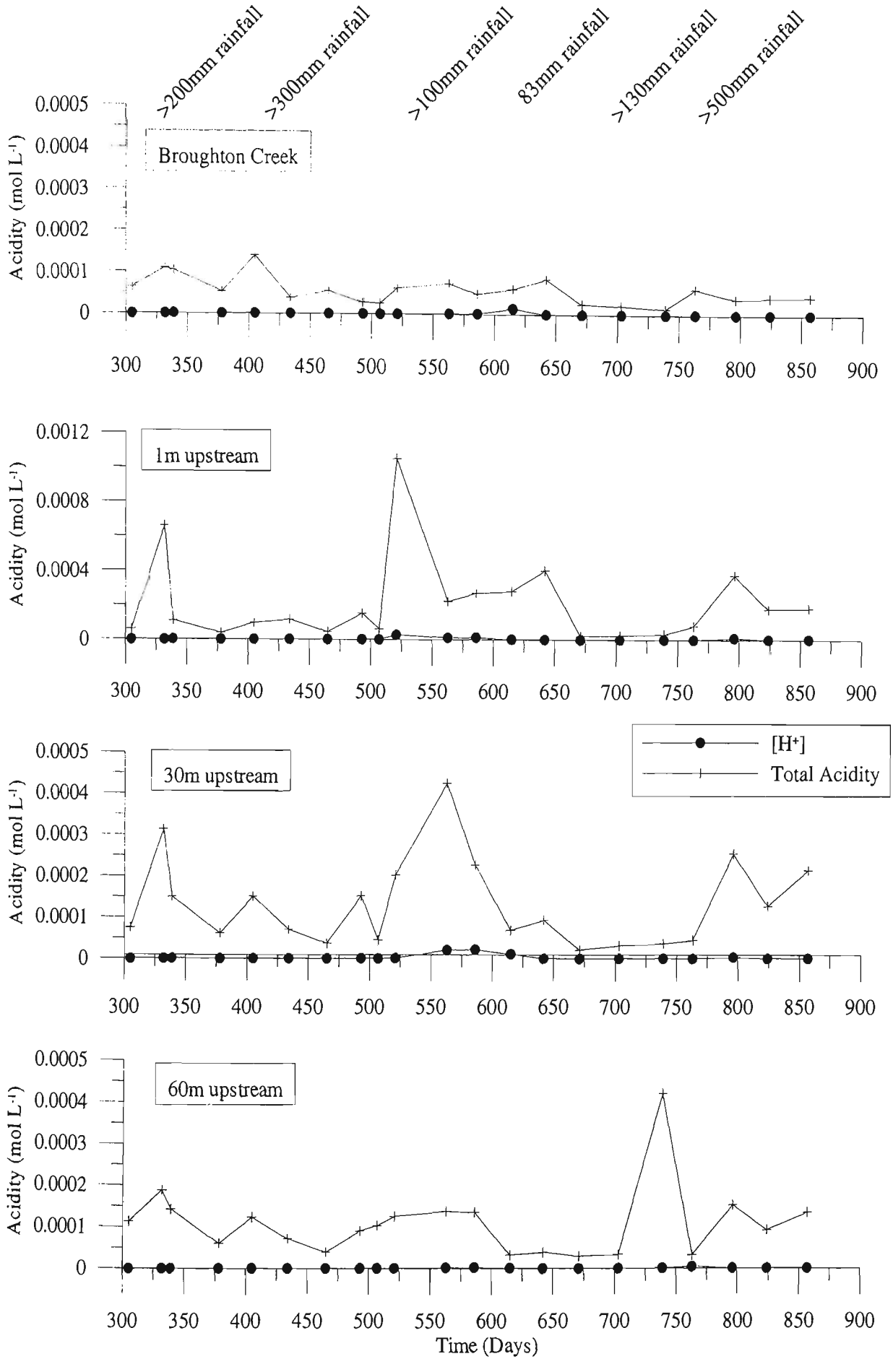

Figure 7.2 Total acidity after floodgate modifications with rainfall.

One of the basic assumptions regarding the post-modification water quality results was that acidic inputs continued to discharge into the study drain after floodgate modifications. Under this premise, the key factor controlling drain water quality was tidal buffering through modified floodgates. To test this assumption, water quality was monitored at both control drains (see Chapter 5 for reference) and in the secondary side drain 45 m upstream of the modified floodgate. As shown in Table 7.1, total acidity within the control, floodgated drain increased significantly during the post modification period. This is important to note because 3 water-retaining structures (v-notch weirs) had been previously installed in this drain to reduce groundwater seepage. Furthermore, total acidity also increased in the non-floodgated drain. These results, as well as the continual discharge of acidic water (median pH 3.03) through the secondary side drain, indicate that the post-modification period was more acidic than the pre-modification period. Moreover, this suggests that improvements within the study drain were solely due to the installation of modified floodgates and the influence of tidal buffering.

7.2.2 Drain water quality: temporal variations

While long-term findings showed significant improvements in water quality, daily measurements fluctuated with changing climatic conditions. Similar to the pre-modification results, large rainfalls (i) flushed neutralising agents from the estuary, (ii) recharged the groundwater table, and (iii) enhanced groundwater seepage. However, in contrast to earlier results where dry periods were typified by extremely acidic conditions, dry periods following floodgate modifications were characterised by neutral pH readings and decreased total acidity. These conditions were attributed to the restoration of tidal flushing within the drain and increased tidal buffering.

The response of drain water quality in regards to rainfall events is shown in Figure 7.3. In this figure, hourly drain water pH and electrical conductivity (EC) measurements taken from datalogger G (1m upstream) are given over the entire post-modification period. Significant rainfall events correspond to major decreases in EC, and, to a lesser extent, declines in pH. As dry conditions returned, EC readings increased from less than 5.0 mS cm^{-1} to greater than 15.0 mS cm^{-1}, which coincides with an increase in pH levels above 6.0. The cyclical nature of these fluctuations for the entire post-modification period is described below.

The installation of modified floodgates triggered immediate improvements in drain water quality. During Days 306-320, pH was consistently above 6.0 and aluminium and iron concentrations decreased. Persistent dry conditions increased bicarbonate concentrations (Figure 7.4) and converted highly ionic sulphuric acid into less ionic carbonic acid. As depicted in Figure 7.5, the change in drain water pH was abrupt. Whereas one week before modifications drain water pH ranged between 3.71-6.3, one week after modifications pH fluctuated between 5.07-7.2. These readings were typical of dry conditions after floodgate modifications, and indicated a significant improvement from pre-modification results.

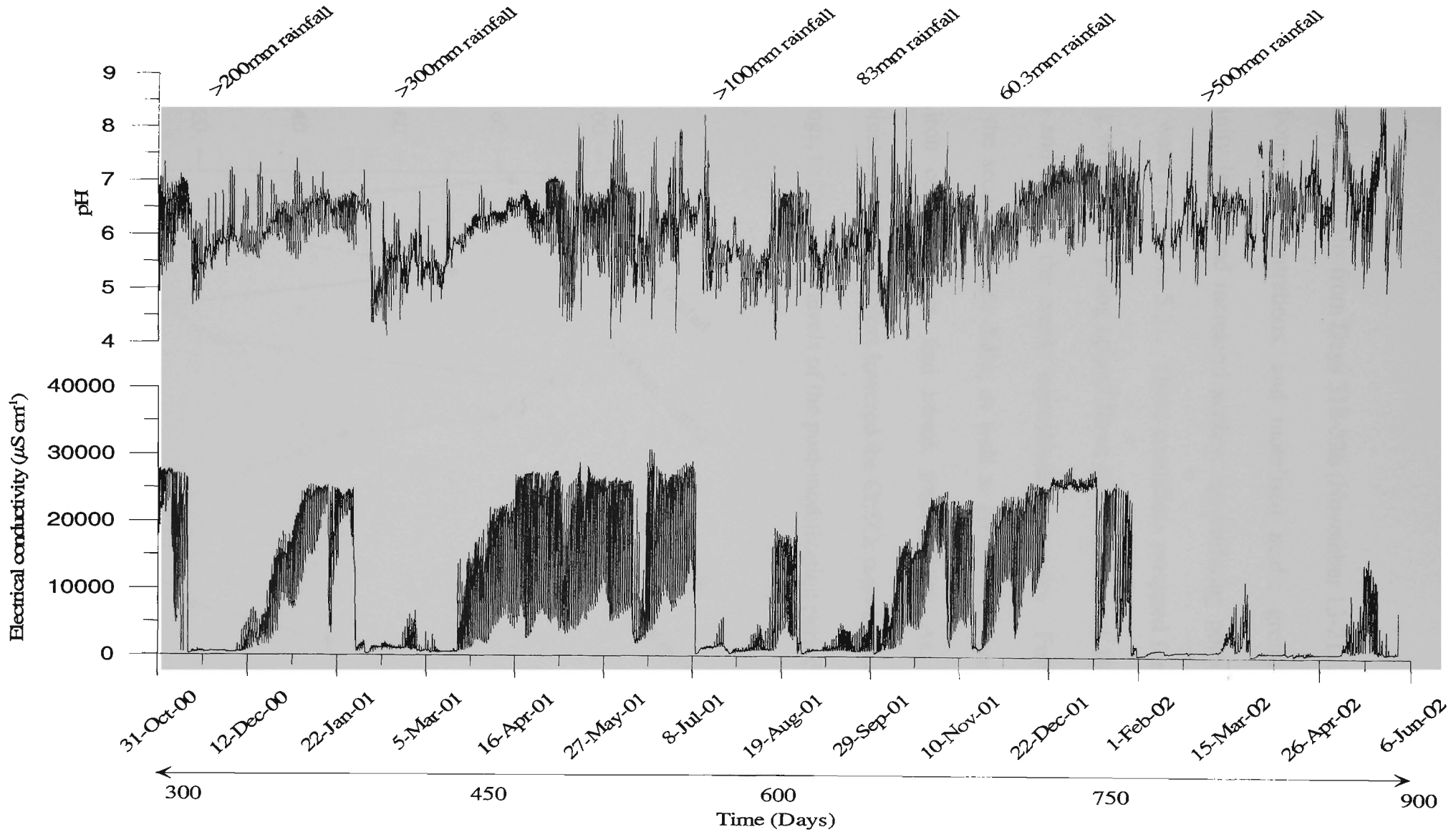

Figure 7.3 Continuous data logger pH and electrical conductivity readings taken 1 m upstream of the modified floodgate with rainfall.

A series of rainfalls from Days 318-326 (November 13-21, 2000) decreased salinity and bicarbonate concentrations, and mobilised acidic groundwater. Due to the low alkalinity levels and increased acidity, the buffering potential decreased and average drain water pH fell to 5.31. These conditions persisted for approximately three weeks during which time strong upland flows (Na: Cl ratio = 1.19, Figure 7.6) restricted tidal reach and limited the creeks neutralisation capacity. Furthermore, acidic discharges from the secondary side drain, as well as groundwater seepage, increased aluminium and iron concentrations, and hence, total acidity. As shown in Figure 7.7, the combination of these factors lowered the $Cl:SO_4$ ratio from characteristically non-acidic readings, to the lowest levels of the post-modification period (1.04, 1 m upstream).

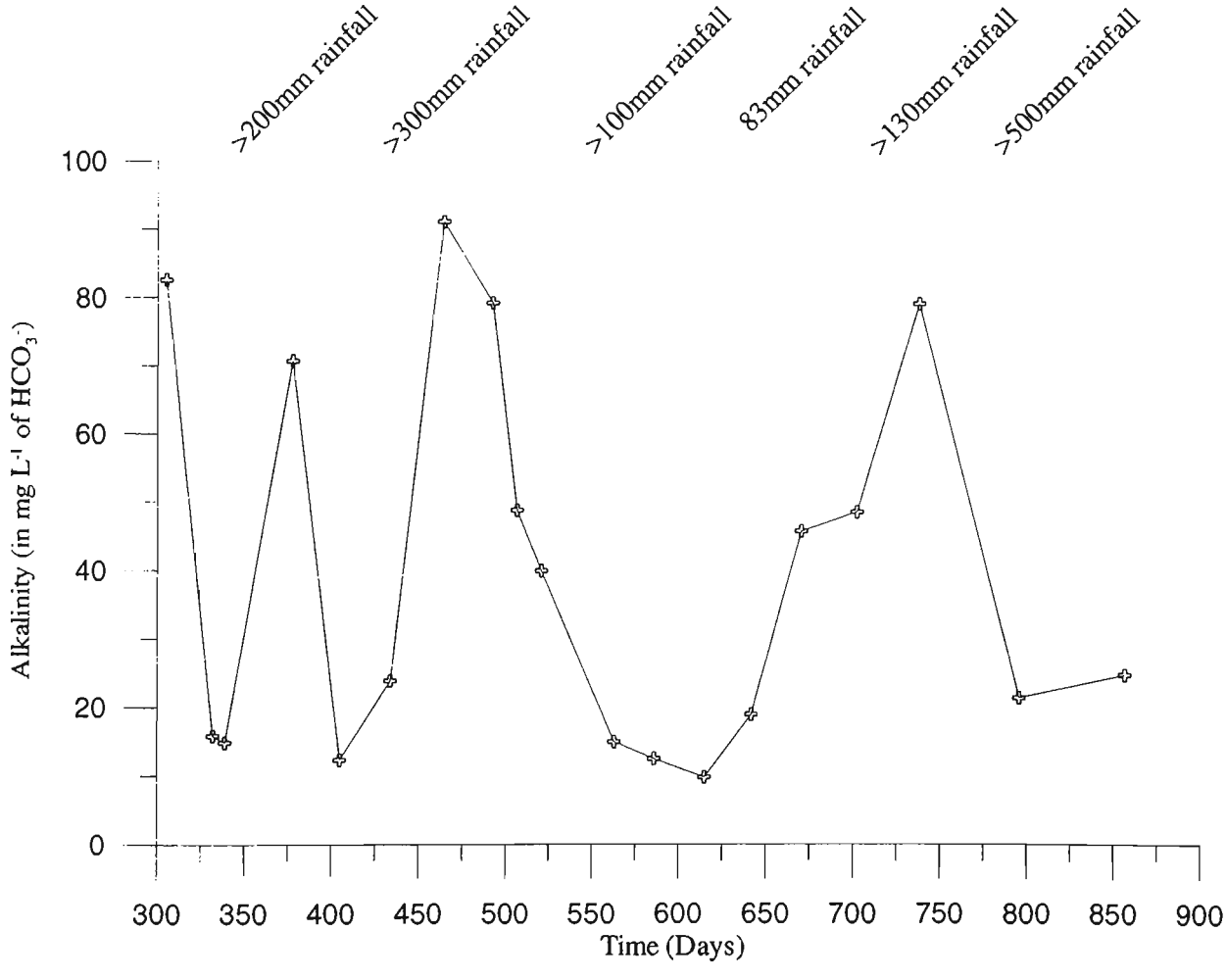

Figure 7.4 Bicarbonate concentrations within the drain after floodgate modifications with rainfall.

Though the wet period increased drain water acidity, the duration and magnitude of these periods was significantly less than similar pre-modification results. By comparison, a smaller rainfall (69 mm versus 208 mm) during Days 182-186 resulted in an average drain water pH of 4.47, which persisted for eleven weeks. The duration of wet periods was reduced because with the reestablishment of the tidal regime, sufficient alkalinity concentrations were available for buffering. Additionally, the minimum alkalinity level necessary to raise drain water pH above 6.0 was low and significant improvements were recorded with only slightly brackish estuarine water (5.0 mS cm^{-1}). Nonetheless, the decrease in water quality during wet periods shows the susceptibility of tidal buffering to extended periods of freshwater flushing. Additional management techniques to combat the reduction in neutralisation capacity during wet periods are discussed at the end of this chapter.

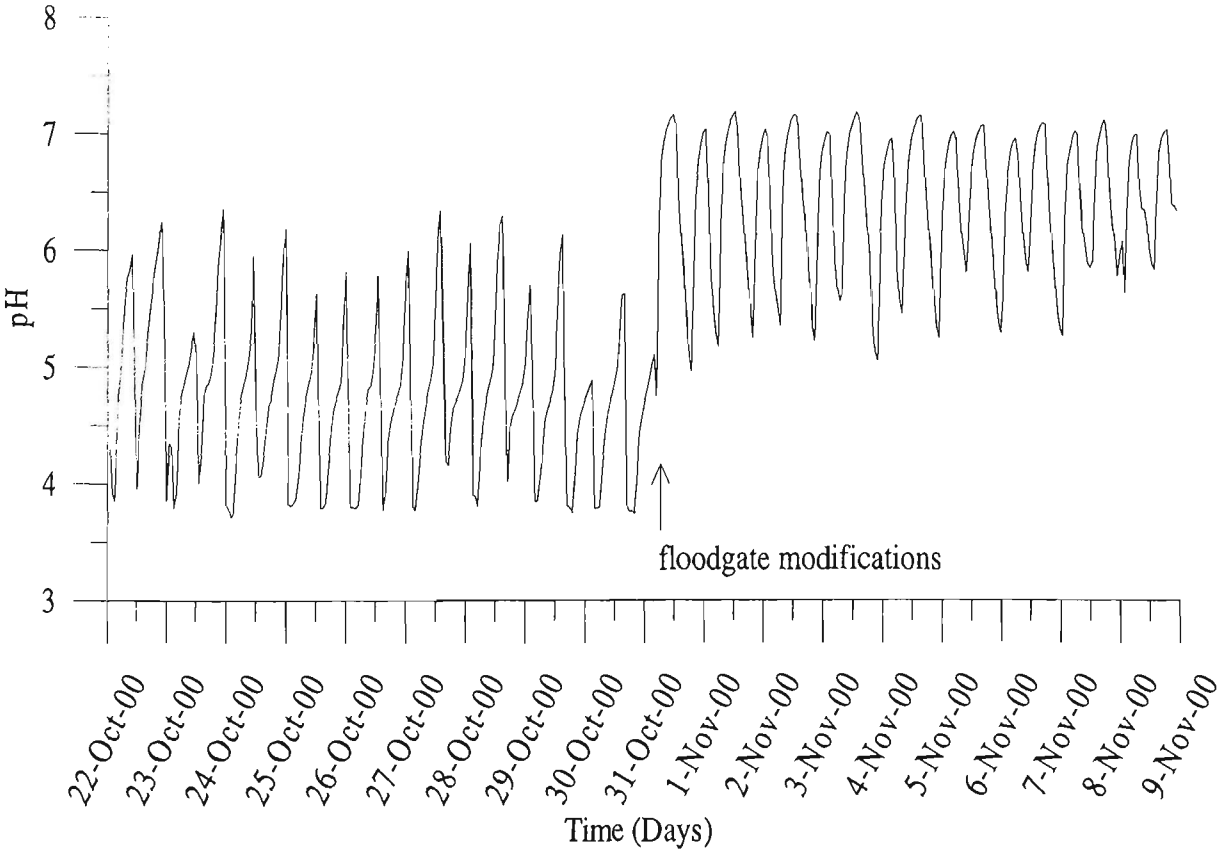

Figure 7.5 In situ drain water pH readings taken immediately before and after floodgate modifications (Days 296-314).

With the return of dry conditions (Na:Cl ratio < 0.9, Figure 7.6), surface water alkalinity increased due to the advection/dispersion of buffering agents within the estuary. During this ten-week period (Days 326-396), bicarbonate concentrations increased from 14.88 mg L^{-1} to 70.55 mg L^{-1} (Figure 7.4). This increase, as well as the reduced acid export, sustained drain water pH above 6.0 and decreased aluminium, iron and total acidity measurements. As bicarbonate readings peaked, the daily fluctuations in pH decreased from > 2.0 units to <1.0, and was in line with ANZECC (1992) guidelines. Moreover, in contrast to acidic readings before floodgate modifications, the overall decrease in total acidity during this dry period suggests that tidal buffering effectively combats acid sulphate soil drainage at the study site.

Climatic variations between wet and dry periods continued throughout the remainder of the post-modification trial; with over 300 mm of rainfall in 22 days, wet conditions returned on Day 396. Similar to previous wet, post-modification conditions, drain water quality was affected by (i) decreased bicarbonate concentrations, (ii) an elevated acidic groundwater table, and (iii) the secondary side drain that discharged acidic water during low tide. In addition, the sodium:chloride ratio (Figure 7.6) increased above 1.0, thus depicting freshwater dominance. Interestingly, during this period the chloride:sulphate ratio was above 10.0 at most sites, which was attributed to chloride salts leaching from the soil matrix following the 10 week period of high salinity. The impact of saline ingress on the soil matrix is further discussed in Chapter 8 and 9.

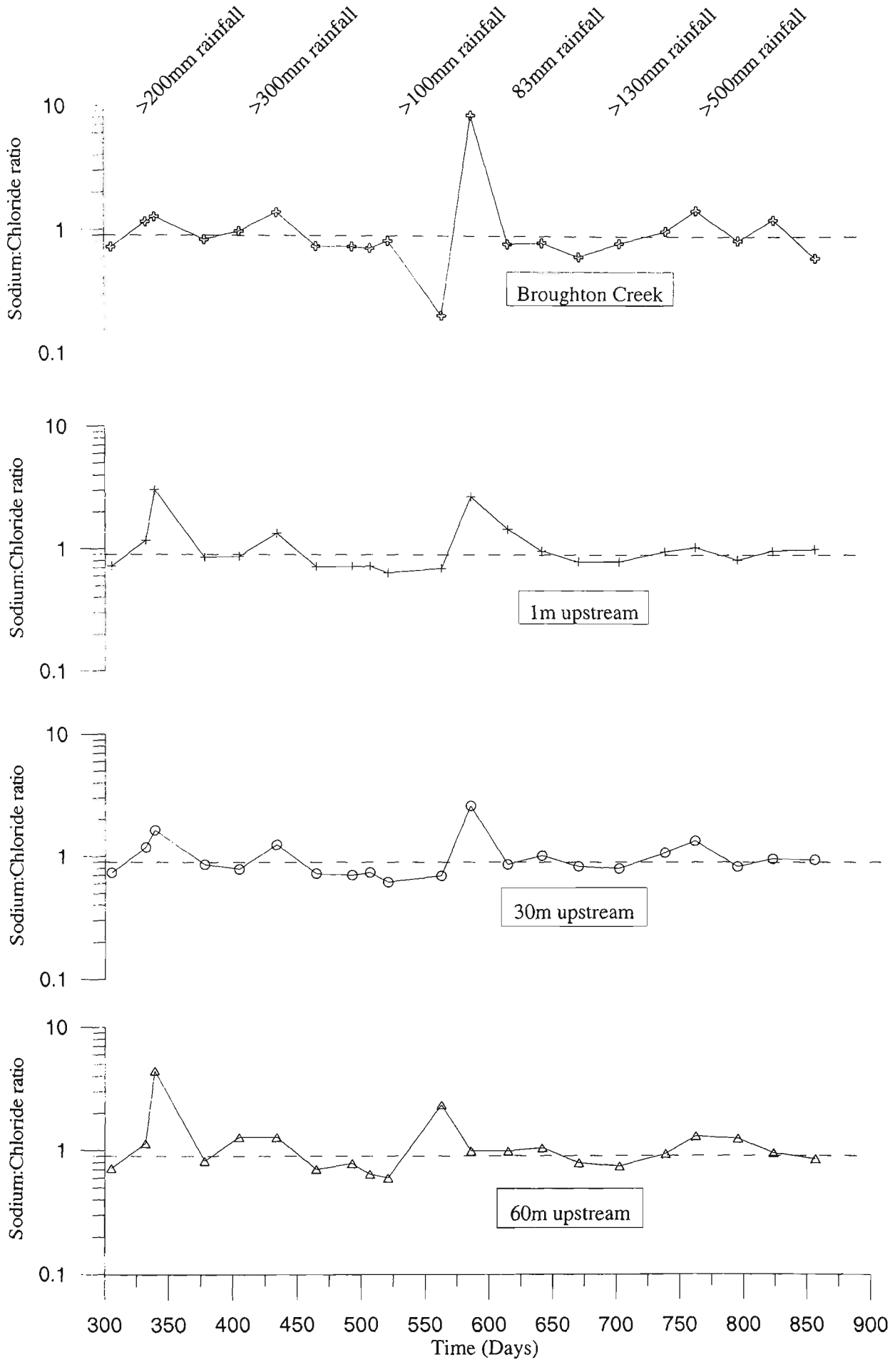

Figure 7.6 Sodium:chloride ratios and rainfall with broken line indicating freshwater versus saline water dominance.

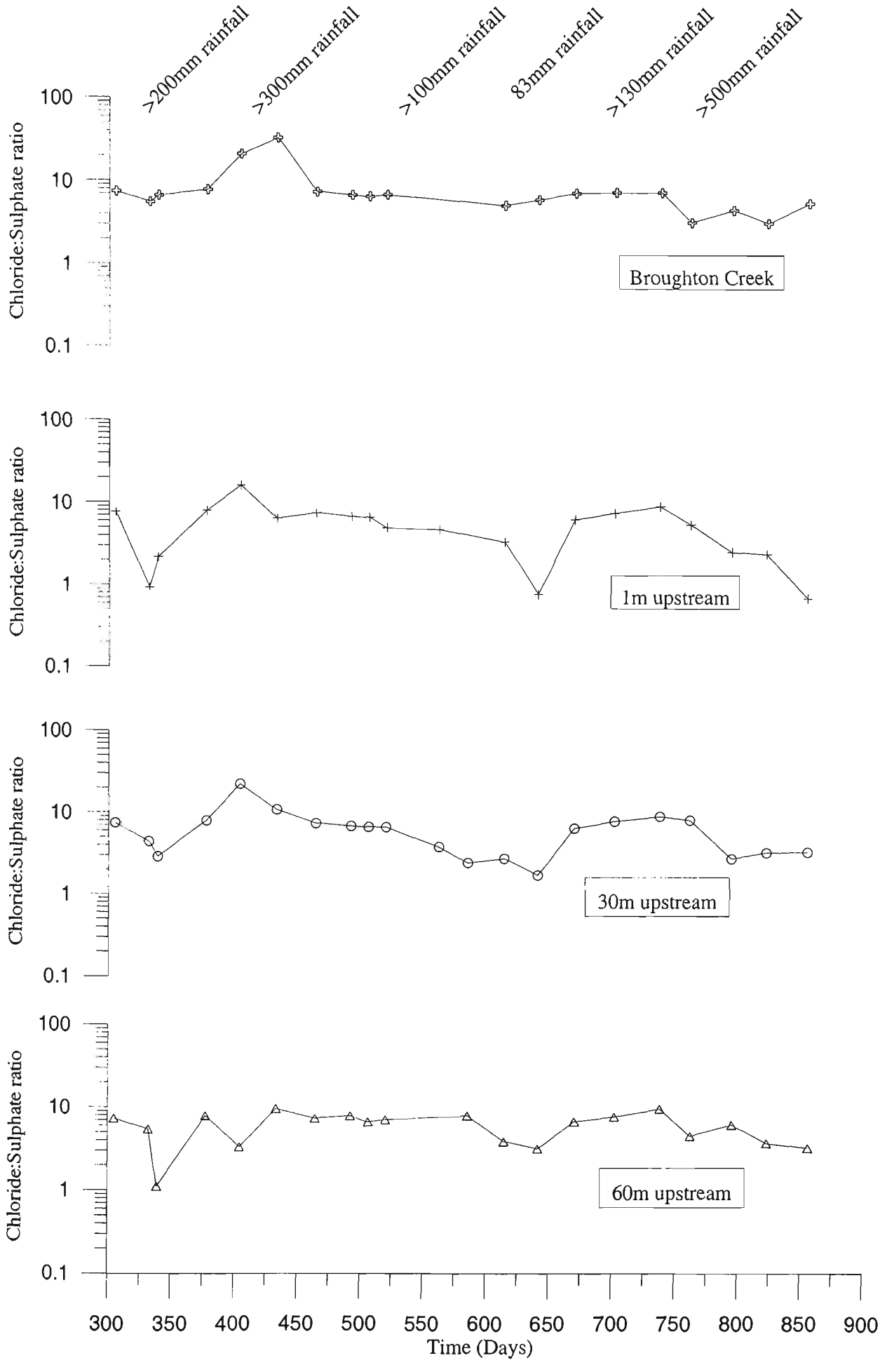

Figure 7.7 Chloride:sulphate ratio of surface water with rainfall.

Though interspersed with several small rainfalls (<50 mm), which briefly increased acidic metal concentrations, the drying conditions from Days 437-555 were typical of water quality fluctuations after modifications. These changes corresponded with the primary objective of floodgate modifications; improvements to water quality during dry periods. Median pH during this period was 6.31 and the average chloride: sulphate ratio was 6.6, which signified that sulphides were not being oxidised and that there was no indication of acid sulphate soils drainage (Mulvey, 1993). Total acidity, including soluble aluminium and iron, remained at this lowest level for the entire study period, with bicarbonate levels peaking at 91.19 mg L^{-1}. These findings infer that during dry periods, highly ionic creek water has the buffering potential to neutralise the majority of acidic constituents to the degree predicted by ion-association models in Chapter 6.

From Day 555 until the end of the study trial, drain water quality was characterised by two wet periods and one prolonged dry period. These periods were typical of wet and dry conditions after floodgate modifications with dry periods characterised by high alkalinity, neutral pH and low total acidity readings, and wet periods depicted by decreased pH and low alkalinity concentrations. Of particular interests during this 302-day period, were two high total acidity events immediately following large rainfalls on Days 556-60 (112 mm rainfall) and Days 747-69 (453 mm). These periods highlight the lack of neutralising capacity available after large rainfall events and the need for additional combative measures. However, considering that pH levels were quickly re-established at near neutral values, the overall affect of total acidity, and particularly aluminium, on marine life was reduced when compared with pre-modification findings.

The concentration of basic cations in drain water was determined by the tidal regime throughout the post-modification period. As shown in Figure 7.8, potassium and magnesium followed the same trend as electrical conductivity. This conservative behaviour indicates that the concentration of these cations was primarily due to physical mixing of tidal waters (seawater concentrations of 380 mg L^{-1}, 400 mg L^{-1} and 1300 mg L^{-1}, for K, Ca and Mg, respectively), and not due to additional inputs such as the breakdown of mature clays under acidic conditions. In contrast, correlations between salinity, soluble Al^{3+} and total dissolved Fe illustrate non-conservative removal as salinity increased. The decline in soluble aluminium was attributed to an increase in buffering concentrations and, as described in Chapter 6, the complexing of aluminium with OH^- ions. Similarly, dissolved iron was primarily removed from solution as iron monosulphides and oxides.

7.3 Hydraulic implications of floodgate modifications

In Chapter 5, one-way tidal floodgates were shown to (i) create acid reservoirs, (ii) maintain stagnant water conditions, and (iii) sustain drain water elevations at the low tide mark. Based on this research, it was hypothesised that restoration of bi-directional tidal flows within the study drain would improve drain hydraulics. To facilitate a concise discussion on this subject, the data presented here is restricted to sampling locations immediately upstream and downstream of the floodgate. Data from other sampling locations is given in Appendix B.

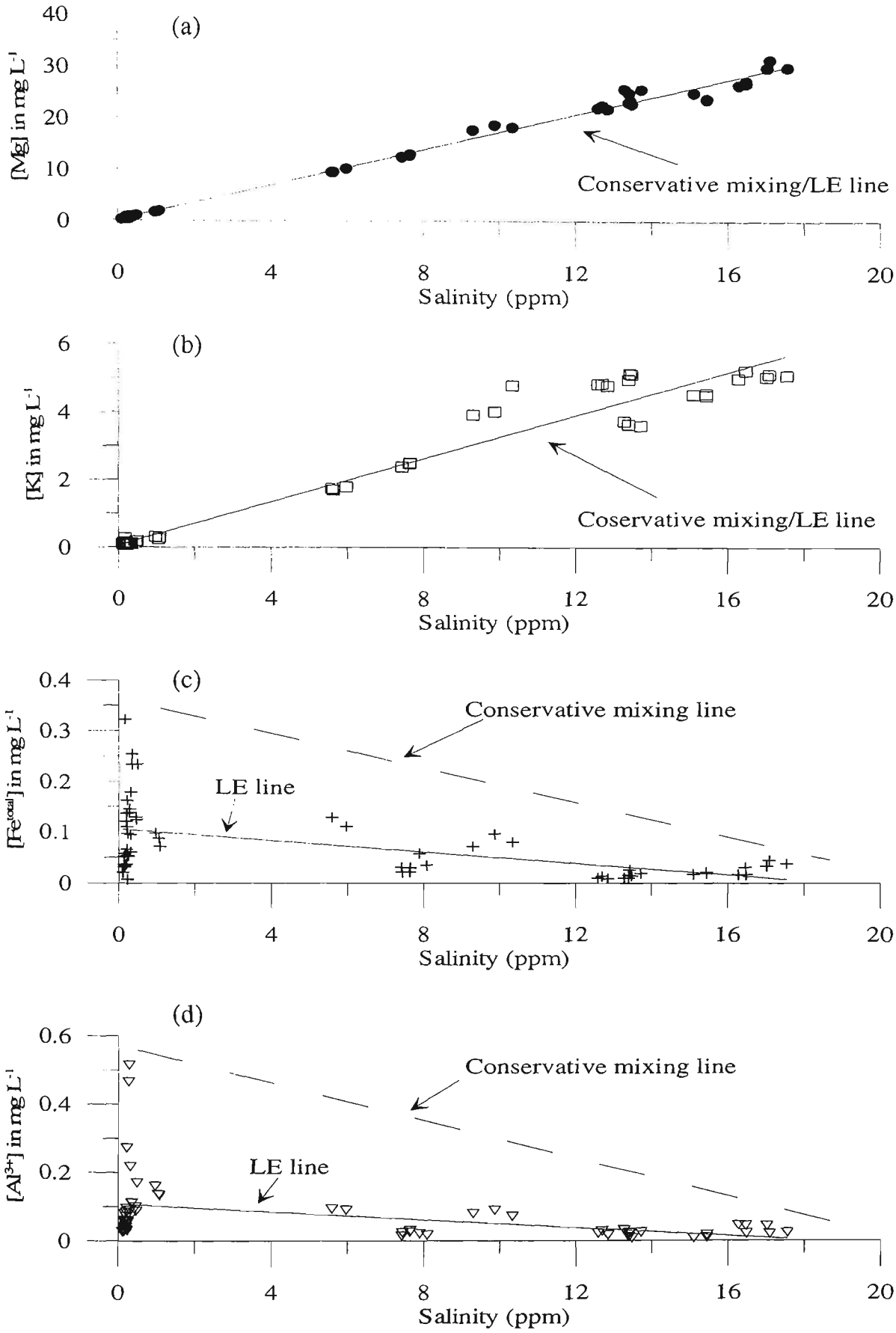

Figure 7.8 Dissolved (a) magnesium, (b) potassium, (c) total iron and (d) monomeric aluminium plotted against salinity, illustrating conservative (a and b) and non-conservative behaviour. The conservative mixing line represents physical mixing with seawater. Linear extrapolation (LE) depicts correlation of data with salinity. When the LE line is below the conservative mixing line (c and d), ion removal from solution is due to additional factors.

7.3.1 Impact of modified floodgates on acid reservoir

As expected, the installation of modified floodgates decreased the disparity between upstream and downstream surface water conditions. A typical cross section of post-modification results (Figure 7.9) shows that pH levels upstream and downstream of the floodgate varied between 0.05 to 0.26 pH units. As ANZECC (1992) guidelines state that water discharging into an estuarine system must be within 0.2 pH units, these readings are a significant improvement over pre-modification results.

The analogous aluminium and iron concentrations upstream and downstream of the modified floodgates decreased metal flocculation. As stated earlier, overall metal concentrations were more than an order of magnitude less during highly ionic periods. Typically, concentrations of aluminium upstream and downstream of the modified floodgate varied in a small range between 0.001-0.003 mmol L^{-1} (Figure 7.10). Considering that pH was predominately above 6.5, both the occurrence of aluminium flocculation and its impact on the aquatic environment was reduced.

Iron flocculation also decreased with upstream and downstream levels fluctuating between 0.01 to 0.0007 mmol L^{-1} (Figure 7.10). This reduction in total soluble iron was due to the decreased solubility of ferrous versus ferric ions under increased Eh and pH conditions at the soil/drain interface. Intermittent spikes in soluble iron recorded upstream of the floodgate during the post-modification period were associated with the mobilisation of iron monosulphides. This was likely because of an increase in surface water velocity, which caused entrainment of the porous flocculant. Nonetheless, whilst before floodgate modifications large plumes of iron flocculant were often seen emanating from the study drain, no acidic plumes were recorded after the modifications.

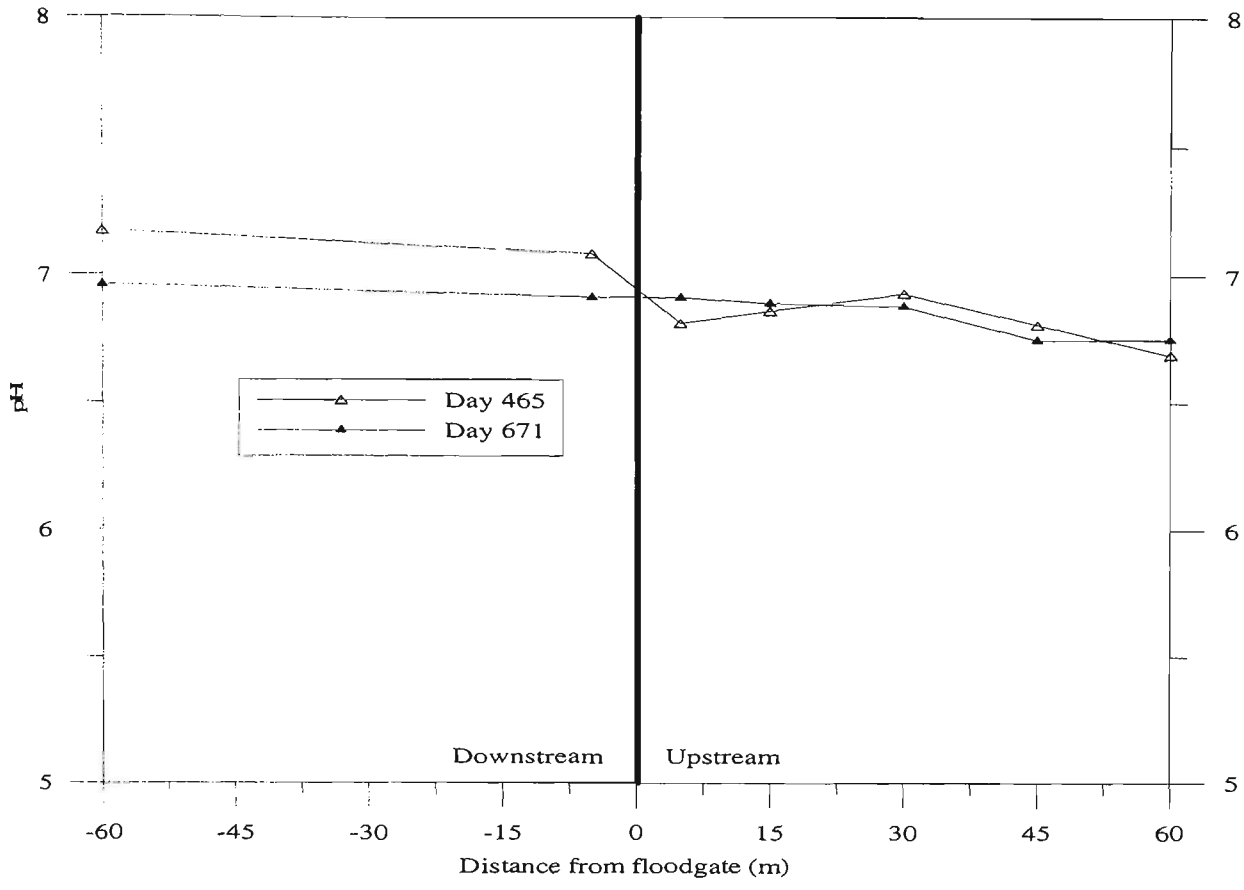

Figure 7.9 pH readings upstream and downstream of the floodgate after floodgate modifications.

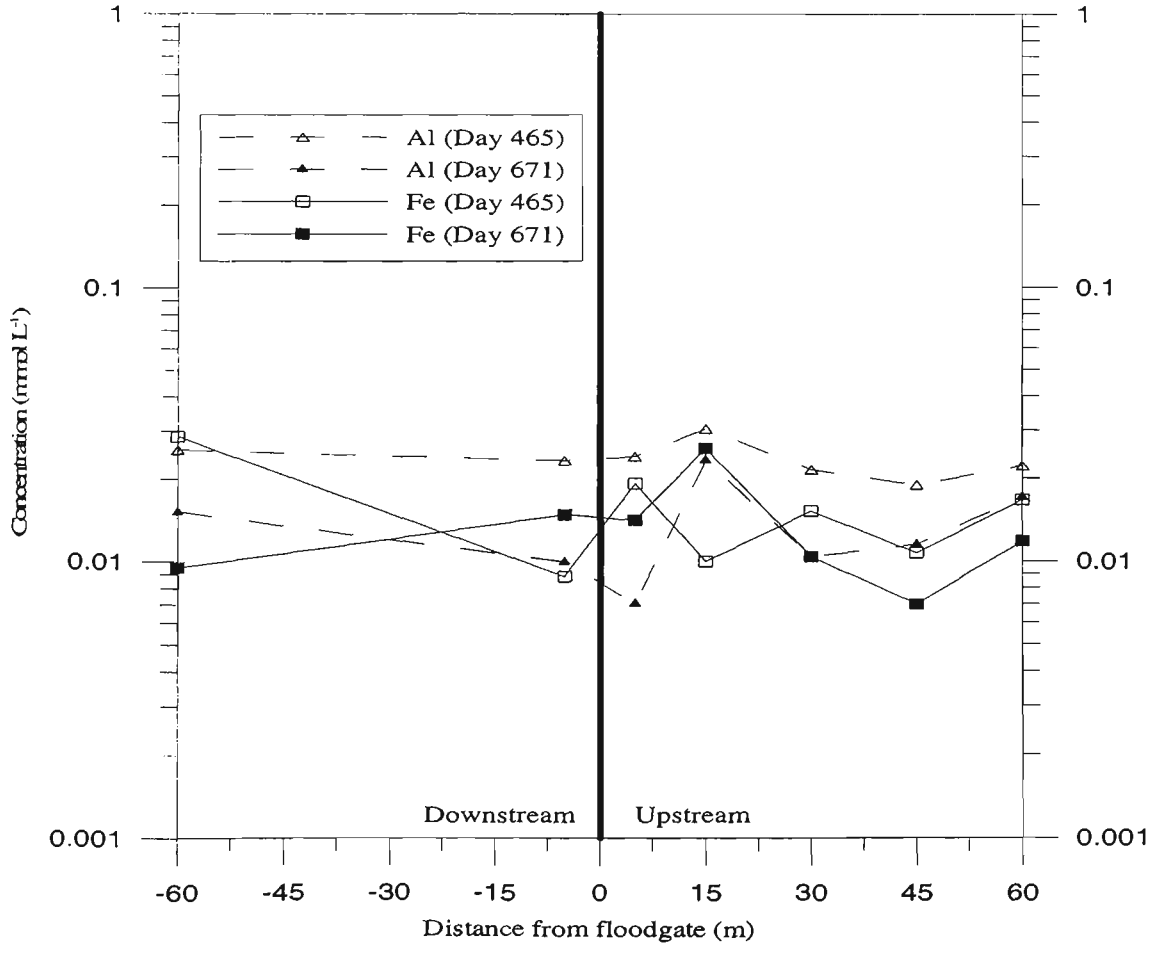

Figure 7.10 Soluble aluminium and iron concentrations upstream and downstream of the modified floodgate.

7.3.2 Impact of tidal restoration on dissolved oxygen conditions

Restoration of tidal flushing to the drainage system increased dissolved oxygen readings. Before modifications, one-way floodgates limited upstream water movement, and, in combination with strong ferrous-ferric oxidation, excessive aquatic weed growth and organic decomposition, dissolved oxygen levels averaged 3.4 ppm. However, after the modifications, dissolved oxygen averaged 7.01 ppm, and strong rainfall events triggered short-term readings below 3.0 ppm. As detailed in Figure 7.11, dissolved oxygen concentrations were inversely related to temperature fluctuations, with higher temperatures corresponding to lower dissolved oxygen readings. This was anticipated due to the temperature dependent metabolic consumption of oxygen by microbial organisms. Interestingly, while a strong inverse relationship commonly exists between chloride concentrations and dissolved oxygen levels, no consistent relationship was found at the study site.

The decrease in dissolved oxygen immediately after floodgate modifications was a result of sediment mobilisation and changes in the drains hydraulic efficiency. Tidal restoration within the drain modified the flow regime (i.e. increased velocity and bi-directional flow), causing monosulphidic black oozes (MBOs) to mobilise. Sullivan *et al.* (2002) and Bush *et al.* (2001) noted that the entrainment of MBOs reduced dissolved oxygen content and was associated with large-scale asphyxiation in fish. This was most common during the post-modification period immediately after opening the floodgates and following large rainfall events (>50 mm). Figure 7.11 shows that dissolved oxygen levels fell below 6.0 ppm in the first 10 days proceeding floodgate modifications, which was attributed to increased surface water flows agitating benthic sediments and mobilising MBOs.

Other periods of low dissolved oxygen readings were recorded immediately after 2 large rainfalls on Days 499 and 767. During these events, high velocity upland flows disturbed bottom sediments and reduced dissolved oxygen (<3.0 ppm). However, the strong flows quickly dispersed the sediments and dissolved oxygen readings were restored above 6.0 ppm within less than 7 days. While the low readings during these periods represent a significant concern, the long-term average DO measurements following floodgate modifications are in line with ANZECC (1992) guidelines.

The transport of MBOs and their subsequent impact on dissolved oxygen levels may also be due to changing hydraulic conditions in the drain. The increased salinity levels and improved water quality affected the aquatic flora and destroyed infestations of the acidophilic sedge- *Eleocharis equisetina.* During storms, damaged weeds were uprooted and discharged from the study drain, which assisted in the transport of MBOs by increasing the drain's hydraulic conductivity and by aerating the sediments during uprooting. While this may only be a temporary concern, it is recommended that drain maintenance/clearing be undertaken some considerable period before commencing future floodgate modifications.

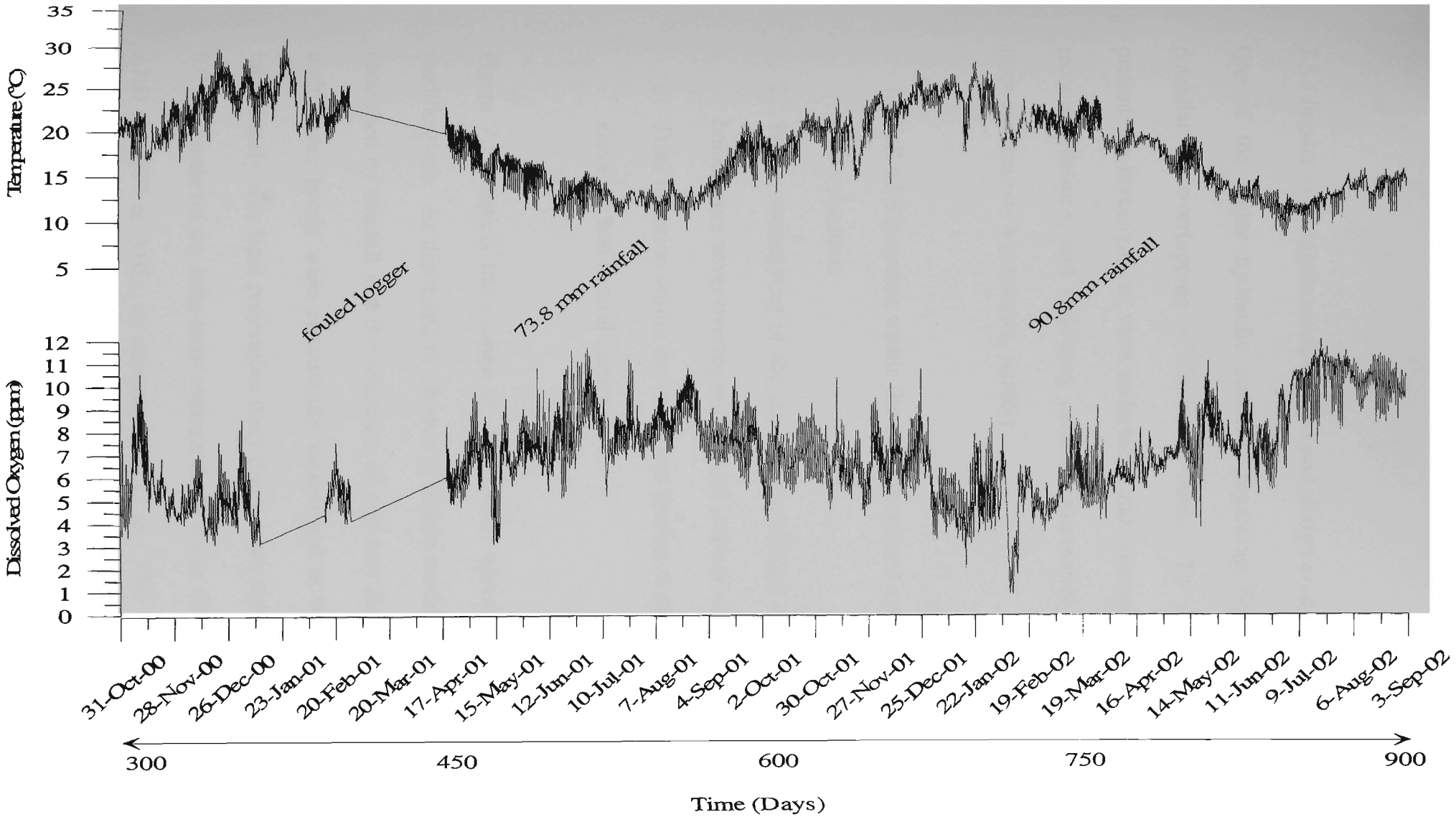

Figure 7.11 Dissolved oxygen and temperature readings upstream of the modified floodgate.

7.3.3 Impact of floodgate modifications and design on drain water elevation

One of the major hydraulic concerns regarding floodgate modifications was the potential for overtopping of the levee bank. To address this concern, extensive preliminary investigations were undertaken and presented in Chapter 6. Based on those recommendations, and following careful examination of post-modification findings, three conclusions were drawn, namely:

1. Full tidal intrusion within the drain increased average drain water elevations and flow velocities;
2. While overtopping of the drain was recorded during rainfall events, the levee banks were never overtopped by tidal (saline) waters;
3. Tidal intrusion within the drain was limited in distance due to changes in surface elevation and natural barriers.

Figure 7.12 depicts the change in drain water elevation before and after floodgate modifications. As discussed in Chapter 5, before modifications drain water levels were controlled by rainfall and the influence of one-way floodgates. As a result, upstream drain water levels were consistently maintained at the low-tide mark. Conversely, immediately after tidal restoration daily drain water elevations fluctuated between 0.63-0.9 m. Furthermore, long-term average drain water elevations increased from 0.056 m AHD to 0.277 m AHD, an increase of 0.22 m. This is important with regards to the hydraulic gradient imposed on the phreatic zone and, hence, acid seepage/transport. The impact of modified drain water levels on acid seepage rates is further discussed in Section 7.4.

Restoration of tidal flushing to the study drain also increased drain water velocity and discharge rates. Before modifications, drain water discharge was difficult to measure during dry periods using conventional propeller driven flow meters, in part because of the dampening effect caused by one-way floodgates, but also because of the 6-hour tidal cycle, which allowed chronic discharges of acid over long periods. However, the ingress of tidal waters after modifications increased the volume of water discharging from the system on the ebb tide. In addition, the installation of a bi-directional Doppler flow meter within the drain showed that flow typically increased on the ebb tide. As detailed earlier, the increase in drain water velocities was related to the decrease in dissolved oxygen readings and the mobilisation of MBOs.

Drain levee overtopping was limited to periods of excessive rainfall and not caused by general tidal fluctuations. These results validated the spatial model findings presented in Chapter 6 and demonstrated that sufficient freeboard was available within the study drain. Indeed, during the 551-day post-modification period, 4 large rainfall events triggered drain water overtopping (see Figure 7.12), but in every instance, the water overtopping the levee banks was less than 4.5 mS cm^{-1}, and therefore, below ANZECC (1992) limits set for irrigation.

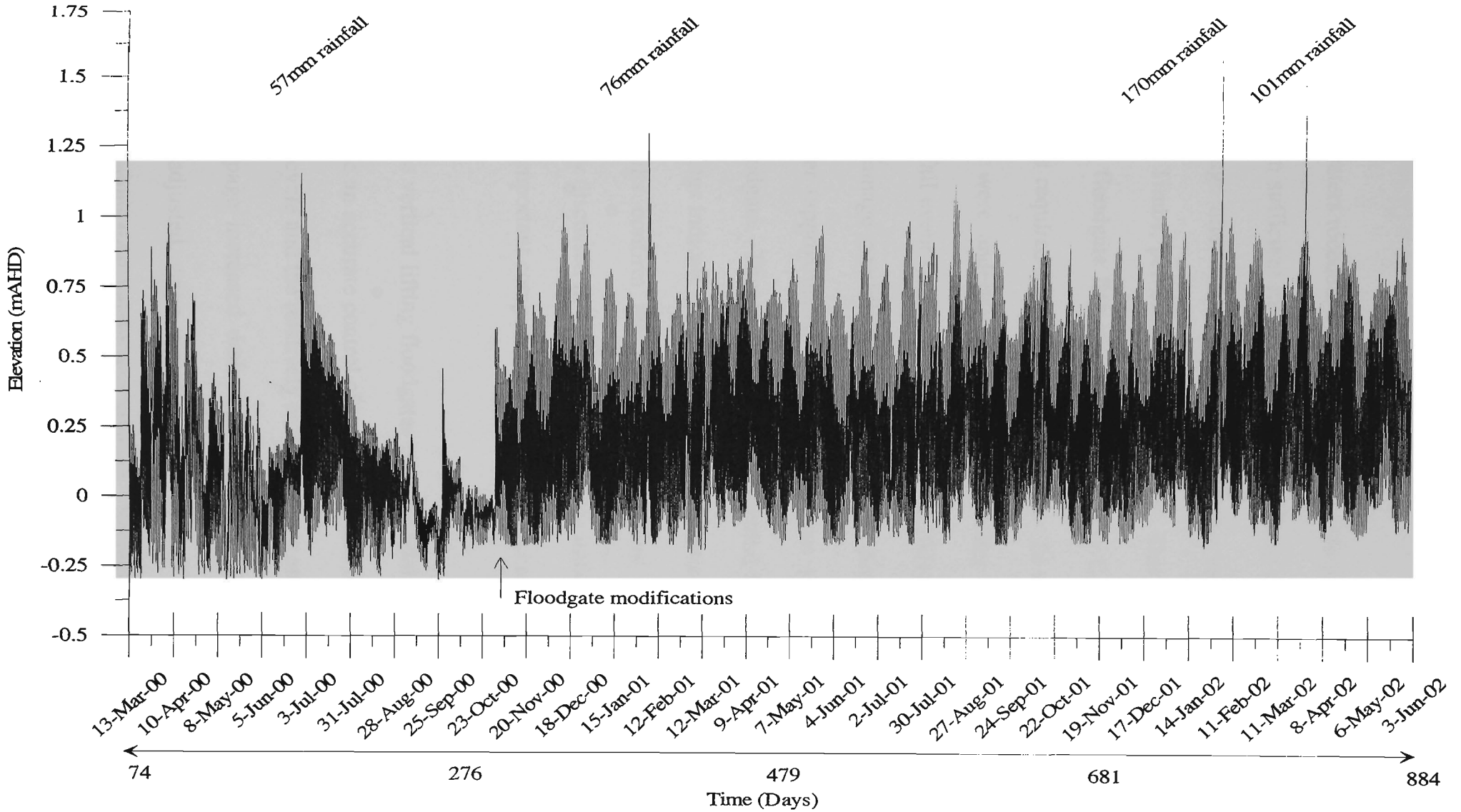

Figure 7.12 Drain water elevation before and after floodgate modifications with 4 overtopping events displayed with rainfall.

As floodwaters receded, a strong hydraulic gradient within the drain quickly established to maintain sufficient runoff. Though difficult to quantify, local landholders suggested that drainage after floods increased when the vertical lifting gates were completely raised (P. Timbs, personal communication). This was attributed to the fact that each individual floodgate flap weighs approximately 0.8 tonnes and significant hydrostatic pressure is required to maintain an opening. To quantify the difference in discharge, field tests were undertaken where surface water velocity was measured following a large rainfall event on Day 609 (31st August 2001). These results indicated that under similar drainage conditions water discharged through the non-floodgated culvert 10 times faster (approximately 1.15 L sec^{-1} versus 12.1 L sec^{-1}) than water through the closed floodgate. Though the rate of preferential flow decreased with falling velocity, these findings indicate an ancillary benefit of vertical lifting gate systems. Furthermore, these results confirm the theoretical treatment of discharge through a flap gate (previously discussed in Chapter 6.4.2), which indicated that the submerged mass of the flap is an important component in relation to discharge.

Though the vertical lifting floodgates restored tidal flushing to the study drain, they did not provide an accurate control of upstream water levels for two reasons. Firstly, the 6-hour tidal cycle and the relatively small drainage area meant that during any time period minor seepage increased drain water height. Therefore, unless the static gate was manually adjusted, water would continue to flow at a constant, albeit low, flow rate until maximum tidal height was attained. Secondly, the rubber sealant that creates a compression seal between the headwall and the floodgate was removed during construction to more efficiently raise and lower the gate. This permitted leakage and decreased control of the upstream water levels.

The lack of upstream water level control affected water retention properties within the study drain. Before floodgate modifications, drain water elevation was consistently low and, in combination with high levee banks, significant water retention was available in the drain during flooding events. However, due to full tidal fluctuations within the study drain, storage capacity was limited and overtopping could occur with reduced upland inflow. Bearing in mind the steep subcatchments in the area and the discharge characteristics of water through straightened and cleared drainage lines, this was considered an important factor. To effectively compensate for these factors, the aforementioned 'Smart Gate' system was designed and installed.

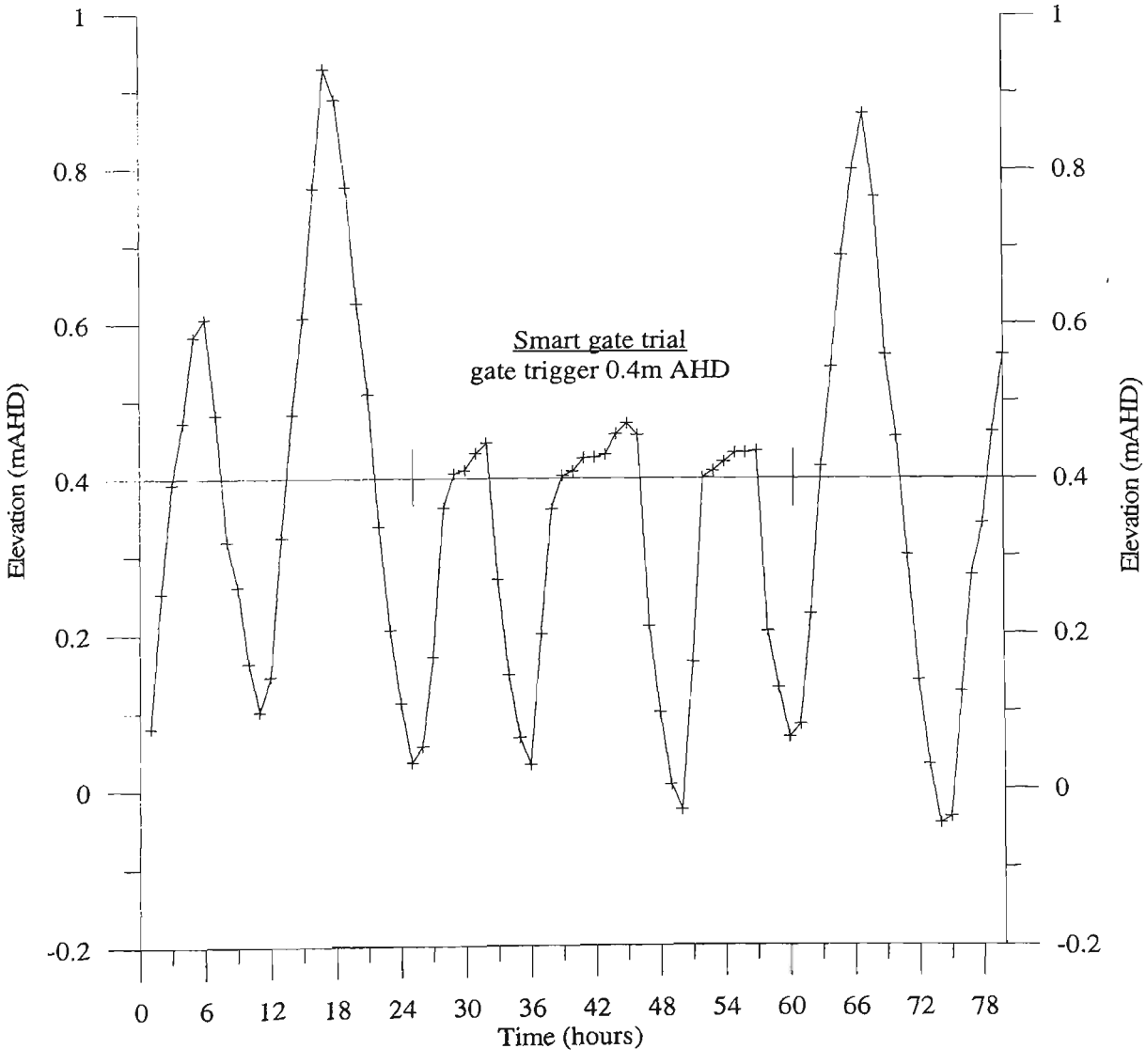

Figure 7.13 Drain water elevations during 'Smart Gate' trials.

The 'Smart Gate' system (see Chapter 6) effectively controlled upstream water levels, but leakage through the vertical lifting gate limited its efficiency. Figure 7.13 depicts a trial period to determine the effectiveness of the 'Smart Gate'. During this trial, the 'Smart Gate' system was programmed to restrict water levels upstream of the floodgate to 0.4 m AHD. In response, the 'Smart Gate' controlled upstream water levels and limited drain water elevation to 0.471 m AHD over three tidal cycles. The discrepancy between the trigger limits and the recorded values was from leakage through one of the remaining vertical lifting gates installed at the site and upstream inflows. It is important to point out that one of the vertical lifting gates remained at the site after installation of the 'Smart Gate' because local landholders wanted to manually control/raise the gate during flooding periods. As a result, although the 'Smart Gate' system successfully operated throughout its installation, unless the vertical lifting gates were manually closed, upstream water levels fluctuated with the tide. Nonetheless, in future applications where leakage is minimised, the ability to remotely control the 'Smart Gates' trigger heights will maintain water retention properties of the drain during flooding events.

The final conclusion drawn from post-modification drain water levels was that tidal intrusion was limited in distance due to changes in surface elevation and natural barriers. Drain water measurements taken 210 m upstream of the floodgate indicated minor (0.017 m) fluctuations over a large (0.962 m) tidal cycle. These results correspond well with spatial modelling techniques (detailed in Chapter 6), which state that tidal fluctuations will be limited to 225 m upstream. Dense stands of phragmatis within the drain also reduced upstream flow energy and decreased tidal forcing, and were associated with the difference between field and simulated results.

7.4 Implications of modified floodgates on the phreatic zone

As detailed above, hydraulic conditions within the drain were significantly modified after tidal restoration. Blunden and Indraratna (2001) showed that as long as a sufficiently moderate hydraulic conductivity exists within the soil matrix, changes to drain water height (i.e. boundary conditions) would influence the phreatic zone. The alteration of drain water boundary conditions on the phreatic zone after floodgate modifications, particularly the hydraulic gradient of groundwater, is detailed in this section. To facilitate a concise discussion, groundwater results are limited to transects B, C, and D; the remaining results can be found in Appendix B.

7.4.1 Groundwater elevation before and after floodgate modifications

Long-term average groundwater elevations before and after floodgate modification are given in Figure 7.14. Before modifications, average groundwater elevations at all sites were below the pyrite layer, which indicated a strong acid producing environment. Furthermore, the average surface of the phreatic zone was similar to the average pre-modification drain water levels (0.056 m AHD versus –0.05 m AHD for drain and groundwater elevations, respectively), which demonstrates that the tidal boundary conditions had a significant impact on groundwater seepage.

After modifications, the groundwater table inundated the acid sulphate soil layer, but fluctuated over a wide range. Groundwater levels were a function of drain water elevations (0.277 m AHD versus 0.201 m AHD for drain and groundwater elevations, respectively), and, by raising the surface of the phreatic zone above the pyrite layer, tidal restoration was shown to be an effective means of controlling future acid

production via atmospheric oxidation. However, fluctuations in groundwater height (as shown by standard deviation bars in Figure 7.14) were significantly stronger during the post-modification period due to the influence of tidal fluctuations on the soil matrix and the increased sample size. Furthermore, it is also important to note the decrease in the hydraulic gradient of groundwater in the post-modification period. Due to the complex nature of groundwater flow over varying climatic and hydraulic factors, this subject is further detailed below and in proceeding chapters.

7.4.2 The influence of altered boundary conditions on the phreatic zone

Fluctuations in the phreatic zone at transect B during the post-modification period are shown in Figure 7.15. These findings indicate that groundwater levels fluctuated above and below the pyritic layer, and their degree of variance decreased with distance from the drain. Specifically, groundwater levels 1 m perpendicular to the drain oscillated more than 0.6 m, whereas 10 m from the drain, groundwater levels varied 0.43 m. The disparity in groundwater height over time was a function of climatic conditions (i.e. rainfall and evapotranspiration) and natural tidal variations.

Climatic and boundary conditions also influenced the hydraulic gradient of groundwater flow. During dry periods, elevated drain water heights reversed the groundwater gradient and, in conjunction with tidal forcing, enhanced recharge of the phreatic zone. This was most apparent on Days 346, 703, and 746 (labelled high tide on Figure 7.15). Importantly, groundwater recharge was never recorded before floodgate modifications; therefore, these findings depict the ability of elevated drain water levels to recharge the phreatic zone during dry periods.

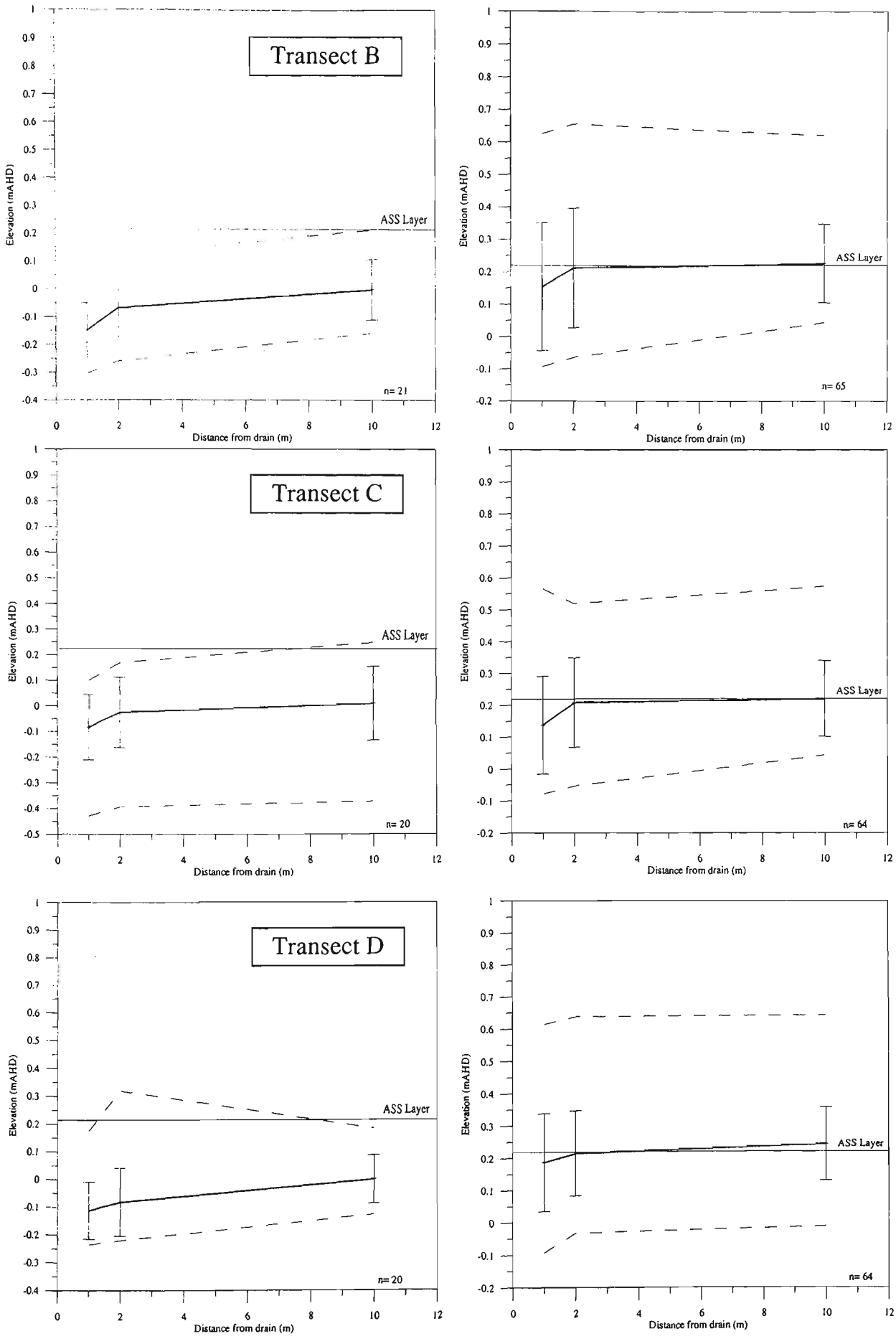

Figure 7.14 Long-term average groundwater elevations at transect B, C, and D before (left column) and after (right column) floodgate modifications. Error bars indicate standard deviation about the mean and the dotted lines show maximum and minimum readings. Note the different Y-axis scale for pre-modification results.

Conversely, during periods of consistently smaller tidal variations or following large rainfalls, the hydraulic gradient sloped towards the drain. This assisted groundwater drainage and reduced surface ponding but also promoted the translocation of acid products. Similar to pre-modification results, groundwater seepage towards the drain was strongest after natural recharge from rainfall. Nonetheless, the slope of the hydraulic gradient was reduced during the post-modification period due to the consistent high tidal levels causing groundwater recharge (Figure 7.14).

The influence of varied boundary conditions on groundwater flow is shown in Figures 7.16 and 7.17. Periods of groundwater recharge due to high drain water levels are depicted in Figure 7.16 (Day 703). Strong tides and a lack of substantial rainfall before this period decreased groundwater elevation and enhanced drain water seepage. In addition, increased velocity vectors nearest the floodgate indicated that the hydraulic gradient decreased with distance because of tidal dampening. Conversely, 83 mm of rainfall during the five days preceding Day 608 (Figure 7.17) raised the groundwater table and promoted groundwater seepage. This was similar to pre-modification results, however, during the post-modification period, groundwater levels were primarily maintained above the pyritic layer.

The above information is useful in determining variations in groundwater height over time, but as previously described, daily tidal variations play an important role in controlling the groundwater gradient. To ascertain the influence of tidal forcing on the phreatic zone, a series of continuously monitoring submersible data loggers were installed in open standpipe piezometers 1 m, 4 m, 8 m, and 16 m perpendicular to the drain over a 12-week period.

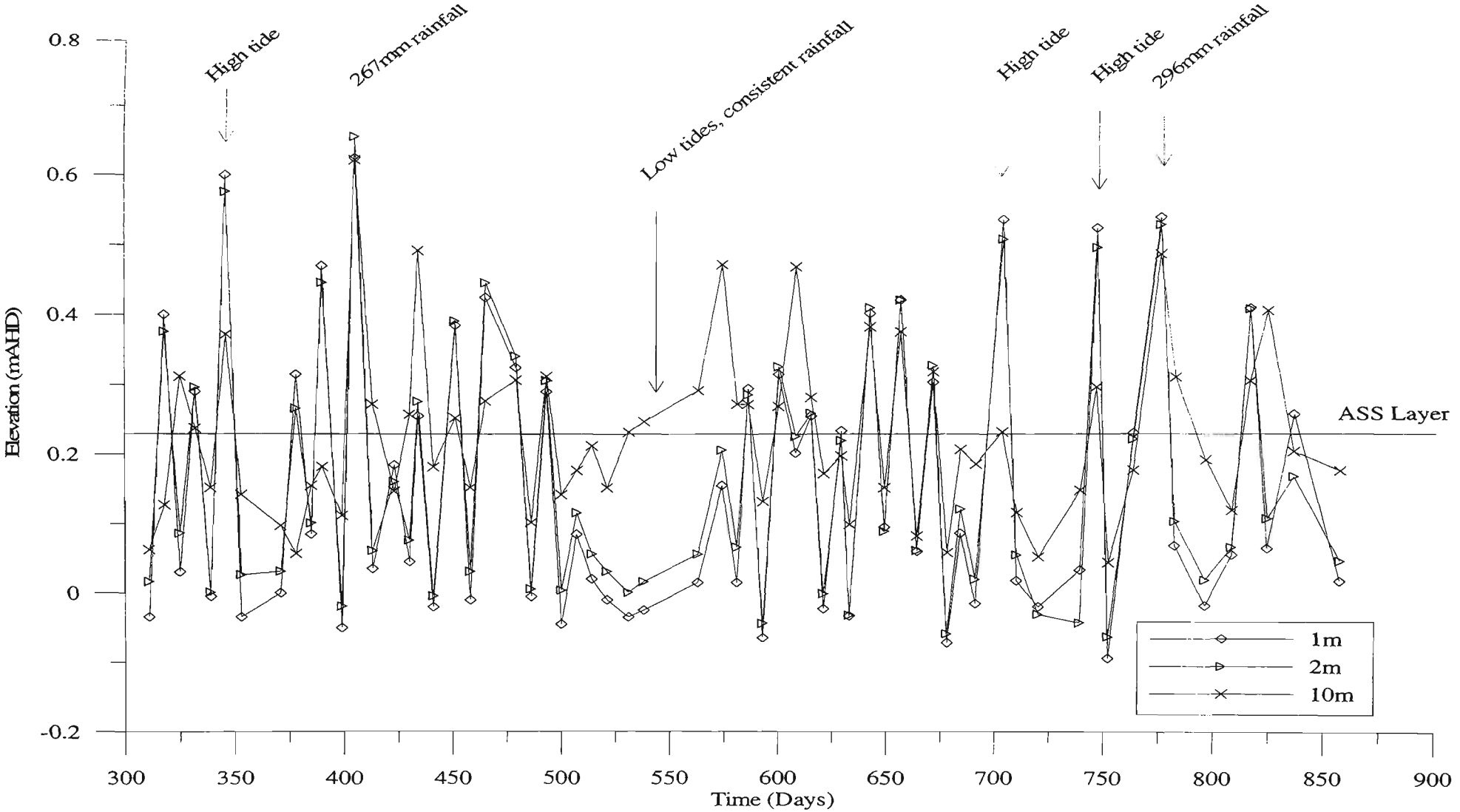

Figure 7.15 Groundwater elevations at transect B after floodgate modifications.

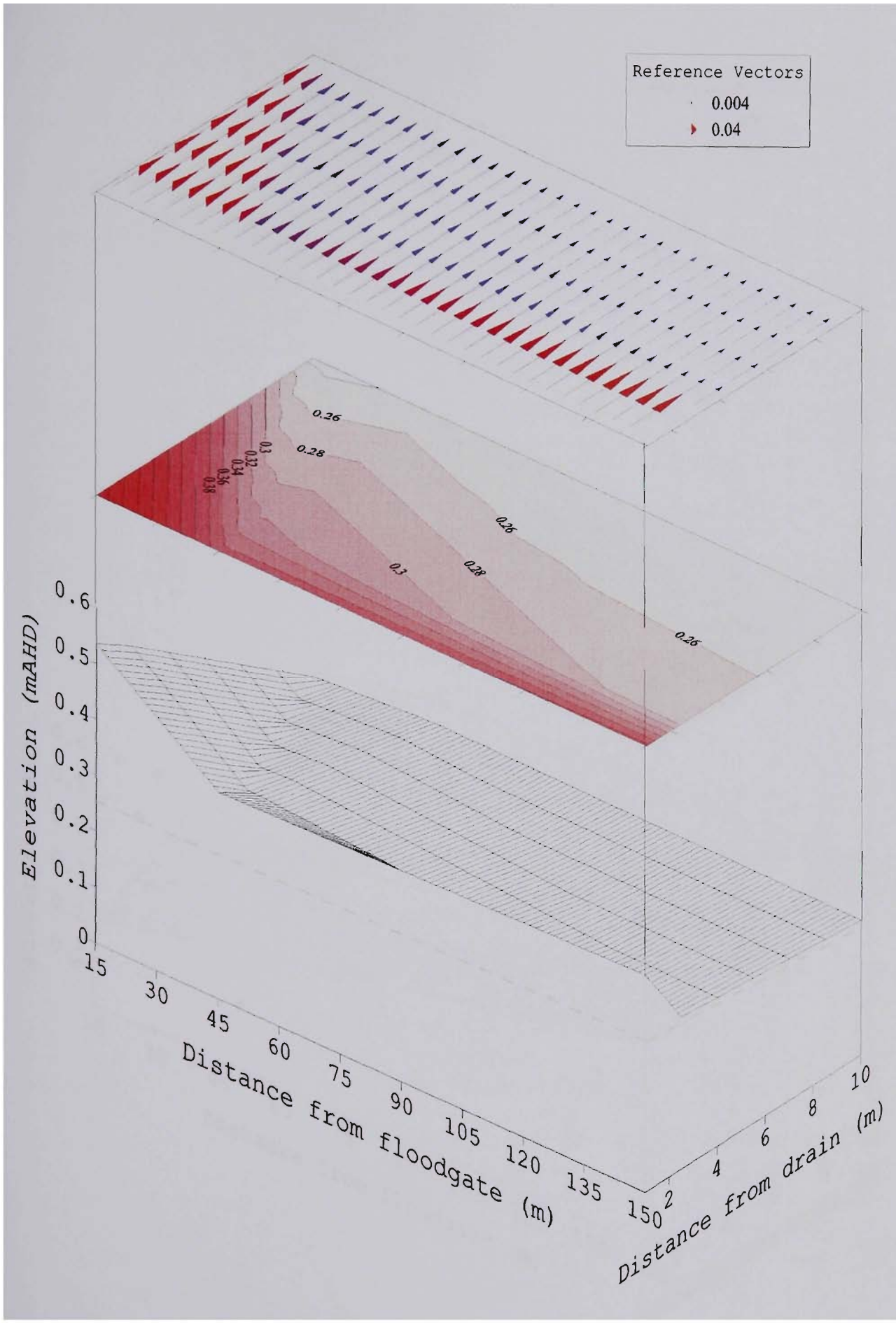

Figure 7.16 Groundwater elevation profile with velocity vectors during Day 703. Note the surface of the pyrite layer is depicted by the green dashed line and that the contour gradient and velocity vectors are in (m/day).

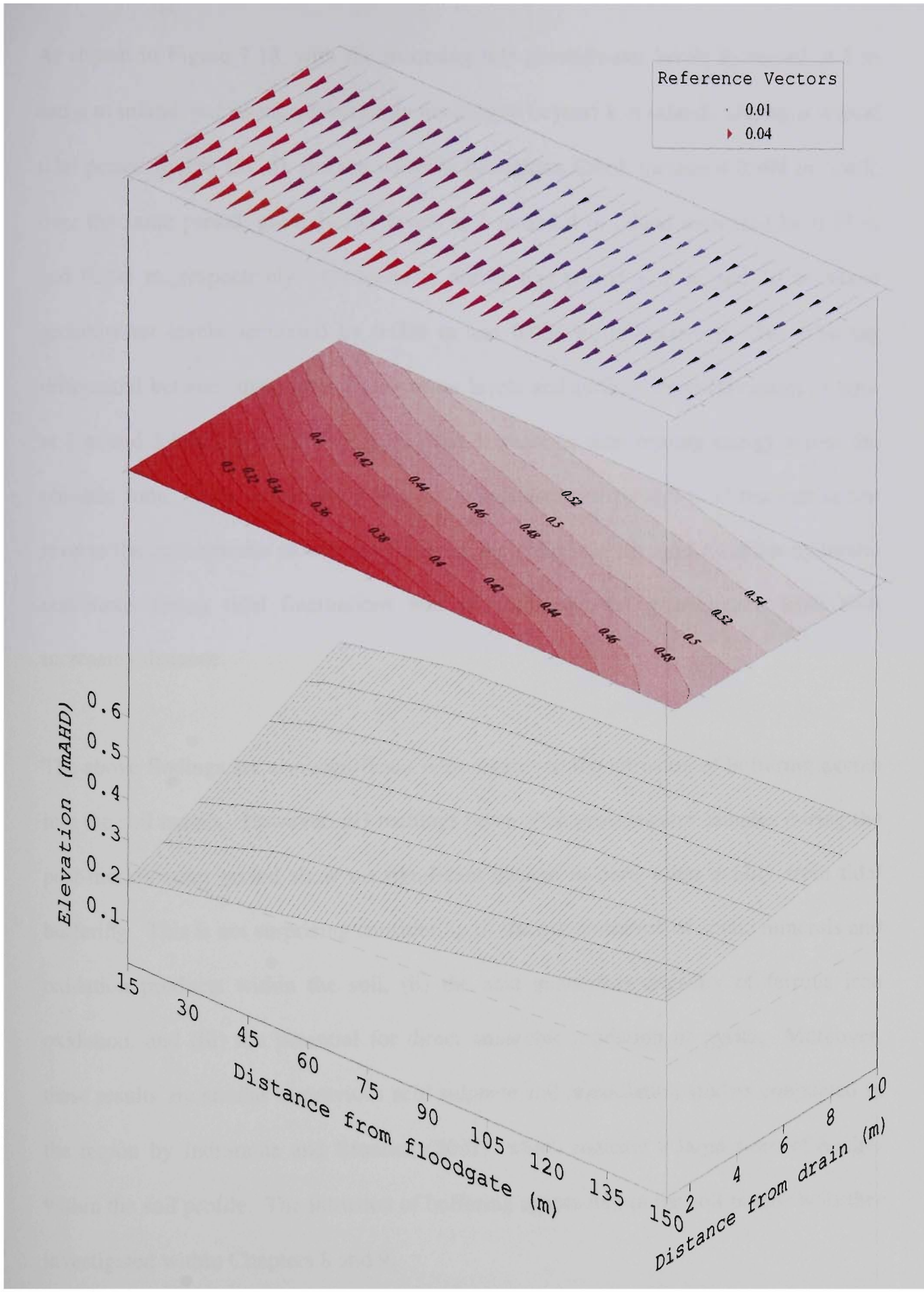

Figure 7.17 Groundwater elevation profile with velocity vectors during Day 608. Note the surface of the pyrite layer depicted by the green dashed line and the contour gradients and velocity vectors are in (m/day).

As shown in Figure 7.18, with the incoming tide groundwater levels increased at 1 m and 4 m inland, but remained relatively unchanged beyond 8 m inland. During a typical tidal period (hours 19-25), surface water in Broughton Creek increased 0.998 m, while over the same period, groundwater levels at 1 m and 4 m inland increased by 0.37 m and 0.205 m, respectively. Conversely, during this period at 8 m and 16 m inland groundwater levels decreased by 0.006 m and 0.008 m, respectively. The time lag differential between maximum groundwater levels and surface water elevations (1 hour at 1 m and 3 hours at 4 m) also depicts the decrease in tidal forcing energy across the phreatic zone. This is important because it indicates that though tidal restoration can reverse the groundwater flow regime nearest the drain (1-6 m), under similar hydraulic conditions strong tidal fluctuations will not influence the groundwater table with increasing distance.

The above findings are also significant with regards to the intrusion of buffering agents into the soil matrix. However, pH readings taken from groundwater samples during the post-modification period show no significant change in pore water acidity from tidal buffering. This is not surprising considering (i) the concentration of acidic minerals and oxidation products within the soil, (ii) the acid generating capacity of ferrous iron oxidation, and (iii) the potential for direct anaerobic oxidation of pyrite. Moreover, these results are similar to previous acid sulphate soil remediation studies conducted in the region by Indraratna and Blunden (2001), which indicate a large store of acidity within the soil profile. The intrusion of buffering agents within the soil profile is further investigated within Chapters 8 and 9.

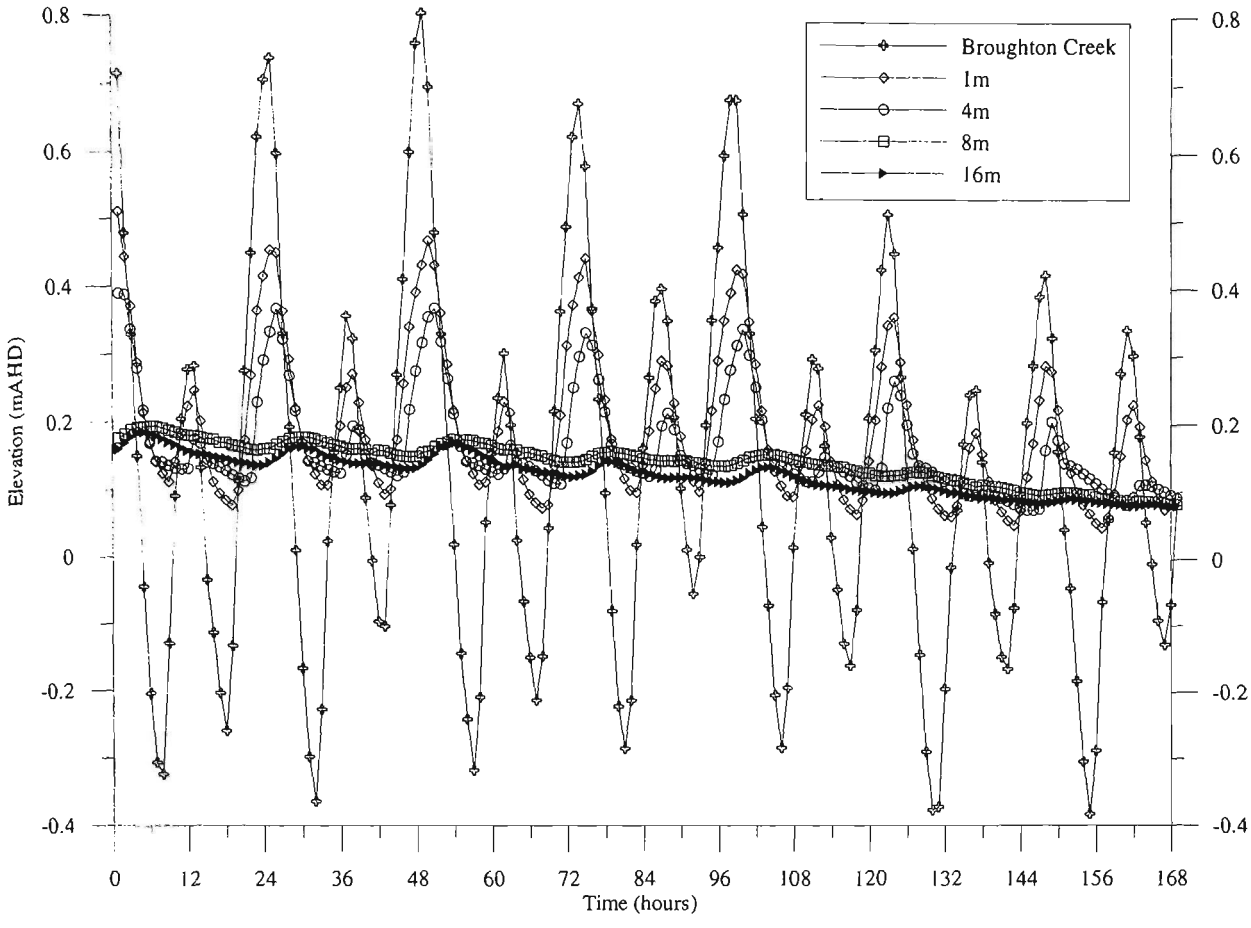

Figure 7.18 Drain and groundwater elevation over a seven-day period in response to tidal forcing.

7.5 Conclusion

The above findings indicate that tidal restoration via modified floodgates is an effective strategy to combat acid sulphate soil drainage. Surface water quality measurements showed that tidal buffering decreased aluminium and iron concentrations and increased drain water pH, especially during prolonged dry periods when increased bicarbonate concentrations were transported in with the tide. The strategy was less effective immediate after large rainfalls because of a decrease in drain water alkalinity and an increase in total acidity. Moreover, while several water quality indicators were still slightly in excess of ANZECC (1992) guidelines, the majority of drain water indicators improved by more than 60%.

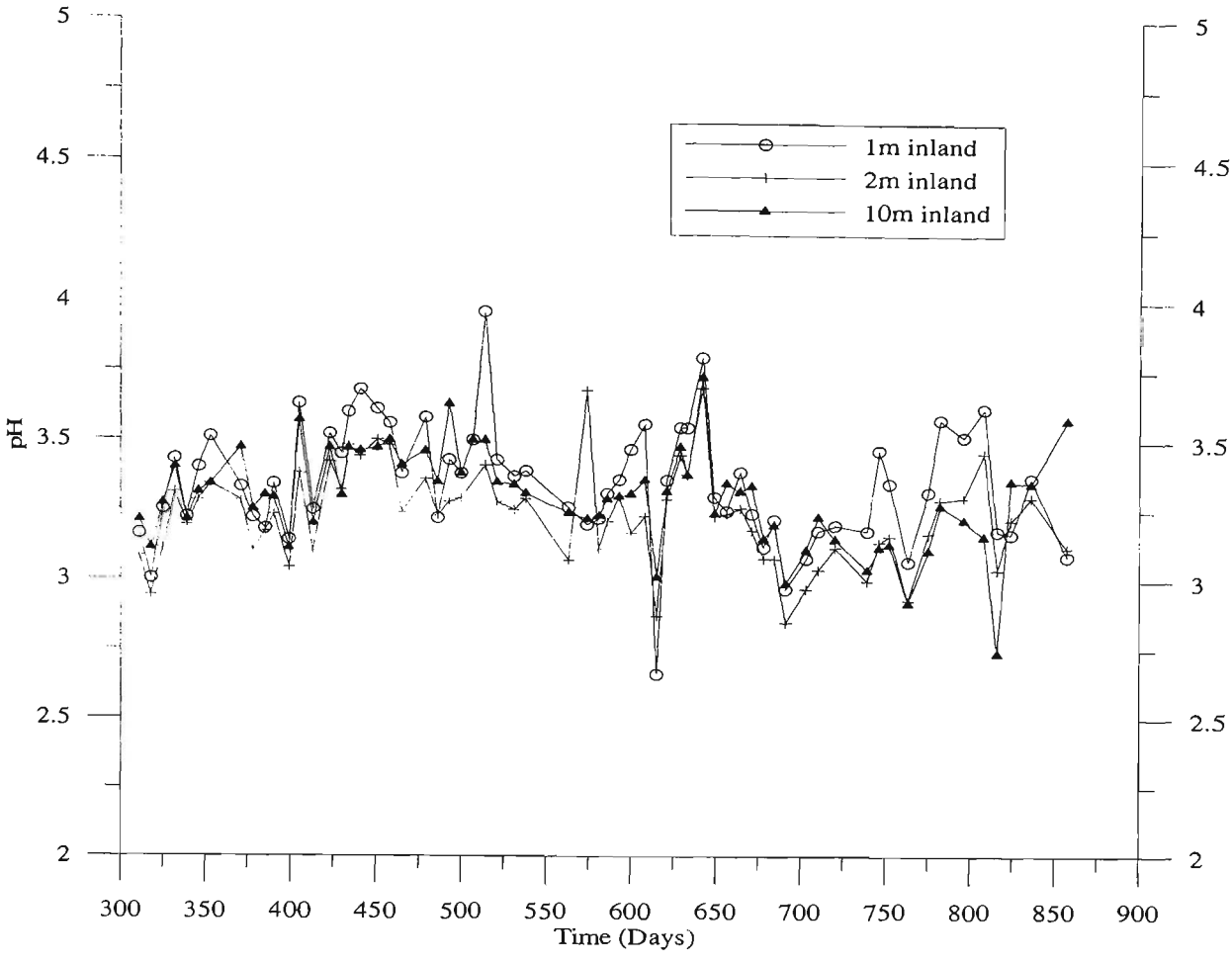

Figure 7.19 Groundwater pH readings at transect B after floodgate modifications.

Post-modification results also demonstrated a decrease in hydraulic related floodgate problems. The installation of modified floodgates eliminated the acid reservoir effect and increased dissolved oxygen levels. Brief declines in dissolved oxygen were attributed to the mobilisation of MBOs and could be reduced in future applications through drain maintenance/clearing prior to civil works. Furthermore, average drain water elevations increased, but drain overtopping was limited to major rainfall events. Installation of a 'Smart Gate' system demonstrated that drain water elevations could be controlled to optimise tidal buffering and hydraulic properties. Finally, tidal intrusion increased the hydraulic efficiency of the drain by eliminating weed growth. The elimination of weeds due to salt stress, and the increased flow rate within the drain, created unfavourable conditions for MBO accumulation.

Altered drain water conditions affected the phreatic zone and average groundwater elevations were above the pyritic layer and significantly higher than pre-modification results. Furthermore, tidal fluctuations fostered groundwater recharge from the drain, but also increased the oxidation zone. Tidal forcing on the soil matrix decreased with distance from the drain and was imperceptible within 8 m. Due to the large store of acid products within the acidic layer, tidal buffering did not alter groundwater acidity levels. These results, however, do not indicate the impact of saline intrusion on the biogeochemical reaction kinetics within the soil. To further address this issue and the impact of contaminant transport under varied lateral hydraulic conductivity rates, extensive field analysis and numerical modelling was undertaken. These findings are presented and discussed in Chapters 8 and 9.

Based on these studies, future floodgate modifications to improve acidic conditions within Broughton Creek are recommended. As stated in Chapter 3, the study drain is the northernmost drain within the Broughton Creek estuary impacted by acid sulphate soils. This means that the transport of buffering agents to the study drain requires the longest recovery period following estuarine flushing after large rainfalls. At other sites closer to the tidal influence, buffering agents are expected to return to the drain within a shorter timeframe, which will reduce both the magnitude and duration of acid discharges during wet periods. Furthermore, the simultaneous installation of water retaining structures (i.e. weirs and dropboards) at strategic locations within a drain will reduce the transport of acidic groundwater products and retain the majority of acid contaminants within the soil matrix until buffering agents are available for neutralisation (5-10 days in most cases). This approach will also reduce fluctuations in groundwater levels and provide water upstream of the weirs during dry periods.

Chapter 8.0 Saline Intrusion within the Soil Matrix: Geochemical Implications of Altered Drainage Hydrology and Tidal Forcing

8.1 Introduction and associated research

Chapter 7 discussed the effects of restoring tidal flushing within a flood mitigation drain to combat acid sulphate soil leachate. These results showed that highly saline surface waters correlated to strong buffering potential. Furthermore, periods of high salinity/high buffering potential were associated with dry conditions due to reduced upland inflow and increased tidal reach. Drain and groundwater hydraulics showed that during prolonged dry periods, tidal forcing recharged the groundwater table. In combination, these 2 phenomena suggest that tidal buffering fosters saline intrusion into the soil matrix. Therefore, the impact of saline intrusion due to advection and dispersion of tidal surface waters on the groundwater regime is detailed in this chapter.

Salinisation of the phreatic zone is a major concern throughout Australia and other parts of the world. In most cases, saline intrusion is enhanced by groundwater extraction, altered drainage conditions or irrigation. The dominant mechanisms that control seawater intrusion are the flow regime in the aquifer above the intruding seawater wedge, the variable density of fluids, and the hydrodynamic forces of dispersion. According to these mechanisms, the freshwater flow rate to the drainage boundary determines the length of the seawater wedge intruding into the aquifer. As the freshwater flow rate is reduced (i.e. by evapotranspiration or pumping), the length of the seawater wedge will increase. Natural replenishment of the aquifer increases mass flux/transport resulting in contaminant removal. The transition zone between saline and freshwater is the result of hydrodynamic dispersion of the dissolved matter and the

spatial variation in hydraulic (primarily lateral) conductivity of the soil. Darcy's Law, (Equation 2.16) governs the mass flux of contaminants based on hydraulic conductivity, and thus, soil layers with higher lateral hydraulic conductivity values will have stronger intrusion/flushing rates. Characteristically, clay soils leach few salts while loamy and sandy soils release contaminants more rapidly.

Saline intrusion alters the biogeochemical conditions within the soil matrix. Four chemical reaction categories can be considered during the hydrologic interactions of saline intrusion, namely: (1) mixing of groundwater and seawater, (2) carbonate precipitation, (3) ionic exchange and silicate diagenesis, and (4) redox reactions (Bear *et al.*, 1999). The chemical reactions associated with the mixing of seawater with freshwater primarily involve the addition of conservative chloride and sodium ions. This is easily tractable by using the ionic ratios of seawater (i.e. Na/Cl ratio) and/or electrical conductivity. Carbonate precipitation is not elaborated in this study due to the acidity of the soil and the undersaturation of carbonate inputs. However, ion exchange and clay diagenesis is an important component of saline intrusion in acid sulphate soil environments, yet instead of the 'typical' ionic exchange between Na^+ and Ca^{2+} ions, aluminium, iron and phosphate ions are exchanged for sodium and magnesium uptake. Finally, redox reactions play a pivotal role during saline intrusion in acid sulphate soil terrains. The intrusion of seawater may produce low redox conditions due to the decomposition of dissolved organic matter, fine suspended organic particulates and/or highly organic sediments, and the reduced ability for water to retain oxygen under elevated chloride concentrations. Custodio *et al.* (1987) suggests that a decrease in redox levels will alter pH and convert dissolved sulphate ions to insoluble H_2S, resulting in low SO_4/Cl ratios. Currently, limited findings are available which examine

the influence of saline intrusion on the above biogeochemical reactions of *in-situ* acid sulphate soil samples.

The management of saline intrusion is a vital issue because of its impact on agricultural productivity. ANZECC (1992) guidelines regarding salinity levels and plant salt tolerance are given in Table 8.1. Considering that most pasture plants in southeastern NSW fall within the medium salinity rating, average root zone chloride concentrations should remain below 4.5 mS cm^{-1}. Concentrations above this level can alter productivity, increase plant death, and stunt growth levels. Additionally, the free energy of water in soil solution is reduced with increasing salinity concentrations, which decreases the uptake of water through the root zone and affects productivity.

Table 8.1 Soil and water salinity criteria (ANZECC, 1992).

Plant Salt Tolerance	Water or Soil Salinity Rating	Average Root Zone Salinity (mS/cm)
Sensitive Crops	Very Low	<0.95
Moderately Sensitive Crops	Low	0.95-1.9
Moderately Tolerant Crops	Medium	1.9-4.5
Tolerant Crops	High	4.5-7.7
Very Tolerant Crops	Very High	7.7-12.2
Non-sensitive Saline Crops	Extreme	>12.2

In microcosm greenhouse experiments, Portnoy and Giblin (1997a and 1997b) investigated the impact of seawater flushing on oxidised acid sulphate soil samples. Their findings indicated that prior to saline flushing, soil/groundwater samples were characterised by low pH, Fe (II) mobilisation, decreased organic content, and abundant levels of sorbed NH_x-N and mineral-bound PO_4. Flushing with saline water increased

porewater pH, alkalinity, dissolved nitrate, orthophosphates, Fe (II), Al^{3+} and ammonium N concentrations, reduced redox levels and contributed to the reestablishment of sulphide and Fe (III) mineral reduction. The highly ionic intruding waters encouraged cation exchange and resulted in a 6-fold rise in soluble Fe (II) and Al, and a 60-fold increase in NO_3-N. While these laboratory experiments indicate that saline intrusion may increase nutrient release and sulphate reduction, they also highlight the mobilisation of soluble aluminium and iron. The results presented in this chapter are the first steps towards validating this research on *in situ* ASS samples.

Based on the previous experiments conducted by Portnoy and Giblin (1997a and 1997b) and groundwater measurements given in Chapter 7, a variety of tests were undertaken to determine the impact of saline intrusion on the soil matrix. First, baseline groundwater conditions obtained before floodgate modifications are compared with post-modification results and climatic data. These results indicate that saline intrusion occurred throughout the study but was limited in distance due to weak tidal forcing and groundwater flushing from rainfall. Second, soil samples are examined before and after floodgate modifications to determine the influence of tidal restoration on soil salinity over time. Finally, multiport piezometer investigations were undertaken to determine the influence of saline intrusion on nutrient release and redox conditions in the vertical and lateral plane. The outcomes from this study were divergent from those of Portnoy and Giblin (1997a, 1997b and 1999) due to varying transport mechanisms under different field conditions and the saline intrusion dynamics. To deliver a concise discussion on the topic, the data presented is restricted to transects B and C (Figure 3.8); the remaining information is given in Appendix B.

8.2 Impact of tidal restoration on groundwater and soil salinity

8.2.1 Groundwater salinity

Weekly sampling of groundwater electrical conductivity levels (EC) were undertaken to determine the saline influence zone. As shown in Figure 8.1, groundwater EC fluctuated over a wide range but was primarily concentrated within 2 m from the drain. Prior to floodgate modifications, groundwater salinity was generally below 5.0 mS cm^{-1} and variances between sampling sites were limited, however, readings at transect B varied because of its proximity to the floodgate. In particular, groundwater EC measurements at a distance of 1 m and 2 m from the drain were often double that of 10 m inland (EC averaged 4.44 mS cm^{-1} versus 2.61 mS cm^{-1} at 1 m and 10 m, respectively). Conversely, the salinity regime at transect C did not follow the same pattern and EC was slightly higher 10 m from the drain (2.7 mS cm^{-1} versus 2.8 mS cm^{-1} at 1 m and 10 m, respectively). Background salinity levels within the groundwater were attributed to high concentrations of soluble Al, Fe (II) and SO_4 ions, and sulphurisation processes that produce ferrous sulphates. These minerals accumulate directly as salt by desiccation or may give rise to other more complex sulphate salts.

As discussed in Chapter 5, the groundwater table before floodgate modifications consistently sloped towards the drain. The seepage of groundwater in this direction limited saline intrusion by advection, and dispersion was the dominant transport mechanism. Dispersion is a much weaker transport mechanism, and following rainfall, the solute mass flux of groundwater towards the drain was greater than the dispersion forces. This flushed the contaminants from the soil matrix and reduced EC levels at all sites (Days 194-208, transect B). Based on this intrusion/flushing cycle, and the low hydraulic conductivity of the soil in the lateral plane (see Chapter 3 for reference), it

was presumed that, while tidal restoration into the study drain may increase groundwater salinity in proximity to the floodgate, the hazard would be limited to subsurface samples nearest the drain.

After floodgate modifications (Day 305), groundwater EC varied within and between transects. EC readings fluctuated with drain water concentrations and significantly increased 1 m and 2 m inland from the drain. EC measurements at 10 m inland from the drain increased to a lesser extent but the change varied significantly between transects B and C (average EC of 5.43 mS cm^{-1} and 3.10 mS cm^{-1} at transects B and C, respectively). Overall, transect B readings were higher than transect C due to increased salinity concentrations at the floodgate and variances in lateral hydraulic conductivity. As previously detailed in Chapter 5, the increase in lateral hydraulic conductivity at transect B was associated with the wetting/drying cycle perpetuated by the one-way floodgates. The low groundwater table beside the floodgate enhanced pyrite oxidation, increased soil development and clay flocculation, which, in turn, increased pore volume and fostered saline ingress. Conversely, the increased pore volume also enhanced flushing of contaminants during high flow, wet periods.

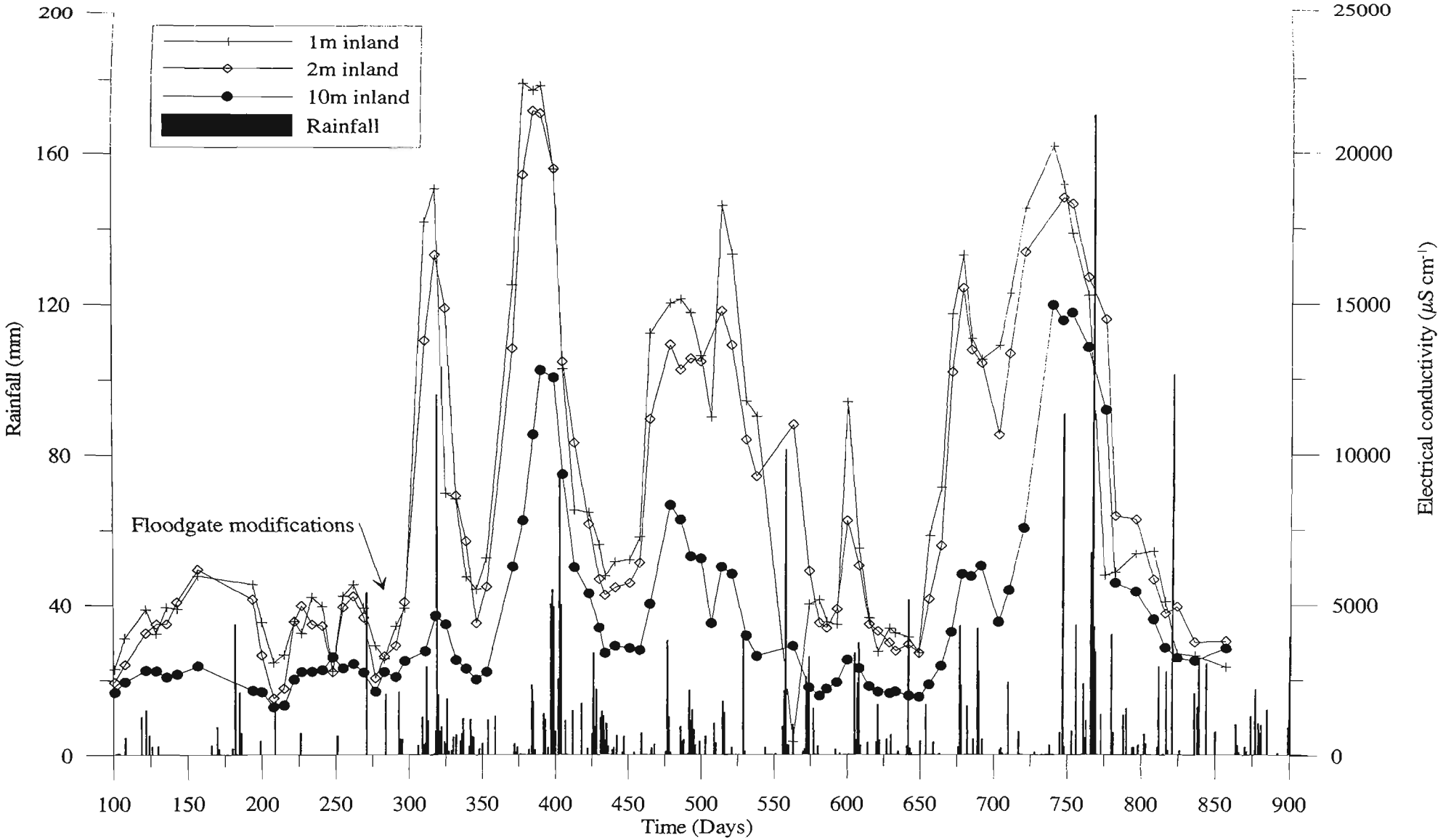

Figure 8.1a Electrical conductivity fluctuations (in mS cm^{-1}) with rainfall at transect B.

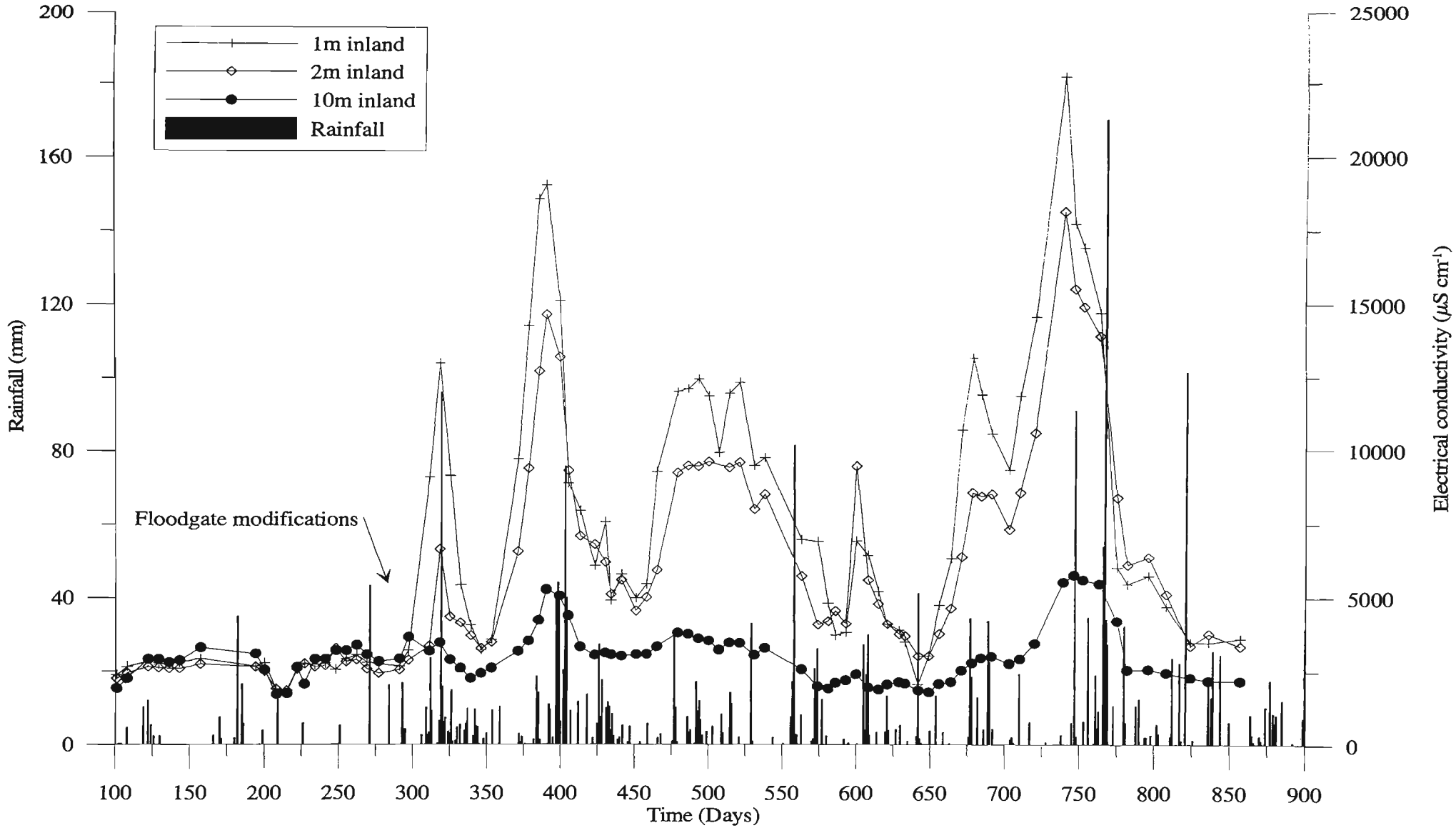

Figure 8.1b Electrical conductivity fluctuations (in mS cm^{-1}) with rainfall at transect C.

The altered drain hydraulics after floodgate modifications changed the salinity transport mechanisms. As shown in Chapter 7, the increased drain water elevations reversed the hydraulic gradient of groundwater flow. Recharging of the phreatic zone assisted contaminant transport by advection as well as dispersion, which resulted in elevated EC readings not previously recorded during dry periods. However, groundwater flushing after rainfall also fostered advective transport of contaminants out of the soil, mainly between Days 739-775, where 502.4 mm of rainfall recharged the phreatic zone, and the resultant flushing returned EC to pre-modification concentrations (decrease of over 15.0 mS cm^{-1}). While this indicates that saline intrusion does not pose a significant threat to the soil matrix, it does not give any indication of the vertical distribution of contaminants within the soil (i.e., impact on root zone), or the biogeochemical inter-relationships.

The chloride/sulphate ratio is commonly used to depict the extent of pyrite oxidising conditions in acid sulphate soils environments (Mulvey, 1993). In this regard, the chloride/sulphate ratio for groundwater samples taken from transects B and C during the entire study period is shown in Figure 8.2. Before floodgate modifications, chloride/sulphate readings were typical of strong oxidising conditions with little or no soil buffering capacity. After floodgate modifications, the chloride/sulphate ratio fluctuated with EC readings, and, during dry periods, $Cl:SO_4$ measurements near the floodgate did not depict acid production. This ratio, however, is not a reliant indicator of the oxidising environment within the soil, because increases in the chloride/sulphate ratio were mainly due to increases in the soluble chloride content. Indeed, dissolved sulphate concentrations during the post-modification period remained relatively stable and any change to the chloride/sulphate ratio was directly attributable to a change in

chloride concentrations. Furthermore, considering the positive correlation between EC and the chloride/sulphate ratio ($r^2 = 0.76$), EC readings were primarily a measurement of chloride concentrations. This is in contrast to the findings of Blunden (2000), who demonstrated that EC measurements in groundwater were directly related to the sum of acidic ions (sulphate, aluminium and iron). Moreover, in combination with the low groundwater pH values given in Figure 7.19, the high chloride/sulphate ratio shown in Figure 8.2 do not affectively estimate groundwater conditions in acid sulphate soil environments that have been exposed to tidal/saline flushing.

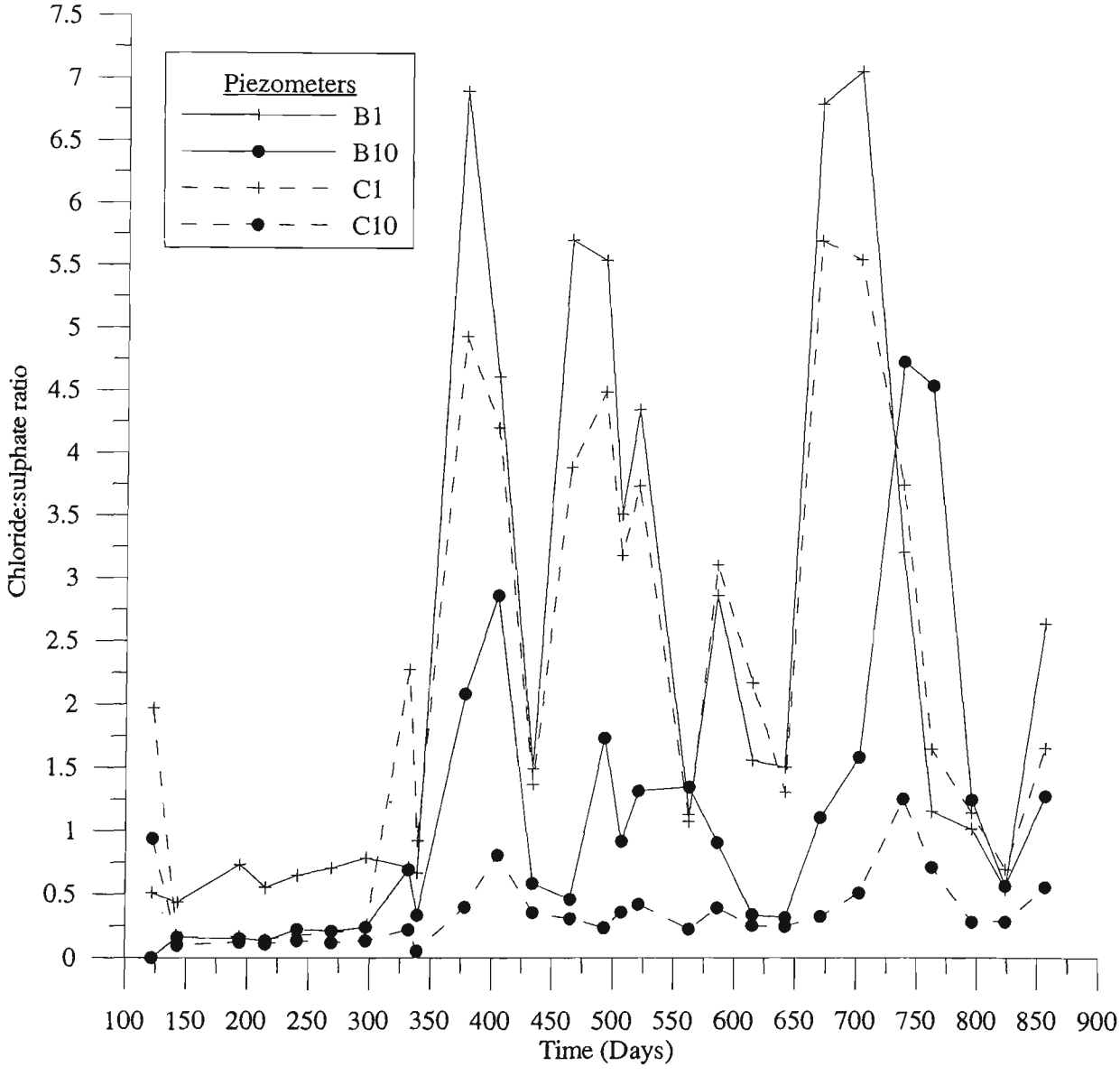

Figure 8.2 Chloride:sulphate ratio at transects B and C over entire study. B1, B10, C1, and C10 denote transect and distance from drain.

8.2.2 Soil salinity

Increased chloride concentrations are an obvious consequence of tidal restoration within the study drain. To determine the impact of Cl^- contamination within the soil, pre-modification and post-modification samples were analysed by the NSW EPA Laboratory using 1:5 water extracts and ion chromatography. Samples were also tested for total sulphate concentrations using 1:5 potassium phosphate extractable digestions and ICPAES.

Laboratory analysis of soil samples showed that chloride concentrations increased in locations nearest to the drain but did not significantly change 10 m inland. Table 8.2 shows that increases in chloride concentrations were particularly evident in the topsoil nearest to the drain due to saline intrusion and capillary rise. Tidal intrusion was not a concern with distance from the drain and chloride concentrations 10 m inland decreased over the study period. This is of particular interest because the 2002 soil samples were obtained during a prolonged drought period (the driest six months in the region since records commenced in 1894), when both low groundwater elevations and high salinity concentrations at the drain boundary fostered chloride transport. It was assumed that the high chloride concentrations at the drain would be flushed from the soil after recharge of the groundwater table by drought breaking rains. This assumption was previously established by Lawrie (1998) who examined the removal of accumulated soil bound contaminants due to irrigation of contaminated effluent waters in the lower Broughton Creek catchment.

Table 8.2 Total chloride and sulphate concentrations in soil samples.

		2000		2002			
Distance to drain (m)	**Depth (m)**	**Total Chloride (mg/kg)**	**Total Sulphate (mg/kg)**	**Total Chloride (mg/kg)**	**Total Sulphate (mg/kg)**	**% Change Chloride**	**% Change Sulphate**
1	0.0-0.5	43	720	250	530	+83	-26
1	0.5-1.0	110	1800	220	1600	+50	-12
1	1.0-1.5	640	1200	857	1740	+25	+32
1	1.5-2.0	920	3500	1200	2700	+24	-23
1	2.0-3.0	1010	980	1200	900	+16	-8
10	0.0-0.5	48	1400	30	1200	-38	-14
10	0.5-1.0	74	1600	84	2200	+12	+27
10	1.0-1.5	250	2200	99	2690	-61	+18
10	1.5-2.0	410	1750	420	2500	+3	+30
10	2.0-3.0	462	1200	280	1100	-40	-8

Due to the slightly elevated chloride concentrations in the topsoil, a detailed analysis of the soil's electrical conductivity was conducted across the study site. Triplicate core samples were collected to 0.5 m below the surface (0.25 m below the root zone), and divided into 0.1 m increments. The samples were then extracted in a 1:5 mixture with deionised water and EC was measured in the field using a calibrated handheld probe. The results, plotted in Figure 8.3, illustrate that soil EC was well below ANZECC (1992) guidelines of 4.5mS cm^{-1} and therefore, agricultural productivity should not be influenced by saline stress or changes in the soil structure.

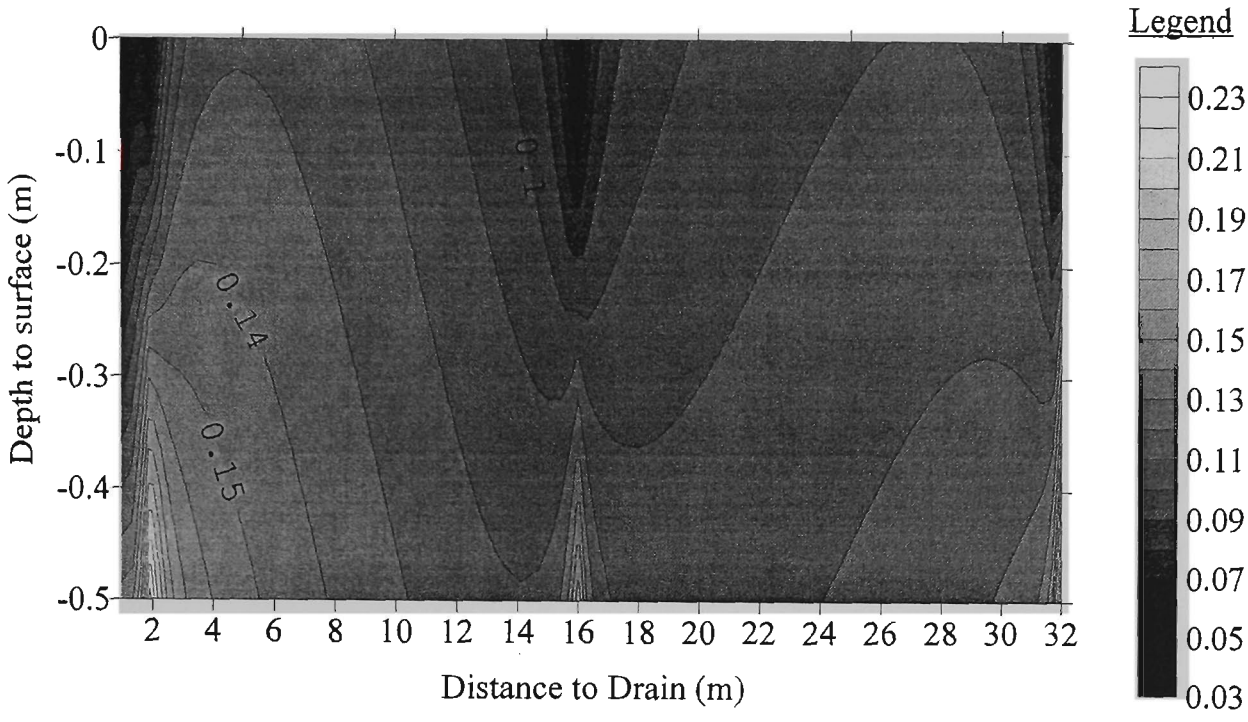

Figure 8.3 Electrical conductivity readings (in mS cm^{-1}) within the root zone.

As expected, total sulphate concentrations differed from total chloride concentrations, but generally sulphate levels increased with distance from the drain and with depth. The high sulphate concentrations were attributed to 'new' acid production due to the aforementioned drought, which lowered the groundwater table below the pyrite layer. Increased sulphate concentrations nearest the drain may also be caused by ingress and flocculation of dissolved sulphates transported into the drain on tidal waters. The biogeochemical impact of saline intrusion, including sulphate reduction, is further examined in Section 8.3.

8.3 Biogeochemical analysis of multi-level piezometer testing

The results discussed above indicate that saline intrusion was limited within the soil matrix and that groundwater recharge flushed contaminants accumulated within the soil matrix after wet periods. However, these findings do not give any indication as to nature of saline contaminants within a 2-dimensional plane or the impact of altered

drainage hydrology on geochemical interactions. To obtain this information, a series of multi-level piezometers were installed at the study site.

8.3.1 Methodology

The design of the multi-level piezometers was based on previously constructed units described by Acworth (1999). First, a section of PVC pipe was cut to length (3 m), slotted with a table saw and covered with geo-technical fabric. Lengths of 12 mm plastic tubing were then attached along the outside of the piezometers at 25 mm intervals, several holes were drilled at the bottom of the plastic tubes to assist water intake, and an abrasive material was inserted to reduce clogging. The plastic tubing was long enough to ensure that the unit could be attached to a vacuum pump. To obtain a representative sample, the vacuum pump first flushed the equivalent volume of each tube and the remaining sample was then transferred from the vacuum pump into a polyethylene sample bottle and immediately stored at 4^0C. Nine sampling ports were attached to each piezometer (1 m to 3 m at 25 mm intervals), and groundwater samples were extracted at individual depths. Details of the multi-port piezometers during construction and the related sampling equipment are shown in Figure 8.4.

For the majority of soil and groundwater analysis, testing was conducted in a manner similar to the methods stated in Chapter 3. In short, pH, electrical conductivity, temperature, and redox conditions for groundwater samples were immediately obtained in the field using calibrated probes. Soluble inorganic monomeric aluminium and total dissolved iron were determined by atomic adsorption spectrometry and soluble chloride and sulphates were analysed using ion chromatography. The elevation of the phreatic

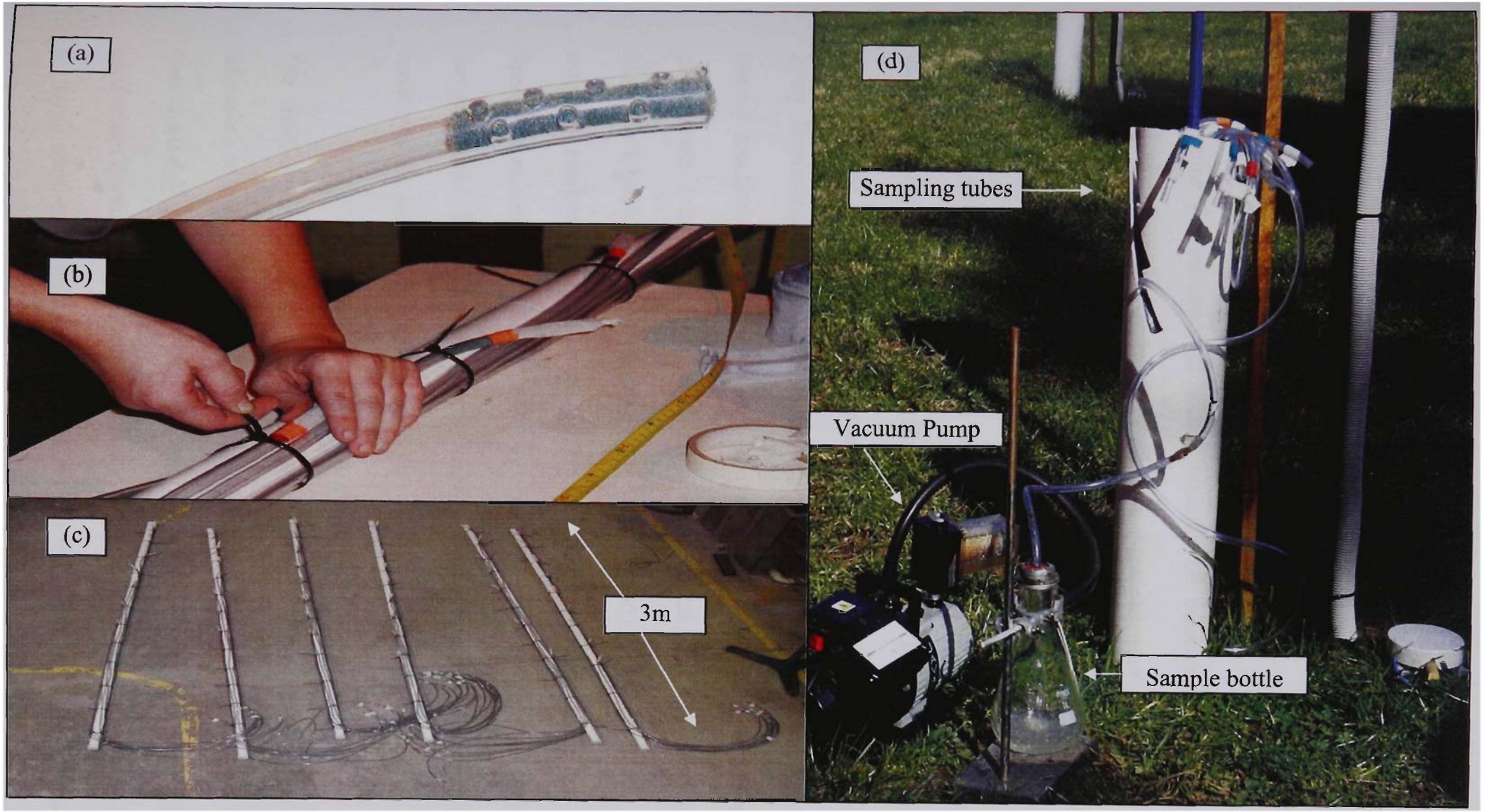

Figure 8.4 Photographs of multi-level piezometers including: (a) sampling nozzle, (b) attachment of individual ports, (c) completed units, and (d) sampling equipment after installation.

zone was calculated by submersible water pressure sensors installed in open standpipe piezometers located adjacent to the multi-port piezometers.

To determine the influence of saline intrusion on nutrient release, total dissolved phosphorous and total dissolved nitrogen concentrations were measured. Within soil, phosphorous is generally found adsorbed to clay particles or as a precipitate with aluminium or iron ions. Similarly, under low pH conditions, nitrogen is typically retained as nitrate or in the form of NH_4 (under high redox conditions), and is unavailable for plant uptake when adsorbed to the clay particle. To establish their concentrations in soil, total phosphorous and water-soluble nitrate were analysed using X-ray fluorescence and an automated colorimetric procedure based on the Griess-Ilosvay reaction, respectively. Furthermore, dissolved reactive phosphorous in the groundwater is immediately available for biological uptake and was measured using the Stannous Chloride Method described in APHA (1985). Soluble nitrate is also an essential nutrient for vegetation growth and was measured using the Ultraviolet Spectrophotometric Screening Method detailed by Valderrama (1981). The Environmental Protection Authority Chemical Laboratories in Lidcombe, NSW, conducted the analytical procedure.

The multi-level piezometers were installed along transect E (see Figure 4.1 for reference) at 1, 2, 4, 8, 16, and 32 m from the drain. Sampling was conducted weekly over a 60-day period from Day 892 to Day 952. The majority of sampling was undertaken during the flood tide, but, due to the time consuming nature of the study and the large number of multi-port piezometers (54 total), sampling from the piezometers often lasted more than 6 hours. Therefore, to avoid samples being influenced by the

tidal cycle, groundwater sampling was always commenced at a location closest to the drain (i.e., at piezometer E1), and, at the beginning and end of each monitoring period, a representative surface water sample was obtained from the drain.

The study trial was conducted during a prolonged dry period. Total rainfall over the 60-day trial was only 68.2 mm in comparison with the long-term average of 245 mm. In addition, the majority of the rainfall was concentrated into one event of 31.4 mm on Day 900. Evapotranspiration over the same period was calculated at 90.5 mm, indicating that groundwater recharge was primarily from drain water seepage. As this increased the likelihood of saline intrusion into the soil matrix, these conditions were deemed optimal to determine its impact on groundwater chemistry.

8.3.2 Results and discussion

The results from the tests were adjusted for changes in surface elevation and incorporated into contour plots based on concentrations. The kriging technique was employed to interpolate across the cross-sectional area because of the high number of samples in the lateral and vertical plane. As this research has not previously been undertaken with *in situ* acid sulphate soils, these findings were contrasted with the aforementioned microcosm experiments conducted by Portnoy and Giblin (1997a, 1997b, and 1999). Plotted results are limited to weeks 1, 3, 5, and 7, however, the remaining data can be found in Appendix B.

8.3.2.1 Electrical conductivity

Electrical conductivity (EC) was used as a measure of saline intrusion due its strong positive correlation (r^2= 0.81) with chloride concentrations. As shown in Figure 8.5,

during the trial period the intrusion zone (denoted by elevated EC measurements) was restricted to 8 m perpendicular to the drain. This is in line with previous data and indicates that the lateral hydraulic conductivity in the soil is sufficiently low to minimise the threat of saline contamination. In addition, the intrusion of chloride salts in a sub-surface wedge limits the impact of salts on agricultural productivity, and, EC readings above 4.5 mS cm^{-1} (the recommended ANZECC guideline for agricultural productivity) were maintained 2 m below the surface.

Fluctuations in groundwater EC during the study were attributed to variations in the hydraulic gradient and boundary salinity concentrations. Differences in the maximum drain water height were due to the natural variance in the tidal cycle (i.e. neap and spring tides), and, as shown in Figure 7.18, the changes in drain water elevation influenced the hydraulic gradient; stronger tides during Weeks 3 and 7 increased advection rates and saline wedge penetration. The salinity concentration at the tidal boundary also increased after rainfall on Day 900, with drain water EC peaking at 29.6 mS cm^{-1} on Day 950. Considering that groundwater EC did not progressively increase with drain water EC, it can be assumed that the mechanism of contaminant transport (i.e. advection or dispersion) is more influential on saline intrusion than the boundary concentration. This is significant to drain management because it demonstrates that restricting surface water height (i.e. by the installation of 'Smart Gate' systems) is more important than controlling drain water salinity.

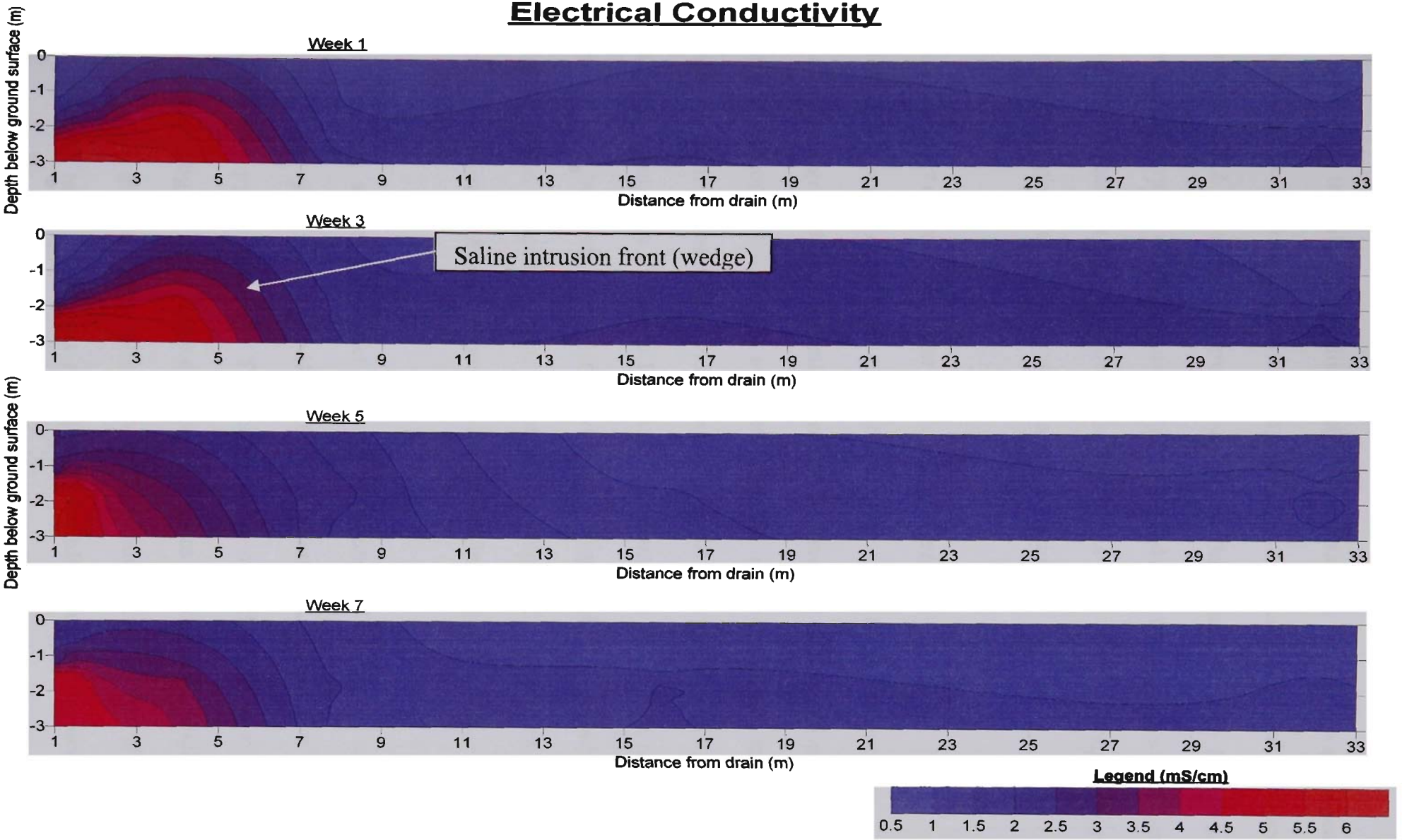

Figure 8.5 Multi-level electrical conductivity values (in mS cm^{-1}).

In addition to the subsurface saline wedge on the drainage boundary, a small peak in EC 16 m from the drain is also worth noting. This increase was likely due to the sandy soil lense found 2 m below the ground surface at this location. The higher hydraulic conductivity values commonly associated with sandy stratums enhance pyrite oxidation, and the increase in EC measurements within this layer were attributed to increased dissolved sulphate, aluminium, and iron concentrations.

8.3.2.2 Impact of saline intrusion on groundwater pH

While not discernible through conventional observation bores, the influence of saline buffering on groundwater oxidation products was marked using multi-port piezometers. Saline intrusion fostered slight acid neutralisation on Weeks 2, 3, 6, and 8, and strong buffering during Weeks 4, 5, and 7 (Selected weeks shown in Figure 8.6). Overall, the buffering extent was limited to less than 2 m inland and below 2 m from the surface. Groundwater buffering was most pronounced during Week 7, which coincided with the highest saline intrusion extent, thereby indicating that elevated EC concentrations within the saline wedge correspond with increased buffering potential.

Areas of high acidity were most apparent 2 m inland and around the sandy lense 16 m inland. The pocket of low pH (<4.0) 2 m inland was likely due to the previous oxidation of pyritic material. The accumulation of acid products within this area is further investigated using finite element simulations in Chapter 9. Slightly elevated pH levels with distance (i.e. >28m) from the drain were associated with a stable groundwater table, which was not as strongly influenced by the drainage boundary conditions.

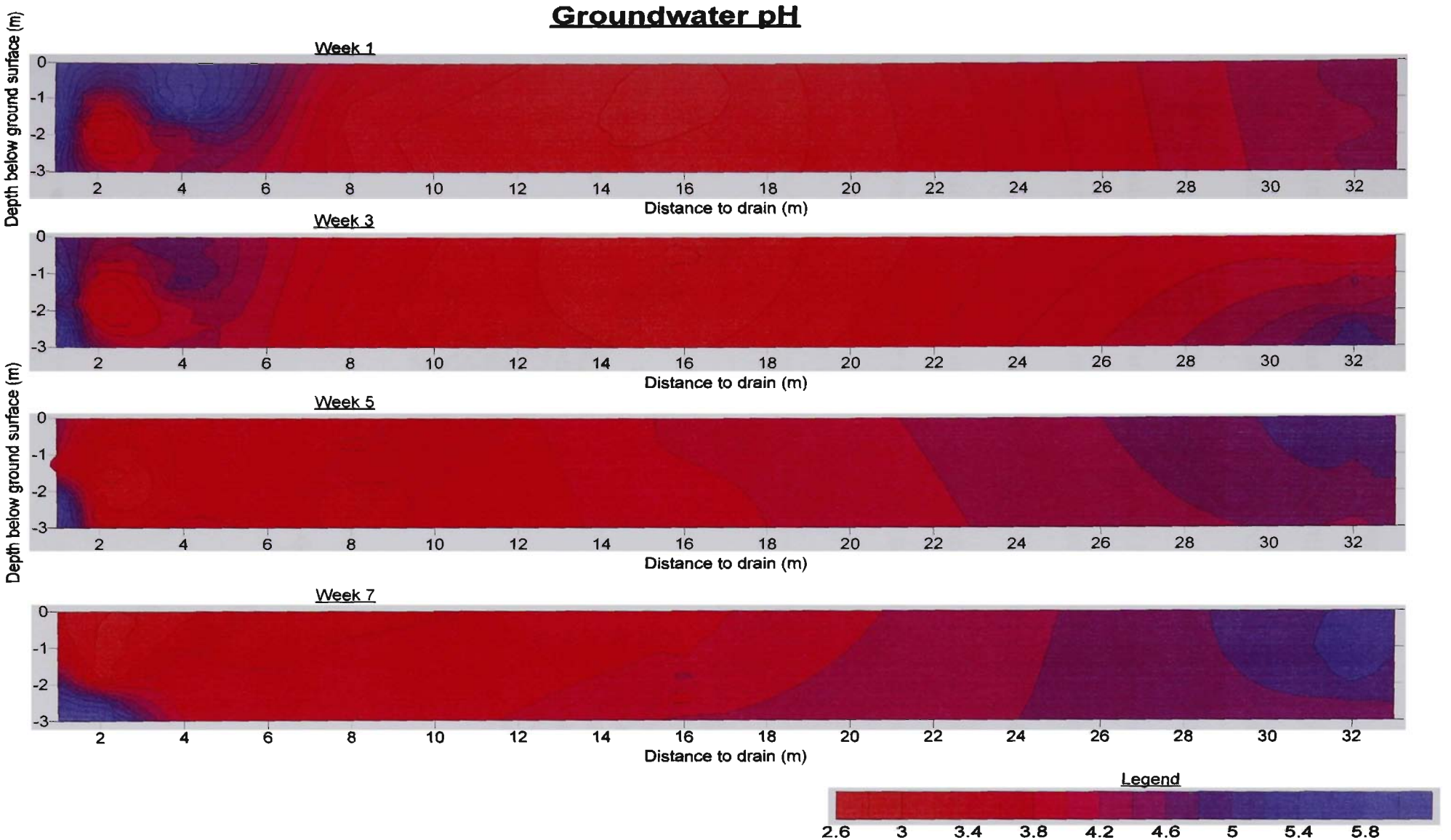

Figure 8.6 Multi-level groundwater pH values.

8.3.2.3 Influence of saline intrusion on redox potential

Redox potential (Eh) is a measure of the potential for water to be either in an oxidised or reduced state. In acid sulphate soil environments, high Eh measurements indicate the potential for pyrite oxidation, and low Eh measurements are favourable for the reduction of sulphate to either innocuous H_2S or FeS_2. Previous researchers (Bear *et al.*, 1999) have reported low Eh readings associated with saline intrusion due to organic decomposition and the poor ability of oxygen to remain dissolved in water under high saline concentrations. However, limited information is available on research involving both redox potential and saline intrusion in acid sulphate soil environments.

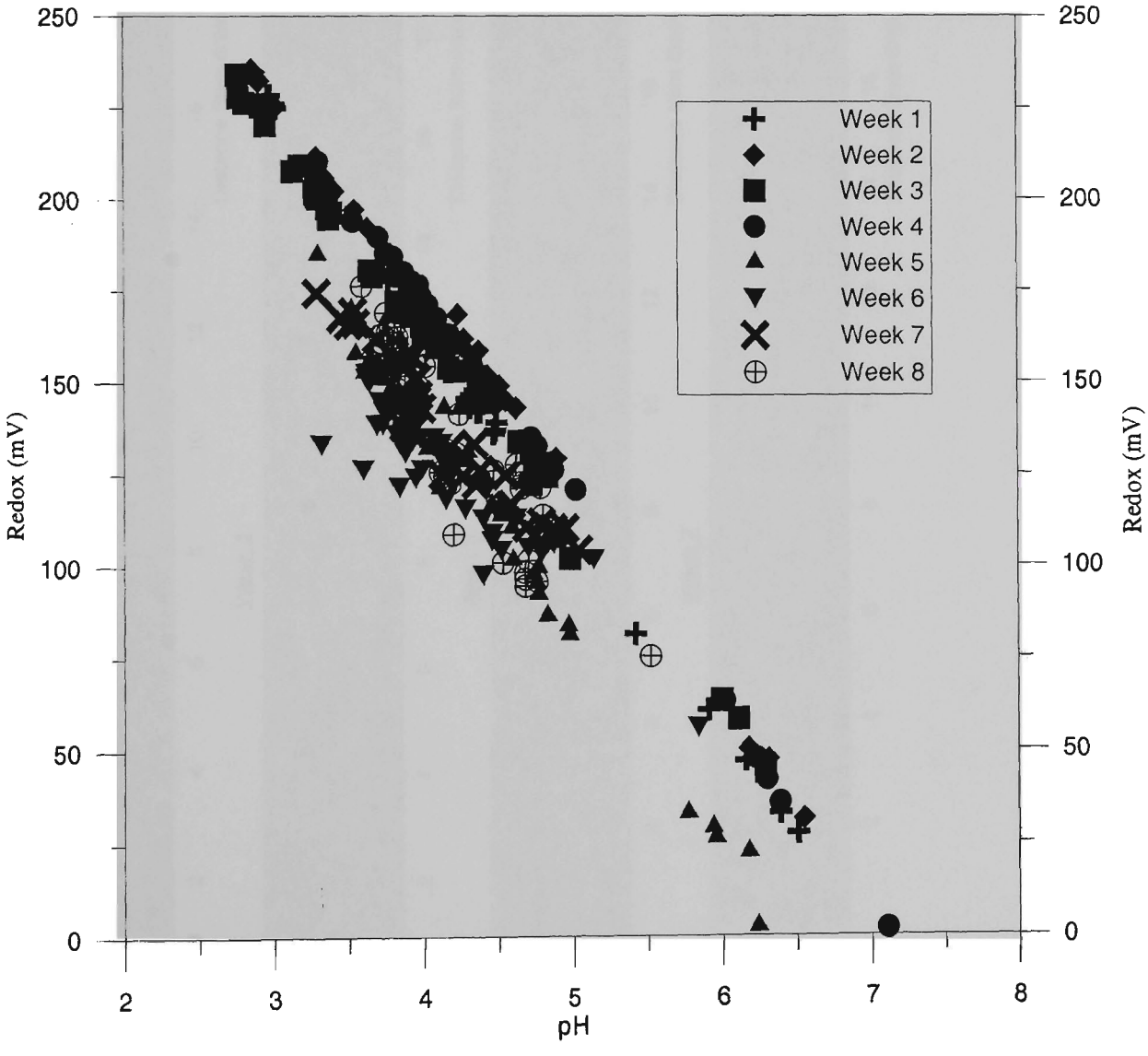

Figure 8.7 pH and redox values during study period.

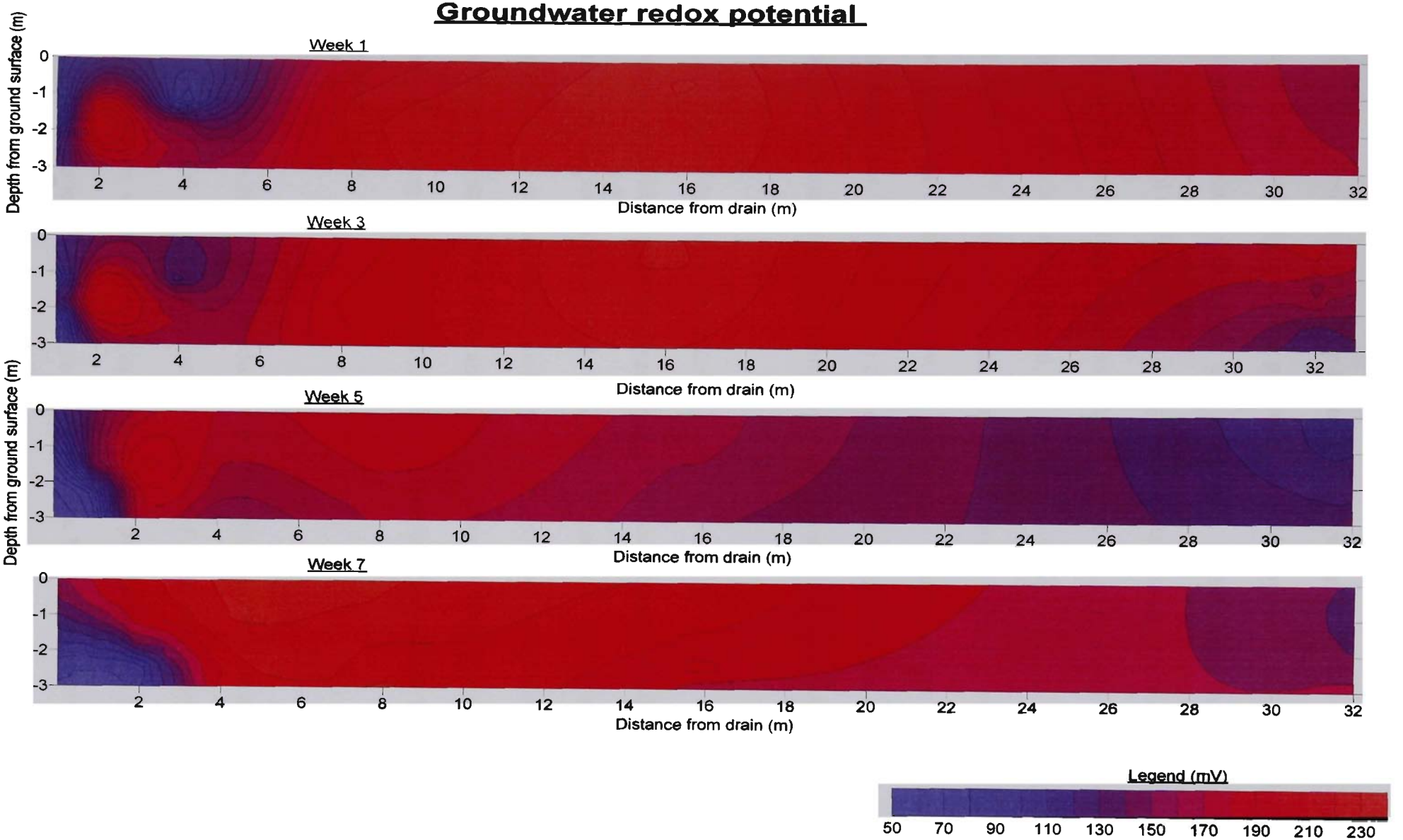

Figure 8.8 Multi-level redox concentrations (in mV).

The strong positive relationship between redox potential and pH readings (Figure 8.7), suggests that acid generation is primarily caused by pyrite oxidation and that a decrease in redox potential will reduce acid production. This was further confirmed by high redox potential readings at the two acidic hotspots (2 m and 16 m inland). To this point, Figure 8.8 shows that low redox measurements were primarily recorded in areas of intense saline intrusion. Indeed, the lowest redox measurements were recorded during Weeks 4 and 7 when saline intrusion was the strongest, but the extent of the low redox measurements was limited with distance. Moreover, the decreased sulphate concentrations, and the reduced capacity for pyrite oxidation due to reducing conditions fostered by saline intrusion, is an additional advantage of tidal restoration.

8.3.2.4 Saline influence on oxidation products

Portnoy and Giblin (1997a) suggest that the lateral intrusion of saline contaminants will influence the solubility of sulphate, aluminium and iron. However, at the study site the limited saline intrusion front meant that changes in solubility were restricted to within the first 8 m inland from the drain. The concentration of dissolved sulphate, aluminium and iron during the trial period is given in Figures 8.9, 8.10 and 8.11, respectively and detailed below.

Soluble sulphate is both a product of pyrite oxidation and a significant component of seawater (2700 mg L^{-1} in seawater). Because of these two sources, abundant sulphate concentrations were measured in areas of high pyrite oxidation (i.e. 16 m inland) and within the saline intrusion wedge. Moreover, the high concentrations of sulphate within the saline wedge differed with previous experiments conducted by Portnoy and Giblin (1997), which found that saline flushing of soil with high soluble iron content

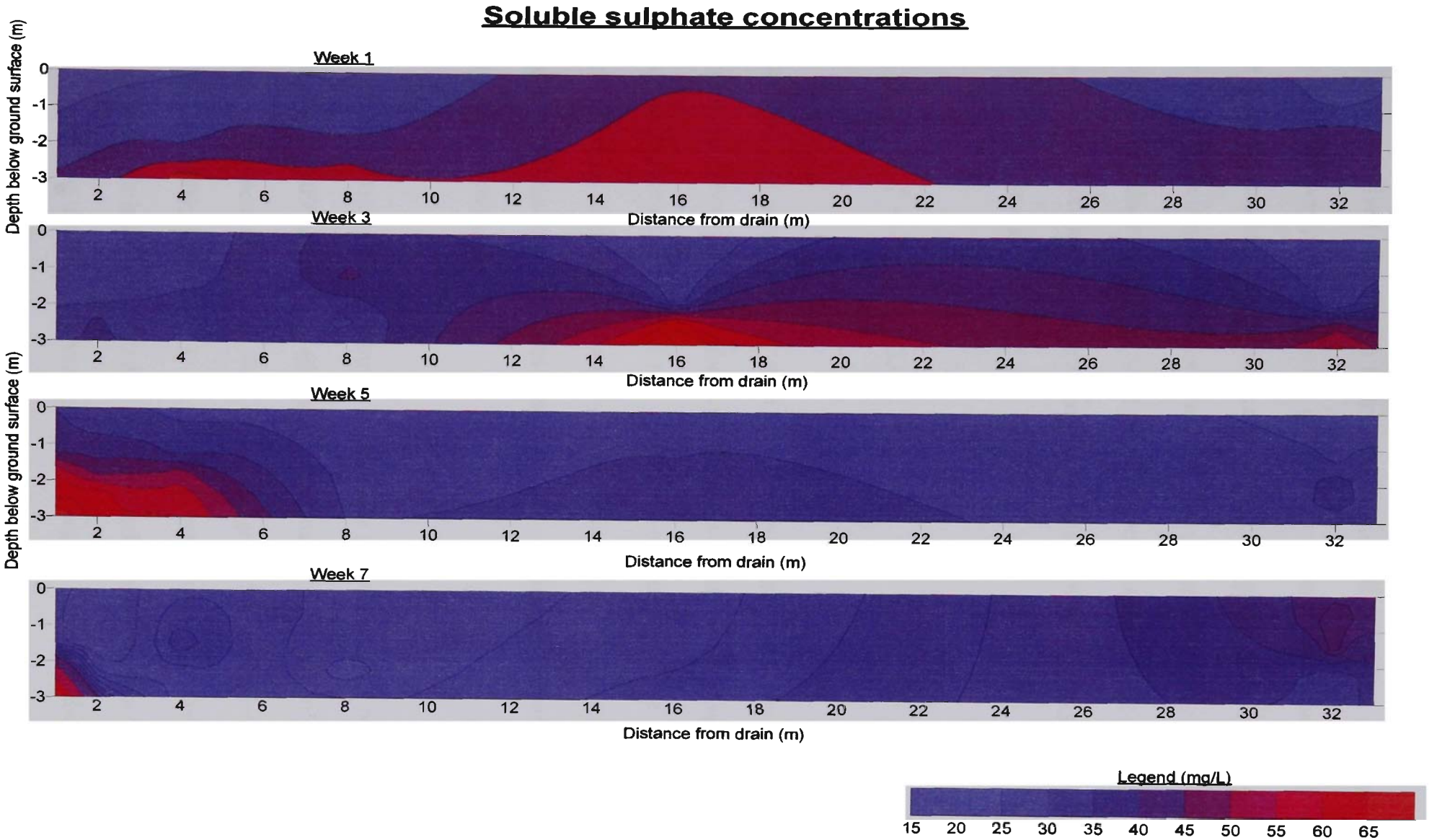

Figure 8.9 Multi-level dissolved sulphate values (in mg L^{-1}).

reduced dissolved sulphate to hydrogen sulphide (H_2S) or iron sulphide (FeS_2). This dissimilarity was partly due to the difference in redox conditions (>0mV) attributed to the transient nature of the groundwater regime, and partly to the low organic content of the soil. In their microcosm experiments, Portnoy and Giblin (1997) reported that the majority of reduced sulphates were found in surface soils with abundant organic matter. Sulphate reduction is more pronounced in regions with high organic content and low redox conditions, as expressed by:

$$2CH_2O + SO_4^{-2} \rightarrow H_2S + 2HCO_3^- \quad (8.1)$$

Therefore, by saturating the pore space with saline water but not simulating tidal movements, Portnoy and Giblin (1997) influenced organic decomposition. These stagnant conditions promoted low redox measurements and the reduction of sulphate ions. Further research is necessary to determine if saline intrusion in soils with high lateral hydraulic conductivities, and thus, more extensive saline fronts, will undergo sulphate reduction.

Within the solid phase, aluminium is primarily found (i) bound to the cation exchange complex (> 90% saturation), (ii) as Al minerals, and (iii) within aluminosilicate clays. While dissolved aluminium does not undergo redox reactions, several researchers (Blunden, 2000; Indraratna *et al.*, 1995) have shown that dissolved aluminium in groundwater is inversely related to pH. This relationship was further confirmed in this study with low aluminium concentrations primarily located within the saline intrusion wedge. This is in contrast with Portnoy and Giblin's (1997) findings, which suggest that tidal flushing increases dissolved Al concentrations due to cation

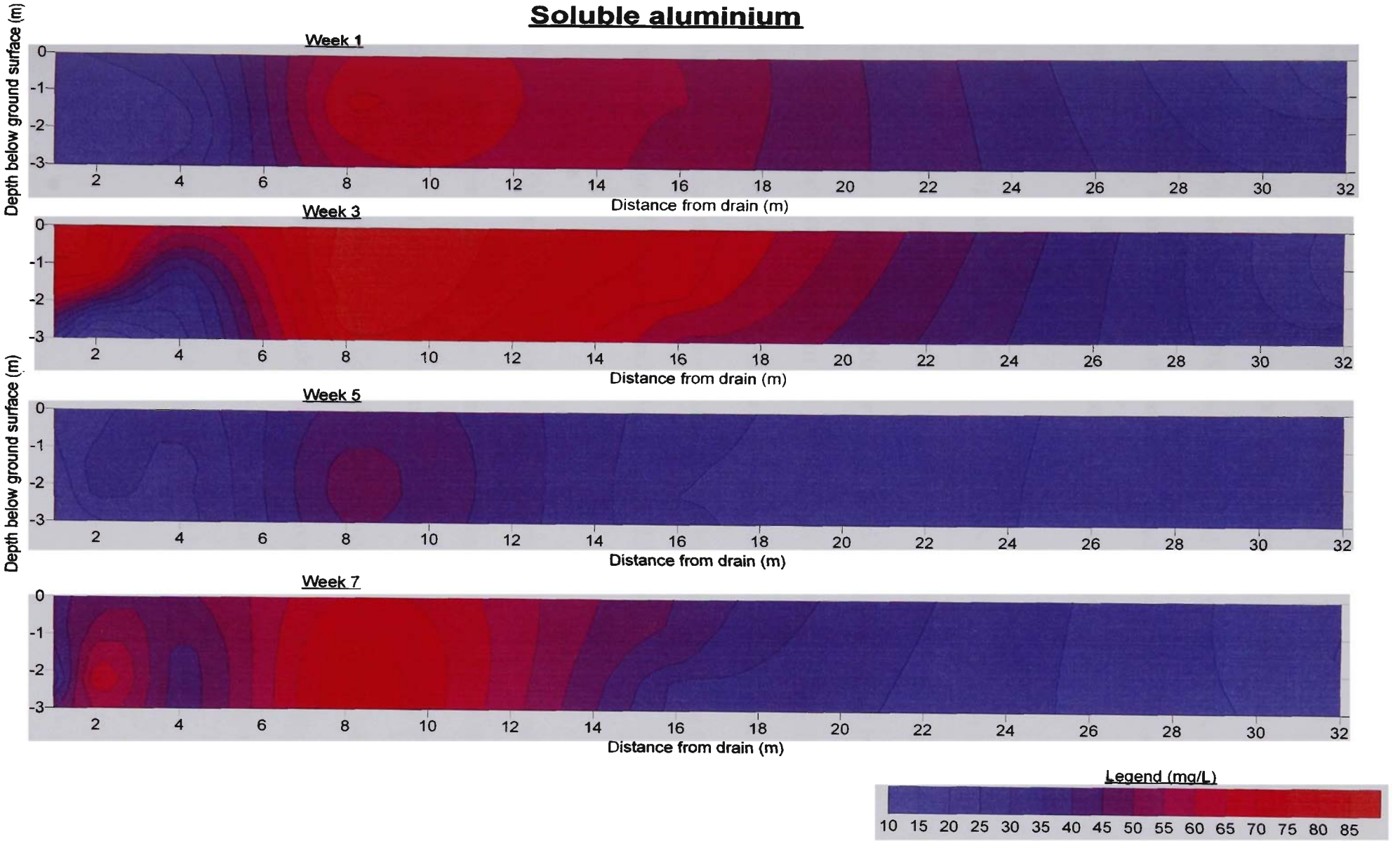

Figure 8.10 Multi-level dissolved aluminium concentrations (in mg L^{-1}).

exchange of the sorbed metal with highly ionic drain water and the dissolution of Al phosphates under reducing conditions. In contrast, the results presented here are in agreement with Nordstrom (1982) who proposed that the solubility of Al is primarily controlled by alunite. Since the saturation indices for alunite increase with pH and redox potential, soluble aluminium concentrations should decrease with saline intrusion.

Similar to sulphate concentrations, total dissolved iron is both a product of pyrite oxidation and susceptible to redox reactions. Figure 8.11 indicates that total iron concentrations increased with distance from the drain due to the fall in the groundwater table with distance away from the groundwater recharge boundary (i.e. drain), and subsequent pyrite oxidation. Furthermore, while soluble iron decreased in proximity to the saline wedge, this decline was not as perceptible as in aluminium concentrations due to the influence of reducing conditions on iron solubility.

Portnoy and Giblin (1997) proposed that seawater would increase total dissolved iron solubility because its high ionic strength promotes the exchange of Fe (II) sorbed onto clay particles, and sulphate reduction lowers Eh which promotes Fe (III) reduction and dissolution. However, at the field site aluminium is the primary ion sorbed onto the clay particles, and sulphate reduction was not reported. Therefore, as long as levee overtopping is restricted and saline water is not permitted within the top sediment, soluble iron concentrations will not be influenced by saline intrusion.

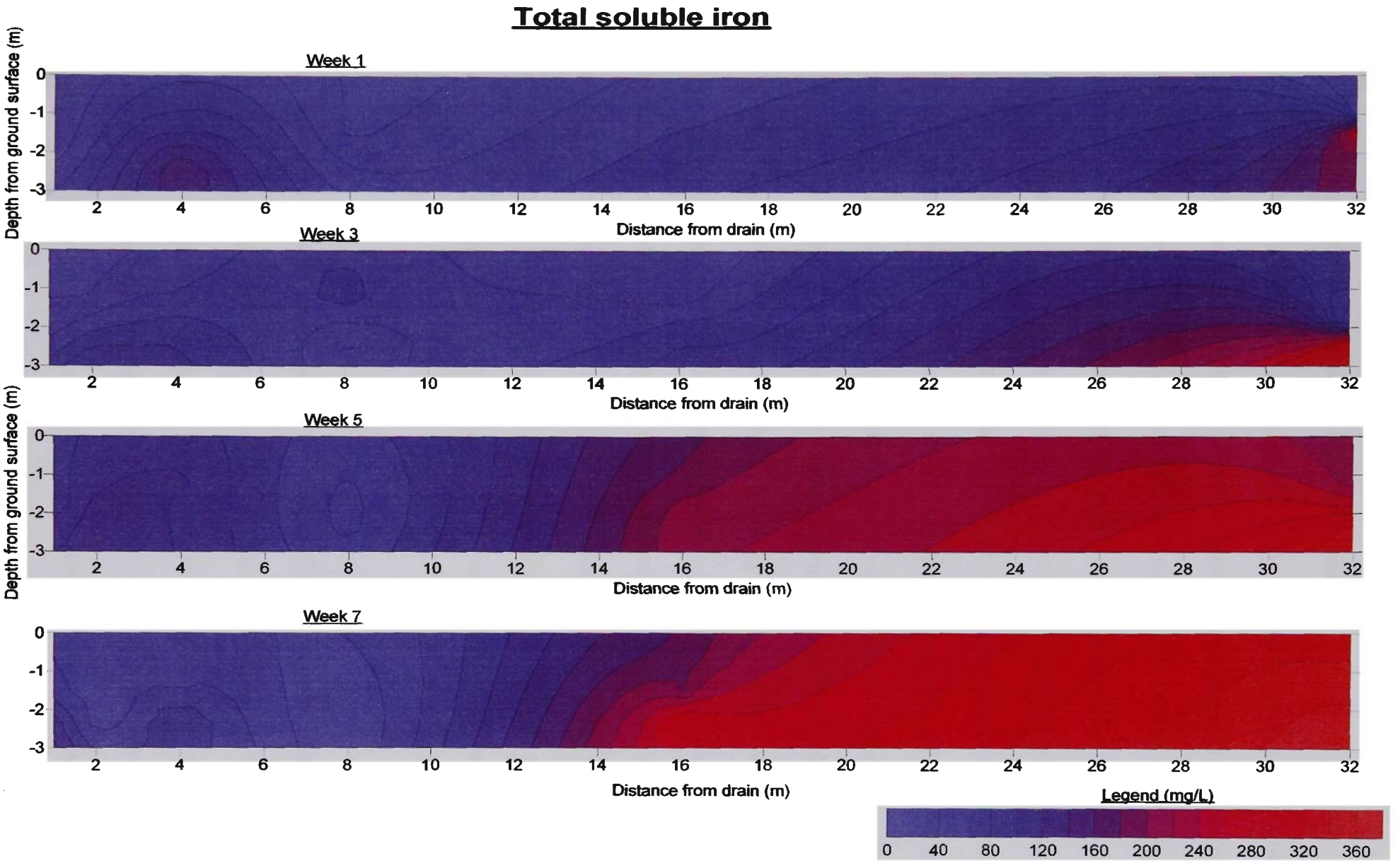

Figure 8.11 Multi-level dissolved iron concentrations (in mg L^{-1}).

8.3.2.5 Influence of saline intrusion on nutrient release

Portnoy and Giblin (1997) studied the impact of seawater flooding on nutrient release in acid sulphate soil sediments and reported that in microcosms experiments with seawater percolation from the surface, soluble nitrates increased 60-fold and dissolved inorganic phosphates increased 20-fold. The retention of N in acidic soils before saline flushing is due to consistently low pH levels inhibiting both nitrification and volatilisation losses of NH_x-N released by aerobic mineralisation. Inorganic P is retained within the soil as Fe and Al phosphates formed at low pH (Dent, 1986). Phosphorous can also be sourced through the application of super-orthophosphates fertilizers applied to stimulate agricultural productivity. Portnoy and Giblin assumed that nutrient release was due to cation exchange with highly ionic waters, declining redox potential, and the reduction of Fe (III) minerals from sulphide precipitation. Though the increase in dissolved nutrients may be beneficial to plant uptake, the accumulation of excess nutrients in receiving waters may cause eutrophication problems. Therefore, one aim of this study was to determine the interaction of nutrients bound within the soil with saline contaminated groundwater and to ascertain if saline intrusion increases nutrient solubility.

Concentrations of total nitrates within the soil profile are given in Table 8.3. Overall, nitrate concentrations across the study site were below 12 mg/kg in both the affected and unaffected zones. While this may be an indication that the majority of nitrates were mobilised within the groundwater, Figure 8.12 shows that soluble nitrates are generally low across the study site. Interestingly, higher concentrations of nitrates were recorded in highly acidic areas, such as the sandy lense at 16 m inland. Nitrates are less likely to adsorb to sandy soils than clays, which explains the peak concentrations in Week 4.

The difference between this study and Portnoy and Giblin's results was attributed to the various forms of dissolved nitrogen and the saline intrusion regime. Under high redox potentials and low pH values, nitrogen complexes with iron and aluminium to form precipitates. Similarly, under high redox values dissolved nitrogen is commonly found as ammonium (NH_4). As it was assumed that saline intrusion would reduce redox potential, high redox potential species such as ammonium were not investigated, and hence, would not of been detected during testing. Furthermore, Portnoy and Giblin (1997) simulated saline intrusion by directly adding seawater to the surface of the testing columns. This application method would have a different influence on the biogeochemical reactions because of the increased organic content in the topsoil. Saline intrusion under a lateral sub-surface wedge does not sufficiently decrease the redox potential and, as with sulphate ions, may not of been sufficient to solubilize nitrogen minerals.

Table 8.3 Concentration of total nitrates and total phosphorus adsorbed to the soil.

	Total Nitrates			Total Phosphates		
Depth (m)	**1m inland**	**4m inland**	**16m inland**	**1m inland**	**4m inland**	**16m inland**
0.0-0.5	<12	16	<12	1200	850	130
0.5-1.0	<12	<12	<12	1400	1200	50
1.0-2.0	<12	<12	<12	300	210	140
2.0-3.0	<12	<12	<12	230	220	170

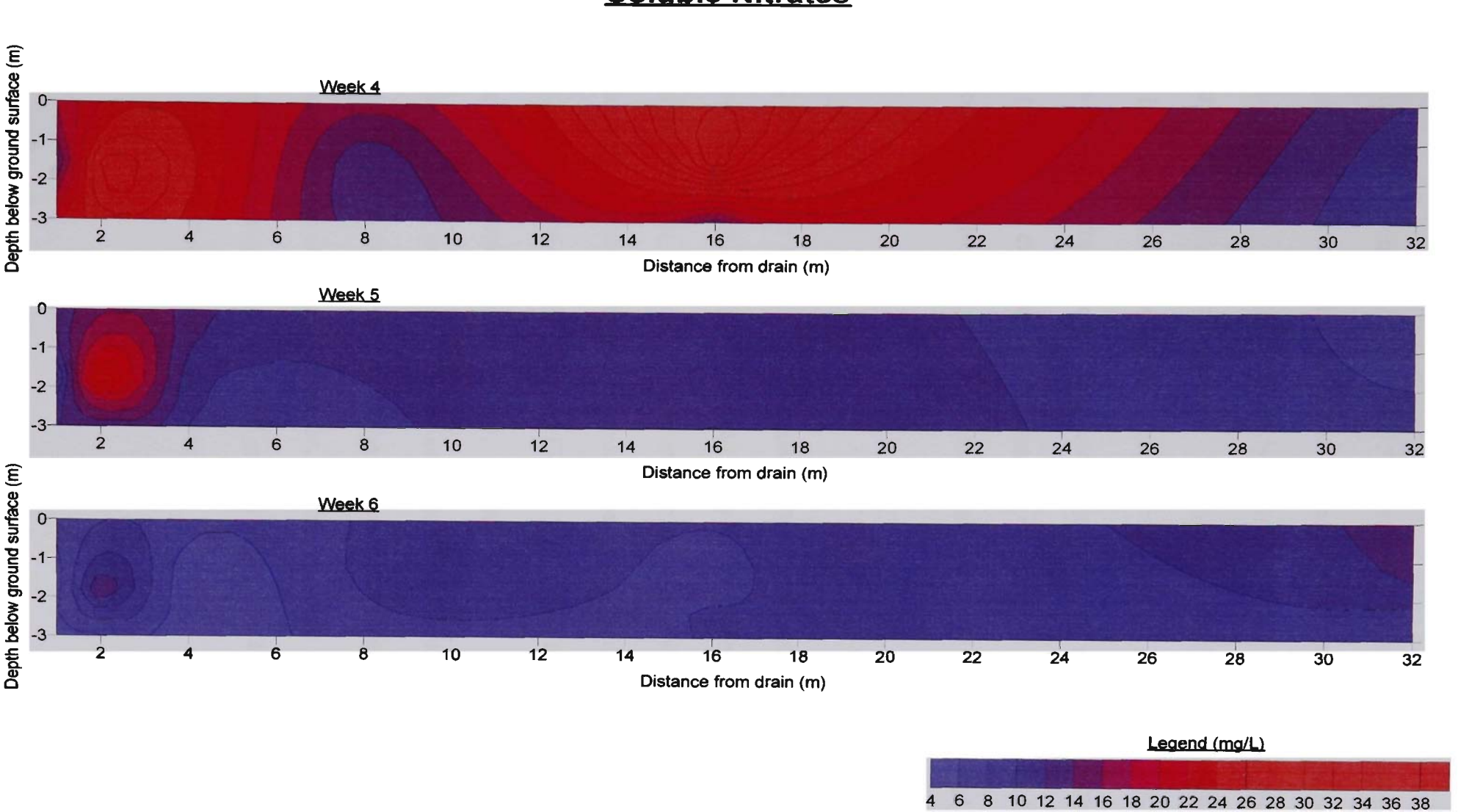

Figure 8.12 Multi-level dissolved nitrate concentrations over selected weeks (in mg L^{-1}).

Laboratory measurements (Table 8.3) indicate that higher concentrations of total phosphorous were adsorbed to the soil in the saline zone than in the region not affected by saline intrusion. This was particularly evident in the top 1 m of the soil profile and was attributed to agricultural practices. For instance, within this paddock the first 10 meters inland from the drain are not cultivated, whereas the remainder of the paddock is sown with a new crop (predominately clover or rye grass) every year. Tilling the soil within the paddock enhances the mobilisation of dissolved phosphorous, but since the perimeter is not tilled, total phosphorous concentrations remain bound to the soil colloid.

Groundwater results showed that inorganic phosphorous concentrations (Figure 8.13) were less than 2 mg L^{-1} across the field site and not correlated with saline intrusion. Throughout the test, the highest readings were recorded within the sandy lense 16m inland and were similar to nitrate contour maps. These results are in contrast with the 20-fold increase found by Portnoy and Giblin (1997), and depict a 10-fold decrease in dissolved phosphorous. Nonetheless, considering that phosphorous solubility is dependant on redox potential, if the saline intrusion front was to overtop the levee bank and inundate the surface layers, it can be presumed that the concentration of dissolved phosphorous would increase. However, as long as drain water height is controlled, dissolved phosphate concentrations will remain below ANZECC (1992) criteria, and not cause a significant threat to receiving waters.

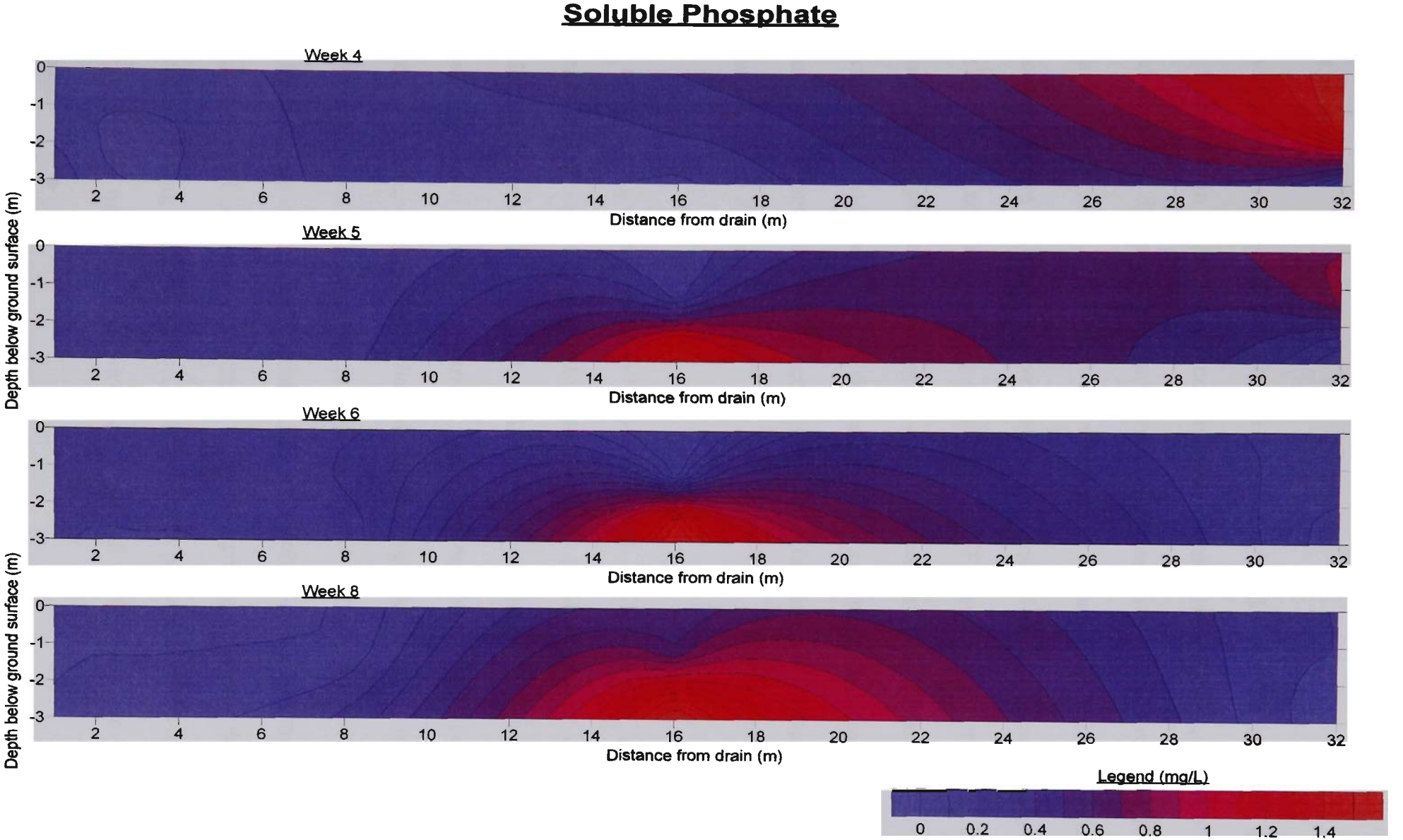

Figure 8.13 Multi-level dissolved inorganic phosphate concentrations from selected sampling weeks (in mg L^{-1}).

8.4 Summary

The results discussed in this Chapter indicate that tidal restoration within the flood mitigation drain caused saline contaminants to intrude into the soil matrix through hydrodynamic dispersion and advection. Increases in soil salinity were limited to samples taken close to the drain and were not in excess of ANZECC guidelines. As shown in Figure 8.5, the intrusion plume was characteristic of a saline wedge bounded by a transition zone rather then a sharp interface. Furthermore, the transition zone was limited to 8 m perpendicular from the drain and remained predominately 2 m below the surface. The transient nature of the saline wedge and the limited contamination plume illustrate that agricultural productivity on the surface should not be affected by tidal flushing within the drain.

In contrast to the findings of Portnoy and Giblin (1997a and 1997b), extensive field measurements indicated that saline intrusion did not increase the quantity of pyrite oxidation products. Within the saline transition zone, pH increased due to the neutralisation of H^+ ions by surface water bicarbonates. Redox potential decreased within the saline wedge due to the inability of oxygen to remain in solution under high saline conditions and the decomposition of organic matter. Increased pH and reduced redox levels decreased soluble aluminium and sulphate concentrations, but did not alter total dissolved iron concentrations. Oxidation products outside the transition zone increased during the study period, and significant pockets of dissolved aluminium and sulphate were measured within a sandy lense and on the landward side of the saline wedge.

In contrast to previous findings, the concentration of dissolved nutrients did not change with increased salinity. While useful in understanding the potential for biogeochemical evolution, the microcosm experiments conducted by Portnoy and Giblin (1997) were not deemed applicable to *in-situ* conditions where saline intrusion is via lateral advection and dispersion forces. Nonetheless, further research is necessary to determine the influence of saline overtopping on nutrient release on *in situ* conditions.

The study trials described in this chapter illustrate that saline intrusion due to altered drain hydrology is limited, and does not adversely influence agricultural productivity. However, this study does not demonstrate the worst-case scenario or depict the response of saline intrusion to large rainfalls. Additionally, while the 2-dimensional figures provide original and detailed description of biogeochemical reactions within acid sulphate soils, they do not shed light on the impact of varying lateral hydraulic conductivity within the soil matrix. This is important as the hydraulic conductivity of the soil can differ, based on the degree of pyrite oxidation and soil development.

To ascertain the impact of saline intrusion over varying climatic and geophysical conditions, a 3-dimensional finite element model was developed. The primary aim of the model was to determine the extent and magnitude of saline intrusion in a worst-case scenario and in response to rainfall events. The model, discussed in the following Chapter, was developed as a predictive tool to quantify the influence of varying lateral hydraulic conductivity on saline intrusion, and highlight the maximum thresholds for restoring tidal intrusion based on physical soil properties.

Chapter 9.0 Numerical Modelling of Saline Intrusion: Maximum Tidal Intrusion and the Influence of Lateral Soil Hydraulic Conductivity

9.1 Introduction

In-depth field testing presented in Chapter 8 illustrated that saline intrusion was prevalent across the study site as a sub-surface saline intrusion front. This Chapter further examines the sub-surface extent and distribution of saline contaminants under varied climatic conditions and soil material properties using a finite element simulation. The coupled flow and transport of saline contaminates into the soil matrix is simulated using a 3-dimensional (3D) finite element model for variably saturated media, FEMWATER, originally developed by Lin *et al.* (1997). The model requires a broad range of initialisation parameters including environmental, climatic and hydraulic information. The climatic and drain water conditions, detailed in Chapter 3, were used as inputs for the surface and drain water boundary conditions. Physical soil properties were sourced from extensive field tests presented in Chapter 4 and previously referenced literature from acid sulphate soil sites within NSW. Once the model was initialised and calibrated, several environmental scenarios were simulated to analyse the saline intrusion process.

Within the first section of this chapter, the background to the numerical model is described, including relevant governing equations and various modifications to the source code. In the second section, material properties and boundary conditions are detailed with reference to the extensive data inputs. The model calibration procedure is then examined and a fourth boundary is introduced to assist in groundwater seepage analysis. Once calibrated, the model is run to simulate the influence of prolonged dry

periods and natural groundwater recharge on the intrusion front. Finally, a series of simulations were performed to calculate the effect of varied lateral soil hydraulic conductivity values on saline ingress. The outputs from the numerical simulations were incorporated into a comprehensive groundwater management plan, which details the effectiveness of different strategies based on the hydraulic conductivity of the soil.

9.2 Method and materials

9.2.1 Flow and transport in FEMWATER

FEMWATER was designed to describe flow and transport through saturated-unsaturated porous media by solving a system of governing equations with initial and boundary conditions. The governing equation for flow was given in Chapter 2 (Equation 2.25), and is derived from the modified Richards equation. Hydraulic conductivity, a key component of this equation, is given by:

$$K = \frac{\rho g}{\mu} k = \frac{(\rho/\rho_o)}{(\mu/\mu_o)} \frac{\rho_o g}{\mu_o} k_s k_r = \frac{\rho/\rho_o}{\mu/\mu_o} K_{so} k_r \qquad (9.1)$$

where, μ = dynamic viscosity of water at chemical concentration C, μ_o = referenced dynamic viscosity at zero chemical concentration, k = permeability, k_s = saturated permeability tensor, k_r = relative permeability or relative hydraulic conductivity, K_{so} = referenced saturated hydraulic conductivity tensor, ρ = water density at chemical concentration C, and ρ_o = referenced water density at zero chemical concentration.

The dynamic viscosity and density of water are functions of chemical concentrations and are assumed to take the following form:

$$\frac{\rho}{\rho_o} = a_1 + a_2 C + a_3 C^2 + a_4 C^3 \tag{9.2}$$

and

$$\mu \frac{\mu}{\mu} = a_5 + a_6 C + a_7 C^2 + a_8 C^3 \tag{9.3}$$

where, a_1, a_2,....a_8 are the parameters employed to define concentration dependence of water density and viscosity, and C is the chemical concentration.

Darcy velocity is determined as:

$$V = -K \cdot \left(\frac{\rho_o}{\rho} \nabla h + \nabla z \right) \tag{9.4}$$

Initial conditions for the flow equation are given by:

$$h = h_i \, (x, y, z) \text{ in } R \tag{9.5}$$

where, R is the region of interest and h_i is the prescribed initial condition that was obtained by field measurements.

The processes governing transport include advection, dispersion/diffusion, adsorption, decay, biodegradation, and source/sink. The governing equation for transport is derived

based on the continuity of mass and flux laws. The governing equation is (Lin *et al.*, 1997):

$$\theta\frac{\partial C}{\partial t}+\rho_b\frac{\partial S}{\partial t}+V\cdot\nabla C-\nabla\cdot(\theta D\cdot\nabla C)=$$
$$-\left(\alpha'\frac{\partial h}{\partial t}+\lambda\right)(\theta C+\rho_b S)-(\theta K_w C+\rho_b K_s S)+ \qquad (9.6)$$
$$m-\frac{\rho^*}{\rho}qC+\left(F\frac{\partial h}{\partial t}+\frac{\rho_o}{\rho}V\cdot\nabla\left(\frac{\rho}{\rho_o}\right)-\frac{\partial\theta}{\partial t}\right)C$$

where,

$S = K_d C$ for linear isotherms,

$S = \frac{S_{max} KC}{1+KC}$ for Langmuir isotherms, and

$S = KC^n$ for Freundlich isotherms.

In the above equation, θ = moisture concentration, ρ_b = bulk density of the medium (M/L^3), C = material concentration in aqueous phase (M/L^3), S = material concentration in adsorbed phase (M/M), t = time, V = discharge, ∇ = del operator, D = dispersion of coefficient tensor, α' = compressibility of medium, h = pressure head, λ = decay constant, m = q C_{in} = artificial mass rate, q = source rate of water, C_{in} = material concentration in the source, K_w = first order biodegradation rate constant through dissolved phase, K_s = first order biodegradation rate through adsorbed phase, F = storage coefficient, S_{max} = maximum concentration of medium in the Langmuir nonlinear isotherm, n = power index in the Freundlich nonlinear isotherm, K = coefficient in the Langmuir or Freundlich nonlinear isotherm.

The dispersion coefficient tensor D in Equation 9.6 is given by:

$$\theta D = a_t |V| \delta + (a_L - a_T) \frac{VV}{|V|} + a_m \theta \tau \delta \tag{9.7}$$

where, $|V|$ = magnitude of V, δ = Kronecker delta tensor, a_T = lateral dispersivity, a_L = longitudal dispersivity, a_m = molecular diffusion coefficient, and τ = tortuosity.

Initial conditions for transport are given by:

$$C = C_i (x, y, z) \text{ in } R \tag{9.8}$$

where, R is the region of interest and C_i is the prescribed initial condition that was obtained by field measurements.

The governing flow equation, subject to initial and boundary conditions, is solved with the Galerkin finite element method. The governing transport equation, also subject to initial and boundary conditions, is solved with the hybrid Lagrangian-Eulerian finite element method. The derived equations and the implementation of numerical approximation of flow and transport problems are further described in detail by Lin *et al.* (1997).

The FEMWATER model is limited in its ability to model large-scale real-time parameter inputs. To overcome these limitations, the FORTRAN code was customised to function within the broad ranging design and field parameters required for flow and

transport of saline contaminants in multi-layered ASS field sites. To incorporate these extensive boundary conditions, a range of modifications were undertaken which include changing the boundary constraints (i.e. the maximum number of data points on each flux rate profile), and the allowable number of nodal points. These modifications were made by grepping through the FORTRAN code for relevant parameters and then modifying the source code to fit the design parameters. The FORTRAN code was then recompiled using Digital Compaq Visual FORTRAN compiler for Windows. The numerical model required a range of modifications and a complete list of design parameters is given in Appendix E.

To determine the initial (steady-state) flow and transport conditions, groundwater data from the study site were incorporated into the model, and an iterative method was used to solve for steady state conditions. This approach begins with an initial estimate of pressure heads and concentrations based on piezometer readings, and then utilises an iterative solver to gradually modify the initial values until they converge to a set of values that satisfy the underlying governing equations. To increase accuracy and model stability, a steady-state simulation was first performed with static boundary conditions and then the simulation output was used as the initial condition for further coupled transient simulations.

9.2.2 FEMWATER boundary and mesh conditions

FEMWATER offers a range of boundary conditions to cover the various environmental conditions encountered in finite element groundwater modelling. To deliver a concise discussion on the subject, only the boundary conditions relating to this study (Dirichlet, flux and variable) will be discussed.

The Dirichlet boundary condition is used when pressure heads or concentrations are known at a given location over the length of the simulation. The Dirichlet boundary is defined as:

$h = h_d (x_b, y_b, z_b, t)$ on B_d for flow equations, and (9.9)

$C = C_d (x_b, y_b, z_b)$ on B_d for transport equations. (9.10)

where, (x_b, y_b, z_b) = spatial coordinates on the boundary, h_d = Dirichlet functional value, B_d = Dirichlet boundary, and C_d = concentration on the Dirichlet boundary.

The Dirichlet boundary condition was employed to simulate flow and transport on the drainage boundary. This was appropriate because the boundary information was sourced from three submersible data loggers installed in the drain which continuously monitored surface water height and salinity at hourly intervals.

The variable boundary condition is generally used when modelling rainfall and evapotranspiration because it is the most robust and allows FEMWATER to change the boundary type to a specified head for both over- and undersaturated conditions. This condition is particularly applicable in transient simulations where the groundwater table fluctuates over the study period. The variable boundary condition is expressed as:

$h = h_p (x_b, y_b, z_b, t)$ on B_v, (9.11)

or

$$-n \cdot K \cdot \left(\frac{\rho_o}{\rho} \nabla h + \nabla z \right) = q_p (x_b, y_b, z_b, t) \text{ on } B_v \quad (9.12)$$

during precipitation periods, or

$$h = h_p\,(x_b, y_b, z_b, t) \text{ on } B_v \tag{9.13}$$

or

$$-n \cdot K \cdot \left(\frac{\rho_o}{\rho} \nabla h + \nabla z \right) = q_e(x_b, y_b, z_b, t) \text{ on } B_v \tag{9.14}$$

during non-precipitation periods.

In the above equation, B_v = variable boundary, h_p = ponding depth, q_p = throughfall of precipitation on the variable boundary, h_m = minimum pressure on the variable boundary, and q_e = evapotranspiration rate on the variable boundary.

The variable boundary condition was employed on the surface boundary to simulate rainfall/evapotranspiration. The climatic data was sourced from the weatherstation located at the field site and was presented in Chapter 3.

The specified flux boundary condition was used to simulate inflow/outflow conditions on the element face. This boundary condition is determined by:

$$-n \cdot K \cdot \left(\frac{\rho_o}{\rho} \nabla h + \nabla z \right) = q_c(x_b, y_b, z_b, t) \text{ on } B_c \tag{9.15}$$

where, q_c = flux value, and B_c = flux boundary.

The specified flux boundary was employed along the base of the model as a calibrating tool to simulate the inflow/outflow of water through the semi-permeable base.

9.2.3 Element types, solution scheme, and mesh generation

The computational discretization utilized by FEMWATER is a three-dimensional finite element mesh (Lin *et al.*, 1997). In this study, triangular prismatic elements (with 6 nodes, each with 3 degrees of freedom) were employed to model the volumetric domain. Individual elements were grouped together into zones representing different stratigraphic units. The typical geometry of an individual element is shown in Figure 9.1.

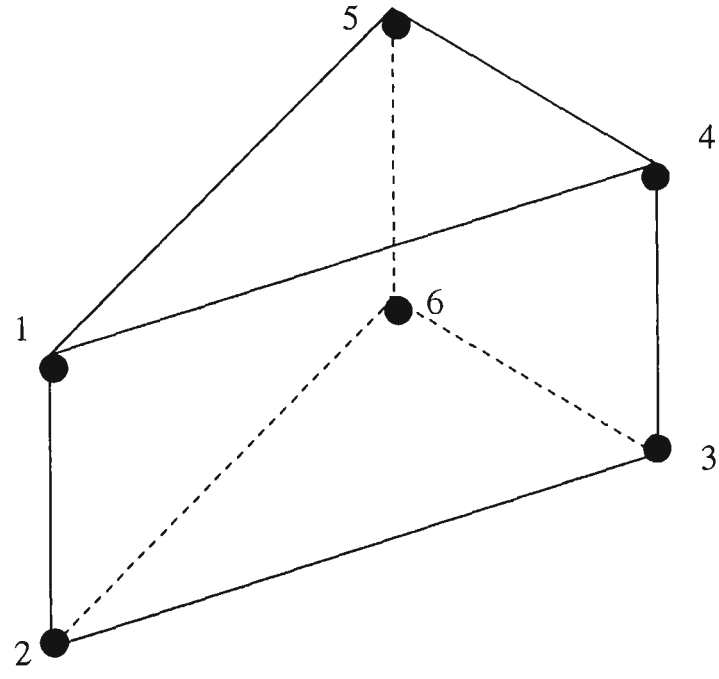

Figure 9.1 Diagram of prismatic element

At all nodes, the Galerkin finite element method was used to solve a non-linear flow equation because the hydraulic conductivity and the water capacity functions are derivatives of the pressure head. Furthermore, a pointwise iterative matrix solver was used in conjunction with a Gaussian quadrature scheme. The pointwise iterative solver uses the basic successive iterative method to solve the matrix equation, including the Gauss-Seidel method, and successive under-relaxation and successive over-relaxation techniques. While convergence may be slow when the matrix is diagonally dominant, the pointwise iterative solver provides a convergent solution. To compensate for the time factor, a maximum of 40 iterations were allowed for solving the non-linear flow equation or until a steady state convergence criteria of 10^{-3} was achieved.

The Langrangian-Eulerian finite element method was used by FEMWATER to solve the transport equation and all transport simulations were conducted in the transient mode. The Gaussian/Gaussian quadrature was used to integrate surface and element selections. The remaining analysis options, including coupled flow and transport parameters are given in Table 9.1.

Table 9.1 FEMWATER criterion for coupled flow and transport simulations.

Run Options:	Parameter:
Quadrature Selection:	Gaussian/Gaussian
Weighting Factor:	Backward Difference
Mass-Lumping:	Selected
Sorption model control (isotherm):	Linear
Type of Simulation:	Initially flow only, then Coupled flow and transport
Steady state or transient:	Initially steady state, then transient (with coupled simulation)
Relaxation parameter of non-linear flow and transport	1.0
Relaxation parameter for linearized for flow and transport	1.0
Solver selection:	Pointwise iterative matrix solver
Iteration Parameters (Flow simulations):	
Max. iterations for non-linear equation:	40
Max. cycles/time steps for variable BC:	10
Max. iterations for linear equations:	400
Steady-state convergence criterion:	0.0001 m
Transient convergence criterion:	0.0001 m
Iteration Parameters (Transport simulations):	
Max. iterations for non-linear equation:	40
Max. iterations for linear equations:	400
Convergence criterion:	0.001
Iteration Parameters (Flow and Transport simulations):	
Max. iterations:	10
Iteration parameter:	0.5
Convergence criterion for head:	0.01m
Convergence criterion of concentration:	0.05 mg/L

The 3-D finite element mesh was developed from a 2-D projection. First, a 2-D mesh was created based on the dimensions of the drain and the expected maximum extent of saline intrusion (150 m long by 30 m wide). The 2-D projection was then contoured by interpolating the surface elevation of the study site (obtained by airborne laser scanning) to the surface layer of the 2-D mesh. The external boundary conditions and the number and distribution of elements were determined based on flow and transport concerns. Fine mesh spacing was located nearest the drain boundary and element size progressively increased with distance from the drain. Once the 2-D mesh was

developed, vertical element spacing was extruded from the mesh to form the 3-D stratigraphic zones. In total, the 3-D mesh (as shown in Figure 9.2) consisted of twelve elemental layers, which represented 6 distinct material zones.

9.2.4 Material properties

Material properties include both fluid properties and soil characteristics. Standard International (SI) units were generally employed, except for time, which was measured in hours rather than seconds. As such, all additional parameters were specified in meters and hours, while mass concentration units were calculated in mg L^{-1} or ppm. To model density driven flow and transport, individual relationships were defined between concentration, density and viscosity. The relationships used by FEMWATER are:

$$\frac{\rho}{\rho_o} = a_1 + a_2 C + a_3 C^2 + a_4 C^3 \tag{9.16}$$

and

$$\frac{\mu}{\mu_o} = a_5 + a_6 C + a_7 C^2 + a_8 C^3 \tag{9.17}$$

where, ρ_o, μ_o = density and viscosity of fresh water, $a_1 \ldots a_8$ = parameters used to define concentration dependence of water density and viscosity, and C = chemical concentration.

Within each of the six soil layers, several physical soil parameters must be defined including the hydraulic conductivity (both vertical and lateral), compressibility, radioactive decay coefficient, the first order biodegradation rate of the dissolved and

absorbed phase, and three water retention curves describing how moisture content, relative conductivity, and water capacity fluctuate with pressure head in the unsaturated zone. The radioactive decay and the first order biodegradation rate of the dissolved and absorbed phase coefficients were ignored due to the conservative nature of chloride ions. Furthermore, the soil matrix was deemed to be incompressible. The remaining parameters were determined by the analysis of field samples shown in Chapter 3 and through the extensive literature review conducted in Chapter 2. A summary of the soil parameters is given in Table 9.2.

Table 9.2 Soil physical properties used for FEMWATER initialisation.

Layer	Depth (m AHD)	θ_r (m^3/m^3)	θ_s (m^3/m^3)	α (1/m)	n	k_v (m/hour)	k_h (m/hour)	ρ_d (kg/m^3)
1	0.35	0.05	0.48	0.281	1.3	0.1653	0.1466	800
2	0.05	0.02	0.35	0.242	1.15	0.1578	0.1668	1110
3	-0.25	0.05	0.34	0.291	1.18	0.0651	0.0398	1050
4	-0.55	0.04	0.50	0.225	1.29	0.0899	0.0426	950
5	-0.85	0.06	0.49	0.474	1.09	0.0766	0.0099	1030
6	-1.85	0.06	0.49	0.474	1.09	0.0083	0.0065	1030

Note, θ_r and θ_s represent residual and saturated volumetric moisture contents, α and n are shape parameters based on the van Gneucthen (1980) equation, k is the hydraulic conductivity in the vertical (k_v) and lateral plane (k_h), and ρ_d is the average dry bulk density. 1m/ hour = 2.77 x 10^{-4} m/sec.

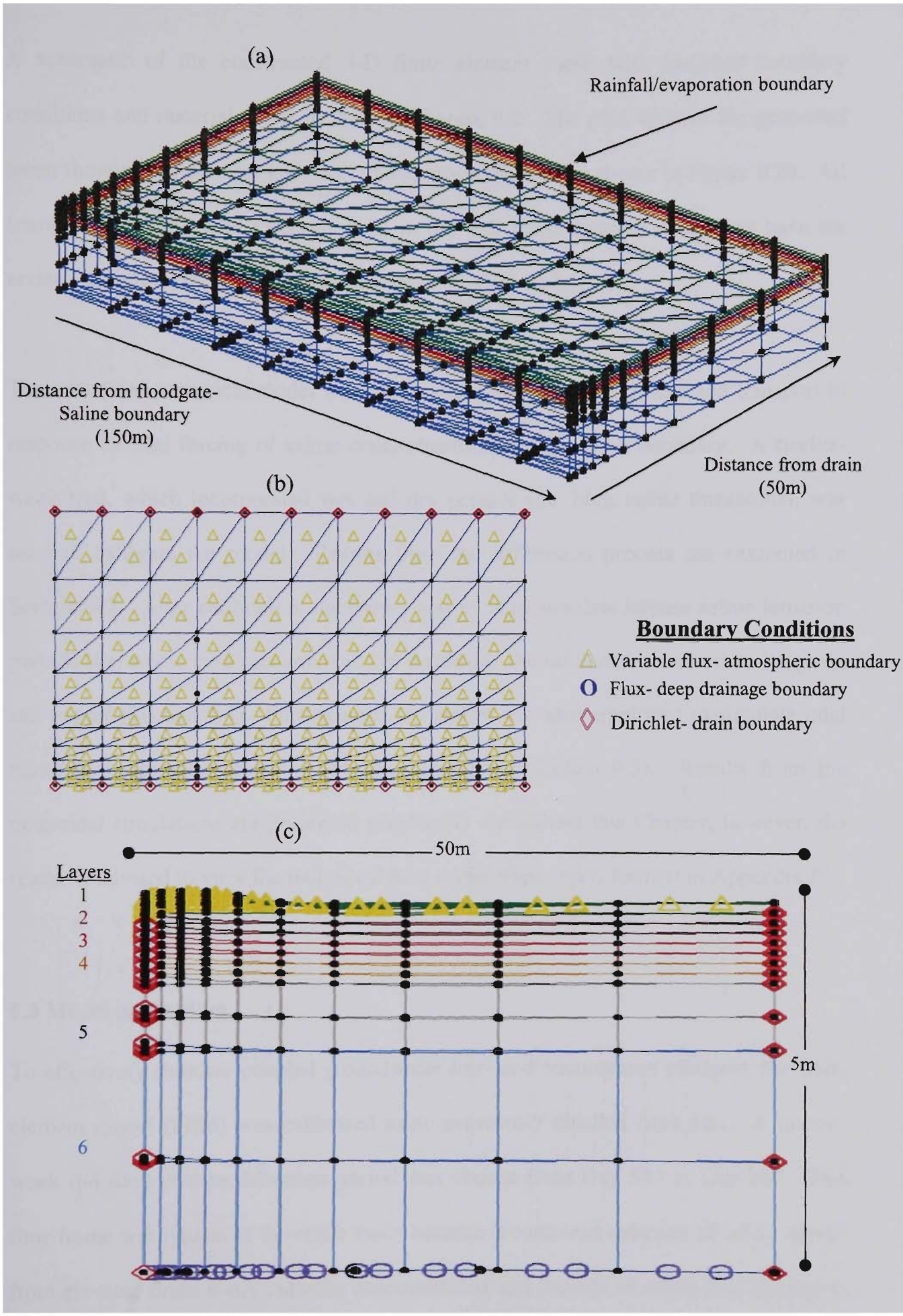

Figure 9.2 Schematic of finite element mesh with (a) nodal distribution, (b) plan view, and (c) detailing material layers and boundary conditions in cross-sectional view.

A schematic of the constructed 3-D finite element mesh with assigned boundary conditions and material zones is shown in Figure 9.2. The plan view of the generated mesh showing the element geometry and location of nodes is shown in Figure 9.2b. All triangular (wedge) solid elements used in the 3-D finite element simulation have six nodes and in total there were 2400 elements and 1573 nodes.

The initialised numerical model was run to simulate groundwater flow and transport in response to tidal forcing of saline contaminants along the drain boundary. A twelve-week trial, which incorporated wet and dry periods (i.e. high saline thresholds), was used to calibrate the model. Results from the calibration process are examined in Section 9.3. After calibration, the model was used to simulate intense saline intrusion periods (i.e. worse case scenarios) and to determine the influence of natural recharge on salt export (Section 9.4). Furthermore, the model was also employed to simulate tidal restoration strategies under varied soil parameters (Section 9.5). Results from the numerical simulations are presented graphically throughout this Chapter, however, the reader is advised to view the individual time series films (*.avi format) in Appendix F.

9.3 Model calibration

To effectively simulate coupled groundwater flow and contaminant transport, the finite element model (FEM) was calibrated using previously detailed field data. A twelve-week (84 day) post-modification period was chosen from Day 581 to Day 665. This time frame was typical of the entire study because it contained episodes of saline ingress from elevated drain water chloride concentrations and periods of saline flushing due to natural groundwater recharge. The climatic conditions of the site, which were used as boundary conditions in the model during the testing period, are shown in Figure 9.3.

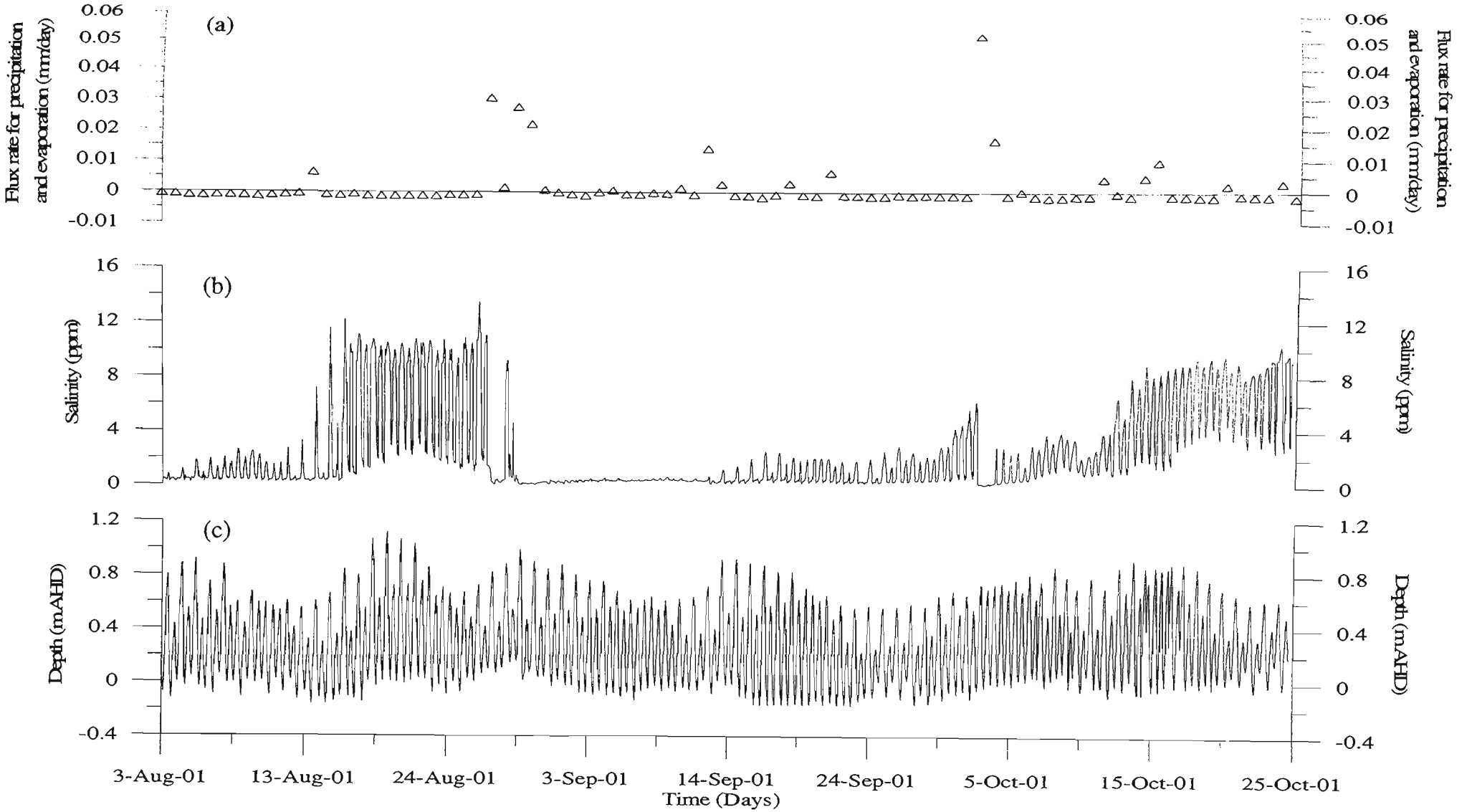

Figure 9.3 Environmental parameters used as boundary conditions including (a) climatic data, (b) salinity and (c) drain water height. Within climatic conditions (a), negative values indicate evaporation while positive values indicate rainfall.

The environmental parameters depicted in Figure 9.3 provide detailed boundary conditions not previously employed in coupled groundwater flow and transport modelling of acid sulphate soils terrains. To obtain this information, multi-parameter submersible data loggers were installed within the study drain at three locations. Hourly depth and electrical conductivity readings were collected, and after conversion to appropriate units (i.e., m AHD), were averaged across the drain. Salinity (ppt) was calculated from non-normalised conductivity values according to the algorithm outlined in 'Standard Methods for the Examination of Water and Wastewater' (2000). The equation for Rt was determined based on the method described by Miller *et al.* (1988). This high level of input data provided detailed modelling accuracy at hourly intervals over the 12 week period, resulting in over 2000 depth and salinity measurements.

Model simulations of groundwater flow strongly agreed with field data (Figure 9.4). The field and numerical simulations show that the phreatic zone fluctuated widely at 1 m and 2 m inland from the drain, and that tidal forcing dissipated with distance (10 m inland). Fluctuations in the saturated zone were primarily associated with daily tidal changes, whereas groundwater recharge was controlled by rainfall. Moreover, the strong agreement between field and calculated results indicated that the constructed finite element model was adequate to simulate groundwater flow throughout the soil matrix to an acceptable accuracy.

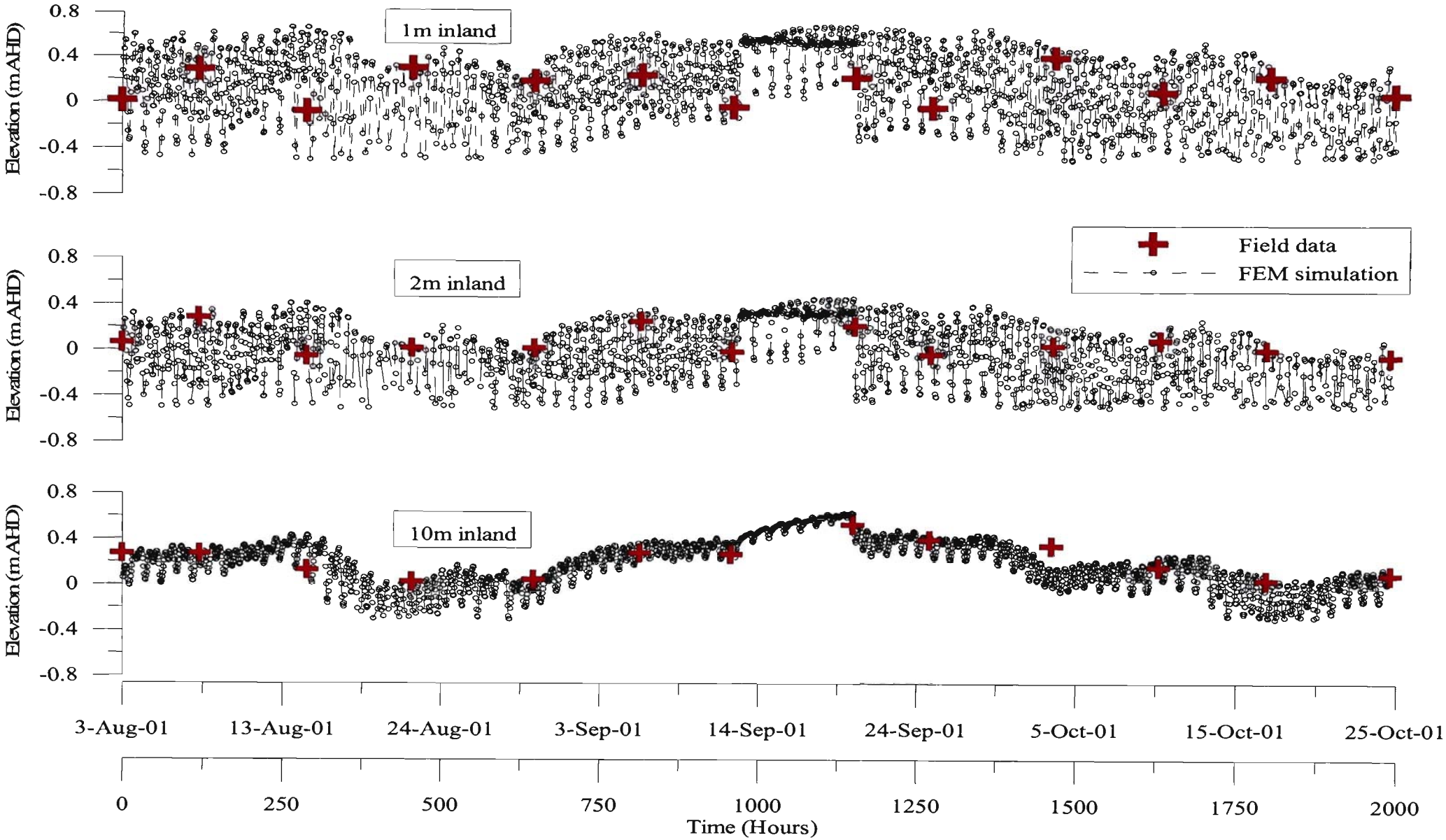

Figure 9.4 Simulated versus field data groundwater elevations with distance from the drain.

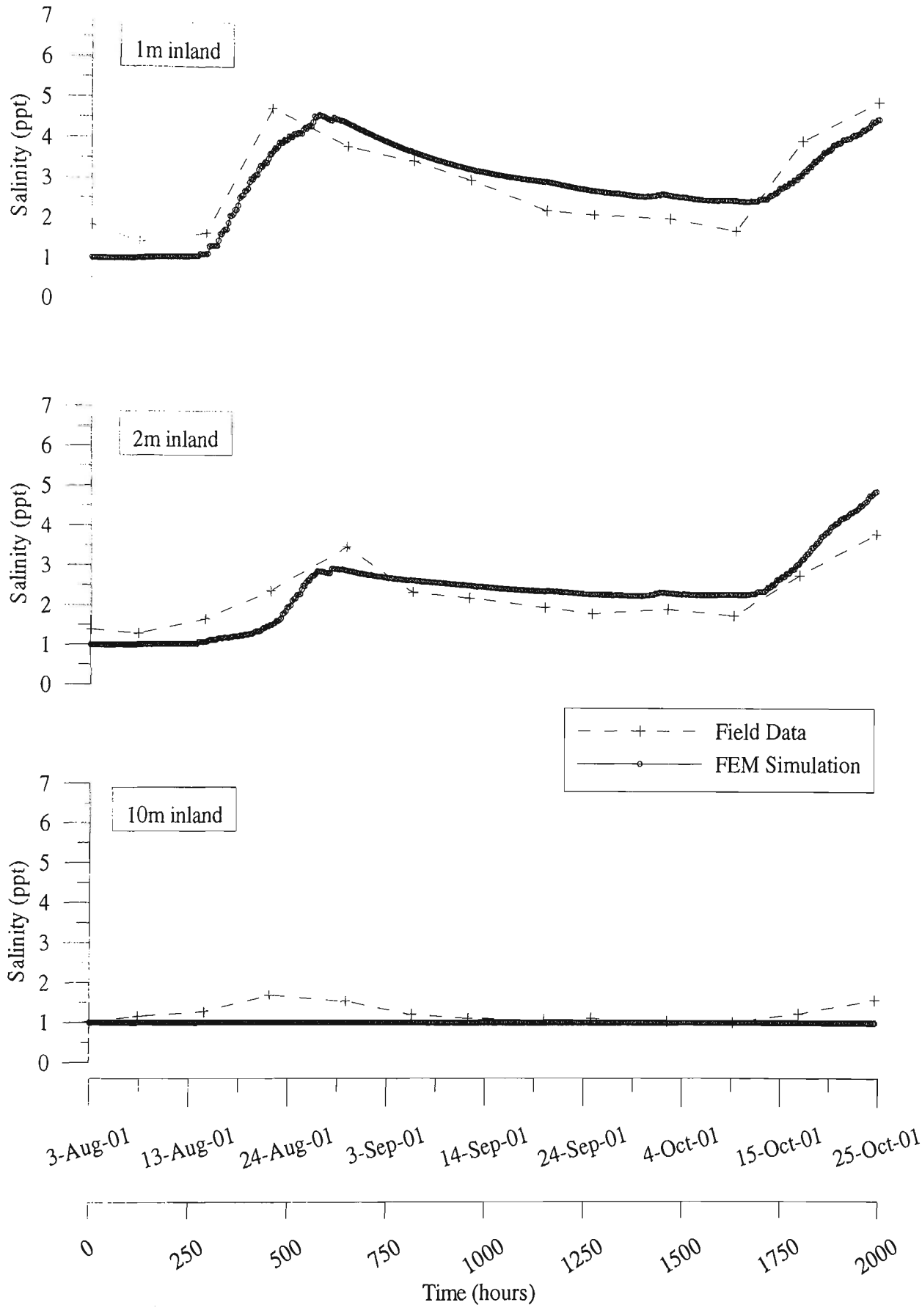

Figure 9.5 Simulated versus field results for transport simulation.

To complete the groundwater simulation mesh, a deep drainage flux boundary was introduced at the bottom layer of the finite elements. This is because FEMWATER has the ability to calculate evaporation but it does not determine the transpiration of groundwater through productive agricultural pastures, or calculate the increased evaporation rates of pore water in large (10 mm) vertical macropores. To compensate for these limitations, an outflow flux boundary was assigned to the face of the bottom elements. This boundary condition was never greater than 2 mm day^{-1} and was not a significant determinant in groundwater movements.

Groundwater field results and numerical simulations were in closer agreement near the drain, which was attributed to the difference in time between field data collection and model simulation outputs. For instance, field data was often collected between hours, whereas to run the model efficiently, the time control parameters were divided into hourly intervals. This was effective because it corresponded with input data and limited the simulation runs to 14 hours on a Pentium III 933MHz processor. Unfortunately, hourly time steps did not exactly correspond to the measured field times (i.e. say 1230, versus 1200 or 100), and lag periods existed between results. This was more apparent nearest the drain because the influence of tidal forcing decreased with distance. Nonetheless, the difference between simulated results and field data findings were within the acceptable criteria limit (5%).

The contaminant transport simulations also agreed with the field results. As shown in Figure 9.5, groundwater salinity fluctuated greatest 1 m inland and decreased with distance from the drain. In all cases, groundwater salinity levels were (i) within ANZECC (1992) criteria, (ii) did not negatively affect the root zone, and, (iii) were

highest during dry periods when elevated salinity concentrations in the drain were drawn into the soil matrix through advection and dispersion. On the other hand, strong rainfall at the 454th time step flushed saline contaminants from the soil zone. This intrusion-flushing cycle, shown in Figure 9.5, is in good agreement with field results.

To compensate for the influence of acidic salts on electrical conductivity, the entire soil matrix was assumed to have an initially low saline concentration. This was because chloride concentrations decreased with distance from the drain yet dissolved sulphate, iron, and aluminium concentrations remained consistent throughout the soil profile. To offset this limitation, a salinity concentration of 1 ppm was assumed across the entire soil matrix prior to initialisation. Following this adjustment, the model accurately simulated the ingress and flushing of chloride contaminants in response to variable salinity levels, groundwater elevations, climatic conditions, and tidal forcing.

The ingress and flushing of a saline intrusion front in response to changing climatic and boundary conditions is best illustrated by a series of 3-dimensional plots (Figure 9.6). For illustration purposes, all 3-D contour graphs are plotted within the entire mesh shown in Figure 9.2 but with the vertical axis magnified five times. In the first plot (Fig. 9.6a), salts are solely concentrated on the drain boundary but as drying conditions persist (Fig. 9.6b), saline contaminants intrude into the subsurface soil matrix in a wedge-like manner. By the 454th hour, the transitional front has reached its maximum intrusion distance (Fig. 9.6c), and, following 83 mm of rainfall, the majority of saline contaminants were flushed from the soil (Fig. 9.6d). As well as depicting the removal of the saline wedge in response to rainfall, these plots also show that the wedge is not a sharp interface, but, instead, a transitional zone between highly saline concentrations at

the drain boundary and low ionic groundwater. The simulation also shows that while rainfall triggers groundwater flushing, it does not completely remove the contaminants. In fact, after rainfall an isolated saline area develops within the soil matrix approximately 1-2 m inland from the drain. Importantly, these results correlate well with findings presented in Chapter 8.3 and illustrate that this area does not represent a significant threat to agricultural activity.

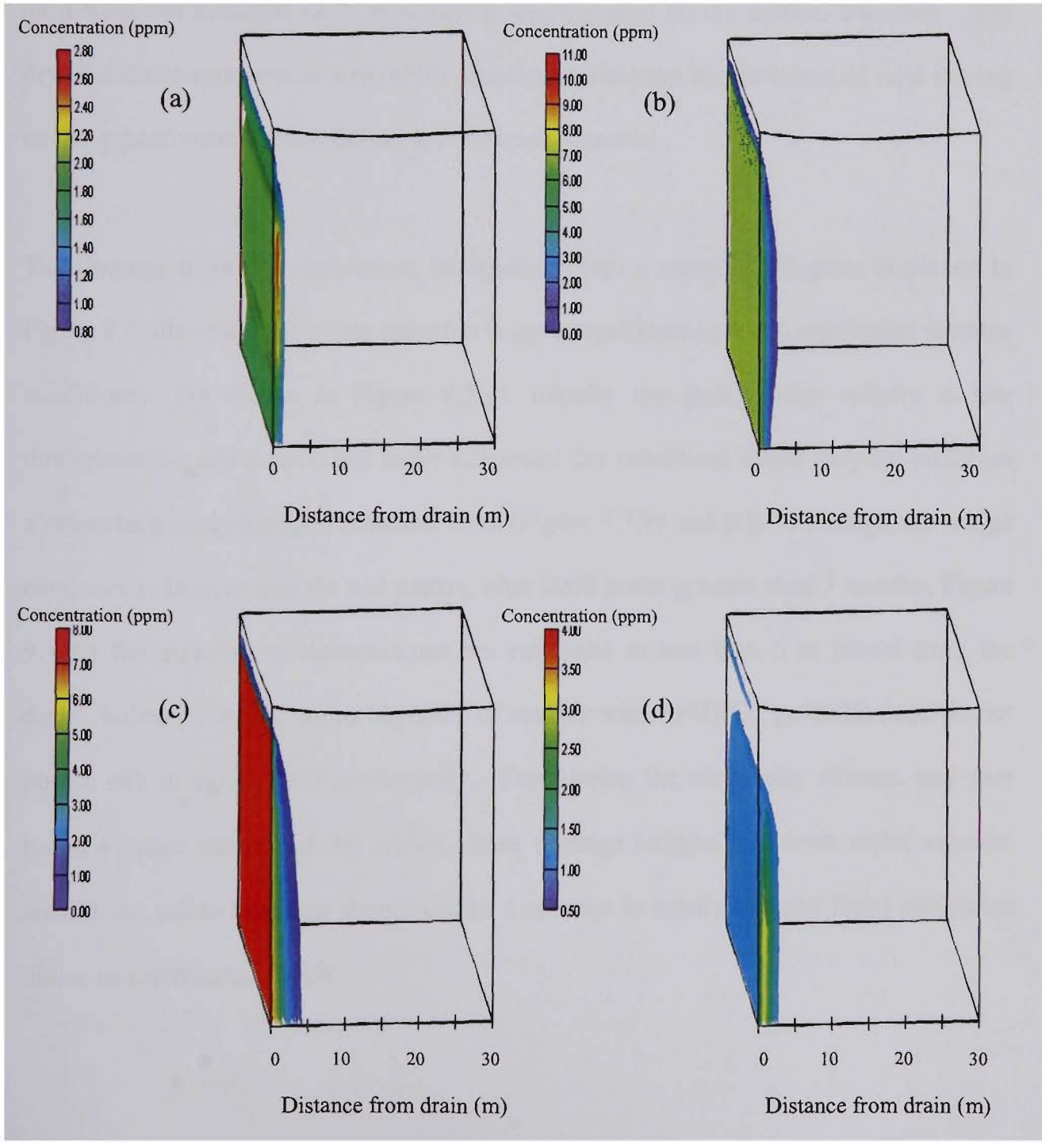

Figure 9.6 Saline intrusion within the finite element mesh during calibration at 1 (a), 1000 (b), 1500 (c) and 2000 (d) hours. Note the plot height is 5m.

9.4 Maximum saline intrusion

Based on the above findings, a series of simulations were undertaken to determine the extent and magnitude of saline intrusion in response to extreme climatic factors. To simulate these conditions, the above 12-week period was modified so that (i) drain water salinity was maintained at 20 ppt throughout the trial, (ii) rainfall was removed from the surface boundary, and (iii) a constant evapotranspiration rate, based on long-term field site averages (2.21 mm day^{-1}), was imposed on the surface boundary. The dry conditions represented within this simulation illustrate the influence of tidal forcing on the groundwater regime during a worst-case scenario.

The findings from this simulation, incorporated into a series of 3D plots displayed in Figure 9.7, illustrate that saline intrusion is not a significant concern even under extreme conditions. As shown in Figure 9.7(a), initially the groundwater salinity is low throughout the soil matrix, but under continued dry conditions saline seepage occurs in a subsurface wedge-shaped intrusion front (Figure 9.7(b) and (c)). Although the wedge continues to intrude into the soil matrix, after 2000 hours (greater than 3 months; Figure 9.7(d)) the majority of contaminants are restricted to less than 6 m inland from the drain. Salinity concentrations beyond 6 m comply with ANZECC guidelines and do not pose a risk to agricultural productivity. Considering the temperate, climate, and year round average rainfall of the region, these findings suggest that even under extreme conditions, saline intrusion should not be a concern in tidally restored flood mitigation drains in southeastern NSW.

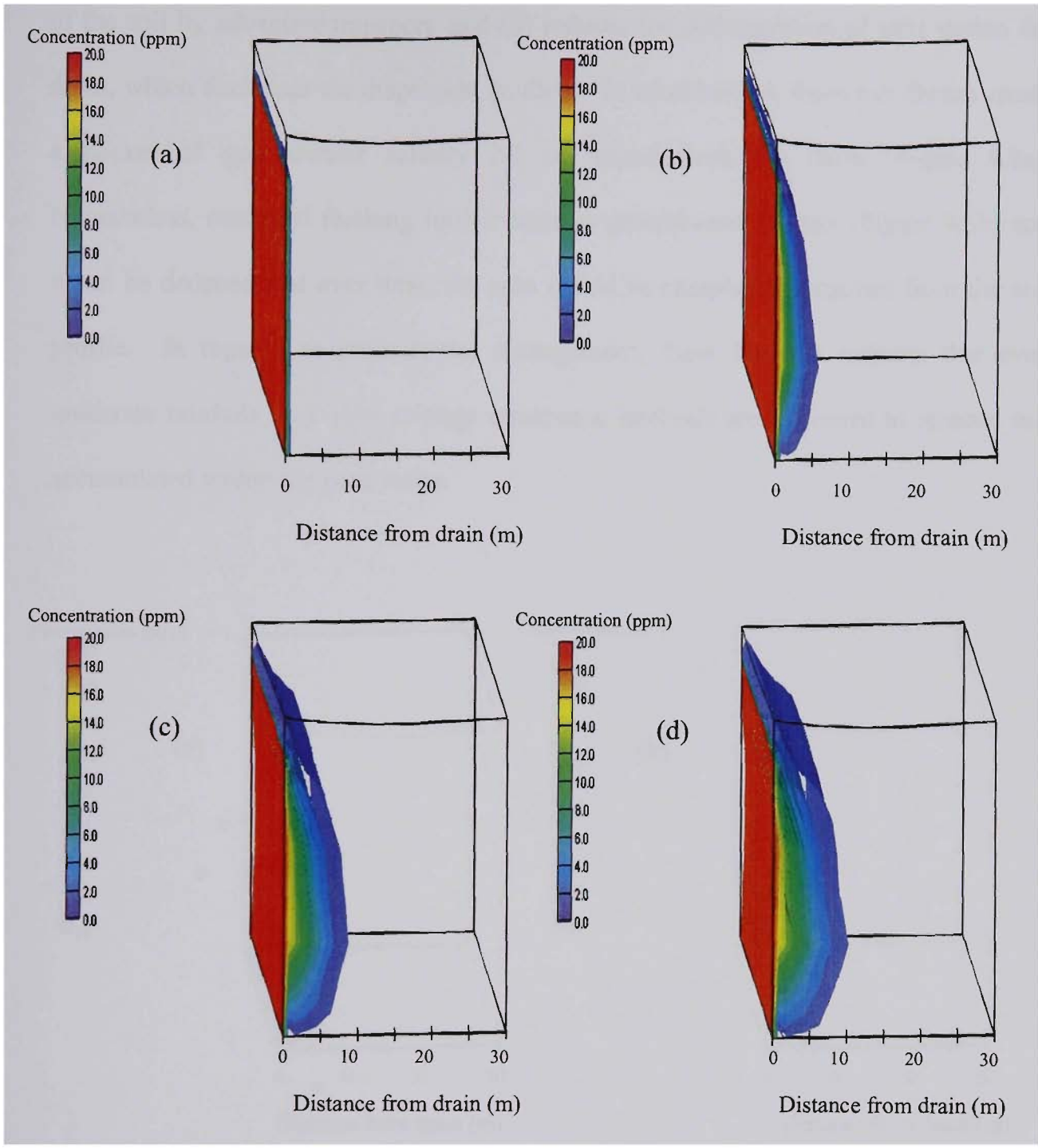

Figure 9.7 Calculated maximum saline intrusion conditions showing (a) initial conditions, (b) conditions at 500 hours, (c) 1000 hours and (d) 2000 hours. Note: Plot height is 5 m.

Using the worse-case scenario shown above (Figure 9.7) as initial conditions, additional simulations were undertaken to illustrate the influence of groundwater recharge (100 mm of rainfall over 2 days) on salts flushing from the soil matrix. These findings, as shown in Figure 9.8, demonstrate that groundwater recharge/flushing (i) decreases pore water salinity by reversing the hydraulic gradient and hence, fostering salt transport out

of the soil by advective transport, and (ii) reduces the concentration of salts within the drain, which decreases the dispersion gradient. In combination, these two forces create a pocket of groundwater salinity 2-3 m inland from the drain (Figure 9.8a). Nonetheless, continual flushing further reduces groundwater salinity (Figure 9.8b) and it can be deduced that over time, the salts would be completely removed from the soil profile. In regards to groundwater management, these findings indicate that even moderate rainfalls (< 1 year average recurrence interval) are sufficient to remove salt accumulated within the pore water.

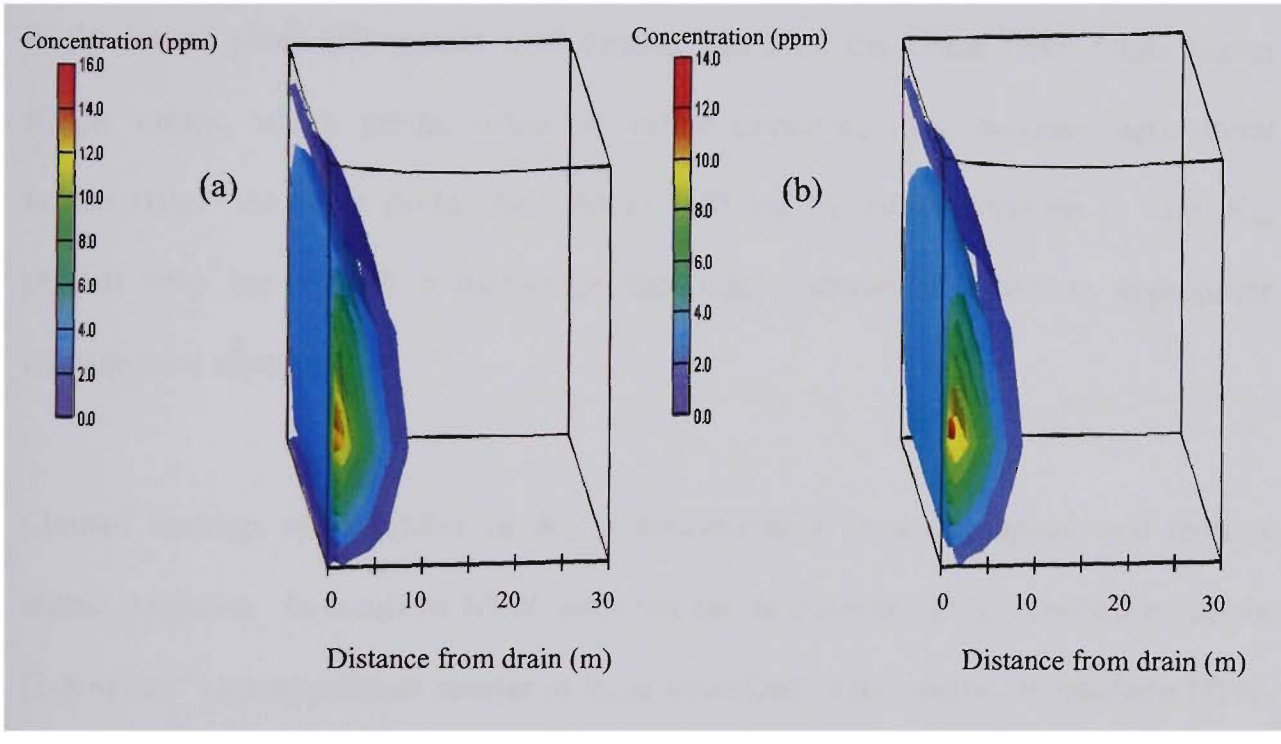

Figure 9.8 Saline conditions within the soil matrix (a) 250 hours and (b) 500 hours after rainfall. Note: Plot height is 5 m.

As expected, Figures 9.7 and 9.8 show that saline intrusion and flushing is greatest in regions with high lateral conductivity ($K_{sat(H)}$) values. At the study site, and in most acid sulphate soil affected floodplains, the highest $K_{sat(H)}$ values are usually measured within the actual acid sulphate soil layer. This is due to the influence of pore water

acidity on the clay lattice structure and natural wetting/drying cycles in the unsaturated zone. In contrast, $K_{sat(H)}$ values within the potential acid sulphate soil layer are lower because of the continual inundation of the clay layer and circum-neutral pH levels. The impact of altered lateral soil hydraulic conductivity values on saline intrusion is discussed below.

9.5 The influence of altered lateral soil hydraulic conductivity on saline intrusion

In terms of groundwater management, lateral soil hydraulic conductivity plays a vital role in determining the extent and distribution of saline contaminates. Low K_{sat} values in the lateral plane (H) restrict tidal forcing and limit the saline front, while higher $K_{sat(H)}$ values, which permit extensive saline intrusion, may decrease agricultural productivity. At some point, the damage inflicted by saline intrusion in high K_{sat} regions may be of such a magnitude that tidal restoration is not an appropriate management strategy.

Limited findings are available on $K_{sat(H)}$ measurements in acid sulphate soil terrains within Australia. In southern NSW, Blunden and Indraratna (2001) reported moderate (2-5 m day^{-1}) measurements similar to those described in this study. In northern NSW, MacDonald *et al.* (2002) reported extremely low $K_{sat(H)}$ values (<0.5 m day^{-1}) in regions underlain by sugarcane, however, in many cases these soils were not extensively drained and had moisture content values in excess of 100%. Conversely, in the Macleay River catchment of northern NSW, Johnson *et al.* (2003) reported $K_{sat(H)}$ measurements in excess of 20 m day^{-1} in oxidised actual acid sulphate soils. Transport within these soils was predominately via macropores formed through the decay of remnant organic root matter or during extensive coagulation of clay particulates.

The influence of altered $K_{sat(H)}$ values on the saline intrusion front was examined by manipulating the material properties within the calibrated model to suite different flow and transport regimes. Three separate conditional states were simulated using $K_{sat(H)}$ values of 1 m/day, 10 m/day, and 20 m/day. Within the material properties, the highest $K_{sat(H)}$ values were assigned to the actual acid sulphate soil layer, and, to maintain model stability, the remaining layers $K_{sat(H)}$ were decreased by 25%. The model was run over a 1500-hour dry period (i.e. no rainfall and high saline concentrations on the drain boundary) to determine the extent and distribution of subsurface saline contaminates. At the 1500^{th} hour, 100 mm of rainfall was applied to the surface boundary over two days. The model was then run for another 500 hours to ascertain the influence of natural recharge on the saline front. It was anticipated that high $K_{sat(H)}$ values would be associated with strong intrusion fronts and enhanced flushing. Each simulation exceeded its design criteria either when groundwater salinity was above 4.5 mS cm^{-1} at 10 m inland or if groundwater salinity concentrations were above 4.5 mS cm^{-1} within the root zone. The range of $K_{sat(H)}$ measurements used as material properties within the numerical simulations are given in Table 9.3.

Table 9.3 Lateral soil hydraulic conductivity measurements used in the numerical simulations.

Soil Layer	$K_{sat(H)}$ = 1m day^{-1}	$K_{sat(H)}$ = 10m day^{-1}	$K_{sat(H)}$ = 20m day^{-1}
Organic topsoil	0.5	5.0	10
Loam-Peat	0.5	5.0	10
Jarosite	0.75	7.5	15
Actual ASS	1.0	10	20
Potential ASS	0.75	7.5	15
Pleistocene Clay	0.5	5.0	10

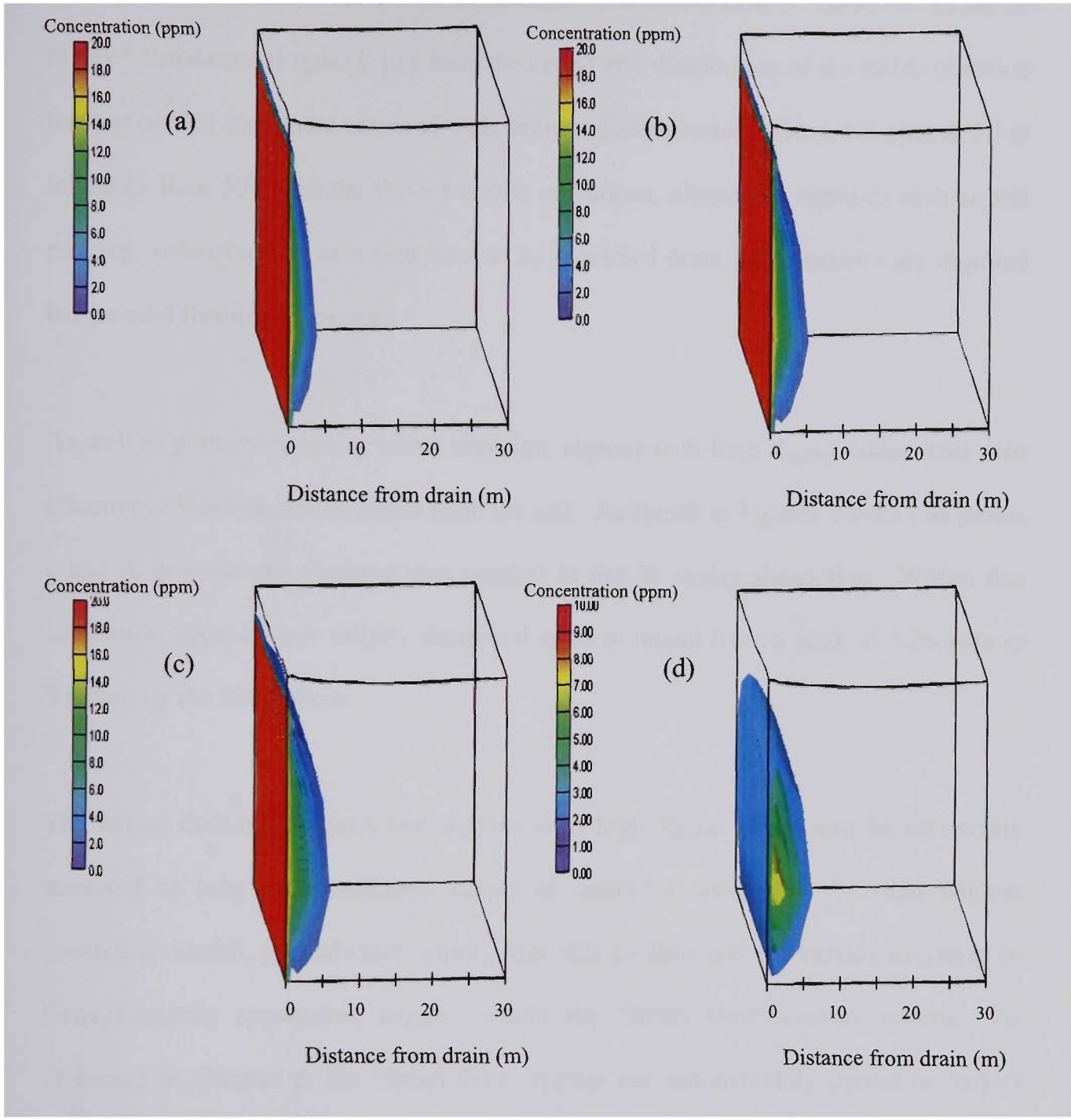

Figure 9.9 Numerical simulations of saline ingress and flushing using a 1 m day^{-1} lateral soil conductivity value. Individual panels depict conditions at (a) 500, (b) 1000, (c) 1500 and (d) 2000 hours. Note: Plot height is 5m.

As expected, the $K_{sat(H)}$ simulations indicated that saline intrusion is limited in regions with low $K_{sat(H)}$ values and more extensive in regions with high $K_{sat(H)}$ levels. In the low K_{sat} simulation (< 10 m day^{-1}), as illustrated in Figure 9.9, by the 1500th hour saline intrusion was limited to 4 m inland and did not impact the root zone. In the 10 m day^{-1} simulation (Figure 9.10), the saline front intruded beyond 15 m inland but groundwater

salinity concentrations were within the acceptable model criterion. However, in the 20 m day^{-1} simulation (Figure 9.11), both the extent and distribution of the saline intrusion front exceeded the model criterion with salinity concentrations above 4.5 ppm at 10 m inland (> hour 509). Under these extreme conditions, alternative methods such as soil packing, subsurface contaminant barriers or restricted drain water salinity are required before tidal flushing is restored.

As well as permitting strong saline intrusion, regions with high $K_{sat(H)}$ values were also effective at flushing contaminants from the soil. As shown in Figures 9.9-9.11 as panels c and d, groundwater flushing was greatest in the 20 m/day simulation. Within this simulation, groundwater salinity decreased at 10 m inland from a peak of 5.26 ppm to 3.6 ppm by the 2000^{th} hour.

The above findings suggests that regions with high $K_{sat(H)}$ values can be effectively managed as long as a consistent supply of rainfall is available. In areas without consistent rainfall, groundwater salinity may still be managed via surface irrigation or through setting appropriate triggers within the 'Smart Gate' control system. As discussed in Chapter 6, the 'Smart Gate' system can automatically permit or restrict tidal flushing based on a series of control triggers (drain water elevation, electrical conductivity, temperature, pH) determined by real-time field measurements.

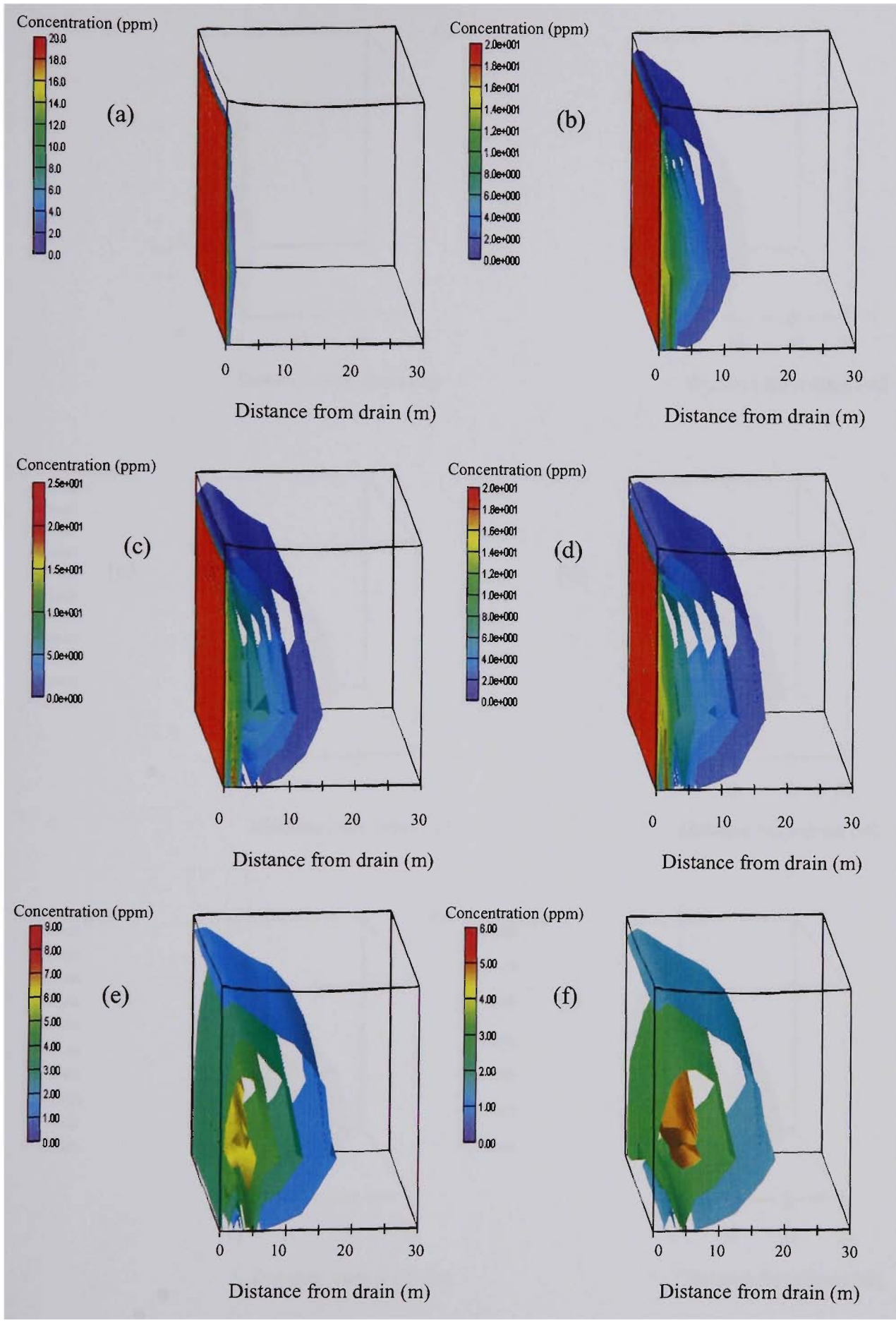

Figure 9.10 Numerical simulations of saline ingress and flushing using a 10 m day^{-1} lateral soil conductivity value. Individual panels depict conditions at hour (a) 1, (b) 500, (c) 1000, (d) 1500, (e) 1750 and (f) 2000. Plot height is 5 m.

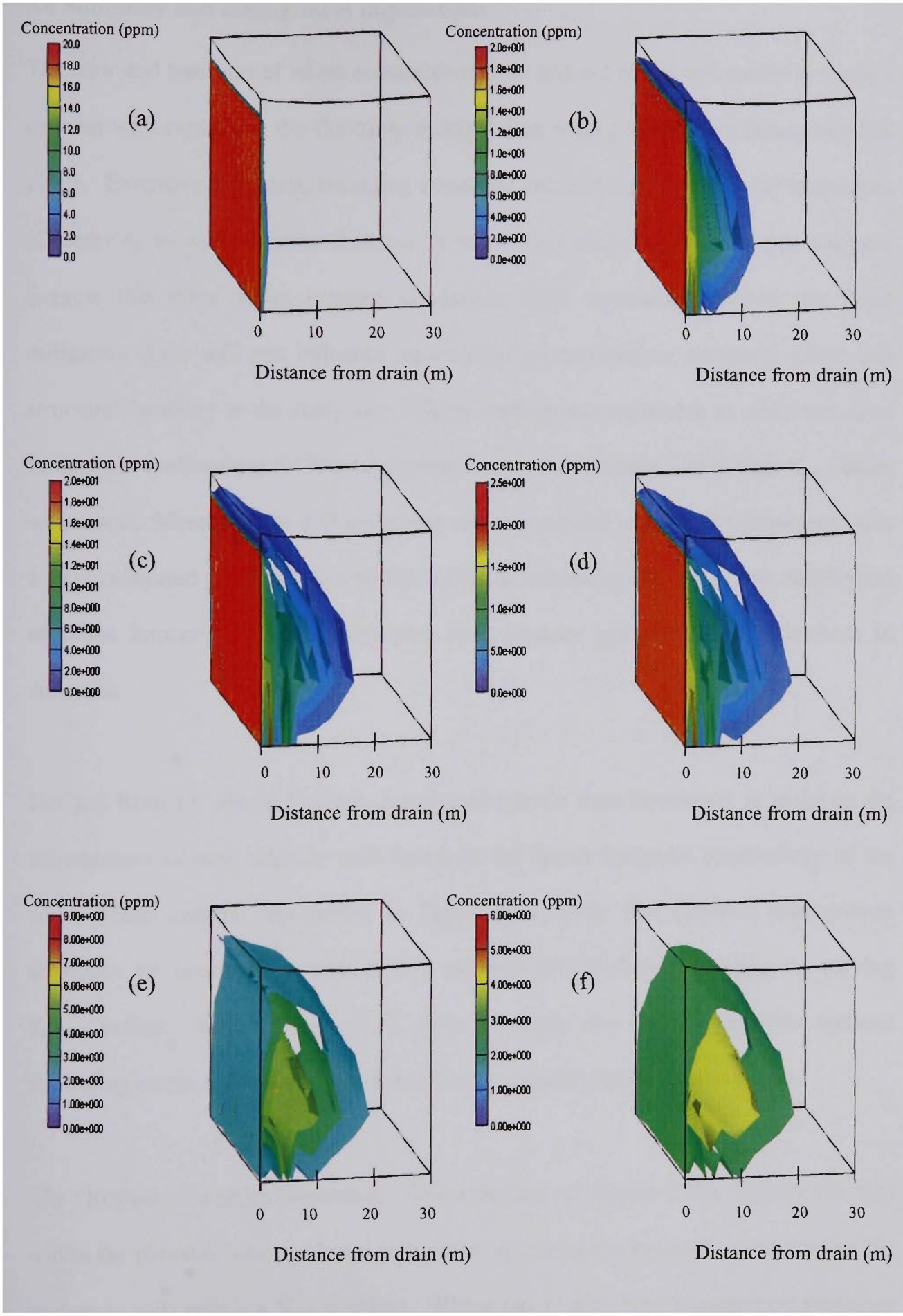

Figure 9.11 Numerical simulations of saline ingress and flushing using a 20 m day^{-1} lateral soil conductivity value. Individual panels depict conditions at hour (a) 1, (b) 500, (c) 1000, (d) 1500, (e) 1750 and (f) 2000. Note: Plot height is 5 m.

9.6 Summary and management implications

The flow and transport of saline contaminants into and out of the soil matrix is a major concern with regards to the floodgate manipulation strategy described throughout this thesis. Extensive field data, including standpipe and multi-port piezometer techniques (Chapter 8) as well as comprehensive finite element analysis shown in this Chapter, suggest that even under extreme conditions, tidal restorations within the flood mitigation drain will not influence agricultural productivity or adversely effect soil structure/chemistry at the study site. These findings are applicable to additional sites throughout southeastern NSW where temperate rainfall patterns and similar K_{sat} values are present. Moreover, the 3-D numerical model presented within this Chapter provides a field calibrated predictive tool that is useful in simulating the extent and distribution of saline intrusion in similar low-lying acid sulphate soil floodplains elsewhere in Australia.

Derived from the above findings, a series of criteria were developed to assist in the management of acid sulphate soils based on the lateral hydraulic conductivity of the soil. These criteria, represented in Figure 9.12, show that different management strategies are necessary to combat acid sulphate soil leachate depending on varying $K_{sat(H)}$ values. Within Figure 9.12, these strategies are divided into two sections depending on the influence of the surface water boundary on the phreatic zone.

The 'Region of evapotranspiration' (lower section of Figure 9.12), depicts the area within the phreatic zone that is not influenced by changes in the surface water boundary such as in soils with low $K_{sat\,(H)}$ values. Within this region, three management strategies can be employed to control acid production and transport.

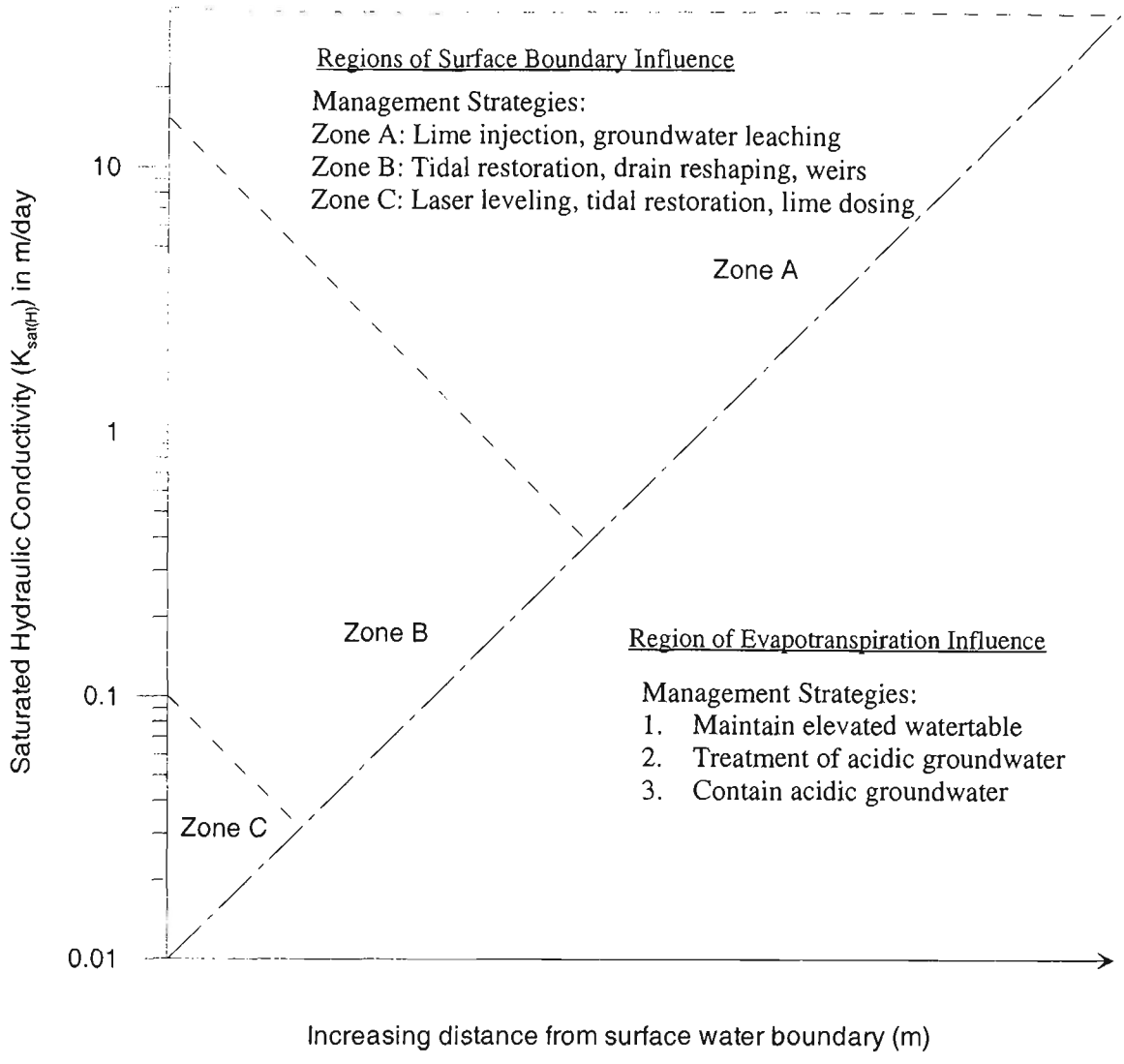

Figure 9.12 Management zones based on varying saturated hydraulic conductivity of the soil in the lateral plane.

First, the watertable should be maintained above the pyritic layer to reduce pyrite oxidation by either agricultural practices (i.e. irrigation) or through geo-technical methods, such as the injection of a subsurface alkaline barrier, which can perch the watertable. The second strategy involves neutralising the groundwater acidity by removal and treatment of acidic products via groundwater pumping or through the injection of subsurface alkaline barriers either in the vertical or lateral direction. The final strategy to control acidic groundwater within the evapotranspiration region is to contain the acidic groundwater and reduce its influence on receiving waters. This can be accomplished by laser levelling of the soil surface, or, where possible, by

maintaining the groundwater table below the sulphidic material. The effectiveness of the above strategies is reliant on several factors including pyrite content, depth to the actual acid sulphate soil layer, groundwater acidity, and agricultural practices.

Within the 'Regions of surface water influence', three sub-regions exist based on the influence of saline ingress and tidal forcing. In areas with low $K_{sat(H)}$ values (<0.1 m/day, zone C, Figure 9.12), the area influenced by the drain is relatively small and acid transport is primarily through overland mass flow during rainfall events. To combat drainage in these regions, the surrounding land should be laser-levelled and lime dosing may be effective. It is worth noting that in these circumstances, tidal restoration would not adversely influence the groundwater zone, and, assuming all other factors are considered, is recommended.

The majority of coastal floodplain sediments within Australia have moderate $K_{sat(H)}$ values which can be characterised by zone B, Figure 9.12. Within these soil conditions, the drainage boundary has a moderate influence on the soil matrix. These soils include those within this study and in other regions of the Broughton Creek floodplain (Blunden and Indraratna, 2001). In regards to management strategies, these soils represent an ideal setting for tidal restoration via modified floodgates and/or maintenance of elevated groundwater tables through drain reshaping or weir installations.

The final sub-zone within the 'Region of surface water influence' includes those soils which have extreme $K_{sat(H)}$ values (> 15 m day^{-1}). These soils cannot be managed by surface water manipulation because of their extreme flow and transport rates, which can influence agriculture productivity through waterlogging or increased salinity

concentrations. Management of these soils is either by leaching of the pyritic sediment over time or by reducing flow rates through lime injection or by soil compaction. Due to their tendency to transport contaminants over large distances, floodplain managers are advised to exercise extreme caution when remediating soils with high $K_{sat(H)}$ values.

The above guidelines are useful in determining individual management strategies based on physical soil parameters. These guidelines were formulated based on the 3-D numerical simulations detailed throughout this chapter. The numerical model denoted here provides a reliable approach in determining the extent and distribution of saline intrusion over varied climatic and physical conditions at the study site following floodgate modifications. Furthermore, as long as the material properties are known, the numerical model can be extended to other low-lying sites with minimal effort.

Chapter 10.0 Conclusions and Recommendations

10.1 Summary

The research presented within this thesis was undertaken to trial a novel acid sulphate soil management strategy, which involved modifying tidal restricting floodgates to restore tidal flushing and increase drain alkalinity in a low-lying flood mitigation drain in southeastern NSW, Australia. Before this study, floodgate manipulation to combat acidic drainage was not substantiated by any long-term field studies and was often conducted on a 'trial and error' basis. This project examined several criteria relating to floodgate management and the effectiveness of the remediation strategy, including:

- Pre-existing baseline surface water and groundwater quality and the impact of one-way floodgates on exacerbating acid drainage.

- Hydrology, environmental, and geo-hydraulic concerns relating to floodgate manipulation using GIS techniques.

- The kinetics of tidal buffering including the development of an aqueous ion speciation model.

- Floodgate design criteria and innovative design techniques to optimise tidal buffering and reduce risk.

- The influence of tidal restoration on drain water quality, and the influence of altered drain hydraulics on the phreatic zone.

- The extent and distribution of saline contaminants within the soil matrix through field analysis (standpipe and multi-port piezometers), and a comprehensive 3-D finite element analysis.

Initial tests showed that a strongly acidic environment existed throughout the soil matrix. High total actual acidity concentrations combined with low pH and low chloride/sulphate ratios (< 1.0) indicated acid production from pyrite oxidation. Chromium reducible sulphur concentrations were in excess of NSW Environmental Protection Authority criteria (Stone *et al.*, 1995) and illustrated that without modifications to the current management strategy acid production would continue. Moreover, the strong hydraulic gradient of groundwater flow towards the drain directly contributed to the acidification of surface waters.

Field work and numerical analysis demonstrated that acidic conditions within the drain were intensified by the hydraulic influence of one-way floodgates, which quickly re-established drain water elevations at the low tide mark after rainfall and enhanced the translocation of acidic products. The one-way floodgates were also linked to low dissolved oxygen conditions, the growth of exotic freshwater weeds, and restricted fish passage. The discharge of acidic drain water into the estuary during the ebb tide caused large plumes of iron and aluminium flocculant which have been associated with fish kills and reduced estuarine health.

Baseline conditions indicated that drain water acidity varied with climatic factors and the efficiency of the floodgate seal. Drain water quality was extremely poor during non-precipitation periods and was characterised by high total acidity levels (sum of soluble aluminium, iron and hydrogen ions) and chronic estuarine acidification. Large rainfalls (>50 mm) diluted drain water acidity, but following recharge of the groundwater table the poorest water quality measurements were reported. The only periods of improved drain water quality were measured when debris accumulated between the floodgate flap and the headwall, and alkaline creek waters were able to intrude upstream of the floodgate. These leakage events suggested that modifying one-way floodgates and restoring full tidal flushing, rather than adding anthropogenic chemicals, would improve the drain water quality.

Before floodgate modifications, several concerns regarding tidal restoration were addressed. Firstly, an ion association mixing model was calibrated with laboratory experiments to investigate the kinetic relationships involved in mixing acidic drain water and circum-neutral creek water. These findings demonstrated that a significant improvement in drain water quality could be made to soluble aluminium, iron, sulphate, and pH concentrations with a 72% increase in mixing. Secondly, a GIS based spatial technique was developed to calculate the exact quantity of water permitted within the drain without overtopping of the levee banks. These calculations showed that sufficient freeboard existed within the primary drain to permit full tidal restoration (and thus 65% mixing), but that the secondary side drains must remain floodgated to reduce flooding of the backswamp area via relict natural drainage lines. Both the water quality and spatial analysis models were confirmed *post facto* through field experiments.

The standardisation and innovation of floodgate design was another major component of this research. First, a series of design criteria were developed pertaining to floodgate installations and hydraulic calculations. Then, using these criteria, two innovative floodgates were designed. The first model provided manual vertical adjustment of the floodgate flap and permitted full tidal intrusion within the drain while maintaining control under varied flow conditions. The second model was built using sophisticated technology that automatically adjusts the gate to control tidal ingress within the drain based on real-time upstream chemical and hydraulic parameters and remote telemetry access. Both models were successfully implemented at the study site and are currently being adapted to other sites throughout the lower Shoalhaven estuary.

After the installation of redesigned floodgates and the establishment of full tidal flushing within the primary drain, water quality significantly improved. Drain water quality was best during prolonged dry periods due to elevated bicarbonate concentrations transported in with the tidal front. Overall, drain water pH increased two orders of magnitude and dissolved aluminium and iron decreased more than 50%. Conversely, dissolved sulphate concentrations did not significantly decrease because of the high concentration of dissolved sulphate in seawater. Tidal flushing also (i) reduced the 'acid reservoir' effect, (ii) increased drain water dissolved oxygen levels, (iii) enhanced fish passage, (iv) decreased exotic freshwater weeds and (v) recharged the phreatic zone during dry periods. Tidal buffering was least effective immediately after large rainfall, when increased acid seepage and decreased creek alkalinity influenced drain water quality.

An extensive analysis of the phreatic zone was also undertaken to determine the extent and distribution of the saline intrusion front due to tidal restoration. Groundwater measurements showed that increased drain water elevations raised the surface of the phreatic zone above the pyrite zone, but tidal fluctuation increased groundwater variance. Tidal forcing on the phreatic zone decreased with distance from the drain, and was imperceptible by 8 m inland. In addition, both multi-port piezometer field studies and finite element analysis indicated that saline intrusion was restricted 2-4 m inland. These tests also showed that rainfall recharged the groundwater table and flushed saline contaminants into the creek. Geochemical field investigations, which were in contrast with previous microcosm research, showed that saline intrusion increased groundwater pH, reduced redox potential, and decreased dissolved aluminium concentrations. Furthermore, the subsoil nature of saline intrusion was shown to have a limited influence on the mineralisation of soil bound phosphate and nitrate levels.

Finite element analysis indicated that saline intrusion is not a concern as long as the hydraulic conductivity of the soil in the lateral plane is below critical levels. The 3-D finite element model was (i) calibrated using extensive field data, (ii) run to simulate maximum saline intrusion during prolonged dry periods and (iii) employed to determine critical lateral hydraulic conductivity levels. Simulations depicted that even under extreme conditions, saline intrusion at the study site was limited to 10 m inland and was predominately flushed out of the soil matrix with drought breaking rain. Variations of the lateral hydraulic conductivity within the model showed that $K_{sat-(H)}$ levels above 10 m day^{-1} were a concern to saline migration. Though this may not be an issue in the study site catchment area, extreme K_{sat} measurements have been reported in northern

NSW, and therefore, an extensive examination of physical soil properties is recommended before future floodgate modifications.

10.2 Guidelines for future management strategies

Based on extensive field research, laboratory experiments, and modelling (including spatial, chemical and numerical simulations) presented in this thesis, the following guidelines are proposed for the restoration of tidal flushing via modified floodgates in flood mitigation drains affected by acid sulphate soil leachate. These guidelines were developed for temperate climates with year-round rainfall patterns but can also be applied to sub-tropical and tropical regions. The proposed guidelines support the hypothesis that tidal restoration is an effective management strategy as long as several initial concerns (detailed in Figure 10.1) are properly investigated.

The flow chart procedure presented in Figure 10.1 is designed to decrease the risks currently involved in tidal restoration via modified floodgates. Using this model, the resultant drain water quality should be determined first using laboratory experiments and aqueous ion speciation models (Chapter 6, Section 6.1 and 6.2). To this point, the ion speciation source code presented in this thesis can be easily adapted to individual study sites with minimal costs. Floodplain managers are advised only to proceed to the next developmental stage if a significant improvement in drain water quality can be achieved. The findings within this thesis indicate that as well as improvements in drain water chemistry, additional secondary benefits need to be considered, including fish passage, improved drain hydraulics, and exotic weed control.

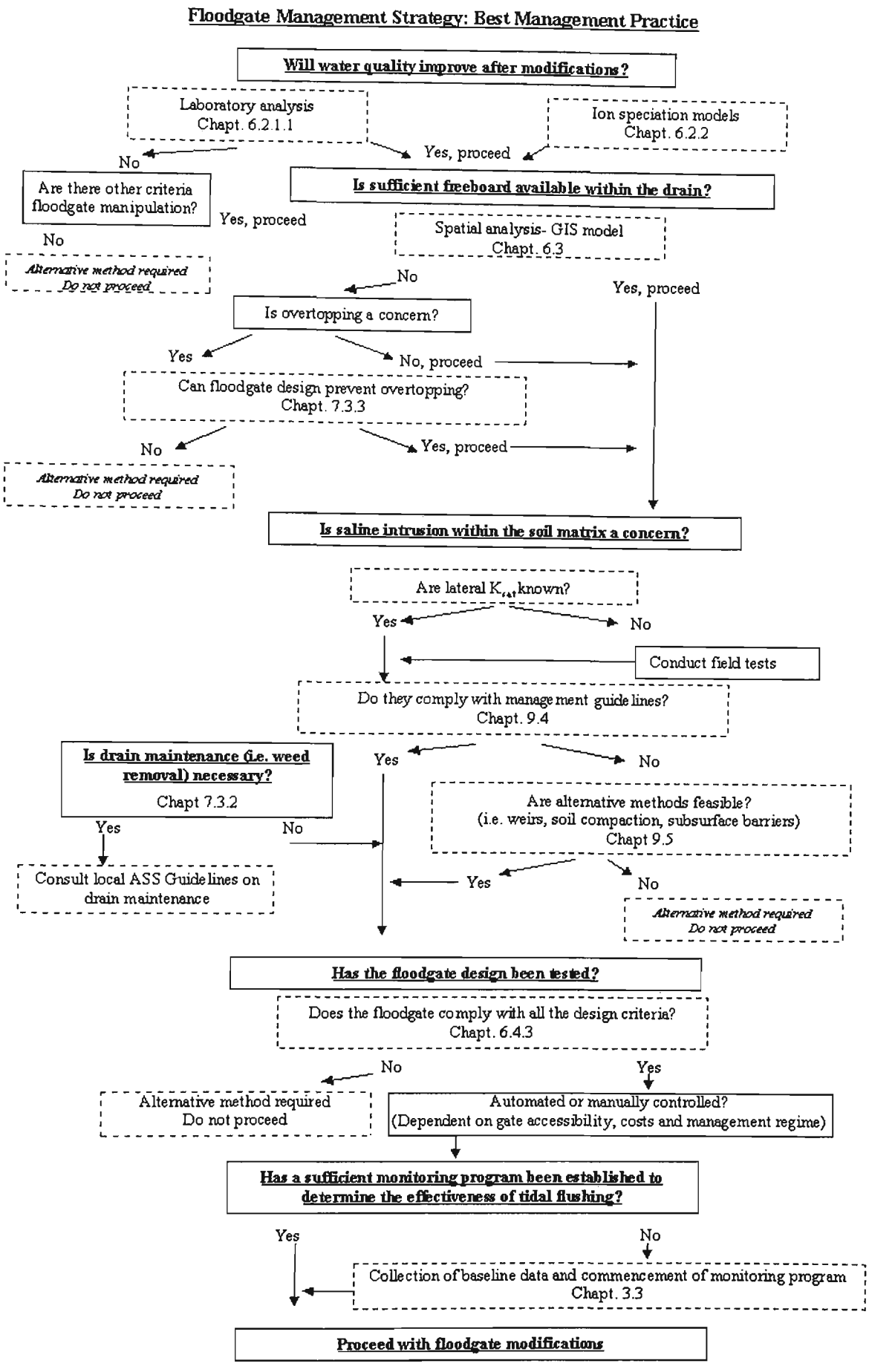

Figure 10.1 Flow chart describing the best management practices relating to tidal restoration and flood modifications.

Once the environmental outcomes are quantified, the second stage entails determining the effect of tidal restoration on drain hydraulics. This mainly involves calculating whether full tidal restoration can be permitted within the drain without overtopping the levee banks. Spatial techniques developed within this thesis (Chapter 6, Section 6.3) provide an accurate estimate of drain levels and are a major improvement on current 'sandbagging' methods. If full tidal flushing cannot be permitted without overtopping then an automated floodgate design, such as the 'Smart Gate' system presented in Chapter 6, Section 6.4, is required.

The third stage of the BMP involves comparing the lateral hydraulic conductivity values ($K_{sat(H)}$) within the soil to the criteria presented in Chapter 9.4. If the $K_{sat(H)}$ measurements are unknown then field tests are clearly required. Once known, the $K_{sat(H)}$ values must be compared with the results in Chapter 9.6, and if in excess of the guidelines, then alternative methods such as subsoil barriers, soil compaction, or weirs are required. In these circumstances, the 'Smart Gate' system can also be used as a remedial measure to control drain water salinity. During this stage, plans should also be made to remove any exotic freshwater weeds which may be destroyed after tidal restoration. Removing the weeds before implementation of weirs and floodgates decreases problems associated with monosulphide mobilisation and organic consumption rates as discussed in Chapter 7.4.

Floodgate design is the final component to consider prior to tidal restoration. The design of the floodgate must comply with all the criteria set out in Chapter 6.5, and the operator must decide whether the unit will be controlled automatically or manually and if accessibility is a concern. It is strongly advised that all floodgate modifications allow

continual and permanent tidal flushing to avoid the problems associated with sporadic floodgate management (Chapter 7.5).

If all of the above criteria are achieved, then floodgate modifications should be undertaken. A rigorous and well designed monitoring program should be designed and commenced before floodgate modifications to ascertain changes in water quality, drain hydraulics, and the effect on the soil matrix both upstream and downstream of the floodgate. Basic drain water parameters that should be monitored include pH, dissolved monomeric aluminium, total dissolved iron, dissolved sulphate, total acidity, alkalinity, salinity, dissolved oxygen, redox potential, water elevation and discharge rates. Important groundwater parameters include pH, redox potential, total dissolved aluminium, dissolved and bound chloride, total dissolved iron and the surface elevation of the phreatic zone.

10.3 Recommendations for future studies

There is considerable scope for major advancements in understanding the complex geo-chemistry of acid sulphate soils, in testing combative strategies, and in developing numerical models of acid transport. Some projects of particular interest include:

Subsurface injection of alkaline barriers: The role of anaerobic acid production via biological oxidation in acid sulphate soils in *in situ* conditions is poorly understood. Recent microcosm research conducted by Rudens (2001) suggests that in acidic groundwater with sufficient organic matter the bacterium *Thiobaccillus Ferooxidians* can directly oxidise pyrite regardless of groundwater height. These findings may

explain why no significant long-term improvements in drain water quality were reported after the installation of weirs at a Broughton Creek field site.

Deep chemical mixing has been conducted in the past by geotechnical engineers and may provide a remedial strategy for anaerobic oxidation. Rudens (2001) suggested that lime treatment might significantly reduce bacterium activity while simultaneously buffering acid products. Within Australia, Indraratna (1996) demonstrated the effectiveness of lime stabilisation and the geochemical kinetics of lime-fly ash slurries. As already demonstrated through preliminary trials, Indraratna (2003) has described the installation of lateral alkaline barriers above the pyritic layer, which have the potential to perch the watertable, neutralise acidic products, and reduce the lateral hydraulic conductivity. The preliminary models developed for lateral alkaline barriers at University of Wollongong incorporate hydraulic fracturing of clay, lime injection pressures, and the rate of lateral diffusion of lime. These may be extended farther in conjunction with advanced numerical modelling.

The coupled application of water retaining structures and modified floodgates to combat acid drainage over varied climatic regimes: Following this thesis and the groundwater management research conducted by Blunden (2000), two remedial measures (weirs and modified floodgates) have been tested to combat acid sulphate soils with varying degrees of success. Strategically placed weirs were found to maintain the groundwater table above the pyritic layer and reduce the translocation of acid products into the drain, yet they do not reduce drain water acidity. As shown throughout this thesis, modified floodgates buffer drain water contaminates via tidal buffering, which is most affective during dry periods and least affective immediately following large rainfalls.

When applied in unison, the two strategies may combine to form a more comprehensive solution. Modified floodgates will enable neutralising agents within the drain (up to the weir headwall) and weirs will retain the groundwater acidity until sufficient buffering agents return to the creek. Trial applications of the dual management strategies are currently underway within the Broughton Creek catchment.

The development of a comprehensive numerical model that simulates both the dispersion of buffering agents throughout an estuary and the chemical interaction with acid contaminants discharged from flood mitigation drains: The application of tidal buffering via modified floodgates to additional low-lying sites is recommended on the basis of the extensive research carried out in this thesis. The effectiveness of tidal buffering is reliant on several complex factors including estuarine hydrodynamics and buffering kinetics. The development of a 2-D numerical surface water flow and transport model is recommended to simulate the transport of buffering agents, the estuarine tidal hydro-dynamics and the hydro-chemical relationship between acidic groundwater and pH neutral surface waters within Broughton Creek. The numerical model would be used to predict the effect of acid discharges and the salinity regime/buffering dynamics in response to fluctuating environmental conditions. The amount of data collected during this thesis, including extensive creek bathymetry information, chemical kinetics and long-term salinity readings from various submersible data loggers located throughout the catchment will assist in the initialisation process.

References

Ahern, C., McElnea, A., Baker, D. (1998) Peroxide Oxidation Combined Acidity and Sulfate (POCAS). In 'Acid Sulfate Soil Manual'. (Eds. Y Stone, C Ahern, B Blunden) NSW Government: Sydney.

Andrews, J. E., Brimblecombe, P., Jickells, T. D., and Liss, P. S. (1996) An introduction to environmental chemistry. Blackwell Science Ltd. Oxford. 208p.

American Public Health Association (1994) Standard Methods for the Examination of Water and Wastewater. 18th Edition, APHA, Washington, DC. pp70.

ANZECC (1992) Australian Water Quality Guidelines for Fresh and Marine Waters. Australian and New Zealand Environment Conservation Council. Canberra.

APHA (1985) *Standard methods for the examination of water and wastewater*, 16th edn. American Public Health Association, Washington DC.

Australian Rainfall and Runoff (1998) A Guide to Flood Estimation. The Institution of Engineers, Australia. Barton, ACT.

Bayley, B. (1975) Shoalhaven- History of the Shire of the Shoalhaven (2nd Edition). South Coast Printers. Port Kembla. Australia.

Bear, J., Cheng, A. H.-D, Sorek, S., Ouazar, D. and Herrara, I. (1999) Seawater intrusion in coastal aquifers- Concepts, Methods and Practices (Volume 14). Kluwer Academic Publishers, Dordrecht, Netherlands.

Blunden, B. G. (2000) Management of Acid Sulfate Soils by Groundwater Manipulation. PhD Thesis, University of Wollongong, NSW Australia.

Blunden, B. and Indraratna, B. (2001) Pyrite oxidation model for assessing groundwater management strategies in acid sulfate soils, *Journal of Geotechnical and Geo-Environmental Engineering-American Society of Civil Engineering,* **127** (2), pp. 146-157.

Blunden, B. and Naylor, S. (1995) Environmental Guidelines: Assessing and Managing Acid Sulphate Soils. Environment Protection Authority Chatswood.

Blunden B, Indraratna B, and Nethery A. (1997) Effect of groundwater table on acid sulphate soil remediation. In 'Geoenvironment 97.' (Eds A Bouazza, I Kodikara B Parker) Balkema, Rotterdam. pp. 549-554.

Blunden, B., Indraratna, B. and Morrison, J. (1998). Problems of acid sulphate soils and their remediation by watertable management. 2nd International Conference on Environmental Management, University of Wollongong, Australia.

Blunden, B. and Indraratna, B. (2000) Evaluation of surface and groundwater management strategies for drained sulfidic soil using numerical simulation models. *Australian Journal of Soil Research, 38*, in press

Blunden, B. and Indraratna, B. (2000) Pyrite oxidation model for assessing groundwater management strategies in acid sulfate soils. *Journal of Geotechnical and Geoenvironmental Research* (accepted).

Bush, R. and Sullivan, L. (1996) Some things standard soil analyses don't reveal about potential acid sulphate soils oxidation. Proceedings 2nd National Conference on Acid Sulphate Soils. (Eds. Smith and Smith). pp. 72-75. Coffs Harbour.

Bohn, H. L., Fu-Young and Huang-Chenge (1989) Hydrogen sulphide sorption by soils. Soil society of America. (**53**) pp. 1914-1917.

Callinan, R. B., Paclibre, J. O., Reantaso, M. B., Lumanlan-mayo, S. C., Fraser, G. C., and Sammut, J. (1995) EUS outbreaks in estuarine fish in Australia and the Philippines: associations with acid sulphate soils, and rainfall, and *Aphanomyces.* In *Diseases in Asian Aquaculture II.* Shariff, M., Arthur, J. R., & Subasinghe, R. P. (eds.), pp. 291-298. Fish Health Section, Asian Fisheries Society, Manilla.

Chapman, S. (1994) Development of a strategy for the management of acid sulphate soils in Berry, NSW. B.E thesis. University of Wollongong.

Custodio, E., Gurgui, A., Ferreira, J., and Lobo, P. (eds) (1988) Groundwater flow and quality modelling, NATO ASI Service C., 224p.

Custodio, E. (1997) Studying, monitoring and controlling seawater intrusion in coastal aquifers. In Guidelines for Study, Monitoring and Control, FAO Water Reports No. 11, 7-23.

Darcy, H. (1856) Les Fontaines Publiques de la Ville de Dijon. Paris: V Dalmont, 647p.

Davis, G. and Ritchie, A. (1986) A model of oxidation in pyritic mine wastes: part 1 equations and approximate solution. *Applied Mathematical Modelling*, **10**, 314-322.

Davison, W., Lishman, J. P. and Hilton, J. (1985) Formation of pyrite in freshwater sediments: implications for C/S ratios. *Geochimica et Cosmochimica Acta*, **49,** 1615-1620.

Davies M., and Mumby, B. (1999) *Acid sulfate soil management priority areas in the Shoalhaven floodplain- Broughton Creek.* Department of Land and Water Conservation, Sydney.

Dent, D. and Bowman, G. (1996) Quick, quantitative assessment of the acid sulfate hazard. Proceedings 2nd National Conference on Acid Sulphate Soils. (Eds. Smith and Smith). pp. 96-98. Coffs Harbour.

Dent, D. and Pons, L. (1993) Acid and muddy thoughts. In '*Proceedings National Conference on Acid Sulfate Soils*'. (Ed. R. Bush). 24-25 June 1993 Coolangatta, NSW, 1-19.

Dent, D. (1992) Reclamation of Acid Sulphate Soils. Springer-Verlag Publishing, New York, USA, 117p.

Dent, D. (1986) Acid Sulphate Soils: a baseline for research and development. IRRI Publication No. 39. Wageningen. The Netherlands.

Dick, T. M. and Osunkoya, O. O. (2000) Influence of tidal restriction floodgates on decomposition of mangrove litter. Aquatic Botany (68) pp. 273-280.

Downey, J. (1997) Shoalhaven City Council Senior Engineer. Personal Communication.

Easton, A., Clesceri, L. and Greenberg, A. (Eds) (1995) Standard Methods for the Examination of Water and Wastewater. American Public Health Association, Washington DC, USA.

Evangelou, V. (1995) Pyrite Oxidation and its Control. CRC Press. New York. USA.

Fanning, D.S. and Fanning M. C. B. (1988) Soil: Morphology, Genesis and Classification. John Wiley and Sons, New York, pp. 395.

Fanning, D. (1993) Salinity problems in acid sulfate coastal soils. In 'Towards the Rational Use of High Salinity Tolerant Plants'. (Eds., Lieth, H. and Masoom, A). Kluwer Academic Publishers. The Netherlands.

Ferguson, A. and Eyre, B. (1995) Local and regional impacts of acid runoff from acid sulfate soils environments in the lower Richmond River catchment. Centre for Coastal Management, Southern Cross University, Lismore.

Ferguson, A., and Eyre, B. D. (1996) Floodplain hydrology and the transport of acid sulfate soil products. In *Proceedings of 2nd National Conference on Acid Sulfate Soils,* Coffs Harbour, 5-6 September 1996, (Eds. R. J. Smith and H. J. Smith), pp. 120-127.

Flemming, W. G. K., Weltman, A. J., Randolph, M. F., and Elson, W. K. (1992) *Piling Engineering*. Blackie and Son, Ltd., London.

Fitzpatrick, R. W., Fritsch, E. and Self, P. G. (1993) Australia's unique saline acid sulphate soils associated with dryland salinity. In Proceeding of National Conference of Acid Sulphate Soils. Coolangatta, Qld. Australia, 24-25 June pp. 41-56.

Food and Agricultural Organisation/United Nations Scientific and Cultural Organisation (1974) Soil Map of the World, Vol 1, Legend, UNESCO, Paris.

Ford, K. (2002) An Evaluation Of The Saline Buffering Principle As An Acid Sulphate Soil Management Technique Using Soil & Water Quality Indicators. Unpublished BE(Honours) thesis. University of Wollongong, NSW.

Glamore, W. and Indraratna, B. (2001) The impact of floodgate modifications on water quality in acid sulphate soil terrains. In *15th Australasian Coastal and Ocean Engineering Conference Proceedings*, 25-28th September, Gold Coast, Australia.

Goldhaber, M. B. and Kaplan, I. R. (1982) Controls and consequence of sulphate reduction rates in recent marine sediments. In J. A. Kittrick, D. S. Fanning and L. R. Hossner (eds.) Acid Sulfate Weathering, pp. 19-36. Soil Science Socity of America Special Publication No. 10, Madison, WI, USA.

Hausmann, M. (1990) Engineering Principles of Ground Modification. McGraw-Hill. pp 632.

Hicks, W., Bowman, G. and Fitzpatrick. J. (1999) East Trinity Acid Sulfate Soils Part 1: Environmental Hazards. CSIRO Land and Water Technical Report 14/99. Canberra.

Host, A. F. van and Westerveld, G. J. W. (1973) Corrosion of concrete foundations in (potential) acid sulphate soils and subsoils in the Netherlands. In H. Dost (ed.) Acid sulphate soils. Proceeding of the International Symposium, International Institute for Land Reclamation and Improvement Publications No. 18. Vol 2 pp. 373-381, Wageningen, Netherlands.

Ikin, D. (2001) Stratification of acid sulphate soil affected waters. Unpublished Bachelor of Engineering Honours thesis, University of Wollongong, NSW Australia.

Indraratna, B., Glamore, W. and Tularam, G. A. (2002) The effects of tidal buffering on acid sulphate soil environments in coastal areas of New South Wales. *Geotechnical and Geological Engineering* **20**(3) pp. 181-199.

Indraratna, B., Glamore, W., Blunden, B., Downey, J. and Tularam, A. (2001). Engineering Strategies for Controlling Problems of Acid Sulphate Soils in Low-lying Coastal Areas. Proc. 2nd Australia-New Zealand Conference on Environmental Geotechnics, Newcastle, (Smith, D.W., Fityus, S.G., and Allman, M.A. editors), Published by Australian Geomechanics Society Inc., pp. 133-146.

Indraratna, B. (1983) Grout properties and methods of grouting under dam foundations. Unpublished MSc thesis, University of London.

Indraratna, B. (1996) Utilization of lime, slag and fly ash for improving colluvial clay soils in NSW. *International Journal of Geotechnical and Geological Engineering*, **14**, 169-191.

Indraratna, B. and Blunden, B. (1997) Remediation of acid sulphate soils by management of groundwater table. In 'Proceedings Second International Green Symposium on Geotechnics and the Environment'. (Ed. Sarsby), pp. 516-524 Thomas Telford Publishers, Krakow, Poland.

Indraratna, B. and Blunden, B. (1999) Nature and properties of acid sulphate soils in drained coastal lowlands in New South Wales. *Australian Geomechanics Journal*, **34**(1), 61-78.

Indraratna, B., Sullivan, J. and Nethery, A. (1995) Effect of groundwater table on the formation of acid sulphate soils. *Minewater and the Environment.* **14**, 71-84.

Indraratna, B. (2003) Installation of lateral lime-flyash barriers in Acid Sulphate Soils. Personal communication and interim reports to Shoalhaven City Council, Nowra.

Johnston, S. G., Slavich, P., and Hirst, P. (2003) Floodgate and drainage system management: opportunities and limitations. An acid export perspective. In *Proceedings of Third International Conference on Acid Sulphate Soils.* 25-31 August 2002, Coolangatta, Qld.

Jones, B. F., Vengosh, A., Rosenthal, E., and Yechieli, Y. (1999) *Seawater Intrusion in Coastal Aquifers- Concepts, Methods and Practices* Bear, J., Cheng, A. H. D., Sorek, S., Ouazar, D., and Herrera, I. (eds.) Kluwer Academic Publishers, London.

Kraus, M. J. (1998) Development of potential acid sulphate paleosols in Paleocene floodplains, Bighorn Basin, Wyoming, USA. Palaeogeography, Palaeoclimatology, and Palaeoecology **144**, 203-224

Lawrie, R. and Murphy, A. (1996) Irrigated cropping on acid sulfate soils of NSW South Coast. In 'Proceedings 2nd National Conference on Acid Sulfate Soils.' (Eds RJ Smith, HJ Smith) 5-6 September, Coffs Harbour, NSW.

Lewis, R. (1997) *Dispersion in Estuaries and Coastal Waters*. John Wiley and Sons, New York, 312p.

Lewin, J. (1995) *Hydraulic gates and valves in free surface flow and submerged outlets.* Thomas Telford Publications, London, 238p.

Lin, C. and Melville, M. (1993) Controls on soils acidification by fluvial sedimentation in an estuarine floodplain, eastern Australia. *Sedimentary Geology*, **85**, 1-13.

Lin, C. and Melville, M. (1994) Acid sulphate soil landscape relationships in the Pearl River Delta, southern China, *Catena*, **22**, 105-120.

Lin, C. Melville, M. White, I. and Wilson, B. (1995) Human and natural controls on the accumulation, acidification and drainage of pyritic sediments: contrasts between the Pearl River delta, China and coastal NSW. *Australian Geographical Studies*, **33**, 77-88.

Lin, H., Richards, D., Talbot, C., Yeh, G., Cheng, J., Cheng, H. and Jones, N. (1997) FEMWATER: A three dimensional finite element computer model for simulating density dependent flow and transport in variably saturated media. Technical Report CHL-97-12 US Army.

Lin, C., Melville, M. D., Islam, M. M., Wilson, B. P., Yang, X., van Oploo, P. (1998) Chemical controls on acid discharges from acid sulfate soils under sugarcane cropping in an eastern Australian estuarine floodplain. *Environmental Pollution*, **103**, 269-276.

Marius, C. (1985) Mangroves du Senegal et de la Gambie, Editions de L'ORSTROM, Institut Francais de Recherche Scientifque pour le Developpement en Cooperation, Travaux et Documents, No. 193, Paris.

Mermut, A. R. and Arshad, M. A. (1987) Significance of sulphide oxidation in soil salinization in Southeastern Saskatchewan. Journal of Soil Science of America (51) pp. 247-251.

Middleton, M. J., Rimmer, M. A., and Williams, R. J. (1996) Structural Flood Mitigation Works and Estuarine Management in New South Wales-Case Study of the Macleay River. *Coastal Zone Management Journal* **13**(1) 1-22.

Miller, R. L., Bradford, W. L. and Peters, N. E. (1988) Specific Conductance: Theoretical considerations and application to analytical quality control. United States Geological Survey Water-Supply Paper 2311. USGS, Federal Center Box 25425, Denver, CO 80225.

Mulvey,. P. (1993) Pollution, prevention and management of sulfuric clays and sands. In '*Proceedings National Conference on Acid Sulfate Soils*'. (Ed. R. Bush). 24-25 June 1993 Coolangatta.

Naylor, S., Chapman, G., Atkinson, G., Murphy, C., Tulau, M., Flewin, T., Milford, H. and Moran, D. (1995) Guidelines for the use of acid sulphate soils risk maps. Soil Conservation Service. Sydney.

Neal, P. (1996) Acid sulfate soils - one dairy farmers experience. *Proceedings 2nd National Conference on Acid Sulphate Soils.* (Eds. Smith and Smith). pp. 172-174. Coffs Harbour.

Nethery, A., Jamieson, P., and Downey, J. (1996) Shoalhaven River Project, In *Proceedings of 2nd National Conference on Acid Sulfate Soils,* Coffs Harbour, 5-6 September 1996, (Eds. R. J. Smith and H. J. Smith), pp. 89-91.

New South Wales State Fisheries (1976) Impact of dam construction and flood mitigation works on the aquatic environment. *NSW State Pollution Control Commission's Technical Advisory Committee*, New South Wales State Fisheries, Sydney, Australia.

Nordstrom, D. (1982) The effect of sulfate on aluminium concentrations in natural waters: some stability relations in the system Al_2O_3-SO_3-H_2O at 298 K. *Geochimica et Cosmochimica Acta*, **46**, 681-692.

Norwood, T. G. (1975) Studies of the acid sulphate soils of the lower Shoalhaven River Floodplain, Unpublished MSc thesis, University of Wollongong, NSW, 114p.

Nriagu, J. (1978) Dissolved silica in pore waters of Lake Ontario, Eire and Superior sediments. *Limnology and Oceanography*, **23**, 53-67.

Parkhurst, D. (1995) PHREEQC - A computer program for speciation, reaction-path, advective transport, and inverse geochemical calculations. *US Geological Survey. Water Resources Investigations Report 95-4227.* Lakewood, Colorado, USA.

Patterson, C., and Smith, R. (2000) Acid sulfate soils program: Design improvements – rural drainage schemes. Final report prepared by Patterson Consultants Pty Limited. 41p.

Pease, M. (1994) Acid sulfate soils and acid drainage Lower Shoalhaven Floodplain, NSW. Unpublished Msc(Hons) thesis. University of Wollongong.

Pease, M., Nethery, A. and Young, A. (1997) Acid sulfate soil and acid drainage, Lower Shoalhaven floodplain, New South Wales. *Wetlands (Australia)* **16**, 56-71.

Pearson, F. H., and MacDonell, A. J. (1975) Limestone Barriers to Neutralise acidic streams. Journal of the Environmental Engineering Division, ASCE Vol. 10, No. EE1, Paper #11131, 139-158.

Pethick, R. J. and Harrison, A. J. W. (1981) The theorectical treatment of the hydraulics of rectangular flap gates. 19th I.A.H.R. Congress, Karlsruhe, subject B (c), paper #12.

Pollard, D. A., and Hannan, J. C. (1994) The ecological effects of structural flood mitigation works on fish habitats and fish communities in the lower Clarence River System of South-Eastern Australia. *Estuaries* **17**(2), 427-461.

Pons, L. (1973) Outline of genesis, classification and improvement of acid sulfate soils. In 'Acid Sulfate Soils: Proceedings of the International Symposium' 13-20 August. IRRI Publication 18 Wageningen, The Netherlands.

Pons, L. J. and van Breeman, N. (1982) Factors influencing the formation of potential acidity in tidal swamps. In H. Dost and N. van Breeman (eds.): *Proceedings of the Bangkok Symposium on acid sulphate soils*, 37-51. IRRI Publication 39 Wageningen, The Netherlands.

Pons, L. J., Breeman, N. van and Driessen, P.M. (1982) Physiography of coastal sediments and development of potential soil acidity. In J. A. Kittrick, D. S. Fanning and L. R. Hossner (eds.) Acid Sulfate Weathering, pp. 1-18. Soil Science Socity of America Special Publication No. 10, Madison, WI, USA.

Portnoy, J. W. (1999) Salt marsh diking and restoration: Biogeochemical implications of altered wetland hydrology. *Environmental Management* **24**(1), 111-120.

Portnoy, J. W. and Giblin, A. E. (1997a) Biogeochemical effects of seawater restoration to diked salt marshes. *Ecological Applications* **7**(3), 1054-1063.

Portnoy, J. W. and Giblin, A. E. (1997b) Effects of historic tidal restrictions on salt march sediment chemistry. *Biogeochemistry* **36**, 275-303.

Pressey, R. L. and Middleton, M. J. (1982) Impacts of flood mitigation works on coastal wetlands in New South Wales. *Wetlands* **2**(1), 27-44.

Rayment, G. and Higginson, F. (1992) Australian Laboratory Handbook of Soil and Water Chemical Methods. Inkata Press. Melbourne.

Read, R. (1974) Broad scale soil survey of eastern flats, Nowra. BCRI, Department of Agriculture, Rydlemere, NSW.

Ritsema, C., Groenenberg, J. and Bisdom, E. (1992) The transformation of potential into actual acid sulphate soils studied in column experiments. *Geoderma*, **55**, 259-271.

Roy, P., Thom, B. and Wright, L. (1980) Holocene sequences on an embayed high-energy coast: an evolutionary model. *Sedimentary Geology*, **26**, 1-19.

Roy, P. (1984) New South Wales estuaries: their origin and evolution. In '*Coastal Geomorphology in Australia.*' (Ed. Thom). Academic Press Australia. Sydney.

Rudens, C. (2001) The role of biotic oxidation on acid production in potential acid sulfate soils in the Shoalhaven floodplain. Unpublished BE(honours) thesis. University of Wollongong, NSW, 85p.

Sammutt, J., and Melville, M. (1994) Impacts of poor water quality on fish. In *Proceedings of Geomorphology and river health in New South Wales*, (Editors Brierley, G. J. and Nagel, F.) October 7th, Macquarie University.

Sammut, J., White, I., and Melville, M. D. (1994) Stratification in acidified coastal floodplain drains. *Wetlands (Australia),* **13**, 49-64.

Sammut, J., Melville, M., Callinan, R. and Fraser, G. (1995) Estuarine acidification: impacts on aquatic biota of draining acid sulfate soils. *Australian Geographical Studies*, **33**, 89-100.

Sammut, J., White, I., and Melville, M. (1996) Acidification of an estuarine tributary in eastern Australia due to drainage of acid sulphate soils. *Marine and Freshwater Research.* **47**, 669-84.

Sbeghen, B. (1995) Acid sulfate soils in the Berry region, NSW - Baseline studies and preliminary assessment of management options. Honours thesis for Master of Environmental Science, Faculty of Science, University of Wollongong, Australia.

Sharman, S. M. (1995) A study on Acid sulfate soils found on agricultural land on the Broughton Creek Floodplain, Berry NSW. Honours thesis for Bachelor of Environmental Science, Faculty of Science, University of Wollongong, Australia.

Simpson, H. J., and Pedini, M. (1985) Brackish water aquaculture in the tropics: the problem of Acid Sulfate Soils. *Food and Agricultural Organisation of the United Nations, Fisheries Circular* No. 791, UNESCO, Rome, 32p.

Spitz, K. and Moreno, J. (1996) *A Practical Guide to Groundwater and Solute Transport Modeling.* John Wiley and Sons, New York, 461p.

State Pollution Control Commission (1978) *Report and findings of the environmental investigation into the environmental impact assessment of flood mitigation works and dams*. State Pollution Control Commission, Sydney, Australia.

Stumm, W. and Morgan, J. J. (1996) *Aquatic Chemistry* (3rd edn). John Wiley and Sons, New York.

Stone, Y., Ahern, C. and Blunden, B. (1998) NSW Acid Sulfate Soil Manual. NSW Government. Sydney.

Sullivan, J. R. (1995) Development of an optimisation strategy for the management of acid sulphate soils in the Illawarra. Unpublished BE(honours) thesis. University of Wollongong, NSW, 102p.

Swales, S. (1982) Environmental effects of river channel works used in land drainage improvements. *Journal of Environmental Management* **14**, 103-126.

Thom, B. G. and Chappell, J. (1975) Holocene sea levels relative to Australia, *Search*, **6**, 90-93.

Toniato, T. (1998) Laboratory testing of pyrite oxidation in column tests. Undergraduate Honours Thesis, University of Wollongong, NSW.

Umitsu, M., Buman, M., Kumiko, K., Woodroofe, C. (2001) Holocene palaeoecology and formation of the Shoalhaven River deltaic-estuarine plains, southeast Australia. *The Holocene* **11**(4), 407-418.

van Breemen, N. (1973) Soil forming processes in acid sulphate soils. In 'Acid Sulphate Soils: Proceeding of the International Symposium on Acid Sulphate'. (Ed. H. Dost) pp 66-129. ILRI, Wageningen, The Netherlands.

Van Breeman, N. (1980) Acid sulphate soils. Problem soils: their reclamation and management. Land Reclamation and water management. ILRI pub. 27, Wageningen, pp. 53-57.

van Breeman, N. (1985) Redox processes of iron and sulfur involved in the formation of acid sulfate soils. In 'Iron in Soils and Clay Minerals'. (Eds, Stucki, J., Goodman, B. and Schwertmann, U.) D. Reidel Publishing Company, Boston, USA. pp 825-841.

van Genuchten, M. (1980) A closed form equation for predicting the hydraulic conductivity of unsaturated soils. *Soil Science Society America Journal*, **44**, 892-898.

van Breeman, N. (1992) Environmental aspects of acid sulfate soils. In 'Selected Papers of the Ho Chi Minh City Symposium on Acid Sulphate Soils.' (Eds Dent and van Mensvoort). pp391-402. ILRI Publication 53. Wageningen.

van der Kevie, W. (1973) Morphology, genesis, occurrence, and agricultural potential of acid sulphate soils in Central Thailand. *Thailand Journal of Agricultural Science*. **5**, 165-182.

Walker, P. (1972) Seasonal and stratigraphic controls in coastal floodplain soils. *Australian Journal of Soil Research*, **10**, 127-142.

Webb, J. A. and Sasowsky, I. D. (1994) The interaction of acid mine drainage with a carbonate terrane: evidence from the Obey River, north central Tennessee. *Journal of Hydrology*, **161**, 327-346.

White, I. and Melville, M. (1993) Treatment and Containment of Acid Sulfate Soils. Technical Report 53, Centre for Environmental Mechanics, CSIRO, Canberra.

White, I., Wilson, B., Melvile, M., Sammut, J. and Lin, C. (1996) Hydrology and drainage of acid sulfate soils. Proceedings 2nd National Conference on Acid Sulphate Soils. (Eds. Smith and Smith). pp. 103-108. Coffs Harbour.

White, I., Melville, M., Sammut, J. and Wilson, B. (1997) Reducing acidic discharges from coastal wetlands in eastern Australia. *Wetlands Ecology and Management*, **5**, 55-72.

Willett, I. and Walker, P. (1982) Soil morphology and distribution of iron and sulfur fractions in a coastal plain toposequence. *Australian Journal of Soil Research*, **20**, 283-294.

Willett, I., Crockford, R., and Milnes, A. (1992) Transformation of iron, manganise and aluminium during oxidation of a sulfidic material from an acid sulfate soil. In 'Biomineralisation Processes of Iron and Manganese - Modern and Ancient Environments' (Eds. Skinner, H. and Fitzpatrick, R.) pp 287-301. Germany, Catena Verlag.

Williams, R. J. and Watford, F. A. (1997) Identification of structures restricting tidal flow in New South Wales, Australia. *Wetlands Ecology*, **5**, 87-97.

Wilson, B. (1995) Soil and hydrological relations to drainage from sugarcane on acid sulfate soils. Unpublished PhD thesis, University of New South Wales, Sydney.

Wilson, B., White, I. and Melville, M. (1999) Floodplain hydrology, acid discharge and water quality change associated with drained acid sulfate soil. *Marine and Freshwater Research* **50**, 149-57.

Woodroffe, C., Buman, M., Kawase, K. and Umitso, M. (2000) Estuarine infill and formation of deltaic plains, Shoalhaven River. *Wetlands (Australia)* **18**(2), 72-84.

Young, R., Bryant, E., Price, D., Wirth, L. and Pease, M. (1993) Theoretical constraints and chronological evidence of Holocene coastal development in central and southern New South Wales, Australia. *Geomorphology*, **7**, 317-329.

Appendix A. Climatic variables

The climatic parameters obtained over the study period are given below. Temperature, windspeed and incoming solar radiation measurements were used to calculate evapotranspiration. Floodgate modifications were undertaken on Day 305.

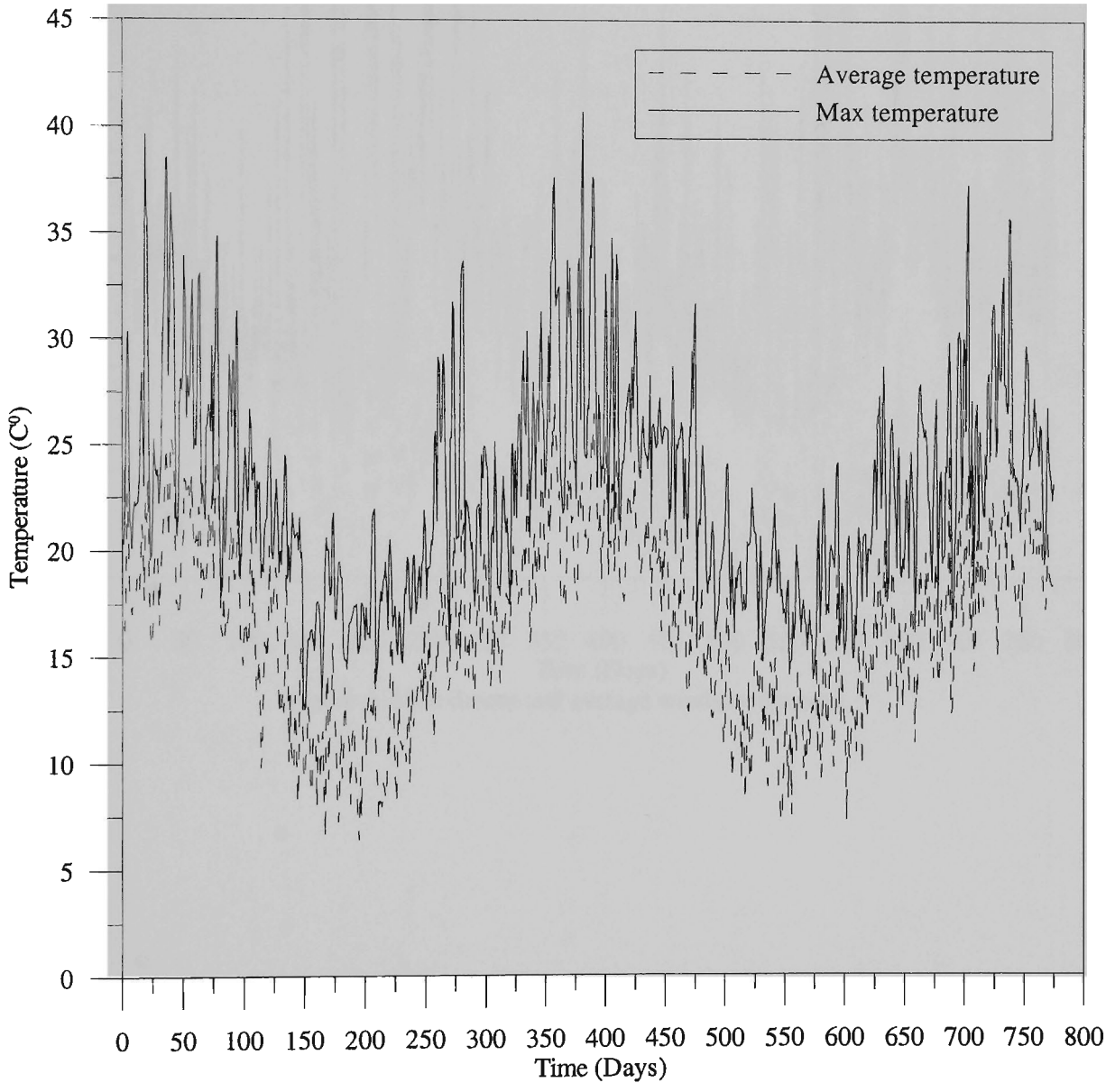

Figure A.1 Maximum and average temperature record.

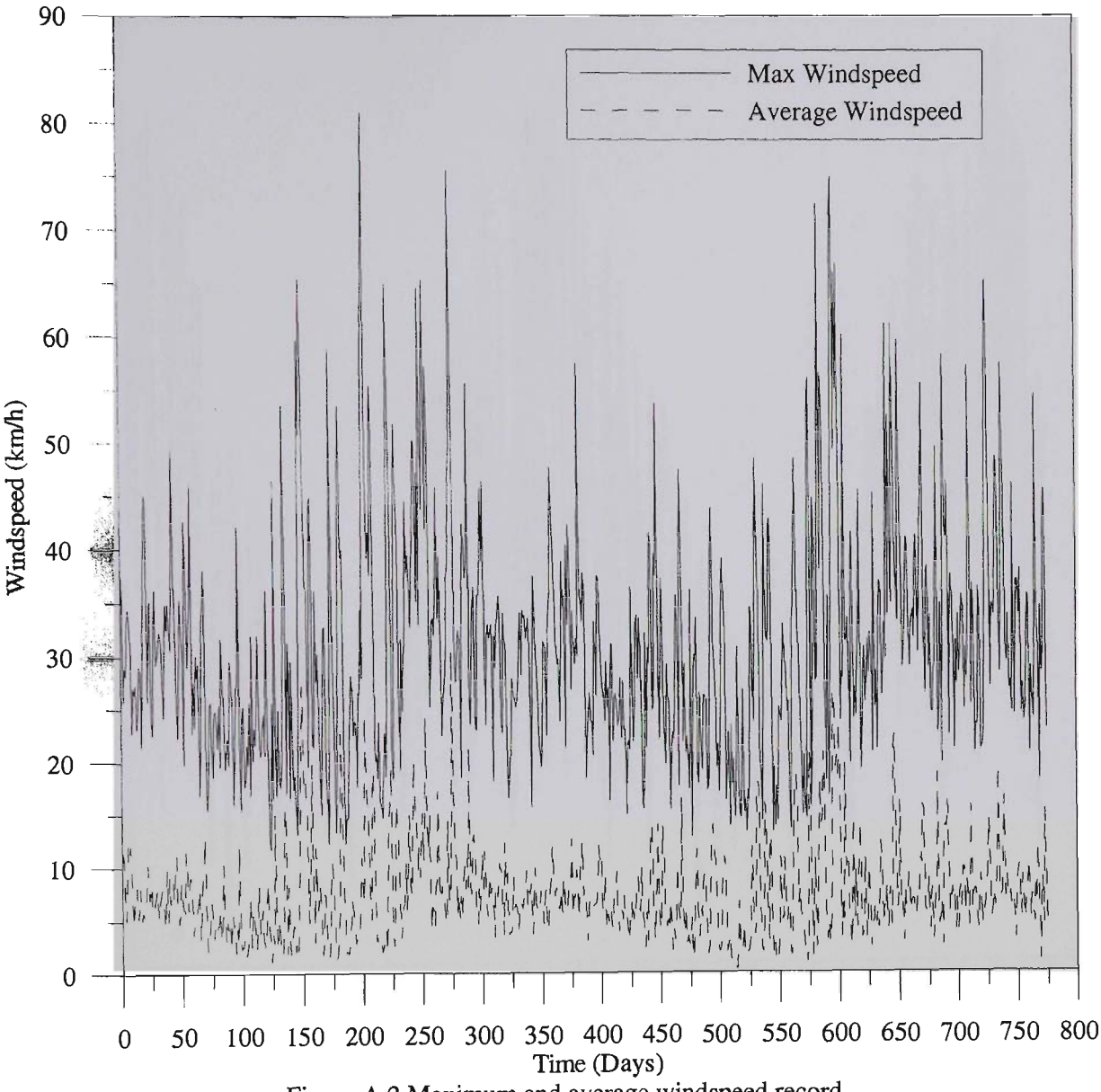

Figure A.2 Maximum and average windspeed record.

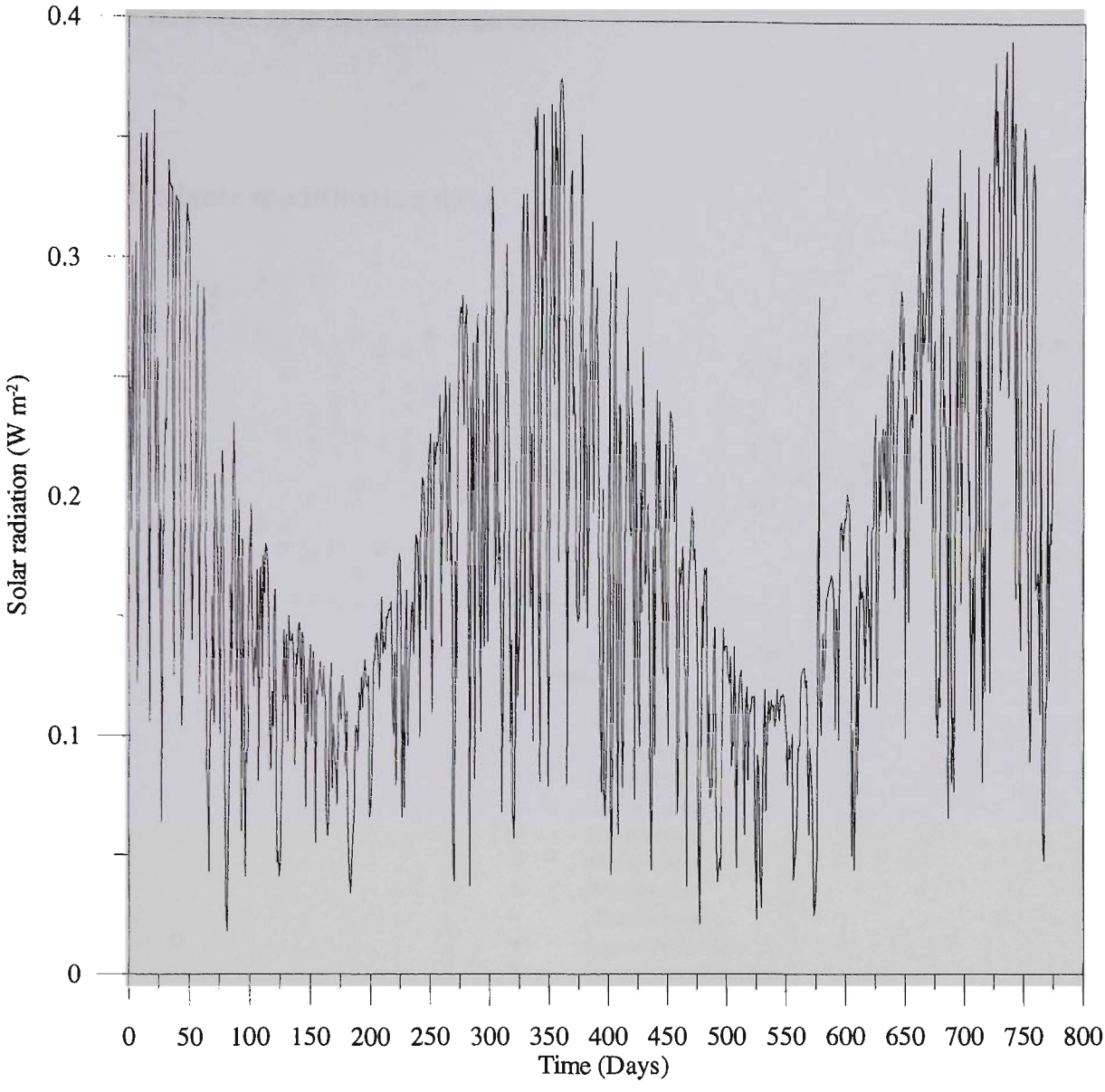

Figure A.3 Incoming solar radiation record.

Appendix B. Field data from all locations

B.1 Pre-floodgate modification data

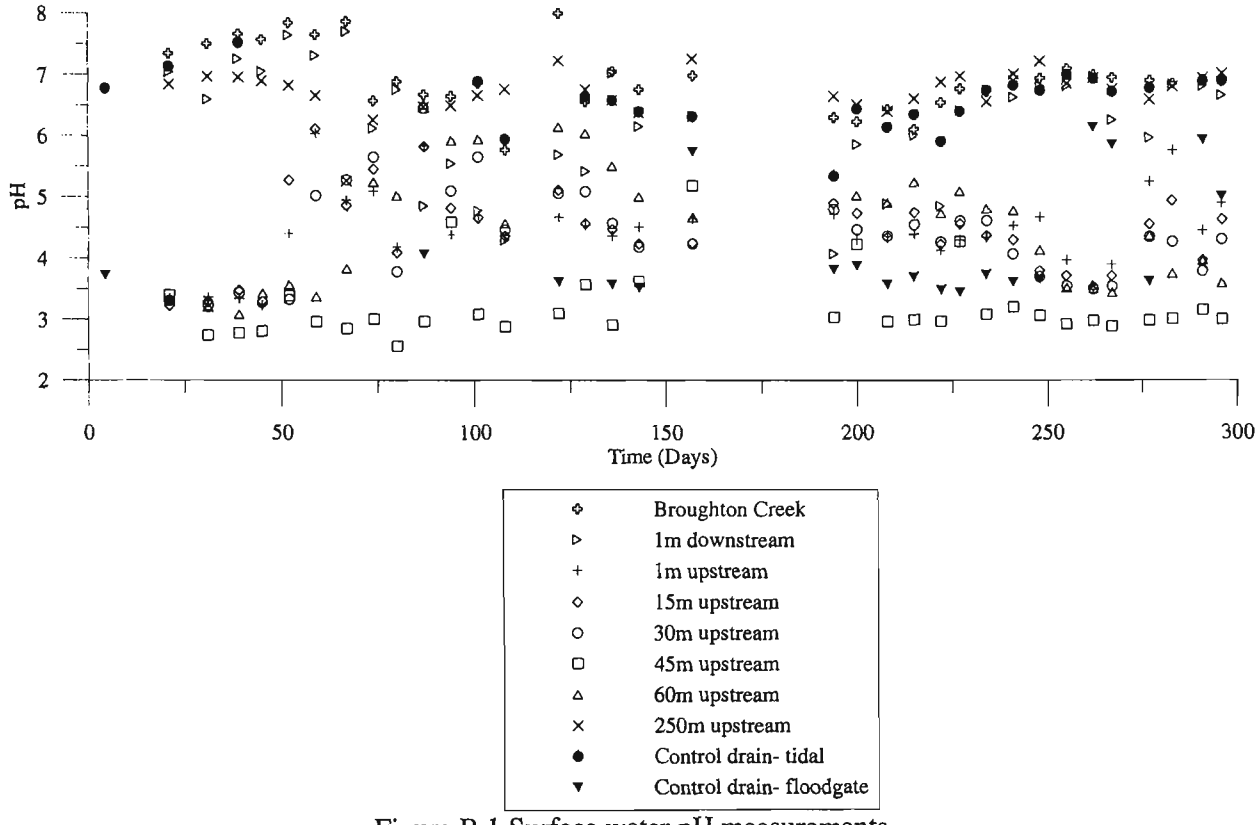

Figure B.1 Surface water pH measurements.

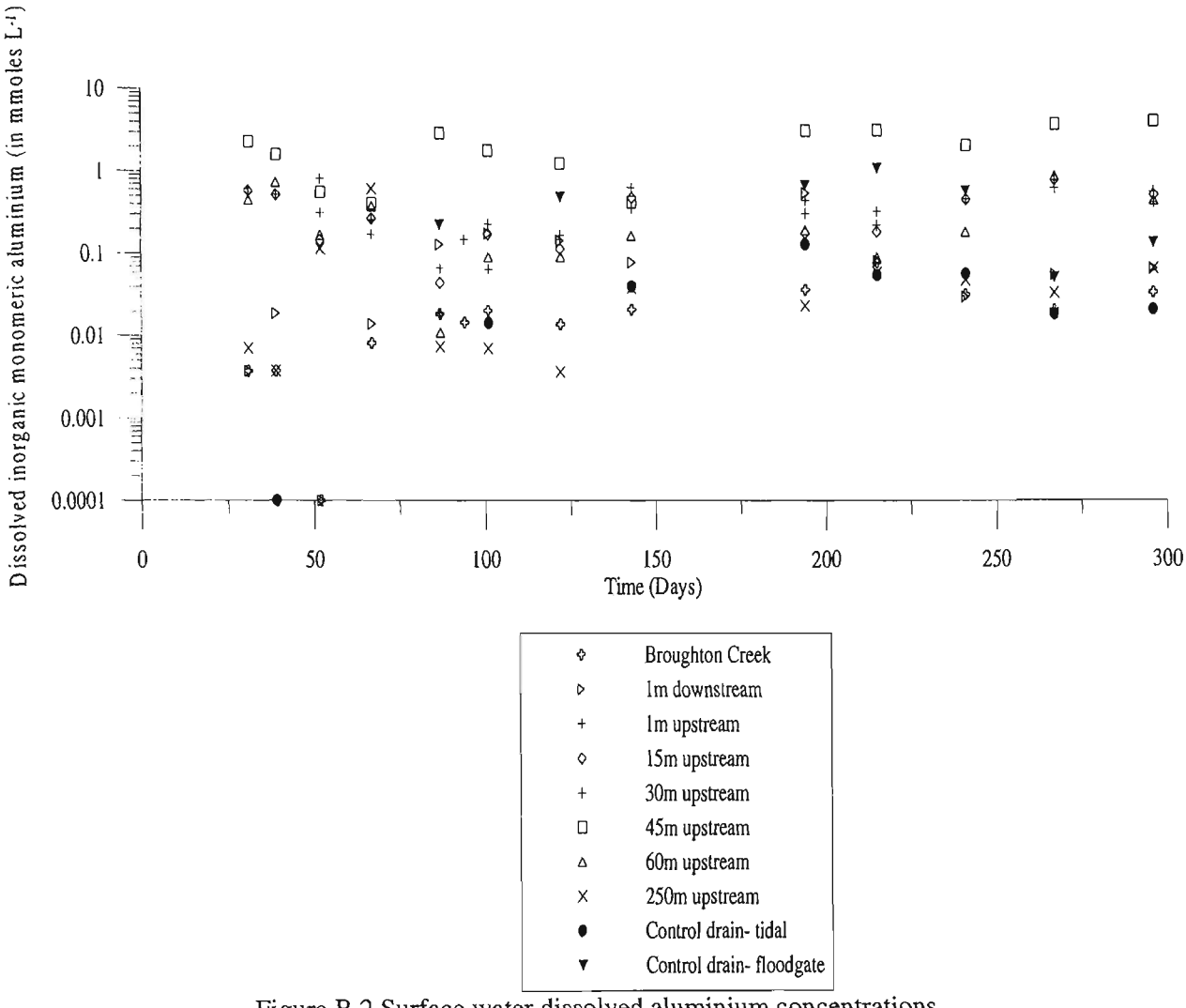

Figure B.2 Surface water dissolved aluminium concentrations.

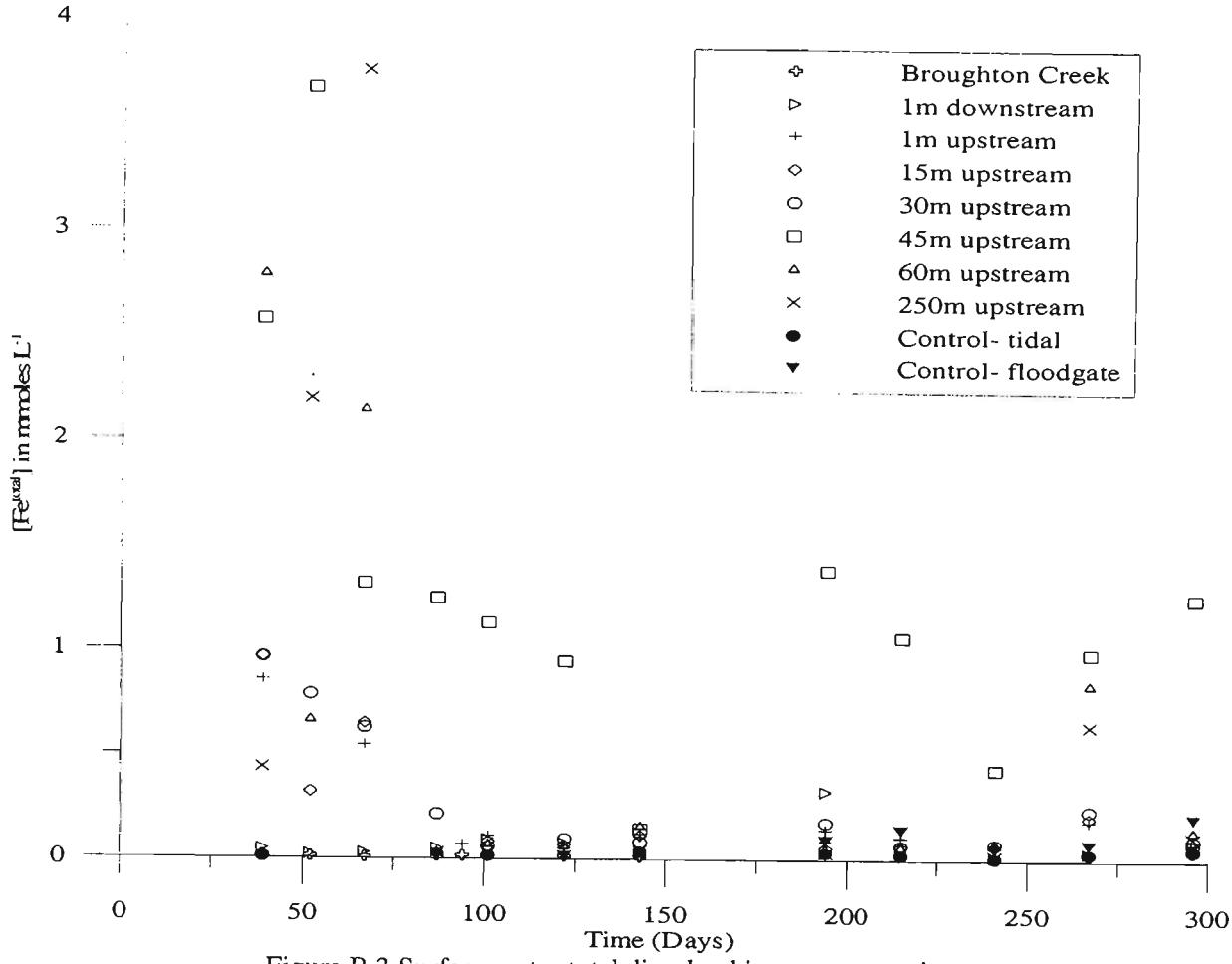

Figure B.3 Surface water total dissolved iron concentrations.

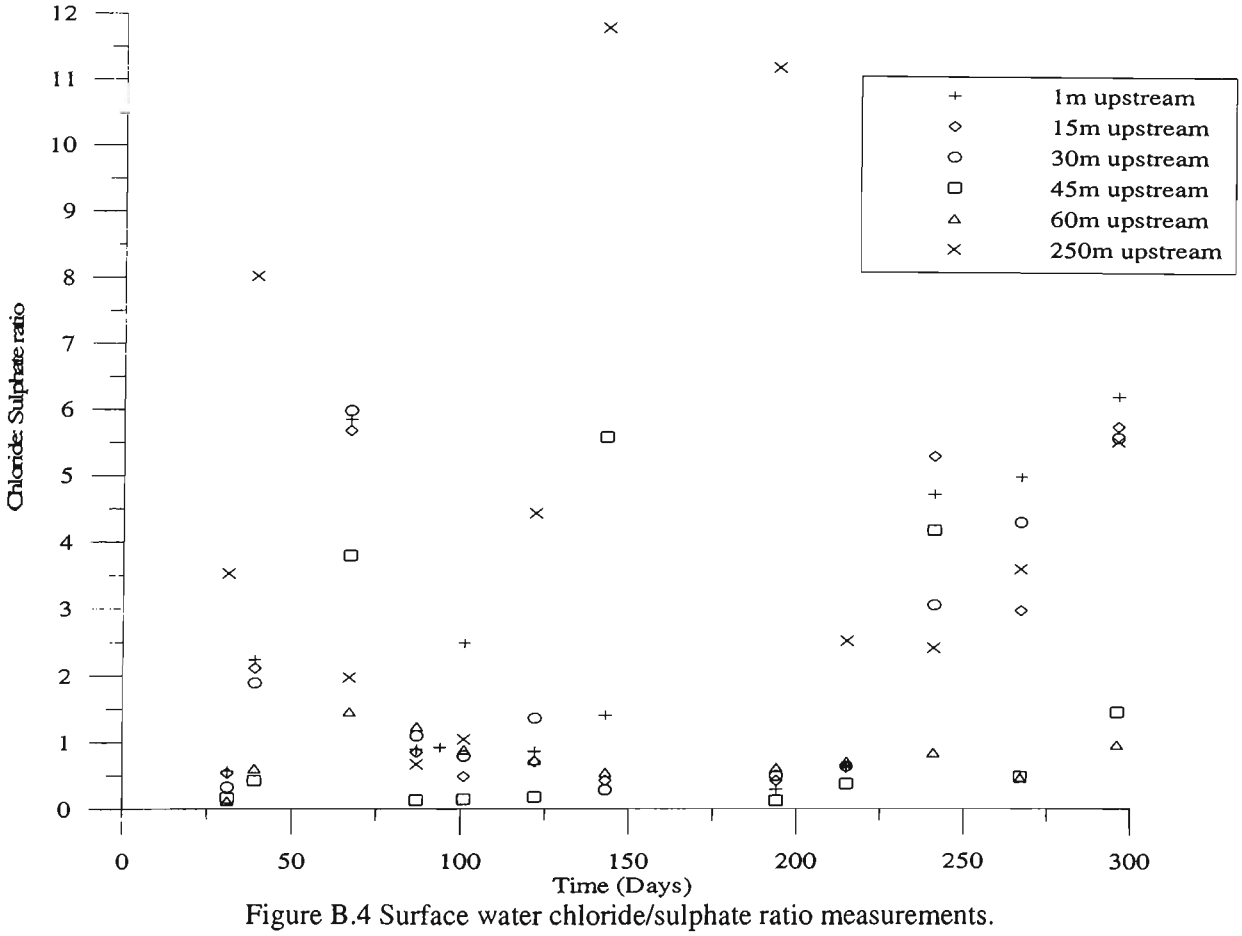

Figure B.4 Surface water chloride/sulphate ratio measurements.

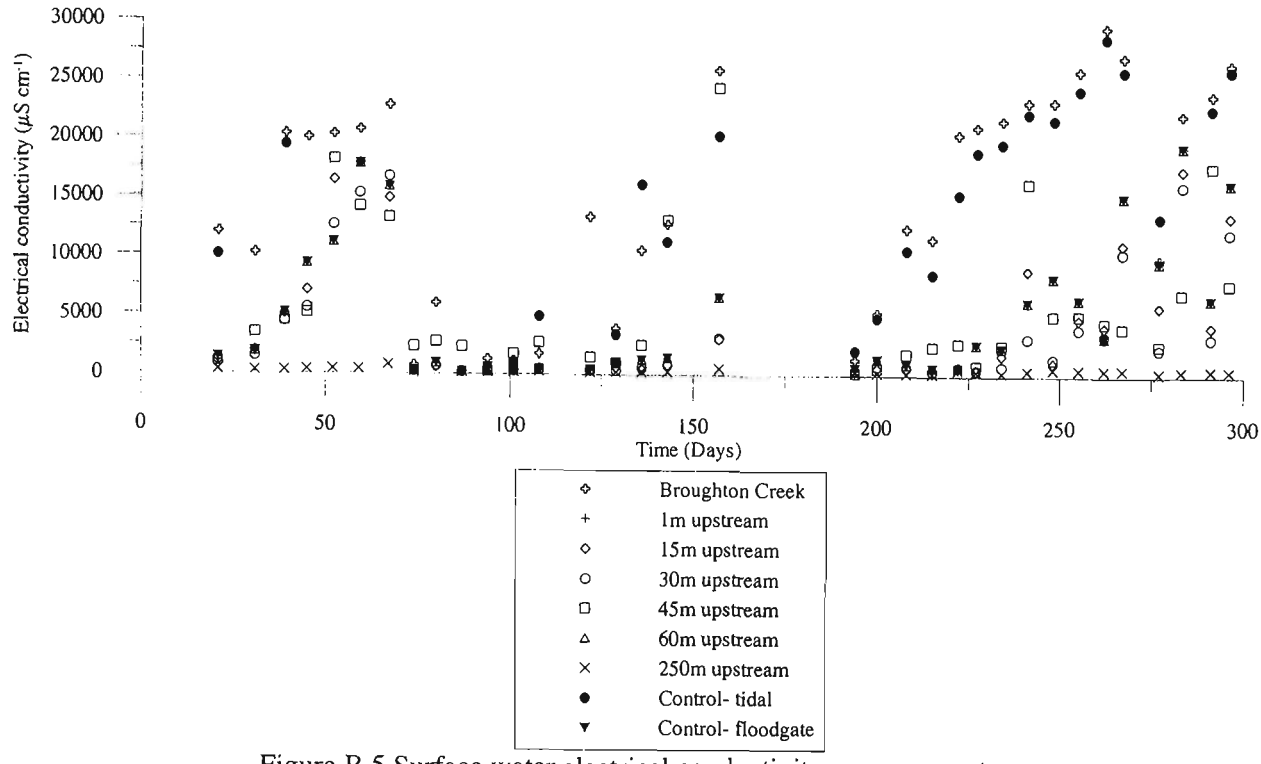

Figure B.5 Surface water electrical conductivity measurements.

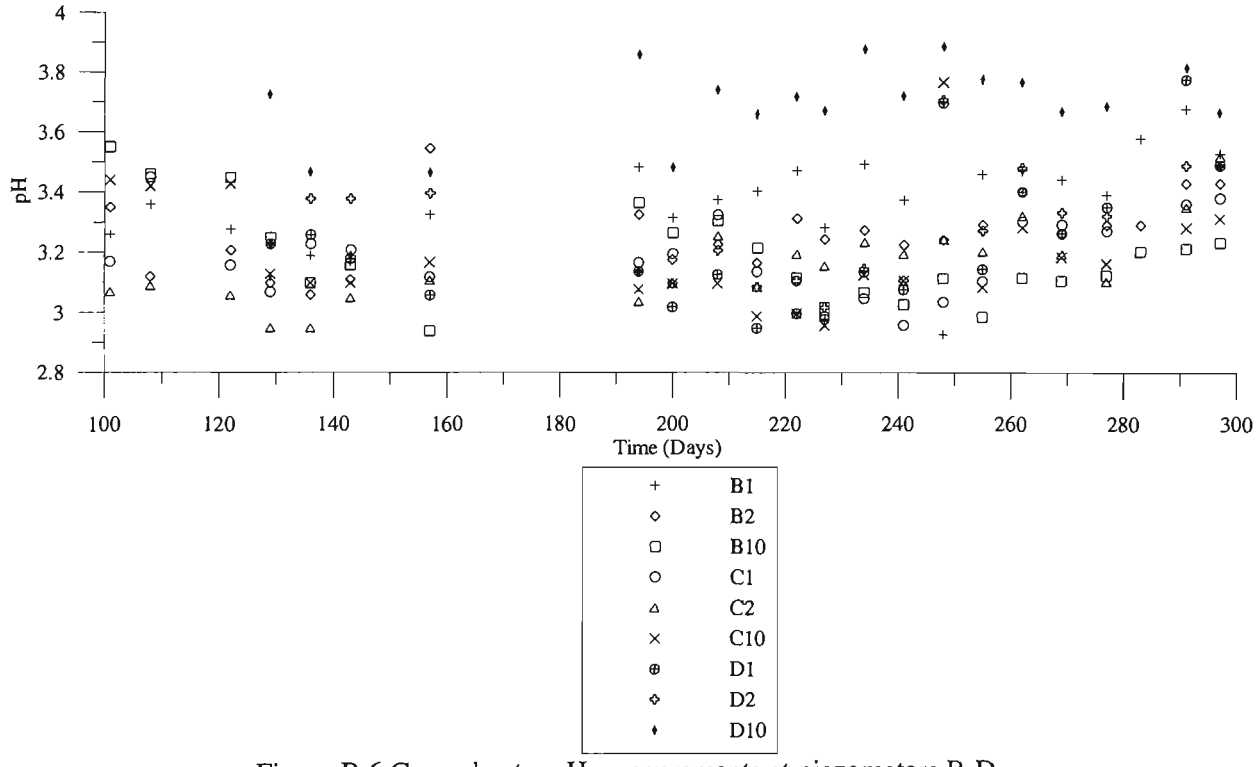

Figure B.6 Groundwater pH measurements at piezometers B-D.

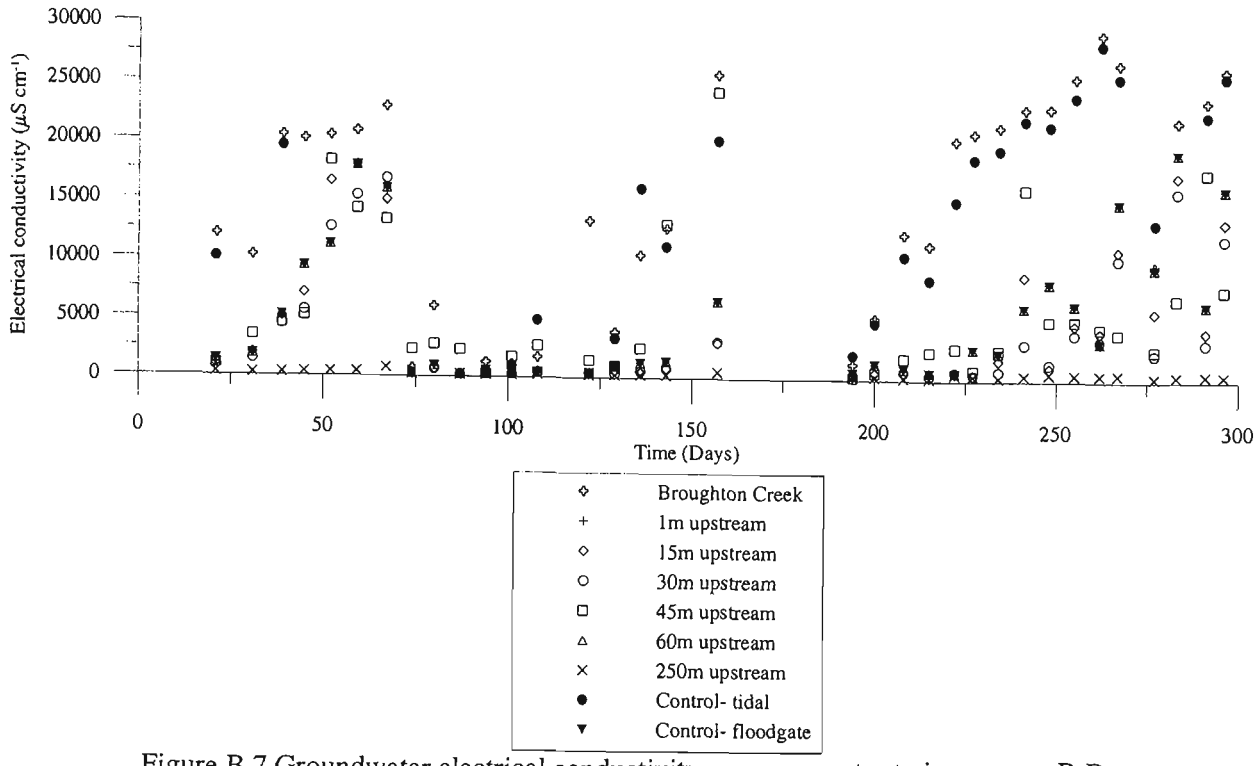

Figure B.7 Groundwater electrical conductivity measurements at piezometers B-D.

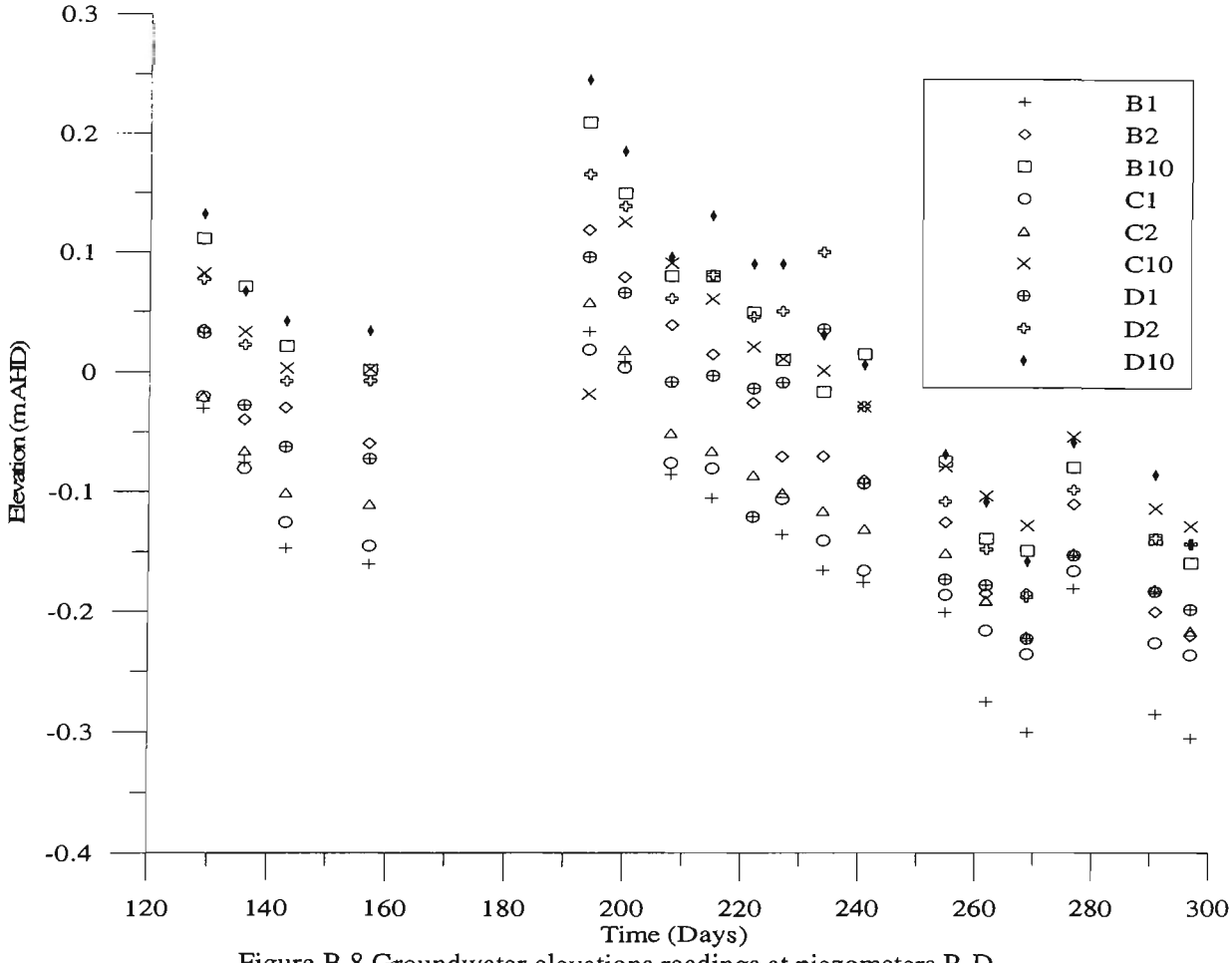

Figure B.8 Groundwater elevations readings at piezometers B-D.

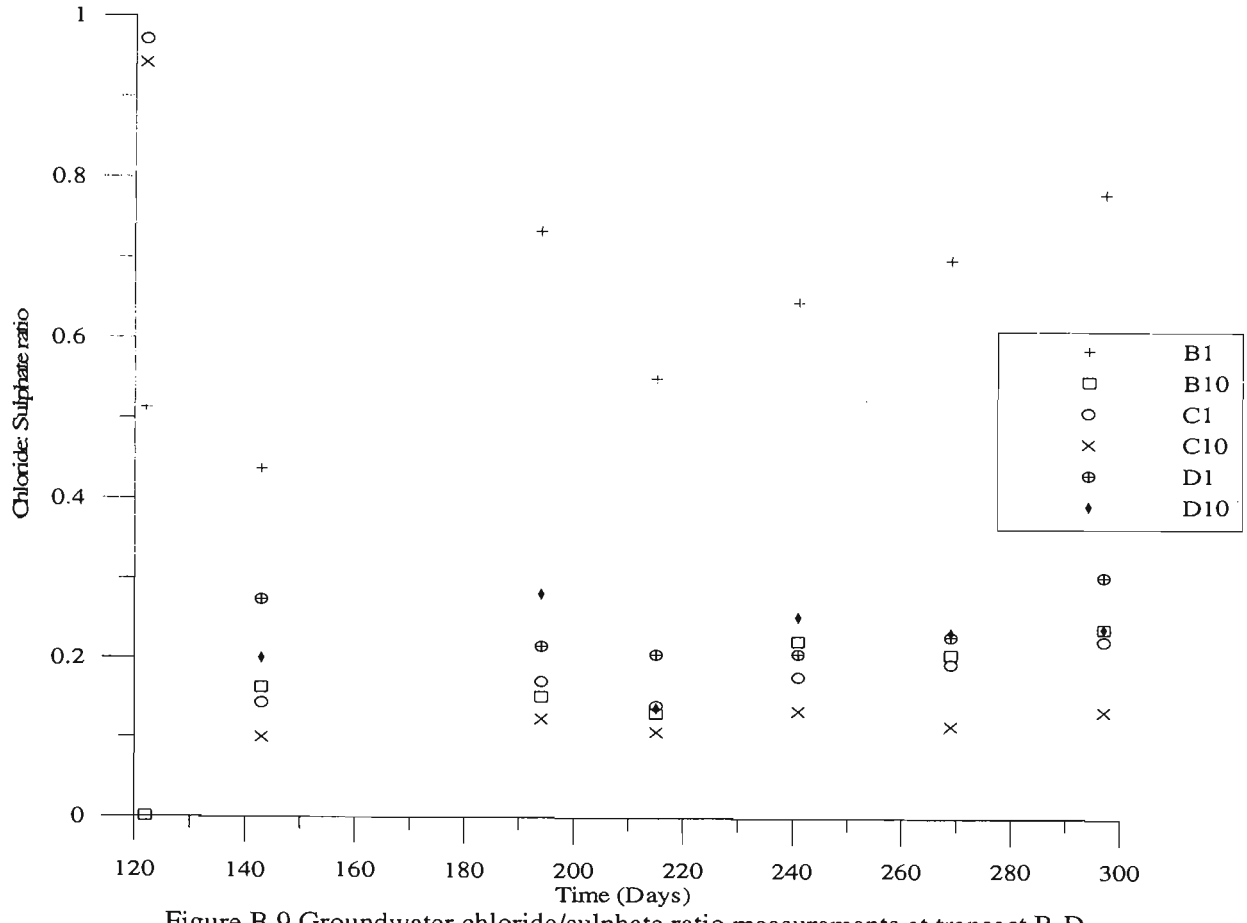

Figure B.9 Groundwater chloride/sulphate ratio measurements at transect B-D.

B.2 Post-floodgate modification data

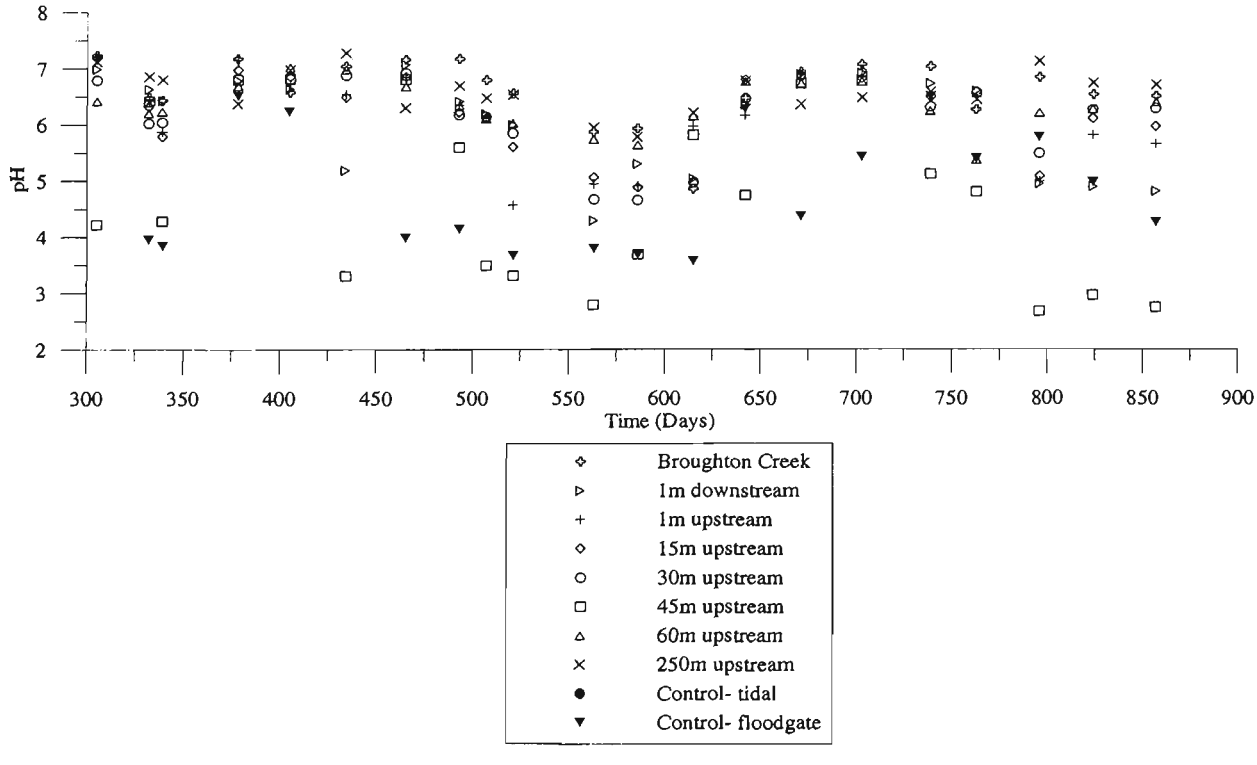

Figure B.10 Surface water pH measurements.

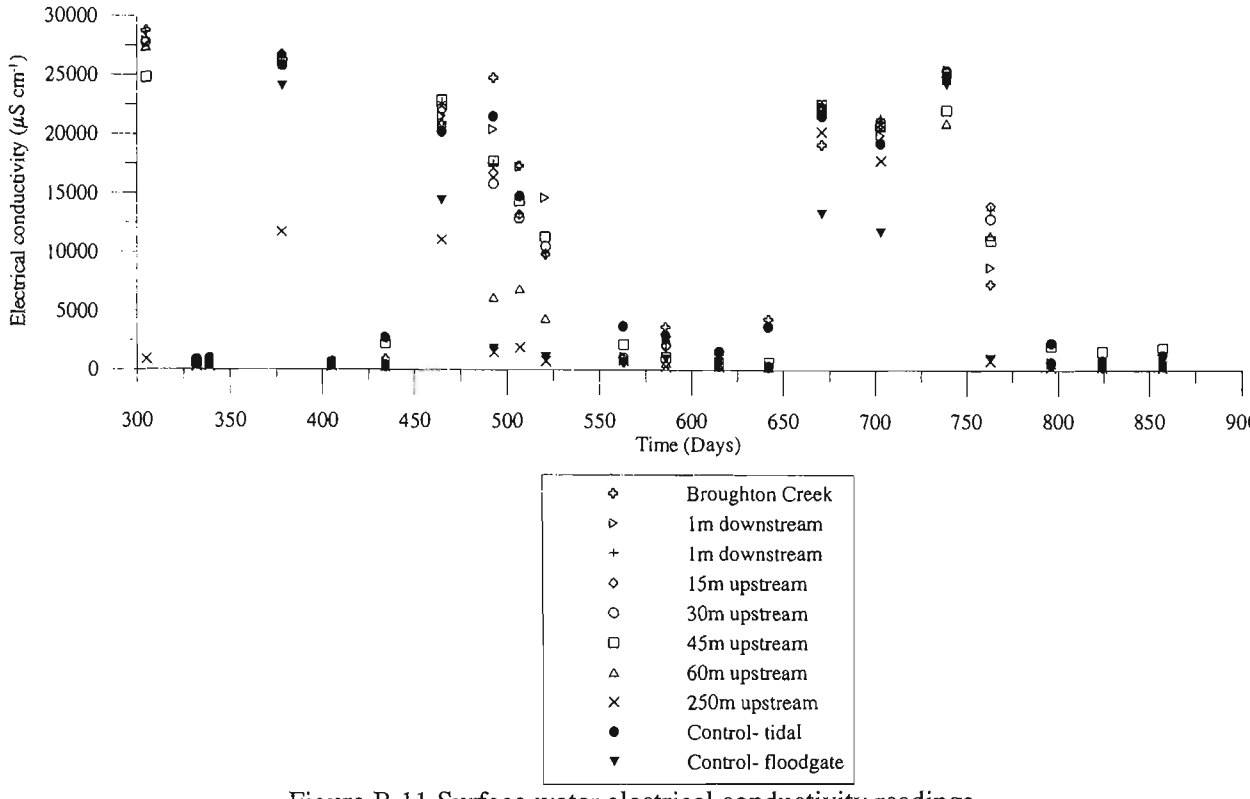

Figure B.11 Surface water electrical conductivity readings.

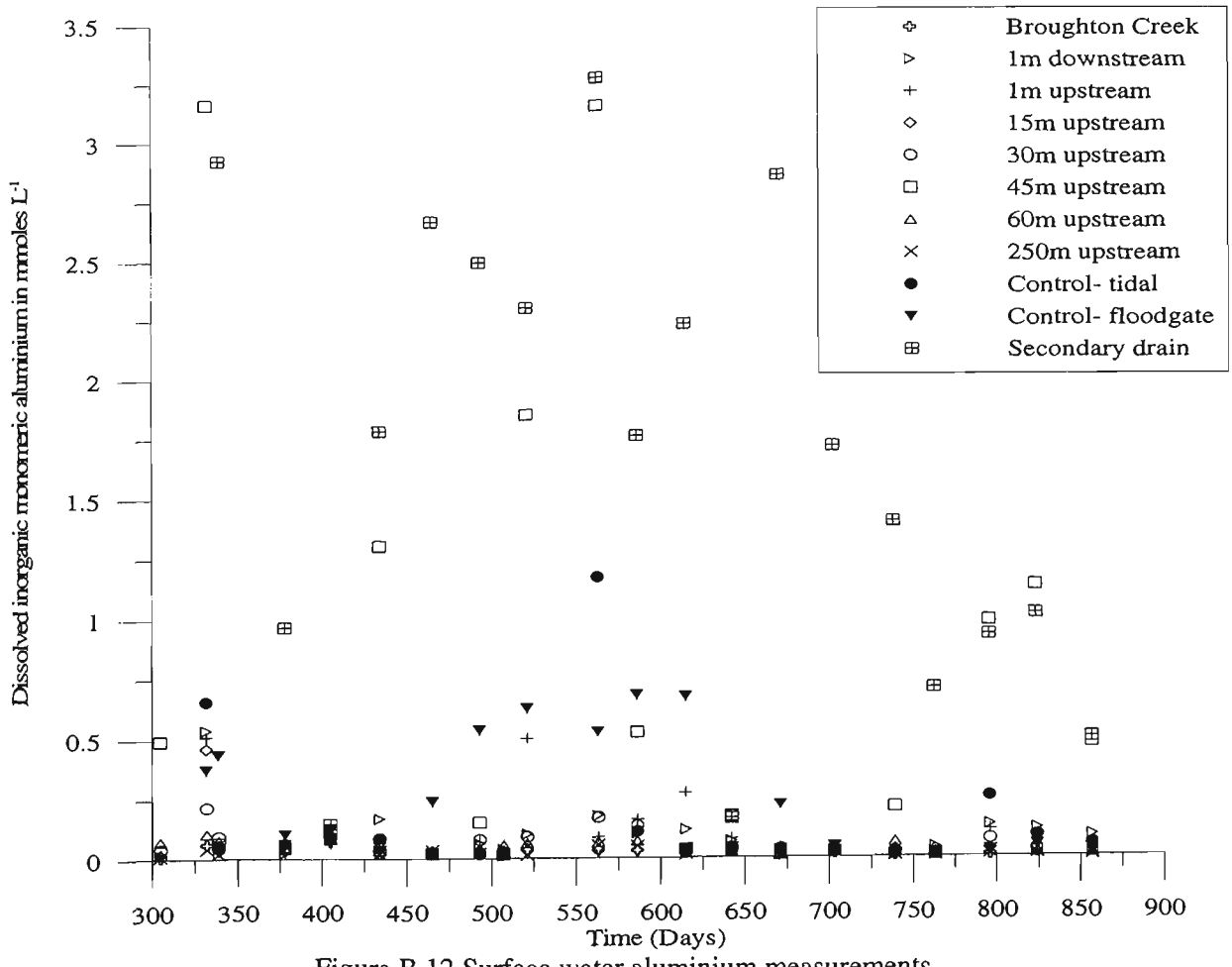

Figure B.12 Surface water aluminium measurements.

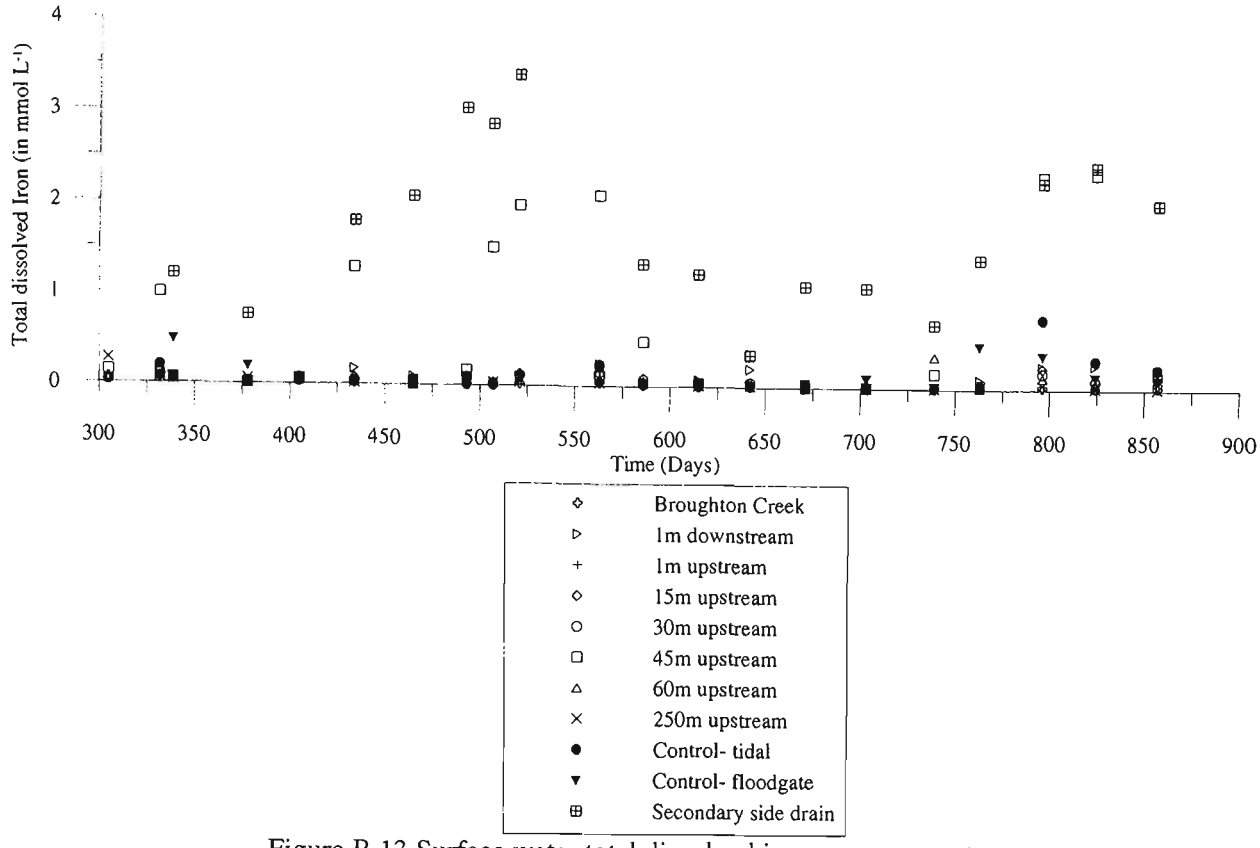

Figure B.13 Surface water total dissolved iron measurements.

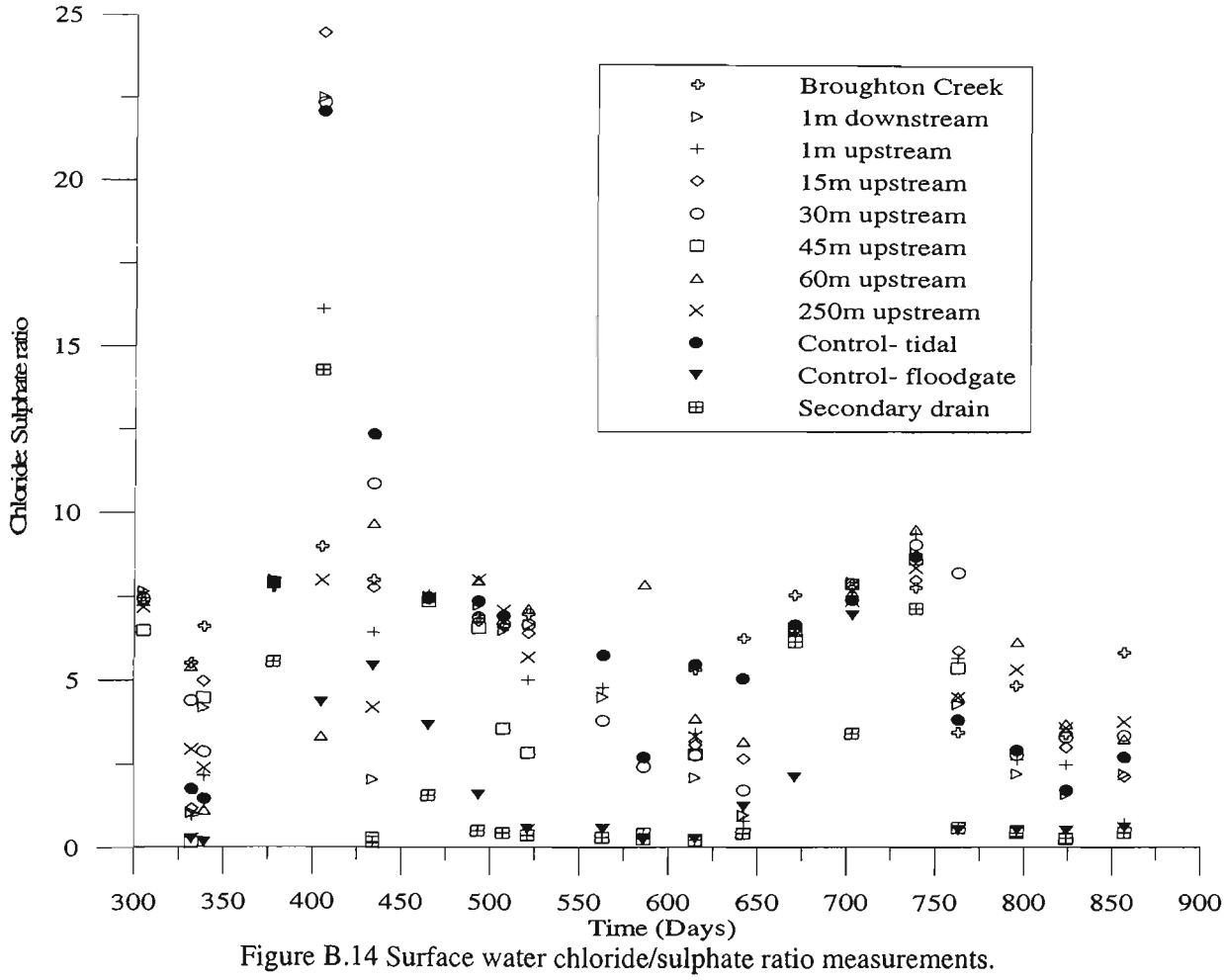

Figure B.14 Surface water chloride/sulphate ratio measurements.

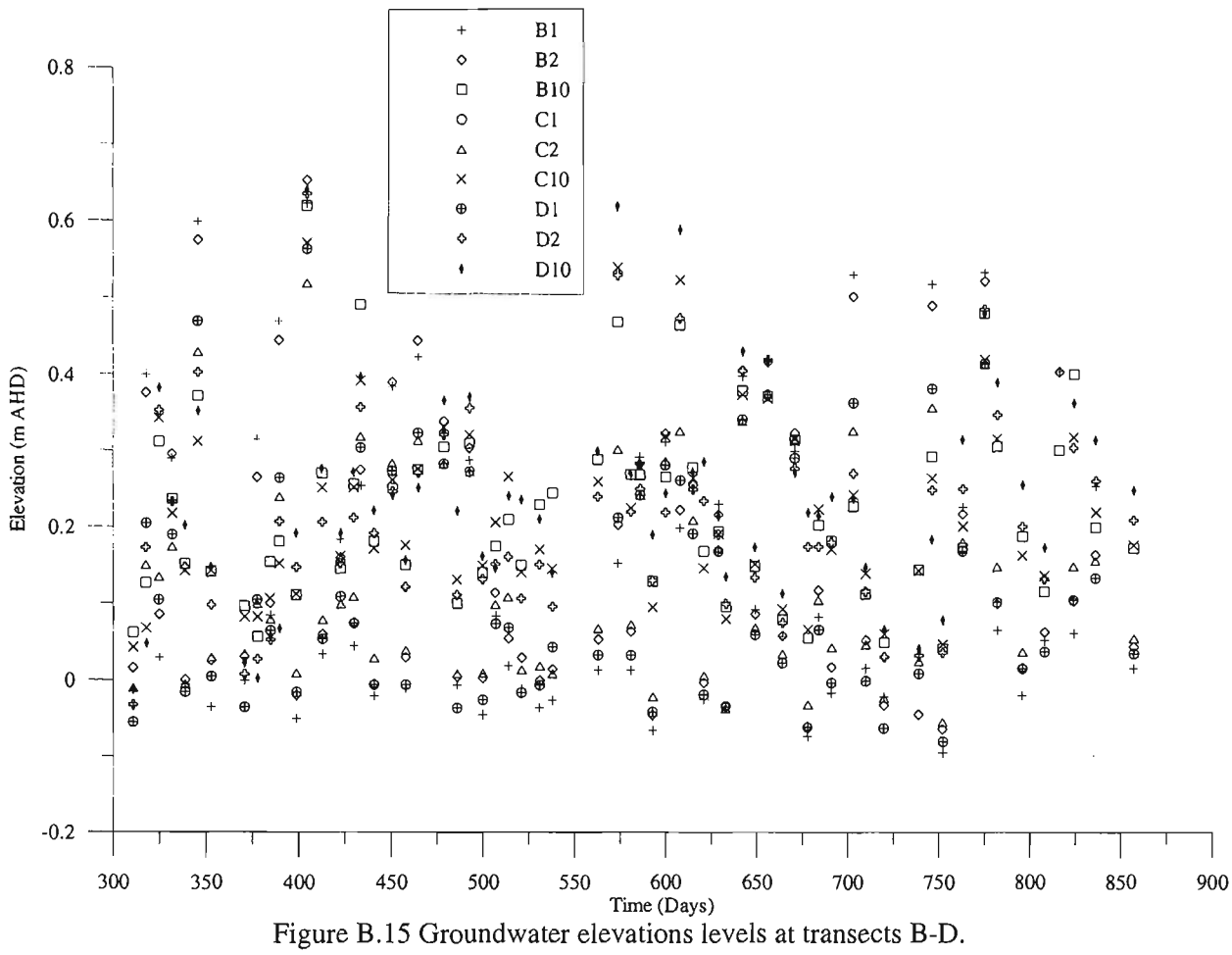

Figure B.15 Groundwater elevations levels at transects B-D.

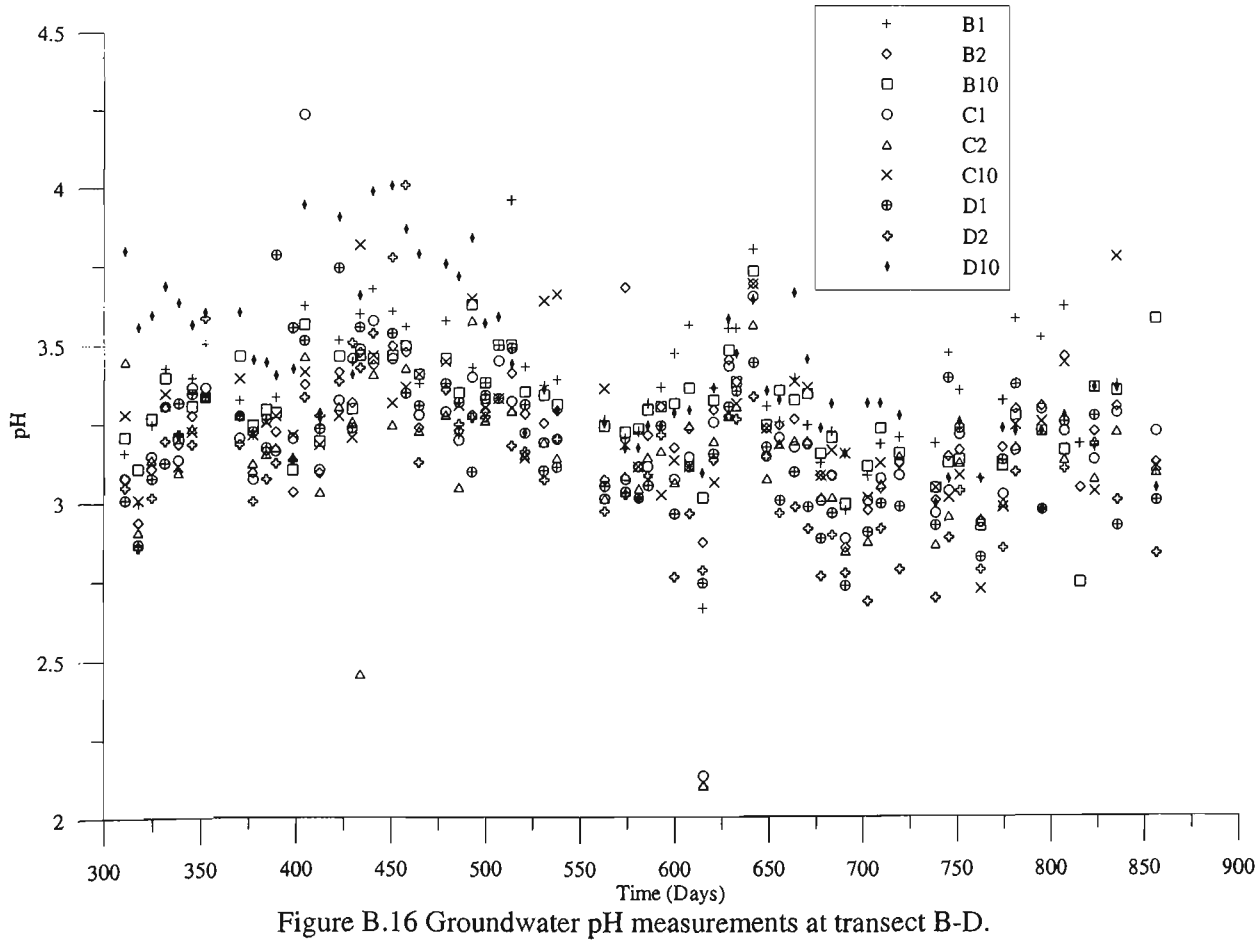

Figure B.16 Groundwater pH measurements at transect B-D.

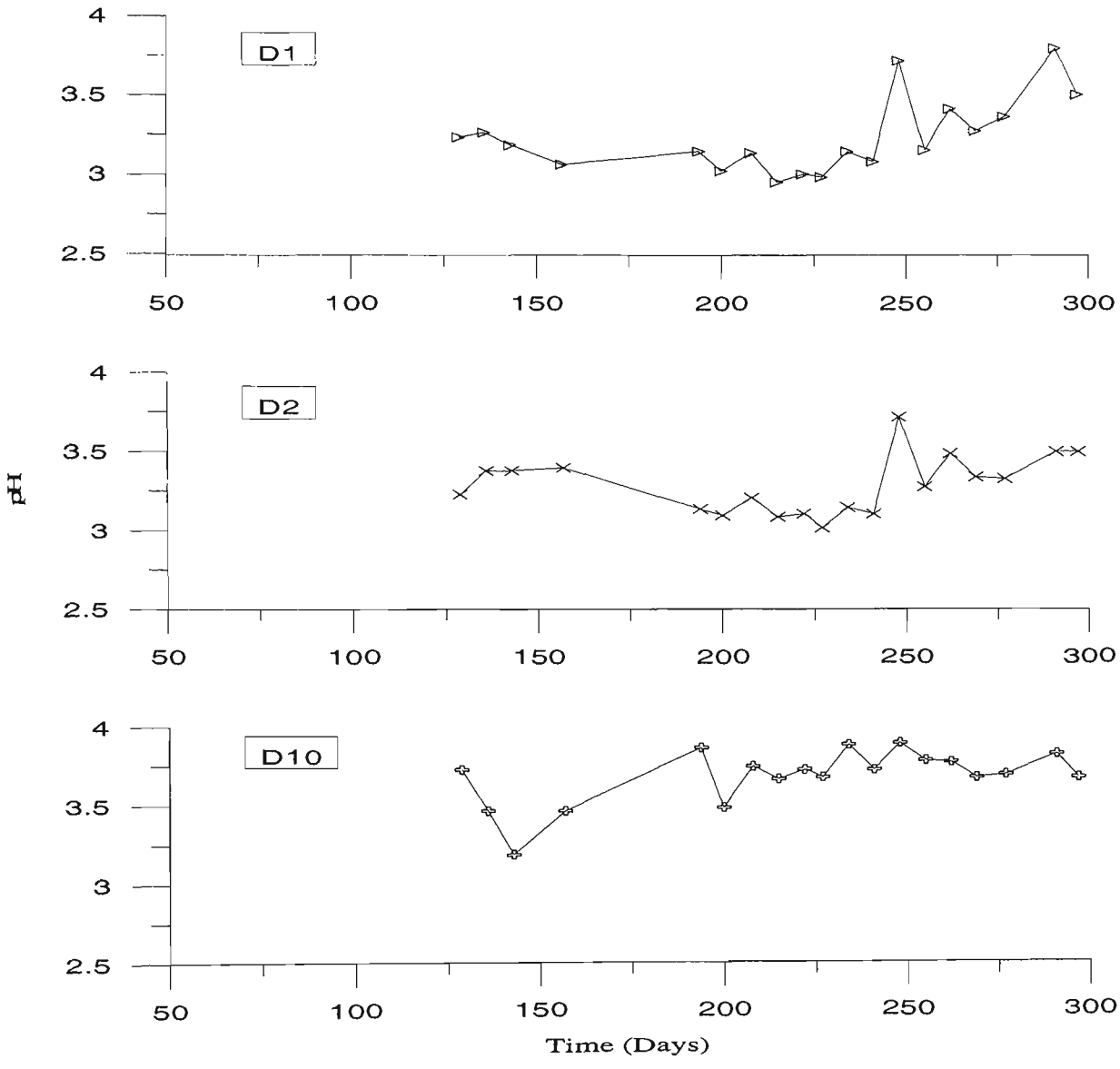

Figure B.17 pH readings from piezometer B1-D10 prior to floodgate modifications.

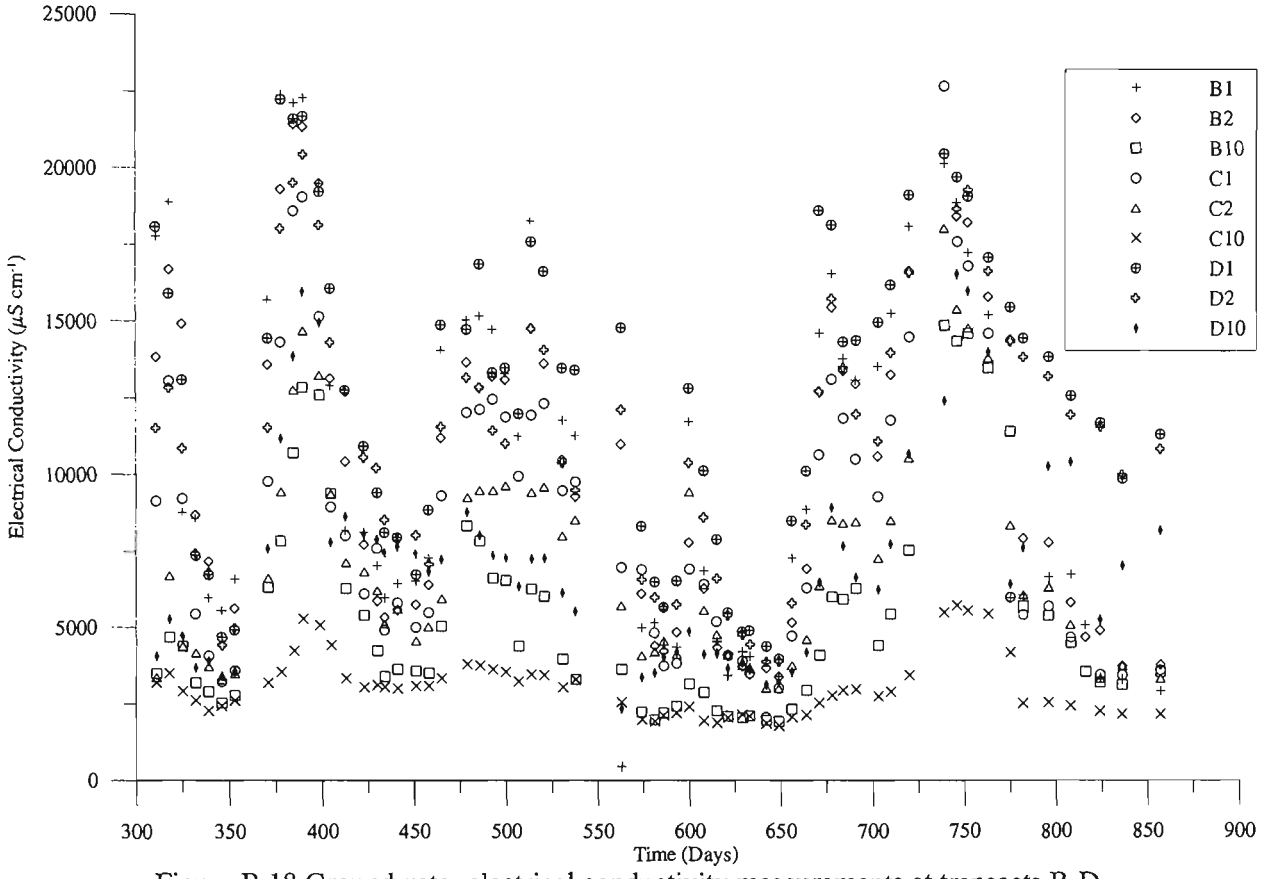

Figure B.18 Groundwater electrical conductivity measurements at transects B-D.

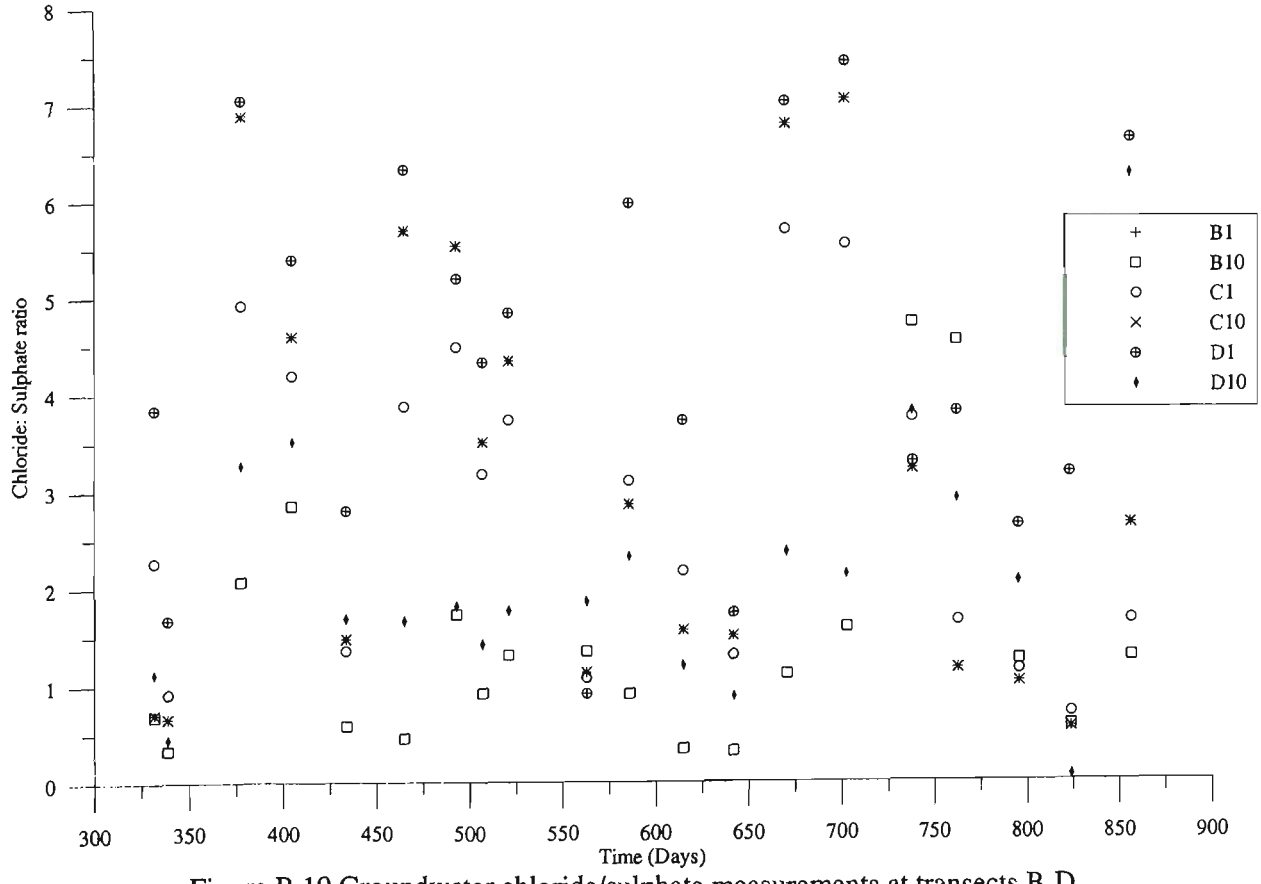

Figure B.19 Groundwater chloride/sulphate measurements at transects B-D.

Appendix C. Ion Speciation Source Code Used in PHREEQC Modelling

The following code was input into the aqueous ion-speciation model PHREEQC version 1.4.07 (Parkhurst, 1995) to calculate the reaction-path kinetics and resultant ion speciation involved in physical mixing of alkaline creek water of varying ionic strength and acidic drain water over increasingly greater proportions (up to 200%).

```
TITLE Drain water versus saline water
SOLUTION 1 Acid water
      units       ppm
      pH          4.49
      temp        20.0
      Ca          83.48
      Al          5.98
      Fe          20.04
      S(6)        428.8
SAVE solution 1
END
TITLE Saline water.
SOLUTION 2 Freshwater
      units       ppm
      pH          6.5
      temp        20.0
      Ca          12.79
      Mg          21.845
      Na          182.3
      K           8.79
      Cl          258.88
      Al          0.617
      Fe          1.3
      Alkalinity 17.98 as HCO3
      S(6)        52.98
SAVE solution 2
END
USER_Graph
-headings pH Ca Mg Na K Cl S(6) Fe Al
-axis_scale x_axis auto auto auto auto auto auto auto auto auto
auto
-axis_scale y_axis auto auto auto auto auto auto auto auto auto
auto
-axis_titles 'pH' 'molality'
-chart_title 'saline mixing'
-grid_offset 1 1
-initial_solutions true
```

```
-start
10 GRAPH_x -LA("H+")
20 GRAPH_Y TOT("Ca"), TOT("Mg"), TOT("Na"), TOT("K"), TOT("Cl"),
TOT("S(6)"), TOT("Fe"), TOT("Al")
-end
TITLE Example 1, mix 10:1.
MIX 1
      1     10
      2     1
SAVE solution 3
END
Title Example 2, mix 10:2.5
MIX 2
      1     10
      2     2.5
Save solution 4
END
Title Example 3 mix 10:5
Mix 3
      1     10
      2     5
Save solution 5
end
Title Example 4, mix 10:7.5
MIX 4
      1     10
      2     7.5
Save solution 6
END
Title Example 5, mix 1:1
MIX 5
      1     1
      2     1
Save solution 7
END
Title Example 6, mix 10:12.5
MIX 6
      1     10
      2     12.5
Save solution 8
END
Title Example 7, mix 10:15
MIX 7
      1     10
      2     15
Save solution 9
END
Title Example 8, mix 10:17.5
MIX 8
      1     10
      2     17.5
Save solution 10
END
Title Example 9, mix 10:20
MIX 9
```

```
     1     10
     2     20
Save solution 11
END

------------------------------------
Reading input data for simulation 1.
------------------------------------

     TITLE Drain water versus saline water
     SOLUTION 1 Acid water
          units       ppm
          pH          4.49
          temp        20.0
          Ca          83.48
          Al          5.98
          Fe          20.04
          S(6)        428.8
     SAVE solution 1
     END
-----
TITLE
-----
 Drain water versus saline water

-------------------------------------------
Beginning of initial solution calculations.
-------------------------------------------
Initial solution 1.   Acid water

-----------------------------Solution composition---------------

     Elements            Molality       Moles
     Al                  2.218e-04   2.218e-04
     Ca                  2.084e-03   2.084e-03
     Fe                  3.590e-04   3.590e-04
     S(6)                4.466e-03   4.466e-03

----------------------------Description of solution-------------
                                       pH  =   4.490
                                       pe  =   4.000
                          Activity of water  =   1.000
                             Ionic strength  =   1.153e-02
                         Mass of water (kg)  =   1.000e+00
                 Total alkalinity (eq/kg)    =  -3.509e-05
                    Total carbon (mol/kg)    =   0.000e+00
                       Total CO2 (mol/kg)    =   0.000e+00
                     Temperature (deg C)     =  20.000
                  Electrical balance (eq)    =  -3.346e-03
 Percent error, 100*(Cat-|An|)/(Cat+|An|)    = -28.91
                                 Iterations  =   5
                                    Total H  = 1.110125e+02
                                    Total O  = 5.552409e+01

----------------------------Distribution of species-------------
```

Species	Molality	Activity	Molality Activity
H+	3.558e-05	3.236e-05	-4.449 -4.490
OH-	2.345e-10	2.098e-10	-9.630 -9.678
H2O	5.551e+01	9.999e-01	-0.000 -0.000
Al	2.218e-04		
AlSO4+	1.567e-04	1.405e-04	-3.805 -3.852
Al+3	4.589e-05	1.954e-05	-4.338 -4.709
Al(SO4)2-	1.176e-05	1.055e-05	-4.930 -4.977
AlOH+2	6.670e-06	4.317e-06	-5.176 -5.365
Al(OH)2+	7.435e-07	6.668e-07	-6.129 -6.176
Al(OH)3	2.070e-09	2.075e-09	-8.684 -8.683
AlHSO4+2	5.981e-10	3.871e-10	-9.223 -9.412
Al(OH)4-	1.268e-10	1.137e-10	-9.897 -9.944
Ca	2.084e-03		
Ca+2	1.600e-03	1.050e-03	-2.796 -2.979
CaSO4	4.843e-04	4.856e-04	-3.315 -3.314
CaOH+	6.006e-12	5.387e-12	-11.221 -11.269
Fe(2)	3.590e-04		
Fe+2	2.850e-04	1.886e-04	-3.545 -3.724
FeSO4	7.406e-05	7.426e-05	-4.130 -4.129
FeHSO4+	1.737e-08	1.558e-08	-7.760 -7.808
FeOH+	1.405e-09	1.260e-09	-8.852 -8.899
Fe(3)	2.255e-10		
Fe(OH)2+	1.896e-10	1.701e-10	-9.722 -9.769
FeOH+2	3.115e-11	2.016e-11	-10.507 -10.695
FeSO4+	3.618e-12	3.245e-12	-11.442 -11.489
Fe(OH)3	5.410e-13	5.425e-13	-12.267 -12.266
Fe+3	3.202e-13	1.363e-13	-12.495 -12.865
Fe(SO4)2-	1.885e-13	1.691e-13	-12.725 -12.772
FeHSO4+2	4.370e-16	2.828e-16	-15.360 -15.549
Fe(OH)4-	1.389e-17	1.246e-17	-16.857 -16.904
Fe2(OH)2+4	7.693e-20	1.350e-20	-19.114 -19.870
Fe3(OH)4+5	1.163e-26	7.669e-28	-25.934 -27.115
H(0)	1.497e-20		
H2	7.483e-21	7.503e-21	-20.126 -20.125
O(0)	0.000e+00		
O2	0.000e+00	0.000e+00	-53.806 -53.805
S(6)	4.466e-03		
SO4-2	3.720e-03	2.430e-03	-2.429 -2.614
CaSO4	4.843e-04	4.856e-04	-3.315 -3.314
AlSO4+	1.567e-04	1.405e-04	-3.805 -3.852
FeSO4	7.406e-05	7.426e-05	-4.130 -4.129
Al(SO4)2-	1.176e-05	1.055e-05	-4.930 -4.977
HSO4-	7.658e-06	6.869e-06	-5.116 -5.163
FeHSO4+	1.737e-08	1.558e-08	-7.760 -7.808
AlHSO4+2	5.981e-10	3.871e-10	-9.223 -9.412
FeSO4+	3.618e-12	3.245e-12	-11.442 -11.489
Fe(SO4)2-	1.885e-13	1.691e-13	-12.725 -12.772
FeHSO4+2	4.370e-16	2.828e-16	-15.360 -15.549

----------Saturation indices----------

Phase	SI log IAP log KT

```
      Al(OH)3(a)        -2.37     8.76    11.13  Al(OH)3
      Anhydrite         -1.25    -5.59    -4.34  CaSO4
      Fe(OH)3(a)        -4.29    13.75    18.03  Fe(OH)3
      Gibbsite           0.37     8.76     8.40  Al(OH)3
      Goethite           1.60    13.75    12.14  FeOOH
      Gypsum            -1.01    -5.59    -4.58  CaSO4:2H2O
      H2(g)            -17.00   -16.98     0.02  H2
      Hematite           4.83    27.49    22.66  Fe2O3
      Melanterite       -4.07    -6.34    -2.27  FeSO4:7H2O
      O2(g)            -50.87    33.96    84.83  O2

------------------------------------
Reading input data for simulation 2.
------------------------------------

      TITLE Saline water.
      SOLUTION 2 Freshwater
            units      ppm
            pH         6.5
            temp       20.0
            Ca         12.79
            Mg         21.845
            Na         182.3
            K          8.79
            Cl         258.88
            Al         0.617
            Fe         1.3
            Alkalinity 17.98 as HCO3
            S(6)       52.98
      SAVE solution 2
      END
-----
TITLE
-----
 Saline water.

------------------------------------------
Beginning of initial solution calculations.
------------------------------------------

Initial solution 2.   Freshwater

-----------------------------Solution composition--------------
      Elements            Molality       Moles

      Al                  2.288e-05   2.288e-05
      Alkalinity          2.948e-04   2.948e-04
      Ca                  3.193e-04   3.193e-04
      Cl                  7.306e-03   7.306e-03
      Fe                  2.329e-05   2.329e-05
      K                   2.249e-04   2.249e-04
      Mg                  8.990e-04   8.990e-04
      Na                  7.934e-03   7.934e-03
      S(6)                5.518e-04   5.518e-04
```

----------Description of solution----------

pH	=	6.500
pe	=	4.000
Activity of water	=	1.000
Ionic strength	=	1.121e-02
Mass of water (kg)	=	1.000e+00
Total carbon (mol/kg)	=	3.722e-04
Total CO2 (mol/kg)	=	3.722e-04
Temperature (deg C)	=	20.000
Electrical balance (eq)	=	2.006e-03
Percent error, 100*(Cat-|An|)/(Cat+|An|)	=	10.52
Iterations	=	8
Total H	=	1.110127e+02
Total O	=	5.550946e+01

----------Distribution of species----------

Species	Molality	Activity	Molality Activity	
H+	3.473e-07	3.162e-07	-6.459	-6.500
OH-	2.395e-08	2.146e-08	-7.621	-7.668
H2O	5.551e+01	9.997e-01	-0.000	-0.000
Al	2.288e-05			
Al(OH)4-	1.290e-05	1.159e-05	-4.889	-4.936
Al(OH)2+	7.227e-06	6.491e-06	-5.141	-5.188
Al(OH)3	2.061e-06	2.066e-06	-5.686	-5.685
AlOH+2	6.312e-07	4.107e-07	-6.200	-6.386
Al+3	4.228e-08	1.817e-08	-7.374	-7.741
AlSO4+	1.920e-08	1.725e-08	-7.717	-7.763
Al(SO4)2-	1.901e-10	1.708e-10	-9.721	-9.768
AlHSO4+2	7.134e-16	4.642e-16	-15.147	-15.333
C(4)	3.722e-04			
HCO3-	2.190e-04	1.974e-04	-3.660	-3.705
CO2	1.501e-04	1.505e-04	-3.824	-3.823
MgHCO3+	1.442e-06	1.295e-06	-5.841	-5.888
NaHCO3	7.888e-07	7.908e-07	-6.103	-6.102
CaHCO3+	5.192e-07	4.680e-07	-6.285	-6.330
FeHCO3+	3.196e-07	2.870e-07	-6.495	-6.542
CO3-2	3.981e-08	2.629e-08	-7.400	-7.580
MgCO3	1.325e-08	1.328e-08	-7.878	-7.877
FeCO3	9.146e-09	9.169e-09	-8.039	-8.038
CaCO3	8.136e-09	8.157e-09	-8.090	-8.088
NaCO3-	3.005e-09	2.699e-09	-8.522	-8.569
Ca	3.193e-04			
Ca+2	3.065e-04	2.023e-04	-3.514	-3.694
CaSO4	1.231e-05	1.234e-05	-4.910	-4.909
CaHCO3+	5.192e-07	4.680e-07	-6.285	-6.330
CaCO3	8.136e-09	8.157e-09	-8.090	-8.088
CaOH+	1.182e-10	1.061e-10	-9.928	-9.974
Cl	7.306e-03			
Cl-	7.306e-03	6.549e-03	-2.136	-2.184
FeCl+	1.463e-07	1.314e-07	-6.835	-6.881
FeCl+2	2.718e-15	1.768e-15	-14.566	-14.752

	FeCl2+	6.767e-17	6.078e-17	-16.170	-16.216
	FeCl3	3.970e-20	3.980e-20	-19.401	-19.400
Fe(2)		2.309e-05			
	Fe+2	2.185e-05	1.454e-05	-4.660	-4.838
	FeSO4	7.532e-07	7.552e-07	-6.123	-6.122
	FeHCO3+	3.196e-07	2.870e-07	-6.495	-6.542
	FeCl+	1.463e-07	1.314e-07	-6.835	-6.881
	FeOH+	1.107e-08	9.938e-09	-7.956	-8.003
	FeCO3	9.146e-09	9.169e-09	-8.039	-8.038
	FeHSO4+	1.724e-12	1.548e-12	-11.764	-11.810
Fe(3)		1.978e-07			
	Fe(OH)2+	1.528e-07	1.372e-07	-6.816	-6.863
	Fe(OH)3	4.466e-08	4.477e-08	-7.350	-7.349
	FeOH+2	2.443e-10	1.590e-10	-9.612	-9.799
	Fe(OH)4-	1.172e-10	1.052e-10	-9.931	-9.978
	FeSO4+	3.674e-14	3.300e-14	-13.435	-13.481
	Fe+3	2.445e-14	1.051e-14	-13.612	-13.979
	FeCl+2	2.718e-15	1.768e-15	-14.566	-14.752
	Fe(SO4)2-	2.527e-16	2.269e-16	-15.597	-15.644
	FeCl2+	6.767e-17	6.078e-17	-16.170	-16.216
	Fe2(OH)2+4	4.681e-18	8.392e-19	-17.330	-18.076
	FeHSO4+2	4.319e-20	2.811e-20	-19.365	-19.551
	FeCl3	3.970e-20	3.980e-20	-19.401	-19.400
	Fe3(OH)4+5	5.642e-22	3.846e-23	-21.249	-22.415
H(0)		1.429e-24			
	H2	7.147e-25	7.166e-25	-24.146	-24.145
K		2.249e-04			
	K+	2.244e-04	2.012e-04	-3.649	-3.696
	KSO4-	4.765e-07	4.280e-07	-6.322	-6.369
	KOH	2.200e-12	2.205e-12	-11.658	-11.657
Mg		8.990e-04			
	Mg+2	8.600e-04	5.716e-04	-3.066	-3.243
	MgSO4	3.759e-05	3.769e-05	-4.425	-4.424
	MgHCO3+	1.442e-06	1.295e-06	-5.841	-5.888
	MgCO3	1.325e-08	1.328e-08	-7.878	-7.877
	MgOH+	4.615e-09	4.145e-09	-8.336	-8.382
Na		7.934e-03			
	Na+	7.921e-03	7.123e-03	-2.101	-2.147
	NaSO4-	1.234e-05	1.108e-05	-4.909	-4.955
	NaHCO3	7.888e-07	7.908e-07	-6.103	-6.102
	NaCO3-	3.005e-09	2.699e-09	-8.522	-8.569
	NaOH	1.484e-10	1.488e-10	-9.829	-9.827
O(0)		0.000e+00			
	O2	0.000e+00	0.000e+00	-45.767	-45.765
S(6)		5.518e-04			
	SO4-2	4.883e-04	3.206e-04	-3.311	-3.494
	MgSO4	3.759e-05	3.769e-05	-4.425	-4.424
	NaSO4-	1.234e-05	1.108e-05	-4.909	-4.955
	CaSO4	1.231e-05	1.234e-05	-4.910	-4.909
	FeSO4	7.532e-07	7.552e-07	-6.123	-6.122
	KSO4-	4.765e-07	4.280e-07	-6.322	-6.369
	AlSO4+	1.920e-08	1.725e-08	-7.717	-7.763
	HSO4-	9.863e-09	8.858e-09	-8.006	-8.053
	Al(SO4)2-	1.901e-10	1.708e-10	-9.721	-9.768
	FeHSO4+	1.724e-12	1.548e-12	-11.764	-11.810

FeSO4+	3.674e-14	3.300e-14	-13.435	-13.481
AlHSO4+2	7.134e-16	4.642e-16	-15.147	-15.333
Fe(SO4)2-	2.527e-16	2.269e-16	-15.597	-15.644
FeHSO4+2	4.319e-20	2.811e-20	-19.365	-19.551

Saturation indices

Phase	SI	log IAP	log KT	
Al(OH)3(a)	0.63	11.76	11.13	Al(OH)3
Alunite	5.86	5.09	-0.77	KAl3(SO4)2(OH)6
Anhydrite	-2.84	-7.19	-4.34	CaSO4
Aragonite	-2.97	-11.27	-8.31	CaCO3
Calcite	-2.82	-11.27	-8.45	CaCO3
CO2(g)	-2.42	-20.58	-18.16	CO2
Dolomite	-5.13	-22.10	-16.97	CaMg(CO3)2
Fe(OH)3(a)	0.63	18.66	18.03	Fe(OH)3
Gibbsite	3.36	11.76	8.40	Al(OH)3
Goethite	6.52	18.66	12.14	FeOOH
Gypsum	-2.61	-7.19	-4.58	CaSO4:2H2O
H2(g)	-21.02	-21.00	0.02	H2
Hematite	14.66	37.32	22.66	Fe2O3
Jarosite-K	-4.80	25.80	30.60	KFe3(SO4)2(OH)6
Melanterite	-6.06	-8.33	-2.27	FeSO4:7H2O
O2(g)	-42.83	42.00	84.83	O2
Siderite	-1.56	-12.42	-10.86	FeCO3

End of input data.

Appendix D. Program for 'Smart Gate' Control System

The following program was written for a Campbell Scientific CR10X data logger in order to operate the 'Smart Gate' system based on the parameters described in Chapter 6. The CSI file below was converted into a DLD file, which removed all of the label text and was uploaded into the primary data logger using the program PC208W.

Program for SMARTGATE control system

```
Primary Objective: To measure two CTDP sensors (with SDI-12 interfaces) and control
gates based on the measurements.

SDI-12 Address summary
+----+-------------------------------------------------------------------+
; | 0  | Uncontrolled side of gate                                         |
; | 1  | Controlled side of gate                                           |
; +----+-------------------------------------------------------------------+
;
; Final storage data array's
; +-----+----------------+-------------------------------------------+
; | ID  |   DESCRIPTION  |  ARRAY OUTPUT                             |
; +-----+----------------+-------------------------------------------+
; | 1   | Motor Posn Chg | 1,Year, Day, HHMM, Sec, MotorOn_T, Postion |
; | 2   | Water Data     | 1,Year, Day, HHMM, Level1, Temp1, EC1, pH1, Offset1,  |
; |     |                |                    Level2, Temp2, EC2, pH2, Offset2.  |
; | 24  | System Stat.   | 24, Year, Day, BatV Av, BatV Min, IntT, Av.           |
; | 500 | ERROR          | 1,Year, Day, HHMM, Sec, ERROR NUM                     |
; |     |                | Where ERROR NUM can be any of the following:          |
; |     |                | 0  No error,                                          |
; |     |                | 1  Pump trying to go to a position it is already at   |
; |     |                | 2  Pump was on too long.  Turned off                  |
; |     |                | 3  Pump drawing too much current.  Turned off         |
; |     |                | 4  No movement direction specified                    |
; |     |                | 5  Both reed switches are closed                      |
; |     |                | 6  System voltage low                                 |
; +-----+----------------+-------------------------------------------------------+
;
; Flag usage
; +----+-------------------------------------------------------------------------+
; | 1  |                                                                         |
; | 2  |                                                                         |
; | 3  |                                                                         |
; | 4  |                                                                         |
; | 5  | Error message reporting bar                                             |
; | 6  |                                                                         |
; | 7  |                                                                         |
; | 8  |                                                                         |
; +----+-------------------------------------------------------------------------+
;
; Control port usage
; +----+-------------------------------------------------------------------------+
; | 1  | Motor Forward/Reverse.  High = Clockwise, Low = Anticlockwise           |
; | 2  | Motor Power                                                             |
; | 3  | Phone Power                                                             |
; | 4  |                                                                         |
```

```
; | 5   | SDI-12 input channel                                                                    |
; | 6   |                                                                                         |
; | 7   | Upper reed switch                                                                       |
; | 8   | Lower reed switch                                                                       |
; +----+-----------------------------------------------------------------------------------------+
;
; Analog input channel usage
; +------+-----------------------------------------------------------------------------------+
; | SE1  |                                                                                   |
; | SE2  |                                                                                   |
; | SE3  |                                                                                   |
; | SE4  |                                                                                   |
; | SE5  |                                                                                   |
; | SE6  |                                                                                   |
; | SE7  |                                                                                   |
; | SE8  |                                                                                   |
; | SE9  |                                                                                   |
; | SE10 |                                                                                   |
; | SE11 |                                                                                   |
; | SE12 |                                                                                   |
; +------+-----------------------------------------------------------------------------------+
;
; Pulse counting input channel usage
; +----+-------------------------------------------------------------------------------------+
; | P1 |                                                                                     |
; | P2 |                                                                                     |
; +----+-------------------------------------------------------------------------------------+
;
; Excitation channel usage
; +----+-------------------------------------------------------------------------------------+
; | E1 | Motor Power                                                                         |
; | E2 | Reed switch excitation                                                              |
; +----+-------------------------------------------------------------------------------------+
;
*Table 1 Program
  01: 1          Execution Interval (seconds)

; The next few instructions are to calculate the execution interval
; so that even if it is changed, it will be figured out correctly
1:  Z=X (P31)
 1: 12        X Loc [ Seconds    ]
 2: 13        Z Loc [ OldSecond  ]

2:  Time (P18)
 1: 0         Seconds into current minute (maximum 60)
 2: 0         Mod/By
 3: 12        Loc [ Seconds    ]

3:  Z=X-Y (P35)
 1: 12        X Loc [ Seconds    ]
 2: 13        Y Loc [ OldSecond  ]
 3: 14        Z Loc [ Time       ]

; If the time is greater than 0 then this must be the proper execution interval
4:  If (X<=>F) (P89)
 1: 14        X Loc [ Time       ]
 2: 3         >=
 3: 1         F
 4: 30        Then Do

    5:  Z=X (P31)
     1: 14        X Loc [ Time       ]
     2: 8         Z Loc [ ExecInt    ]

6:  End (P95)

; Clear the error location
7:  Z=F (P30)
 1: 0         F
 2: 0         Exponent of 10
 3: 7         Z Loc [ ERROR      ]

; and its associated value location
8:  Z=F (P30)
 1: 0         F
 2: 0         Exponent of 10
```

```
 3: 46        Z Loc [ VALUE     ]

; ************************************************************
; *                                                          *
; *                                                          *
; *                                                          *
; *   Load program constants here                            *
; *                                                          *
; *                                                          *
; *                                                          *
; ************************************************************
9:  If Flag/Port (P91)
 1: 28        Do if Flag 8 is Low
 2: 30        Then Do

    ; System trigger points
    10:  Z=F (P30)
     1: 7.0       F
     2: 0         Exponent of 10
     3: 15        Z Loc [ TRIG_ph_U ]

    11:  Z=F (P30)
     1: 20000     F
     2: 0         Exponent of 10
     3: 16        Z Loc [ TRIG_EC_U ]

    12:  Z=F (P30)
     1: 0.5       F
     2: 0         Exponent of 10
     3: 17        Z Loc [ TRIG_LvlU ]

    13:  Z=F (P30)
     1: -0.3      F
     2: 0         Exponent of 10
     3: 18        Z Loc [ TRIG_LvlL ]

    ; Position constants
    14:  Z=F (P30)
     1: 1         F
     2: 0         Exponent of 10
     3: 2         Z Loc [ HIGH      ]

    15:  Z=F (P30)
     1: 0         F
     2: 0         Exponent of 10
     3: 3         Z Loc [ MIDDLE    ]

    16:  Z=F (P30)
     1: -1        F
     2: 0         Exponent of 10
     3: 4         Z Loc [ LOW       ]

    ; Load the maximum time that the pump can be on for, before stopping and alarming
    17:  Z=F (P30)
     1: 30        F
     2: 0         Exponent of 10
     3: 9         Z Loc [ MaxOnTime ]

    ; Load the maximum current
    18:  Z=F (P30)
     1: 5000      F
     2: 0         Exponent of 10
     3: 11        Z Loc [ MaxCurrnt ]

    ; Reset error codes
    19:  Z=F (P30)
     1: 0         F
     2: 0         Exponent of 10
     3: 7         Z Loc [ ERROR     ]

    ; Clear error value
    20:  Z=F (P30)
     1: 0         F
     2: 0         Exponent of 10
     3: 46        Z Loc [ VALUE     ]
```

```
    ; Load the two pressure sensor offsets
    21:  Z=F (P30)
     1: -1        F
     2: 0         Exponent of 10
     3: 37        Z Loc [ Offset_1  ]

    22:  Z=F (P30)
     1: 0         F
     2: 0         Exponent of 10
     3: 38        Z Loc [ Offset_2  ]

    ; Load the phone power up time
    23:  Z=F (P30)
     1: 0         F
     2: 0         Exponent of 10
     3: 40        Z Loc [ PhoneOn   ]

    ; Load the phone power down time
    24:  Z=F (P30)
     1: 1430      F
     2: 0         Exponent of 10
     3: 41        Z Loc [ PhoneOff  ]

    25:  Z=F (P30)
     1: 11.5      F
     2: 0         Exponent of 10
     3: 47        Z Loc [ BatV_Min  ]

    ; Set high flag 8 so that this code is only executed once
    26:  Do (P86)
     1: 18        Set Flag 8 High

27:  End (P95)

; ************************************************************
; *                                                          *
; *                                                          *
; *                                                          *
; *   Phone power control section                            *
; *                                                          *
; *                                                          *
; *                                                          *
; ************************************************************
28:  Time (P18)
 1: 1         Minutes into current day (maximum 1440)
 2: 0         Mod/By
 3: 39        Loc [ Minutes   ]

29:  If (X<=>Y) (P88)
 1: 39        X Loc [ Minutes   ]
 2: 3         >=
 3: 41        Y Loc [ PhoneOff  ]
 4: 30        Then Do

    30:  Do (P86)
     1: 53        Set Port 3 Low

31:  Else (P94)

    32:  If (X<=>Y) (P88)
     1: 39        X Loc [ Minutes   ]
     2: 3         >=
     3: 40        Y Loc [ PhoneOn   ]
     4: 43        Set Port 3 High

33:  End (P95)

; ************************************************************
; *                                                          *
; *                                                          *
; *                                                          *
; *   Sensor measurement section                             *
; *                                                          *
; *                                                          *
; *                                                          *
; ************************************************************
```

```
34:  Batt Voltage (P10)
 1: 42       Loc [ BatV      ]

; Check to see if battery voltage is ok or not
35:  If (X<=>Y) (P88)
 1: 42       X Loc [ BatV      ]
 2: 4        <
 3: 47       Y Loc [ BatV_Min  ]
 4: 30       Then Do

    ; Set error code
    36:  Z=F (P30)
     1: 6        F
     2: 0        Exponent of 10
     3: 7        Z Loc [ ERROR     ]

    37:  Z=X (P31)
     1: 42       X Loc [ BatV      ]
     2: 46       Z Loc [ VALUE     ]

    ; Log the error data
    38:  Do (P86)
     1: 3        Call Subroutine 3

39:  End (P95)

40:  Internal Temperature (P17)
 1: 43       Loc [ IntT      ]

41:  If time is (P92)
 1: 0        Minutes (Seconds --) into a
 2: 10       Interval (same units as above)
 3: 30       Then Do

    ; Measure first sensor
    42:  SDI-12 Recorder (P105)
     1: 0        SDI-12 Address
     2: 0        Start Measurement (aM0!)
     3: 5        Port
     4: 19       Loc [ SDI_Mes1  ]
     5: 1.0      Mult
     6: 0.0      Offset

    ; If the value is not -6999 then move it into the appropriate location
    43:  If (X<=>F) (P89)
     1: 19       X Loc [ SDI_Mes1  ]
     2: 3        >=
     3: -6000    F
     4: 30       Then Do

        44:  Z=X (P31)
         1: 19       X Loc [ SDI_Mes1  ]
         2: 27       Z Loc [ Press_1   ]

        ; Apply the pressure sensor offset to get the actual level
        45:  Z=X+Y (P33)
         1: 37       X Loc [ Offset_1  ]
         2: 27       Y Loc [ Press_1   ]
         3: 35       Z Loc [ Level_1   ]

        46:  Z=X (P31)
         1: 20       X Loc [ SDI_Mes2  ]
         2: 28       Z Loc [ Temp_1    ]

        47:  Z=X (P31)
         1: 21       X Loc [ SDI_Mes3  ]
         2: 29       Z Loc [ EC_1      ]

        48:  Z=X (P31)
         1: 22       X Loc [ SDI_Mes4  ]
         2: 30       Z Loc [ pH_1      ]

    49:  End (P95)

    ; Measure second sensor
;    46:  SDI-12 Recorder (P105)
```

```
;     1: 1         SDI-12 Address
;     2: 0         Start Measurement (aM0!)
;     3: 5         Port
;     4: 19        Loc [ SDI_Mes1   ]
;     5: 1.0       Mult
;     6: 0.0       Offset

    ; If the value is not -6999 then move it into the appropriate location
    50:  If (X<=>F) (P89)
     1: 19        X Loc [ SDI_Mes1   ]
     2: 3         >=
     3: -6000     F
     4: 30        Then Do

        51:  Z=X (P31)
         1: 19        X Loc [ SDI_Mes1   ]
         2: 31        Z Loc [ Press_2    ]

        ; Apply the pressure sensor offset to get the actual level
        52:  Z=X+Y (P33)
         1: 38        X Loc [ Offset_2   ]
         2: 31        Y Loc [ Press_2    ]
         3: 36        Z Loc [ Level_2    ]

        53:  Z=X (P31)
         1: 20        X Loc [ SDI_Mes2   ]
         2: 32        Z Loc [ Temp_2     ]

        54:  Z=X (P31)
         1: 21        X Loc [ SDI_Mes3   ]
         2: 33        Z Loc [ EC_2       ]

        55:  Z=X (P31)
         1: 22        X Loc [ SDI_Mes4   ]
         2: 34        Z Loc [ pH_2       ]

    56:  End (P95)

57:  End (P95)

; ************************************************************
; *                                                          *
; *                                                          *
; *                                                          *
; *   Gate movement section                                  *
; *                                                          *
; *                                                          *
; *                                                          *
; ************************************************************
; Determine where we are...
; Update the position location
58:  Z=X (P31)
 1: 3         X Loc [ MIDDLE     ]
 2: 5         Z Loc [ Position   ]

; If the upper switch is closed then this is where we are
59:  If Flag/Port (P91)
 1: 47        Do if Port 7 is High
 2: 30        Then Do

    60:  Z=X (P31)
     1: 2         X Loc [ HIGH       ]
     2: 5         Z Loc [ Position   ]

61:  End (P95)

; If the lower switch is closed then this is where we are
62:  If Flag/Port (P91)
 1: 48        Do if Port 8 is High
 2: 30        Then Do

    63:  Z=X (P31)
     1: 4         X Loc [ LOW        ]
     2: 5         Z Loc [ Position   ]

64:  End (P95)
```

```
; if pH > 7.0 then
65:  If (X<=>Y) (P88)
 1: 30       X Loc [ pH_1      ]
 2: 3        >=
 3: 15       Y Loc [ TRIG_ph_U ]
 4: 30       Then Do

    ; If the gate is currently at the upper switch position then we need to move it.
    66:  If (X<=>Y) (P88)
     1: 5        X Loc [ Position  ]
     2: 1        =
     3: 2        Y Loc [ HIGH      ]
     4: 30       Then Do

        ; Set the gate to move down
        67:  Z=X (P31)
         1: 4        X Loc [ LOW       ]
         2: 6        Z Loc [ Direction ]

        ; Set flag 1 high to move the gate
        68:  Do (P86)
         1: 11       Set Flag 1 High

    69:  End (P95)

70:  Else (P94)

    ; if EC > 20,000 then
    71:  If (X<=>Y) (P88)
     1: 29       X Loc [ EC_1      ]
     2: 3        >=
     3: 16       Y Loc [ TRIG_EC_U ]
     4: 30       Then Do

        ; If the gate is currently at the upper switch position then we need to move it.
        72:  If (X<=>Y) (P88)
         1: 5        X Loc [ Position  ]
         2: 1        =
         3: 2        Y Loc [ HIGH      ]
         4: 30       Then Do

            ; Set the gate to move down
            73:  Z=X (P31)
             1: 4        X Loc [ LOW       ]
             2: 6        Z Loc [ Direction ]

            ; Set flag 1 high to move the gate
            74:  Do (P86)
             1: 11       Set Flag 1 High

        75:  End (P95)

    76:  Else (P94)

        ; if Level > 1.0m then
        77:  If (X<=>Y) (P88)
         1: 35       X Loc [ Level_1   ]
         2: 3        >=
         3: 17       Y Loc [ TRIG_LvlU ]
         4: 30       Then Do

            ; If the gate is currently at the upper switch position then we need to move
it.
            78:  If (X<=>Y) (P88)
             1: 5        X Loc [ Position  ]
             2: 1        =
             3: 2        Y Loc [ HIGH      ]
             4: 30       Then Do

                ; Set the gate to move down
                79:  Z=X (P31)
                 1: 4        X Loc [ LOW       ]
                 2: 6        Z Loc [ Direction ]

                ; Set flag 1 high to move the gate
```

```
                80:  Do (P86)
                 1: 11       Set Flag 1 High

            81:  End (P95)

        82:  Else (P94)

            ; if Level < 0.75m then
            83:  If (X<=>Y) (P88)
             1: 36       X Loc [ Level_2    ]
             2: 4        <
             3: 18       Y Loc [ TRIG_LvlL ]
             4: 30       Then Do

                ; If the gate is currently at the lower switch position then we need to
move it.
                84:  If (X<=>Y) (P88)
                 1: 5        X Loc [ Position  ]
                 2: 1        =
                 3: 4        Y Loc [ LOW       ]
                 4: 30       Then Do

                    ; Set the gate to move up
                    85:  Z=X (P31)
                     1: 2        X Loc [ HIGH      ]
                     2: 6        Z Loc [ Direction ]

                    86:  Do (P86)
                     1: 11       Set Flag 1 High

                87:  End (P95)

            88:  End (P95)

        89:  End (P95)

    90:  End (P95)

91:  End (P95)

; Check to see if both switches are detecting the magnet at the same time
92:  If Flag/Port (P91)
 1: 48       Do if Port 8 is High
 2: 30       Then Do

    93:  If Flag/Port (P91)
     1: 47       Do if Port 7 is High
     2: 30       Then Do

        ; Set error code
        94:  Z=F (P30)
         1: 5        F
         2: 0        Exponent of 10
         3: 7        Z Loc [ ERROR     ]

        95:  Z=X (P31)
         1: 5        X Loc [ Position  ]
         2: 46       Z Loc [ VALUE     ]

        ; Log the error data
        96:  Do (P86)
         1: 3        Call Subroutine 3


    97:  End (P95)

98:  End (P95)

;If the motor has stopped then we are clear to look at moving it if we want
99:  If Flag/Port (P91)
 1: 52       Do if Port 2 is Low
 2: 30       Then Do

    ; If flag 1 is high then we need to move the motor
    100:  If Flag/Port (P91)
     1: 11       Do if Flag 1 is High
```

```
 2: 30       Then Do

    ; Only attempt to move the gate if there is a direction specified
    101:  If (X<=>F) (P89)
     1: 6        X Loc [ Direction ]
     2: 1        =
     3: 0        F
     4: 30       Then Do

        ; Set error code
        102:  Z=F (P30)
         1: 4        F
         2: 0        Exponent of 10
         3: 7        Z Loc [ ERROR     ]

        ; Log the error data
        103:  Do (P86)
         1: 3        Call Subroutine 3

    104:  Else (P94)

        105:  Do (P86)
         1: 1        Call Subroutine 1

    106:  End (P95)

    ; Clear the flag to indicate that this has been successful
    107:  Do (P86)
     1: 21       Set Flag 1 Low

108:  End (P95)

; Otherwise it is still operating so we need to update the information
109:  Else (P94)

    ; Increment the counter
    110:  Z=X+Y (P33)
     1: 1        X Loc [ MotorOn_T ]
     2: 8        Y Loc [ ExecInt   ]
     3: 1        Z Loc [ MotorOn_T ]

    ; Check to see if the motor has been on longer than the maximum allowed time
    111:  If (X<=>Y) (P88)
     1: 1        X Loc [ MotorOn_T ]
     2: 3        >=
     3: 9        Y Loc [ MaxOnTime ]
     4: 30       Then Do

        ; If so, turn it off now and send out a message saying the move was unsuccessful
        112:  Do (P86)
         1: 52       Set Port 2 Low

        ; Allow a brief stop and then turn the direction relay off
        113:  Excitation with Delay (P22)
         1: 1        Ex Channel
         2: 1        Delay W/Ex (units = 0.01 sec)
         3: 0        Delay After Ex (units = 0.01 sec)
         4: 0        mV Excitation

        114:  Do (P86)
         1: 51       Set Port 1 Low

        ; Set error code
        115:  Z=F (P30)
         1: 2        F
         2: 0        Exponent of 10
         3: 7        Z Loc [ ERROR     ]

        116:  Z=X (P31)
         1: 1        X Loc [ MotorOn_T ]
         2: 46       Z Loc [ VALUE     ]

        ; Stop the counter
        117:  Z=F (P30)
         1: 0        F
         2: 0        Exponent of 10
```

```
     3: 1        Z Loc [ MotorOn_T ]

    ; Log the error data
    118:  Do (P86)
     1: 3        Call Subroutine 3

119:  End (P95)

; Measure the current being drawn by the pump
120:  Volt (Diff) (P2)
 1: 1        Reps
 2: 2        7.5 mV Slow Range
 3: 1        DIFF Channel
 4: 10       Loc [ Pump_I    ]
 5: 1.0      Mult
 6: 0.0      Offset

121:  Z=X (P31)
 1: 10       X Loc [ Pump_I    ]
 2: 48       Z Loc [ Pump_Curr ]

122:  Z=F (P30)
 1: 0        F
 2: 0        Exponent of 10
 3: 10       Z Loc [ Pump_I    ]

; Check to see if the current consumption of the motor is higher than whats allowed
123:  If (X<=>Y) (P88)
 1: 10       X Loc [ Pump_I    ]
 2: 3        >=
 3: 11       Y Loc [ MaxCurrnt ]
 4: 30       Then Do

    ; If so, turn it off now and send out a message saying the move was unsuccessful
    124:  Do (P86)
     1: 52       Set Port 2 Low

    ; Allow a brief stop and then turn the direction relay off
    125:  Excitation with Delay (P22)
     1: 1        Ex Channel
     2: 1        Delay W/Ex (units = 0.01 sec)
     3: 0        Delay After Ex (units = 0.01 sec)
     4: 0        mV Excitation

    126:  Do (P86)
     1: 51       Set Port 1 Low

    ; Set error code
    127:  Z=F (P30)
     1: 3        F
     2: 0        Exponent of 10
     3: 7        Z Loc [ ERROR     ]

    128:  Z=X (P31)
     1: 10       X Loc [ Pump_I    ]
     2: 46       Z Loc [ VALUE     ]

    ; Log the error data
    129:  Do (P86)
     1: 3        Call Subroutine 3

    ; Stop the counter
    130:  Z=F (P30)
     1: 0        F
     2: 0        Exponent of 10
     3: 1        Z Loc [ MotorOn_T ]

131:  End (P95)

132:  End (P95)

; ************************************************************
; *                                                          *
; *                                                          *
; *                                                          *
; *   Data output section                                    *
```

```
; *                                                              *
; *                                                              *
; *                                                              *
; ****************************************************************

133:  If time is (P92)
 1: 0        Minutes (Seconds --) into a
 2: 60       Interval (same units as above)
 3: 10       Set Output Flag High (Flag 0)

134:  Set Active Storage Area (P80)
 1: 1        Final Storage Area 1
 2: 2        Array ID

135:  Real Time (P77)
 1: 1220     Year,Day,Hour/Minute (midnight = 2400)

136:  Sample (P70)
 1: 1        Reps
 2: 35       Loc [ Level_1    ]

137:  Sample (P70)
 1: 1        Reps
 2: 28       Loc [ Temp_1     ]

138:  Resolution (P78)
 1: 1        High Resolution

139:  Sample (P70)
 1: 1        Reps
 2: 29       Loc [ EC_1       ]

140:  Resolution (P78)
 1: 0        Low Resolution

141:  Sample (P70)
 1: 1        Reps
 2: 30       Loc [ pH_1       ]

142:  Sample (P70)
 1: 1        Reps
 2: 37       Loc [ Offset_1   ]

143:  Sample (P70)
 1: 1        Reps
 2: 36       Loc [ Level_2    ]

144:  Sample (P70)
 1: 1        Reps
 2: 32       Loc [ Temp_2     ]

145:  Resolution (P78)
 1: 1        High Resolution

146:  Sample (P70)
 1: 1        Reps
 2: 33       Loc [ EC_2       ]

147:  Resolution (P78)
 1: 0        Low Resolution

148:  Sample (P70)
 1: 1        Reps
 2: 34       Loc [ pH_2       ]

149:  Sample (P70)
 1: 1        Reps
 2: 38       Loc [ Offset_2   ]

150:  If time is (P92)
 1: 0        Minutes (Seconds --) into a
 2: 1440     Interval (same units as above)
 3: 10       Set Output Flag High (Flag 0)

151:  Set Active Storage Area (P80)
 1: 1        Final Storage Area 1
```

```
 2: 24       Array ID

152:  Real Time (P77)
 1: 1220     Year,Day,Hour/Minute (midnight = 2400)

153:  Average (P71)
 1: 1        Reps
 2: 42       Loc [ BatV      ]

154:  Minimum (P74)
 1: 1        Reps
 2: 0        Value Only
 3: 42       Loc [ BatV      ]

155:  Average (P71)
 1: 1        Reps
 2: 43       Loc [ IntT      ]

; *************************************************************
; *                                                           *
; *                                                           *
; *                                                           *
; *   SMS Activation section                                  *
; *                                                           *
; *                                                           *
; *                                                           *
; *************************************************************
; If the ERROR does not equal zero then a message needs to be sent out, so allow
; that to happen.
156:  If (X<=>F) (P89)
 1: 7        X Loc [ ERROR     ]
 2: 2        <>
 3: 0        F
 4: 30       Then Do

    157:  Do (P86)
     1: 25       Set Flag 5 Low

    ; Check to see if the phone is turned on, if not, turn it on!
    ; Leave the phone turned on afterwards incase someone wants
    ; to dial into the system to check it out
    158:  If Flag/Port (P91)
     1: 53       Do if Port 3 is Low
     2: 30       Then Do

        159:  Do (P86)
         1: 43       Set Port 3 High

        160:  Excitation with Delay (P22)
         1: 1        Ex Channel
         2: 1000     Delay W/Ex (units = 0.01 sec)
         3: 0        Delay After Ex (units = 0.01 sec)
         4: 0        mV Excitation

    161:  End (P95)

162:  End (P95)

163:  Initiate Telecommunications (P97)
 1: 72       Generic Phone Modem
 2: 5        Disabled when User Flag 5 is High
 3: 20       Seconds Call Time Limit
 4: 0        Seconds Before Fast Retry
 5: 0        Fast Retries
 6: 0        Minutes before Slow Retry
 7: 45       Failures Loc [ FAIL_____ ]
 8: 0000     Call-back ID

164:  Extended Parameters 4 digit (P68)
 1: 87       Option ;Wait
 2: 10       Option ;1 sec before retry
 3: 69       Option ;Tx with echo [E{n}]
 4: 21       Option ; 21 chars
 5: 65       Option ;A
 6: 84       Option ;T
 7: 43       Option ;+
```

```
 8: 67        Option ;C

165:  Extended Parameters 4 digit (P68)
 1: 77        Option ;M
 2: 71        Option ;G
 3: 83        Option ;S
 4: 61        Option ;=
 5: 34        Option ;"
 6: 48        Option ;0
 7: 52        Option ;4
 8: 51        Option ;3

166:  Extended Parameters 4 digit (P68)
 1: 56        Option ;8
 2: 50        Option ;2
 3: 56        Option ;8
 4: 52        Option ;4
 5: 55        Option ;7
 6: 56        Option ;8
 7: 48        Option ;0
 8: 34        Option ;"

167:  Extended Parameters 4 digit (P68)
 1: 13        Option ;
 2: 82        Option ;Rx chars
 3: 3         Option ; 3 chars
 4: 10        Option ;LF
 5: 62        Option ;>
 6: 32        Option ;space
 7: 69        Option ;Tx with echo [E{n}]
 8: 19        Option ; 19 chars

168:  Extended Parameters 4 Digit (P68)
 1: 83        Option ;S
 2: 89        Option ;Y
 3: 83        Option ;S
 4: 84        Option ;T
 5: 69        Option ;E
 6: 77        Option ;M
 7: 32        Option ;
 8: 65        Option ;A

169:  Extended Parameters 4 Digit (P68)
 1: 76        Option ;L
 2: 65        Option ;A
 3: 82        Option ;R
 4: 77        Option ;M
 5: 33        Option ;!
 6: 32        Option ;
 7: 13        Option ;NEW LINE
 8: 73        Option ;I

170:  Extended Parameters 4 Digit (P68)
 1: 68        Option ;D
 2: 58        Option ;:
 3: 32        Option ;
 4: 76        Option ;Tx location with echo [L{loc}]
 5: 7         Option ; Location ID
 6: 69        Option ;Tx with echo [E{n}]
 7: 9         Option ; X chars
 8: 32        Option ;

171:  Extended Parameters 4 Digit (P68)
 1: 13        Option ;NEW LINE
 2: 86        Option ;V
 3: 97        Option ;a
 4: 108       Option ;l
 5: 117       Option ;u
 6: 101       Option ;e
 7: 58        Option ;:
 8: 32        Option ;

172:  Extended Parameters 4 Digit (P68)
 1: 76        Option ;Tx location with echo [L{loc}]
 2: 159       Option ; location Value
 3: 69        Option ;Tx with echo [E{n}]
```

```
 4: 1        Option ; 1 char
 5: 26       Option ; CTRL-Z
 6: 0000     Option
 7: 0000     Option
 8: 0000     Option


*Table 2 Program
  02: 0.0000    Execution Interval (seconds)

*Table 3 Subroutines
; ************************************************************
; *                                                          *
; *                                                          *
; *                                                          *
; *   SUBROUTINE SECTION                                     *
; *                                                          *
; *                                                          *
; *                                                          *
; ************************************************************
; Move the gate - checking first to see if it is required.
1:  Beginning of Subroutine (P85)
 1: 1        Subroutine 1

    ; Make sure that the motor has stopped
    2:  Do (P86)
     1: 52       Set Port 2 Low

    ; Allow a brief stop and then turn the direction relay off
    3:  Excitation with Delay (P22)
     1: 1        Ex Channel
     2: 1        Delay W/Ex (units = 0.01 sec)
     3: 0        Delay After Ex (units = 0.01 sec)
     4: 0        mV Excitation

    4:  Do (P86)
     1: 51       Set Port 1 Low

    ; Clear the timer
    5:  Z=F (P30)
     1: 0        F
     2: 0        Exponent of 10
     3: 1        Z Loc [ MotorOn_T ]

    ; If we want to head up, check that we are not already there!
    6:  If (X<=>Y) (P88)
     1: 6        X Loc [ Direction ]
     2: 1        =
     3: 2        Y Loc [ HIGH      ]
     4: 30       Then Do

        ; Check that the upper reed switch is not closed
        7:  If Flag/Port (P91)
         1: 57       Do if Port 7 is Low
         2: 30       Then Do

            ; Set the motor to go in the up position
            8:  Do (P86)
             1: 41       Set Port 1 High

            ; Have a short delay to make sure that the position relay has changed
            9:  Excitation with Delay (P22)
             1: 1        Ex Channel
             2: 1        Delay W/Ex (units = 0.01 sec)
             3: 0        Delay After Ex (units = 0.01 sec)
             4: 0        mV Excitation

            ; Start the motor
            10:  Do (P86)
             1: 42       Set Port 2 High

            ; Log the data
            11:  Do (P86)
             1: 2        Call Subroutine 2

        12:  Else (P94)
```

```
        ; We are trying to go to a position we are already at!
        ; so log the information

        13:  Z=F (P30)
         1: 1         F
         2: 0         Exponent of 10
         3: 7         Z Loc [ ERROR      ]

        ; Log the error data
        14:  Do (P86)
         1: 3         Call Subroutine 3

        ; And  clear this direction
        15:  Z=F (P30)
         1: 0         F
         2: 0         Exponent of 10
         3: 6         Z Loc [ Direction ]


    16:  End (P95)

17:  End (P95)

; If we want to head up, check that we are not already there!
18:  If (X<=>Y) (P88)
 1: 6         X Loc [ Direction ]
 2: 1         =
 3: 4         Y Loc [ LOW       ]
 4: 30        Then Do

    19:  If Flag/Port (P91)
     1: 58        Do if Port 8 is Low
     2: 30        Then Do

        ; Set the motor to go in the down position
        20:  Do (P86)
         1: 51        Set Port 1 Low

        ; Have a short delay to make sure that the position relay has changed
        21:  Excitation with Delay (P22)
         1: 1         Ex Channel
         2: 1         Delay W/Ex (units = 0.01 sec)
         3: 0         Delay After Ex (units = 0.01 sec)
         4: 0         mV Excitation

        ; Start the motor
        22:  Do (P86)
         1: 42        Set Port 2 High

        ; Log the data
        23:  Do (P86)
         1: 2         Call Subroutine 2

    24:  Else (P94)

        ; We are trying to go to a position we are already at!
        ; so log the information
        25:  Z=F (P30)
         1: 1         F
         2: 0         Exponent of 10
         3: 7         Z Loc [ ERROR      ]

        ; Log the error data
        26:  Do (P86)
         1: 3         Call Subroutine 3

        ; And clear this direction
        27:  Z=F (P30)
         1: 0         F
         2: 0         Exponent of 10
         3: 6         Z Loc [ Direction ]

    28:  End (P95)

29:  End (P95)
```

```
30:  End (P95)

; Log position data
31:  Beginning of Subroutine (P85)
 1: 2        Subroutine 2

    32:  Do (P86)
     1: 10       Set Output Flag High (Flag 0)

    33:  Set Active Storage Area (P80)
     1: 1        Final Storage Area 1
     2: 1        Array ID

    34:  Real Time (P77)
     1: 1221     Year,Day,Hour/Minute,Seconds (midnight = 2400)

    35:  Sample (P70)
     1: 1        Reps
     2: 1        Loc [ MotorOn_T ]

    36:  Sample (P70)
     1: 1        Reps
     2: 5        Loc [ Position  ]

37:  End (P95)

38:  Beginning of Subroutine (P85)
 1: 3        Subroutine 3

    39:  Do (P86)
     1: 10       Set Output Flag High (Flag 0)

    40:  Set Active Storage Area (P80)
     1: 1        Final Storage Area 1
     2: 500      Array ID

    41:  Real Time (P77)
     1: 1221     Year,Day,Hour/Minute,Seconds (midnight = 2400)

    42:  Sample (P70)
     1: 1        Reps
     2: 7        Loc [ ERROR     ]

43:  End (P95)

44:  Beginning of Subroutine (P85)
 1: 97       Subroutine 97

    ; Indicate our position
    45:  Z=X (P31)
     1: 2        X Loc [ HIGH      ]
     2: 5        Z Loc [ Position  ]

    ; Only stop the pump if the position matches the direction
    46:  If (X<=>Y) (P88)
     1: 6        X Loc [ Direction ]
     2: 1        =
     3: 5        Y Loc [ Position  ]
     4: 30       Then Do

        ; turn motor off
        47:  Do (P86)
         1: 52       Set Port 2 Low

        ; Log this stoppage information
        48:  Do (P86)
         1: 2        Call Subroutine 2

        49:  Z=F (P30)
         1: 0        F
         2: 0        Exponent of 10
         3: 1        Z Loc [ MotorOn_T ]

        ; Allow a brief stop and then turn the direction relay off
        50:  Excitation with Delay (P22)
```

```
          1: 1         Ex Channel
          2: 1         Delay W/Ex (units = 0.01 sec)
          3: 0         Delay After Ex (units = 0.01 sec)
          4: 0         mV Excitation

        ; Set the direction back to zero as we have finished moving
        51:  Do (P86)
          1: 51        Set Port 1 Low

        52:  Z=F (P30)
          1: 0         F
          2: 0         Exponent of 10
          3: 6         Z Loc [ Direction ]

    53:  End (P95)

54:  End (P95)


55:  Beginning of Subroutine (P85)
 1: 98        Subroutine 98

    ; Indicate our position
    56:  Z=X (P31)
     1: 4         X Loc [ LOW       ]
     2: 5         Z Loc [ Position  ]

    ; Only stop the pump if the position matches the direction
    57:  If (X<=>Y) (P88)
     1: 6         X Loc [ Direction ]
     2: 1         =
     3: 5         Y Loc [ Position  ]
     4: 30        Then Do

        ; turn motor off
        58:  Do (P86)
          1: 52        Set Port 2 Low

        ; Log this stoppage information
        59:  Do (P86)
          1: 2         Call Subroutine 2

        ; Stop the counter
        60:  Z=F (P30)
          1: 0         F
          2: 0         Exponent of 10
          3: 1         Z Loc [ MotorOn_T ]

        ; Allow a brief stop and then turn the direction relay off
        61:  Excitation with Delay (P22)
          1: 1         Ex Channel
          2: 1         Delay W/Ex (units = 0.01 sec)
          3: 0         Delay After Ex (units = 0.01 sec)
          4: 0         mV Excitation

        ; Set the direction back to zero as we have finished moving
        62:  Do (P86)
          1: 51        Set Port 1 Low

        63:  Z=F (P30)
          1: 0         F
          2: 0         Exponent of 10
          3: 6         Z Loc [ Direction ]


    64:  End (P95)

65:  End (P95)


End Program

-Input Locations-
1 MotorOn_T 1 4 6
2 HIGH      1 7 1
3 MIDDLE    1 1 1
```

```
4 LOW        1 7 1
5 Position   1 8 5
6 Direction  1 5 8
7 ERROR      1 2 9
8 ExecInt    1 1 1
9 MaxOnTime  1 1 1
10 Pump_I    1 3 2
11 MaxCurrnt 1 1 1
12 Seconds   1 2 1
13 OldSecond 1 1 1
14 Time      1 2 1
15 TRIG_ph_U 1 1 1
16 TRIG_EC_U 1 1 1
17 TRIG_LvlU 1 1 1
18 TRIG_LvlL 1 1 1
19 SDI_Mes1  1 4 2
20 SDI_Mes2  1 2 0
21 SDI_Mes3  1 2 0
22 SDI_Mes4  1 2 0
23 SDI_Mes5  0 0 0
24 SDI_Mes6  0 0 0
25 SDI_Mes7  0 0 0
26 SDI_Mes8  0 0 0
27 Press_1   1 1 1
28 Temp_1    1 1 1
29 EC_1      1 2 1
30 pH_1      1 2 1
31 Press_2   1 1 1
32 Temp_2    1 1 1
33 EC_2      1 1 1
34 pH_2      1 1 1
35 Level_1   1 2 1
36 Level_2   1 2 1
37 Offset_1  1 2 1
38 Offset_2  1 2 1
39 Minutes   1 2 1
40 PhoneOn   1 1 1
41 PhoneOff  1 1 1
42 BatV      1 4 1
43 IntT      1 1 1
44 _____     1 0 0
45 FAIL_____ 1 0 1
46 VALUE     1 0 6
47 BatV_Min  1 1 1
48 Pump_Curr 1 0 1
-Program Security-
0000
0000
0000
-Mode 4-
-Final Storage Area 2-
0
-CR10X ID-
0
-CR10X Power Up-
3
```

Appendix E. Modified Fortran Parameters

The following parameters were modified by grepping through the FORTRAN source code, and then adjusting the parameters to suite the model. The FORTRAN code was then recompiled with Digital Compaq Visual FORTRAN compiler for Windows. A description of each parameter is also given.

3-D MESH

PARAMETER (NX=45,NY=28,NZ=16)

ARRAY DIMENSIONS DECLARATIONS

1. FOR BOTH FLOW AND TRANSPORT

PARAMETER (MAXNPK=3500, MAXELK=6000)

PARAMETER (MXBNPK=2*(NX*NY+NX*(NZ-2)+(NY-2)*(NZ-2)))

PARAMETER (MXBESK=5000)

PARAMETER (MXTUBK= 4*MXBNPK, MXJBDK=51, MXKBDK=35, MXNTIK=50)

PARAMETER (MXMATK=15, MXRMPK=8, MXDTCK=200)

2. FOR FLOW SOURCE/SINK, BOUNDARY CONDITIONS

PARAMETER (MXWNPH=20, MXWPRH=20, MXWDPH=50)

PARAMETER (MXDNPH=3500, MXDPRH=100, MXDDPH=2200)

PARAMETER (MXCNPH=2*NX*NZ+2*(NY-2)*NZ)

PARAMETER (MXCESH=2*(NX-1)*(NZ-1)+2*(NY-1)*(NZ-1))

PARAMETER (MXCPRH=10,MXCDPH=2200)

PARAMETER (MXVNPH=NX*NY, MXVESH=(NX-1)*(NY-1))

PARAMETER (MXVPRH=10,MXVDPH=365)

PARAMETER (MXNNPH=2*NX*NZ+2*(NY-2)*NZ)

PARAMETER (MXNESH=2*(NX-1)*(NZ-1)+2*(NY-1)*(NZ-1))

PARAMETER (MXNPRH=10,MXNDPH=2200)

PARAMETER (MXRNPH=NX*NY, MXRPRH=10, MXRDPH=50, MXRMAH=10)

PARAMETER (MXRESH=(NX-1)*(NY-1))

3. FOR TRANSPORT SOURCE/SINK, BOUNDARY CONDITIONS, AND MATERIALS

PARAMETER (NXG=1, NYG=1, NZG=1)

PARAMETER (MXNPWK= (NXG+1)*(NYG+1)*(NZG+1), MXELWK= NXG*NYG*NZG)

PARAMETER (MXWNPC=20, MXWPRC=20, MXWDPC=50)

PARAMETER (MXDNPC=3500, MXDPRC=100, MXDDPC=2200)

PARAMETER (MXCNPC=2*NX*NZ+2*(NY-2)*NZ)

PARAMETER (MXCESC=2*(NX-1)*(NZ-1)+2*(NY-1)*(NZ-1))

PARAMETER (MXCPRC=10, MXCDPC=2200)

PARAMETER (MXVNPC= NX*NY, MXVESC= (NX-1)*(NY-1), MXVPRC= 10, MXVDPC= 2200)

PARAMETER (MXNNPC=2*NX*NZ+2*(NY-2)*NZ)

PARAMETER (MXNESC=2*(NX-1)*(NZ-1)+2*(NY-1)*(NZ-1))

PARAMETER (MXNPRC=10, MXNDPC=2200)

4. FOR XY1 SERIES CARD

PARAMETER (MXXYS=500,MXXYP=2500,MXSPMK=MXXYP)

5. FOR WORKING ARRAY

PARAMETER (MXRSCB=1500, KTMP=4*MXRSCB)

6. FOR POST-PROCESSING ARRAY

PARAMETER (MXPOST=100)

DESCRIPTION OF PARAMETERS

The list and definition of the control parameters required for the model are given below:

MAXNPK = maximum number of nodes in the 3-D mesh

MAXELK = maximum number of element in the 3-D mesh

MXBESK = maximum number of boundary-element surfaces

MXBNPK = maximum number of nodal points at the boundary

MXJBDK = maximum number of element for node connectivity

MXKBDK = maximum number of element for element connectivity

Material and Soil Properties

MXMATK = maximum number of soil types

MXSPMK = maximum number of data points to describe soil characteristic curve in unsaturated zone

MXMPMK = maximum number of material properties per material (hydraulic conductivity)

MXRMPK = maximum number for coefficients of the viscosity and density functions

HEAD Boundary Conditions

For flow simulation:

MXDNPH = maximum number of head nodal points

MXDPRH = maximum number of head profiles

MXDDPH = maximum number of data points on each profile

For transport simulation:

MXDNPC = maximum number of concentration nodal points

MXDPRC = maximum number of concentration profiles

MXDDPC = maximum number of data points on each profile

NXG = maximum number of grids for element tracking in x-direction

NYG = maximum number of grids for element tracking in y-direction

NZG = maximum number of grids for element tracking in z-direction

FLUX Boundary Conditions

1. Cauchy flux boundary condition:

For flow simulations:

MXCNPH = maximum number of flux nodal points

MXCESH = maximum number of flux element surfaces

MXCPRH = maximum number of flux rate profiles

MXCDPH = maximum number of data points on each flux rate profile

For transport simulations:

MXCNPC = maximum number of nodal points for concentration

MXCESC = maximum number of element surfaces for concentration

MXCPRC = maximum number of concentration profiles

MXCDPC = maximum number of data points on each concentration profile

2 Neumann flux boundary condition:

For flow simulations:

MXNNPH = maximum number of flux nodal points

MXNESH = maximum number of flux element surfaces

MXNPRH = maximum number of fluxrate profiles

MXNDPH = maximum number of data points on each flux rate profile

For transport simulations:

MXNNPC = maximum number of nodal points for concentration

MXNESC = maximum number of element surfaces for flux rate

MXNPRC = maximum number of concentration profiles

MXNDPC = maximum number of data points on each flux rate profile

3. Rainfall-Seepage Boundary Conditions

For flow simulations:

MXVNPH = maximum number of ground nodal points

MXVESH = maximum number of ground element surfaces

MXVPRH = maximum number of rainfall-seepage profile

MXVDPH = maximum number of data points on each rainfall-seepage profile

For transport simulations:

MXVNPC = maximum number of ground nodal points

MXVESC = maximum number of ground element surfaces

MXVPRC = maximum number of rainfall-seepage profile

MXVDPC = maximum number of data points on each rainfall-seepage profile

Source/Sink Boundary Conditions

For flow simulations:

MXWNPH = maximum number of well nodal points

MXWPRH = maximum number of well source/sink profiles

MXWDPH = maximum number of data points on each well source/sink profile

For transport simulations:

MXWNPC = maximum number of well nodal points for concentration

MXWPRC = maximum number of well source/sink profiles for concentration

MXWDPC = maximum number of data points on each well source/sink profile

The FEMWATER program is limited to allow NX*NY*NZ nodes. There are NX nodes along the x-direction, NY nodes long the y-direction, and NZ nodes along the z-direction.

Appendix F. Films of Saline Intrusion Taken From Finite Element Simulations

See Attached CD.